UNIVERSITY OF WOLLONGONG AUSTRALIA

Following the DNA damage response in *Escherichia coli*

Single-molecule studies of proteins in live cells

Sarah Sylviane Henrikus

Supervisors:

Dr Andrew Robinson and Distinguished Professor Dr Antoine M. van Oijen

This thesis is presented as part of the requirement for the conferral of the degree:

Doctor of Philosophy

The University of Wollongong

Molecular Horizons Institute and School of Chemistry and Molecular Bioscience

August 2019

Abstract

Bacterial resistance to antibiotics has become a major health problem worldwide. The rapid development of drug-resistant strains to clinically used antibiotics and the slow rate of development of new treatment options threaten a healthcare catastrophe. Currently, 700,000 deaths per year are attributable to antimicrobial resistance. By 2050, antibiotic resistance is estimated to contribute to the deaths of 10 million people per year. In recent years, bacteria have emerged resistance to all classes of antibiotics. More than ever, there is a necessity for new antibiotics, exploring new mechanisms of action.

In the search for new drug targets, it is fundamentally important to understand how bacteria battle and develop resistance to antibiotics used in the clinic. It is possible that by understanding the mechanisms of the DNA damage response that promote resistance to antibiotics, new drug targets may be identified. The scope of this thesis is to characterise DNA repair and damage tolerance pathways in *Escherichia coli*, focusing on the interconnectivity between error-prone DNA polymerases and homologous recombination. Using single-molecule fluorescence live-cell imaging, it has been possible to monitor proteins involved in these pathways directly and in real time.

Monitoring proteins at the single-molecule level in live cells has allowed me to make significant new discoveries. My PhD work challenges long-standing models in the fields of translesion synthesis (TLS) and homologous recombination in *Escherichia coli*. The error-prone DNA polymerase IV (pol IV) has long been assumed to mainly carry out TLS at stalled replication forks. My live-cell work has revealed that pol IV primarily acts at recombination intermediates and rarely, if ever, binds at replisomes. The resection of DNA double-strand breaks is crucial to pol IV activity in cells, suggesting that pol IV could be a recombination protein. Strikingly, this requirement is shared for cells treated with antibiotics that have different primary targets in cells. The common element appears to be surges in cellular ROS levels, which induce DNA breakage and thus create substrates for pol IV.

My real-time live-cell imaging approach also allowed me to functionally dissect the RecFOR pathway for homologous recombination. Conventionally, the recombination mediators RecF, RecO and RecR have been described to collectively load the RecA recombinase on single-stranded DNA. Contrary to this model, single-molecule imaging revealed that RecF and RecO rarely form a complex *in vivo* and indicated that RecF and RecO have distinct functions. RecF binds mainly at replisomes while RecO binds to DNA in the region between the nucleoid and membrane, the same region of the cell in which large RecA bundles form in cells carrying DNA damage. Following RecF, I further showed that RecF impacts on pol IV binding at the replisome; a new link connecting the fields of TLS and homologous recombination. This Thesis provides unprecedented single-molecule level insight into the mechanisms of TLS and homologous recombination in *Escherichia coli* cells suffering DNA damage and, importantly, reveals new and unexpected links between the two processes.

Context statement

This Thesis summarizes studies at the interface of translesion synthesis (TLS) and homologous recombination, revealing that in many ways the pathways are interlinked. Throughout there is a focus on understanding mutation-promoting processes and their potential roles in antimicrobial resistance development. By understanding how repair enzymes within different pathways contribute to resistance, new drug targets may be identified. To observe repair enzymes within living cells, I employed single-molecule fluorescence live-cell imaging, in combination with microfluidic devices, monitoring proteins as they bind to their targets in real time during the dynamic DNA repair response. To follow each protein of interest, fluorescent protein fusion constructs were used, where the protein of interest is covalently coupled to a fluorescent protein due to genetic alterations. The motion of repair enzymes was then determined by following the signal of their fluorescent protein tag. This approach is very powerful when combined with genetics approaches as mutants that cause alterations to protein binding behavior give clues about how that protein may function within living cells.

Live-Cell Imaging Revolution. Single-molecule microscopy went through a revolution during the last decades. The discovery of the green fluorescent protein, GFP, started the revolution, pushing the experimental tools in life sciences.

The 'green revolution' created the platform for novel functional imaging of live probes and for single-molecule fluorescence microscopy. In 1997, the Moerner lab demonstrated single GFP molecules blinking upon laser exposure, where bleached GFP molecules could be switched back on following laser exposure. With the blinking phenomenon and the advantage that GFP can mature *in vivo*, protein-based fluorescent probes became attractive as fluorescent biological labels. In the following years, the development in molecular cloning techniques generated numerous GFP mutants with improved photophysical characteristics, improving for instance photostability for longer measurement time in life cells. Molecular cloning techniques also made it possible to generate genetically encoded fluorescent probes, where the protein of interest is covalently linked with a fluorescent protein. This approach enabled researchers to follow proteins by watching the fluorescent protein tag in cells. This approach is called detection-by-localisation. To allow the detection of all locations of target molecules, which can be limited due to photobleaching, photoactivatable probes were developed which can be repeatedly activated and imaged. These probes lead to the development of new imaging approaches such as photoactivated localization microscopy (PALM) and stochastic optical reconstruction microscopy (STROM).

Localisation microscopy with either non-photoactivatable or photoactivatable fluorescent fusion protein constructs allowed researchers to measure several previously inaccessible parameters which are however required to understand cellular processes. For example, analysis of focus lifetimes can allow binding kinetics to be measured as individual proteins bind to their substrates in live cells. To untangle the function of proteins within biological processes, mutants can be employed to alter protein functions, and the resulting changes in focus lifetimes can be monitored. Localisation microscopy can also be used to determine the stoichiometry of a protein complex, where the known intensity of a single fluorescent protein can be used to determine the number of proteins in a focus. A prominent example for this

measurement was published by Reyes-Lamothe *et al.*, where the authors determined the composition of the *Escherichia coli* replisome. Furthermore, the known intensity of a single fluorescent protein together with the fluorescent intensity measured for single cells can be used to determine the number of molecules per cell; a useful approach to monitoring changes in protein expression levels, or transcription bursts.

At the beginning of my PhD in 2016, a small collection of single-molecule live-cell imaging studies has been performed using these approaches. Besides determining the replisome composition in *Escherichia coli* and localizing proteins to the fork, other systems were studied such as the role of the CI repressor in regulating the expression of λ genes in *Escherichia coli* (Hensel *et al.*). Another example is the visualization of the hexameric state of the FtsK N-terminal domain at the division site in *Escherichia coli* (Bisicchia *et al.*). In the van Oijen group, single-molecule live-cell imaging began with a study of the error-prone DNA polymerase V in *Escherichia coli*, revealing a novel type of spatiotemporal regulation that is induced upon response to DNA damage (Robinson *et al.*). This study laid the basis for further *in vivo* studies to be conducted in live cells, investigating other low-abundance systems in *Escherichia coli*, in particular those responsible for DNA replication and repair.

Thesis context. Two major DNA repair and damage tolerance pathways were of interest for this Thesis: those involving error-prone translesion synthesis polymerases (TLS polymerases) and the homologous recombination system responsible for the repair of single-stranded DNA gaps, comprised by the RecF, RecO and RecR proteins. The goal of my Thesis was to understand how DNA damage filters through these two seemingly independent pathways. My thesis is based on four specific aims: **1.** Identify major substrates of the error-prone DNA polymerase IV (pol IV) in *Escherichia coli*. At the beginning of my studies, pol IV was most often described to work in TLS at stalled replisomes, assisting in the recovery of DNA replication in cells experiencing extensive DNA damage. Thus, I initially focused on replisomes as a pol IV binding target and later investigated the role of pol IV in homologous recombination. **2.** Determine the composition of the RecFOR complex following DNA damage induction, where RecFOR facilitated homologous recombination reactions. The main open questions were whether a RecFOR complex exists and whether RecF and RecO have the same binding targets. 3**.** Compare pol IV to other error-prone DNA polymerases such as DNA polymerase V (pol V). Therefore, I investigated if these polymerases, both being error-prone, work on the same DNA substrate; or rather bind to different substrates. **4.** Determine mechanistic differences between pol V and its homolog pol V_{ICE}, which is much more error-prone than pol V. To investigate these four aims, I primarily employed single-molecule live-cell imaging, allowing me to determine expression levels, localisations, co-localisation against other markers, stoichiometries and binding lifetimes.

This Thesis presents single-molecule live-cell imaging studies on pol IV, pol V, pol V_{ICE}, RecF and RecO. The findings presented begin to draw a broad picture of how bacterial cells deal with DNA damage, starting to understand how DNA damage is distributed to different pathways for repair or damage tolerance. In particular, my findings reveal that the major role of pol IV is in double-strand break repair, intertwining the fields of TLS and homologous recombination. We are just beginning to scratch the surface of these systems, and all the other systems into which single-molecule imaging can provide new insight. My work represents important first steps in this endeavor.

Chapter 1 broadly reviews current literature on the development of antibiotic resistance, written in my 1st year and expanded over the course of my PhD. My supervisors Andrew Robinson and Antoine M. van Oijen monitored my progress and provided assistance in writing this review. Briefly, cells have evolved different DNA repair and damage tolerance pathways to overcome endogenous and exogenous damage. This literature review primarily elaborates on error-prone DNA polymerases which generate mutations, as well as, the major DNA repair pathway, homologous recombination. Historically, error-prone polymerases have been described to carry out TLS at stalled replisomes. Pol IV has however also been described to work on single-stranded DNA gaps originating from replisomal lesion skipping, stalled transcription complexes and recombination intermediates.

The study described in **Chapter 2** measures the DNA binding activities of the error-prone DNA polymerase IV close to, and away from replisomes *in vivo*. Using different DNA damaging agents (methylmethane sulfonate [MMS] and ciprofloxacin) and UV light, this study shows that the majority of DNA polymerase IV (pol IV) activity occurs outside of replisomes, presumably at substrates other than stalled replisomes. This study demonstrates that only 5–10% of foci induced by DNA damage form nearby replisomes, indicating that pol IV predominantly works in a non-replisomal context. In addition, replisomal formed pol IV foci exhibit a broad distribution of colocalisation distances, suggesting that pol IV carries out postreplicative TLS in gaps behind the replisome, or carries out activities at other structures that form close behind replication forks. For this study, Elizabeth A. Wood (from Michael M. Cox's lab, Department of Biochemistry, University of Wisconsin-Madison, Madison, United States) constructed the majority of strains by using λ_{RED} recombination. I was also involved in the construction of strains, transducing alleles produced by Wood into selected cell lines and carrying out transformations to introduce plasmids. Using these strains, I carried out plate-based spot assays to measure cell survival upon antibiotic treatment, determining whether cells expressing fluorescent protein fusions exhibited similar tolerance to stressors as wild-type cells, or if the presence of the fluorescent protein impaired the activity of the tagged repair enzymes. I further carried out ciprofloxacin resistance assays to compare rates of ciprofloxacin-resistance evolution in the various strains. After characterization, I recorded all the microscopy data that forms the main basis of the study. Live-cell single-molecule experiments were carried out in either quartz- or PDMS-based flow-cells, which were home-built. Single-colour time-lapse movies of pol IV were recorded to characterize its up-regulation in cells exposed to DNA-damaging agents, while video rate movies were collected to investigate the nucleoid-binding behavior of pol IV. I further recorded two-colour time-lapse movies to quantify rates of pol IV focus formation at, and away from replisomes. Analysis of data utilised scripts from past and present lab members, as well as scripts that I wrote myself in MATLAB and java, then run in ImageJ. Western blotting of DinB expression levels was carried out by John P. McDonald in Roger Woodgate's lab, Laboratory of Genomic Integrity, National Institute of Child Health and Human Development, National Institutes of Health, Bethesda, United States. The manuscript was drafted by myself, Andrew Robinson, Michael M. Cox, Roger Woodgate, Myron F. Goodman. Antoine van Oijen edited drafts and contributed intellectually to the study design and data interpretation.

Chapter 3 reviews different models of error-prone DNA polymerase activities that have been described in *Escherichia coli*, in particular activities other than TLS at stalled replication forks. The

review was inspired by the findings of the study described in Chapter 2; if pol IV rarely works at replication forks, where might it (and other TLS polymerases) work? Genetic and biochemical studies have generated evidence for TLS polymerases being involved in nucleotide excision repair, homologous recombination and transcription pathways. In addition, treatments with cell stressors (compounds that damage DNA, deplete the nucleotide pool, inhibit cell wall synthesis etc.) are known to result in accumulation of reactive oxygen species within cells, oxidizing the nucleotide pool. Oxidation of the nucleotide pool increases mutation rates by promoting TLS. The review was written by me with input from Andrew Robinson. Antoine van Oijen reviewed the manuscript.

In **Chapter 4**, I show that processing of DNA double-strand breaks via the RecBCD pathway is crucial for both the damage-induced upregulation of pol IV expression, and for the binding of pol IV to its substrates on the nucleoid. The study utilized two antibiotics, ciprofloxacin and trimethoprim, which both promote the formation of double-strand breaks, but have different mechanisms of action. Both antibiotics induce SOS-mediated upregulation of pol IV in cells. The SOS signal originates from double-strand breaks, some of which are dependent of reactive-oxygen species (ROS). Formation of ROS-dependent double-strand breaks is a known property of many antibiotics. These observations support that pol IV primarily works in DSB repair in cells. Ultimately, ROS-induced DSBs may contribute to pol IV activity in mutagenic DSB repair. This project evolved from observations that I made and I drove the study. It is important to point out, however, that Camille Henry (from Michael M. Cox's lab, Department of Biochemistry, University of Wisconsin-Madison, Madison, United States) also played a key role in the development of this study, bringing in her knowledge about the accumulation of ROS during antibiotic treatment. Strain construction was a collaborative effort between Camille Henry, Steven T. Bruckbauer and Elizabeth A. Wood (all three from Michael M. Cox's lab, Department of Biochemistry, University of Wisconsin-Madison, Madison, United States), Roger Woodgate (Laboratory of Genomic Integrity, National Institute of Child Health and Human Development, National Institutes of Health, Bethesda, United States) and Megan E. Cherry (PhD student in the Robinson/van Oijen lab, School of Chemistry and Molecular Bioscience, University of Wollongong, Wollongong, Australia), and myself. ROS reporter plasmids and MuGam-PAmCherry vector were constructed by Camille Henry, Steven T. Bruckbauer and Elizabeth A. Wood. The MuGam vector is based on a plasmid construct from Harshad Ghodke (PostDoc in the van Oijen lab, School of Chemistry and Molecular Bioscience, University of Wollongong, Wollongong, Australia). Fluorescent protein fusion constructs were characterized by Camille Henry, employing DNA damaging agent sensitivity assays. I carried out the survival assay for the MuGam-PAmCherry vector, to determine the induction level for single-molecule imaging, choosing a non-toxic expression range. All plate-reader assays were carried out by me, measuring increases in intracellular ROS and SOS induction levels. In addition, I carried out all single-molecule experiments of this live-cell study, performing experiments in home-build quartz flow cells. From previous work by Yvonne Hellmich, a former intern (now PhD student at Institute of Biochemistry, Goethe Universität, Frankfurt, Germany), I adapted trimethoprim concentrations used for single-molecule live-cell imaging. Time-lapse experiments were recorded to follow pol IV, pol V, replisome markers and SOS induction levels. Two-colour video rate movies of pol IV were recorded to determine if pol IV binds longer at or away from replisomes, comparing cells before and after DNA damage induction. I performed the data analysis by

using MATLAB and java scripts from past and present members of the van Oijen lab, as well as scripts that I wrote myself. Western blotting was carried out by John P. McDonald in Roger Woodgate's lab. I drafted the manuscript, which was initially edited by Camille Henry, Harshad Ghodke and Andrew Robinson. Roger Woodgate, Michael M. Cox and Antoine van Oijen reviewed later versions of the manuscript.

Subchapter 4.8 contains additional data obtained during this study, which link the nucleoid-binding activities of pol IV with the recombination mediator protein RecF. Cells lacking RecF show increased colocalization between pol IV and replisome markers, suggesting that RecF normally inhibits pol IV binding near replisomes. Strain construction and experiments for this subchapter involved Elizabeth A. Wood and myself. I wrote the subchapter.

The study described in **Chapter 5** shows that RecA and UmuD cleavage modulate the binding activity of pol IV, providing a possible model for regulation of the error-prone activity of pol IV. The recombinase RecA, in particular RecA* nucleoprotein filament structures, recruit pol IV to the nucleoid. Up to 40% of pol IV foci colocalised with the RecA* probe mCI. It has been reported that RecA modulates the mutagenic activity of pol IV (i.e. during DSB repair). Based on these reports, pol IV might be expected to incorporate nucleotides with low fidelity when acting at these RecA* structures. The results described in this chapter further support the notion that pol IV primarily works in homologous recombination. Furthermore, Chapter 5 also investigates the UmuD protein as another regulator of pol IV mutagenicity *in vivo*. In the absence of DNA damage, full-length UmuD promotes error-free, long-lived pol IV binding events which last for some seconds. Following DNA damage, RecA* filaments promote the autocleavage of UmuD to its cleaved form UmuD′. In the presence of UmuD′, pol IV is known to generate -1 frameshift mutations at an elevated rate. However, I found that UmuD′ also reduces pol IV binding, suggesting that UmuD′ helps to control the mutagenic activity of pol IV by reducing its binding to the nucleoid. For this study, the strain construction involved Elizabeth A. Wood (from Michael M. Cox's lab, Department of Biochemistry, University of Wisconsin-Madison, Madison, United States), Roger Woodgate (Laboratory of Genomic Integrity, National Institute of Child Health and Human Development, National Institutes of Health, Bethesda, United States) and me. Plasmids for single-molecule imaging experiments were designed and constructed by John P. McDonald from Roger Woodgate's lab and Roger Woodgate himself. All single-molecule experiments were carried out and analyzed by me using the previously established analysis pipeline. Time-lapse experiments revealed that pol IV foci colocalise with the RecA* probe after DNA damage indcution. Rapid video-rate movies showed that pol IV foci are promoted in different backgrounds such as *recA*E38K cells and cells expressing the uncleavable UmuDK96A enzyme. My single-molecule observations brought forward the idea that we should test if pol IV directly interacts with RecA*, which required purification of pol IV and RecA. Proteins were expressed and purified Matthew L. Ritger (former intern in Michael M. Cox's lab) and Phuong T. Pham (Assistant Professor in Myron F. Goodman's lab, Departments of Biological Sciences and Chemistry, University of Southern California, Los Angeles, United States). The interaction between pol IV and RecA* was tested through surface plasmon resonance experiments. These experiments confirmed that pol IV can associate with RecA* filaments on DNA, intriguingly, pol IV can even bind to filaments formed on double-stranded DNA when using RecAE38K mutant. The same mutant

promotes the formation of pol IV foci in cells, even in the absence of exogenous DNA damage. Together the observations support a physical interaction between pol IV and RecA* *in vivo*. These experiments were performed by Amy E. McGrath (PostDoc in Nicholas E. Dixon's and Aaron J. Oakley's lab, School of Chemistry and Molecular Bioscience, University of Wollongong, Wollongong, Australia) and Slobodan Jergic (Senior PostDoc in the van Oijen lab, School of Chemistry and Molecular Bioscience, University of Wollongong, Wollongong, Australia). These experiments were designed by Harshad Ghodke and Slobodan Jergic (both at School of Chemistry and Molecular Bioscience, University of Wollongong, Wollongong, Australia). To support that RecAE38K filaments form on double-stranded DNA, Matthew L. Ritger from Michael M. Cox's lab performed the LexA cleavage assay and ATPase assay. Ritger showed that RecAE38K filaments formed on double-stranded DNA can cleave LexA, which is the signal for SOS induction in cells. This finding is consistent with *recA*E38K cells constitutively having the SOS response turned on. I drafted the manuscript, which was initially edited by Amy E. McGrath, Harshad Ghodke and Andrew Robinson. Myron F. Goodman, Michael M. Cox and Antoine van Oijen reviewed the manuscript.

Chapters 4 and 5 revealed new links between pol IV and RecA-dependent processes. **Chapter 6** investigates recombination mediator proteins that are thought to assist in loading RecA onto single-stranded DNA gaps. During the repair of ssDNA gaps, the proteins RecF, RecO and RecR have been described to load RecA recombinase on ssDNA gaps as a complex. The study described in Chapter 6 sought to resolve a long-standing controversy in the field; whether or not RecF, RecO and RecR act independently, or as a complex. The study revealed that RecF and RecO rarely colocalize in cells, implying that they do not form a complex *in vivo*. Single-molecule imaging revealed several differences in the spatiotemporal behaviours of RecF and RecO, suggesting that RecF and RecO have distinct functions in cells. RecF frequently binds at sites of replisomes, whereas RecO binds to DNA in a region of the cell between the main nucleoid mass and the cell membrane. This is the same region in which large bundles of RecA protein have been observed by others. In addition, the study revealed that RecF dimerizes in cells exposed to UV irradiation, and that RecF focus formation depends on RecR. This observation, together with previous published reports, implies that RecF and RecR act as a complex *in vivo*. Beyond this, stalling of active replicative by using a temperature-sensitive helicase mutant, results in the loss of replisome, RecF and RecO foci. This observation might be consistent with RecF and/or RecO working around post-replicative gaps and/or being physically coupled to the replisome. Interestingly, initial findings suggest that the RecF may exclude pol IV from its binding sites close to replisomes. This project originates from the lab of Michael M Cox (Department of Biochemistry, University of Wisconsin-Madison, Madison, United States), who developed the project together with Elizabeth A. Wood. Strains used in this study were constructed by Elizabeth A. Wood, Camille Henry (both from Michael M. Cox's lab, Department of Biochemistry, University of Wisconsin-Madison, Madison, United States), Harshad Ghodke (from the van Oijen lab, School of Chemistry and Molecular Bioscience, University of Wollongong, Wollongong, Australia) and me. Camille Henry together with undergraduate interns Neema Mbele, Roopashi Saxena,and Upasana Basu, measured growth curves and fitness values of fusion strain constructs, determining if fusion constructs behave similar to wild-type cells. For fitness measurements, they used a modified growth competition assay described by Lenski *et al.*, a two-colour colony assay

using tetrazolium arabinose indicator plates. They further conducted UV survival, SOS induction assays using mytomycin C and plate-based sensitivity assays. I carried out all microscopy experiments, recording time-lapse movies of RecF, RecO and replisome markers, capturing their spatiotemporal behaviour. In addition, I recorded video-rate movies of RecF and RecO, to determine if they exist in a monomeric or dimeric form. With the exception of the autocorrelation analysis, which was carried out by Andrew Robinson, I analyzed all other data using MATLAB and java scripts written by past and present van Oijen lab members and by myself. I drafted the manuscript together with Camille Henry and Michael M. Cox. Initial edits were made by Andrew Robinson and Harshad Ghodke. Antoine van Oijen reviewed the manuscript.

Subchapter 6.7 explains additional data, imaging RecF and RecO in context of the RecA* probe mCI, which binds to RecA* filaments, the intermediates of recombination reactions. Strain construction and experiments involved Elizabeth A. Wood, Harshad Ghodke and me. I wrote this subchapter.

The study described in **Chapter 7** investigates another class of RecA-dependent process, DNA synthesis by the highly error-prone polymerase V (pol V) and its homolog encoded on an integrative conjugative element, pol V_{ICE391}. Besides RecA* being a key regulator for pol IV activity, it has long been understood that RecA* filaments are required for the activation of pol V and pol V_{ICE391}. Both of the pol V enzymes investigated in this chapter are highly mutagenic. Pol V_{ICE391} is however more efficient at promoting spontaneous mutagenesis than pol V; it is the most potent pol V mutator reported to date. To understand how the high mutagenicity of pol V_{ICE391} materializes from events occurring at the molecular level, we compared polV_{ICE391} with pol V behavior via single-molecule imaging. We observed that both polymerases bind repetitively to the nucleoid, with pol V_{ICE391} binding to its substrates for longer periods than pol V. Additionally, pol V_{ICE391} also incorporates nucleotides much faster than pol V. For these slow polymerases, it is unlikely that every binding event leads to the incorporation of nucleotides, however the probability is increased for pol V_{ICE391}, which binds for longer and act faster. This study further utilizes a steric gate pol V_{ICE391} variant (pol V_{ICE391}_Y13A), which exhibits increased mutation rates due to its ability to incorporate ribonucleotides into the *E. coli* genome. In cells that conduct ribonucleotide excision repair (RER), mutation rates are minimized because active RER removes misincorporated ribonucleotides. When removing RNase HII, nucleotide excision repair (NER) contributes to the removal of misincorporated ribonucleotides. Most RNaseHII and NER-independent RER are found on the lagging strand, which is an important activity in genome maintenance. This project was developed by Roger Woodgate and his laboratory (Laboratory of Genomic Integrity, National Institute of Child Health and Human Development, National Institutes of Health, Bethesda, United States). Bacterial strains and plasmids were made by John P. McDonald, Roger Woodgate (both Woodgate lab), Thomas J. Armstrong and me (both PhDs student in the Robinson/van Oijen lab, School of Chemistry and Molecular Bioscience, University of Wollongong, Wollongong, Australia). Quantitative spontaneous mutagenesis was measured by Erin Walsh. Western blotting to detect plasmid encoded UmuC and RumB proteins was performed by John P. McDonald (in Laboratory of Genomic Integrity, National Institute of Child Health and Human Development, National Institutes of Health, Bethesda, United States). He also expressed and purified pol V_{ICE391}_Y13A and conducted the *in vitro* replication assays. Measurements of leading vs lagging strand *lacZ* mutagenesis were performed by Alexandra Vaisman, Karolina Makiela-Dzbenska,

Krystian Łazowski, Piotr Jonczyk and Iwona J. Fijalkowska (Institute of Biochemistry and Biophysics, Polish Academy of Science, Warsaw, Poland). Live-cell single-molecule experiments were performed by Thomas J. Armstrong and me (PhD student in the van Oijen lab, School of Chemistry and Molecular Bioscience, University of Wollongong, Wollongong, Australia). Both of us analyzed data. The autocorrelation analysis was carried out by Andrew Robinson. The manuscript was drafted by Erin Walsh and Roger Woodgate and initially edited and finally reviewed by every other collaborating author including me.

Emerging Themes. This Thesis, as with many studies before it, puts RecA at the center of the DNA damage response. The TLS polymerases clearly have an intimate relationship with RecA. It is a key player in the SOS-induced upregulation of pol IV. RecA* structures recruit pol IV to the nucleoid. Double-strand break resection and a physical interaction with RecA are crucial for focus formation by pol IV. Thus RecA* structures, particularly those formed during double-strand break repair, regulate pol IV activity at multiple levels. My finding is that pol IV predominantly works in recombination intermediates in live cells opposed to assisting in the restart of stalled replisomes. RecA* filaments also play important roles in regulating the activity of pol IV. RecA is required for the damage-induced upregulation of pol V subunits, the auto-cleavage of one of those subunits, UmuD, which allows the polymerase-containing subunit UmuC to escape the membrane, and for the production of the catalytically competent complex pol V Mut ($UmuD'_2$- UmuC-RecA-ATP). Observations described in Chapter 4 suggest that pol V does not act in double-strand break repair, as pol IV does. The involvement of RecA* nucleoprotein filaments in regulating pol V, together with a previously described observation that pol V does not act at replisomes, make other recombination intermediates prime candidates as substrates for pol V activity in cells. Thus far, however, the substrates for pol V-dependent synthesis remain to be identified.

The work described in this Thesis agrees with a recent model of TLS polymerases being specialized for specific DNA substrates. Pol IV and pol V appear to work differently in a cellular context. For instance, ROS-induced DSBs promote pol IV focus formation but not pol V focus formation, consistent with pol IV, and not pol V, working on ROS-induced DSBs or pol IV activity being promoted following oxidation of the nucleotide pool. Furthermore, pol IV and pol V differ in their SOS-mediated upregulation. Pol IV is upregulated following trimethoprim treatment, where the nucleotide pool is depleted from thymine and ROS covert single-stranded gaps into DSBs. Pol V is neither unregulated nor activated upon trimethoprim treatment. Intriguingly, RecA* filaments, which are essential for pol V Mut activation, are however potentially formed in trimethoprim-treated cells; SOS induction is observed which requires RecA* filament formation to cleave the SOS-repressor LexA. This Thesis opens up questions about the regulation of error-prone DNA polymerases in *Escherichia coli*, informing about possible mutagenesis promotors. Furthermore, observations about pol IV and pol V open questions about the third TLS polymerase in *Escherichia coli*, DNA polymerase II (pol II). Single-molecule microscopy will likely reveal the main targets of pol II and its regulation in living cells.

This Thesis begins to suggest that bacterial error-prone DNA polymerases could be involved in many DNA repair and damage tolerance pathways. Besides RecA*, other recombination mediators appear to regulate pol IV focus formation such as RecF, suggesting another degree of interconnectivity

between translesion synthesis homologous recombination. Other studies have indicated that pol IV activity might also feed into base excision repair (BER), incorporating oxidized nucleotides. Two closely spaced oxidized guanines can be removed by enzymes of the BER pathway, thereby, possibly creating DSBs and fueling pol IV activity. Overall, repair and damage tolerance pathways appear to operate not as neatly as described in text books, making it fundamentally necessary to study each enzyme involved in depth. In the future, multidisciplinary projects are likely to uncover molecular mechanisms, where single-molecule microscopy will likely play a valuable role in assessing the merits of mechanistic models with in living cells.

Acknowledgments

My journey through science has been an exciting time – watching my favorite proteins every day. This experience I owe to all those who shaped my way through my PhD. Firstly, I would like to thank my supervisors Dr. Andrew Robinson and Prof. Antoine van Oijen for their encouragement and support which let me grow to an independent researcher, thereby especially thanking Andrew Robinson. I would like to extend my gratitude to lab members of the greater van Oijen/Dixon/Oakley/Tolun lab, past and present. I would like to especially thank Dr. Harshad Ghodke, Dr. Amy McGrath, Megan Cherry and Dr. Slobodan ('Boban') Jergic for all your advice, which helped me immensely over the past years. My gratitude also goes out to Thomas Armstrong for his support and help throughout my PhD.

I also would like to thank all collaborators for their support and critiques, which helped me tremendously to grow as a scientist. I would like to particularly thank Prof. Michael Cox, Dr. Camille Henry, Elizabeth Wood, Dr. Roger Woodgate, Dr. John McDonald, Prof. Myron Goodman and Dr. Malgorzata ('Gosia') Jaszczur.

I would like to address my thanks to my close friends: Dr. Caroline Wern, Nathalie Luckas, Barbara Gress, Monja Gillmann, Anke Lauterbach, Yvonne Hellmich, Pascal Schorr, Timon Geib and Laura Müller for being there whenever I needed them.

I owe sincere gratitude to my parents, Otmar and Friederike, for their encouragement and support throughout my life. Thank you.

I would also like to especially thank my partner Michael who has been my rock throughout this journey. Thank you for always being there for me, bringing the balance between life and work. I would like to extend my thanks to Michael's mother Michelle who always had an open ear for me over the past years.

Certification

I, Sarah Sylviane Henrikus, declare that this thesis submitted in fulfilment of the requirements for the conferral of the degree Doctor of Philosophy, from the University of Wollongong, is wholly my own work unless otherwise referenced or acknowledged. This document has not been submitted for qualifications at any other academic institution.

This thesis consists of a number of chapters, as listed below, each based on papers published in, accepted by, under review at, or in preparation for, peer-reviewed journals.

Chapter 1 Literature review.

Chapter 2 DNA polymerase IV primarily operates outside of DNA replication forks in *Escherichia coli.* **Sarah S. Henrikus**, Elizabeth A. Wood, John P. McDonald, Michael M. Cox, Roger Woodgate, Myron F. Goodman, Antoine M. van Oijen, Andrew Robinson. Published in *PLoS Genet.*, 2018; 14(1):e1007161.

Chapter 3 Specialised DNA polymerases in *Escherichia coli*: roles within multiple pathways. **Sarah S. Henrikus**, Antoine M. van Oijen, Andrew Robinson. Published in *Curr Genet.*, 2018; https://doi.org/10.1007/s00294-018-0840-x.

Chapter 4 DNA double-strand breaks induced by reactive oxygen species promote DNA polymerase IV activity in *Escherichia coli.* **Sarah S. Henrikus**, Camille Henry, John P. McDonald, Yvonne Hellmich, Steven T. Bruckbauer, Megan E. Cherry, Elizabeth A. Wood[3], Roger Woodgate, Michael M. Cox, Antoine M. van Oijen, Harshad Ghodke, Andrew Robinson. *bioRχiv* 2019, https://www.biorxiv.org/content/ 10.1101/533422v2.

Chapter 5 UmuD and RecA* modulate the DNA-binding activity of DNA polymerase IV in *Escherichia coli*. **Sarah S. Henrikus**, Amy E. McGrath, Slobodan Jergic, Matthew L. Ritger, Phuong T. Pham, Elizabeth A. Wood, Myron F. Goodman, Michael M. Cox, Antoine M. van Oijen, Harshad Ghodke, Andrew Robinson. *bioRχiv*, 2019, https://doi.org/10.1101/620195.

Chapter 6 RecFOR epistasis group: RecF and RecO have distinct localisations and functions in *Escherichia coli.* **Sarah S. Henrikus**, Camille Henry, Harshad Ghodke, Elizabeth A. Wood, Neema Mbele, Roopashi Saxena, Upasana Basu, Antoine M. van Oijen, Michael M. Cox, and Andrew Robinson**.** Published in *Nucleic Acid Research*, **47**, 2946-2965 (2019).

Chapter 7 Role of RNase H enzymes in maintaining genome stability in *Escherichia coli* expressing a steric-gate mutant of pol V_{ICE391}. Erin Walsh, **Sarah S. Henrikus**, Alexandra Vaisman, Karolina Makiela-Dzbenska, Thomas J. Armstrong, Krystian Łazowski, John P. McDonald, Myron F. Goodman[5], Antoine M. van Oijen, Piotr Jonczyk, Iwona J. Fijalkowska, Andrew Robinson, Roger Woodgate. Accepted in *DNA Repair*.

Chapter 8 Concluding remarks.

All collaborating authors are listed below, where either each individual signed or the corresponding author/supervisor.

Thomas J. Armstrong
Megan E. Cherry
Dr Harshad Ghodke
Dr Amy McGrath
Dr Slobodan Jergic
Dr Andrew Robinson
Prof Antoine van Oijen
Yvonne Hellmich
Matthew L. Ritger
Neema Mbele
Roopashi Saxena
Upasana Basu
Dr Camille Henry
Dr Steven T. Bruckbauer
Elizabeth A. Wood
Prof Michael M. Cox
Dr Erin Walsh
Dr John P. McDonald
Dr Roger Woodgate
Prof Phuong T. Pham
Prof Myron F. Goodman
Dr Alexandra Vaisman
Krystian Łazowski
Dr Karolina Makiela-Dzbenska
Dr Piotr Jonczyk
Prof Iwona J. Fijalkowska

Sarah Sylviane Henrikus
6th August 2019

Table of Contents

List of Publications

Walsh, E.; **Henrikus, S. S.**; Vaisman, A.; Makiela-Dzbenska, K.; Armstrong, T. J.; Łazowski, K.; McDonald, J. P.; Goodman, M. F.; van Oijen, M. M; Jonczyk, P.; Fijalkowska, I. J.; Robinson, A.; Woodgate, R. Role of RNase H enzymes in maintaining genome stability in *Escherichia coli* expressing a steric-gate mutant of pol V_{ICE391}. *(accepted in DNA Repair).*

Sommer, R.; Rox, K.; Wagner, S.; Hauck, D.; **Henrikus, S. S.**; Newsad, S.; Arnold, T.; Ryckmans, T.; Brönstrup, M.; Imberty, A.; Varrot, A.; Hartmann, R. W.; Titz, A. Anti-biofilm agents against *Pseudomonas aeruginosa*: a structure-activity relationship study of C-glycosidic LecB inhibitors. *(submitted to The Journal of Medical Chemistry)*. (*Master program*)

Henrikus, S. S.; McGrath, A. E.; Jergic, S.; Ritger, M. L.; Pham, P. T.; Wood, E. A.; Goodman, M. F.; Cox, M. M.; van Oijen, A. M.; Ghodke, H.; Robinson, A. UmuD and RecA* modulate the DNA-binding activity of DNA polymerase IV in *Escherichia coli*. *(bioRχiv: https://www.biorxiv.org/content/10.1101/620195v2* 2019*)*

Henrikus, S. S.; Henry, C.; McDonald, J.; Hellmich, Y.; Wood, E. A.; Cox, M. M.; Woodgate, R.; van Oijen, A. M.; Ghodke, H.; Robinson, A. DNA double-strand breaks induced by reactive oxygen species promote DNA polymerase IV activity in *Escherichia coli*. *(bioRχiv: https://www.biorxiv.org/content/10.1101/533422v2* 2019).

Henrikus, S. S.; Henry, C.; Ghodke, H.; Wood, E. A.; Mbele, N.; Saxena, R.; Basu, U.; van Oijen, A. M.; Cox, M. M.; Robinson, A. The *Escherichia coli* RecF and RecO proteins: Distinct cellular localisation and function within a putative epistasis group. *Nucleic Acid Research.* **47**, 2946-2965 (2019). ***Publication Of the Month Award for January 2019 from Illawarra Health & Medical Research Institute.***

Smit, J.; van der Velde, J.; Huang, J.; Trauschke, V.; **Henrikus, S. S.**; Chen, S.; Eleftheriadis, N.; Warszawik, E.; Herrmann, A.; Cordes, T. On the impact of competing intra- and intermolecular triplet-state quenching on photoswitching kinetics of organic fluorophores. *Physical Chemistry Chemical Physics.* Advance Article (2019). (*Master program*)

Henrikus, S. S.; van Oijen, A. M.; Robinson, A. Specialised DNA polymerases in *Escherichia coli*: roles within multiple pathways. *Current Genet*. **64**, 1169-1189 (2018).

Henrikus, S. S., Single-molecule imaging: observing cellular processes in live bacterial cells. *Syntrophy Newsletter*, **19**, 3 (2018). ***Becton Dickinson finalist article.***

Henrikus, S. S.; Wood, E. A.; McDonald, J. P.; Cox, M. M.; Woodgate, R.; Goodman, M. F.; van Oijen, A. M.; Robinson, A. DNA polymerase IV primarily operates outside of DNA replication forks in *Escherichia coli*. *PLoS Genet.* **14,** e1007161 (2018).

Huynh, A. M., Müller, A., Kessler, S. M., **Henrikus, S. S.**, Hoffmann, C., Kiemer, A. K., Bücker, A., Jung, G. Small BODIPY Probes for Combined Dual ^{19}F MRI and Fluorescence Imaging. *ChemMedChem*, **11**, 1568-1575 (2016). (*Master program*)

List of Conference Presentations

Henrikus, S. S.; Henry, C.; McGrath, A. E.; McDonald, J.; Hellmich, Y.; Wood, E. A.; Woodgate, R.; Cox, M. M.; Goodman, M.; van Oijen, A. M.; Ghodke, H.; Robinson, A. DNA double-strand breaks induced by reactive oxygen species promote DNA polymerase IV activity in *Escherichia coli*. 44th Lorne Conference on Protein Structure and Function - Australia (2019). ***Poster presentation. Funded by Travel Scholarship from the Sydney Protein Group: Lorne Travelling.***

Henrikus, S. S.; Henry, C.; Hellmich, Y.; Cox, M. M.; Woodgate, R.; van Oijen, A. M.; Robinson, A. Reactive oxygen species promote DNA polymerase IV activity in *Escherichia coli*. 5th DNA Polymerase meeting – The Netherlands (2018). ***Oral presentation. Selected by abstract, funded by SMAH HDR Travel Grant.***

Henrikus, S. S.; Henry, C.; Ghodke, H.; Wood, E. A.; Mbele, N.; Saxena, R.; Basu, U.; van Oijen, A. M.; Cox, M. M.; Robinson, A. Single-molecule studies reveal different loci for RecF and RecO in *Escherichia coli* cells. 84th Harden Conference: Single-molecule bacteriology – UK (2018). ***Oral presentation. Selected by abstract, funded by SMAH HDR Travel Grant.***

Henrikus, S. S. Single-molecule studies of DNA repair in live *Escherichia coli.* School of Chemistry Annual Conference – Australia (2017). ***Oral presentation. Peer* Award *for Best Oral Presentation. Highly Commended Talk by a Second-Year PhD Student.***

Henrikus S. S.; van Oijen, A. M.; Robinson, A. Single-molecule studies of DNA repair in live *Escherichia coli*. Single-molecule club meeting – Australia (2017). ***Oral presentation.***

Henrikus, S. S.; Wood, E. A.; Cox, M. M.; Woodgate, R.; Goodman, M.; van Oijen, A. M.; Robinson, A. A short window of opportunity: DNA polymerase IV is granted limited access to stalled replication forks in *Escherichia coli*. Australian Society for Microbiology Annual Scientific Meeting - Australia (2017). ***Poster presentation.***

Henrikus, S. S.; Wood, E. A.; Cox, M. M.; Woodgate, R.; Goodman, M.; van Oijen, A. M.; Robinson, A. A short window of opportunity: DNA polymerase IV is granted limited access to stalled replication forks in *Escherichia coli*. 42nd Lorne Conference on Protein Structure and Function - Australia (2017). ***Poster presentation.***

Henrikus S. S.; van Oijen, A. M.; Robinson, A. Single-molecule studies of TLS polymerases in *Escherichia coli*. Single-molecule club meeting – Australia (2016). ***Oral presentation.***

1 Literature review (1st year report)

1.1 Glossary

adaptation	An organism evolves to become better suited to a new environment.
clonal interference	Competition for survival between populations of different cell types, for example between wild-type cells and newly arising mutant cells.
collateral sensitivity	Susceptibility for resistance development when exposed to drugs because a resistance to another drug is already gained.
combination therapy	Therapy in which the patient is treated with more than one type of antibiotic at the same time.
conjugation	Transfer of genetic material between cells through physical contact, also known as "bacterial sex". DNA is passed from the donor cell to the recipient through a proteinaceous tube called a pilus.
epistatic interaction	An effect on the function of a gene that is exerted by one or more other genes present in the cell.
fitness	The capacity for an organism to survive in a particular environment. For a pure culture, the fitness is directly related to growth rate. In a complex environment, *fitness* also encompasses the ability of an organism to compete for resources with other organisms.
fitness landscape	The distribution of fitness values of different genotypes (e.g. mutants of a parent organism) in a particular environment.
gene amplification	Increase in the copy number of a gene on the chromosome due to recombination between repeat sequences. Gene amplification allows the cell to produce more of the protein encoded by that gene. Further amplification of the gene allows the cell to even produce more protein.
genomic rearrangement	Movement, deletion or amplification of parts of the chromosome *via* recombination.
horizontal gene transfer	Transfer of genetic material between cells, including cells of different species, *via conjugation*, *transformation* or *transduction*. Also known as *lateral gene transfer.*
mutation	Technically speaking, any change in DNA sequence. In the context of this report *mutation* refers to relatively small changes, such as insertion or deletion of one or two nucleotides, or change in sequence of a single base-pair.

mutation supply rate	The number of new mutations evolving in a particular amount of time; typically the generation time. For example, *E. coli* has a mutation supply rate of 1×10^{-3} mutations per genome per generation.
selection pressure	Environmental conditions that cause cells (more accurately genes) with particular attributes to survive and others to perish.
sequential therapy	Therapy in which the patient is treated with one type of antibiotic, administered one after the other, or in regular cycles.
stress-induced mutagenesis	Increase in the mutation rate induced in response to environmental factors, in particular those that cause DNA damage.
transduction	Transfer of genetic material between cells through viral infection. Host DNA is inadvertently packaged into the virus particle and upon reinfection is transferred to a new host cell.
transformation	Direct uptake of genetic material from the environment

1.2 Antibiotic resistance is a major challenge to world health

Antibiotics drugs are used to treat diseases caused by pathogenic bacteria (1). Antibiotics work either by killing bacteria (bactericidal antibiotics) and/or by stopping their growth (bacteriostatic antibiotics) (2–7). Since their introduction in the 1930s, antibiotics have saved countless lives. Unfortunately however, extensive use (and overuse) of antibiotics has led bacterial pathogens to evolve resistance to these drugs, in turn causing treatments to fail. Antibiotic resistance is genetic: once a bacterium develops drug resistance, it can pass its genes on to its progeny and even to other unrelated bacteria (8)

A particularly serious situation arises when life-threatening organisms become drug-resistant, for example extensively drug-resistant *Mycobacterium tuberculosis* (XDR-TB) and Methicillin-resistant *Staphylococcus aureus* (MRSA). Some strains of each organism have become resistant to virtually all available antibiotics and thus no treatment options exist for infected patients (1). Antibiotic resistant bacteria are already estimated to kill 700,000 people every year. Unfortunately, as the rate of antibiotic resistance continues to rise, projections indicate that this number could rise to 10 million by 2050. Beyond the challenge this poses for world health, antibiotic resistance costs world economies billions each year (9). In the USA alone, resistant bacteria are estimated to cost the health system $20 billion per year (1).

Why has antibiotic resistance become such a big problem? As soon as pharma developed antibiotics as a way to fight antimicrobial pathogens, the issue of resistance development was already reported (1). Despite this, neither companies nor the government have invested in finding a solution for antimicrobial resistance and the pipeline for developing new antibiotics has been allowed to stagnate. It is also important to note that antibiotic resistance is driven by antibiotic use. Importantly, there are no rapid diagnostic tests available for detecting and characterising bacterial infections, meaning most prescriptions are issued “just in case” the patient has a bacterial infection. Existing antibiotics have been badly misused, partly through inappropriate prescribing practices, but also through extensive use of sub-therapeutic doses of antibiotics as growth-enhancers in agriculture (10). Furthermore, the need to treat antibiotic resistance as a global risk has only been recognised recently. Globalization of trade and increased travel has increased the rate at which resistant microorganisms spread around the world (11).

Despite the fact that antibiotic resistance is predicted to soon become the biggest challenge to human health, we know little about the evolutionary dynamics and mechanisms that lead to resistance generation. There is an urgent need to better understand how antibiotic treatment leads to the evolution of resistant pathogens.

1.3 How do bacteria become resistant to antibiotics?

The emergence of resistant pathogens is a process of *adaptation* (see Glossary) (12). Bacteria become resistant to antibiotics in one of three ways. Bacteria can acquire resistance genes from other organisms in a process known as *horizontal gene transfer* (HGT, see Glossary). Here, resistance genes are passed from one organism to another on mobile genetic elements such as plasmids, transposons and integrons. Because transfer can occur across species boundaries, resistance genes can be taken from a

very large gene pool (known as the mobile metagenome) (13). Horizontal gene transfer is the most common mechanism by which antibiotic resistance spreads in hospital pathogens. A famous example is the gene encoding extended spectrum beta-lactamase (ESBL), which travels between organisms on plasmids and provides resistance to nearly all antibiotics in the beta-lactam family (14,15). HGT is facilitated by bacteriophage transduction, conjugation or transformation (16). In *transduction*, DNA is passed from one bacterium to another by a virus or a viral vector. *Conjugation* involves the transfer of genetic material via physical contact between two cells and is mediated by a tube-like structure called a pilus. *Transformation* describes genetic alteration due to the direct incorporation of exogenous genetic material, absorbed from the surroundings through the cell membrane. The mobile genetic elements acquired by bacteria during HGT often contain multiple resistance genes, leading to multi-drug resistance (17,18).

A second route for antibiotic resistance to arise is through *genomic rearrangement*, in particular *gene amplification* (12,19,20). Here, the copy number of a gene on the chromosome is increased due to recombination between repeat sequences. One recombination event duplicates the gene, doubling its copy number and allowing the cell to produce more of the protein encoded by that gene. Subsequent recombinations further amplify the gene, producing even more protein. If the protein is the target of an antibiotic, this amplification process allows to cell to tolerate higher concentrations of drug. Resistance to the drug trimethoprim commonly occurs in this way (21). Trimethoprim inhibits the enzyme dihydrofolate reductase, blocking a key step in the production of folate (22,23). As folate is required for the synthesis of the nucleotide bases that comprise DNA, this leads to inhibition of DNA replication. Cells develop resistance to trimethoprim by amplifying the gene that encodes dihydrofolate reductase, *dhfr*, allowing higher amounts of the enzyme to be produced and thus higher concentrations of trimethoprim to be tolerated.

A third route towards antibiotic resistance is *mutation* (12). Here, errors in DNA replication lead to changes in the DNA sequence of the bacterium. Most mutations are non-beneficial for drug survival, however in rare cases mutations occur that increase survival in the presence of antibiotic. For example, resistance to the drug rifampicin occurs commonly by mutation (24). Rifampicin inhibits cell growth by binding to RNA polymerase and thus inhibiting transcription. Resistance occurs when mutations arise in the *rpoB* gene, altering the structure of RNA polymerase such that it no longer binds rifampicin, yet remains competent for transcription. A common example is the mutation *rpoB*(S531L), in which a change in the *rpoB* gene sequence causes a change from serine to leucine at position 531 of the RpoB protein (the β-subunit of RNA polymerase), which reduces the efficiency of rifampicin. In many organisms, including *Mycobacterium tuberculosis*, mutation represents the major route through which drug resistance is developed. In addition, mutations in repressor genes or mutations that activate regulons can alter expression of efflux pumps, leading to increased efflux transport of antibiotics (25).

1.4 How does antibiotic use influence the way bacteria evolve?

Antibiotics apply strong *selection:* they kill, or completely inhibit the growth of, any non-resistant bacteria, while resistant bacteria continue to grow normally (12). The serious consequence for health is that antibiotic use rapidly selects for resistant cells, allowing them to quickly become the

dominant species in the environment. The strength of the selection pressure applied varies with the drug and its concentration. Strength of selection pressure, however, is not the only factor that shapes how organisms evolve. To understand how antibiotics use encourages antibiotic resistance, we need to understand the complex interplay between cells, population genetics and environmental factors that occur in patients, agricultural animals and the wider environment.

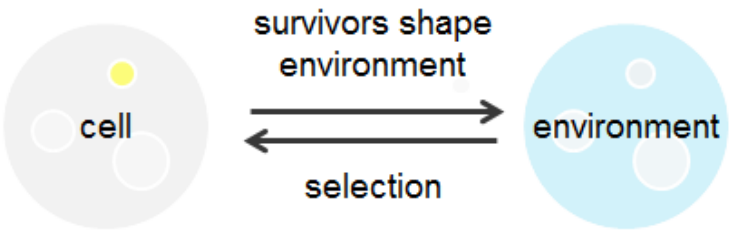

Figure 1: Evolution is self-referential. The environment shapes the cell population and the survivors shape the environment.

An antibiotic dose represents a change in a bacterium's environment. In order to survive the new environment, the species must adapt to the new conditions. How do cells adapt to environmental changes? Like all evolution events, resistance development involves the complex interplay of many factors (12). Evolution is uniquely self-referential (26): changing the environment affects the survival of organisms within that environment, while at the same time the organisms that survive in an environment play an important role in shaping that environment (Figure 1).

An important factor that influences the rate of evolution is the *mutation supply rate*: the rate at which cells evolve mutations (12). In general higher mutation rates promote faster evolution. High mutation rates cause populations to rapidly diversify. Since antibiotics supply strong selective pressure, members of the population that develop mutations that increase fitness in the presence of antibiotic are strongly selected. Different mutants in a population hold different fitness levels: some are better suited to the environmental conditions than others. This distribution of fitness amongst different variants (or potential variants) is known as the *fitness landscape* (27). For some antibiotics the fitness landscape will contain broad peaks: many different mutations may lead to an increase in fitness. For other antibiotics, the fitness landscape may contain sharp peaks. Here a few rare mutations may dramatically increase fitness, whereas most are of little or no benefit. It may therefore be 'easier' to find resistance mutations for some antibiotics than for others.

It was recently demonstrated that resistance development can be driven along a concentration gradient of antibiotics, i.e. along changes in the 'selection landscape' (12). High-level resistance to antibiotics often requires that cells accumulate a series of mutations within several genes. In situations where the change from low to high concentrations is very sharp, either in time or in space, cells need to somehow accumulate all the necessary mutations for high-level resistance before they can survive antibiotic exposure. Even with high mutation supply rates, the likelihood of producing all necessary mutations prior to selection by the antibiotic is extremely low. If there is a more gradual gradient in antibiotic concentration, however, cells can accumulate the mutations one at a time, becoming resistant to

a slightly higher antibiotic concentration in each step. Gradients in antibiotic concentration may thus accelerate the development of drug resistance.

Selective pressure also interacts with population effects (12). As shown in Figure 2, a particularly important parameter is the population size. Under very strong selection pressure (top two panels), resistance mutations have a large fitness benefit and thus come to dominate the population even when extremely rare. Under weaker selection pressures (bottom two panels), the fitness benefit of resistance mutants is low relative to the original cells. Here, the size of the population becomes important. In small populations, a single resistant cell represents a sizeable proportion of the population and thus has a high probability of survival. In very large populations, however, any resistant mutants that arise will most likely be out-competed for nutrients by the other members of the population. Thus small population sizes allow rare mutations to fix in the population with much higher probability than it would in a large population.

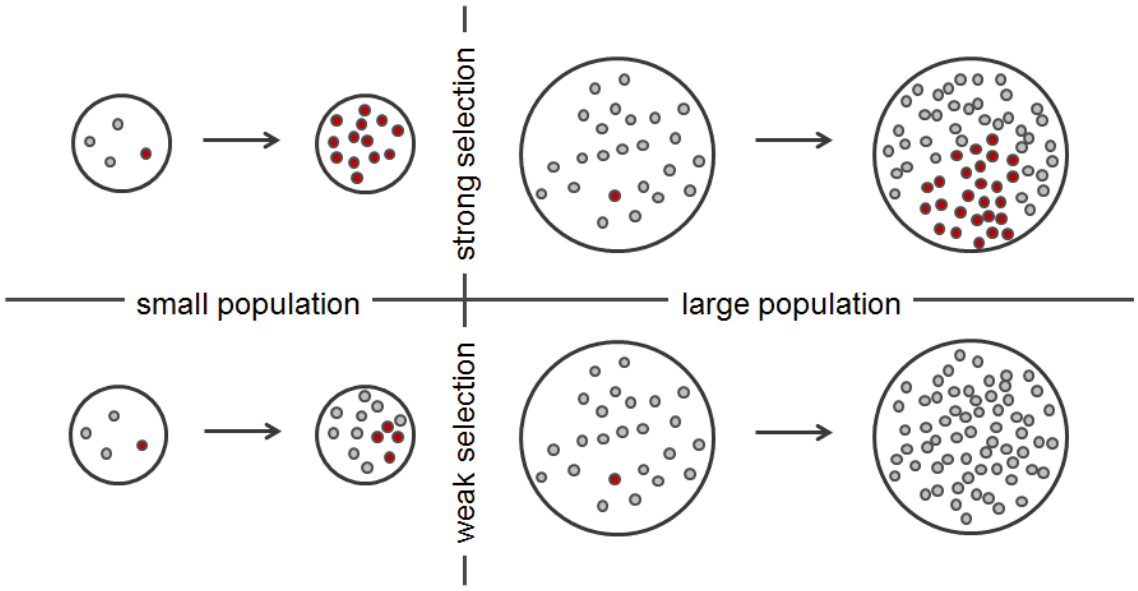

Figure 2: A small (left panel) and large population (right panel) are shown under a weak (lower panel) and strong selective pressure (upper panel). A fitter mutant is indicated by a red circles and the remaining population of wild-type cells are indicated by grey circles. Applying strong selective pressure results in the domination of the population by the red fitter mutant in both large and small populations (upper panels). Under weak selection pressure, the red, resistant variant grows best, however its advantage over wild-type cells is small. Thus in large populations it has a high probability of being out-competed by wild-type cells, despite its higher fitness (lower-right panel). Rare mutations have a higher probability of fixing in small populations (lower-left panel).

Importantly, in order to circumvent drug resistance, patients are often treated with more than one type of antibiotic at the same time (12). This treatment is known as *combination therapy*. Other therapies involve cycling between drugs or drug combinations (28). This is known as *sequential therapy*. While these strategies have seen great successes in the short-term, their long-term outcomes in terms of drug resistance are unclear. The potential for multi-drug resistance to arise from combination or succession therapies is of particular concern and requires further study (29).

1.5 Some antibiotics cause bacteria to mutate faster

Mutation supply rates are generally considered to be constant. However, use of some types of antibiotics has been shown to result in *stress-induced mutagenesis*, i.e. the bacteria increase their mutation rate upon coming in contact with the antibiotic (30). As shown in Figure 3, this may allow bacteria to adapt to the presence of the antibiotic faster than if the mutation rate was constant. Under stress-induced mutagenesis, exposure of a population of cells to an antibiotic causes cells to increase their mutation rates, leading diversification the population. In figure 3, newly arising cells containing different mutations are indicated in red, black and light yellow, while the remaining wild-type cells appear grey. The antibiotic also applies selection; non-beneficial mutations (in this case those in the black and yellow cells), as well as the wild-type cells, are quickly outcompeted by the resistant (red) mutant. Stress-induced mutagenesis is expected to be important in situations where genetic diversity limits the rate of evolution.

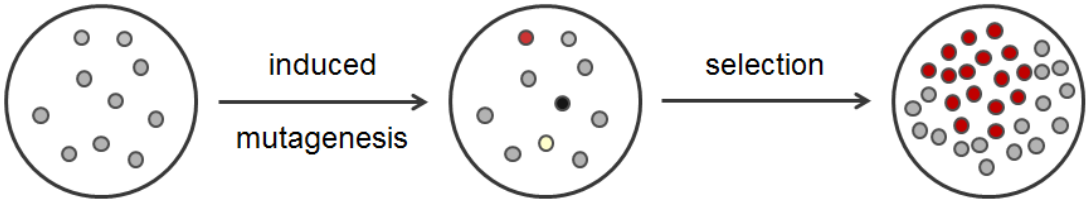

Figure 3: Increased mutagenesis can be induced by exposure to antibiotics as a result of the SOS response (first arrow). This produces a range of different mutants (red, light yellow, black and grey circles) with in the population. Selection pressure applied by the antibiotic selects for the most beneficial mutations, i.e. those that provide antibiotic resistance.

The commonly used antibiotics ciprofloxacin, nitrofurantoin and trimethoprim are all thought to cause stress-induced mutagenesis (31). The common thread between these drugs is that they inhibit DNA replication and induce the SOS response. The obvious question is whether the increased mutagenesis induced by these drugs promotes the evolution of drug resistance. This seemingly simple question is extremely difficult to answer experimentally, primarily because the systems that regulate the mutation rate in cells also regulate proteins that repair DNA. It is therefore difficult to design experiments that separate the effects of mutagenesis from those of DNA damage tolerance. To address the question properly, the complex interplay of evolutionary factors has to be understood. In this light, a better understanding of how and when mutations are produced, and how they influence evolution dynamics, would be particularly beneficial.

1.6 DNA repair and damage tolerance

How does DNA damage channel through the different DNA repair and damage tolerance mechanisms? How does stress-induced mutagenesis occur? Many elements of DNA repair are directed by the SOS response; a transcriptional response to DNA damage in which a set of genes (~40 in *E. coli*) are up-regulated (32). Most of these genes encode DNA repair proteins and are involved in error-free DNA repair pathways such as homologous recombination. Recombinational DNA repair is the exchange of nucleotide sequences between similar or identical strands. Classically, two main types of homologous

recombination were described: the RecBCD pathway and the RecF pathway. Both are involved in maintaining the genome. In addition to error-free repair pathways, many bacteria also express specialised, error-prone DNA polymerases during the SOS response. These polymerases carry out a special type of DNA replication on damaged DNA, known as translesion synthesis (TLS). TLS polymerases tend to be error-prone and are largely responsible for the increase in mutagenesis brought on by SOS induction. While it is clear that many antibiotics induce the SOS response, not much is known about how DNA damage feeds into DNA repair and damage tolerance. Recombination is shown to play a critical role; however, it is unknown where, when and how recombination takes places. Moreover, TLS polymerases and increased mutation rates go hand in hand but the level of TLS activity that results and where in the cell TLS occurs remain open questions.

1.6.1 DNA replication in the absence of antibiotics

The SOS response is induced when chromosomal DNA replication becomes interrupted by the presence of damage in the template DNA. In the absence of damage, DNA replication is performed by a complex multi-protein machine known as the replisome (33). The process of DNA replication is initiated at the origin (*oriC*). The initiator protein DnaA binds to the origin and separates the two strands of the parental DNA (see Figure 4). The primosome ($DnaB_6$-$DnaG_3$), composed of the primase (DnaG) and the 5' → 3' DNA helicase (DnaB), is assembled at the melted origin and loaded on both ssDNA substrates (see Figure 4). DnaB unwinds the dsDNA bidirectional and DnaG synthesises RNA primers. Once the template is primed, DNA polymerase III (Pol III) holoenzyme (HE) is assembled, completing the replisome complex (34). One strand, the leading strand, is replicated by Pol III HE continuously. As replication only occurs in the 3' → 5' direction, the other strand, known as the lagging strand, is replicated discontinuously as Okazaki fragments.

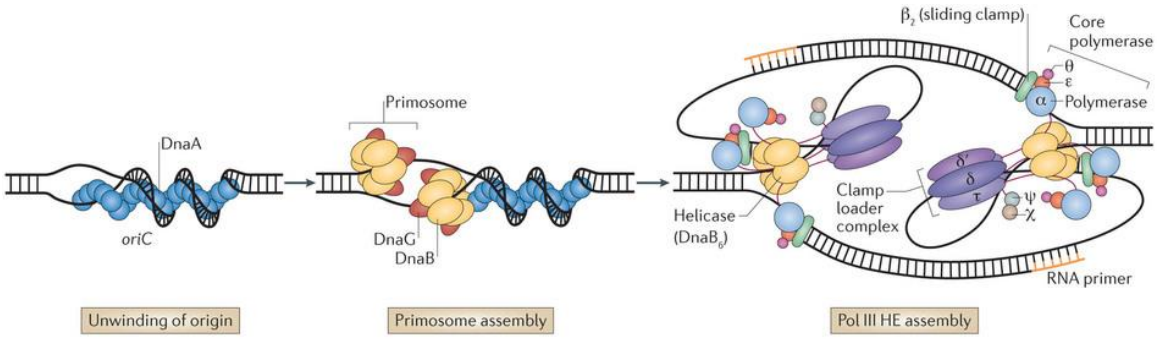

Figure 4: Initiation of DNA replication in *Escherichia coli*. Unwinding of the origin by DnaA leads to melting of the two strands (left panel). This is followed by assembly of the primosome (middle panel), consisting of the primase DnaG (shown in red) and the DNA helicase DnaB (shown in yellow). The next step is Pol III HE assembly (right panel) to begin the elongation phase. Pol III HE consists of the clamp loader complex shown in violet, the sliding clamp shown in green and the core (αεθ). The core is composed of the α- (blue subunit), the ε- (red subunit) and the θ-subunit (purple subunit) (33) .

Pol III HE is assembled from a series of subcomplexes – two or three Pol III cores (αεθ), which are each connected to the clamp loader complex ($\tau_n\gamma_{3-n}\delta\delta'\chi\psi$)(32,34,35). Each Pol III core is composed of an α-subunit (family C polymerase from the DnaE family), an ε-subunit (3'→5' proofreading exonuclease from the DnaQ family) and a θ-subunit (stabilising role for ε). While synthesising DNA,

each Pol III core interacts with a homodimeric β-sliding clamp processivity factor (β_2), through contacts on the α- and ε-subunits. Importantly, the β-sliding clamp also interacts with a series of other DNA-processing proteins, including TLS polymerases.

1.6.2 DNA damage inhibits replication and induces the SOS response

Pol III HE is a fast, processive and accurate DNA copier. However, if the template DNA becomes damaged (for example by exposure to UV light or certain antibiotics), Pol III HE stalls (32). In some cases, replication restarts downstream of the damage, in a process known as lesion-skipping (37). Both stalling and lesion-skipping lead to accumulation of ssDNA gaps, which ultimately represents the signal that triggers the SOS response (38). In the first step, the recombinase protein RecA is loaded onto ssDNA regions, displacing the single-stranded binding protein SSB, producing nucleoprotein filaments known as RecA* (see Figure 5a). Similarly to gaps, resected double-strand breaks serve as a substrate for RecA* nucleoprotein filaments (see Figure 5b) (39). These activated RecA* filaments co-catalyse self-cleavage of the transcriptional repressor protein LexA. In the resting state, LexA represses the expression of SOS genes as it binds to their SOS repressor boxes. RecA*-mediated cleavage of LexA inactivates the repressor and thus leads to increased expression of SOS genes. LexA however has different affinities for different SOS repressor boxes, regulating when which SOS gene is induced. The earliest SOS genes to be induced constitute non-mutagenic DNA repair pathways such as homologous recombination. If damage persists beyond these early stages, a mutagenic stage is initiated in which TLS polymerases become (more highly) activated. LexA is also highly expressed during the SOS response, allowing the system to reset once the DNA damage has been repaired.

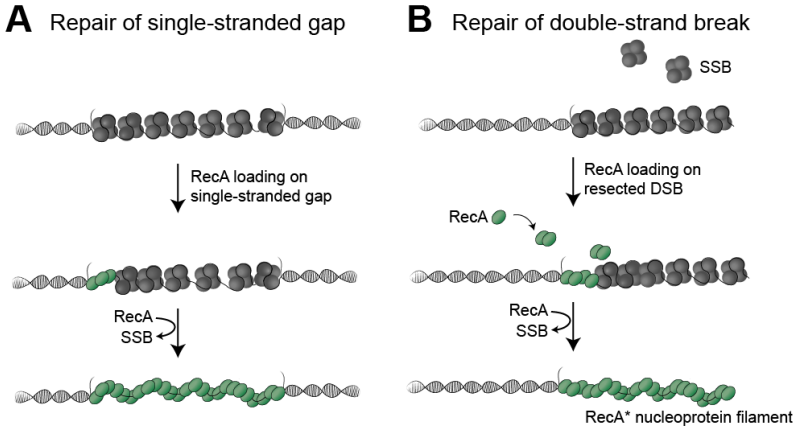

Figure 5: RecA loading onto SSB-coated ssDNA regions with filament growth from 5'-to-3'. (A) Single-stranded DNA gap is coated with the single-stranded binding protein SSB. SSB is replaced by the recombinase RecA, forming a RecA* nucleoprotein filament. (B) RecA is loaded onto a resected double-strand break.

1.6.3 Recombinational DNA repair: a strongly regulated pathway

To maintain genomic integrity, ssDNA regions have to be repaired error-free. In bacteria, the major error-free repair pathway is homologous recombination (HR, see Figure 6). In this pathway, RecA-coated ssDNA undergoes homology search to pair this ssDNA region with its complementary duplex,

leading to strand invasion and the formation of a displacement loop (D-loop) (39). Following DNA synthesis, the HR intermediate is resolved.

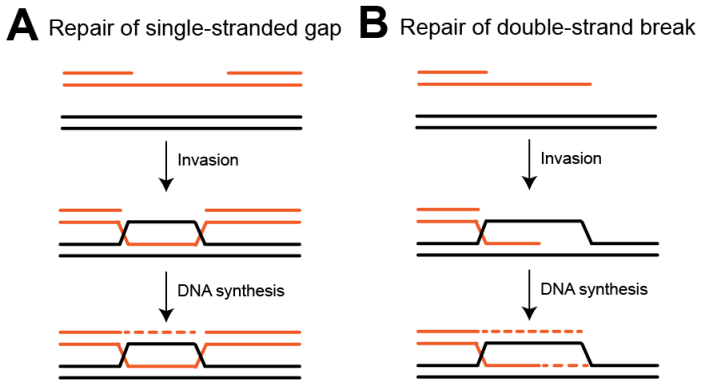

Figure 6: Homologous recombination. Recombinant ssDNA invades complementary duplex forming a displacement loop. The invading 3' end primes DNA synthesis. (A) Repair of single-stranded gap. (B) Repair of double-strand break.

RecA loading and filament growth are temporally and spatially regulated otherwise leading to deleterious consequences for genomic integrity (39). Although being one key regulator of the SOS response, RecA is controlled within the SOS regulon. RecA is a high abundant protein with approximately 7,000-15,000 molecules per cell in undamaged cells and up to 10^5–10^6 molecules per cell after SOS induction (40–44). Another level of regulation is RecA's autoregulation by supressing its activities under certain conditions. Beyond this, RecA activity is regulated on various levels by several proteins that ensure that RecA activities are directed.

1.6.3.1 RecF, RecO and RecR proteins facilitate RecA loading and stabilisation

Historically, RecF, RecO and RecR are commonly described as working together in a RecFOR complex to facilitate RecA loading and stabilise RecA filaments (39,45–56). This pathway is called the RecFOR pathway or RecF pathway (39,44–56). RecF, RecO and RecR play a key role in post-replicative gap repair which is important for DNA damage repair and restart of stalled replication forks. The study described in chapter 6 of this thesis, however, indicates that RecF and RecO function independently.

Mutants of *recF* exhibit UV sensitivity showing impaired DNA repair (58,59). The RecF protein has a weak ATPase activity; the ADP bound form of RecF has a lower affinity for dsDNA (60). Without ATP present, RecF forms aggregates. Interestingly, RecF interacts with RecR, forming a complex with stoichiometry $RecF_2RecR_4$ (61–63). RecF and RecR together have been described to confine RecA filament extension to the single strand gap (64). Furthermore, RecF is necessary for processing DNA damage-induced replication fork regression (65). The *recF* gene is also associated with operons encoding replisome components such as *dnaN* and *dnaA*, suggesting that *recF* is linked to replication at the level of genomic organisation (65,66). Besides, the 3′ end of the *recF* gene includes the promotor sequence for the *gyrB* gene downstream, which encodes for the DNA gyrase B subunit (67). DNA gyrase removes positive supercoils in DNA, relieving topological stress that arises from the translocation of transcription and replication complexes along DNA (68,69). Genomic organisation of *recF and gyrB* suggests a role for RecF in supercoiling.

Similar to RecF, RecO has been identified as a recombinational protein using UV sensitivity assays in combination with *recBC* mutants (58). RecO also forms a complex with RecR, however, has no ATPase activity and is monomeric in solution (46,47,70–73). RecO and RecR together catalyse the nucleation step of RecA proteins onto SSB-coated ssDNA which is slowed by RecO competing off SSB (73). Besides, RecO mediates the renaturation of complementary single-stranded DNA independently of ATP which is also enhanced with SSB in the reaction (70,74). RecR however reduces this efficiency suggesting that RecR competes with RecO for SSB binding sites (74).

Mutants of *recR* exhibit the same sensitivity to UV light as *recF* and *recO* mutants (59,75,76). The RecR protein itself has no ATPase activity but slows down the ATP dependent dissociation of RecF from dsDNA (60). In solution, *E. coli* RecR is dimeric, whereas, the structure of *D. radiodurans* RecR revealed a tetrameric ring structure which might allow sliding on dsDNA suggesting a DNA clamp like function (47,61). Additionally, RecR forms complexes with RecO and RecF. Alike RecF, RecR is required to protect and maintain the replication fork upon DNA damage induction (65). The *recR* gene is also closely associated with operons otherwise encoding components of the replication system and is co-transcribed with the *dnaX* gene (66).

1.6.3.2 Mechanism of RecA loading at gaps

The RecFOR proteins are grouped in the same pathway due to *in vivo* and *in vitro* experiments. *In vivo*, deletion mutants alone or in combination show similar phenotypes using UV sensitivity assays (58). *In vitro*, polymerisation and the ATPase activity of RecA are enabled by RecFOR and are also enhanced under some conditions when all three are combined (48). RecR however can only interact with either RecF or RecO suggesting that RecF and RecO compete for binding to RecR (77). Beyond this, RecO and RecR together are sufficient for RecA loading onto SSB-coated ssDNA (47,78). A recent study has shown that RecA loading is only dependent on RecOR in *B. subtilis* (79). RecO binds for few hundred milliseconds after DNA damage induction (80). These binding sites are spread over the whole chromosome and do not form repair hubs. Furthermore, the compaction of the nucleoid in response to UV damage is only dependent of RecOR as it is of RecA (81). Within this context, RecF has a catalytic function; it speeds up RecA loading and the process of nucleoid compaction upon UV damage induction.

These facts open questions such as: What is the function of RecF/RecFR? Is RecOR involved in RecA filament nucleation or also RecA filament growth? Which recombination mediator proteins load RecA in ssDNA gaps? Understanding the function of RecF, RecO and RecR *in vivo* would possibly reveal the mechanism of RecA loading.

1.6.3.3 Mechanism of RecA loading at double-strand breaks

In *Escherichia coli*, double-strand breaks are processed by RecBCD helicase/nuclease (82,83). The activity of the RecBCD enzyme is regulated by a unique DNA sequence, known as Chi (83). Once reaching the Chi site, RecBCD creates a new 3′ end and loads RecA on to the resected DSB, making a recombinant ssDNA strand. Thereby, the RecBC enzyme (also called exonuclease V) has an ATP-dependent nuclease function (83). RecD is required for Chi hot spot activity (83). In a *recB* deficient mutant, RecJ nuclease is essential for SOS induction after introduction of a DSB (84). In a *recBC* mutant,

the helicase RecQ and the gap repair proteins RecJ, RecF, RecO and RecR can catalyse DSB resection and repair (82). It however still remains unclear which recombination mediator proteins load RecA on resected double-strand breaks *in vivo*.

In comparison to RecFOR, RecBCD is found less frequently over genomes (82). Some bacteria use different proteins than RecBCD, for instance *Bacillus subtilis* utilises AddAB (82).

1.6.4 Translesion DNA synthesis: an important source of mutations

DNA damage that is not repaired during the early stages of the SOS response channels into the mutagenic stage, the damage tolerance pathway. Furthermore, cells increase the accumulation of the sigma factor RpoS, activating the RpoS general stress response (85). During this stage, TLS polymerases are expressed. In *E. coli* this includes: Pol II, encoded by *polB*; Pol IV encoded by *dinB*; and Pol V, encoded by the *umuDC* operon (86,87).

1.6.4.1 TLS polymerases work on damaged DNA

Unlike Pol III HE, TLS polymerases have the ability to insert nucleotide bases opposite DNA lesions (see Figure 3). Chapter 3 reviews the activities of TLS polymerases in *Escherichia coli*.

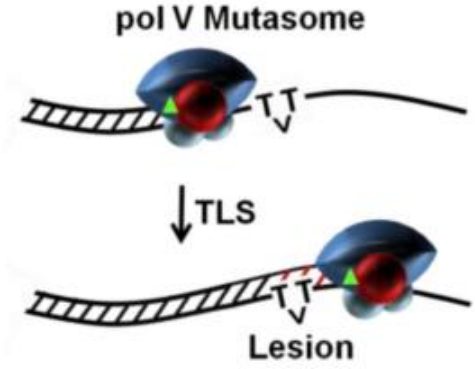

Figure 5: Translesion DNA synthesis: insertion of nucleotide bases opposite a DNA lesion by Pol V Mut (87).

This activity allows ssDNA gaps to be filled in, thus the cell avoids potentially catastrophic problems brought on by long-term stalling of replication and transcription. Importantly, damaged nucleotide bases are not removed during TLS; it represents a damage tolerance mechanism, as opposed to a repair mechanism. Another consequence of TLS is that often the base inserted opposite the lesion by a TLS polymerase is incorrect, producing a mutation (89). For example, when Pol V carries out TLS at a T-T cyclopyrimidine dimer (a lesion consisting of a covalently cross-linked pair of thymidine bases, which is commonly produced by UV irradiation), it frequently inserts the sequence GA, rather than the canonical AA (90,91). This type of mutation, occurring at a lesion, is called targeted mutation (92). Even on undamaged portions of DNA, however, TLS polymerases tend to be much less accurate than Pol III HE and thus contribute to an increased mutation rate. This untargeted mutagenesis may lead to a significant number of mutations under SOS conditions. Thus, both targeted and untargeted mutagenesis by TLS polymerases are likely to factor into the evolution of antibiotic resistance. As described below,

TLS polymerases each have different mutational signatures, producing characteristic mutations at different types of lesions.

In undamaged *E. coli* cells, DNA polymerase II is estimated to be expressed at a level of 50 molecules per cell. Upon SOS induction, its production is assessed to increase around seven-fold, reaching approximately 350 molecules per cell (34,88). Pol II is a relatively high-fidelity enzyme, possessing the capacity for proof-reading through its 3'→5' exonuclease activity. While Pol II generally carries out error-free TLS, it can produce mutations in cells exposed to N^2-acetylaminofluorene (AAF). In this case, Pol II bypass of AAF-adducts of guanine lead to a -2 frameshift, i.e. deletion of two nucleotides (89,93).

Pol IV has been estimated to be the most abundant polymerase with approximately 250 molecules per cell in undamaged cells and up to 2,500 molecules per cell after SOS induction by western blotting (94). Pol IV is devoid of 3'→5' proofreading activity and, once overexpressed *in vivo* after alkylation damage, responsible for -1 frameshifts, i.e. deletion of a single nucleotide (93,95). These however are supressed when co-overexpressing UmuD (pol V subunit) (96). Furthermore, Mallik *et al.* found that adducts to the N^2 position of guanines are primarly bypassed by Pol IV even in a mostly error-free fashion (94). These lesions can be induced by addition of benzo(α)pyrene or 4-nitroquinoline-1-oxide (NQO), a DNA damaging agent. Pol IV also bypasses a variety of alkylation lesions, most often without inducing mutations (97). Additionally, pol IV is involved in transcription-coupled repair (98) and double strand break-repair repair (99–102), and contributes significantly to cell fitness in late stationary phase cultures in the absence of any exogenous DNA damage (103). The study described in chapter 4 and 5 of this thesis, however, indicates that pol IV primarily works at recombination intermediates.

The third TLS polymerase, pol V, can replicate past a wide variety of chemical and radiation-induced DNA lesions. Pol V is devoid of proofreading activity and is highly mutagenic (32,104). Its fidelity on undamaged templates is far lower than Pols III and IV. It also promotes targeted mutagenesis. For example, Pol V has a strong tendency to insert G opposite the 3'-T of a TT(6-4) photoproduct dimer (92). In undamaged cells, pol V is rarely abundant with less than 15 copies per cell (105). After inducing SOS, fewer than 200 molecules are present per cell (105). Recent findings by Robinson *et al.* provide key insight into mechanisms that limit DNA polymerase V activity during the SOS response (32). Accumulation of pol V is shown relatively late during SOS response. Moreover, time-lapse analyses show three tightly regulated, distinct phases within UV-irradiated cells. First, a small amount of UmuC is produced that is primarily bound to the cell membrane, away from the DNA. In phase II, the *umuDC* operon is depressed by cleavage of LexA. As a consequence, the UmuC molecules in cells increase to a large extent, but remain associated with the cell membrane. During the last phase, the UmuC is release into the cytosol in its active form, Pol V Mut (a complex of UmuC with the doubly-cleaved form of $UmuD_2$, called $UmuD'_2$, and a molecule of RecA bound to ATP; $UmuD'_2$C-RecA-ATP). In total Pol V activity is thus limited by its induction late in the SOS response, requirement for RecA*-dependent cleavage of UmuD, membrane binding and requirement for extracting a RecA-ATP from a RecA* filament. Once activated, pol V Mut inserts only a few bases before the complex dynamically deactivates and dissociates from the DNA. Besides pol V, $RumA'_2B$ (also known as pol V_{ICE391}) also belong to the *umu* family of error-prone polymerases (106,107). This polymerase however has a much higher mutation

rate than pol V, despite being a pol V orthologue. To date, it remains unknown why RumA′$_2$B incorporates many more mutations than pol V. Possibilities might be 1. RumA′$_2$B might be more error-prone than pol V. 2. RumA′$_2$B might be more processive than pol V, incorporating many more nucleotides. 3. RumA′$_2$B might have a higher affinity for the DNA template than pol V, and thus, this polymerase might be bound to DNA for a longer time, incorporating many more nucleotides. Unpublished *in vitro* studies have however shown that RumA′$_2$B is as error-prone as pol V. The study described in chapter 7 reveals that Rum polymerase is bound to DNA for a longer time than pol V, suggesting that Rum could be more processive than pol V *in vivo*.

1.6.3.4 Mutagenic double-strand break repair

The activation of the RpoS general stress response is also a mutagenic switch for homologous recombination (30,99,102,108). Then, error-prone DNA polymerases participate in repairing DSBs, inducing mutations. Consistent with RpoS regulating DSB repair dependent stress-induced mutations, the deletion of *rssB*, a negative regulator for RpoS, strongly increases mutations during starvation (109). In addition, for I-SecI endonuclease induced DSB during starvation, error-prone DSB repair is a major source of spontaneous mutations which strongly depends on DNA polymerase IV (109). The study described in chapter 4 and 5 support a role for pol IV in DSB repair. DSB processing is crucial for pol IV DNA binding activity *in vivo*.

Double-strand breaks are mutagenic hotspots in stressed cells (99,102,109,110). At DSBs, TLS polymerases are involved in strong local mutation hotspotting covering a range of ~60 kb. TLS polymerases however also provide long-distance hotspotting over ~1 Mb (100). In addition, strong local hotspotting at DSB requires RecBCD-mediated degradation from DSB ends. *In vivo*, mutations arising from DSB repair have been shown to depend on pol II and pol IV activity (111). Single-molecule *in vivo* assays also revealed that DNA polymerase IV localises to an induced DSB site and also localises to RecA structures (93). *In vitro*, DNA polymerases IV is highly proficient in copying DNA in recombination intermediates (D-loops) (112). This activity is called error-prone recombination-directed replication. Besides, long-distance hotspotting might be induced by break-induced replication.

1.6.4.2 Regulation and activity of DNA polymerases

How are TLS polymerases regulated? Pol V is regulated on several levels before being released into the cytosol as active pol V Mut (32). This opens up the question of a regulatory system for pol II and pol IV activities. Recent studies suggest that UmuD affects pol IV's mutagenic activity by enclosing its open site and thus preventing -1 frameshifts (96). In chapter 5, the study shows that UmuD promotes long-lived pol IV binding events while UmuD′ inhibits pol IV binding to DNA.

Furthermore, where do TLS polymerases actually act inside cells? It has long been assumed that TLS polymerases are recruited to stalled replicated forks to facilitate the restart of DNA replication. In recent years, however, evidence was found showing that these specialised polymerases also act on other substrates than replisomes. For example, Pol V Mut mostly binds away from replication forks inside live cells (32). Are there proteins that facilitate lesion-skipping and thus create lesion containing gaps left behind the replication fork? These structures could be a TLS polymerase target. It remains an open

question which TLS polymerases act behind the replisomes, which TLS polymerases act at replisomes, and which act at other structures. Nonetheless, there is compelling evidence that Pol IV does act at replisomes, competing for binding sites with Pol III HE (94). Chapter 2 elaborates on the activity of pol IV at replisomes. It remains also unknown if TLS polymerases have cofactors that allow these polymerases into replisomes. With UmuD binding pol IV and UmuD being proposed to inhibit the bond between α and β, UmuD might make it easier for pol IV to get into the replisome (113). The role of UmuD in the replisomal activity of pol IV is further discussed in chapter 5.

To determine the relevance of mutagenic TLS polymerase activity in the evolution of antibiotic resistance, we need to better understand where these polymerases work and how these proteins compete with other proteins, in the presence of antibiotics.

1.7 Single-molecule imaging: observing cellular processes in live bacterial cells

Sarah S. Henrikus

Published in *ASM NSW-ACT Branch Syntrophy Newsletter*, 2018; 19(2):3.

Single-molecule microscopy is a powerful new technique for studying molecular processes in bacterial cells. Recent advances in camera technology and the availability of high power laser excitation sources allow us to construct wide-field microscopes with such high sensitivity that the dynamics of individual molecules can be observed within live cells in real time. Most commonly the molecules being observed are proteins, which are fused to a bright fluorescent protein such as YPet, which is 2.5 x brighter than eGFP. This is typically accomplished by modifying the gene encoding a protein of interest so that the protein is fused to a fluorescent protein when expressed. The fluorescent protein signal in cells then informs on the spatio-temporal behaviour of the protein in question. Provided that the modification leaves regulatory sequences intact, fluorescence levels can be used to accurately monitor gene expression (114).

Single-molecule microscopy yields information that is not accessible through traditional microscopy techniques. The most important difference is that diffusion modes of individual molecules can be observed directly when imaging at the single-molecule level (115). Depending on the imaging rate employed and the behaviour of the target protein, some molecules within cells will be detected as punctate foci whereas others will be blurred. In other words, the diffusion behaviour of the protein imparts contrast in the images. This contrast can yield information on protein activity. For instance, video-rate movies recorded at 30 frames per second (30 Hz) cannot resolve a freely diffusing protein in the cytoplasm as it moves too quickly ($D \approx 10\ \mu m^2/s$). Consequently, a freely diffusing protein appears as a blur not a distinct feature (see Fig. 6A). On the other hand, a molecule will diffuse more slowly when bound to another molecule or to a larger structure. For example, a molecule bound to DNA moves slowly in time and space ($D \approx 10^{-5}\ \mu m^2/s$). Thus when imaging at video rate, this molecule appears as a distinct, bright feature, a static focus that can be resolved against a background of up to ~100 freely diffusing molecules (see Figure 6B). Similarly, a protein in a multiprotein complex associated with DNA forms a focus.

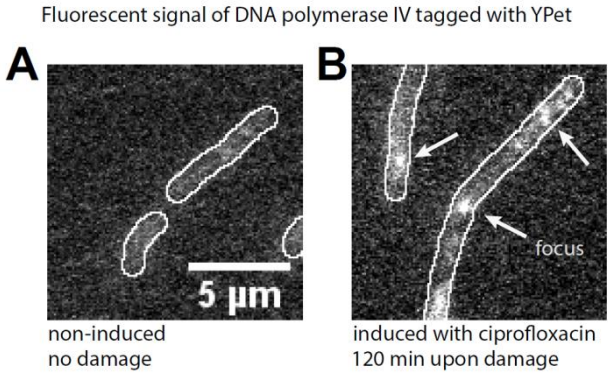

Figure 6: Blur vs distinct focus: features of the error-prone DNA polymerase IV tagged with the fluorescent protein YPet. (A) In the absence of DNA damage, error-prone DNA polymerase IV has no substrate to bind to. The fluorescent signal appears as a blur and not a distinct focus (B) After damage induction using the antibiotic ciprofloxacin, binding sites for DNA polymerase IV open. Consequently, this error-prone polymerase binds to DNA which is observed as distinct focus.

The concept described above is known as detection by localisation and allows us to observe proteins as they carry out their cellular activities. Thus far the approach has most often been applied to study DNA repair proteins and DNA polymerases, which are typically expressed at relatively low levels (<1000 copies) and produce large diffusional contrast as they bind to, and dissociate from, sites on the DNA (116).

Single-molecule microscopy allows for measurement of several parameters that cannot be extracted with other techniques but are highly important to understand cellular processes. For example, binding kinetics for individual proteins can be observed by analysing focus lifetimes (117). In combination with mutants, binding modes can be correlated with its specific task in a cellular process. Moreover, by increasing the image capture rate the position of a single protein can be tracked to reveal microscopic changes in diffusive behaviour.

Detection by localisation can also be used to determine the stoichiometry of a protein complex by correlating the intensity of a focus to the known intensity of a single fluorescent protein. This additional information leads to a better understanding of how molecular machines might actually work. For instance, single-molecule imaging allowed the composition and architecture of the *Escherichia coli* replisome complex to be measured in live cells (33,36,116). Historically, the active replisome was believed to contain two polymerase subunits. The live-cell imaging revealed that the replisome actually can contain two or three.

Recently, my co-workers and I published on the error-prone *Escherichia coli* DNA polymerase IV (pol IV) (118). Here we used two-colour co-localisation measurement to test competing models for translesion DNA synthesis. In the most-cited model, translesion polymerases, such as pol IV, should mainly act within the replisome and assist in lesion bypass. Our data demonstrated, however, that when pol IV binds to DNA, it mainly does so outside of replisomes. Based on these observations and a previous study on a second polymerase, pol V, we hypothesise that translesion polymerases primarily contribute to DNA damage tolerance through post-replicative gap filling and other pathways, rather than by rescuing stalled replisomes.

1.8 References

1. O'Neill J. Tackling drug-resistant infections globally: final report and recommendations. *Rev Antimicrob Resist*. 2016;1–84.
2. Silva F, Lourenço O, Queiroz JA, Domingues FC. Bacteriostatic versus bactericidal activity of ciprofloxacin in *Escherichia coli* assessed by flow cytometry using a novel far-red dye. *J Antibiot*. 2011;64:321–325.
3. Rahal JJ, Simberkoff MS. Bactericidal and bacteriostatic action of chloramphenicol against meningeal pathogens. *Antimicrob Agents Chemother*. 1979;16:13–18.
4. Pankey GA, Sabath LD. Clinical relevance of bacteriostatic versus bactericidal mechanisms of action in the treatment of gram-positive bacterial infections. *Clin Infect Dis*. 2004;38:864–870.
5. Barry AL, Craig WA, Nadler H, Reller LB, Sanders CC, Swenson JM. Methods for determining bactericidal activity of antimicrobial agents; approved guideline. *The National Committee for Clinical Laboratory Standards*. 1999.
6. Peterson LR, Shanholtzer CJ. Tests for bactericidal effects of antimicrobial agents: Technical performance and clinical relevance. *Clin Microbiol Rev*. 1992;5:420–432.
7. Ocampo PS, Lázár V, Papp B, Arnoldini M, Zur Wiesch PA, Busa-Fekete R, et al. Antagonism between bacteriostatic and bactericidal antibiotics is prevalent. *Antimicrob Agents Chemother*. 2014;58:4573–4582.
8. Andersson DI, Hughes D. Selection and transmission of antibiotic-resistant bacteria. *Microbiol Spectr*. 2017;5.
9. WHO. Antibiotic resistance - Fact sheet October 2015 (http://www.who.int/mediacentre /factsheets/antibiotic-resistance/en/, 24/08/2016, 7:36 am).
10. Luedtke BE, Bosilevac JM, Harhay DM, Arthur TM. Effect of direct-fed microbial dosage on the fecal concentrations of enterohemorrhagic *Escherichia coli* in feedlot cattle. *Foodborne Pathog Dis*. 2016;13:190–195.
11. WHO. Drug resistance (http://www.who.int/features/factfiles/antimicrobial_resistance/facts /en/index7.html, 12/06/2016, 02:34 pm)..
12. Hughes D, Andersson DI. Evolutionary consequences of drug resistance: shared principles across diverse targets and organisms. *Nat Rev Genet*. 2015;16:459–471.
13. Robinson A, Wu PSC, Harrop SJ, Schaeffer PM, Dosztányi Z, Gillings MR, et al. Integron-associated mobile gene cassettes code for folded proteins: The structure of Bal32a, a new member of the adaptable α + β barrel family. *J Mol Biol*. 2005;346:1229–1241.
14. Sanders CC, Sanders WE. Emergence of resistance to cefamandole: Possible role of cefoxitin-inducible beta-lactamases. *Antimicrob Agents Chemother*. 1979;15:792–797.
15. Spadafino JT, Cohen B, Liu J, Larson E. Temporal trends and risk factors for extended-spectrum

beta-lactamase-producing *Escherichia coli* in adults with catheter-associated urinary tract infections. *Antimicrob Resist Infect Control* . 2014;3:39.

16. O'Connell MP. Genetic transfer in prokaryotes: Transformation, transduction, and conjugation. In: *Advanced Molecular Genetics*. 1984. p. 2–13.

17. Aly SA, Boothe DM, Suh S-J. A novel alanine to serine substitution mutation in SoxS induces overexpression of efflux pumps and contributes to multidrug resistance in clinical *Escherichia coli* isolates. *J Antimicrob Chemother*. 2015;70:2228–2233.

18. Zhou X-Y, Ye X-G, He L-T, Zhang S-R, Wang R-L, Zhou J, *et al. In vitro* characterization and inhibition of the interaction between ciprofloxacin and berberine against multidrug-resistant *Klebsiella pneumoniae*. *J Antibiot*. 2016;1–6.

19. Slack A, Thornton PC, Magner DB, Rosenberg SM, Hastings PJ. On the mechanism of gene amplification induced under stress in *Escherichia coli. PLoS Genet*. 2006;2:385–398.

20. Sandegren L, Andersson DI. Bacterial gene amplification: implications for the evolution of antibiotic resistance. *Nat Rev Microbiol*. 2009;7:578–588.

21. Vellinga A, Tansey S, Hanahoe B, Bennett K, Murphy AW, Cormican M. Trimethoprim and ciprofloxacin resistance and prescribing in urinary tract infection associated with *Escherichia coli*: A multilevel model. *J Antimicrob Chemother*. 2012;67:2523–2530.

22. Jacobs MR. 5.7 Folic acid metabolism inhibitors. In: *Antimicrobial Drug Resistance: Clinical and Epidemiological Aspects*, Volume 2. 2009. p. 789–790.

23. Queener SF, Cody V, Pace J, Torkelson P, Gangjee A. Trimethoprim resistance of dihydrofolate reductase variants from clinical isolates of *Pneumocystis jirovecii*. *Antimicrob Agents Chemother*. 2013;57:4990–4998.

24. Taniguchi H, Aramaki H, Nikaido Y, Mizuguchi Y, Nakamura M, Koga T, *et al.* Rifampicin resistance and mutation of the *rpoB* gene in *Mycobacterium tuberculosis*. *FEMS Microbiol Lett.* 1996;144:103–108.

25. Webber MA, Piddock LJV. The importance of efflux pumps in bacterial antibiotic resistance. *J Antimicrobial Chemotherapy.* 2003;51:9–11.

26. Wallace R. A formal approach to evolution as self-referential language. *BioSystems.* 2011;106:36–44.

27. de Visser JAGM, Krug J. Empirical fitness landscapes and the predictability of evolution. *Nat Rev Genet*. 2014;15:480–490.

28. Nooka A, Lonial S. Sequential or combination therapy for multiple myeloma. *Expert Rev Hematol*. 2012;5:533–545.

29. Vinué L, Corcoran MA, Hooper DC, Jacoby GA. Mutations that enhance the ciprofloxacin resistance of *Escherichia coli* with *qnrA1*. *Antimicrob Agents Chemother*. 2016;60:1537–1545.

30. Foster PL. Stress-induced mutagenesis in bacteria. *Crit Rev Biochem Mol Biol*. 2007;42:373–397.

31. Chevereau G, Dravecká M, Batur T, Guvenek A, Ayhan DH, Toprak E, *et al*. Quantifying the determinants of evolutionary dynamics leading to drug resistance. *PLoS Biol*. 2015;13:1–18.

32. Robinson A, McDonald JP, Caldas VEA, Patel M, Wood EA, Punter CM, *et al*. Regulation of mutagenic DNA polymerase V activation in space and time. *PLoS Genet*. 2015;11:e1005482.

33. Robinson A, van Oijen AM. Bacterial replication, transcription and translation: mechanistic insights from single-molecule biochemical studies. *Nat Rev Microbiol*. 2013;11:303–315.

34. Bloom LB, Chen X, Fygenson DK, Turner J, O'Donnell M, Goodman MF. Fidelity of *Escherichia coli* DNA polymerase III holoenzyme. *J Biol Chem*. 1997;272:27919–27930.

35. Banach-Orlowska M, Fijalkowska IJ, Schaaper RM, Jonczyk P. DNA polymerase II as a fidelity factor in chromosomal DNA synthesis in *Escherichia coli*. *Mol Microbiol*. 2005;58:61–70.

36. Lewis JS, Slobodan J, Dixon NE. Chapter Two - The *E . coli* DNA replication fork. In: *The Enzymes*. 2016. p. 1–57.

37. Gabbai CB, Yeeles JTP, Marians KJ. Replisome-mediated translesion synthesis and leading strand template lesion skipping are competing bypass mechanisms. *J Biol Chem.* 2014;289:32811–32823.

38. Janion C. Inducible SOS response system of DNA repair and mutagenesis in *Escherichia coli* . *Int J Biol Sci*. 2008;4:338–344.

39. Cox MM. Regulation of bacterial RecA protein function. *Crit Rev Biochem Mol Biol.* 2007;42:41–63.

40. Boudsocq F, Campbell M, Devoret R, Bailone A. Quantitation of the inhibition of Hfr x F- recombination by the mutagenesis complex UmuD′C. *J Mol Biol*. 1997;270:201–211.

41. Courcelle J, Khodursky A, Peter B, Brown PO, Hanawalt PC. Comparative gene expression profiles following UV exposure in wild-type and SOS-deficient. *Genetics*. 2001;158:41–64.

42. Stohl EA, Brockman JP, Burkle KL, Morimatsu K, Kowalczykowski SC, Seifert HS. *Escherichia coli* RecX inhibits RecA recombinase and coprotease activities in vitro and *in vivo*. *J Biol Chem*. 2003;278:2278–2285.

43. Renzette N, Gumlaw N, Nordman JT, Krieger M, Yeh S-P, Long E, *et al*. Localization of RecA in *Escherichia coli* K-12 using RecA-GFP. *Mol Microbiol.* 2005;57:1074–1085.

44. Salles B, Paoletti C. Control of UV induction of RecA protein. *Proc Natl Acad Sci USA*. 1983;80:65–69.

45. Kowalczykowski SC, Krupp RA. Effects of *Escherichia coli* SSB protein on the single-stranded DNA-dependent ATPase activity of *Escherichia coli* RecA protein: Evidence that SSB protein facilitates the binding of RecA protein to regions of secondary structure within single-stranded DNA. *J Mol Biol*. 1987;193:97–113.

46. Umezu K, Chi N-W, Kolodner RD. Biochemical interaction of the *Escherichia coli* RecF , RecO , and RecR proteins with RecA protein and single-stranded DNA binding protein. *Proc Natl Acad*

Sci USA. 1993;90:3875–3879.

47. Umezu K, Kolodner RD. Protein interactions in genetic recombination in *Escherichia coli*. J Biol Chem. 1994;269(47):30005–30013.

48. Morimatsu K, Kowalczykowski SC. RecFOR proteins load RecA protein onto gapped DNA to accelerate DNA strand exchange: A universal step of recombinational repair. *Mol Cell.* 2003;11:1337–1347.

49. Morimatsu K, Wu Y, Kowalczykowski SC. RecFOR proteins target RecA protein to a DNA gap with either DNA or RNA at the 5' terminus: Implication for repair of stalled replication forks. *J Biol Chem*. 2012;287:35621–35630.

50. Laureti L, Demol J, Fuchs RP, Pagès V. Bacterial proliferation: Keep dividing and don't mind the gap. *PLoS Genet*. 2015;11:1–16.

51. Naiman K, Pagès V, Fuchs RP. A defect in homologous recombination leads to increased translesion synthesis in *E. coli*. *Nucleic Acids Res.* 2016;44:7691–7699.

52. Gupta R, Shuman S, Glickman M. RecF and RecR play critical roles in the homologous recombination and single-strand annealing pathways of Mycobacteria. *J Bacteriol.* 2015;197:3121–3132.

53. Lisboa J, Andreani J, Sanchez D, Boudes M, Collinet B, Liger D, *et al*. Molecular determinants of the DprA-RecA interaction for nucleation on ssDNA. *Nucleic Acids Res.* 2014;42:7395–7408.

54. Morimatsu K, Kowalczykowski SC. RecQ helicase and RecJ nuclease provide complementary functions to resect DNA for homologous recombination. *Nucleic Acids Res.* 2014;42:7395–7408.

55. Tang Q, Liu YP, Yan XX, Liang DC. Structural and functional characterization of Cys4 zinc finger motif in the recombination mediator protein RecR. *DNA Repair*. 2014;24:10–14.

56. Johnston C, Mortier-Barriere I, Granadel C, Polard P, Martin B, Claverys JP. RecFOR is not required for pneumococcal transformation but together with XerS for resolution of chromosome dimers frequently formed in the process. *PLoS Genet*. 2015;11:e1004934.

57. Sakai A, Cox MM. RecFOR and RecOR as distinct RecA loading pathways. *J Bio*. 2009;284:3264–3272.

58. Ivančić-Baće I, Peharec P, Moslavac S, Škrobot N, Salaj-Šmic E, Brčić-Kostić K. RecFOR function is required for DNA repair and recombination in a RecA loading-deficient *recB* mutant of *Escherichia coli. Genetics.* 2003;16:485–494.

59. Horii Z, Clark AJ. Genetic analysis of the recF pathway to genetic recombination in *Escherichia coli* K12: isolation and characterization of mutants. *J Mol Biol.* 1973;80:327–344.

60. Webb BL, Cox MM, Inman RB. An interaction between the *Escherichia coli* RecF and RecR proteins dependent on ATP and double-stranded DNA. *J Biol Chem*. 1995;270:31397–31404.

61. Lee B Il, Kim KH, Park SJ, Eom SH, Song HK, Suh SW. Ring-shaped architecture of RecR: implications for its role in homologous recombinational DNA repair. *EMBO J.* 2004;23:2029–

2038.

62. Makharashvili N, Mi T, Koroleva O, Korolev S. RecR-mediated modulation of RecF dimer specificity for single- and double-stranded DNA. J Biol Chem. 2009;284:1425–1434.

63. Koroleva O, Makharashvili N, Courcelle CT, Courcelle J, Korolev S. Structural conservation of RecF and Rad50 : implications for DNA recognition and RecF function. *EMBO J.* 2007;26:867–877.

64. Webb BL, Cox MM, Inman RB. Recombinational DNA repair: The RecF and RecR proteins limit the extension of RecA filaments beyond single-strand DNA gaps. Cell. 1997;91:347–356.

65. Courcelle J, Carswell-Crumpton C, Hanawalt PC. *recF* and *recR* are required for the resumption of replication at DNA replication forks in *Escherichia coli*. Proc Natl Acad Sci USA. 1997;94:3714–19.

66. Flower AM, McHenry CS. Transcriptional organization of the *Escherichia coli dnaX* gene. *J Mol Biol*. 1991;220(3):649–658.

67. Macián F, Pérez-Roger I, Armengod ME. An improved vector system for constructing transcriptional *lacZ* fusions: analysis of regulation of the *dnaA*, *dnaN*, *recF* and *gyrB* genes of *Escherichia coli. Gene*. 1994;145:17–24.

68. Drlica K, Zhao X. DNA gyrase, topoisomerase IV, and the 4-quinolones. *Microbiol Mol Biol Rev*. 1997;61:377–392.

69. Champoux JJ. DNA topoisomerases: structure, function, and mechanism. *Annu Rev Biochem*. 2001;70:369–413.

70. Luisi-DeLuca C, Kolodner R. Purification and characterization of the *Escherichia coli* RecO protein. Renaturation of complementary single-stranded DNA molecules catalyzed by the RecO protein. *J Mol Biol*. 1994;236:124–138.

71. Luisi-DeLuca C. Homologous pairing of single-stranded DNA and superhelical double-stranded DNA catalyzed by RecO protein from *Escherichia coli*. J Bacteriol. 1995;177:566–572.

72. Bork JM, Cox MM, Inman RB. The RecOR proteins modulate RecA protein function at 5' ends of single-stranded DNA. *EMBO J*. 2001;20:7313–7322.

73. Hobbs MD, Sakai A, Cox MM. SSB protein limits RecOR binding onto single-stranded DNA. *J Biol Chem*. 2007;282:11058–11067.

74. Kantake N, Madiraju MVVM, Sugiyama T, Kowalczykowski SC. *Escherichia coli* RecO protein anneals ssDNA complexed with its cognate ssDNA-binding protein: A common step in genetic recombination. *Proc Natl Acad Sci USA*. 2002;99:15327–15332.

75. Kolodner R, Fishel RA, Howard M. Genetic recombination of bacterial plasmid DNA: Effect of RecF pathway mutations on plasmid recombination in *Escherichia coli*. *J Bacteri.* 1985;163:1060–1066.

76. Clark AJ. *rec* genes and homologous recombination proteins in *Escherichia coli. Biochimie*.

1991;73:523–532.

77. Honda M, Inoue J, Yoshimasu M, Itp Y, Shibata T, Mikawa T. Identification of the RecR Toprim domain as the binding site for both RecF and RecO. *J Biol Chem.* 2006;281:18549–18559.

78. Shan Q, Bork JM, Webb BL, Inman RB, Cox MM. RecA protein filaments: End-dependent dissociation from ssDNA and stabilization by RecO and RecR proteins. *J Mol Biol*. 1997;265:519–540.

79. Lenhart JS, Brandes ER, Schroeder JW, Sorenson RJ, Showalter HD, Simmons LA. RecO and RecR are necessary for RecA loading in response to DNA damage and replication fork stress. *J Bacteriol*. 2014;196:2851–2860.

80. Rösch TC, Altenburger S, Oviedo-Bocanegra L, Pediaditakis M, Najjar N El, Fritz G, *et al.* Single molecule tracking reveals spatio-temporal dynamics of bacterial DNA repair centres. *Sci Rep*. 2018;8:16450.

81. Odsbu I, Skarstad K. DNA compaction in the early part of the SOS response is dependent on RecN and RecA. Microbiology. 2014;160:872–82.

82. Rocha EPC, Cornet E, Michel B. Comparative and evolutionary analysis of the bacterial homologous recombination systems. *PLoS Comput Biol*. 2005;1:e15.

83. Smith GR. How RecBCD Enzyme and Chi promote DNA break repair and recombination: a molecular biologist's view. *Microbiol Mol Biol Rev*. 2012;76:217–228.

84. Vlašić I, Ivančić-Baće I, Imešek M, Mihaljević B, Brčić-Kostić K. RecJ nuclease is required for SOS induction after introduction of a double-strand break in a RecA loading deficient *recB* mutant of Escherichia coli. Biochimie. 2008;90:1347–55.

85. Battesti A, Majdalani N, Gottesman S. The RpoS-mediated general stress response in *Escherichia coli*. *Annu Rev Microbiol*. 2011;65:189–213.

86. Al Mamun AAM, Humayun MZ. *Escherichia coli* DNA polymerase II can efficiently bypass 3,$N^{(4)}$-ethenocytosine lesions *in vitro* and *in vivo*. *Mutat Res*. 2006;593:164–176.

87. Napolitano R, Janel-Bintz R, Wagner J, Fuchs RPP. All three SOS-inducible DNA polymerases (Pol II, Pol IV and Pol V) are involved in induced mutagenesis. *EMBO J.* 2000;19:6259–6265.

88. Jaszczur MM, Bertram JG, Robinson A, van Oijen AM, Woodgate R, Cox MM, et al. Mutations for worse or better: Low fidelity DNA synthesis by SOS DNA polymerase V is a tightly-regulated double-edged sword. *Biochemistry*. 2016;2:2309–2318.

89. Goodman MF. Error-prone repair DNA polymerases in prokaryotes and eukaryotes. *Annu Rev Biochem*. 2002;71:17–50.

90. Hawver LA, Tehrani M, Antczak NM, Kania D, Muser S, Sefcikova J, *et al.* Point mutations in *Escherichia coli* DNA pol V that confer resistance to non-cognate DNA damage also alter protein-protein interactions. *Mutat Res*. 2015;780:1–14.

91. Walker GC. Mutagenesis and inducible responses to deoxyribonucleic acid damage in

Escherichia coli. Microbiol Rev. 1984;48:60–93.

92. Tang M, Pham P, Shen X, Taylor JS, O'Donnell ME, Woodgate R, et al. Roles of *E. coli* DNA polymerases IV and V in lesion-targeted and untargeted SOS mutagenesis. *Nature*. 2000;404:1014–1018.

93. Goodman MF, Woodgate R. Translesion DNA polymerases. *Cold Spring Harb Perspect Biol*. 2013;5:a010363.

94. Mallik S, Popodi EM, Hanson AJ, Foster PL. Interactions and localization of *Escherichia coli* error-prone DNA polymerase IV after DNA damage. *J Bacteriol*. 2015;197:2792–2809.

95. Wagner J, Gruz P, Kim SR, Yamada M, Matsui K, Fuchs RPP, et al. The *dinB* gene encodes a novel E. coli DNA polymerase, DNA pol IV, involved in mutagenesis. *Mol Cell*. 1999;4:281–286.

96. Godoy VG, Jarosz DF, Simon SM, Abyzov A, Walker GC. UmuD and RecA directly modulate the mutagenic potential of the Y-family DNA polymerase DinB. *Mol Cell*. 2007;28:1058–1070.

97. Bjedov I, Dasgupta CN, Slade D, Le Blastier S, Selva M, Matic I. Involvement of *Escherichia coli* DNA polymerase IV in tolerance of cytotoxic alkylating DNA lesions *in vivo*. *Genet Soc Am*. 2007;176:1431–440.

98. Cohen SE, Godoy VG, Walker GC. Transcriptional modulator NusA interacts with translesion DNA polymerases in *Escherichia coli*. *J Bacteriol*. 2009;191:665–672.

99. Ponder RG, Fonville NC, Rosenberg SM. A switch from high-fidelity to error-prone DNA double-strand break repair underlies stress-induced mutation. *Mol Cell*. 2005;19:791–804.

100. Shee C, Gibson JL, Rosenberg SM. Two mechanisms produce mutation hotspots at DNA breaks in *Escherichia coli. Cell Rep*. The Authors; 2012;2:714–721.

101. Shee C, Ponder R, Gibson JL, Rosenberg SM. What limits the efficiency of double-strand break-dependent stress-induced mutation in *Escherichia coli*? *J Mol Microbiol Biotechnol*. 2012;21:8–19.

102. Rosenberg SM, Shee C, Frisch RL, Hastings PJ. Stress-induced mutation *via* DNA breaks in *Escherichia coli*: A molecular mechanism with implications for evolution and medicine. *Bioessays*. 2012;34:885–892.

103. Corzett CH, Goodman MF, Finkel SE. Competitive fitness during feast and famine: How SOS DNA polymerases influence physiology and evolution in *Escherichia coli*. *Genetics*. 2013;194:409–420.

104. Frank EG, Ennis DG, Gonzalez M, Levine a S, Woodgate R. Regulation of SOS mutagenesis by proteolysis. *Proc Natl Acad Sci USA*. 1996;93:10291–10296.

105. Fijalkowska IJ, Schaaper RM, Jonczyk P. DNA replication fidelity in *Escherichia coli*: a multi-DNA polymerase affair. *FEMS Microbiol Rev*. 2012;36:1105–1121.

106. Szekeres Jr. ES, Woodgate R, Lawrence CW. Substitution of *mucAB* or *rumAB* for *umuDC* alters

the relative frequencies of the two classes of mutations induced by a site-specific T-T cyclobutane dimer and the efficiency of translesion DNA synthesis. *J Bacteriol*. 1996;178:2559–2563.

107. Mead S, Vaisman A, Valjavec-Gratian M, Karata K, Vandewiele D, Woodgate R. Characterization of polVR391: A Y-family polymerase encoded by rumA′B from the IncJ conjugative transposon, R391. *Mol Microbiol*. 2007;63:797–810.

108. Battesti A, Majdalani N, Gottesman S. The RpoS-mediated general stress response in *Escherichia coli*. *Annu Rev Microbiol.* 2011;65:189–213.

109. Shee C, Gibson JL, Darrow MC, Gonzalez C, Rosenberg SM. Impact of a stress-inducible switch to mutagenic repair of DNA breaks on mutation in *Escherichia coli*. *Proc Natl Acad Sci USA.* 2011;108:13659–13664.

110. Motamedi MR, Szigety SK, Rosenberg SM. Double-strand-break repair recombination in *Escherichia coli*: physical evidence for a DNA replication mechanisms *in vivo. Genes Dev*. 1999;13:2889–2903.

111. Frisch RL, Su Y, Thornton PC, Gibson JL, Rosenberg SM, Hastings PJ. Separate DNA Pol II- and Pol IV-dependent pathways of stress-induced mutation during double-strand-break repair in *Escherichia coli* are controlled by RpoS. *J Bacteriol.* 2010;192:4694–4700.

112. Pomerantz RT, Kurth I, Goodman MF, O'Donnell M. Preferential D-loop extension by a translesion DNA polymerase underlies error-prone recombination. *Nat Struct Mol Biol.* 2013;20:748–755.

113. Chaurasiya KR, Ruslie C, Silva MC, Voortman L, Nevin P, Lone S, et al. Polymerase manager protein UmuD directly regulates Escherichia coli DNA polymerase III α binding to ssDNA. *Nucleic Acids Res*. 2013;41:8959–8968.

114. Yu J, Xiao J, Ren X, Lao K, Xie SX. Probing gene expression in live cells, One Protein Molecule at a Time. *Science*). 2006;311:1600–1604.

115. Reyes-Lamothe R, Possoz C, Danilova O, Sherratt DJ. Independent positioning and action of *Escherichia coli* replisomes in live cells. *Cell.* 2008;133:90–102.

116. Reyes-Lamothe R, Sherratt DJ, Leake MC. Stoichiometry and architecture of active DNA replication machinery in *Escherichia coli. Science*. 2010;328:498–501.

117. Gebhardt JCM, Suter DM, Roy R, Zhao ZW, Chapman AR, Basu S, *et al.* Single molecule imaging of transcription factor binding to DNA in live mammalian cells. *Nat Methods*. 2013;10:421–426.

118. Henrikus SS, Wood EA, McDonald JP, Cox MM, Woodgate R, Goodman MF, et al. DNA polymerase IV primarily operates outside of DNA replication forks in *Escherichia coli. PLoS Genet*. 2018;14:e1007161.

2 DNA polymerase IV primarily operates outside of DNA replication forks in *Escherichia coli*

Sarah S. Henrikus, Elizabeth A. Wood, John P. McDonald, Michael M. Cox, Roger Woodgate, Myron F. Goodman, Antoine M. van Oijen, Andrew Robinson

Published in *PLoS Genet.*, 2018; 14(1):e1007161.

In *Escherichia coli*, damage to the chromosomal DNA induces the SOS response, setting in motion a series of different DNA repair and damage tolerance pathways. DNA polymerase IV (pol IV) is one of three specialised DNA polymerases called into action during the SOS response to help cells tolerate certain types of DNA damage. The canonical view in the field is that pol IV primarily acts at replisomes that have stalled on the damaged DNA template. However, the results of several studies indicate that pol IV also acts on other substrates, including single-stranded DNA gaps left behind replisomes that re-initiate replication downstream of a lesion, stalled transcription complexes and recombination intermediates. In this study, we use single-molecule time-lapse microscopy to directly visualize fluorescently labelled pol IV in live cells. We treat cells with the DNA-damaging antibiotic ciprofloxacin, Methylmethane sulfonate (MMS) or ultraviolet light and measure changes in pol IV concentrations and cellular locations through time. We observe that only 5–10% of foci induced by DNA damage form close to replisomes, suggesting that pol IV predominantly carries out non-replisomal functions. The minority of foci that do form close to replisomes exhibit a broad distribution of colocalisation distances, consistent with a significant proportion of pol IV molecules carrying out postreplicative TLS in gaps behind the replisome. Interestingly, the proportion of pol IV foci that form close to replisomes drops dramatically in the period 90–180 min after treatment, despite pol IV concentrations remaining relatively constant. In an SOS-constitutive mutant that expresses high levels of pol IV, few foci are observed in the absence of damage, indicating that within cells access of pol IV to DNA is dependent on the presence of damage, as opposed to concentration-driven competition for binding sites.

I carried out and analysed all in vivo single-molecule experiments, 4-nitroquinolone-1-oxide survival assays and ciprofloxacin resistance assays. I was involved in strain construction, analysis of Western blotting and the preparation of the manuscript.

2.1 Author Summary

Translesion DNA polymerases play a critical role in DNA damage tolerance in all cells. In *Escherichia coli*, the translesion polymerases include DNA polymerases II, IV, and V. At stalled replication forks, DNA polymerase IV is thought to compete with, and perhaps displace the polymerizing subunits of DNA polymerase III to facilitate translesion replication. The results of the current fluorescence microscopy study challenge that view. The results indicate that DNA polymerase IV acts predominantly at sites away from the replisome. These sites may include recombination intermediates, stalled transcription complexes, and single-stranded gaps left in the wake of DNA polymerase III replisomes that re-initiate replication downstream of a lesion.

2.2 Introduction

Translesion synthesis (TLS) DNA polymerases are produced at elevated levels in bacteria as part of the SOS response to DNA damage (1). They have historically been thought to serve as a last resort DNA damage-tolerance mechanism, re-starting replication forks that have stalled at damage sites on the DNA (1–7). TLS polymerases are highly error prone: inducing their activities leads to increased rates of mutation (error rates of up to 1 in every 100 nucleotides incorporated into DNA). TLS is an important source of mutations that fuel bacterial evolution (8–13). For several species of bacteria, deleting genes for TLS polymerases dramatically reduces rates of antibiotic resistance development in laboratory measurements, and in some cases even reduces infectivity (9,14–22). Many of the drugs used to treat bacterial infections cause an increase in mutation rates as a result of TLS (16). It remains unclear, however, whether TLS polymerases contribute to resistance by providing damage tolerance, increasing cell survival and thus the chances that a resistant mutant will be found, or by facilitating adaptive mutation – selectively increasing mutation rates to speed the evolution of drug resistance (14–19).

DNA polymerase (pol) IV is thought to be the most abundant TLS polymerase in *E. coli*. From Western blots, it has been estimated that levels of pol IV increase from approximately 250 molecules per cell in the absence of DNA damage, to 2500 molecules per cell upon activation of the SOS damage response (23,24). Pol IV promotes TLS on a variety of different lesion-containing DNA substrates, although its tendency for misincorporation varies with lesion type (25–32). Pol IV bypasses adducts to the N^2 position of guanines and a variety of alkylation lesions in a mostly error-free fashion (28–30,33–35). When overexpressed, pol IV induces -1 frameshift mutations in cells treated with alkylating agents (36). In addition to these lesion bypass activities, pol IV participates in transcription (37–40) and double strand break-repair repair (41–45), and contributes significantly to cell fitness in late stationary phase cultures in the absence of any exogenous DNA damage (8). Pol IV is also reported to be required for formation of adaptive point mutations in the *lac* operon and was found to be a major determinant in the development of ciprofloxacin resistance in a laboratory culture model (9,46).

Visualisation of pol IV within live bacterial cells would make it possible to better understand how pol IV activity is regulated in response to DNA damage and test proposed models for its TLS activity at replisomes. Here, we report a single-molecule time-lapse approach to investigate pol IV dynamics and kinetics in live *E. coli* cells under normal growth conditions and following treatment with the antibiotic

ciprofloxacin, the DNA-damaging agent MMS, or ultraviolet (UV) light. Our analysis indicates that most pol IV molecules carry out DNA synthesis predominantly outside replisomes and that access of pol IV to DNA is governed by more than simple concentration-action driven polymerase exchange.

2.3 Results

2.3.1 Construction and validation of a chromosomal *dinB-YPet* fusion

To visualise time-dependent changes in pol IV activity in response to DNA damage, we constructed an *E. coli* strain in which pol IV is fluorescently labelled, then imaged the resulting cells on a purpose-built single-molecule fluorescence microscope (47). We created the pol IV-labelled strain in two steps. We started with a plasmid-based *dinB-eYFP* construct, shown previously to be active for pol IV-dependent DNA damage tolerance and mutagenesis by Mallik *et al*. (30). We first replaced the gene for eYFP with the gene for the similar, but brighter, fluorescent protein, YPet. We then replaced the native *dinB* gene on the *E. coli* K12 MG1655 chromosome with the *dinB-YPet* fusion gene using λ_{RED} recombineering to create the strain EAW633. These cells express pol IV from its natural promoter, at its native chromosomal locus, but with YPet fused to its C-terminus through a twenty-amino acid linker (**Fig 1A**). To facilitate two-colour imaging of pol IV and replisomes, we also produced two strains with DNA polymerase III holoenzyme (pol III HE) markers. These strains expressed red fluorescent protein fusions of the pol III HE τ-subunit (EAW643; *dnaX-mKate2 dinB-YPet*) and ε-subunit (EAW641; *dnaQ-mKate2 dinB-YPet*) respectively. We have previously used *dnaX-YPet* and *dnaQ-YPet* fusions to indicate the position of replisomes (47). Both the *dnaX-mKate2* and *dnaQ-mKate2* alleles used here are fully functional, having no impact on the growth of cells and showing no tendency for fluorescent protein-induced aggregation (48).

The expression and activity of the DinB-YPet fusion protein was verified using a series of three assays. First, we carried out Western blots using anti-DinB antibodies in order to compare the expression levels of DinB-YPet to those of untagged DinB (pol IV) in wild-type cells (**Fig 1B, Supplementary figure 1**). In cells treated with ciprofloxacin, DinB-YPet is expressed at levels equivalent to wild-type DinB, although a small amount (~20%) is proteolysed to two shorter fragments within the cells. The larger fragment is probably produced via cleavage between the linker sequence and YPet, yielding YPet and DinB-linker. The smaller fragment migrates similarly to DinB and is probably produced via cleavage between the linker and DinB, yielding DinB and linker-YPet.

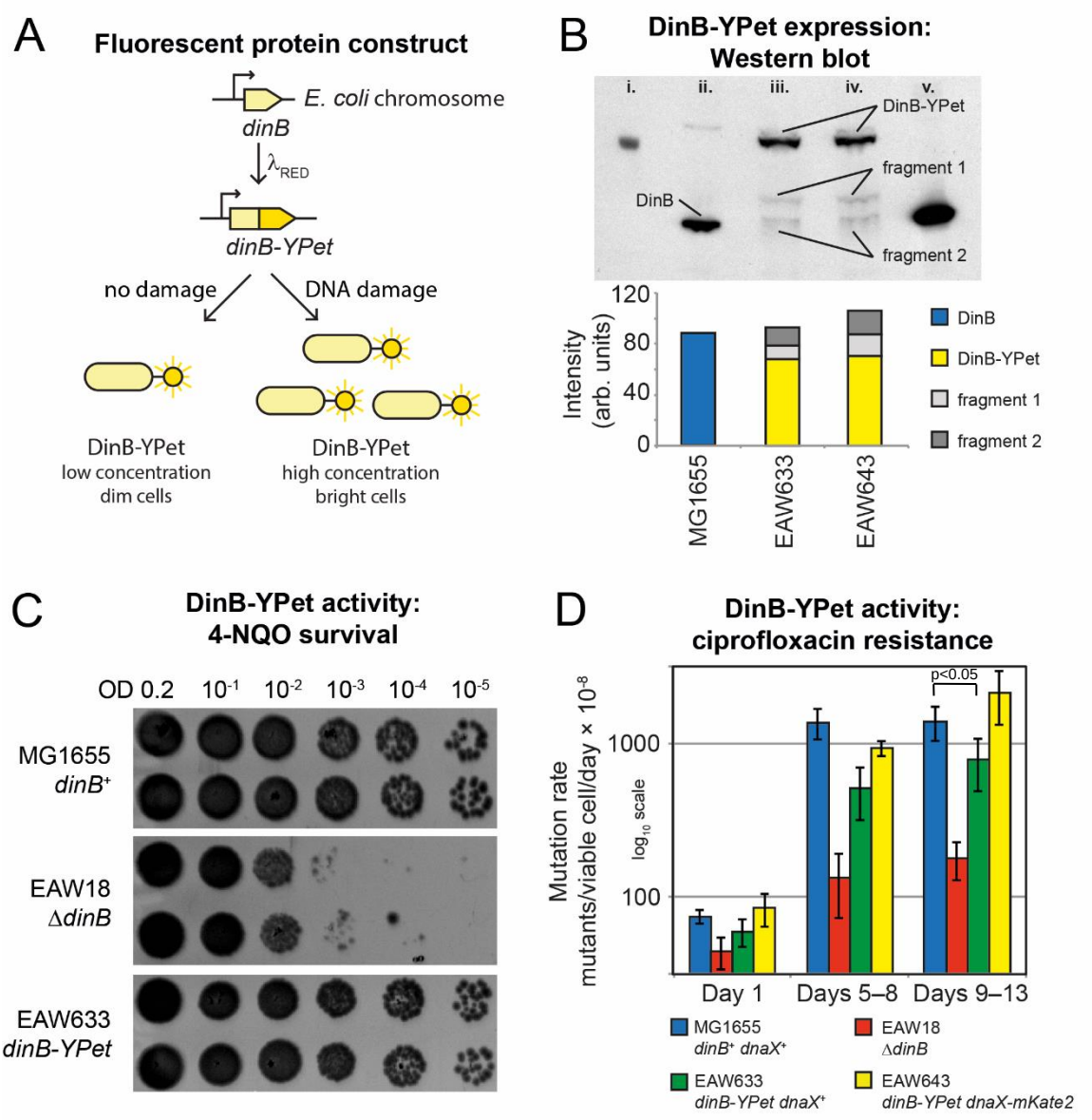

Figure 1. Construction of *E. coli* cells expressing labelled pol IV and analysis of bypass and mutagenic functions. (A) Construction of EAW633 (*lexA*$^+$ *dinB-YPet*). The *dinB* gene of *E. coli* K12 MG1655 was modified using λ_{RED} recombineering so that pol IV is expressed as a fusion with the bright yellow fluorescent protein YPet (DinB-YPet). (B) Confirmation of DinB-YPet expression in ciprofloxacin-treated cells. (Upper part) Western blot of extracts from cells (treated with 30 ng/ml ciprofloxacin for 120 min), developed using anti-DinB antibodies. Lanes: i) molecular weight marker; ii) MG1655; iii) EAW633 (*dinB-YPet*); iv) EAW643 (*dinB-YPet dnaX-mKate2*); v) BL21 pLysS pET-DinB (uninduced cell extract). Bands corresponding to full length DinB-YPet are clearly visible in lanes ii and iii. A small amount of two DinB-containing fragments are also visible. Fragment 1 corresponds to DinB+linker. Fragment 2 corresponds to DinB +/- one or two residues. (Lower part) Results of densitometry measurements for lanes ii–iv. DinB-YPet is expressed at levels equivalent to wild-type DinB, however ~20% is proteolysed within the cells. (C) DinB-YPet retains lesion bypass activity. Strains were grown to exponential growth phase (OD_{600} = 0.2), serial diluted, and spotted onto LB agar plates containing 8 μM of 4-nitroquinolone-1-oxide (NQO). Because of an inability to bypass lesions induced by NQO, cells lacking *dinB* are sensitized by 3 orders of magnitude relative to wild type cells. Cells expressing DinB-YPet survival to levels equivalent to wild-type cells, indicating that DinB-YPet retains full lesion bypass activity. (D) DinB-YPet facilitates mutation to ciprofloxacin resistance. Approximately 10^8 log-phase cells were spread onto LB agar plates containing 40 ng/ml ciprofloxacin and incubated at 37°C for 13

days. Colonies appearing on the plates were counted on days 4, 8 and 13. The number of new colonies appearing between each interval was determined and normalised against viable cell counts, as described in reference (9). Cells lacking *dinB* produced only 10% as many ciprofloxacin-resistant colonies as wild-type cells. DinB-YPet expressing cells produced similar number of resistant colonies as wild-type cells, indicating that DinB-YPet supports mutagenic pol IV activities. $p < 0.05$ in two-sample t test for differences of means of MG1655 and EAW633, 9-13 days.

We next exposed cells to the DNA damaging agent 4-nitroquinoline-1-oxide (NQO) and measured survival using plate-based dilution assays (**Fig 1C**). As has been observed previously (29,44), cells lacking pol IV (Δ*dinB*) were much more sensitive to NQO than wild-type cells. Cells expressing the DinB-YPet fusion (EAW633) showed similar survival as wild-type cells, indicating that DinB-YPet retains pol IV-dependent lesion bypass activity.

When plated on LB agar containing an inhibitory concentration of the antibiotic ciprofloxacin, *E. coli* cells produce colonies of resistant mutants over the course of 13 days (9). It was found previously that cells lacking pol IV activity give rise to fewer resistant mutants than wild-type cells (9). We repeated these measurements and found that cells lacking pol IV (Δ*dinB*) produced only 10% as many ciprofloxacin-resistant mutants as wild-type cells (**Fig 1D**). Cells expressing DinB-YPet (EAW633 and EAW 643) produced similar numbers of resistant mutants as wild-type cells, indicating that DinB-YPet also remains active for pol IV-dependent mutagenesis.

2.3.2 Direct observation of pol IV activity during the SOS response

We imaged EAW643 cells in the context of home-built flow-cells, which enable continuous flow of media throughout our measurements. For this study, we recorded two types of fluorescence movies: rapid-acquisitions, which capture the motions of molecules on the milliseconds–seconds timescale; and time-lapse measurements, which capture changes in pol IV behaviour over the course of hours. Single-molecule level measurements allow us to observe binding of pol IV molecules to DNA or pol IV as part of a DNA-bound multiprotein complex. On our imaging timescale (34 ms exposures), proteins moving freely through the cytosol diffuse quickly ($D \approx 10$ μm^2/s) and thus appear as a blur (**Fig 2A)**. Any pol IV molecules bound to specific binding sites on the DNA, however, should move much more slowly; their motion will be dictated by the motion of the binding site. In *E. coli*, individual sites on the chromosome have an apparent diffusion constant $D \approx 10^{-5}$ μ m^2/s (49). As pol IV requires ~100 ms to incorporate a single nucleotide, we expect that any molecules synthesising DNA will appear relatively static in our images and thus produce bright foci.

In the absence of damage, we observed small, but measureable DinB-YPet signals within cells, consistent with continuous low-level production of pol IV (**Fig 2B**). It is possible to calibrate the fluorescence intensities of cells against the intensity of individual molecules in order to determine the number of molecules in each cell (**see Experimental Procedures**). We calculated that EAW643 cells express 20 ± 3 molecules of DinB-YPet per cell (STD = 36; n = 105 cells) in the absence of damage. Using cell size parameters measured from bright-field images it is further possible to determine the volume of each cell, and subsequently to determine the DinB-YPet concentration. We calculate that in the absence of damage the DinB-YPet concentration is 6 ± 1 nM.

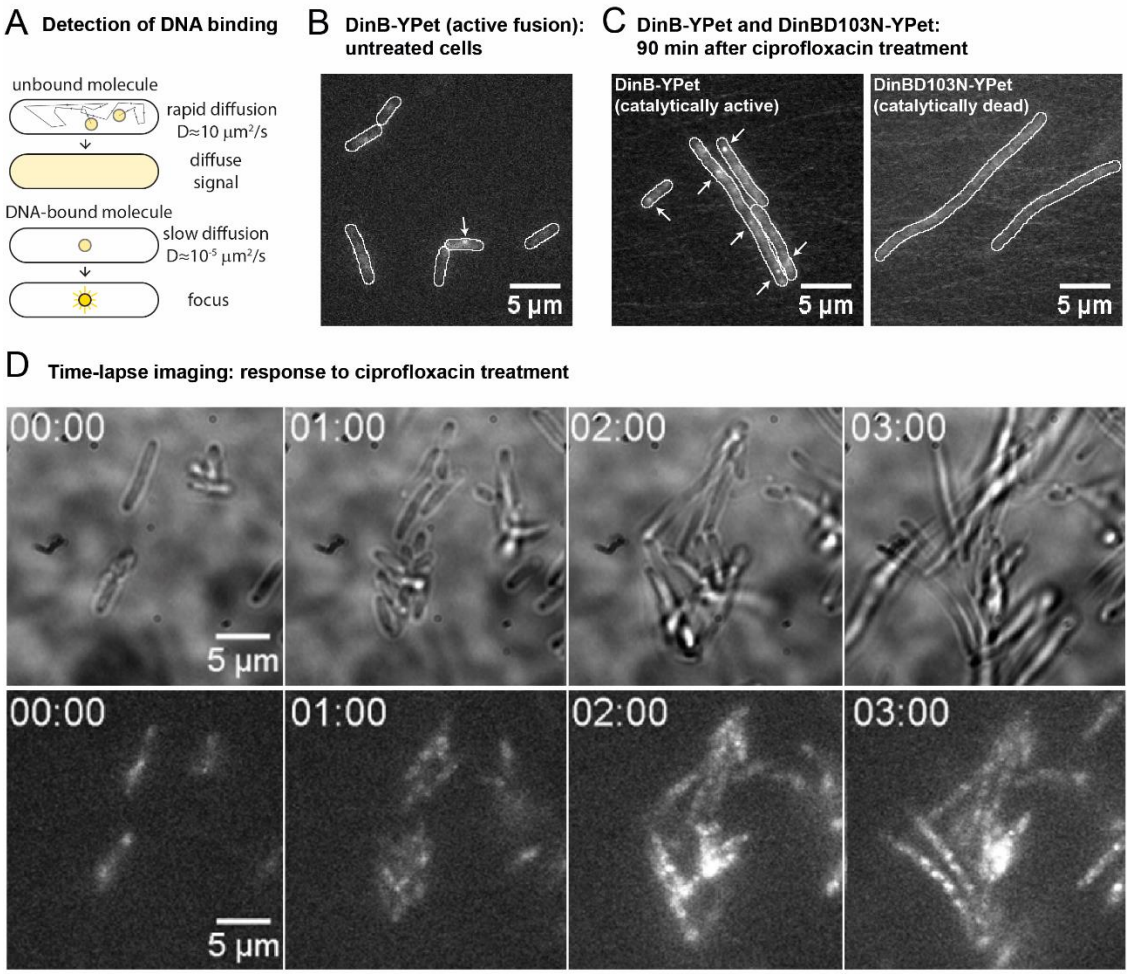

Figure 2. Single-molecule imaging of cells expressing DinB-YPet. (A) Detection of DNA-bound molecules in single-molecule images. Molecules of DinB-YPet that are not bound to DNA will diffuse quickly ($D \approx 10\ \mu m^2/s$ for a typical cytosolic protein) and thus signals from individual molecules will blur over the entire cell in our images (exposure time = 30–100 ms). Molecules of DinB-YPet that are bound to DNA, however, experience greatly reduced motion and thus appear as punctate foci. Because of this diffusional contrast, it is possible to detect individual molecules of DinB-YPet when bound to DNA. (B) Single-molecule sensitive fluorescence image of undamaged EAW643 cells showing low-level DinB-YPet signals at 50 ms exposure time. (C) Average projection of rapid acquisition (effective exposure time 306 ms) for DinB-YPet (left) and DinBD103N-YPet (right). (D)Time-lapse imaging of pol IV up-regulation in response to ciprofloxacin treatment. Images shown are a montage of a three-hour time-lapse series. Cells were initially grown in rich medium in the absence of exogenous DNA damage. At t = 0 min, the flow cell inlet was switched to medium containing 30 ng/ml ciprofloxacin. At each field-of-view, a bright-field image and a DinB-YPet fluorescence image were collected every 5 min for 180 min. Time stamps indicate hours after ciprofloxacin addition.

The pol IV levels measured here by microscopy are somewhat lower than previous estimates of 250 molecules of pol IV per cell, based on Western blots (24). It has been demonstrated previously that under conditions similar to those used here that >90% of YPet molecules are in the mature, fluorescently active form (50). The small amount of proteolysis of DinB-YPet observed in the Western blot (**Fig 1B**) would be expected to yield an intact YPet fragment. Thus, the microscopy-based measurements should still produce an accurate measure of DinB levels. At worst, DinB levels would be underestimated by ~20%. To probe this discrepancy further, we repeated the Western blot analysis (**Supplementary figure 1**). The values we

calculated varied considerably between replicates, reflecting the difficulties associated with quantifying Western blots of low abundance proteins. All values were, however, significantly lower than those determined in the Kim *et al*. study and were consistent with the fluorescence microscopy results. Taking the mean of two independent blots, the current Westerns indicate that MG1655 contain 33 molecules of DinB per cell on average. The strain used in the Kim *et al*. study, YG2247 (a derivative of P90C) returns similar value: 30 molecules per cell on average. DinB-YPet was measured at 19 molecules per cell. The fluorescence microscopy measurements presented here are much more sensitive, and far less variable, than Western blotting and likely to provide more accurate results. We therefore conclude that the value measured by fluorescence microscopy, 20 molecules of DinB per cell, is correct and that the original value of 250 was an overestimation (24).

In rapid acquisition movies, we observe that the DinB-YPet signal is primarily diffuse (**Fig 2B**): cells contain 0.5 ± 0.5 foci per cell on average (i.e. one focus for every two cells; STD 1.11; n = 105 cells).

We then induced DNA damage by switching to medium containing 30 ng/mL ciprofloxacin, an antibiotic that inhibits DNA gyrase and forms covalent adducts on the DNA (51). These inhibit DNA replication and lead to induction of the SOS response. Under these conditions, we observed that cells were longer and exhibited stronger DinB-YPet signals (**Fig 2C**). This observation is consistent with increasing production of pol IV as part of the SOS response, leading to higher concentrations of pol IV in the cell. Punctate foci were visible after ciprofloxacin addition, consistent with pol IV binding to DNA. Cells expressing a catalytically dead variant of pol IV (52,53), DinB(D103N)-YPet, did not produce foci when imaged under the same conditions (**Fig 2C**). We therefore conclude that ciprofloxacin treatment leads to a significant increase in the number of pol IV binding events on the DNA.

Time-lapse analysis indicated that cells filament and exhibit a strong increase in DinB-YPet fluorescence, beginning approximately 20 min after the addition of ciprofloxacin (**Fig 2D**; **Fig3A–B, Supplementary Movie 1**). From 90–180 min, the DinB-YPet concentrations plateaus. We calculate that at this point, cells contain an average of 279 ± 33 DinB-YPet molecules per cell (STD 28; n = 105 cells). Thus, ciprofloxacin-treated cells contain 14 times more molecules of DinB-YPet than undamaged cells. Due to damage-induced filamentation, however, the ciprofloxacin-treated cells are 2.5 times larger in volume. Thus, the concentration of DinB-YPet after treatment with ciprofloxacin is 34± 3 nM, is only 5.5 times higher than in the absence of damage. The number of pol IV molecules per cell that we measure by microscopy after ciprofloxacin treatment is lower than previous estimates of pol IV expression (~2500 molecules per cell) based on Western blotting of MMS-treated cells (24). Values measured by Western blot during the current study were highly variable, but all were significantly lower than the previous estimate of 2500 molecules per cell. The values measured here, ~100 molecules per cell following treatment with 30 ng/ml ciprofloxacin for 2 h, are more consistent with those measured by fluorescence microscopy (**Supplementary figure 1**). We conclude that the value originally published by Kim *et al*. is likely to be overestimated. Based on the microscopy results, which are likely to be more accurate than those of Western blots, we concluded that there are 250 molecules of DinB per cell following ciprofloxacin treatment.

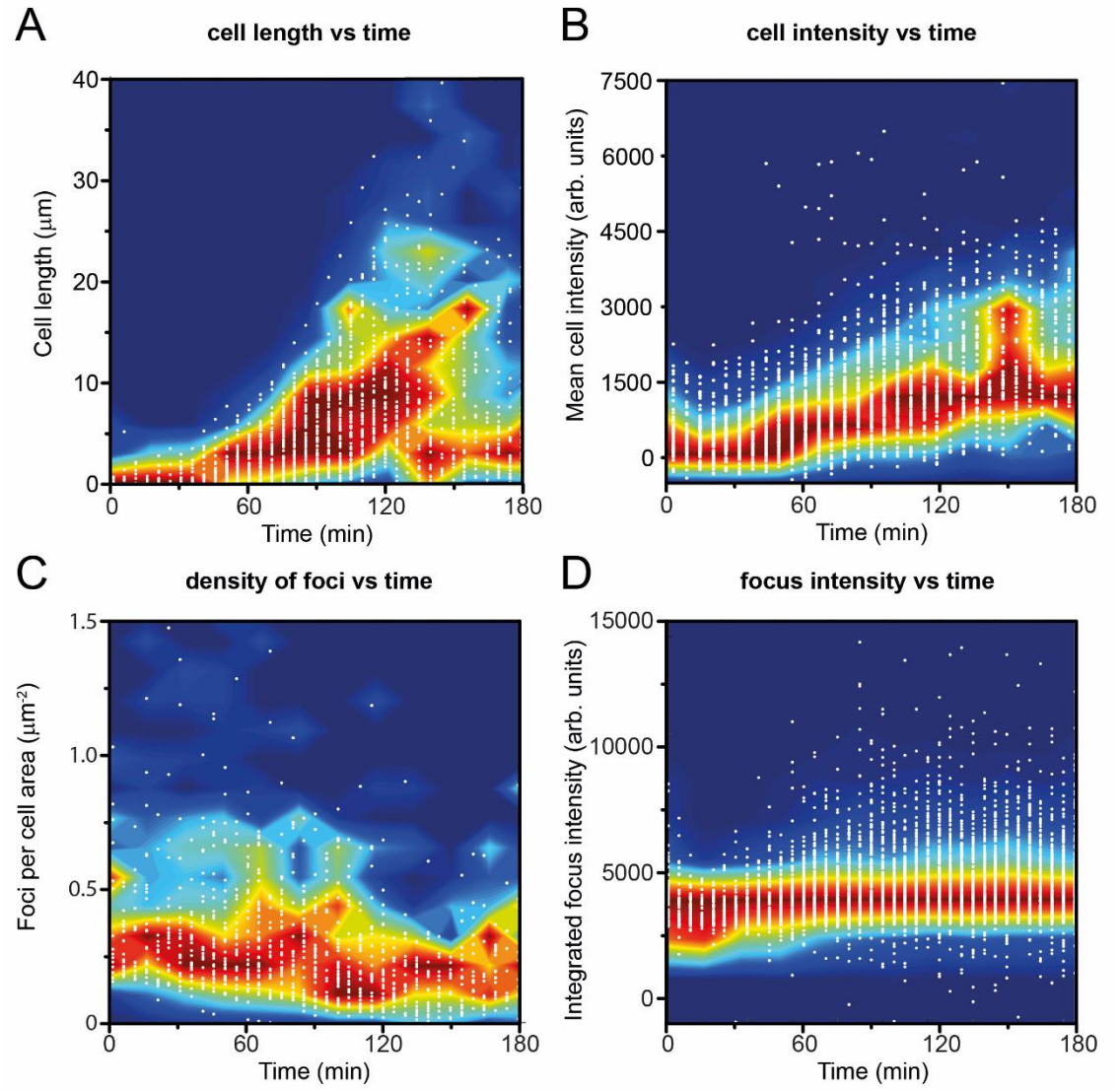

Figure 3. Scatter plots of cell-size and fluorescence signal parameters from time-lapse imaging of DinB-YPet cells treated with ciprofloxacin. White points indicate individual data-points, while blue-to-red contours indicate frequencies of observations. Blue areas indicate regions of the plot containing few data points; red areas indicate regions containing a large number of data points. Frequencies were normalised at each time-point to the maximum value at that time-point. (A) Distribution of cell lengths based on bright-field images, showing ciprofloxacin-induced filamentation. (B) DinB-YPet fluorescence per cell, measured as the mean pixel intensity within each cell, showing up-regulation of DinB-YPet. (C) Density of DinB-YPet foci, measured as the number of foci per cell area (μm^2), showing the density remains relatively constant over the three-hour measurement. (D) Integrated fluorescence intensity of foci. Each focus was fit with a 2D Gaussian function; the volume under this function represents the integrated fluorescence intensity. Foci become brighter over the course of the measurement, indicating that a higher number of DinB-YPet molecules bind at each binding site. We conservatively estimate that >100 cells were used in each measurement.

We next measured as a function of time the number of DinB-YPet foci per cell area (i.e. the density of foci throughout the cell) and their intensities. The density of DinB-YPet foci in cells remained relatively constant (**Fig 3C**), the intensities of foci increased slightly over time (**Fig 3D**), following a similar trend as the increase in pol IV concentration (**Fig 3B**). These observations indicate that the number of binding sites for pol IV in each cell remains relatively constant from 30–180 min after ciprofloxacin addition,

whereas the number of molecules bound at each binding site increases in time. Comparing the intensities of DinB-YPet foci to the intensity of a single YPet molecule, we calculate that in the early stages of the response (30–90 min, foci contain 1–2 DinB-YPet molecules while in the later stages (90–180 min), foci contain 2–4 molecules (**Supplementary Figure 2**).

2.3.3 Colocalisation between pol IV and replisomes

Two models have been proposed for pol IV activity in the vicinity of replisomes. In the first and most widely cited model, pol IV acts within the replisome (1–7). Here the pol IV exchanges with a pol III that has stalled at a lesion in the template, bypasses the lesion, then exchanges back out of the replisome, allowing pol III to continue with processive DNA synthesis. In the second model pol IV carries out postreplicative TLS at gaps left in the wake of replisomes that skip over lesions (54–56). In principal both mechanisms could be at play within cells. In addition to these (near) replisomal activities, a number of studies have implicated pol IV in a variety of other cellular processes, including transcription and recombination (30,37–45).

To further examine the activities of pol IV inside and outside the replisomal context, we imaged both DinB-YPet and a replisome marker, either DnaX-mKate2 or DnaQ-mKate2, which allowed us to visualise the position of pol III HE complexes. The DnaX (τ-subunit) and DnaQ (ε-subunit) proteins are stably associated within the pol III HE in *E. coli*; they do not exchange in and out of the complex (48). We assume that foci formed by DnaX-mKate2 and DnaQ-mKate2 exclusively indicate the positions of pol III HE complexes acting within replisomes. From this point, we make reference to replisome markers and replisome foci. These refer to DnaX-mKate2 foci unless otherwise stated. As the pol III HE contains (at least) two polymerases, we expect that if pol IV exchanges with one of the pol III cores, pol III HE will remain bound and the pol IV and replisome markers will colocalise. On the other hand, if pol III HE does fully dissociate from the DNA as pol IV binds at the replication fork, the DinB-YPet and replisome foci would not colocalise. In this case we would expect that as the number of DinB-YPet foci in cells increased, there would be a significant decline in the number of replisome foci.

We recorded two-colour time-lapse movies and measured the number of replisome and pol IV foci as a function of time, as well as their colocalisation (**Fig 4**). Two forms of analysis were carried out. To further investigate whether pol IV acts within or behind replisomes, we measured pair-wise distances between pol IV foci and replisome markers. To investigate the balance between (near) replisomal and non-replisomal activities of pol IV, we measured time-dependent changes in the proportion of pol IV foci that tightly colocalised with replisome markers.

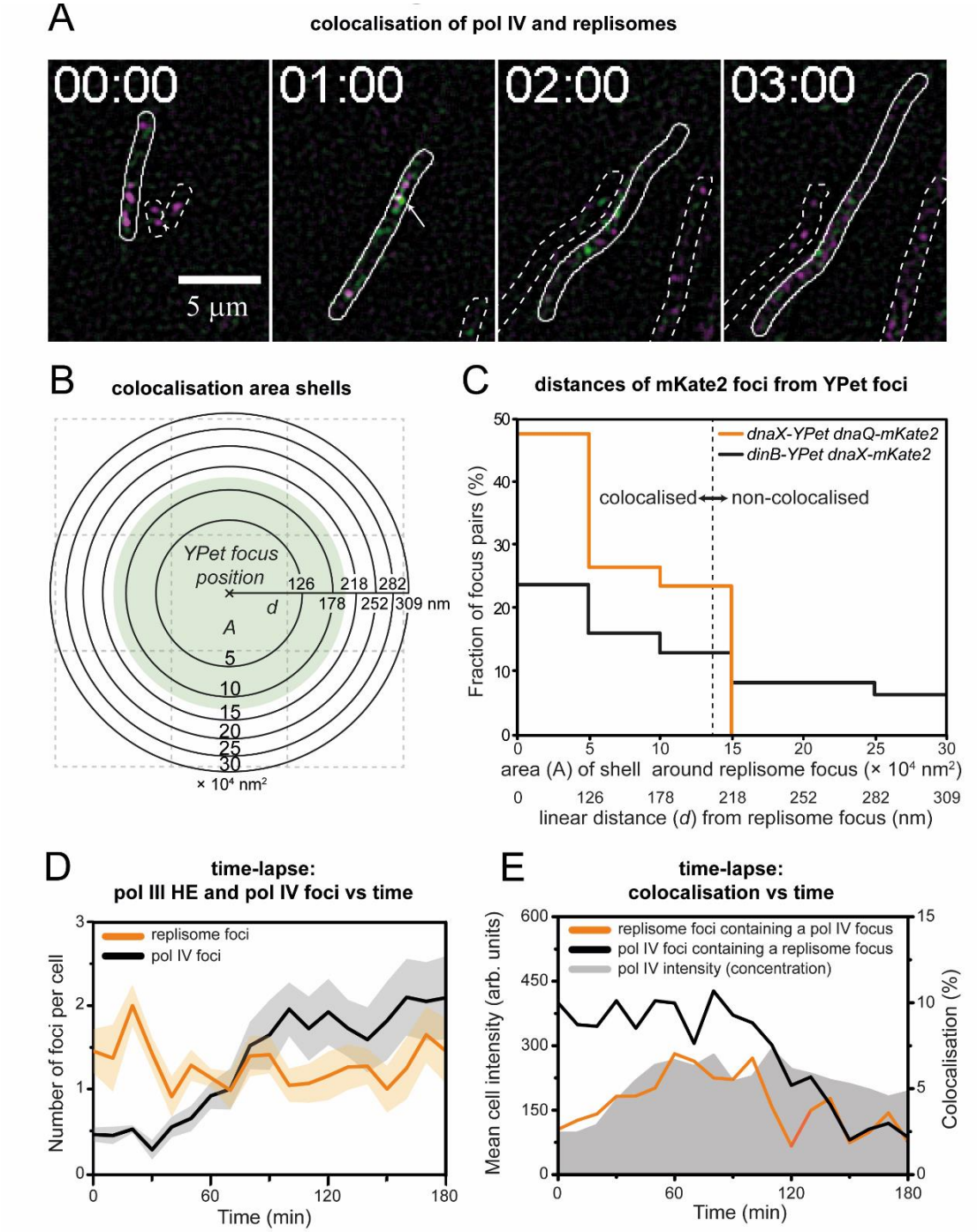

Figure 4. Colocalisation of pol IV with replisomes**.** (A) Montage of two-colour time-lapse movie recorded after treatment 30 ng/mL ciprofloxacin. Pol IV (DinB-YPet) foci appear green and replisome (DnaX-mKate2) foci appear in magenta. Colocalised foci appear white. For display purposes, images were subjected to spatial filtering to enhance foci (47). (B-C) Analysis of colocalisation distances for foci detected in two-colour images. (B) Diagram of area shells used for colocalisation analysis. As colocalisation is a radial measurement, histograms of colocalisation distances are constructed using bins of linearly increasing area rather than distance. (C) Histograms of colocalisation distances for foci within a doubly labelled replisome strain (EAW203; *dnaX-YPet dnaQ-mKate2*) and a two-colour pol IV/replisome strain (EAW643; *dinB-YPet dnaX-mKate2*). As expected, distances between DnaX-YPet and DnaQ-mKate2 foci fall within a narrow distribution, indicative of 'tight' colocalisation. Distances between DinB-YPet and DnaX-mKate2 foci present a much broader distribution, indicative of 'loose' colocalisation. (D) Plot of the number of pol IV and replisome foci per EAW643 cell as a function of time. Data were compiled from ten technical replicates. Shaded areas indicate the standard error of the

mean between these replicates. Some cells were lost from the coverslip surface during the measurement. A total of 188 cells remained bound and were analysed over the full course of the measurement. (E) Plots of mean cell intensity and colocalisation between pol IV and replisome foci. The mean cell intensity (grey shaded area) is a direct measure of the pol IV concentration in cells. Foci located within 200 nm of each other were defined as being colocalised. Colocalisation was measured in two ways: the proportion of pol IV foci that contain a colocalised replisome focus (black line), and the proportion of replisome foci that contain a colocalised pol IV focus (orange line). Data were compiled from ten technical replicates. Shaded areas indicate the standard error of the mean between these replicates. The total number of cells analysed were not determined in these measurements. We conservatively estimate that >1000 cells were used in each measurement. The analysis includes a total of 17005 DnaX-mKate2 foci and 12408 DinB-YPet foci.

If pol IV carries out replicative TLS (within the replisome), one would expect to observe 'tight' colocalisation of pol IV foci with replisome foci; a histogram of pair-wise distances between DinB-YPet and DnaX-mKate2 foci would be expected to produce a relatively sharp peak. One might also expect enrichment of pol IV foci close to replisomes if pol IV instead carries out postreplicative TLS in gaps left behind the replisome. In this case however, replisomes would be expected to rapidly move away from gaps after they are created. This would lead to a type of 'loose' colocalisation that would manifest as a broad distribution of distances between pol IV foci and replisome markers.

We first measured pair-wise distances between foci in the strain EAW203 (*dnaX-YPet dnaQ-mKate2*) as a control. In this strain, the replisomes are labelled in two colours, producing a very high degree of colocalisation in two-colour images (48). Pair-wise distances between DnaX-YPet and DnaQ-mKate2 foci were plotted as a histogram. As colocalisation is a radial measurement there is a higher probability of detecting pairs separated by longer distances because longer search radii will cover a larger area of the image. To account for this, we assigned histogram bins based on shells of regularly increasing area rather than binning by linear distances (**Fig 4B**). For the two-colour replisome strain, the histogram contained a sharp peak (**Fig 4C**). All mKate2 foci fell within 218 nm of a YPet focus (i.e. they fell within a 15×10^4 nm^2 area shell). The width of the peak reports on the colocalisation error, which is a product of the localisation errors associated with fitting the YPet and mKate2 foci and any sample motion that occurs in the interval between collecting images in each colour channel (~2 s). We then repeated the analysis for the two-colour pol IV/replisome strain. A histogram of pair-wise distances for pol IV and replisome foci showed a considerably broader peak (**Fig 4C**), indicative of 'loose' colocalisation. Together these observations suggest that many DinB-YPet foci form close to, but not at replisomes. Thus, the results of this analysis are consistent with pol IV carrying out postreplicative TLS. With the current data, it is not possible to determine if pol IV carries out postreplicative TLS exclusively, or if both replicative and postreplicative TLS occur.

We next analysed time-dependent changes in colocalisation behaviour. Based on the histogram of pair-wise distances for the two-colour replisome strain (**Fig 4C**), we defined foci detected in time-lapse analyses as being colocalised if their fitted centroid positions fell within 200 nm of each other. We found that following ciprofloxacin treatment the number of replisome spots in cells remained relatively constant over time, indicating that pol III HE was not being removed from replisomes to a large extent (**Fig 4D**). We determined colocalisation in both directions, i.e. we measured the proportion of DinB-YPet foci that overlapped with a replisome focus, as well as the proportion of replisome foci that overlapped with a pol

IV focus. From 0–100 min after ciprofloxacin addition, 10% of pol IV foci colocalise with replisomes (**Fig 4E**), significantly above levels expected by chance (~5%, **see Experimental Procedures**), but well below levels expected if pol IV predominantly operates in the vicinity of replisomes. This observation suggests that the majority of pol IV's activities could be non-replisomal (**see Discussion**). Additionally, we found that in the late stages of the SOS response there was an even higher proportion of non-replisomal pol IV foci: from 100 min the proportion of pol IV foci that colocalise with replisomes falls to just 2.5%. Similar behaviour is observed when measuring colocalisation in the other direction. From 0–60 min, the proportion of replisomes that contain pol IV increases to 7%, tracking the increase in pol IV concentration within that period. From 60–100 min, the colocalisation plateaus at this level (modestly above the level expected by chance), in line with a plateau in the pol IV concentration. From 100–180 min, however, the proportion of replisomes that contain pol IV falls sharply; the average colocalisation is ~3% between 110–180 min, close to levels expected by chance. In contrast, the pol IV concentration remains elevated during this period. For both replisomes and pol IV, a plot of the number of foci per cell shows no evidence of a sharp transition at 100 min (**Fig 4D**), ruling out the possibility that the drop in colocalisation (**Fig 4E**) results from sudden loss of replisome or pol IV foci. Throughout the first 100 min, the concentration of pol IV increases, whereas the proportion of pol IV foci that colocalise with a replisome marker remains relatively constant. This indicates that the proportion of pol IV molecules that bind near replisomes is independent of the pol IV concentration. Similar results were obtained using EAW641, in which replisomes are marked by expression of DnaQ-mKate2 rather than DnaX-mKate2 (**Supplementary figure 3**).

To determine which DinB-YPet foci are likely to represent catalytically active molecules, we measured colocalisation using a longer (300 ms) exposure time. Pol IV molecules engaged in DNA synthesis may remain associated with the DNA for longer than molecules that bind non-productively to DNA or to other factors. In 300 ms images, foci are visible in DinB-YPet cells, but not in cells expressing catalytically dead DinB(D103N)-YPet (**Fig 2C**). In time-lapse images we detected fewer foci than when using 50 ms exposures (**Supplementary figure 4**), however the proportion of foci that colocalised with replisomes in 300 ms images (5%; **Supplementary Figure 4**) was similar to that observed in 50 ms exposures (10%; **Fig 4E**). Furthermore, a similar drop in colocalisation at 100 min was observed. From 0-90 min, 5% of pol IV foci overlap with a replisome (**Supplementary figure 4**). From 100-180 min, the colocalisation drops to 1.5%. Colocalisation of replisomes with pol IV shows a similar trend. From 0-90 min, 0.5% of replisomes have a pol IV focus, however, after 90 min only 0.2% of replisomes contain a pol IV focus. The fact that colocalisation was similar for both the 50 ms and 300 ms exposures indicates that there is no major difference in the lifetimes of foci formed near to, or away from replisomes and suggests that pol IV engages in DNA synthesis at sites both near to, and away from replisomes.

2.3.4 Pol IV activity is not governed by mass action-driven competition

In light of the observation that the colocalisation of pol IV and replisomes does not track with pol IV concentration, it is unlikely that access of pol IV to different DNA substrates is governed by mass action-driven competition alone. To explore this issue further, we altered the expression levels of pol IV in two different ways and examined the effects on pol IV focus formation and colocalisation with

replisomes. We first increased the amount of pol IV in cells by transforming SSH001 cells (Δ*dinB dnaQ-mKate2*) with the DinB-eYFP plasmid used by Mallik *et al* (30). Within this plasmid, pol IV is expressed from its natural promoter. However, because the plasmid is maintained at ~5–10 copies per cell, pol IV levels are expected to be much higher than when it is expressed from the chromosome.

We repeated the time-lapse analysis for this plasmid-containing strain and observed much higher levels of fluorescence (**Fig 5A**). We calculated that cells contain approximately 7000 molecules of DinB-eYFP after 90 min; already 14-fold higher than in cells expressing only DinB-YPet from the chromosome (280 molecules per cell) after >120 min. Despite this large change in the amount of pol IV, we observed the same time-dependent loss of colocalisation as before, although colocalisation in the initial stages of SOS was somewhat higher (**Fig 5B**). In the plasmid-containing strain, we found that the proportion of replisomes that contained a pol IV focus increased from 3 to 20 % within the first 90 min after ciprofloxacin addition. Similarly, the proportion of pol IV that colocalise with a replisome focus is 25–30 % from 0 – 90 min. We found that pol IV foci were noticeably brighter in the presence of the pol IV-expressing plasmid than in its absence, especially after 100 min (**Supplementary Figure 5A**). We calculated that each focus contains ~3-10 molecules of pol IV, while at the later stages foci contain > 30 molecules of pol IV (**Supplementary Figure 5B**). Cells that carried the *dinB-eYFP* plasmid only (i.e. they lacked a chromosomal copy of *dinB*) produced foci that showed similar levels of colocalisation with replisomes as cells that contained both *dinB-YPet* and *dinB-eYFP* (**Supplementary Figure 6**).

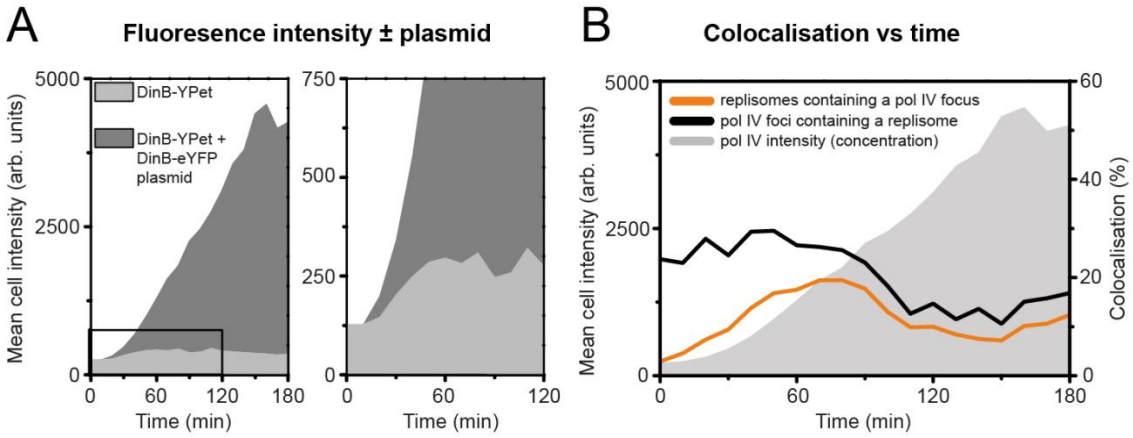

Figure 5. Colocalisation of pol IV with replisomes in the presence of additional fluorescently labelled pol IV expressed from a plasmid. (A) Mean cell intensity measurements for EAW643 cells (Pol IV^{+}; light grey line) and EAW643 cells containing pPFB1188 (expressing additional DinB-eYFP from the *dinB* promoter; Pol IV^{++}; dark grey line). Cells containing pFB1188 clearly express much higher levels of labelled pol IV, however because cells contain an unknown ratio two different YFPs (DinB-YPet and DinB-eYFP), it is not possible to measure the pol IV concentration. (B) Plots of mean cell intensity and colocalisation between pol IV (DinB-YPet/DinB-eYFP) foci and replisome (DnaX-mKate2) foci. The mean cell intensity (grey shaded area) is a convoluted measure of the combined DinB-YPet and DinB-eYFP concentrations in cells. Colocalisation was measured in two ways: the proportion of pol IV foci that contain a colocalised replisome focus (black line), and the proportion of replisome foci that contain a colocalised pol IV focus (orange line). Data were compiled from ten technical replicates. The total number of cells analysed were not determined in these measurements. We conservatively estimate that >500 cells were used in each measurement. The analysis includes a total of 27651 DnaX-mKate2 foci and 31978 DinB-YPet/DinB-eYFP foci.

Importantly, we found that the *dinB-eYFP* plasmid is toxic to cells during the late SOS response. We observed that 17% of cells carrying the *dinB-eYFP* plasmid lysed upon ciprofloxacin treatment (**Supplementary Figure 7**). In comparison, <3% of wild-type MG1655 or EAW643 cells lysed during the measurements. We also noted that cells containing the DinB-eYFP plasmid elongated at a much slower rate than the either EAW643 lacking the plasmid or wild-type cells. These observations suggest that in the presence of the *dinB-eYFP* plasmid, pol IV reaches concentrations high enough above wild-type levels that it begins to interfere with cell growth.

We next examined pol IV behaviour in *lexA*(Def) cells. This background contains a mutation that inactivates the LexA repressor protein, causing cells to constitutively express high levels of all proteins within the SOS regulon, including pol IV (23,57,58). To prevent cell death from constitutive SOS-driven filamentation, we also introduced a *sulA*$^{-}$ mutation. The *lexA*(Def) background allowed us to investigate if high concentrations of pol IV allow it to bind to DNA in the absence of DNA damage. In the *lexA*(Def) background, we calculate the concentration of pol IV to be 96.5 ± 7.29 nM (STD 53.54 nM, n = 54 cells), 15.6 times higher than undamaged wild-type cells, and 2.8 times higher than wild-type cells treated with ciprofloxacin for 2h. The elevated concentrations of DinB-YPet in the *lexA*(Def) background created a high background of diffuse fluorescence signal, making it difficult to observe pol IV foci directly (**Fig 6A**). Instead, we recorded fluorescence movies at high time resolution as DinB-YPet photobleached. Once ~50% of the DinB-YPet had bleached, it was possible to observe foci. These foci, however, were extremely transient, rarely persisting beyond a single 34 ms frame, indicative of only short-lived events on the DNA. It appeared that very few of these transient foci colocalised with replisomes. To examine this more closely, we analysed time-dependent fluctuations in DinB-YPet signals at replisomes, and away from replisomes, and compared signals from undamaged *lexA*(Def) cells against signals from wild-type cells treated with ciprofloxacin (**Fig 6B; Supplementary figures 8-9**). The trajectories indicate some transient binding of DinB-YPet at replisomes in the *lexA*(Def) strain, however these trajectories appear comparable to those for regions-of-interest placed outside of replisomes. In comparison, replisome trajectories in the ciprofloxacin-treated wild-type cells often indicated pol IV binding events lasting >1s before dissociation or photobleaching occurs. These observations clearly indicate that even the highest concentrations of pol IV that could naturally occur in cells at the height of the SOS response are not enough to allow pol IV to enter replisomes and productively synthesise DNA. Pol IV either requires DNA damage, or additional factors that accumulate in response to damage, to be recruited to DNA.

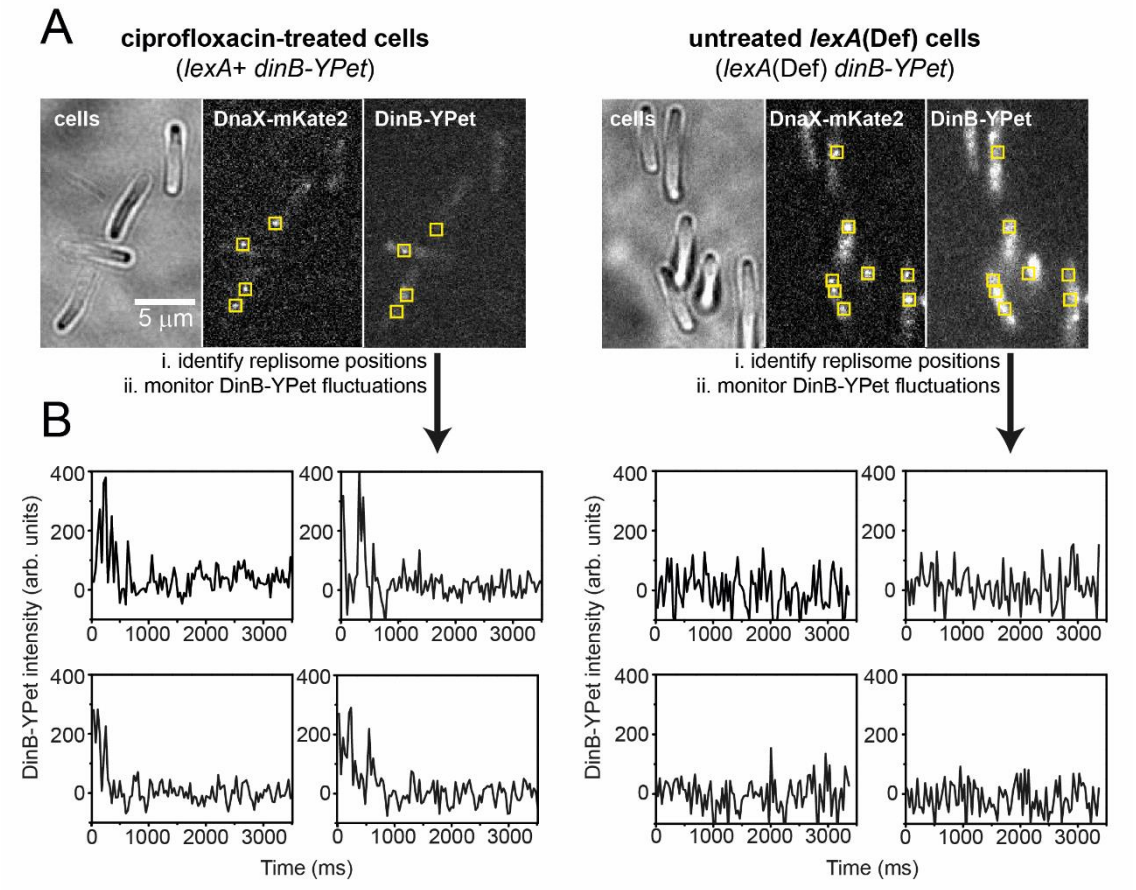

Figure 6. Comparison of DinB-YPet behaviour in untreated, *lexA*(Def) cells and ciprofloxacin-treated *lexA*$^+$ cells. (A) Representative images of ciprofloxacin-treated *lexA*$^+$ cells (left) and untreated *lexA*(Def) cells (right). (B) Representative intensity vs time trajectories for DinB-YPet signals in the vicinity of replisomes. Additional, randomly selected trajectories appear in **Supplementary figure 7** (ciprofloxacin-treated *lexA*$^+$ cells) and **Supplementary figure 8** (untreated *lexA*(Def) cells). 5×5 pixel regions of interest were placed at replisome foci, then used to monitor fluctuations in DinB-YPet signals (see panel A). In ciprofloxacin-treated *lexA*$^+$ cells, DinB-YPet signals are elevated in the vicinity of replisomes for multiple frames, indicating long-lived binding events. In untreated *lexA*(Def) cells no events are visible in which the DinB-YPet is elevated in the vicinity of replisomes for more than a single 34 ms frame, indicating no long-lived binding events.

2.4 Discussion

2.4.1 Non-replisomal activities of pol IV

We observed that only 5–10% of pol IV foci tightly colocalise with replisome markers. Assuming that these foci indicate sites of pol IV binding (short- and long-lived binding events) to the DNA, this observation implies that the vast majority of pol IV molecules could work on other, as yet unidentified substrates. What other DNA structures might pol IV work at? Do the mutagenic and non-mutagenic lesion-bypass activities of pol IV relate to its action at replisomes, as is often assumed, or do they relate to activities at other DNA structures? Pol IV has been previously found to be involved in a range of different pathways, including rescue of stalled transcription complexes (38), double-strand break repair (30,59), adaptive mutation (46,60) and stationary phase fitness (8). It is possible that the non-

replisomal DinB-YPet foci that we observe represent pol IVs participation in these pathways. Determining how pol IV activity is distributed amongst these various pathways is far beyond the scope of this study. It is clear, however, that two-colour fluorescence imaging has a large part to play in characterising the range of substrates used by pol IV in cells.

2.4.2 Replisome-proximal activities of pol IV: TLS is predominantly postreplicative

The minority of pol IV foci that do form near replisomes show only loose colocalisation: there is a very broad distribution of distances between pol IV foci and replisomes. This result is inconsistent with the notion that pol IV-dependent TLS exclusively takes place at replications forks that have stalled at a damage site on the template DNA (1–7). The results strongly suggest that pol IV is capable of carrying out post-replicative TLS within gaps behind the fork. The results do not indicate, however, whether pol IV acts purely in a post-replicative sense, or whether both replicative and post-replicative TLS are possible. Although the DinB-YPet fusion behaves like wild-type pol IV in the NQO-survival and ciprofloxacin resistance assays, we cannot formally rule out the possibility that the addition of YPet to pol IV somehow alters the balance between TLS at replication forks vs TLS within gaps.

There is a well-established, and growing, body of literature that points to replisomal lesion skipping as a major mechanism of DNA damage tolerance in bacteria (54–56; 61–68). The idea that pol IV participates in post-replicative TLS is consistent with the lesion-skipping scenario, as proposed previously (69–72). Rather than replisomes stalling when they encounter lesions, they simply re-prime the template and continue synthesis downstream of the lesion. In its wake, the replisome leaves a lesion-containing single stranded DNA gap. Such gaps could not be repaired by pathways that work on double stranded DNA, such as nucleotide excision repair, and would instead be initially bypassed, either by TLS, or by *recFOR*-mediated daughter strand gap repair. Based on a lack of colocalisation with replisome markers, we have previously hypothesised that another TLS polymerase, pol V, also carries out post-replicative TLS in single stranded DNA gaps (47). It would of considerable interest to determine if the third TLS polymerase in *E. coli*, pol II, also shows loose colocalisation with replisomes in cells carrying DNA damage.

2.4.3 Pol IV does not access replisomes through mass action-driven exchange with pol III HE

A conventional view has been that pol IV gains access to replisomes upon SOS induction because it is produced at higher concentrations, allowing it to better compete with pol III HE for binding to replication forks (1–7,54). Observations made during the current study are inconsistent with this simple mass action-driven mechanism.

The most direct evidence comes from the analysis of SOS-constitutive *lexA*(Def) cells (**Fig 6**). Introduction of the *lexA*(Def) mutation increased the concentration of DinB-YPet to nearly 100 nM; more than 15-times higher than the concentration present in undamaged *lexA*$^{+}$ cells. Despite this increase in concentration, there were almost no pol IV foci visible in the *lexA*(Def) cells. This indicates that pol IV concentrations up to 100 nM are insufficient for pol IV to enter the replisome, or for that matter, any other

binding site on the DNA. In contrast, pol IV is able to access the DNA in cells treated with DNA damaging agents, even when the pol IV concentration was significantly below 100 nM. Thus, it appears that DNA damage is required for pol IV to access the DNA, at least within the concentration regimes expected to occur in wild-type cells. Interestingly, the pol IV concentration did affect the number of pol IV molecules that bound to each binding site on the DNA. Expression of DinB-eYFP from a low-copy plasmid increased the concentration of labelled pol IV up to 14-fold relative to when DinB-YPet was expressed from the chromosome. This induced only a mild increase in the proportion of pol IV foci that colocalised with replisomes, however the number of molecules present within each focus increased: in the absence of damage there were 1–2 DinB-YPet molecules per focus, increasing to 3–10 molecules per focus when DinB-eYFP was expressed from the plasmid; in the presence of damage there were 3–4 DinB-YPet molecules per focus, increasing to >30 molecules per focus when DinB-eYFP was expressed from the plasmid. Thus, within the bounds of cellular pol IV concentrations, higher pol IV concentrations do not open up new binding sites at replisomes, or any other site on the DNA. High concentrations do, however, allow more pol IV to bind at each binding site.

2.4.4 Pol IV is granted only temporary access to replisome regions

We conclude that pol IV has very limited access to the region close to replisomes, even after the induction of the SOS response. Access to the replisome region, be it direct access to the replisome or access to ssDNA gaps, is restricted to the first 100 minutes after induction of the SOS response (colocalisation drops after this point), and involves only a small subset of the replisomes and pol IV molecules. What factors could temporarily licence pol IV to enter the area of cells close to replication forks?

In eukaryotes, TLS polymerases are licenced to enter replisomes at least in part through ubiquitination of the PCNA sliding clamp (73). To our knowledge, pol IV and replisome components are not altered biochemically during the SOS response. Pol IV is currently thought to access replisomes through a series of physical interactions that it forms with the β-sliding clamp and pol III (74–78). Such interactions could conceivably provide pol IV with access to gaps behind the replisome. These gaps are unlikely to contain pol III HE. There is, however, evidence supporting that three pol III core subunits present at the fork in *E. coli* allow for shorter Okazaki fragment (79). Perhaps pol III cores compete with pol IV for binding to gaps and the previously described interactions between the two facilitate switching in that context.

It is assumed that when the replisome skips a lesion it leaves a β-sliding clamp behind at the gap. The known interactions of pol IV with the β-sliding clamp are likely to be involved during post-replicative TLS by pol IV. It is difficult to imagine, however, how these interactions could be modulated to provide access to gaps during early stages of the SOS response, while excluding pol IV in late stages of the SOS response. One possibility is that the gaps are no longer created during late stages of the SOS response. Another possibility is that a protein (or complex) binds to either pol IV, or the β-sliding clamp during the late SOS response and prevents pol IV from acting at gaps. Alternatively, a protein (or complex) that is active only during the early stages of SOS could help to recruit pol IV to gaps.

2.4.5 SOS progresses through periods of distinct enzyme activities

A new model of the bacterial SOS-response is emerging in which different proteins are put into play during discrete time periods, as depicted in Figure 7. In the current study, we revealed that pol IV is permitted access to the region close to replisomes 30–100 min after ciprofloxacin addition, after which it is excluded from these regions. This behaviour is not limited to ciprofloxacin treatment: we observe a similar series of events following treatment with both MMS and ultraviolet light (**Supplementary figure 10**). Interestingly, the time-point where pol IV is ejected from the replisome region matches well with the timing of a key event in the regulation of another TLS polymerase, pol V (47). We previously discovered that pol V becomes activated for TLS 90–120 min after cells are damaged with ultraviolet light. We found that the pol V subunit, UmuC, is produced ~45 min after irradiation. However, the protein is sequestered at the inner membrane, keeping it away from the DNA. From ~90 min after damage, the other critical component of pol V, $UmuD'_2$, is produced by RecA*-mediated autoproteolysis of $UmuD_2$ (78). As this point, the pol V complex ($UmuD'_2$-UmuC) forms, becomes activated to pol V Mut ($UmuD'_2$-UmuC-RecA-ATP) through interaction with a RecA* nucleoprotein filament, and is released from the membrane to catalyse TLS. This same series of events occurs when treating pol V-labelled cells with ciprofloxacin (**Supplementary figure 11**).

That the ejection of pol IV from the replisome region occurs at ~90–100 min, the same time-point at which pol V is released from the membrane (**Fig 7**), suggests a possible functional link between the two enzymes. In the previous study, we demonstrated that pol V Mut does not act at replisomes, ruling out the possibility that pol IV is excluded from replisome regions because it is out-competed by pol V. Based on far-Western blots and pull-down experiments, it has been previously suggested that pol IV interacts with both $UmuD_2$ and $UmuD'_2$ (78). $UmuD_2$ (and presumably $UmuD'_2$) are produced in excess over UmuC, at concentrations similar to pol IV. It is therefore tempting to speculate that $UmuD_2$, $UmuD'_2$, or both, modulate the access of pol IV to replisome regions. This hypothesis will be tested further in future work. Put together, the results of our previous and current studies suggest that the SOS response progresses through (at least) three stages: an early period (0–30 min) of predominantly error-free repair; a middle period (30–90 min) that includes pol IV-catalysed TLS at gaps behind the replication fork; and finally, a mutagenic period (>90 min) in which pol V Mut is active.

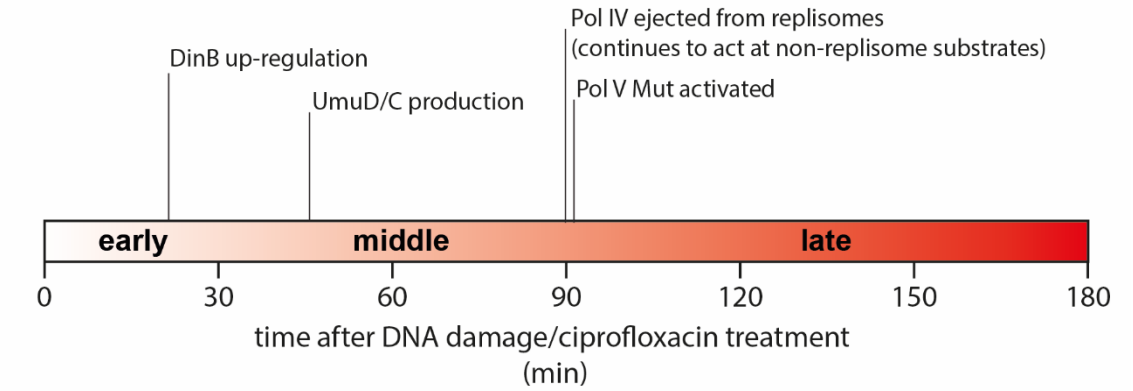

Figure 7. Timeline of translesion DNA synthesis based on single-molecule imaging studies. Pol IV is expressed relatively early after DNA damage is incurred and is allowed access to replisomes until cells abruptly transition into the late stage. At this transition, pol IV is ejected from replisomes and a second TLS polymerase, pol V Mut becomes activated. Pol IV continues to act on non-replisome substrates. The timescale indicated for these transitions is likely to be specific to our growth conditions (EZ glucose medium; APTES-treated flow cell; 37°C). We anticipate that under different conditions the same transitions would be observed, but at different time-points.

2.5 Experimental procedures

2.5.1 Cell constructs and plasmids

EAW633 is *E. coli* K-12 MG1655 *dinB-YPet* (80). It was made by λ_{RED} recombination (81), replacing the wild-type *dinB* gene with *dinB-YPet* and a mutant FRT-Kanamycin resistance-wt FRT cassette. Positive colonies were selected for kanamycin resistance. The fusion gene *dinB-YPet* encodes pol IV, a C-terminal twenty amino acid spacer (as used in (29)), followed by YPet.

EAW641 and EAW643 are two-colour strains derived from EAW633. The kanamycin resistance marker in EAW633 was removed via FLP-FRT recombination using the plasmid pLH29 (81). To construct EAW643, λ_{RED} recombination was used to replace the *dnaX* gene of EAW633 with *dnaX-mKate2* and a mutant FRT-Kanamycin resistance-wt FRT cassette. Colonies were selected for kanamycin resistance. The *dnaX-mKate2* fusion encodes the τ-subunit of pol III HE, a C-terminal 11 amino acid linker followed by mKate2. EAW641 was constructed in a similar manner, replacing the *dnaQ* gene in EAW633 with a *dnaQ-mKate2* fusion.

To increase the intracellular concentration of labelled pol IV, we used the plasmid pPFB1188, which expresses DinB-eYFP (pol IV labelled at its C-terminus with eYFP, through a twenty amino-acid linker; (30)). To generate EAW643 pPFB1188 cells, we transformed EAW643 cells with pPFB1188, selecting for ampicillin resistance. Cells carrying a replisome marker, but lacking *dinB* were used in control measurements. SSH001 is *E. coli* MG1655 *dnaQ-mKate2 lexA*$^+$ *dinB*::kan^R. It was made by transferring *dinB*::kan^R by P1 transduction from SF2006 (8) into EAW192 (48). SSH001 pPFB1188 was generated by transforming SSH001 cells with pPFB1188 (30).

RW1594 is *E. coli* MG1655 *dinB-YPet dnaX-mKate2 lexA*(Def) *sulA*::kan^R. It was made in two steps: first the wild-type *sulA*+ gene of EAW643 was replaced with *sulA*::kan by P1 transduction from EAW26 (47), to create RW1588; then *lexA51*(Def) *malB*::Tn*9* was transferred from DE406 (82) into RW1588 by P1 transduction, selecting for chloramphenicol resistance. To confirm the presence of the

lexA(Def) genotype, colonies were then screened for high levels of RecA expression by Western blotting with anti-RecA antibodies (83).

Strain	Relevant Genotype	Parent strain	Source/technique
MG1655	*dinB*$^+$ *lexA*$^+$	-	(79)
EAW18	Δ*dinB*	MG1655	Lambda RED recombination
EAW26	*sulA*$^-$ *lexA*(Def)	MG1655	(47)
EAW633	*dinB-YPet lexA*$^+$	MG1655	Lambda RED recombination
EAW830	*dinB*(D103N)-*YPet lexA*$^+$	MG1655	Lambda RED recombination
EAW641	*dinB-YPet dnaQ-mKate2 lexA*$^+$	EAW633	Lambda RED recombination
EAW643	*dinB-YPet dnaX-mKate2 lexA*$^+$	EAW633	Lambda RED recombination
EAW643/pPFB1188	*dinB-YPet dnaX-mKate2 lexA*$^+$ + pPFB1188 (*dinB-eYFP*)	EAW643	Transformation of EAW643 with pPFB1188 (29)
EAW192	*dinB*$^+$ *dnaQ-mKate2 lexA*$^+$	MG1655	(48)
EAW203	*dnaX-YPet dnaQ-mKate2 dinB*$^+$ *lexA*$^+$	JJC5945	(48)
SSH001	Δ*dinB dnaQ-mKate2 lexA*$^+$	EAW192	Transduction of EAW192 with P1 grown on SF2006 (8)
SSH001/pPFB1188	Δ*dinB dnaQ-mKate2 lexA*$^+$ + pPFB1188 (*dinB-eYFP*)	SSH001	Transformation of SSH001 with pPFB1188 (29)
RW1588	*dinB-YPet dnaX-mKate2 sulA*::kan^R	EAW643	Transduction of EAW643 with P1 grown on EAW26
RW1594	*dinB-YPet dnaX-mKate2 sulA*::kan^R *lexA*(Def) Cm^R	RW1588	Transduction of RW1588 with P1 grown on DE406
EAW282	*dnaX-YPet umuC-mKate2 lexA*$^+$	JJC5945	(47)
CC108	*dinB*$^+$; F' plasmid *dinB*$^+$	-	(24)
FC1243	Δ*dinB*; F' plasmid Δ*dinB*	CC108	(24)
YG2247	*dinB*$^+$; F' plasmid Δ*dinB*	CC108	(24)

Table 1. Strains used in this study.

2.5.2 Western blotting for DinB expression levels

Cell cultures were grown in Luria-Bertani media at 37°C. The following morning, they were diluted 1:100 in fresh media until they reached exponential phase (OD_{600} ~0.5). Where noted, cultures were treated with 30ng/mL ciprofloxacin for 2 hours prior to harvesting. After cells were harvested by centrifugation, the cell pellet was resuspended in NuPage LDS sample buffer (Novex) and freeze-thawed

to produce whole cell extracts. Dilutions of purified pol IV protein were made in FC1243 (Δ*dinB*) whole cell extracts. Aliquots of whole cell extracts, representing approximately 1.5×10^8 cells, or DinB dilutions (containing 0.5 – 8 ng of purified DinB (42)), were electrophoresed in NuPage 4-12% Bis-Tris gels (Novex). Proteins were transferred to an Invitrolon PVDF membrane (Novex) which was probed with a 1:5000 dilution of purified rabbit anti-DinB antibodies (a kind gift from Patricia Foster (30)) and subsequently probed with a 1:5000 dilution of Goat Anti-Rabbit IgG (H+L)-AP Conjugate (BioRad). Using the CDP-Star chemiluminescent assay (Applied Biosystems), the DinB proteins were visualized on Carestream Biomax XAR film after various exposure times.

2.5.3 4-nitroquinolone-1-oxide survival assay

Cells (MG1655, EAW18, and EAW633) were grown in LB overnight at 37ºC. The next day, a 1/1000 dilution of each culture was grown to mid log phase (OD_{600} = 0.2), then stored on ice. These cultures were then serially diluted by factors of ten down to 10^{-5}. A spot (5 μL) of the OD 0.2 culture and each dilution was plated on an agar plate containing 8 μM NQO. The plate was incubated at 37ºC for 18h.

2.5.4 Ciprofloxacin resistance assay

The assay was carried out as described in reference (9). Cells (MG1655, EAW18, EAW633, EAW643) were grown in LB at 37ºC for 25h. For each culture, a 10^{-6} dilution was prepared. 150 μL of diluted cells were plated on a LB agar plate and incubated overnight at 37ºC to count for viable cells. The mutagenesis assay was performed by plating 150 μL of each saturated overnight culture (corresponding to approximately 10^8 cells) on an LB agar plate containing 40 ng/mL ciprofloxacin. For each strain 5 plates were prepared and incubated at 37 ºC.

On day one, all colonies of the LB agar plates were counted to determine the number of viable cells that were originally present in each overnight culture. On day 4, colonies on the ciprofloxacin containing plates were counted. These were interpreted as pre-existing mutations (9). Colonies were counted again on day 8 and 13 and interpreted as resistant colonies formed as a result of mutagenesis induced by ciprofloxacin. The numbers of new colonies appearing between days 4–8 and 8–13 were calculated and normalised against the number of viable cells in each culture. The number of viable cells as a function of time was determined using the count taken at day 1 and loss-of-viability rates measured previously (9).

2.5.5 Fluorescence microscopy

Wide-field fluorescence imaging was performed on an inverted microscope (IX-81, Olympus with a 1.49 NA 100x objective) in an epifluorescence configuration, as described previously (47). Continuous excitation is provided using semidiode lasers (Sapphire LP, Coherent) of the wavelength 514 nm (150 mW max. output) and 568 nm (200 mW max. output). DnaX-mKate2 and DnaQ-mKate2 were imaged using yellow excitation light (λ = 568 nm) at high intensity (2750 Wcm^{-2}), collecting emitted light between 610–680 nm (ET 645/75m filter, Chroma) on a 512 × 512 pixel EM-CCD camera (C9100-13, Hamamatsu). For DinB-YPet and DinB-eYFP imaging, we used green excitation (λ = 514 nm) at lower

power (160 Wcm^{-2}) for DinB-YPet strains (EAW641 and EAW 643) and 60 Wcm^{-2} for the DinB-YPet+DinB-eYFP strain EAW643 pPFB1188, collecting light emitted between 525–555 nm (ET540/30m filter, Chroma).

Rapid acquisitions (movies of 300 × 34 ms frames, continuous excitation with 514 nm light) were collected to characterise the motions of DinB-YPet and DinBD103N-YPet molecules, and to determine the number of DinB-YPet molecules per cell. Time-lapse movies were recorded to visualise changes in DinB-YPet expression and measure colocalisation with replisome markers. For EAW641 and EAW643 cells, sets of three images were recorded (bright-field [34 ms exposure], YPet fluorescence [50 ms exposure]; mKate2 fluorescence [100 ms exposure]) at an interval of 5 min for 3h. All images were analysed with ImageJ (65).

2.5.6 Flow cell designs

All imaging was carried out on cultures growing in home-built flow cells. Most imaging was carried out in quartz-based flow cells, similar to those used in our previous study (47). These flow cells were assembled from a no. 1.5 coverslip (Marienfeld, REF 0102222), a quartz top piece (45x20x1 mm) and PE-60 tubing (Instech Laboratories, Inc.). Prior to flow-cell assembly, coverslips were silanized with aminopropyltriethoxy silane (Sigma Aldrich, Alfa Aeser). First, coverslips were sonicated for 30 min in a 5M KOH solution to clean and activate the surface. The cleaned coverslips were rinsed thoroughly with MilliQ water, then treated with a 5% (v/v) solution of amino-propyl-triethoxysilane in MilliQ water. The coverslips were subsequently rinsed with ethanol and sonicated in ethanol for 20 seconds. Afterwards, the coverslips were rinsed with MilliQ water and dried in a jet of N_2. Silanised slides were stored under vacuum prior to use.

To assemble each flow cell, polyethylene tubing (BTPE-60, Instech Laboratories, Inc.) was glued (BONDiT B-482, Reltek LLC) into two holes that were drilled into a quartz piece. After the glue solidified overnight, double-sided adhesive tape was stuck on two opposite sides of the quartz piece to create a channel. Then, the quartz piece was stuck to an APTES-treated coverslip. The edges were sealed with epoxy glue (5 Minute Epoxy, DEVCON home). Each flow cell was stored in a desiccator under mild vacuum while the glue dried. Typical channel dimensions were 45 mm × 5 mm × 0.1 mm (length × width × height).

Data shown in **Figures 2–3** were collected in a three-channel PDMS-based flow cell. A commercial PDMS kit (Dow Corning, SYLGARD 184 silicone elastomer kit) was used to obtain a 10:1 (polymer:curing agent) mixture. The mixed resin was poured in an aluminium mold that has three ridges, creating PDMS blocks with channel dimensions (0.1 mm, 0.5 mm and 1.9 mm). After pouring, the polymer was allowed to solidify at 65°C overnight. The next day, 1 mm holes were punched in the PDMS block for the in- and outlet tubing. Then, the PDMS block was covalently attached to a clean glass coverslip (KOH treated as above) by plasma treatment. After plasma bonding, PE60 tubing was pushed into each hole. As a final step, the flow cell surface was silanised by pulling 5% (v/v in water) amino propyl triethoxy silane solution through the channel with a syringe. The silanization reaction was allowed to proceed for 15 min before the channels were flushed with MilliQ water.

2.5.7 Imaging in flow cells

For all imaging experiments, cells were grown at 37°C in EZ rich defined medium (Teknova) that contained 0.2% (w/v) glucose. EAW633, EAW641 and EAW643 cells were grown in the presence of kanamycin (25 μg/mL), EAW643 pPFB1188 was grown in the presence of ampicillin (100 μg/mL) and RW1594 was grown in the presence of chloramphenicol (25 μg/mL). Cells were loaded into flow cells, allowed a few minutes to associate with the APTES surface, then loosely associated cells were removed by pulling through fresh medium. The experiment was then initiated by either changing the input solution to medium containing 30 ng/mL ciprofloxacin or 0.2 ng/ml MMS, or by irradiating cells *in situ* with 254 nm UV light from a mercury lamp (UVP) at a fluence of 30 $J.m^{-2}$. In each case, medium was pulled through the flow cell throughout the measurement using a syringe pump, at a rate of 50 μL/min.

2.5.8 Analysis of pol IV upregulation

We selected regions of images occupied by cells to obtain information about pol IV upregulation upon ciprofloxacin treatment (>200 cells; all 5 min frames during the 3h experiment). MicrobeTracker 0.937 (84), a MATLAB script, was used to create cell outlines as regions of interest (ROI). We manually curated cell outlines designated by MicrobeTracker to ensure accuracy and to ensure that only non-overlapping, in-focus cells were selected for analysis. These ROI were imported in ImageJ 1.50i (85). The cell outlines were then used to measure mean cell intensities, cell lengths and the number of foci per cell. Parameters describing foci (number, positions and intensities) were obtained using a Peak Fitter plug-in, described previously (47).

2.5.9 Analysis of colocalisation events of pol IV with replisomes

Foci were classed as colocalised if their centroid positions (determined using our peak fitter tool) fell within 2 px (200 nm) of each other. We determined that for DinB-YPet–DnaX-mKate2 localisation the background of pol IV foci expected to colocalise with replisomes purely by chance is ~4%. This was calculated by taking the area of each cell occupied by replisome foci (including the colocalisation search radius) and dividing by the total area of the cell. The value of 4% corresponds to the mean of measurements made over >300 cells. As the number of pol IV foci changes in time, the proportion of replisome foci expected to colocalise with pol IV foci by chance also changes in time. At the beginning of the measurement, there are almost zero pol IV foci, thus there is close to zero chance that a replisome focus will colocalise with a pol IV focus. At t = 30 min, chance colocalisation is expected to be 5% and at t = 120 min, the chance for co-localisation 3%.

2.5.10 Analysis of pol IV copy numbers per cell

The number of pol IV molecules per cell and thus the intracellular concentration is extracted from the change in integrated intensity under each cell outline during rapid acquisition photobleaching measurements, as described previously (47). The intensity decay for each cell includes contributions not

just from YPet bleaching, but also from cellular auto-fluorescence and background signals from the flow cell surface. To obtain a background-free measure of the YPet photobleaching rate, we measured the number of foci detected over hundreds of cells during bleaching. The number of foci over time followed a single exponential decay with τ = 6 s. Returning to the integrated cell intensity decays, we found that signals followed a two-exponential decay, with τ_1 = 6 s and $\tau_2 \approx$ 60 s. Wild-type cells, expressing no YPet, gave single-exponential decays with $\tau \approx$ 60 s, indicating that the τ = 6 s decay seen for YPet-expressing cells arises purely due to YPet bleaching. It was therefore possible to easily extract the YPet intensity from the slower decaying auto-fluorescence and background by fitting with a two-exponential function.

First, the images were corrected for the electronic offset and flattened to correct for inhomogeneity of the excitation beam. We then fit the cellular intensity decay with a two exponential function f(x), fixing τ_1 to 6 s^1:

$$f(x) = A_1 \cdot \exp(-x/\tau_1) + A_2 \cdot \exp(-x/\tau_2).$$

For each cell, the amplitude A_1 is an accurate measure of the mean YPet signal per pixel. Multiplying by the cell area gives the integrated YPet intensity, which was used to determine the number of YPet molecules per cell.

The mean intensity of individual YPet molecules was determined by analysing single-molecule return events (see **Supplementary figure 1**). For each cell, the number of DinB-YPet molecules was then calculated by dividing the integrated YPet intensity, measured by two-exponential fitting of cell-area decays, by the mean single-molecule intensity. The concentration was calculated using the volume of each cell, determined during cell outline assignation in MicrobeTracker.

2.6 Supporting information legends

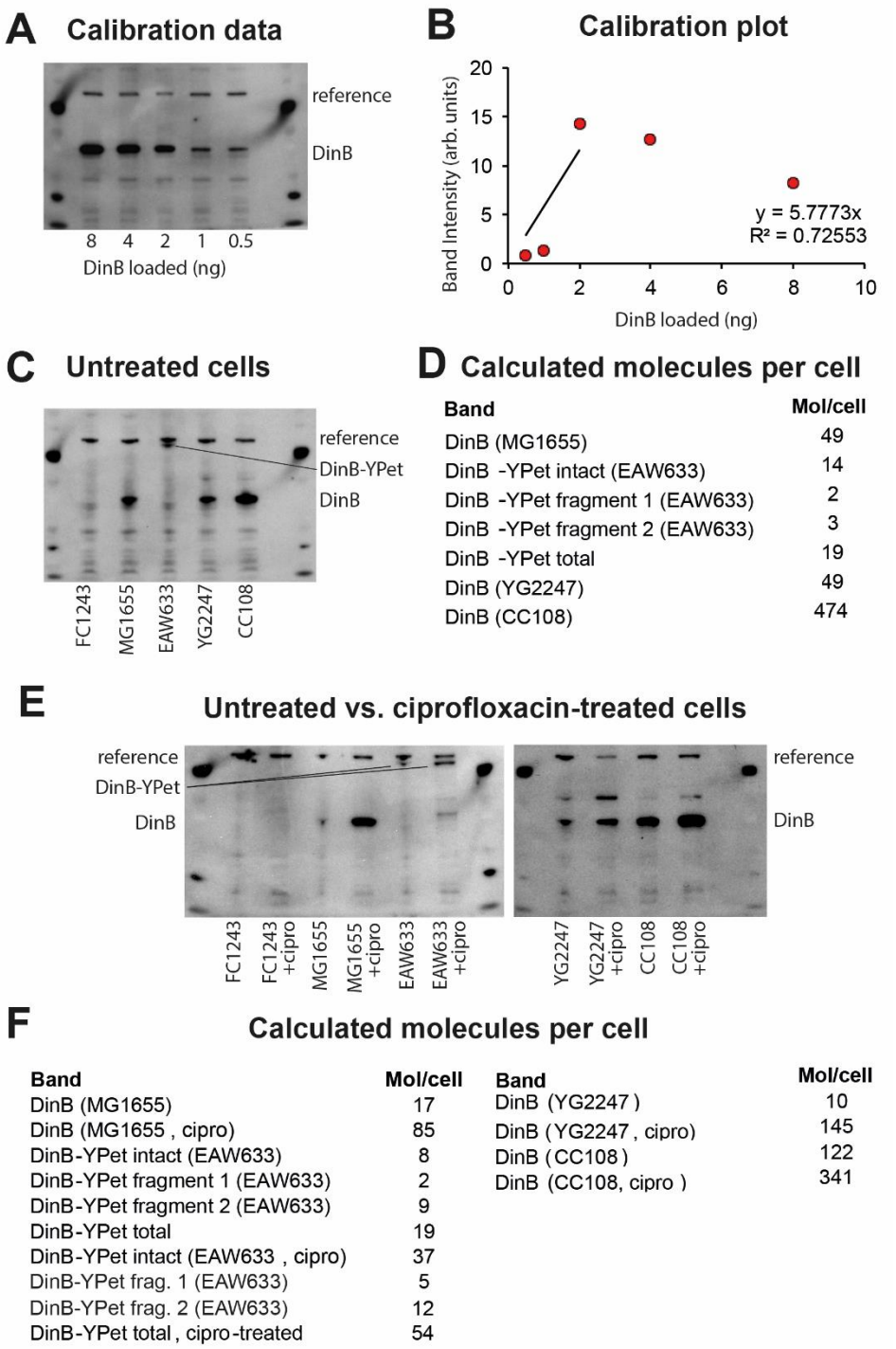

Supplementary Figure 1. Measurement of DinB and DinB-YPet molecules per cell in different backgrounds. Western blots were developed using anti-DinB antibodies. In addition to DinB-specific bands, a series of bands for cross-reacting species were observed. The slowest migrating of these was used as an internal reference for the amount of cell extract loaded in each lane. (A) Calibration for DinB loading. Lanes: i) molecular weight marker, ii) 8 ng DinB, iii) 4 ng DinB, iv) 2 ng DinB, v) 1 ng DinB, vi) 0.5 ng DinB, vii) molecular weight marker. (B) Corresponding calibration plot: band intensity is plotted against loaded DinB (ng). Lanes with 0.5 ng, 1 ng and 2 ng DinB were included in calibration plot, 4 ng and 8 ng were excluded due to saturation. The intensities plotted for each band are the integrated intensity of the DinB band divided by the integrated intensity of the reference band. Amounts

of DinB present in cell extracts (C–F) were calculated from a line of best fit (y = 5.7773x; R^2 = 0.72553). (C) Western blot of extracts from untreated cells. Lanes: i) molecular weight marker, ii) FC1243 (*ΔdinB*), iii) MG1655 (*dinB*$^+$), iv) EAW633 (*dinB-YPet*), v) YG2247 (*dinB*$^+$; F' plasmid - *ΔdinB*), vi) CC108 (*dinB*$^+$; F' plasmid - *dinB*$^+$), vii) molecular weight marker. Bands corresponding to full length DinB-YPet are clearly visible in lane iv. A small amount of two DinB-containing fragments are also visible. Fragment 1 corresponds to DinB+linker. Fragment 2 corresponds to DinB +/- one or two residues. (D) Calculated molecules per cell for untreated cells (Western blot, panel C). Total DinB levels in EAW633 (DinB-YPet) cells are similar to wild-type DinB levels, although ~25% is proteolysed within the cells. YG2247 have DinB at equivalent levels to MG1655, whereas, CC108 have tenfold higher levels than MG1655. This is due to the fact that CC108 cells contain the F' plasmid, which provides a second copy of *dinB*. Levels in CC108 may be somewhat underestimated due to saturation of DinB bands. (E) Two Western blots of extracts from cells. Lanes from left Western blot: i) molecular weight marker, ii) FC1243 (*ΔdinB*) untreated, iii) FC1243 (*ΔdinB*) ciprofloxacin-treated, iv) MG1655 (*dinB*$^+$) untreated, v) MG1655 (*dinB*$^+$) ciprofloxacin-treated, vi) EAW633 (*dinB-YPet*) untreated, vii) EAW633 (*dinB-YPet*) ciprofloxacin-treated, viii) molecular weight marker. Bands corresponding to full length DinB-YPet are clearly visible in lane vi-vii. A small amount of two DinB-containing fragments are also visible. Lanes from right Western blot: i) molecular weight marker, ii) YG2247 (*dinB*$^+$) untreated, iii) YG2247 (*dinB*$^+$; F' plasmid - *ΔdinB*) ciprofloxacin-treated, iv) CC108 (*dinB*$^+$; F' plasmid - *dinB*$^+$) untreated, v) CC108 (*dinB*$^+$) ciprofloxacin-treated, vi) molecular weight marker. (F) Calculated molecules per cell for untreated and ciprofloxacin-treated cells (two Western blots, panel E). In untreated cells, DinB-YPet is expressed at levels equivalent to wild-type DinB, however ~58% is proteolysed within the cells. In comparison to MG1655, YG2247 expresses similar levels of DinB, whereas, CC108 have tenfold higher expression levels. The band for CC108 is saturated, however, and thus likely to be underestimated. In ciprofloxacin-treated EAW633 (DinB-YPet) cells, levels are similar to wild-type DinB levels, however ~31% is proteolysed within the cells. Comparing to MG1655, YG2247 expressed ~1.7 fold more DinB, whereas, CC108 have fourfold higher expression levels. This however might be an underestimate due to the saturated band.

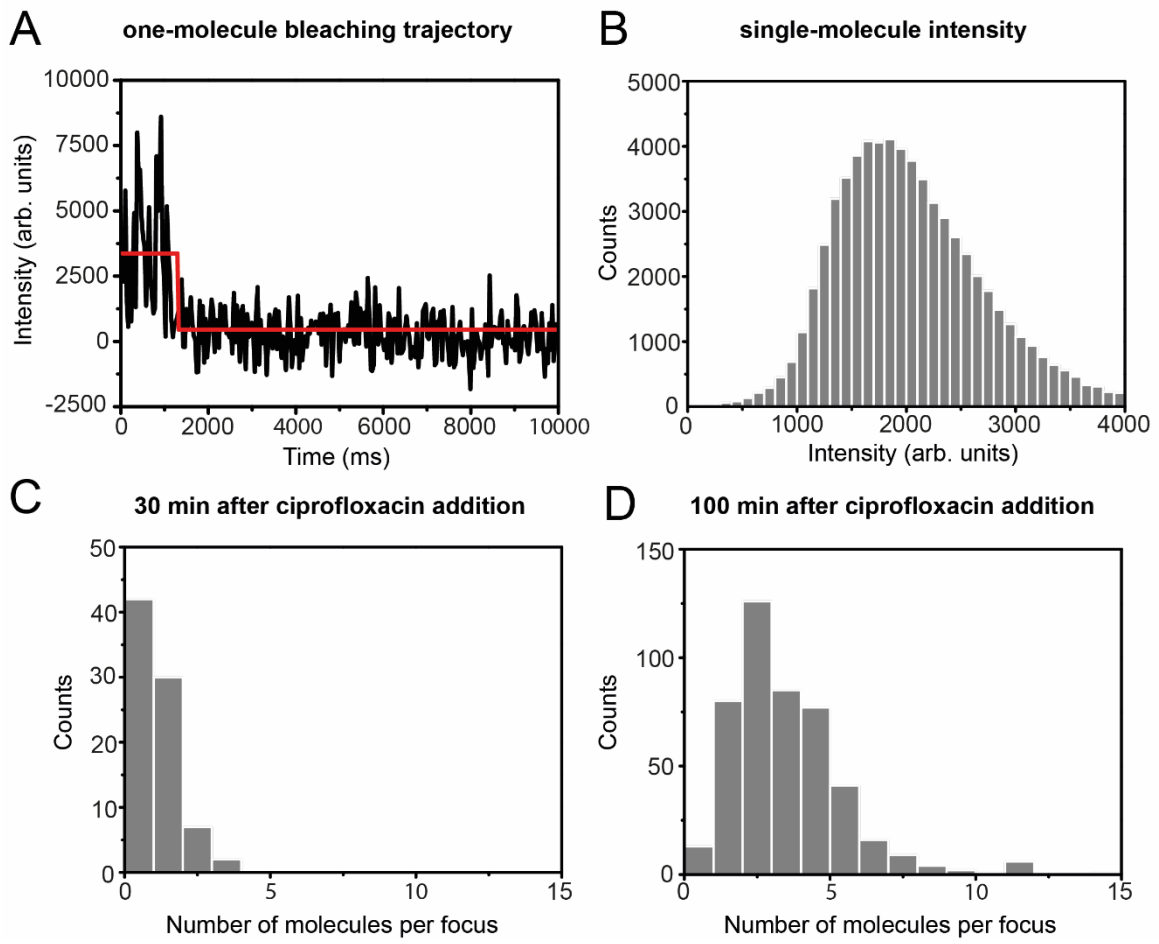

Supplementary Figure 2. Measurement of the number of DinB-YPet molecules per focus by analysis of photobleaching trajctories. (A) Representative photobleaching trajectory showing bleaching of a single DinB-YPet molecule. For each focus, the intensity within a 5 × 5 pixel selection box was monitored as a function of time as foci photobleached. Each measurement was locally background-corrected by subtracting the mean intensity within a 2 pixel-wide ring outside each focus. The red line indicates a fit of intensity levels derived from change-point analysis (47). (B) Histogram of single-molecule intensities. Once the majority of DinB-YPet in cells had photobleached, foci occasionally appeared as individual molecules returned to the bright (fluorescent) state. These foci were fit with 2D Gaussian functions to determine the integrated fluorescence intensities. The measured intensities were narrowly distributed, with a mean value of 1850 arbitrary units. This value represents the mean intensity of a single DinB-YPet molecule. (C–D) Histograms of intensities for DinB-YPet foci, 30 min (C) and 100 min (D) after addition of ciprofloxacin. The initial intensities of foci were determined from photobleaching trajectories using change-point analysis (47). This value was then divided by the single-molecule intensity 1850 to obtain the number of molecules present in each focus.

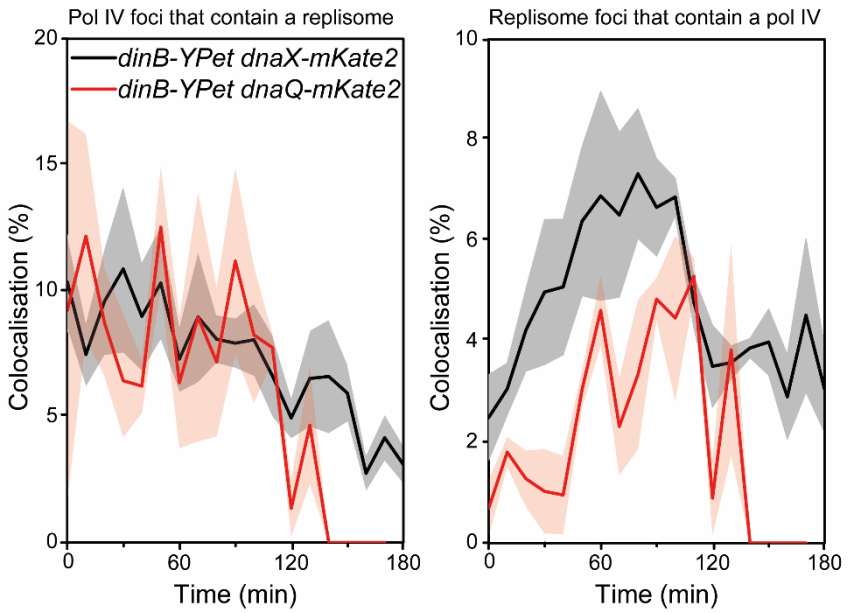

Supplementary Figure 3. Comparison of pol IV-replisome colocalisation in EAW641 and EAW643. Foci located within 200 nm of each other were defined as being colocalised. (A) Graph indicating the proportion of pol IV foci that contain a colocalised replisome focus in EAW641 cells (red line) and EAW643 cells (black line). (B) Graph indicating the proportion of replisome foci that contain a colocalised pol IV focus in EAW641 cells (red line) and EAW643 cells (black line). Shaded areas (A–B) indicate the standard error of the proportion. The total number of cells analysed were not determined in these measurements. We conservatively estimate that >300 cells were used in each measurement. The DnaX-mKate2 dataset includes a total of 17005 DnaX-mKate2 foci and 12408 DinB-YPet foci. The DnaQ-mKate2 dataset includes 7451 DnaQ-mKate2 foci and 3166 DinB-YPet foci.

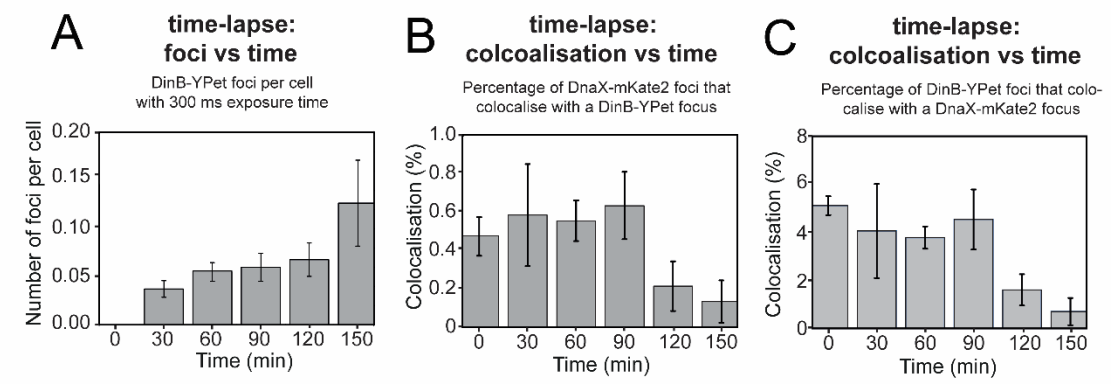

Supplementary Figure 4. Colocalisation measurements for images of EAW643 cells recorded with a longer (300 ms) exposure time. Foci located within 200 nm of each other were defined as being colocalised. (A) Plot of the number of pol IV and replisome foci per EAW643 cell as a function of time. Some cells were lost from the coverslip surface during the measurement. A total of 134 cells remained bound and were analysed over the full course of the measurement. (B) Graph indicating the proportion of replisome foci that contain a colocalised pol IV focus. (C) Graph indicating the proportion of pol IV foci that contain a colocalised replisome focus. Error bars (B–C) indicate the standard error of the proportion. The total number of cells analysed were not determined in these measurements. We conservatively estimate that >300 cells were used in each measurement. The analysis includes a total of 7160 DnaX-mKate2 foci and 1027 DinB-YPet foci.

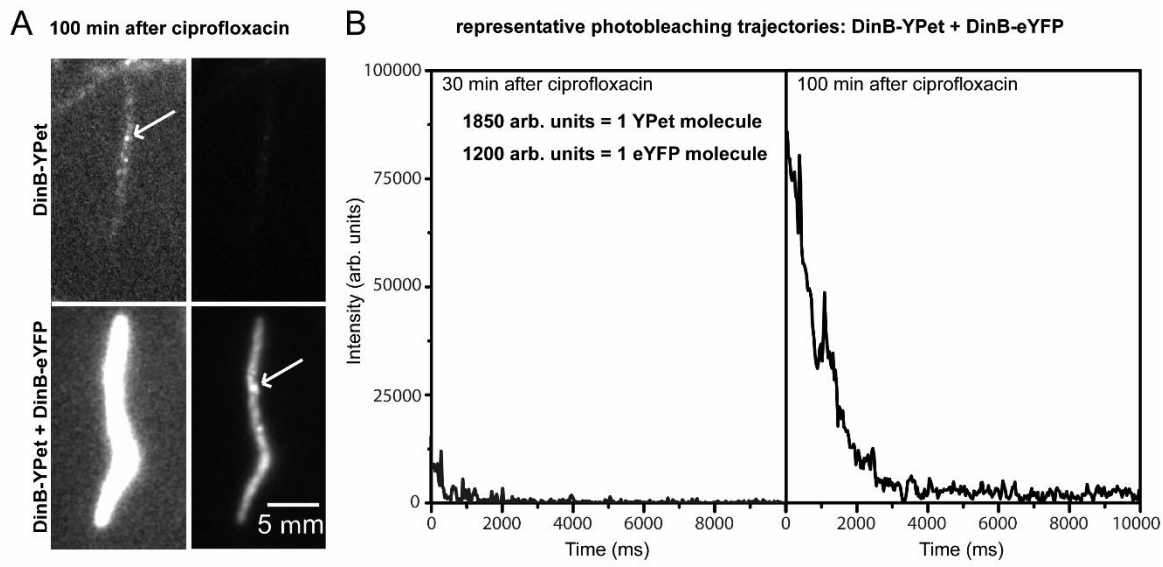

Supplementary Figure 5. Pol IV behaviour in cells expressing both DinB-YPet (from the *dinB* locus on the chromosome) and DinB-eYFP (from the plasmid pPFB1188). (A) Representative microscope images comparing yellow fluorescent protein signals in EAW643 (DinB-YPet only; top row) and EAW643 pPFB1188 (DinB-YPet + DinB-eYFP; bottom row) cells, 100 min after ciprofloxacin addition. The left and right columns contain the same images, but with different intensity ranges displayed. (B) Photobleaching trajectories for DinB foci in EAW643 pPFB1188 (DinB-YPet + DinB-eYFP) cells. Trajectories were measured as illustrated in Supplementary figure 1. Derivation of the intensity of a single YPet molecule (1850 arbitrary units) is shown in Supplementary figure 1B. The intensity of a single eYFP molecule (1200 arbitrary units) was estimated based on the relative extinction coefficients and quantum yields of YPet and eYFP (85).

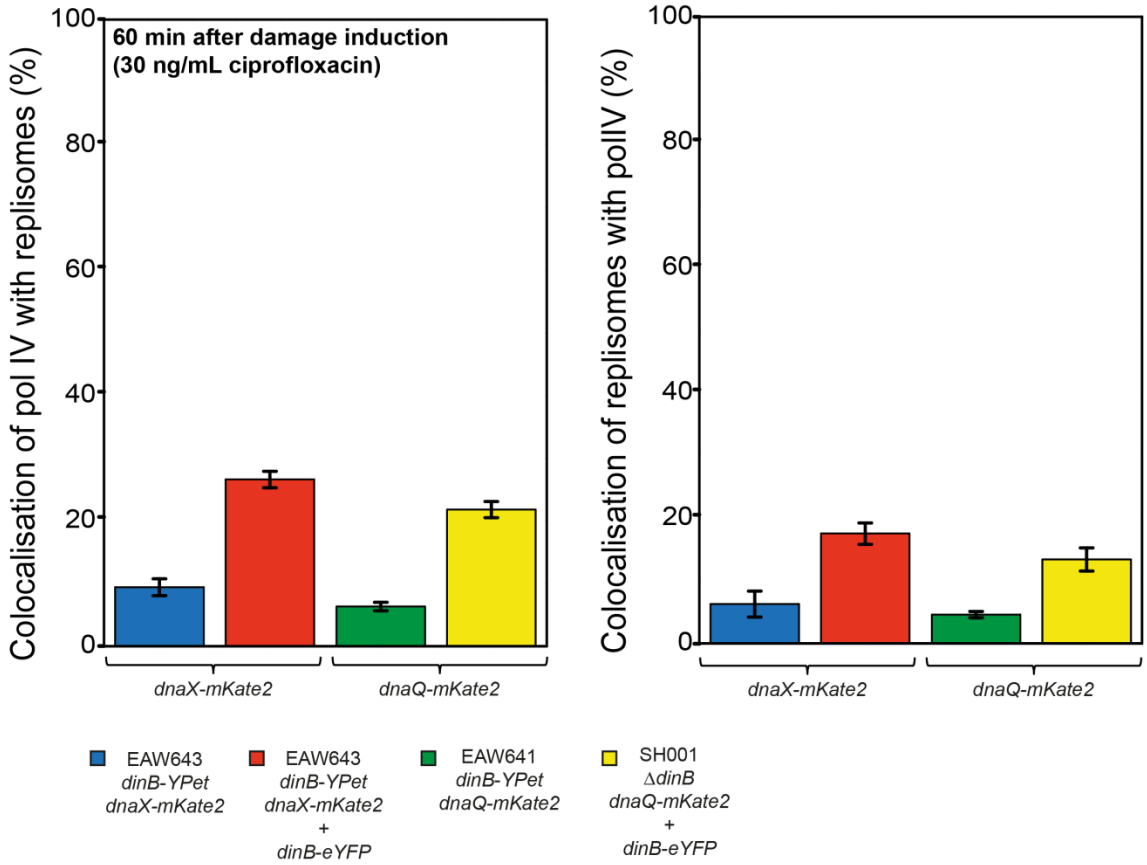

Supplementary Figure 6. Comparison of pol IV-replisome colocalisation in cells expressing labelled pol IV from the chromosome (DinB-YPet), a plasmid (DinB-eYFP), or both. Foci located within 200 nm of each other were defined as being colocalised. Measurements were made on cells treated with 30 ng/ml ciprofloxacin for 60 min in the context of a flow cell. (A) Bar graph indicating the proportion of pol IV foci that contain a colocalised replisome focus. (B) Bar graph indicating the proportion of replisome foci that contain a colocalised pol IV focus. Bar colours (A–B) indicate cell type: EAW643 (blue), EAW643 pPFB1188 (red), EAW641 (green) and SSH001 pPFB1188 (yellow). Error bars indicate the standard error of the proportion. The total number of cells analysed were not determined in these measurements. We conservatively estimate that >300 cells were used in each measurement. The DnaX-mKate2 DinB-YPet dataset includes a total of 1178 DnaX-mKate2 foci and 907 DinB-YPet foci. The DnaX-mKate2 DinB-YPet + DinB-eYFP dataset includes 1165 DnaX-mKate2 foci and 1264 DinB-YPet/DinB-eYFP foci. The DnaQ-mKate2 DinB-YPet dataset includes a total of 739 DnaQ-mKate2 foci and 413 DinB-YPet foci. The DnaQ-mKate2 DinB-YPet + DinB-eYFP dataset includes 386 DnaQ-mKate2 foci and 280 DinB-YPet/DinB-eYFP foci.

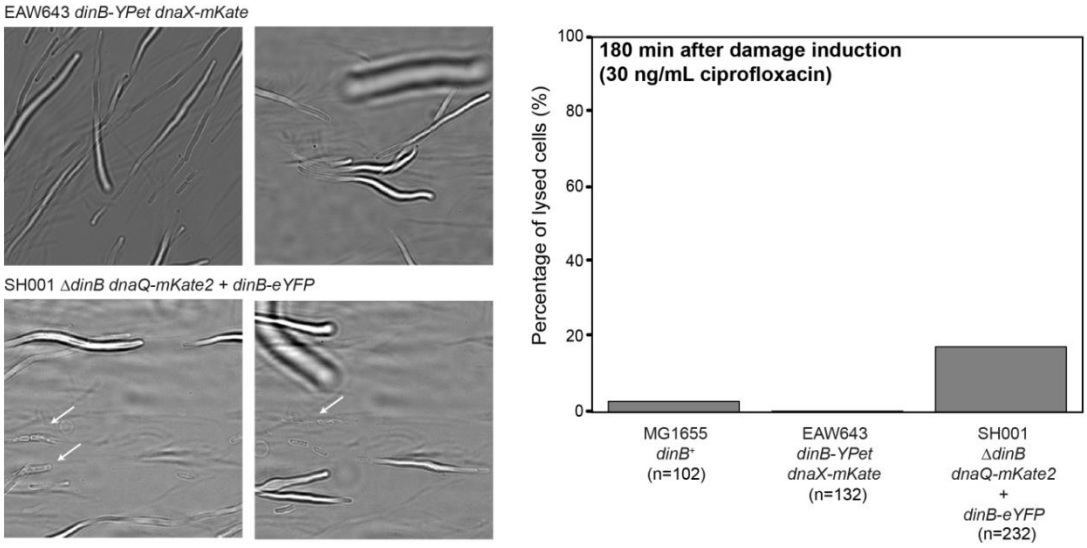

Supplementary Figure 7. Increased rates of lysis in cells expressing DinB-eYFP from pPFB1188. (A) Representative bright-field images of EAW643 cells (top two panels) and SSH001 pPFB1188 cells (bottom two panels), 180 min after the addition of 30 ng/ml ciprofloxacin. Arrows indicate the positions of cells that have lysed. (B) Bar graph showing the percentage of cells that lyse by the 180 min time-point for MG1655, EAW643 and SSH001 pPFB1188 cells. The number of cells that were tracked were as follows: MG1655, 102 cells; EAW643, 132 cells; SSH001 pPFB1188, 232 cells.

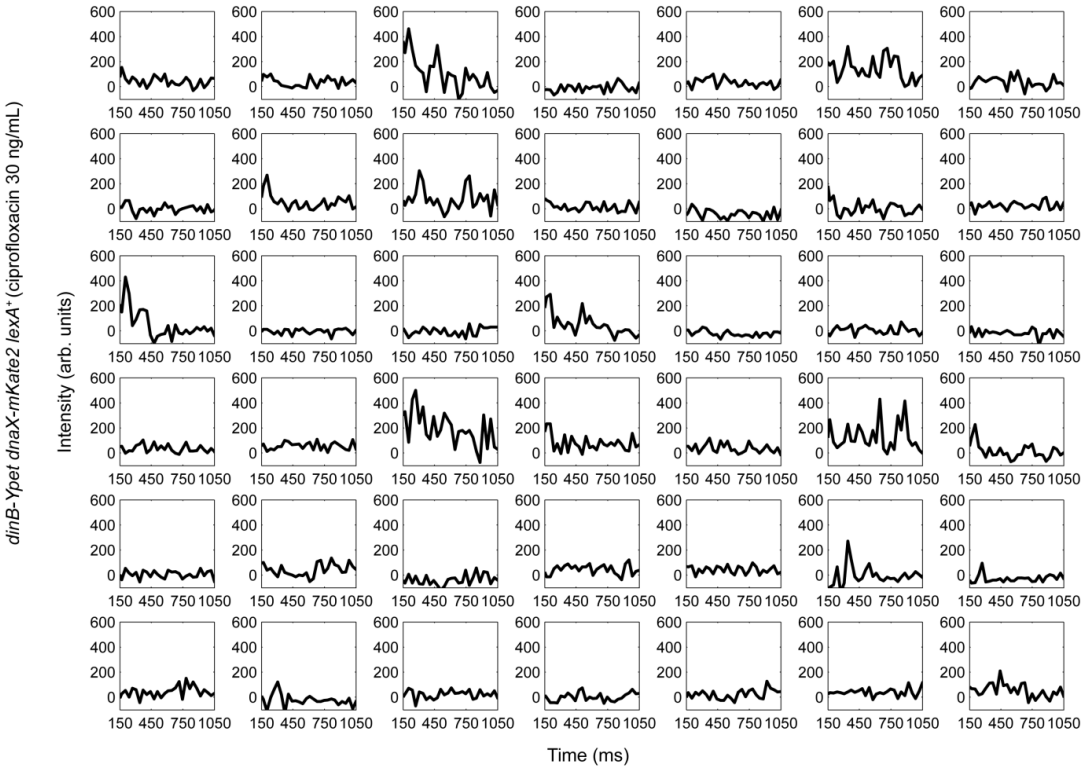

Supplementary Figure 8. Intensity vs time trajectories for DinB-YPet signals in the vicinity of replisomes in ciprofloxacin-treated EAW643 cells. 5×5 pixel regions of interest were placed at replisome foci, then used to monitor fluctuations in DinB-YPet signals (see Fig 6A). A subset of 42 trajectories were selected randomly from a total of 470 trajectories. To allow comparison with DinB-YPet singles in *lexA*(Def) cells, where expression levels are too high to observe single-molecule foci, we present only a portion of each trajectory, starting at a time-point (150 ms) where ~50% of DinB-YPet molecules have already photobleached. In ciprofloxacin-treated EAW643 cells, DinB-YPet signals are frequently elevated in the vicinity of replisomes for multiple frames, indicating long-lived binding events.

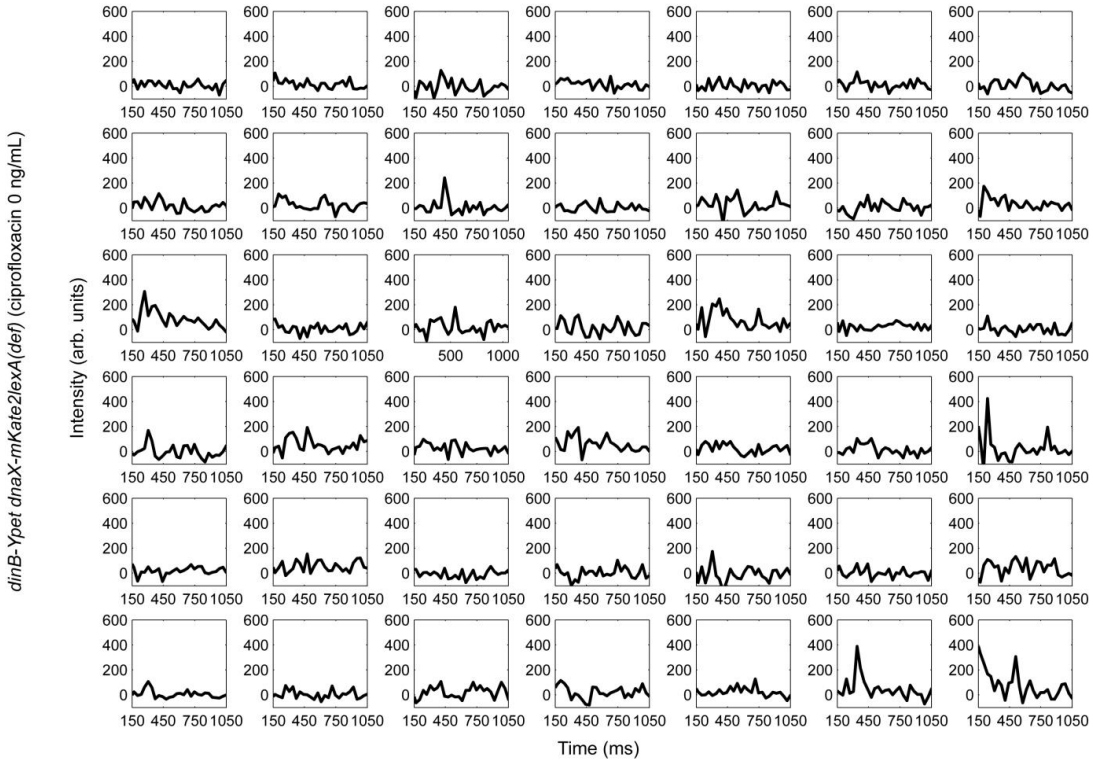

Supplementary Figure 9. Intensity vs time trajectories for DinB-YPet signals in the vicinity of replisomes in untreated *lexA*(Def) cells. 5×5 pixel regions of interest were placed at replisome foci, then used to monitor fluctuations in DinB-YPet signals (see Fig 6A). A subset of 42 trajectories were selected randomly from a total of 65 trajectories. A portion of each trajectory is presented, starting at a time-point (150 ms) where ~50% of DinB-YPet molecules have already photobleached, allowing single-molecule foci to be observed. In untreated *lexA*(Def) cells few events are visible in which the DinB-YPet is elevated in the vicinity of replisomes for more than a single 34 ms frame, indicating few long-lived binding events.

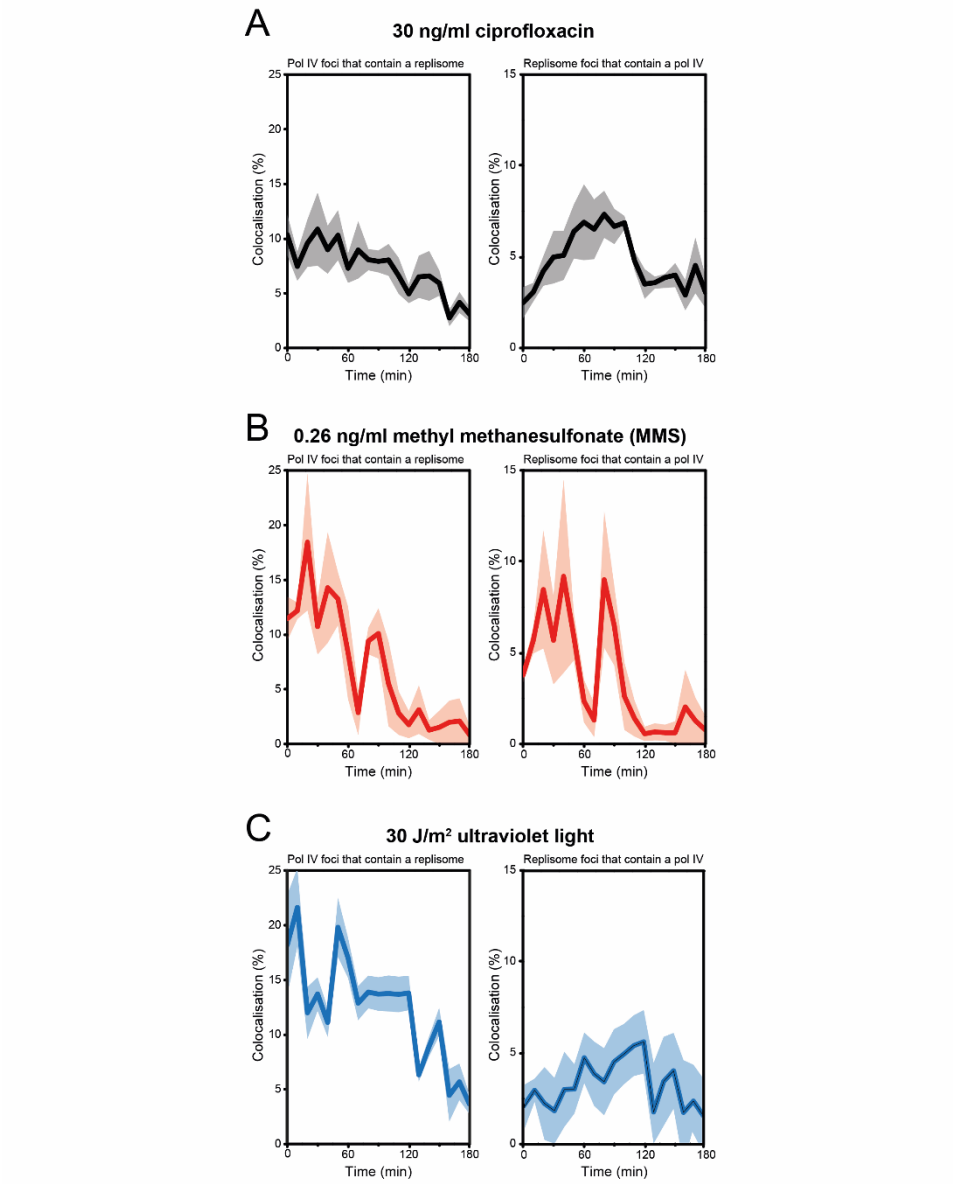

Supplementary Figure 10. Comparison of pol IV-replisome colocalisation in cells treated with different DNA-damaging agents: (A) 30 ng/ml ciprofloxacin, (B) 0.26 ng/ml methyl methanesulfonate, (C) ultraviolet light (fluence = 30 J/m^2, flux density = 3.3 W/m^2, λ = 254 nm). Colocalisation (A–C) was measured in two ways: the proportion of DinB-YPet foci that contain a colocalised DnaX-mKate2 (replisome) focus, and the proportion of DnaX-mKate2 foci that contain a colocalised DinB-YPet focus. Shaded areas indicate the standard error of the proportion. All DNA-damaging agents produce a distinctive drop in colocalisation 90–120 min after treatment. We conservatively estimate that >200 cells were used in each measurement.

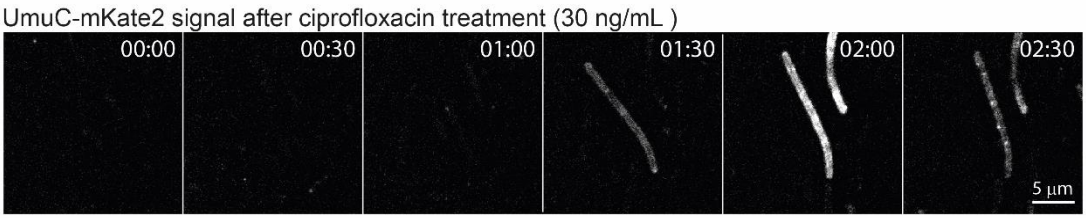

Supplementary Figure 11. Time-lapse imaging of pol V-labelled EAW282 (*dnaX-YPet umuC-mKate2*) cells following treatment with 40 ng/ml ciprofloxacin. We previously discovered that pol V is spatially regulated: the UmuC protein accumulates at the cell membrane, until the active form pol V Mut ($UmuD'_2$-UmuC-RecA-ATP) is formed and released into the cytosol (47). This was monitored by observing the change in cellular localisation of UmuC-mKate2 as a function of time. When cells are instead treated with ciprofloxacin, UmuC-mKate2 goes through a very similar progression of localisation states. In the example shown in this figure, UmuC-mKate2 is initially absent (0–1 h), then membrane associated (1.5-2 h), then cytosolic (2.5–3 h). The timing of these transitions varies from cell to cell. Typically, no UmuC-mKate2 is visible until 45-90 min after ciprofloxacin treatment. From 45-150 min, UmuC-mKate2 is membrane-associated. UmuC-mKate2 typically remains membrane-associated for approximately 30 min before being released into the cytosol.

Supplementary Movie 1. Time-lapse imaging of pol IV up-regulation in response to ciprofloxacin treatment. Cells were initially grown in rich medium in the absence of exogenous DNA damage. At t = 0 min, the flow cell inlet was switched to medium containing 30 ng/ml ciprofloxacin. At each field-of-view, a bright-field image and a DinB-YPet fluorescence image were collected every 5 min for 180 min. Time stamp indicates hours after ciprofloxacin addition.

2.7 References and Notes:

1. Friedberg EC, Walker GC, Siede W. DNA Repair and mutagenesis. 1995.

2. Goodman MF, Woodgate R. Translesion DNA polymerases. *Cold Spring Harb Perspect Biol*. 2013;5: a010363

3. Goodman MF. Error-prone repair DNA polymerases in prokaryotes and eukaryotes. *Annu Rev Biochem*. 2002;71: 17–50.

4. Fuchs RP, Fujii S. Translesion DNA syntheis and mutagenesis in prokaryotes. *Cold Spring Harb Perspect Biol*. 2013;5: a012682.

5. Waters LS, Minesinger BK, Wiltrout ME, D'Souza S, Woodruff R V, Walker GC. Eukaryotic translesion polymerases and their roles and regulation in DNA damage tolerance. *Microbiol Mol Biol Rev*. 2009;73: 134–154.

6. Simmons LA, Foti JJ, Cohen SE, Walker GC. The SOS regulatory network. *EcoSal Plus*. 2008;3: doi:10.1128/ecosalplus.5.4.3.

7. Fuchs RP. Tolerance of lesions in *E. coli*: chronological competition between translesion synthesis and damage avoidance. *DNA Repair*. 2016;44: 51–58.

8. Corzett CH, Goodman MF, Finkel SE. Competitive fitness during feast and famine: how SOS DNA polymerases influence physiology and evolution in *Escherichia coli*. *Genetics*. 2013;194: 409–420.

9. Cirz RT, Chin JK, Andes DR, De Crécy-Lagard V, Craig WA, Romesberg FE. Inhibition of mutation and combating the evolution of antibiotic resistance. *PLoS Biol*. 2005;3: e176.

10. Andersson DI, Koskiniemi S, Hughes D. Biological roles of translesion synthesis DNA polymerases in eubacteria. *Mol Microbiol*. 2010;77: 540–548.

11. Napolitano R, Janel-Bintz R, Wagner J, Fuchs RP. All three SOS-inducible DNA polymerases (Pol II, Pol IV and Pol V) are involved in induced mutagenesis. *EMBO J.* 2000;19: 6259–65.

12. Foster PL. Stress-induced mutagenesis in bacteria. Crit Rev Biochem Mol Biol. 2007;42: 373–397.

13. MacLean RC, Torres-Barceló C, Moxon R. Evaluating evolutionary models of stress-induced mutagenesis in bacteria. *Nat Rev Genet*. 2013;14: 221–227.

14. Aranda J, López M, Leiva E, Magán A, Adler B, Bou G, *et al*. Role of *Acinetobacter baumannii* UmuD homologs in antibiotic resistance acquired through DNA damage-induced mutagenesis. *Antimicrob Agents Chemother*. 2014;58: 1771–1773.

15. Boshoff HIM, Reed MB, Barry CE, Mizrahi V. DnaE2 polymerase contributes to *in vivo* survival and the emergence of drug resistance in *Mycobacterium tuberculosis*. *Cell.* 2003;113: 183–193.

16. Cirz RT, Romesberg FE. Controlling mutation: intervening in evolution as a therapeutic strategy. *Crit Rev Biochem Mol Biol*. 2007;42: 341–354.

17. Henderson-Begg SK, Livermore DM, Hall LMC. Effect of subinhibitory concentrations of antibiotics on mutation frequency in *Streptococcus pneumoniae*. *J Antimicrob Chemother*. 2006;57: 849–854.

18. Sanders LH, Rockel A, Lu H, Wozniak DJ, Sutton MD. Role of *Pseudomonas aeruginosa dinB*-encoded DNA polymerase IV in mutagenesis. *J Bacteriol*. 2006;188: 8573–8585.

19. Torres-Barceló CT, Kojadinovic M, Moxon R, MacLean RC. The SOS response increases bacterial fitness, but not evolvability, under a sublethal dose of antibiotic. *Proc R Soc B Biol Sci*. 2015;282: 20150885.

20. Warner DF, Ndwandwe DE, Abrahams GL, Kana BD, Machowski EE, Venclovas C, *et al*. Essential roles for *imuA'*- and *imuB*-encoded accessory factors in DnaE2-dependent mutagenesis in *Mycobacterium tuberculosis*. *Proc Natl Acad Sci USA*. 2010;107: 13093–13098.

21. Chevereau G, Dravecká M, Batur T, Guvenek A, Ayhan DH, Toprak E, *et al*. Quantifying the determinants of evolutionary dynamics leading to drug resistance. *PLoS Biol*. 2015;13: 1–18.

22. Gawel D, Seed PC. Urinary tract infection drives genome instability in uropathogenic *Escherichia coli* and necessitates translesion synthesis DNA polymerase IV for virulence. *Virulence*. 2011;2: 222–232.

23. Janion C. Inducible SOS response system of DNA repair and mutagenesis in *Escherichia coli*. *Int J Biol Sci*. 2008;4: 338–344.

24. Kim SR, Matsui K, Yamada M, Gruz P, Nohmi T. Roles of chromosomal and episomal *dinB* genes encoding DNA pol IV in targeted and untargeted mutagenesis in *Escherichia coli*. *Mol Genet Genomics*. 2001;266: 207–215.

25. Tang M, Pham P, Shen X, Taylor J-S, O'Donnell ME, Woodgate R, et al. Roles of *E. coli* DNA polymerases IV and V in lesion-targeted and untargeted SOS mutagenesis. *Nature.* 2000;404: 1014–1018.

26. Wagner J, Gruz P, Kim SR, Yamada M, Matsui K, Fuchs RPP. The *dinB* gene encodes a novel *E. coli* DNA polymerase, DNA pol IV, involved in mutagenesis. *Mol Cell*. 1999;4: 281–286.

27. Kuban W, Banach-orlowska M, Schaaper RM, Jonczyk P, Fijalkowska IJ. Role of DNA polymerase IV in *Escherichia coli* SOS mutator activity. *J Bacteriol*. 2006;188: 7977–7980.

28. Kenyon CJ, Walker GC. DNA-damaging agents stimulate gene expression at specific loci in

Escherichia coli. *Proc Natl Acad Sci USA*. 1980;77: 2819–2823.

29. Kumari A, Minko IG, Harbut MB, Finkel SE, Goodman MF, Lloyd RS. Replication bypass of interstrand cross-link intermediates by *Escherichia coli* DNA polymerase IV. *J Biol Chem*. 2008;283: 27433–27437.

30. Mallik S, Popodi EM, Hanson AJ, Foster PL. Interactions and localization of *Escherichia coli* error-prone DNA polymerase IV after DNA damage. *J Bacteriol*. 2015;197: 2792–2809.

31. Jarosz DF, Godoy VG, Delaney JC, Essigmann JM, Walker GC. A single amino acid governs enhanced activity of DinB DNA polymerases on damaged templates. Nature. 2006;439: 225–8.

32. Zhou BL, Pata JD, Steitz TA. Crystal structure of a DinB lesion bypass DNA polymerase catalytic fragment reveals a classic polymerase catalytic domain. *Mol Cell*. 2001;8: 427–437.

33. Ikeda M, Furukohri A, Philippin G, Loechler E, Akiyama MT, Katayama T, et al. DNA polymerase IV mediates efficient and quick recovery of replication forks stalled at N^2-dG adducts. *Nucleic Acids Res*. 2014;42: 8461–8472.

34. Yuan B, Cao H, Jiang Y, Hong H, Wang Y. Efficient and accurate bypass of N^2-(1-carboxyethyl)-2'-deoxyguanosine by DinB DNA polymerase *in vitro* and *in vivo*. *Proc Natl Acad Sci USA*. 2008;105: 8679–8684.

35. Cafarelli TM, Rands TJ, Godoy VG. The DinB-RecA complex of *Escherichia coli* mediates an efficient and high-fidelity response to ubiquitous alkylation lesions. *Environ Mol Mutagen Mutagen*. 2014;55: 92–102.

36. Kim SR, Maenhaut-Michel G, Yamada M, Yamamoto Y, Matsui K, Sofuni T, et al. Multiple pathways for SOS-induced mutagenesis in *Escherichia coli*: an overexpression of *dinB/dinP* results in strongly enhancing mutagenesis in the absence of any exogenous treatment to damage DNA. *Proc Natl Acad Sci USA*. 1997;94: 13792–13797.

37. Cohen SE, Godoy VG, Walker GC. Transcriptional modulator NusA interacts with translesion DNA polymerases in *Escherichia coli*. *J Bacteriol*. 2009;191: 665–672.

38. Cohen SE, Walker GC. The transcription elongation factor NusA is required for stress-induced mutagenesis in *Escherichia coli*. *Curr Biol*. 2010;20: 80–85.

39. Cohen SE, Lewis CA, Mooney RA, Kohanski MA, Collins JJ, Landick R, et al. Roles for the transcription elongation factor NusA in both DNA repair and damage tolerance pathways in *Escherichia coli*. *Proc Natl Acad Sci USA*. 2010;107: 15517–15522.

40. Cohen SE, Walker GC. New discoveries linking transcription to DNA repair and damage tolerance pathways. *Transcription*. 2011;2: 37–40.

41. Lovett ST. Replication arrest-stimulated recombination: dependence on the RecA paralog,

RadA/Sms and translesion polymerase, DinB. *DNA Repair*. 2006;5: 1421–1427.

42. Pomerantz RT, Goodman MF, O'Donnell ME. DNA polymerases are error-prone at RecA-mediated recombination intermediates. *Cell Cycle*. 2013;12: 2558–2563.

43. Shee C, Ponder R, Gibson JL, Rosenberg SM. What limits the efficiency of double-strand break-dependent stress-induced mutation in *Escherichia coli*? *J Mol Microbiol Biotechnol*. 2012;21: 8–19.

44. Williams AB, Hetrick KM, Foster PL. Interplay of DNA repair, homologous recombination, and DNA polymerases in resistance to the DNA damaging agent 4-nitroquinoline-1-oxide in *Escherichia coli*. *DNA Repair*. 2010;9: 1090–1097.

45. Pomerantz RT, Kurth I, Goodman MF, O'Donnell M. Preferential D-loop extension by a translesion DNA polymerase underlies error-prone recombination. *Nat Struct Mol Biol*. 2013;20: 748–755.

46. McKenzie GJ, Lee PL, Lombardo M, Hastings PJ, Rosenberg SM. SOS mutator DNA polymerase IV functions in adaptive mutation and not adaptive amplification. *Mol Cell.* 2001;7: 571–579.

47. Robinson A, McDonald JP, Caldas VEA, Patel M, Wood EA, Punter CM, et al. Regulation of mutagenic DNA polymerase V activation in space and time. *PLoS Genet*. 2015;11: 1–30.

48. Lewis JS, Spenkelink LM, Jergic S, Wood EA, Monachino E, Horan NP *et al*. Single-molecule visualization of fast polymerase turnover in the bacterial replisome. *eLife*. 2017;22: e23932.

49. Reyes-Lamothe R, Possoz C, Danilova O, Sherratt DJ. Independent positioning and action of *Escherichia coli* replisomes in live cells. Cell. 2008;133: 90-102. doi: 10.1016/j.cell.2008.01.044

50. Reyes-Lamothe R1, Sherratt DJ, Leake MC. Stoichiometry and architecture of active DNA replication machinery in *Escherichia coli. Science*. 2010;328: 498-501.

51. Drlica K, Malik M, Kerns RJ, Zhao X. Quinolone-mediated bacterial death. Antimicrob Agents Chemother. 2008;52: 385–392. doi:10.1128/AAC.01617-06

52. Benson RW, Cafarelli TM, Rands TJ, Linn I, Godoy VG. Selection of *dinB* alleles supressing survival loss upon *dinB* overexpression in *Escherichia* coli. *J Bacteriol*. 2014;196: 3023-3035.

53. Scotland MK, Heltzel JMH, Kath JE, Choi JS, Berdis AJ, Loparo JJ, et al. A genetic selection for *dinB* mutants reveals an interaction between DNA polymerase IV and the replicative polymerase that is required for translesion synthesis. *PLoS Genet*. 2015;11: e1005507.

54. Gabbai CB, Yeeles JTP, Marians KJ. Replisome-mediated translesion synthesis and leading strand template lesion skipping are competing bypass mechanisms. *J Biol Chem*. 2014;289: 32811–32823.

55. Yeeles JTP, Marians KJ. Dynamics of leading-strand lesion skipping by the replisome. *Mol Cell*. 2013;52: 855–865.

56. Yeeles JT, Marians KJ. The *Escherichia coli* replisome is inherently DNA damage tolerant. *Science*. 2011;334: 235–238.

57. Fernández De Henestrosa A, Ogi T, Ferna AR, Aoyagi S, Chafin D, Hayes JJ. *et al*. Identification of additional genes belonging to the LexA regulon in *Escherichia coli*. *Mol Microbiol*. 2000;35: 1560–1572.

58. Walker GC. Mutagenesis and inducible responses to deoxyribonucleic acid damage in *Escherichia coli*. *Microbiol Rev*. 1984;48: 60–93.

59. Ponder RG, Fonville NC, Rosenberg SM. A switch from high-fidelity to error-prone DNA double-strand break repair underlies stress-induced mutation. *Mol Cell*. 2005;19: 791–804.

60. Cairns J, Foster PL. Adaptive reversion of a frameshift mutation in *Escherichia coli*. *Genetics*. 1991;128: 695–701.

61. Hall JD, Howard-Flanders P. Temperature-sensitive *recA* mutant of *Escherichia coli* K-12: deoxyribonucleic acid metabolism after ultraviolet irradiation. *J Bacteriol*. 1975;121: 892-900.

62. Rothman RH, Clark AJ. The dependence of postreplication repair on *uvrB* in a *recF* mutant of *Escherichia coli* K-12. *Mol Gen Genet*. 1977;155: 279-286.

63. Rothman RH, Clark AJ. Defective excision and postreplication repair of UV-damaged DNA in a *recL* mutant strain of *E. coli* K-12. *Mol Gen Genet*. 1977;155: 267-277.

64. Rupp WD, Howard-Flanders P. Discontinuities in the DNA synthesized in an excision-defective strain of *Escherichia coli* following ultraviolet irradiation. *J Mol Biol*. 1968;31: 291-304.

65. Sedgwick SG. Genetic and kinetic evidence for different types of postreplication repair in *Escherichia coli* B. *J Bacteriol*. 1975;123: 154-161.

66. Youngs DA, Smith KC. Genetic control of multiple pathways of post-replicational repair in *uvrB* strains of *Escherichia coli* K-12. *J Bacteriol*. 1976;125: 102-110.

67. Lehmann AR, Fuchs RP. Gaps and forks in DNA replication: Rediscovering old models. *DNA Repair*. 2006;5: 1495-1498.

68. Wang TC. Discontinuous or semi-discontinuous DNA replication in *Escherichia coli*? *Bioessays*. 2005;27: 633-6.

69. Indiani C, O'Donnell M. A proposal: Source of single strand DNA that elicits the SOS response. *Front Biosci*. 2013;18: 312-323.

70. Fuchs RP. Tolerance of lesions in *E. coli*: Chronological competition between translesion synthesis and damage avoidance. *DNA Repair*. 2016;44: 51-58.

71. Waters LS, Walker GC. The critical mutagenic translesion DNA polymerase Rev1 is highly expressed during G(2)/M phase rather than S phase. *Proc Natl Acad Sci USA*. 2006;103: 8971-8976.

72. Quinet A, Vessoni AT, Rocha CR, Gottifredi V, Biard D, Sarasin A, Menck CF, Stary A. Gap-filling and bypass at the replication fork are both active mechanisms for tolerance of low-dose ultraviolet-induced DNA damage in the human genome. *DNA Repair*. 2014;14: 27-38.

73. Vaisman A, Woodgate R. Translesion DNA polymerases in eukaryotes: what makes them tick? *Crit Rev Biochem Mol Biol*. 2017;52: 1–30.

74. Kath JE, Jergic S, Heltzel JMH, Jacob DT, Dixon NE, Sutton MD, et al. Polymerase exchange on single DNA molecules reveals processivity clamp control of translesion synthesis. *Proc Natl Acad Sci USA*. 2014;111: 7647–7652.

75. Heltzel JMH, Maul RW, Wolff DW, Sutton MD. *Escherichia coli* DNA polymerase IV (Pol IV), but not Pol II, dynamically switches with a stalled Pol III* replicase. *J Bacteriol*. 2012;194: 3589–3600.

76. Maki H, Kornberg A. The polymerase subunit of DNA polymerase III of *Escherichia coli*. II. Purification of the α subunit, devoid of nuclease activities. *J. Biol. Chem*. 1985;260: 12987–12992.

77. Nohmi T, Battista JR, Dodson LA, Walker GC. RecA-mediated cleavage activates UmuD for mutagenesis: mechanistic relationship between transcriptional derepression and posttranslational activation. *Proc Natl Acad Sci USA*. 1988;85: 1816–1820.

78. Godoy VG, Jarosz DF, Simon SM, Abyzov A, Walker GC. UmuD and RecA directly modulate the mutagenic potential of the Y-family DNA polymerase DinB. *Mol Cell*. 2007;28: 1058–1070.

79. Georgescu RE, Kurth I, O'Donnell ME. Single-molecule studies reveal the function of a third polymerase in the replisome. *Nat Struct Mol Biol*. 2012;19: 113–116.

80. Blattner FR, Plunkett III G, Bloch CA, Perna NT, Burland V, Riley M, *et al*. The complete genome sequence of *Escherichia coli* K-12. *Science*. 1997;277: 1453–1474.

81. Huang LC, Wood EA, Cox MM. Convenient and reversible site-specific targeting of exogenous DNA into a bacterial chromosome by use of the FLP recombinase: The FLIRT system. *J Bacteri*ol. 1997;179: 6076–6083.

82. Ennis DG, Amunsden SK, Smith GR. Genetic functions promoting homologous recombination in *Escherichia coli*: A study of inversions in phage λ. *Genetics*. 1987;115: 11–24.

83. Frank EG, Hauser J, Levine AS, Woodgate R. Targeting of the UmuD, UmuD', and MucA' mutagenesis proteins to DNA by RecA protein. *Proc Natl Acad Sci USA*. 1993;90: 8169–8173.

84. Sliusarenko O, Heinritz J, Emonet T, Jacobs-Wagner C. High- throughput, subpixel-precision analysis of bacterial morphogenesis and intracellular spatio-temporal dynamics. *Mol. Micro*, 2011;80: 612:627.

85. Schneider CA, Rasband WS, Eliceiri KW. NIH Image to ImageJ: 25 years of image analysis. *Nat Methods*. 2012;9: 671–675.

86. Shaner NC, Steinbach PA, Tsien RY. A guide to choosing fluorescent proteins. *Nat Methods*. 2005;2: 905–909.

3 Specialised DNA polymerases in *Escherichia coli*: roles within multiple pathways

Sarah S. Henrikus, Antoine M. van Oijen and Andrew Robinson

Published in *Curr Genet.*, 2018; https://doi.org/10.1007/s00294-018-0840-x.

In many bacterial species, DNA damage triggers the SOS response; a pathway that regulates the production of DNA repair and damage tolerance proteins, including error-prone DNA polymerases. These specialised polymerases are capable of bypassing lesions in the template DNA, a process known as translesion synthesis (TLS). Specificity for lesion types varies considerably between the different types of TLS polymerases. TLS polymerases are mainly described as working in the context of replisomes that are stalled at lesions or in lesion-containing gaps left behind the replisome. Recently, a series of single-molecule fluorescence microscopy studies have revealed that two TLS polymerases, pol IV and pol V, rarely colocalise with replisomes in *Escherichia coli* cells, suggesting that most TLS activity happens in a non-replisomal context. In this review we re-visit the evidence for the involvement of TLS polymerases in other pathways. A series of genetic and biochemical studies indicates that TLS polymerases could participate in nucleotide excision repair, homologous recombination and transcription. In addition, oxidation of the nucleotide pool, which is known to be induced by multiple stressors, including many antibiotics, appears to favours TLS polymerase activity and thus increases mutation rates. Ultimately, participation of TLS polymerases within non-replisomal pathways may represent a major source of mutations in bacterial cells and calls for more extensive investigation.

I drafted this review article on translesion DNA polymerases in Escherichia coli. I edited the manuscript according to the review comments.

3.1 Review article

Replication of the *Escherichia coli* genome is a fast and accurate process. On undamaged DNA, the primary polymerase, DNA polymerase III, inserts close to 1000 nucleotides per second, with an error rate of only one in one billion (1,2). Damaged DNA templates, however, lead to replication problems as the primary polymerase is inhibited by the presence of lesions in the template DNA (3). Since cells are frequently exposed to endogenous and exogenous sources of DNA damage, they have evolved error-free repair pathways to remove and replace DNA lesions (4). Some lesions, however, escape these pathways and are encountered by replication forks. Depending on conditions, this leads to either replication fork arrest or re-priming and continued synthesis downstream of the lesion (known as lesion skipping) (3–12). Both pathways lead to the accumulation of single-stranded DNA (ssDNA) gaps which are either repaired or processed into double-strand breaks (DSBs) (8–10,13,14). DSBs are particularly toxic to cells (4). As an overall consequence of DNA damage, the SOS response is triggered (15). The SOS response increases the expression levels of many proteins involved in DNA repair mechanisms (9,15). The earliest SOS genes to be induced participate in non-mutagenic DNA repair pathways. If damage is not resolved during this stage, mutagenic pathways are initiated (16,17). Mutagenesis arises from the upregulation of specialised DNA polymerases that are able to bypass lesions, a process known as translesion synthesis (TLS) (3,4,19,20,5–11,18).

TLS polymerases generate mutations. In contrast to the primary polymerase, TLS polymerases are capable of efficient lesion bypass. This activity is made possible by the architecture of their template-binding sites, which are more open than that of the primary polymerase (21). This also, however, makes TLS polymerases highly error-prone as they are less likely to discriminate between correct and incorrect nucleotides which can lead to misincorporations. Insertion of the incorrect base can lead to a mutation being established during subsequent rounds of replication (4).

Mutations caused by TLS polymerases acting on undamaged portions of DNA are called untargeted mutations (22). Overexpression of TLS polymerases often leads to increased mutation rates in the absence of damage, suggesting that a drastic increase in TLS polymerase concentration tilts the balance towards TLS activity. For instance, *E. coli* DNA polymerase IV, encoded by the *dinB* gene, is an error-prone polymerase and induces -1 frameshift mutations when highly overexpressed (23,24). Similarly, overexpression of *Bacillus subtilis* DNA polymerase Pol Y1, encoded by *yqjH*, results in increased mutagenesis in a rifampicin resistance assay (25,26). TLS polymerases increase the genetic diversity of bacterial populations growing in the absence of external damage (27), implying that TLS polymerases may produce untargeted mutations at a low, but significant, rate.

TLS polymerases are specialised because they can extend primed lesion-containing templates (3,28). The incorporation of an incorrect base opposite the lesion can lead to mutation. This type of mutation is called a targeted mutation (22,29). TLS polymerases carry out a variety of error-free and mutagenic TLS activities (detailed below). It is important to note that in most cases the biological context(s) for lesion bypass (stalled replisomes, ssDNA gaps, recombination intermediates etc.) remains poorly understood.

TLS polymerases copy a variety of lesion-containing templates. DNA lesions originate from endogenous or exogenous sources, for instance some antibiotics, other DNA damaging compounds (e.g.

methyl methanesulfonate), or ultraviolet light (UV light)(3,17). Lesions can include chemically altered nucleo-bases or changes in the sugar-phosphodiester backbone. Common lesions include abasic sites, alkylated bases, oxidised bases and adducts to the N^2 position of guanines (11). Certain DNA lesions are only bypassed by a particular TLS polymerase, indicating that the active site of each TLS polymerase differently accommodates different lesion types (21).

Ultraviolet light generates covalently cross-linked pairs of thymidine bases, most commonly forming cyclobutane pyrimidine dimers (CPDs) and single cross-linked (6–4) photoproducts (4,29). In *E. coli*, UV lesions are bypassed by DNA polymerase V (pol V) (30,31). This TLS polymerase is encoded by *umuDC* and belongs to the Y-family polymerases (UmuC subfamily). Pol V is a highly error-prone polymerase that is responsible for almost all UV-induced mutagenesis. When carrying out TLS at CPDs, pol V frequently inserts the sequence GA opposite the TT-CPD lesion, rather than the canonical AA (5,32–34). A second polymerase in *E. coli*, pol II (encoded by *polB*), plays a role in restarting replication in UV-irradiated cells; cells lacking pol II show delayed recovery of DNA synthesis after irradiation (17,35,36). The biochemical nature of this activity remains unclear. In *B. subtilis* Pol Y2 is essential for UV-induced mutagenesis, whereas Pol Y1 is not (25). Polymerases of the UmuC subfamily appear to be generally necessary for UV-induced mutagenesis (37–41). While deletion of *E. coli dinB* (encoding pol IV) does not yield effects on UV survival, UV-induced mutagenesis or replication restart after UV arrest (42), biochemical measurements indicate that pol IV is capable of error-free bypass of CPD lesions (43).

Alkylating agents, such as methyl methanesulfonate (MMS) modify nucleo-bases in DNA, producing both cytotoxic and mutagenic effects (44). In *E. coli* pol IV contributes to survival upon MMS treatment (44). This activity appears to stem from error-free bypass of MMS lesions. Pol V is involved in error-prone bypass of the MMS-induced lesions N^1-methyl-deoxyadenosine (1meA) and N^3-methyl-deoxycytosine (3meC) (45).

Certain compounds generate bulky adducts to the N^2 position of deoxyguanosine (N^2-dG), for instance benzo[*a*]pyrene, nitrofurazone (NFZ), 4-nitroquionoline 1-oxide (4-NQO) and 2-acetylaminofluorene (22,46,47). TLS polymerases do not contribute equally to survival of N^2 modifications. *Escherichia coli* pol V contributes to mutagenesis upon *N*-ethyl-*N*-nitrosourea treatment(48), whereas, pols II and IV contribute greatly to 4-NQO survival (22,49,50). N^2acetylaminofluorene guanine adducts (N^2-AAFdG) can be bypassed by pol II, often inducing -2 frameshift mutations (51). In cells carrying benzo[*a*]pyrene lesions, both pols IV and V have been shown to be active using genetics and *in vitro* reconstitution assays, each contributing to both error-free TLS and -1 frameshifts (52,53).

N^2 adducts can also originate from methylglyoxal, a by-product of the glycolysis pathway (54). These N^2-(1-carboxyethyl)-2'-deoxyguanosine adducts (N^2-CEdG) are accurately bypassed by pol IV suggesting that in cells pol IV might frequently carry out error-free TLS on N^2-dG adducts that arise during normal metabolism. Moreover, bulky N^2-N^2-guanine cross-links are bypassed by pol IV with high fidelity (55).

Modified nucleotide triphosphates may favour TLS polymerase activity. DNA lesions are also induced by reactive oxygen species (ROS). For instance, guanine is often oxidised to 8-oxo-guanine (56,57). Such oxidised nucleotides form altered DNA base pairs and are commonly mutagenic (57,58).

The amount of ROS in cells can vary considerably according to several factors, including for example metabolic rates and oxygen concentrations. There is some evidence that in cells growing aerobically, increased ROS levels lead to increased numbers of lesions (58). This, presumably, would cause an increase in TLS activity. In fact, levels of pol V-dependent mutagenesis in *E. coli* appear to be markedly higher in aerobic conditions than in anaerobic conditions (59). It is not clear, however, whether the extra mutations that arise under aerobic conditions derive from targeted mutagenesis at oxidised base pairs or whether the conditions favour untargeted mutagenesis. It has been directly demonstrated that pol IV incorporates 8-oxo-dGs into the DNA (56). Whether pol V is similarly capable of incorporating oxidised nucleotides requires further investigation.

Cellular stress is also known to increase ROS levels (60). For instance, ROS increasingly accumulate in response to treatment with several antibiotics or in the case of thymine starvation and in both cases strongly contribute to killing (61,62). The killing mechanism appears to depend on ROS-induced conversion of ssDNA regions into toxic DSBs (61,62). Stress-induced increases in ROS also increase mutation rates and TLS polymerases are involved (56,62,63). It remains unclear, however, if this involvement relates to incorporation of oxidised nucleotides into the DNA, mutagenic TLS at sites of oxidised bases already present in the DNA, error-prone synthesis by TLS polymerases during break repair, or some combination of the three. In general, the incorporation of non-canonical dNTPs into the DNA by DNA polymerases is an important area that remains under-investigated.

Replicative vs post-replicative translesion synthesis. Two models have been proposed for TLS activity upon encounters of replisomes with lesions on the leading strand (see **Fig. 1A**). In the most cited model, known as replicative TLS, TLS polymerases assist stalled replisomes by exchanging for the arrested pol III and bypassing the lesion (Heltzel et al. 2012; Fuchs and Fujii 2013; Scotland et al. 2015). Following TLS, the polymerases exchange back, allowing pol III to resume replication. This model was primarily built upon the results of *in vitro* reconstitution assays and led to the proposal of molecular mechanisms invoking polymerase switching on the β clamp (65–69). In the other model, TLS polymerases are involved in post-replicative translesion synthesis. Here the replisome is proposed to skip over lesions (by re-priming downstream), creating lesion-containing gaps behind the replisome (43,70). These gaps are templates for TLS polymerases, which bypass lesions and thus allow the gaps to be filled (11,71,72).

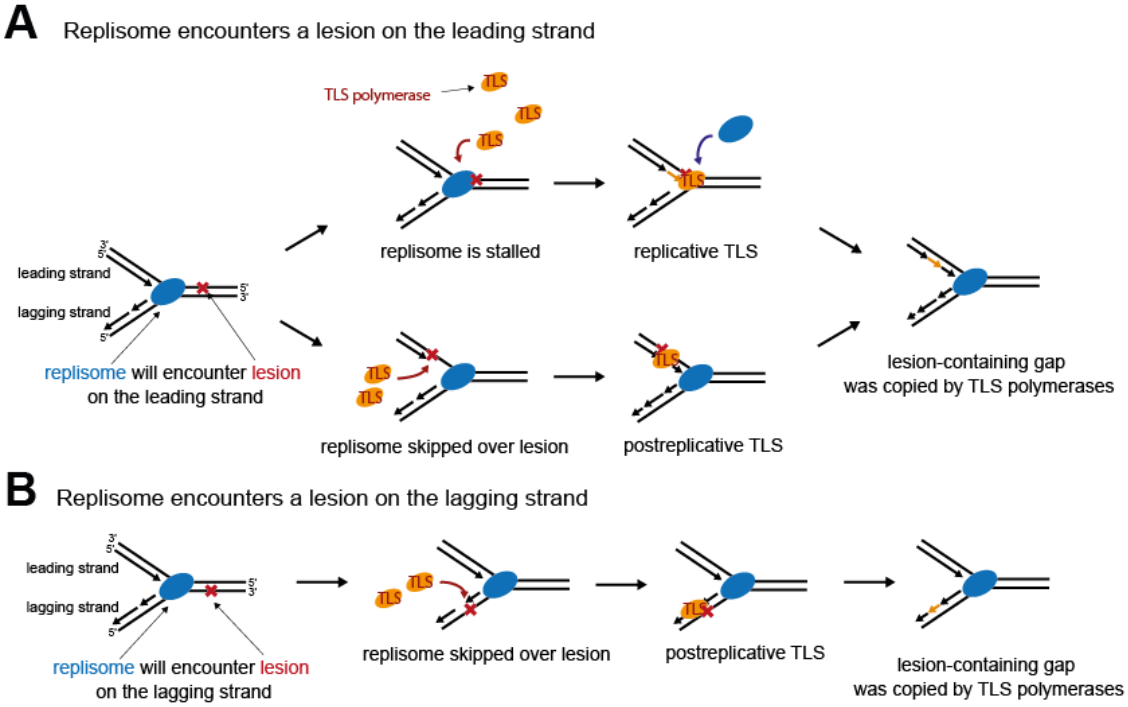

Figure 1. Potential outcomes of replisome-lesion encounters. Schematic diagram describing commonly envoked models for TLS triggered by the replisome encounters with a lesion on the leading strand (a) and lagging strand (b).

Studies conducted *in vitro* have concluded that skipping of lagging strand lesions is an inherent property of the replisome (see **Fig. 1B**) (73,74). In light of new observations that demonstrate that Pol III* (three Pol III cores plus clamp loader complex, i.e. $[\alpha\varepsilon\theta]_3\tau_3\delta\delta'\chi\psi$) exchanges readily at replication forks (75,76), the conclusions of these studies may need to be revisited. The Higuchi and McInerney studies demonstrated that lagging strand lesions did not block the progress of the replisome in bulk-level biochemical assays. From this they each concluded that the replisome simply skips over lagging lesions. In the absence of exogenous DNA damage, Pol III* exchanges readily *in vivo* (75,76). This opens an alternative explanation for the Higuchi and McInerney data: the lagging strand polymerase actually stalled at the lesion, but the stalled Pol III* was replaced by another molecule from the bulk. There are only ~20 molecules of Pol III* available in each cell (75,76), thus exchange could easily become limiting in the presence of damage. It would be of interest to examine the capacity of the replisome to skip lagging strand lesions under dilute conditions, or in pre-assembled single-molecule assays, where exchange of Pol III* would be limited.

TLS polymerases are involved in other DNA repair pathways. Historically, error-prone polymerases have mainly been examined in the context of the replisome. Several studies, however, implicate the TLS polymerases are also involved in other DNA repair mechanisms, for instance, transcription coupled repair (77–79), nucleotide excision repair (42,50) and homologous recombination (80–83). Additionally, TLS polymerases play a role in adaptive mutagenesis (84–87).

In addition to DNA replication, DNA damage is also a hindrance to transcription. Lesion-containing gaps on the template strand result in RNA polymerase stalling. Work by Cohen *et al.* revealed that RNA polymerases stalled at gaps may recruit TLS polymerases to close the gap and allow

transcription to continue (see **Fig. 2A**). The group found that the *E. coli* transcription modulator NusA genetically interacts with both Y-family polymerases pol IV and pol V (77,78). NusA physically interacts with pol IV (79). NusA functions in both termination and antitermination of transcription and in both cases is bound to the RNA polymerase (RNAP). In the Cohen transcription-coupled TLS model, NusA recruits TLS polymerases to RNAPs stalled at gaps generated when the replisome encounters a lesion in the nontranscribed strand (77). TLS polymerases could then fill the gap in the template strand and rescue the stalled RNAP. In contrast, RNAPs stalled at lesions on the transcribed strain would be resolved by transcription-coupled repair (77).

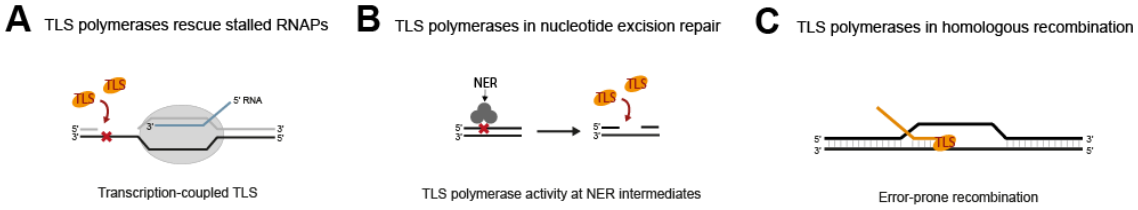

Figure 2. TLS polymerases are potentially involved in non-replisomal activities. Schematic diagrams depicting TLS and/or primer exten- sion by TLS polymerases. (a) TLS polymerases rescue stalled RNAPs. (b) TLS polymerases in nucleotide excision repair. (c) TLS polymerases in homologous recombination

Nucleotide excision repair (NER) can remove a variety of bulky DNA lesions, leaving behind ssDNA gaps which, in principle, could be substrates for TLS polymerases (see **Fig. 2B**). In fact, *E. coli* pol IV is involved in both NER-dependent and -independent pathways in cells treated with 4-NQO (50). Pol IV and NER are also proposed to work cooperatively on N^2-N^2-guanine interstrand DNA cross-links (ICLs) (55). In another study, ICLs induced by exposure of cells to nitrogen mustard were proposed to be repaired by pol II in concert with NER (88). The role of pol IV in processing of nitrogen mustard ICLs has not yet been investigated.

Aside from NER, another major determinant of NQO survival is homologous recombination (50). Although homologous recombination has been described as an error-free repair pathways, several studies have proposed that TLS polymerases can participate in homologous recombination and make the process error-prone (see **Fig. 2C**) (63,89). *In vitro* experiments demonstrated that *E. coli* pol IV can proficiently extend D-loops (83). Interestingly, synthesis at D-loops has markedly lower fidelity than at standard primed-template structures. At D-loops, pol II appears to be proficient in correcting errors introduced by pol IV, presumably due to its exonuclease function. Consequently, pol II is proposed to supresses error-prone recombination (83). Similar to pol IV, DNA polymerase I (pol I) is less accurate at RecA-mediated recombination intermediates (90). This suggests that certain polymerases might generally be error-prone at these unstable recombination intermediates which might be driving error-prone recombination and, conceivably, could represent a major determinant in the development of antibiotic resistance through mutation (90).

Single-molecule microscopy reveals that TLS polymerases mainly act away from replisomes. Considering TLS polymerases being involved in several DNA repair pathways, we investigated if TLS polymerases predominantly act in the vicinity of replisomes using single-molecule imaging in live *E. coli*

cells (91,92). Single molecule microscopy allows TLS polymerase activity to be observed as individual TLS polymerase molecules bind to DNA or replisomes and dissociate.

Using the SOS-inducing agents ciprofloxacin, UV light and MMS, we showed that the concentration of pol IV increases upon damage induction (91). The increase in concentration was correlated with cell filamentation rate and increased pol IV binding activity at DNA. In contrast to the textbook model, we found that pol IV mainly binds away from replisomes suggesting that the majority of pol IV activity could be non-replisomal. Furthermore, pol IV molecules bound in the vicinity of replisomes were often close to, rather than at, replisomes. These results, and those of others (93), support the model of post-replicative TLS, although do not completely exclude the possibility that pol IV is involved in replicative TLS. Since pol IV mostly binds away from replisomes, pol IV might predominantly work in other pathways such as transcription (77), nucleotide excision repair (42,50) and homologous recombination (80–82,90) as proposed in several studies. In a microscopy study in which cells were treated with NQO or nalidixic acid, pol IV foci were been shown to colocalise with certain RecA structures and also with DSBs, supporting the idea that pol IV is involved in DSB repair (80). It is important to note, however, that in this study pol IV was expressed at somewhat higher levels than in wild-type cells. The pol IV colocalisation with RecA agglomerates was observed at a relatively late stage of the DNA damage response, around 180 min after damage induction. It would be of considerable interest to repeat these measurements with higher time resolution, to determine if pol IV acts at RecA structures earlier in the SOS response.

We have also investigated the regulation of pol V and its role in replicative translesion synthesis upon UV damage (92). Pol V is a highly error-prone polymerase and thus underlies several stages of temporal and spatial regulation. After activation, pol V has little activity at replisomes and rather binds away from replisomes, similar to pol IV. However, in a *recA*(E38K) mutant, where pol V is constitutively activated in the absence of damage, many pol V molecules are bound at replisomes. In *recA*(E38K) UV irradiation however, additional binding sites away from replisomes open for pol V. Since pol IV binds at RecA structures upon SOS induction, it would be of interest to determine whether it also works on recombination intermediates.

The third TLS polymerase, pol II, is different to pol IV and V in that it has an exonuclease function. Pol II has been shown to suppress the error-prone activity of pol IV at recombination intermediates, presumably due to pol II proof-reading errors introduced by pol IV. To date, live cell single-molecule studies on pol II have not yet been published. It would be interesting to know whether pol II shows a different behaviour to pol IV and V especially because of pol II's exonuclease activity.

Conclusions. Single-molecule live cell imaging reveals that 90% of pol IV foci and 95% of pol V foci form at sites on the DNA that are spatially distinct from replisomes (91,92). Of the remaining 5–10% of foci, many appear close to replisomes rather than at replisomes. The data appear to indicate that TLS polymerases frequently participate in mechanisms other than replicative TLS. Based on other studies, these extra-replisomal activities could include post-replicative TLS, incorporation of oxidised dNTPs, rescue of stalled RNA polymerase complexes or participation in NER or homologous recombination.

3.2 References

1. Lewis JS, Slobodan J, Dixon NE. Chapter Two - The *E . coli* DNA replication fork. In: *The Enzymes*. 2016. p. 1–57.
2. Drake JW. A constant rate of spontaneous mutation in DNA-based microbes. *Proc Natl Acad Sci USA*. 1991;88:7160–7164.
3. Goodman MF, Woodgate R. Translesion DNA polymerases. *Cold Spring Harb Perspect Biol*. 2013;5:a010363.
4. Friedberg EC, Walker GC, Siede W. DNA Repair and Mutagenesis. 1995.
5. Goodman MF. Error-prone repair DNA polymerases in prokaryotes and eukaryotes. *Annu Rev Biochem*. 2002;71:17–50.
6. Simmons LA, Foti JJ, Cohen SE, Walker GC. The SOS regulatory network. *EcoSal Plus*. 2008;3:doi:10.1128/ecosalplus.5.4.3.
7. Waters LS, Minesinger BK, Wiltrout ME, D'Souza S, Woodruff R V, Walker GC. Eukaryotic translesion polymerases and their roles and regulation in DNA damage tolerance. *Microbiol Mol Biol Rev*. 2009;73:134–154.
8. Yeeles JTP, Marians KJ. The *Escherichia coli* replisome is inherently DNA damage tolerant. *Science*. 2011;14:235–238.
9. Fuchs RP, Fujii S. Translesion DNA syntheis and mutagenesis in prokaryotes. *Cold Spring Harb Perspect Biol*. 2013;5:a012682.
10. Gabbai CB, Yeeles JTP, Marians KJ. Replisome-mediated translesion synthesis and leading strand template lesion skipping are competing bypass mechanisms. *J Biol Chem*. 2014;289:32811–32823.
11. Fuchs RP. Tolerance of lesions in E. coli: Chronological competition between translesion synthesis and damage avoidance. *DNA Repair*. 2016;44:51–8.
12. Lloyd RG, Rudolph CJ. 25 years on and no end in sight: a perspective on the role of RecG protein. *Curr Genet*. 2016;62:827–840.
13. Heltzel JMH, Maul RW, Wolff DW, Sutton MD. Escherichia coli DNA polymerase IV (Pol IV), but not Pol II, dynamically switches with a stalled Pol III* replicase. *J Bacteriol.* 2012;194:3589–3600.
14. Scotland MK, Heltzel JMH, Kath JE, Choi JS, Berdis AJ, Loparo JJ, et al. A genetic selection for dinB mutants reveals an interaction between DNA polymerase IV and the replicative polymerase that is required for translesion synthesis. *PLoS Genet*. 2015;11:e1005507.
15. Henestrosa A, Ogi T, Ferna AR, Aoyagi S, Chafin D, Hayes JJ. Identification of additional genes belonging to the LexA regulon in *Escherichia coli*. *Mol Biol.* 2000;35:1560–1572.
16. Foster PL. Stress-induced mutagenesis in bacteria. Crit Rev *Biochem Mol Biol.* 2007;42:373–397.
17. Goodman MF. Error-prone repair DNA polymerases in prokaryotes and eukaryotes. *Annu Rev Biochem*. 2002;71:17–50.
18. Napolitano R, Janel-Bintz R, Wagner J, Fuchs RPP. All three SOS-inducible DNA polymerases (Pol II, Pol IV and Pol V) are involved in induced mutagenesis. *EMBO J*. 2000;19:6259–6265.
19. Yeiser B, Pepper ED, Goodman MF, Finkel SE. SOS-induced DNA polymerases enhance long-

term survival and evolutionary fitness. *Proc Natl Acad Sci USA*. 2002;99:8737–8741.

20. Michel B, Sandler SJ. Replication restart in bacteria. J Bacteriol. 2017;199(13):e00102-17.
21. Yang W, Gao Y. Translesion and repair DNA polymerases: Diverse structure and mechanism. *Annu Rev Biochem.* 2018;87:12.1-12.23.
22. Kim SR, Matsui K, Yamada M, Gruz P, Nohmi T. Roles of chromosomal and episomal *dinB* genes encoding DNA pol IV in targeted and untargeted mutagenesis in E*scherichia coli. Mol Genet Genomics*. 2001;266:207–215.
23. Kim SR, Maenhaut-Michel G, Yamada M, Yamamoto Y, Matsui K, Sofuni T, et al. Multiple pathways for SOS-induced mutagenesis in *Escherichia coli*: an overexpression of *dinB*/*dinP* results in strongly enhancing mutagenesis in the absence of any exogenous treatment to damage DNA. *Proc Natl Acad Sci USA.* 1997;94:13792–13797.
24. Kuban W, Banach-Orlowska M, Bialoskorska M, Lipowska A, Schaaper RM, Jonczyk P, et al. Mutator phenotype resulting from DNA polymerase IV overproduction in *Escherichia coli*: Preferential mutagenesis on the lagging strand. *J Bacteriol.* 2005;187:6862–6866.
25. Duigou S, Ehrlich SD, Noirot P, Noirot-Gros MF. Distinctive genetic features exhibited by the Y-family DNA polymerases in *Bacillus subtilis. Mol Microbiol*. 2004;54:439–451.
26. Sung HM, Yeamans G, Ross CA, Yasbin RE. Roles of YqjH and YqjW, homologs of the *Escherichia coli* UmuC/DinB or Y superfamily of DNA polymerases, in stationary-phase mutagenesis and UV-induced mutagenesis of *Bacillus subtilis. J Bacteriol.* 2003;185:2153–2160.
27. Corzett CH, Goodman MF, Finkel SE. Competitive fitness during feast and famine: How SOS DNA polymerases influence physiology and evolution in *Escherichia coli*. *Genetics*. 2013;194:409–420.
28. Vaisman A, Woodgate R. Translesion DNA polymerases in eukaryotes: what makes them tick? *Crit Rev Biochem Mol Biol*. 2017;52:274–303.
29. Tang M, Pham P, Shen X, Taylor JS, O'Donnell M, Woodgate R, et al. Roles of *E . coli* DNA polymerases IV and V in lesion-targeted and untargeted SOS mutagenesis. *Nature*. 2000;404:1014–1018.
30. Krishna S, Maslov S, Sneppen K. UV-induced mutagenesis in *Escherichia coli* SOS response: A quantitative model. *PLoS Comput Biol*. 2007;3:e41:0451-0462.
31. Patel M, Jiang Q, Woodgate R, Cox MM, Goodman MF. A new model for SOS-induced mutagenesis: How RecA protein activates DNA polymerase V. *Crit Rev Biochem Mol Biol*. 2010;45:171–184.
32. Banerjee SK, Christensen RB, Lawrence CW, LeClerc JE. Frequency and spectrum of mutations produced by a single cis-syn thymine-thymine cyclobutane dimer in a single-stranded vector. *Proc Natl Acad Sci USA.* 1988;85:8141–8145.
33. Banerjee SK, Borden A, Christensen RB, LeClerc JE, Lawrence CW. SOS-dependent replication past a single trans-syn T-T cyclobutane dimer gives a different mutation spectrum and increased error rate compared with replication past this lesion in uninduced cells. *J Bacteriol.* 1990;172:2105–2112.
34. Timms AR, Muriel W, Bridges BA. A UmuD,C-dependent pathway for spontaneous G:C to C:G

transversions in stationary phase *Escherichia coli mutY*. *Mutat Res*. 1999;435:77–80.

35. Rangarajan S, Woodgate R, Goodman MF. A phenotype for enigmatic DNA polymerase II: a pivotal role for pol II in replication restart in UV-irradiated *Escherichia coli*. *Proc Natl Acad Sci USA*. 1999;96:9224–9229.
36. Wang F, Yang W. Structural insights into translesion synthesis by DNA Pol II. *Cell*. 2009;139:1279–1289.
37. Woodgate R, Levine AS. Damage inducible mutagenesis: recent insights into the activities of the Umu family of mutagenesis proteins. *Cancer Surv*. 1996;28:117–140.
38. Hauser J, Levine AS, Ennis DG, Chumakov KM, Woodgate R. The enhanced mutagenic potential of the MucAB proteins correlates with the highly efficient processing of the MucA protein. *J Bacteriol*. 1992;174:6844–6851.
39. Szekeres Jr. ES, Woodgate R, Lawrence CW. Substitution of *mucAB* or *rumAB* for *umuDC* alters the relative frequencies of the two classes of mutations induced by a site-specific T-T cyclobutane dimer and the efficiency of translesion DNA synthesis. *J Bacteriol.* 1996;178:2559–2563.
40. Woodgate R, Rajagopalan M, Lu C, Echols H. UmuC mutagenesis protein of *Escherichia coli*: Purification and interaction with UmuD and UmuD′. *Proc Natl Acad Sci USA*. 1989;86:7301–7305.
41. Thomas SM, Crowne HM, Pidsley SC, Sedgwick SG. Structural characterization of the *Salmonella typhimurium* LT2 *umu* operon. J Bacteriol. 1990;172(9):4979–87.
42. Courcelle CT, Belle JJ, Courcelle J. Nucleotide excision repair or polymerase V-mediated lesion bypass can act to restore UV-arrested replication forks in *Escherichia coli*. *J Bacteriol*. 2005;187:6953–6961.
43. Gabbai CB, Yeeles JTP, Marians KJ. Replisome-mediated translesion synthesis and leading strand template lesion skipping are competing bypass. *J Biol Chem*. 2014;289:32811–32823.
44. Bjedov I, Dasgupta CN, Slade D, Le Blastier S, Selva M, Matic I. Involvement of *Escherichia coli* DNA polymerase IV in tolerance of cytotoxic alkylating DNA lesions *in vivo*. *Genet Soc Am*. 2007;176:1431–1440.
45. Sikora A, Mielecki D, Chojnacka A, Nieminuszczy J, Wrzesiński M, Grzesiuk E. Lethal and mutagenic properties of MMS-generated DNA lesions in *Escherichia coli* cells deficient in BER and AlkB-directed DNA repair. *Mutagenesis.* 2010;25:139–147.
46. Pagès V, Fuchs RPP. How DNA lesions are turned into mutations within cells? *Oncogene*. 2002;21:8957–8966.
47. Jarosz DF, Godoy VG, Delaney JC, Essigmann JM, Walker GC. A single amino acid governs enhanced activity of DinB DNA polymerases on damaged templates. *Nature*. 2006;439:225–228.
48. Fix D. *N*-ethyl-*N*-nitrosourea-induced mutagenesis in *Escherichia coli*: multiple roles for UmuC protein. *Mutagen Res*. 1993;294:127–138.
49. Sanders LH, Rockel A, Lu H, Wozniak DJ, Sutton MD. Role of *Pseudomonas aeruginosa dinB*-encoded DNA polymerase IV in mutagenesis. *J Bacteriol*. 2006;188:8573–8585.
50. Williams AB, Hetrick KM, Foster PL. Interplay of DNA repair, homologous recombination, and DNA polymerases in resistance to the DNA damaging agent 4-nitroquinoline-1-oxide in

Escherichia coli. DNA Repair. 2010;9:1090–1097.

51. Becherel OJ, Fuchs RPP. Mechanism of DNA polymerase II-mediated frameshift mutagenesis. *Proc Natl Acad Sci USA*. 2001;98:8566–8571.
52. Ikeda M, Furukohri A, Philippin G, Loechler E, Akiyama MT, Katayama T, et al. DNA polymerase IV mediates efficient and quick recovery of replication forks stalled at N^2-dG adducts. *Nucleic Acids Res*. 2014;42:8461–8472.
53. Lenne-Samuel N, Janel-Bintz R, Kolbanovskiy A, Geacintov NE, Fuchs RPP. The processing of a Benzo(*a*)pyrene adduct into a frameshift or a base substitution mutation requires a different set of genes in *Escherichia coli*. *Mol Microbiol.* 2000;38:299–307.
54. Yuan B, Cao H, Jiang Y, Hong H, Wang Y. Efficient and accurate bypass of N^2-(1-carboxyethyl)-2'-deoxyguanosine by DinB DNA polymerase *in vitro* and *in vivo. Proc Natl Acad Sci USA*. 2008;105:8679–9684.
55. Kumari A, Minko IG, Harbut MB, Finkel SE, Goodman MF, Lloyd RS. Replication bypass of interstrand cross-link intermediates by *Escherichia coli* DNA polymerase IV. *J Biol Chem.* 2008;283:27433–27437.
56. Foti JJ, Devadoss B, Winkler JA, Collins JJ, Walker GC. Oxidation of the guinine nucleotide pool underlies cell death by bactericidial antibiotics. *Science*. 2012;336:315–319.
57. Sekiguchi M, Tsuzuki T. Oxidative nucleotide damage: Consequences and prevention. *Oncogene*. 2002;21:8895–8904.
58. Sakai A, Nakanishi M, Yoshiyama K, Maki H. Impact of reactive oxygen species on spontaneous mutagenesis in *Escherichia coli. Genes to Cells.* 2006;11:767–778.
59. Bhamre S, Gadea BB, Koyama CA, White SJ, Fowler RG. An aerobic *recA*-, *umuC*-dependent pathway of spontaneous base-pair substitution mutagenesis in *Escherichia coli*. *Mutat Res*. 2001;473:229–247.
60. Matic I. The major contribution of the DNA damage-triggered reactive oxygen species production to cell death: implications for antimicrobial and cancer therapy. *Curr Genet.* 2018;64:567-569.
61. van Acker H, Coenye T. The role of reactive oxygen species in antibiotic-mediated killing of bacteria. *Trends Microbiol.* 2017;25:456–466.
62. Hong Y, Li L, Luan G, Drlica K, Zhao X. Contribution of reactive oxygen species to thymineless death in *Escherichia coli. Nat Microbiol*. 2017;2:1667–1675.
63. Moore JM, Correa R, Rosenberg SM, Hastings PJ. Persistent damaged bases in DNA allow mutagenic break repair in *Escherichia coli. PLoS Genet*. 2017;13:e1006733.
64. Fuchs RP, Fujii S. Translesion DNA synthesis and mutagenesis in prokaryotes. *Cold Spring Harb Perspect Biol*. 2013;5:a012682.
65. Becherel OJ, Fuchs RPP. Pivotal role of the β-clamp in translesion DNA synthesis and mutagenesis in *E . coli* cells. DNA Repair. 2002;1:703–708.
66. Furukohri A, Goodman MF, Maki H. A dynamic polymerase exchange with *Escherichia coli* DNA polymerase IV replacing DNA polymerase III on the sliding clamp. *J Biol Chem.* 2008;283:11260–11269.
67. Kath JE, Jergic S, Heltzel JMH, Jacob DT, Dixon NE, Sutton MD, et al. Polymerase exchange on

single DNA molecules reveals processivity clamp control of translesion synthesis. P*roc Natl Acad Sci USA*. 2014;111:7647–7652.

68. Lenne-Samuel N, Wagner J, Etienne H, Fuchs RPP. The processivity factor β controls DNA polymerase IV traffic during spontaneous mutagenesis and translesion synthesis *in vivo. EMBO Rep*. 2002;3:45–9.
69. Wagner J, Fujii S, Gruz P, Nohmi T, Fuchs RPP. The beta clamp targets DNA polymerase IV to DNA and strongly increases its processivity. *EMBO Rep*. 2000;1:484–8.
70. Yeeles JTP, Marians KJ. Dynamics of leading-strand lesion skipping by the replisome. *Mol Cell*. 2013;52:855–865.
71. Waters LS, Walker GC. The critical mutagenic translesion DNA polymerase Rev1 is highly expressed during G2/M phase rather than S phase. *Proc Natl Acad Sci USA*. 2006;103:8971–8976.
72. Indiani C, O'Donnell M. A Proposal: Source of single strand DNA that elicits the SOS response. *Front Biosci*. 2013;18:312–323.
73. Higuchi K, Katayama T, Iwai S, Hidaka M, Horiuchi T, Maki H. Fate of DNA replication fork encountering a single DNA lesion during oriC plasmid DNA replication *in vitro. Genes to Cells*. 2003;8:437–449.
74. McInerney P, O'Donnell M. Functional uncoupling of twin polymerases. *J Biol Chem*. 2004;279:21543–21551.
75. Lewis JS, Spenkelink LM, Jergic S, Wood EA, Monachino E, Horan NP, et al. Single-molecule visualization of fast polymerase turnover in the bacterial replisome. *Elife*. 2017;6:e23932.
76. Beattie TR, Kapadia N, Nicolas E, Uphoff S, Wollman AJM, Leake MC, et al. Frequent exchange of the DNA polymerase during bacterial chromosome replication. *Elife*. 2017;6:e21763.
77. Cohen SE, Lewis CA, Mooney RA, Kohanski MA, Collins JJ, Landick R, et al. Roles for the transcription elongation factor NusA in both DNA repair and damage tolerance pathways in *Escherichia coli. Proc Natl Acad Sci USA.* 2010;107:15517–15522.
78. Cohen SE, Walker GC. New discoveries linking transcription to DNA repair and damage tolerance pathways. *Transcription*. 2011;2:37–40.
79. Cohen SE, Godoy VG, Walker GC. Transcriptional modulator NusA interacts with translesion DNA polymerases in *Escherichia coli. J Bacteriol.* 2009;191:665–672.
80. Mallik S, Popodi EM, Hanson AJ, Foster PL. Interactions and localization of *Escherichia coli* error-prone DNA polymerase IV after DNA damage. *J Bacteriol.* 2015;197:2792–2809.
81. Ponder RG, Fonville NC, Rosenberg SM. A switch from high-fidelity to error-prone DNA double-strand break repair underlies stress-induced mutation. *Mol Cell*. 2005;19:791–804.
82. Shee C, Gibson JL, Darrow MC, Gonzalez C, Rosenberg SM. Impact of a stress-inducible switch to mutagenic repair of DNA breaks on mutation in *Escherichia coli. Proc Natl Acad Sci USA.* 2011;108:13659–13664.
83. Pomerantz RT, Kurth I, Goodman MF, O'Donnell M. Preferential D-loop extension by a translesion DNA polymerase underlies error-prone recombination. *Nat Struct Mol Biol.* 2013;20:748–755.

84. McKenzie GJ, Lee PL, Lombardo MJ, Hastings PJ, Rosenberg SM. SOS mutator DNA polymerase IV functions in adaptive mutation and not adaptive amplification. *Mol Cell*. 2001;7:571–579.
85. Cairns J, Foster PL. Adaptive reversion of a frameshift mutation in *Escherichia coli*. *Genetics*. 1991;128:695–701.
86. Wagner J, Gruz P, Kim SR, Yamada M, Matsui K, Fuchs RPP, et al. The *dinB* gene encodes a novel *E. coli* DNA polymerase, DNA pol IV, involved in mutagenesis. *Mol Cell*. 1999;4:281–286.
87. Rosenberg SM. Evolving responsively: adaptive mutation. *Nat Rev Genet*. 2001;2:504–515.
88. Berardini M, Foster PL, Loechler EL. DNA polymerase II (polB) is involved in a new DNA repair pathway for DNA interstrand cross-links in *Escherichia coli*. *J Bacteriol*. 1999;181:2878–2882.
89. Lovett ST. Replication arrest-stimulated recombination: Dependence on the RecA paralog, RadA/Sms and translesion polymerase, DinB. *DNA Repair*. 2006;5:1421–1427.
90. Pomerantz RT, Goodman MF, O'Donnell ME. DNA polymerases are error-prone at RecA-mediated recombination intermediates. *Cell Cycle*. 2013;12:2558–2563.
91. Henrikus SS, Wood EA, McDonald JP, Cox MM, Woodgate R, Goodman MF, et al. DNA polymerase IV primarily operates outside of DNA replication forks in *Escherichia coli*. *PLoS Genet*. 2018;14:e1007161.
92. Robinson A, McDonald JP, Caldas VEA, Patel M, Wood EA, Punter CM, et al. Regulation of mutagenic DNA polymerase V activation in space and time. *PLoS Genet*. 2015;11:e1005482.
93. Thrall ES, Kath JE, Chang S, Loparo JJ. Single-molecule imaging reveals multiple pathways for the recruitment of translesion polymerases after DNA damage. *Nat Commun*. 2017;8.

4 DNA double-strand breaks induced by reactive oxygen species promote DNA polymerase IV activity in *Escherichia coli*

Sarah S. Henrikus, Camille Henry, John P. McDonald, Yvonne Hellmich, Steven T. Bruckbauer, Megan E. Cherry, Elizabeth A. Wood[3], Roger Woodgate, Michael M. Cox, Antoine M. van Oijen, Harshad Ghodke, Andrew Robinson

bioRχiv 2019, https://www.biorxiv.org/content/10.1101/533422v2.

Under many conditions the killing of bacterial cells by antibiotics is potentiated by damage induced by reactive oxygen species (ROS). In most bacteria, ROS primarily target biomolecules such as proteins and DNA. Damage to DNA, particularly in the form of double-strand breaks (DSBs), is a major contributor to cell death. DNA polymerase IV (pol IV), an error-prone DNA polymerase produced at elevated levels in cells experiencing DNA damage, has been implicated both in ROS-dependent killing and in DSB repair (DSBR). Here, we show using single-molecule fluorescence microscopy that ROS-induced DSBs promote pol IV activity in two ways. First, exposure to the DNA-damaging antibiotics ciprofloxacin and trimethoprim triggers an SOS-mediated increase in intracellular pol IV concentration that is strongly dependent on both ROS and DSBR. Second, in cells that constitutively express pol IV, co-treatment with a ROS mitigator dramatically reduces the number of DSBs as well as pol IV foci formed, indicating a role of pol IV in the repair of ROS-induced DSBs.

I carried out and analysed all in vivo single-molecule experiments and plate reader assays. I was involved in strain construction, plate-based survival assays and the preparation of the manuscript.

4.1 Significance

Many antibiotics induce an accumulation of reactive oxygen species (ROS) in bacterial cells. ROS-induced damage to DNA, in particular formation of double-strand breaks (DSBs), potentiates killing by several bactericidal antibiotics. Here we used single-molecule fluorescence microscopy to reveal new links between ROS-induced DSBs and the activity of error-prone DNA polymerase IV (pol IV). We found that antibiotic-induced up-regulation of pol IV production requires active formation of DSB intermediates and can be supressed by ROS mitigators. The formation of pol IV foci, which reflect DNA-binding events, also requires DSB repair. Our findings support a major role for pol IV in DSB intermediates and reveal new details of how antibiotic treatment can potentially drive the development of antibiotic resistance in bacteria.

4.2 Main

Many antibiotics induce the accumulation of reactive oxygen species (ROS) within bacterial cells (1–4). These highly reactive molecules cause widespread damage to biomolecules. It is becoming clear that secondary DNA lesions induced by ROS, such as double-strand breaks (DSBs) (5,6) and oxidized nucleotides (7,8), potentiate killing by bactericidal antibiotics. This phenomenon of secondary lesion formation, which has been described for several antibiotic classes with different primary modes of action, is known as a common killing mechanism (8–15). A well-studied model of the common killing mechanism is the fluoroquinolone antibiotic ciprofloxacin, a DNA gyrase inhibitor, for which killing is strongly potentiated by ROS accumulation (12). A second well-studied model of the common killing mechanism is trimethoprim (13), an antibiotic that inhibits folic acid production and consequently induces thymineless death (TLD). Recent work indicates that TLD involves the accumulation of ROS, which lead to the formation of DSBs (5).

Two mechanisms for ROS-induced DSB formation have been proposed in *E. coli*. The first invokes oxidization of the cellular nucleotide pool, leading to increased incorporation of oxidized nucleotide triphosphates (e.g. 8-oxo-dGTP) into the DNA, for instance, by DNA polymerase IV (7,16). Subsequent initiation of base-excision repair (BER) creates single-stranded DNA (ssDNA) gaps. In cases where BER is initiated at nearby sites, DSBs may be formed (7,15,16). Evidence for a second mechanism of ROS-dependent DSB formation has emerged from a recent mechanistic study of TLD in *Escherichia coli* (5,13). The ROS-driven potentiation of killing by both antibiotic treatment and TLD can be abrogated through the addition of ROS mitigators to the culture medium (1,5,12). For example, dimethyl sulfoxide (DMSO) and 2,2'-bipyridine (BiP), both, effectively mitigate the accumulation of antibiotic-induced ROS (5,17). Using microscopy to quantify ssDNA gaps and DSBs in cells undergoing TLD, Hong and co-workers discovered that thymine starvation initially leads to the accumulation of ssDNA gaps, which are subsequently converted to DSBs in an ROS-dependent process (5). In cells treated with ROS mitigators, gaps were not converted to DSBs and thymine starvation was largely abolished (5). For ciprofloxacin, a DNA gyrase inhibitor, a second, ROS-independent pathway exists in which gyrase-stabilized cleavage complexes dissociate, creating a DSB directly (9–11,18).

Several lines of evidence implicate pol IV in ROS-dependent DSB formation and processing. Pol IV efficiently incorporates 8-oxo-dGTP into DNA *in vitro* (7). Cells over-expressing pol IV exhibit ROS-dependent lethality (7,16,19). Similarly, cells lacking pol IV and pol V are partially protected against killing by ampicillin under conditions where ROS concentrations are increased (7). These observations suggest that pol IV promotes the formation of DBSs due to the BER-mediated removal of closely spaced 8-oxo-dGTPs incorporated by pol IV (16). Other studies indicate that pol IV has a role in the repair of DSBs (20,21,30,31,22–29): First, pol IV physically interacts with the RecA recombinase and RecA nucleoprotein filaments (RecA*); a key player in DSB repair (DSBR) (26,32). This interaction might facilitate pol IV to function in strand exchange (33). Second, fluorescently labelled pol IV colocalizes with RecA extensively at sites of induced DSBs when expressed from a low-copy plasmid (27). Similarly, in cells treated with ciprofloxacin, pol IV highly colocalizes with RecA* structures (32). Third, genetic studies reveal that the gene encoding pol IV, *dinB*, is required for both induced and spontaneous error-prone DSBR (20–25). Fourth, intermediates of DSBR known as recombination D-loops are efficiently utilized as substrates by pol IV *in vitro* (28,34).

Interestingly, the mutagenic potential of pol IV is modulated by UmuD and the recombinase RecA (26,29–31). UmuD induces error-free synthesis of pol IV (26), promoting long-lived association of pol IV with the DNA (32). Following UmuD cleavage, pol IV however operates error-prone (26) and pol IV association with DNA is inhibited (32). Furthermore, pol IV operates in an error-prone manner in recombination intermediates *in vitro* (29). Error-prone activity of pol IV in recombination intermediates might be induced due to the interaction of pol IV with RecA (26,29). Beyond this, RecA promotes DNA synthesis by pol IV in replisomes *in vitro* (30). In the presence of RecA, pol IV can also bypass alkylation lesions more efficiently (31). In addition, RecA nucleoprotein formation on single-stranded DNA is a major trigger for SOS induction and thus increased pol IV expression (35). For some antibiotics, it has however been shown that the SOS response is mostly triggered following DSB processing by RecBCD (36,37). Notably, upon induction of the SOS response, the cellular concentration of pol IV increases significantly (38,39). Despite these observations, it remains unclear if pol IV primarily works in recombination intermediates or in the context of replisomes in cells.

Here, we used single-molecule fluorescence microscopy to investigate whether ROS, and ROS-mediated DSBs, influence pol IV expression and association with the nucleoid in cells. We used two antibiotics which alter DNA replication and for which killing is known to involve ROS generation; ciprofloxacin and trimethoprim (5,12). We further showed that DSB resection is necessary for the formation of pol IV foci, even in cells expressing high concentrations of pol IV (constitutive SOS, *lexA51* mutants, here: *lexA*[Def] mutants), suggesting that pol IV mainly operates on recombination intermediates.

4.3 Results

4.3.1 ROS potentiate the expression levels and activity of pol IV

We set out to investigate the influence of antibiotic-induced ROS on pol IV activity by monitoring fluorescently-tagged single pol IV molecules in cells. Toward that objective, we first

compared pol IV expression levels and its dynamic behavior under normal conditions (no DMSO) and ROS-mitigating conditions (DMSO added) in response to antibiotic treatment. Cells were treated with i) ciprofloxacin alone, ii) ciprofloxacin and DMSO in combination, iii) trimethoprim alone or iv) trimethoprim and DMSO in combination (**Fig. 1**, *SI Appendix*, Fig. 1*A*).

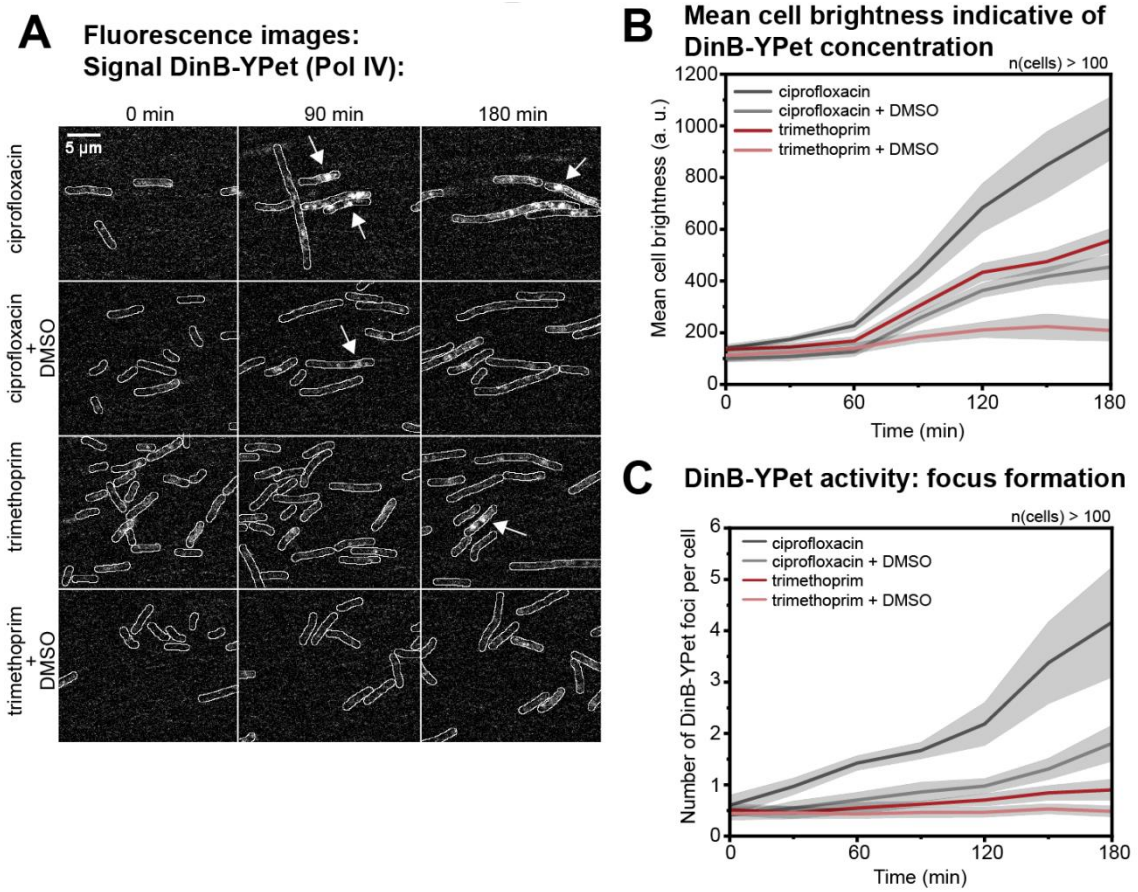

Figure 1. Pol IV concentration and activity following ciprofloxacin or trimethoprim treatment under normal conditions or ROS-mitigating conditions. (*A*) Fluorescence images showing cells expressing DinB-YPet (Pol IV) at 0, 90 and 180 min (left to right) after ciprofloxacin-alone, ciprofloxacin-DMSO, trimethoprim-alone or trimethoprim-DMSO treatment (top to bottom). Scale bar represents 5 µm. (*B*) Concentration of DinB-YPet during stress. Mean cell brightness is plotted against time (ciprofloxacin-alone: dark grey line, ciprofloxacin-DMSO: light grey line, trimethoprim-alone: magenta line, trimethoprim-DMSO: light magenta line). At each time-point, data are derived from >100 cells. Grey shaded error bands represent standard error of the mean. (*C*) Number of DinB-YPet foci per cell are plotted against time (ciprofloxacin-alone: dark grey line, ciprofloxacin-DMSO: light grey line, trimethoprim-alone: red line, trimethoprim-DMSO: light red line). At each time-point, data are derived from >100 cells. Grey shaded error bands represent standard error of the mean.

Prior to live-cell imaging, we first established that cells expressing fluorescent protein fusions of DinB, τ (replisome marker) and UmuC (component of DNA polymerase V, pol V) exhibited wild-type oxidative stress responses upon antibiotic treatment (ciprofloxacin or trimethoprim) administered either alone or along with the ROS mitigator (DMSO) (*SI Appendix*, Fig. 2). In the presence of ROS, *E. coli* cells induce the peroxide and/or superoxide stress responses in which expression of superoxide dismutase, alkyl hydroperoxidase and Fe^{3+} enterobactin transporter genes are upregulated (reviewed in (3,4,40–44)).

Therefore, we developed an assay to monitor expression of *gfp* from ROS-regulated and iron-responsive promoters in cells treated with ciprofloxacin, trimethoprim or hydrogen peroxide (as a control). We further tested if the addition of DMSO suppressed the accumulation of ROS (*SI Appendix*, Fig. 3, 4, 5). For this purpose, we constructed three plasmids that express GFP (fast-folding GFP, *sf-gfp* (45)) from the ROS-regulated promoters of *sodA* (notably regulated by superoxides/redox active compound *via* SoxRS and by the iron (Fe^{2+}) concentration via Fur (4,45), *SI Appendix*, Fig. 3*A*), *ahpC* (regulated by OxyR (4,42,43), *SI Appendix*, Fig. 4*A*) or *fepD* (regulated by Fur pathway; iron homeostasis (44), *SI Appendix*, Fig. 5*A*). Following hydrogen peroxide treatment, the addition of DMSO reduced the expression of the GFP reporter from the plasmid-based *sodA* and *fepD* promoters by 30% (30 mM hydrogen peroxide at t = 8 h, *SI Appendix*, Fig. 3*C*, 4*D*). This reduction in GFP signal is not due to DMSO quenching fluorescence (*SI Appendix*, Fig. 6). Increased expression from the *ahpC* promotor was delayed by ~3 h (30 and 100 mM hydrogen peroxide, *SI Appendix*, Fig. 4*D*). For ciprofloxacin-treated cells, the addition of DMSO reduced expression from the *fepD* promotor by 50% (5, 10, 20 and 40 ng/mL at t = 8 h, *SI Appendix*, Fig. 5*B*). For trimethoprim-treated cells, the addition of DMSO reduced the expression from the *ahpC* and *fepD* promotors by 50% (0.1 and 0.3 μg/mL at t = 8 h, *SI Appendix*, Fig. 4*B*, 5*B*). Together, these results indicate that (i) ciprofloxacin and trimethoprim generate ROS in cells (consistent with previous work (5,46)) and (ii) DMSO reduced the expression from ROS-sensitive promoters, following hydrogen peroxide, ciprofloxacin and trimethoprim treatment, implying that ROS levels were effectively reduced by the addition of DMSO.

Following antibiotic addition, we recorded time-lapse movies capturing fluorescence from *Escherichia coli* cells expressing a functional, YPet fusion of the DinB gene from its native promoter (*SI Appendix*, Fig. 1*B, C*, Materials and Methods) (39,47). We then monitored pol IV concentrations by measuring the fluorescence intensity of DinB-YPet within cells in the presence or absence of DMSO (2% v/v) and monitored DNA binding activities by counting the number of pol IV foci per cell. Treatment with ciprofloxacin resulted in cell filamentation accompanied by a clear increase in DinB-YPet intensity, indicating an increase in the intracellular DinB-YPet concentration (seven-fold increase from 140 to 990 DinB-YPet fluorescence, **Fig. 1*A***, ***B*****;** *SI Appendix*, Fig. 7). In a previous study (39), following ciprofloxacin treatment, cells exhibited a similar increase in DinB-YPet concentration; an increase in intracellular DinB-YPet (pol IV) concentrations was measured from 6 ± 1 nM prior to treatment (standard error of the mean, SE) to 34 ± 3 nM (SE) 180 min after ciprofloxacin addition. Interestingly, in this present study, we showed that inclusion of DMSO led to a significant reduction in the expression level of DinB-YPet in ciprofloxacin-treated cells. DMSO was added at the concentration previously tested (*SI Appendix*, Fig. 3, 4, 5). 180 min after ciprofloxacin addition in the presence of DMSO, cellular DinB-YPet intensities were only four-fold higher than basal levels (intensity increase from 100 to 454, **Fig. 1*A*, *B***). This final intensity corresponds to a concentration of DinB-YPet equalling 19 ± 2 nM (SE, see *Materials and Methods*), corresponding to a reduction of about 15 nM of ciprofloxacin-induced pol IV. Treatment with trimethoprim alone led to a significant increase in DinB-YPet fluorescence; 180 min after trimethoprim addition, the mean fluorescence intensity increased by more than four-fold (fluorescence intensity increase from 135 to 557, **Fig. 1*A*, *B***), corresponding to a final intracellular pol IV concentration of 23 ± 2 nM. Inclusion of DMSO led to a significant reduction in trimethoprim-induced pol IV up-

regulation; cellular DinB-YPet fluorescence intensities increased only slightly from 113 to 209, corresponding to a final pol IV concentration of 9 ± 2 nM. Thus, for both antibiotics, addition of DMSO resulted in a significant reduction in the steady state levels of pol IV in response to treatment.

Cells exhibit distinct pol IV foci when individual DinB-YPet molecules bind to DNA and thus experience decreased diffusional mobility (48). Since cells expressing fluorescently tagged catalytically dead pol IV molecules do not exhibit foci (39), the foci observed in response to antibiotic treatment represent pol IV molecules engaged in catalytic functions. Prior to the addition of ciprofloxacin, cells contained on average 0.6 ± 0.2 foci per cell (SE) in the absence of DMSO, and 0.4 ± 0.1 foci per cell in the presence of DMSO (**Fig. 1*C***). Following treatment with ciprofloxacin alone, the number of foci steadily increased. By 180 min, cells had 4.2 ± 1.1 foci per cell. Upon ciprofloxacin-DMSO treatment, cells contained 1.8 ± 0.4 foci per cell; a > 50% reduction compared to ciprofloxacin-alone measurements. Prior to the addition of trimethoprim, cells contained on average 0.5 ± 0.1 foci (SE) in the absence of DMSO and 0.4 ± 0.1 foci in the presence of DMSO. Trimethoprim-alone treatment induced a slight increase in the number of DinB-YPet foci with 0.9 ± 0.2 per cell (SE) at 180 min. This is lower than the number of foci observed for ciprofloxacin-DMSO treatment (1.8 ± 0.4 per cell), despite the measured pol IV concentration being marginally higher after trimethoprim-alone treatment (**Fig. 1*C***). Strikingly, cells treated with both trimethoprim and DMSO did not show any increase in DinB-YPet foci after trimethoprim addition (0.5 ± 0.1 foci per cell at 180 min; **Fig. 1*C***). Together, these results demonstrate that for cells treated with ciprofloxacin or trimethoprim, addition of DMSO supresses the drug-induced increases in DinB-YPet concentration, as well as the binding of pol IV to DNA, as evidenced by a reduction in the number of DinB-YPet foci. Importantly, the concentration of pol IV and its extent of DNA-binding are not directly correlated as the trimethoprim-alone and ciprofloxacin-DMSO treatments induced similar DinB-YPet concentrations, but different numbers of DinB-YPet foci.

4.3.2 ROS-induced double-strand breaks trigger the SOS response

Reasoning that the decreased induction of *dinB-YPet* expression in cells co-treated with DMSO likely resulted from attenuation of the SOS response, we repeated the time-lapse experiments (*SI Appendix*, Fig. 1*B, C*) on cells that carried an SOS-reporter plasmid, in which GFP is expressed from the SOS-inducible *sulA* promoter (pUA66 P_{sulA}-*gfp*; fast-folding GFP, *gfpmut2* (49)). In the absence of any antibiotic treatment, cells exhibit very low fluorescence intensity, consistent with the repression of the *sulA* promoter in the absence of exogenously applied DNA damage (**Fig. 2*A*,** '0 min'). SOS levels were similarly low for cells grown in the presence of DMSO. Cells exhibited robust SOS induction upon treatment with ciprofloxacin as evidenced by the increase in GFP fluorescence in the 180 min time window after addition of ciprofloxacin (170 fold induction, **Fig. 2*B***). Consistent with our hypothesis, SOS induction was strongly inhibited upon inclusion of DMSO during ciprofloxacin treatment (13 fold induction at 180 min; **Fig. 2*B***). A similar reduction in ROS and SOS levels has been observed in cells following co-administration of ciprofloxacin with another ROS mitigator, *N*-acetylcysteine (51). Cells exposed to trimethoprim exhibited a delay in SOS induction, however, even in this case, high levels of

SOS induction (100 fold induction) were supressed by the addition of DMSO (2 fold induction for combined treatment with trimethoprim and DMSO; **Fig. 2*B***). Notably, the addition of a different ROS mitigator, 2,2'-bipyridine (BiP, 0.35 mM, 0.5 x MIC (5)), similarly supressed the induction of the SOS response (**Fig. 2**). These results were also confirmed using plate-reader assays (*SI Appendix*, Fig. 8).

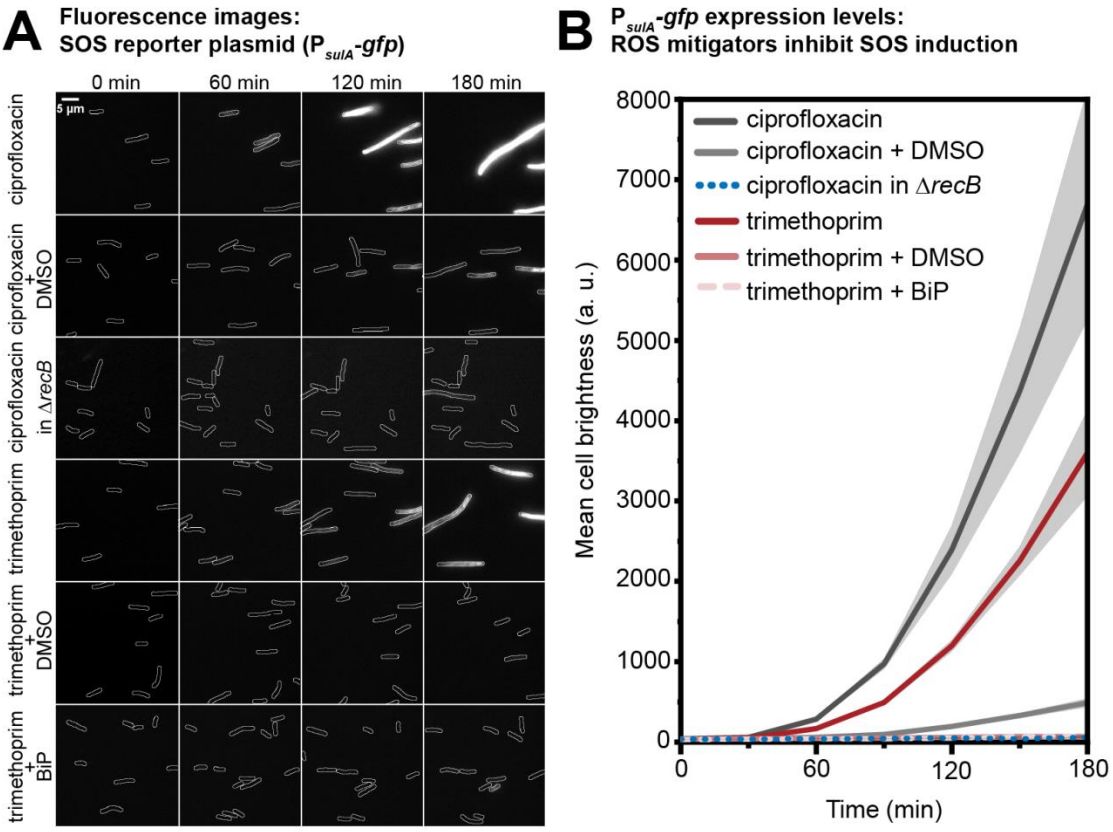

Figure 2. P_{sulA}-*gfp* expression levels (SOS response levels) following ciprofloxacin or trimethoprim treatment under normal or ROS-mitigating conditions in different genetic backgrounds. (*A*) Fluorescence images showing the expression of GFP from a SOS reporter plasmid (P_{sulA}-*gfp*) at 0, 60, 120 and 180 min (left to right) after ciprofloxacin-alone, ciprofloxacin-DMSO, ciprofloxacin-alone in Δ*recB*, trimethoprim-alone, trimethoprim-DMSO or trimethoprim-BiP treatment (top to bottom). Scale bar represents 5 µm. (*B*) GFP expression levels from the *sulA* promotor during stress. Mean cell intensity is plotted against time (ciprofloxacin-alone: dark grey line, ciprofloxacin-DMSO: light grey line, ciprofloxacin in Δ*recB*: purple, dotted line, trimethoprim-alone: red line, trimethoprim-DMSO: light red line, trimethoprim-BiP: rose-colored, dashed line). At each time-point, data are derived from >100 cells. Grey shaded error bands represent standard error of the mean.

We reasoned that the suppression of SOS by ROS mitigators might reflect a reduction in the formation and processing of DSBs. Cells lacking *recB* fail to induce SOS upon treatment with nalidixic acid, suggesting that end-resection products formed by RecBCD might be sites of SOS induction (36,37). Since ciprofloxacin and nalidixic acid both target DNA gyrase (9,11,51), we repeated the GFP reporter measurements in cells lacking *recB* (SSH111, Δ*recB* P_{sulA}-*gfp*) to determine if SOS induction by ciprofloxacin is also dependent on DSB processing. The deletion of *recB* strongly inhibited the SOS response following ciprofloxacin treatment (0.4 fold induction at 180 min in comparison to $recB^+$, **Fig. 2,**

SI Appendix, Fig. 9). While *recB* deletions are known to reduce survival in cells treated with ciprofloxacin (52), we observed that most cells lacking *recB* continued to grow and divide during the 180 min time-lapse measurement (*SI Appendix*, Fig. 7, 9), indicating that the lack of SOS induction observed for ciprofloxacin-treated *recB*-deficient cells did not stem from gross inhibition of all cellular functions. Plate reader assays did not reveal a sustained increase in cell mass for *recB* deletion cells following ciprofloxacin treatment (*SI Appendix*, Fig. 8*A*, last column), suggesting that the initial growth observed by microscopy stagnates soon after the 180 min observation window.

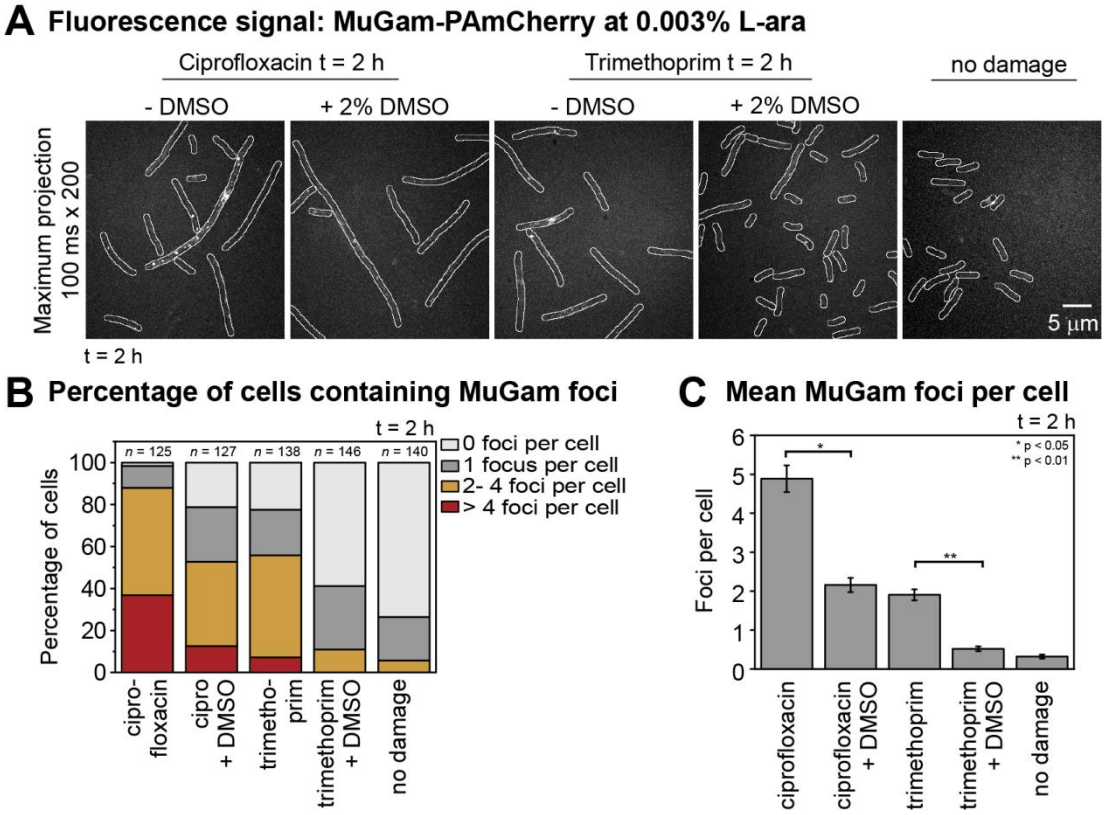

Figure 3. Number of MuGam-PAmCherry foci per cell following ciprofloxacin or trimethoprim treatment under normal conditions or ROS-mitigating conditions in different genetic backgrounds. (*A*) Fluorescence signal from MuGam-PAmCherry at 0.003% L-arabinose: Maximum projections over 100 ms x 200 frames showing MuGam-PAmCherry foci. From left to right: MuGam signal after 2 h treatment with ciprofloxacin, ciprofloxacin + DMSO, trimethoprim, trimethoprim + DMSO, no damage. (*B*) Percentage of cells containing MuGam foci: 0 foci (light grey), 1 focus (grey), 2-4 foci (amber) and > 4 foci (red). Cells were treated with ciprofloxacin (n = 125), ciprofloxacin + DMSO (n = 127), trimethoprim (n = 138), trimethoprim + DMSO (n = 146), or experienced no damage (n = 140). (*C*) Mean number of MuGam foci per cell. Cells were treated with ciprofloxacin (n = 125), ciprofloxacin + DMSO (n = 127), trimethoprim (n = 138), trimethoprim + DMSO (n = 146), or experienced no damage (n = 140). The error bars represent standard error of the mean over the number of cells. * for $p < 0.05$; ** for $p < 0.01$.

To more directly investigate if ROS create DSBs following ciprofloxacin and trimethoprim treatment, we imaged cells expressing a fluorescent fusion of the DSB reporter MuGam (53) to the photoactivatable mCherry protein (PAmCherry1 (54), *SI Appendix*, Fig. 1A, *C*). MuGam-PAmCherry

was expressed from a plasmid (**Fig. 3*A***). For these single-molecule microscopy experiments, expression of MuGam was induced using 0.003% L-arabinose at MuGam expression levels that had minimal effects on survival upon drug treatment (*SI Appendix*, Fig. 10). In the absence of antibiotic, cells exhibited 0.3 ± 0.1 MuGam foci per cell with 74% of cells containing no foci (**Fig. 3b, c**). Two hours after ciprofloxacin treatment, cells contained increased number of MuGam foci per cell (4.9 ± 0.3 foci with 1.6% of cells containing no foci, **Fig. 3*C***). Consistent with DMSO mitigating ROS, DMSO addition reduced the number of MuGam foci per cell (2.2 ± 0.2 foci with 21% of cells containing no foci, **Fig. 3*C***), indicating a significant contribution of ROS to the formation of DSBs during ciprofloxacin treatment. In agreement with a previous study (5), we observed that trimethoprim treatment generates DSBs (1.9 ± 0.1 MuGam foci with 22% of cells containing no foci, **Fig. 3*C***). These DSBs are ROS-induced as the addition of DMSO prevents the formation of these DSBs (0.5 ± 0.1 foci with 59% of cells containing no foci, **Fig. 3*C***). In contrast, in a recent study using sub-inhibitory concentrations of ciprofloxacin, reactive oxygen species do not induce additional DSBs (57).

Taken together our measurements indicate that antibiotic-induced ROS generate DSBs and potentiate the SOS response. Furthermore, SOS induction levels are dependent on *recB* DSB processing in cells treated with ciprofloxacin. Together the results are consistent with a model in which the SOS response is triggered or potentiated in antibiotic-treated cells via ROS-induced DSBs, leading to increased levels of pol IV in cells.

4.3.3 Double-strand break resection creates substrates for pol IV

Having established conditions under which ROS create a majority of DSBs in cells as well as binding sites for pol IV upon antibiotic treatment, we next set out to characterize pol IV behavior during DSBR in response to antibiotic treatment. To that end, we tested if pol IV primarily forms foci following DSB resection, suggestive of pol IV having a major role in DSBR. Therefore, we examined the extent of DinB-YPet focus formation in ciprofloxacin and trimethoprim treated cells, comparing backgrounds that permitted (*recB*$^{+}$) or prevented (Δ*recB*) DSB processing. Additionally, we monitored the formation of DinB-YPet foci while using DMSO to modulate the number of antibiotic-induced DSBs (**Fig. 3**). To separate effects on focus formation from effects on DinB-YPet expression, these measurements were carried out in a *lexA*(Def) background (56) (*dinB-YPet dnaX-mKate2 lexA*[Def]). These cells constitutively express DinB-YPet at levels consistent with SOS induced levels, even in the absence of DNA damage (39). To capture DinB-YPet binding events on the time-scale of seconds, we recorded burst acquisitions of the DinB-YPet signal (300 x 50 ms exposures taken every 100 ms, *SI Appendix*, Fig. 1*A*, *D*).

Consistent with the results from our previous study (39), close to zero DinB-YPet foci were observed in *lexA*(Def) cells in the absence of antibiotic (0.08 ± 0.05 foci per cell, **Fig. 4**). In contrast, *lexA*(Def) cells treated with ciprofloxacin for 60 min exhibited clear foci (1.83 ± 0.15 foci per cell, **Fig. 4*B, C***). Co-treatment with ciprofloxacin and DMSO yielded fewer foci (1.02 ± 0.13 foci per cell, **Fig. 4 *B, C***). The deletion of *recB* resulted in a striking loss of DinB-YPet foci (0.23 ± 0.05 foci per cell, **Fig. 4 *B, C***). *lexA*(Def) cells treated with trimethoprim for 60 min contained multiple DinB-YPet foci (2.6 ±

0.18 foci per cell), whereas cells treated with both trimethoprim and DMSO contained few foci (0.19 ± 0.06). Trimethoprim-treated Δ*recB* cells also contained very few foci (0.14 ± 0.05). Similar effects were observed in *lexA*$^{+}$ cells, although reductions in focus formation were conflated with reductions in DinB-YPet expression levels (**Fig. 1*C***). Taken together these results demonstrate that pol IV is normally active at ROS-induced, RecBCD-processed DSBs in cells treated with ciprofloxacin or trimethoprim. Consistent with this, we have demonstrated that pol IV co-localizes with RecA* features in cells treated with ciprofloxacin (32).

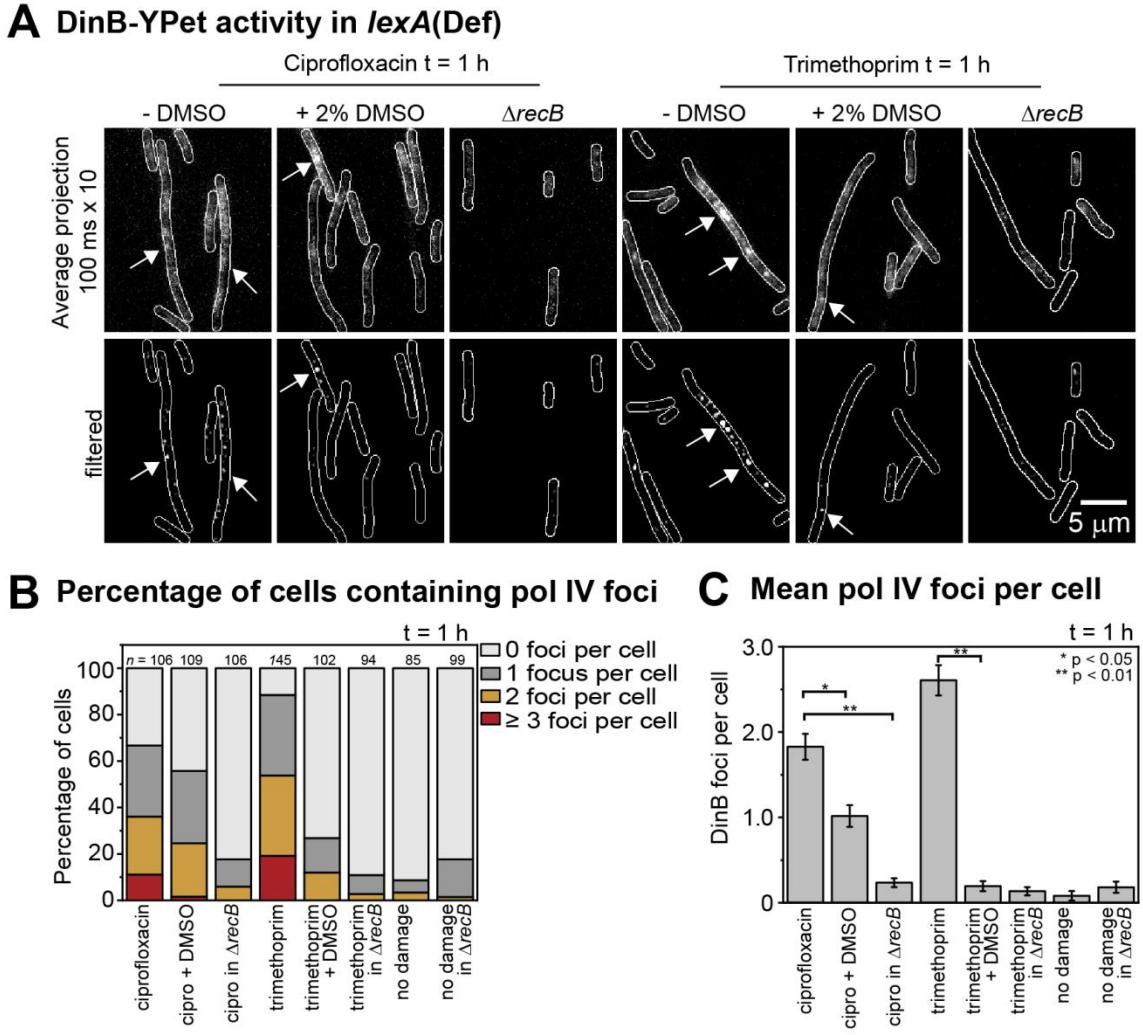

Figure 4. Number of pol IV foci per cell in *lexA*(Def) cells following ciprofloxacin or trimethoprim treatment under normal conditions or ROS-mitigating conditions. (*A*) Upper row: Average projection in time (100 ms x 10 frames) showing DinB-YPet (pol IV) foci. Bottom row: Discoidal filtered projections. Cells were treated for 60 min prior to imaging. (*B*) Percentage of cells containing pol IV foci: 0 foci (light grey), 1 focus (grey), 2 foci (amber) and ≥ 3 foci (red). Cells were treated with ciprofloxacin (*n* = 106), ciprofloxacin + DMSO (*n* = 109), ciprofloxacin in Δ*recB* (*n* = 106), trimethoprim (*n* = 145), trimethoprim + DMSO (*n* = 102), trimethoprim in Δ*recB* (*n* = 94) experienced no damage for wild-type (*n* = 85) and Δ*recB* (*n* = 99). (*C*) Number of DinB-YPet foci per cell. Error bars represent standard error of the mean. Number of cells included in analysis: *n*(ciprofloxacin) = 106, *n*(ciprofloxacin-DMSO) = 109, *n*(ciprofloxacin in Δ*recB*) = 106, *n*(trimethoprim) = 145, *n*(trimethoprim-DMSO) = 102, *n*(trimethoprim in Δ*recB*) = 94, *n*(untreated *recB*$^{+}$) = 85, *n*(untreated Δ*recB*) = 99. * for p < 0.05; ** for p < 0.01.

In a previous study (39), we showed that pol IV primarily forms foci away from replisomes, indicating that pol IV has a minor role in facilitating replication restart of stalled replisomes. To investigate if these non-replisomal pol IV foci are ROS-induced, we next determined the percentage of DinB-YPet foci that form in the vicinity of replisomes (fluorescent protein fusion of the pol III τ-subunit, τ -mKate2). For each experiment, when recording the DinB-YPet signal in *recB*$^{+}$ cells, we also recorded the position of τ -mKate2 as in the previous study (39). Ciprofloxacin treatment, which rapidly halts DNA synthesis (57,58), causes 10% of pol IV foci to bind near replisomes (39). Here we observed that the inclusion of DMSO dramatically increased the relative colocalization of DinB-YPet with replisomes in both *lexA*$^{+}$ and *lexA*(Def) cells treated with ciprofloxacin (*SI Appendix*, Fig. 11, 12). For long-lived pol IV foci (detectable within a 10 s average projection image, **Fig. 5*B***, right panel) in the *lexA*(Def) background, 80% of foci colocalized with replisomes under ciprofloxacin-DMSO conditions (**Fig. 5*B***). This is consistent with the addition of DMSO having removed the vast majority of non-replisomal substrates for pol IV-dependent DNA synthesis. This observation appears to be consistent with a recent proposal that ROS-mitigation reduces rates of pol IV-dependent mutagenesis (55). For *lexA*(Def) cells treated with trimethoprim, addition of DMSO abolished long-lived pol IV foci entirely (**Fig. 5*A, C***).

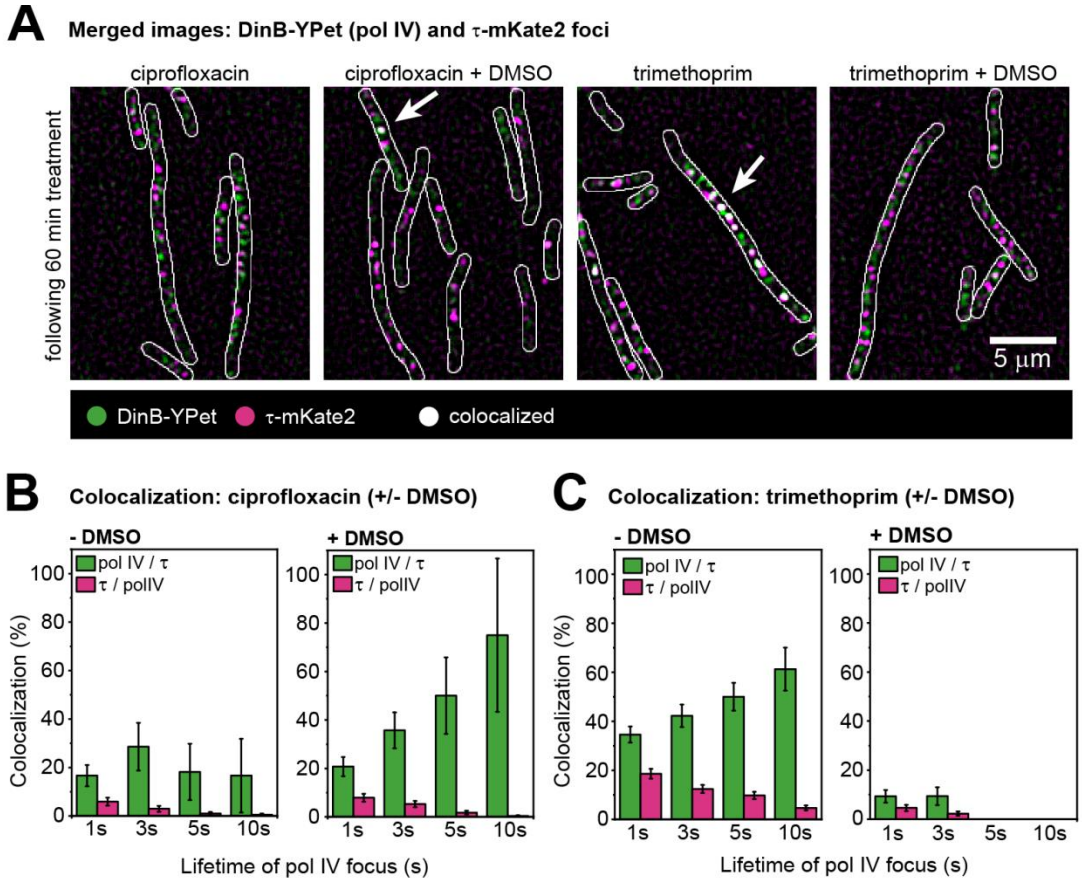

Figure 5. Measuring the colocalization of pol IV and replisomes following ciprofloxacin or trimethoprim treatment ± DMSO in *lexA*(Def) cells. (*A*) DinB-YPet activity at replisomes in *lexA*(Def) cells. Cells were treated for 60 min prior to imaging. Merged images showing DinB-YPet foci in green and τ-mKate2 foci in magenta following ciprofloxacin-alone (*n* = 106), ciprofloxacin-DMSO (*n* = 109), trimethoprim-alone (*n* = 145) and trimethoprim-DMSO (*n* = 102) treatment (from left to right). White arrow points at colocalization event (white focus). Data were collected over three biologically independent experiments.

Scale bar represents 5 μm. (*B*) Colocalization percentages of pol IV foci that bind at replisomes (green bars) and colocalization percentages of replisomes that contain a pol IV focus (magenta bars) for cells treated with ciprofloxacin-alone (left) or ciprofloxacin-DMSO (right). Colocalization was measured with sets of pol IV foci that last 1, 3, 5 and 10 s. Error bars represent the standard error of the mean. (*C*) Colocalization percentages of pol IV foci that bind at replisomes (green bars) and colocalization percentages of replisomes that contain a pol IV focus (magenta bars) for cells treated with trimethoprim-alone (left) or trimehtoprim-DMSO (right). Colocalization was measured with sets of pol IV foci that last 1, 3, 5 and 10 s. Error bars represent the standard error of the mean.

4.3.4 ROS do not promote pol V activity

Finally, we explored if ROS-induced DSBs promote a change in the binding activity of the other major error-prone polymerase pol V ($UmuD'_2C$) in real time (59). Since pol V is also a member of the SOS regulon (35), we use a *lexA*(Def) background (RW1286, *umuC-mKate2 dnaX-YPet lexA*[Def]) to separate effects on focus formation from effects on UmuC-mKate2 expression.

UmuC foci might form at two stages during the activation of pol V Mut at RecA* filaments and when active pol V Mut complexes synthesize DNA. As before, *lexA*(Def) cells were treated for 60 min with ciprofloxacin-alone, ciprofloxacin-DMSO, trimethoprim-alone or trimethoprim-DMSO (*SI Appendix*, Fig. 1*A*). Burst acquisitions of the UmuC-mKate2 signal were recorded (*SI Appendix*, Fig. 1*D*, 300 x 50 ms exposures taken every 100 ms).

Few UmuC-mKate2 foci were observed in the absence of antibiotic in *lexA*(Def) cells (about 0.32 ± 0.08 foci per cell, *SI Appendix*, Fig. 12). In *lexA*(Def) cells treated with ciprofloxacin or trimethoprim for 60 min, foci were clearly visible (ciprofloxacin: 1.24 ± 0.16 foci per cell; trimethoprim 1.39 ± 0.21 foci per cell). In both cases, co-treatment with DMSO had little effect on the number of UmuC-mKate2 foci (ciprofloxacin-DMSO: 0.99 ± 0.12 foci per cell; trimethoprim-DMSO 1.26 ± 0.16 foci per cell) or on the overall levels of UmuC-mKate2 fluorescence in the cells. Thus in contrast to the effects observed for pol IV, the addition of DMSO had little effect on the formation of UmuC foci. Interestingly, in $lexA^+$ cells, which express SOS normally, trimethoprim treatment (with or without DMSO) did not lead to the formation of pol V (*SI Appendix*, Fig. 13*A*, *C*). Consistent with this, cleavage of UmuD to UmuD′ was far less efficient in trimethoprim-treated cells than in ciprofloxacin-treated cells (compare *SI Appendix*, Fig. 14*B*, *D*). This suggests that RecA* structures that induce SOS (i.e. increase in the expression levels of SulA and pol IV) may be different from those that mediate the formation of pol V through UmuD cleavage. This result is discussed further below and warrants further investigation.

4.4 Discussion

4.4.1 ROS-mediated DSBs induce high intracellular concentrations of pol IV

We observed that ROS mitigators reduced levels of SOS induction, and thus, pol IV concentrations, adding to a growing body of evidence linking ROS and mutational resistance to antibiotics (14,50,60,61). ROS mitigators reduced the number of MuGam foci per cell, indicative of fewer DSBs being formed. ROS accumulation is a major trigger for SOS induction in trimethoprim treated cells and is mediated through RecBCD-dependent resection of ROS-induced DSBs. When a ROS mitigator is

including during treatment, the SOS response is not induced even though ssDNA regions are likely to be generated by trimethoprim-induced TLD (5,62,63). Thus, the formation of double-strand breaks is essential for SOS induction in trimethoprim-treated cells. During thymine starvation, ssDNA regions are converted to DSB due to ROS activity (5). Our results indicate that a similar pathway is at play in trimethoprim-treated cells as previously proposed (5).

In ciprofloxacin-treated cells, the deletion of *recB* almost fully inhibited the SOS response. Ciprofloxacin and nalidixic acid both target DNA gyrase (9,11,52). It was previously observed that induction of SOS by the antibiotic nalidixic acid was completely blocked in cells that carried a *recB* mutation and were therefore incapable of processing DSBs through the RecBCD end-resection nuclease complex (36,37). This implies that SOS induction is also primarily triggered by DSB processing in nalidixic acid-treated cells. Consistent with this result, we showed here that the SOS response in ciprofloxacin-treated cells is *recB*-dependent, consistent with a requirement for DSB processing. Cells lacking *recB* still exhibit very low levels of SOS induction, which could arise from RecA structures assembled on ssDNA regions or by alternative DSB end-resection pathways, for instance *via* a RecJ-dependent pathway proposed previously (64,65)

Our findings raise the question of whether ssDNA gaps truly represent the major source of SOS induction in *E. coli*. Under our conditions, DSB processing – most often induced by ROS – acts as the major trigger of the SOS response. The results presented here highlight a need that further studies are necessary to fully understand the regulation of the SOS response, in particular the role RecA* structures formed on ssDNA gaps versus DSBs (54,66–68). The observation by Hong *et al*. that ssDNA gaps are converted to DSBs under conditions of thymine starvation (5), highlights ROS-dependent gap-to-break conversion as a potential complicating factor in studies that seek to differentiate events that take place at gaps from those that take place at breaks.

4.4.2 DSB processing is critical for the formation of pol IV foci

We showed that the processing of ROS-induced DSBs promotes DinB-YPet focus formation. The observations are consistent with a model in which ROS-induced DSBs promote pol IV activity by inducing the SOS response and by generating substrates for pol IV in the form of recombination intermediates.

Few DinB-YPet foci were observed in cells treated with a combination of trimethoprim and DMSO. Based on events that occur during the analogous process of TLD (5,62), treatment with trimethoprim should induce the formation of ssDNA gaps in the wake of the replisome. In the presence of ROS these would be rapidly converted to DSBs, whereas under ROS mitigated conditions the gaps would persist. The low extent of focus formation observed under trimethoprim-DMSO conditions implies that pol IV rarely acts at these ssDNA gaps.

Following ciprofloxacin treatment, cells exhibited reduced numbers of DinB foci under low ROS conditions. However, ciprofloxacin also induces the formation of end-stabilized DNA-gyrase complexes, which halt DNA synthesis, slowing down cell growth (57,58). When deleting *recB*, and thus blocking DSB resection at both ROS-induced and ROS-independent DSBs, cells exhibited a very low number of

DinB foci, equivalent to numbers present in the absence of damage. Moreover, the colocalization of DinB-YPet with replisomes was substantially increased in the presence of DMSO. It is possible that replisome-proximal DinB-YPet foci, that are insensitive to ROS, reflect pol IV molecules that are recruited to replisomes that have stalled at end-stabilized DNA-gyrase complexes.

4.4.3 Pol V is not activated by ROS-induced damage

In contrast to the observations made for pol IV, mitigation of ROS produces only a marginal effect on pol V levels in ciprofloxacin-treated cells. Pol V levels barely increase following trimethoprim treatment. Thus unlike pol IV, the repair of ROS-induced DSBs does not directly lead to increased levels of pol V. One possibility is that the mechanisms of SOS induction are different during trimethoprim and ciprofloxacin treatments, with the RecA* structures formed during trimethoprim treatment being insufficient for the up-regulation of pol V. A second and perhaps more likely possibility is that the RecA* structures that trigger LexA cleavage (and thus SOS induction) are different from those that trigger UmuD cleavage (and thus pol V activation). In this scenario, ciprofloxacin treatment may produce both types of RecA* structure, whereas trimethoprim induces only the form competent for SOS induction. In this case, poor cleavage of UmuD would be expected to prevent the accumulation of UmuC due a previously identified system of targeted proteolysis, which limits UmuC accumulation in the absence of $UmuD'_2$ (69).

Interestingly, the formation of pol V foci was not affected by adding DMSO to supress DSB formation. This implies that DSBR intermediates are not major substrates for pol V in ciprofloxacin- or trimethoprim-treated cells. In a previous study, we observed that pol V rarely colocalizes with replisomes (48). Together our observations hint at a potential division of labor between pols IV and V, with pol IV often acting at DSBR intermediates and pol V acting at other, as yet unidentified structures, which may include ssDNA gaps or daughter strand gap repair intermediates.

4.5 Materials and Methods

4.5.1 Strain construction

EAW102 is *E. coli* K-12 MG1655 Δ*recB* and was constructed using λ_{RED} recombination. The kanamycin resistance marker in EAW102 was removed via FLP-FRT recombination (70) using the plasmid pLH29 to obtain kanamycin sensitive HG356.

SSH091, SSH111 and MEC030 (*dinB*$^+$ *lexA*$^+$ *recB*$^+$ + pUA66-*sulA*-gfp, *dinB*$^+$ *lexA*$^+$ Δ*recB::FRT* + pUA66-*sulA*-gfp and *recA730 sulA*$^-$ + pUA66-*sulA*-gfp) were created by transforming MG1655, EAW102 and EAW287 with pUA66-*sulA*-gfp (49).

RW1286 is *E. coli* MG1655 *umuC-mKate2 dnaX-YPet sulA*$^-$::kan^R *lexA51*(Def)::Cm^R and was made in two steps: first the wild-type *sulA*+ gene of EAW282 was replaced with *sulA*$^-$::kan by P1 transduction from EAW13 (47), to create EAW282 *sulA*$^-$; then *lexA51*(Def) *malB*::Tn*9* was transferred

from DE406 (71) into EAW282 *sulA*$^-$ by P1 transduction, selecting for chloramphenicol resistance. To confirm the presence of the *lexA*(Def) genotype, colonies were then screened for high levels of RecA expression by Western blotting with anti-RecA antibodies (72).

EAW1144 is *E. coli* K-12 MG1655 *dinB-YPet dnaX-mKate2 sulA*$^-$ *lexA51*(Def) Δ*recB* and was constructed in three steps: *sulA*$^-$ FRT-Kan-FRT was P1 transduced in EAW643 (KanS) using a P1 lysate grown on EAW13 to obtain the strain EAW1134. The Kan cassette was removed using pLH29 (70). Then, *lexA51*(Def) *malB*::Tn*9* was transduced into EAW1134 using a P1 lysate grown on DE406 to obtain the strain EAW1141. Finally, Δ*recB* FRT-KanR-FRT was transduced into EAW1141using P1 lysate grown on EAW102 to obtain EAW1144. All mutations introduced were confirmed by PCR.

The pBAD-*MuGam* vector (pEAW1159) was constructed using a PCR-amplified *muGam* gene fragment (us=GGATATCCATATGGCTAAACCAGCAAAACGTA consisting of a NdeI site and the beginning of the *muGam* gene, and MuGam ds= GCGAATTCTTAAATACCGGCTTCCTGTTCA consisting of an *Eco*RI site and the end of the *muGam* gene) from EAW727 (MG1655 Founder (73) Δe14 with chromosomal *muGam-gfp* in the *att*Tn*7* site). EAW727 was constructed by transducing *muGam-gfp* into Founder Δe14 using a P1 lysate grown on SMR14350 (54). The PCR product was digested with *Nde*I and *Eco*RI and inserted into pBAD *Nde*I which was cut with the same enzymes. pBAD *Nde*I is pBAD/Myc-HisA (Invitrogen) that has been mutated to add a *Nde*I site in place of the original *Nco*I site. All other *Nde*I sites were filled in before the mutagenesis. The resulting plasmid was directly sequenced to confirm presence of wt *muGam* gene

The pBAD-*MuGam-PAmCherry* vector (pEAW1162) was constructed by using two PCR fragments: 1. *Nde*I-MuGam-linker-*Eco*RI generated from pEAW1159 using the following PCR primers: MuGam us=GGATATCCATATGGCTAAACCAGCAAAACGTA consisting of a *Nde*I site and the beginning of the *muGam* gene, and MuGam ds no stop link= GGATATCGAATTCGCCAGAACCAGCAGCGGAGCCAGCGGAAATACCGGCTTCCTGTTCAAA TG consisting of an *Eco*RI site, an 11aa linker, and the end of the *muGam* gene without a stop codon. The PCR product was digested with *Nde*I and *Eco*RI. 2. *Eco*RI-PAmCherry-*Hind*III generated from pBAD-*PAmCherry-mCI* (54) using the following PCR primers PAmCherry usEco = GGATATCGAATTCATGGTGAGCAAGGGCGAGGAG consisting of an *Eco*RI site and the beginning of mCherry, and PAmCherry dsHind= GGATATCAAGCTTTTACTTGTACAGCTCGTCCAT consisting of a *Hind*III site and the end of the *mCherry* gene. The PCR product was digested with *Eco*RI and *Hind*III. Both PCR products were ligated to pBAD *Nde*I that had been digested with *Nde*I and *Hind*III. The resulting plasmid was directly sequenced to confirm the presence of *muGam-PAmCherry.*

Table 1. Strains used in this study.

Strain	Relevant Genotype	Parent strain	Source/technique
MG1655	*dinB*$^+$ *dnaX*$^+$ *recB*$^+$ *lexA*$^+$	-	published (74)
EAW102	Δ*recB*::Kan^R	MG1655	Lambda Red recombination
HG356	Δ*recB*::FRT	MG1655	EAW102
SSH091	*dinB*$^+$ *lexA*$^+$ *recB*$^+$ + pUA66-*sulA*-gfp	MG1655	Transformation of MG1655 with pUA66-P$_{sulA}$-*gfp* (49)

SSH111	*dinB*$^+$ *lexA*$^+$ Δ*recB*::FRT + pUA66-P$_{sulA}$-*gfp*	HG356	Transformation of HG356 with pUA66-P$_{sulA}$-*gfp* (49)
EAW18	Δ*dinB*::Kan^R	MG1655	published (39)
RW120	*recA*$^+$ *sulA*$^-$ *lexA*$^+$ Δ*umuDC*::Cm^R	RW118	published (75)
RW546	*recA*+ *sulA*$^-$ *lexA51*(Def) Δ*umuDC*::Cm^R	RW542	published (76)
RW880	Δ*umuDC*::Cm^R	MG1655	Transduction of MG1655 with P1 grown on RW120 (75)
JJC5945	*dnaX-YPet*::Kan^R	MG1655	published (47)
EAW642	*dnaX-mKate2*::Kan^R	MG1655	published (39)
EAW633	*dinB-YPet*::Kan^R	MG1655	published (39)
EAW643	*dinB-YPet*::FRT *dnaX-mKate2*::Kan^R	EAW633	published (39)
EAW191	*umuC-mKate2*::Kan^R	MG1655	published (47)
EAW282	*umuC-mKate2*::FRT *dnaX-YPet*::Kan^R	JJC5945	published (47)
EAW13	*sulA*$^-$::Kan^R	MG1655	published (47)
EAW282 *sulA*$^-$	*umuC-mKate2*::FRT *dnaX-YPet*::FRT *sulA*$^-$::Kan^R	EAW282	Transduction of EAW282 with P1 grown on EAW13 (47)
RW1286	*umuC-mKate2*::FRT *dnaX-YPet*::FRT *sulA*$^-$::Kan^R *lexA51*(Def)::Cm^R	EAW282 *sulA*$^-$	Transduction of EAW282 *sulA*$^-$ with P1 grown on DE406 (71)
RW1594	*dinB-YPet dnaX-mKate2 sulA*$^-$::Kan^R *lexA51*(Def)::Cm^R	RW1588	published (39)
EAW1134	*dinB-YPet*::FRT *dnaX-mKate2*::FRT *sulA*$^-$::Kan^R	EAW643	Transduction of EAW643 with P1 grown on EAW13
EAW1141	*dinB-YPet*::FRT *dnaX-mKate2*::FRT *sulA*$^-$::FRT *lexA51*(Def)::Cm^R	EAW1134	Transduction of EAW1134 with P1 grown on DE406 (71)
EAW1144	*dinB-YPet*::FRT *dnaX-mKate2*::FRT *sulA*$^-$::FRT *lexA51*(Def)::Cm^R Δ*recB*::Kan^R	EAW1141	Transduction of EAW1141 with P1 grown on EAW102
EAW287	*recA730 sulA*$^-$::FRT	MG1655	published (47)
MEC030	*recA730 sulA*$^-$ + pUA66-P$_{sulA}$-*gfp*	EAW287 Kan^S	Transformation of EAW287 with pUA66-P$_{sulA}$-*gfp* (50)
MG1655 + pEAW1162	pBAD-MuGam-PAmCherry	MG1655	Transformation of MG1655 with pBAD-MuGam-PAmCherry
MG1655 + pSTB-*sodA-gfp*	P$_{sodA}$-*sf-gfp*	MG1655	Transformation of MG1655 with pSTB-*sodA-gfp*
MG1655 + pCJH0008	P$_{ahpC}$-*sf-gfp*	MG1655	Transformation of MG1655 with pQCJH0008
MG1655 + pCJH0009	P$_{fepD}$-*sf-gfp*	MG1655	Transformation of MG1655 with pCJH0009

4.5.2 ROS reporter fusions construction

Three promoters of genes regulated by changes in ROS or iron levels were cloned and fused to the *sf-gfp* gene (45) into a pQBI63 plasmid (Qbiogene). Briefly, upstream regions of *sodA* gene (consisting of the 284 nt intergenic region of *rhaT* and *sodA*) regulated by *soxS* and Fur (4,41), or *ahpC* gene (- 372 to -1 nt of ATG) regulated by OxyR (4,42,43), or *fepD* gene (-170 to -1 nt of ATG) regulated by Fur (44), were amplified and cloned into the pQBI63 plasmid using *Bgl*II/*Nhe*I restriction enzyme to generate respectively pSTB-*sodA-gfp*, pCJH0008 and pCJH0009. All constructions were confirmed by sequencing.

4.5.3 DNA damaging agent sensitivity assay

Cells were grown in EZ glucose medium overnight at 37ºC. The next day, a dilution 1/1000 of each culture was grown in EZ glucose (at 37ºC, 150 rpm) until reaching mid log phase (OD_{600} = 0.3). Six aliquots of 300 µL of each culture were transferred in 24 microplates. The first aliquot was used as control of no treatment, 2% DMSO (282 mM, 0.2 x MIC (5)), 30 ng/mL ciprofloxacin, 30 ng/mL ciprofloxacin + 2% DMSO, 1 µg/mL trimethoprim or 1 µg/mL trimethoprim + 2% DMSO were added in the others. Samples of 150 uL were taken at 0 and 60 min; samples at 0 h were taken just before treatment. Each sample was serial diluted in PBS by factor ten down to 10^{-6} and dilutions 10^{-1} to 10^{-6} were spotted on fresh LB plates (Difco brand). Plates were incubated overnight at 37ºC in the dark.

4.5.4 Survival assay following MuGam-PAmCherry expression

To test the effect of MuGam-PAmCherry expression levels on lethality following ciprofloxacin and trimethoprim exposure, seven cells cultures were set up, expressing different levels of MuGam-PAmCherry from a pBAD plasmid. Cells cultures 1-7 (each 1 mL) were grown in EZ glycerol medium in the presence of ampicillin (100 µg/mL) and different L-arabinose concentrations (0, 0.001, 0.003, 0.01, 0.03, 0.1%) and cell culture 8 (1 mL) was grown EZ glucose medium in the presence of ampicillin (100 µg/mL) in overnight at 37ºC, 950 rpm. The next day, a 10/1000 dilution of each culture (final volume of 1.5 mL) was grown under the same conditions as over-night growth for 3 h. Each culture was split in three and no drug, 30 ng/mL ciprofloxacin or 1 µg/mL trimethoprim was added. These cultures were grown (at 37ºC, 950 rpm) for 2 h. Then, cultures were spin down (5 min; 5,000 g) and cell pellets were resuspended in 0.5 mL corresponding EZ medium; centrifugation and resuspension was carried out three times. Each cell culture was serial diluted in PBS by factor ten down to 10^{-5} and dilutions 10^{-1} to 10^{-5} were spotted on fresh LB plates containing 100 µg/mL ampicillin (Difco brand). Plates were incubated overnight at 37ºC in the dark. For each condition, biological triplicates were performed. From these experiments, an L-arabinose concentration of 0.003% was chosen for fluorescence microscopy experiments because this L-arabinose concentration showed no drastic decrease in survival compared to the sample grown in the presence of glucose.

4.5.5 Plate reader assay

Cells were grown in EZ glucose medium overnight at 37ºC. The next day, a dilution 10/1000 of each culture was grown in EZ glucose (at 37ºC, 950 rpm) for 3 h. These cultures were diluted to 1/200. Then, 10 µL of these diluted cultures were added to a total volume of 200 µL medium in each well of a 96-well plate. These 200 µL of media contained antibiotic, or hydrogen peroxide, and/or ROS mitigators (final concentration: 5, 10, 20 and 40 ng/mL ± 2% DMSO or ± 0.35 mM BiP; 0.1, 0.3, 1 and 3 µg/mL ± 2% DMSO or ± 0.35 mM BiP; 30, 100, 300 and 500 mM hydrogen peroxide [H_2O_2] ± 2% DMSO). For experiments with antibiotics and/or ROS mitigators, antibiotics and/or ROS mitigators were added just before cells were added. For experiments with hydrogen peroxide, hydrogen peroxide was added subsequently after cells were added. For each well, absorbance (OD_{600}) is measured every 30 min over 17 h or 18 h. The fluorescence signal was measured at each time point ($\lambda_{excitation}$ = 470 ± 15 nm, $\lambda_{emission}$ = 515 ± 20 nm). For cells carrying P*sulA*-gfp, experiments were carried out in 96-well plates from Nalge Nunc International (no. 265301). For cells carrying P*sodA*-sf-gfp, P*ahpC*-sf-gfp or P*fepD*-sf-gfp, experiments were carried out in 96-well plates from Thermo Scientific (no. 165305). The experiments were carried out using the CLARIOstar plate reader (BMG Labtech; settings: orbital reading 4 mm (for 96-well plates from Nalge Nunc International) or 2 mm (for 96-well plates from Thermo Scientific), orbital shaking at 200 rpm, at 37 ºC).

Cell cultures were also serial diluted and plated on LB agar plates in order to calculate the number of cells added to each well. To each well, when adding wild-type cells, 10^5 – 10^6 cells were added at the beginning of the experiment. For experiments when adding Δ*recB* cells, 10^5 cells were added at the beginning of the experiment.

4.5.6 Fluorescence microscopy

For all experiments except for experiments including imaging of MuGam-PAmCherry (**Fig. 3**), wide-field fluorescence imaging was conducted on an inverted microscope (IX-81, Olympus with a 1.49 NA 100x objective) in an epifluorescence configuration (47). Continuous excitation is provided using semidiode lasers (Sapphire LP, Coherent) of the wavelength 514 nm (150 mW max. output) and 568 nm (200 mW max. output). τ-mKate2 in EAW643 and UmuC-mKate2 in EAW282 were imaged using yellow excitation light (λ = 568 nm) at high intensity (2750 Wcm^{-2}), collecting emitted light between 610–680 nm (ET 645/75m filter, Chroma) on a 512 × 512 pixel EM-CCD camera (C9100-13, Hamamatsu). Images of UmuC-mKate2 in RW1286 were recorded at 275 Wcm^{-2}. For DinB-YPet imaging of EAW643, we used green excitation (λ = 514 nm) at 160 Wcm^{-2} collecting light emitted between 525–555 nm (ET540/30m filter, Chroma). For DinB-YPet imaging of RW1594, cells were imaged at 51 Wcm^{-2}. τ-YPet imaging (EAW282, RW1286) was performed at 51 Wcm^{-2}. Cells carrying the SOS reporter plasmid pUA66-*sulA*-gfp (SSH091, SSH111) were imaged at 16 Wcm^{-2}.

For experiments including imaging of MuGam-PAmCherry (**Fig. 3**), imaging was conducted on an inverted microscope (Nikon Eclipse-Ti), equipped with a 1.49 NA 100× objective and a 512 × 512 $pixel^2$ Photometrics Evolve CCD camera (Photometrics, Arizona, US). NIS-Elements equipped with JOBS module was used to operate the microscope (Nikon, Japan). Continuous excitation is provided

using semidiode lasers of the wavelength 405 nm (OBIS, Coherent, 200 mW max. output) and 568 nm (Sapphire LP, Coherent, 200 mW max. output). MuGam-PAmCherry was imaged by simultaneous illumination with the activation laser 405 nm (1–5 W cm^{-2}) and 568 nm readout laser (540 W cm^{-2}), a PALM (photoactivation localization microscopy) acquisition protocol, collecting emitted light from 590 nm (ET590LP, Chroma).

Two-color time-lapse movies were recorded to visualize if DinB-YPet foci overlap with τ-mKate2 foci (EAW643). Sets of three images were recorded (bright-field [34 ms exposure], mKate2 fluorescence [100 ms exposure], YPet fluorescence [50 ms exposure]) at an interval of 10 min for 3 h. To measure colocalization between UmuC-mKate2 with the replisome marker τ-YPet (EAW282), we recorded time-lapse movies at the same intervals but different exposures for the replisome marker (bright-field [34 ms exposure], mKate2 fluorescence [100 ms exposure], YPet fluorescence [500 ms exposure]).

Burst acquisitions of DinB-YPet (movies of 300 × 50 ms frames taken every 100 ms light at 514 nm) were collected, subsequently to each burst acquisition, an image of τ-mKate2 (568 nm) was taken (imaging sequence for RW1594). With this imaging sequence, we analysed activity of DinB-YPet at replisomes. RW1286 was imaged similarly; we recorded burst acquisitions of UmuC-mKate2 (568 nm) followed by a snapshot of τ-YPet (514 nm). All images were analysed with ImageJ (77).

The MuGam-PAmCherry imaging acquisition was recorded as a set of two acquisitions, 1. bright-field image (100 ms exposure), 2. PAmCherry fluorescence [simultaneous illumination with the activation laser 405 and 568 nm readout laser for 200 frames each with 100 ms exposure]). This protocol was only executed once for a field-of-view to minimize laser damage. Consequently, before and after antibiotic treatment shows a new set of cells. Images taken after antibiotic addition were recorded following 2 h of antibiotic treatment.

4.5.7 Flow cell designs

All imaging experiments were carried out in home-built quartz-based flow cells. These flow cells were assembled from a no. 1.5 coverslip (Marienfeld, REF 0102222, for imaging on IX-81, Olympus) or (Marienfeld, REF 0107222, for imaging on Nikon Eclipse-Ti), a quartz top piece (45x20x1 mm) and PE-60 tubing (Instech Laboratories, Inc.). Prior to flow-cell assembly, coverslips were silanized with (3-aminopropyl)triethoxysilane (APTES, from Alfa Aeser). First, coverslips were sonicated for 30 min in a 5M KOH solution to clean and activate the surface. The cleaned coverslips were rinsed thoroughly with MilliQ water and then treated with a 5% (v/v) solution of APTES in MilliQ water. The coverslips were subsequently rinsed with ethanol and sonicated in ethanol for 20 seconds. Afterwards, the coverslips were rinsed with MilliQ water and dried in a jet of N_2. Silanized slides were stored under vacuum prior to use.

To assemble each flow cell, polyethylene tubing (BTPE-60, Instech Laboratories, Inc.) was glued (BONDiT B-482, Reltek LLC) into two holes that were drilled into a quartz piece. After the glue solidified overnight, double-sided adhesive tape was stuck on two opposite sides of the quartz piece to create a channel. Then, the quartz piece was stuck to an APTES-treated coverslip. The edges were sealed with epoxy glue (5 Minute Epoxy, PARFIX). Each flow cell was stored in a desiccator under mild vacuum while the glue dried. Typical channel dimensions were 45 mm × 5 mm × 0.1 mm (length × width × height).

4.5.8 Preparation of cell cultures for microscopy

The day before each experiment, for all experiments, an over-night culture was grown from a freezer stock for each cell culture. Cells that did not carry the MuGam-PAmCherry plasmid were grown at 37^{0}C in EZ rich defined medium (Teknova) that contained 0.2% (w/v) glucose. All strains that have a *Kan*^{R} cassette were grown in the presence of kanamycin (20 μg/mL). Cells that carried the MuGam-PAmCherry plasmid were grown at 37^{0}C in EZ rich defined medium (Teknova) that contained 0.2% (w/v) glycerol and 0.001% L-arabinose, in the presence of ampicillin (100 μg/mL).

At the day of the experiment, for all imaging experiments excluding imaging of MuGam fusion, cells were grown at 37^{0}C in EZ rich defined medium (Teknova) that contained 0.2% (w/v) glucose. All strains that have a *Kan*^{R} cassette were grown in the presence of kanamycin (20 μg/mL). Cultures used for imaging under ROS-mitigating conditions were grown in the presence of the particular mitigator used for the experiment (DMSO [2% v/v, 282 mM, 0.2 x MIC (5)] or BiP [0.35 mM, 0.5 x MIC (5)], culture time ~3 h for *recB*$^+$ *lexA*$^+$, ~4 h for Δ*recB lexA*$^+$ and ~6 h for Δ*recB lexA*[Def]). For imaging experiments of the MuGam fusion, cells were grown at 37^{0}C in EZ rich defined medium (Teknova) that contained 0.2% (w/v) glycerol and 0.001% L-arabinose. All strains were grown in the presence of ampicillin (100 μg/mL). Cultures used for imaging under ROS-mitigating conditions were grown in the presence of DMSO [2% v/v, 282 mM, 0.2 x MIC (5)] for ~3 h culture time.

4.5.9 Imaging in flow cells

Cells were loaded into flow cells (*SI Appendix*, Fig. 1*A*), allowed a few minutes to associate with the APTES surface, then loosely associated cells were removed by pulling through fresh medium. The experiment was then initiated by adding either an antibiotic alone or in combination with DMSO to the medium (30 ng/ mL ciprofloxacin, 30 ng/ mL ciprofloxacin with 2% (v/v) DMSO, 1 μg/mL trimethoprim, 1 μg/mL trimethoprim with 2% (v/v) DMSO or 1 μg/mL trimethoprim with 0.35 mM BiP). Throughout the experiment, medium was pulled through the flow cell using a syringe pump, at a rate of 50 μL/min. For each condition, triplicate measurements were recorded.

4.5.10 Analysis of cell filamentation, concentrations, SOS induction level and number of foci

We selected single cells to obtain information about SOS induction, DinB and UmuC levels upon UV irradiation (>100 cells for every time point). MicrobeTracker 0.937 (78), a MATLAB script, was used to create cell outlines as regions of interest (ROI). We manually curated cell outlines designated by MicrobeTracker at t = 0 min (time point of antibiotic addition) and at 30 min time intervals until 180 min. By obtaining cell outlines manually, we ensure accuracy and purely select non-overlapping, in-focus cells for analysis. These ROI were imported in ImageJ 1.50i. The cell outlines were then used to measure mean cell intensities, cell lengths and the number of foci per cell. Parameters describing foci (number, positions and intensities) were obtained using a Peak Fitter plug-in, described previously (39,47). Prior to determining DinB-YPet foci UmuC-mKate2 per cell from burst acquisition movies in *lexA*(Def), average

projections in time were curated from frame 1 to 101 (10 x 100 ms = 1 s). Prior to determining MuGam-PAmCherry foci per cell from burst acquisition movies, maximum projections in time were curated over the entire movie, capturing all binding events of MuGam-PAmCherry.

Using information of mean cell brightness derived from DinB-YPet expressing cells, we also calculated DinB-YPet concentrations of cells grown in the absence or presence of antibiotic. In a previous study (39), we calculated the DinB-YPet concentration which correlates with a certain mean cell brightness (in the absence of ciprofloxacin: 6 ± 1 nm [SE]; 180 min after ciprofloxacin treatment: 34 ± 3 nM [SE]). We utilized these values to calculate the DinB-YPet concentration for ciprofloxacin ± DMSO or trimethoprim ± DMSO treated cells.

4.5.11 Analysis of colocalization events

Foci were classed as colocalized if their centroid positions (determined using our peak fitter tool) fell within 2.18 px (218 nm) of each other. When treating with ciprofloxacin, we determined that for DinB-YPet–τ-mKate2 localization the background of DinB foci expected to colocalize with replisomes purely by chance is ~4% at 180 min. This was calculated by taking the area of each cell occupied by replisome foci (including the colocalization search radius) and dividing by the total area of the cell. The value of 4% corresponds to the mean of measurements made over 121 cells. Since the foci density of replisomes stays fairly constant following ciprofloxacin treatment, the chance colocalization of DinB-YPet foci with τ-mKate2 is ~4% during the experiment (39). Chance colocalization of τ-mKate2 with DinB-YPet is however not constant over time because most cells contain no pol IV foci in the absence of any DNA damage. Chance colocalization is close to zero at 0 min; at 60 min, chance colocalization is ~5%; at 120 min, chance colocalization is ~3%. Moreover, chance colocalization of τ-mKate2 with DinB-YPet is overall reduced under ROS-mitigating conditions due to a reduced number of foci per cell (chance colocalization close to zero at 0 min; at 120 min, ~2%). Chance colocalization of τ-mKate2 with DinB-YPet in trimethoprim-treated cells amounts to ~1% from 60-90 min (close to zero before 60 min). Under ROS-mitigating conditions, chance colocalization is always close to zero because the number of pol IV foci per cell does not increase post treatment as well as cell size (**Fig. 1**).

The chance colocalization of UmuC-mKate2 with τ-YPet is similar to the chance colocalization of DinB-YPet with τ-mKate2 (chance colocalization: ~4%). The expected colocalization of τ-YPet with UmuC-mKate2 by background is close to zero until 90 min. UmuC-mKate2 is neither upregulated nor released from the membrane (*SI Appendix*, Fig. 13*A*). Chance colocalization is ~3% at 180 min after ciprofloxacin treatment and ~2% after the combinational treatment of ciprofloxacin/DMSO.

4.5.12 Western blotting

Overnight *E. coli* LB cultures of RW120/pRW154 and RW546/pRW154 (75) were diluted 1 to 100 in fresh LB with appropriate antibiotics and grown to mid-log (~OD 0.5, ~3 hrs). Aliquots were then taken for the untreated samples. Either ciprofloxacin (30 ng/mL) or trimethoprim (1 µg/mL) was added to the remaining culture and incubated with or without the addition of 2% DMSO. Samples were taken at 1, 2 and 3 hours. Whole cell extracts were made by centrifuging 1.5 mL of culture and adding 90 µl of

sterile deionized water and 30µL of NuPAGE LDS sample buffer (4X) (Novex, Life Technologies) to the cell pellet. Five cycles of freeze/thaw on dry ice and in a 37^0C water bath were performed to lyse the cells. Extracts were boiled for 5 minutes prior to loading. Samples were run on NuPAGE 4-12% Bis-Tris gels (Novex Life Technologies) and transferred to Invitrolon PVDF (0.45 µm pore size) membranes (Novex Life Technologies). Membranes were incubated with anti-UmuD antibodies (1:5,000 dilution) at room temperature overnight. Then the membranes were incubated with goat anti-rabbit IgG (H+L) alkaline phosphatase conjugate (1:10,000 dilution) (BIO-RAD). Subsequently, the membranes were treated with the CDP-Star substrate (Tropix). Membranes were then exposed to BioMax XAR film (Carestream) to visualize UmuD protein bands.

4.6 Supplementary Information Text and Legends

Sequence of pBAD-MuGam-PAmCherry (pEAW1162).

AAGAAACCAATTGTCCATATTGCATCAGACATTGCCGTCACTGCGTCTTTTACTGGCTCTTCT
CGCTAACCAAACCGGTAACCCCGCTTATTAAAAGCATTCTGTAACAAAGCGGGACCAAAGC
CATGACAAAAACGCGTAACAAAAGTGTCTATAATCACGGCAGAAAAGTCCACATTGATTAT
TTGCACGGCGTCACACTTTGCTATGCCATAGCATTTTTATCCATAAGATTAGCGGATCCTACC
TGACGCTTTTTATCGCAACTCTCTACTGTTTCTCCATACCCGTTTTTTGGGCTAACAGGAGGA
ATTAACATATGGCTAAACCAGCAAAACGTATCAAGAGTGCCGCAGCGGCTTATGTGCCACA
AAACCGCGATGCGGTGATTACCGATATTAAACGCATCGGGGATTTACAGCGCGAAGCATCA
CGTCTGGAAACGGAAATGAATGATGCCATCGCGGAAATTACGGAGAAATTTGCGGCCCGGA
TTGCACCGATTAAAACCGATATTGAAACCCTTTCAAAAGGCGTTCAGGGATGGTGTGAAGCG
AACCGCGACGAACTGACGAACGGCGGCAAAGTGAAGACGGCGAATCTTGTCACCGGTGATG
TATCGTGGCGGGTCCGTCCACCATCAGTAAGTATTCGTGGTATGGATGCAGTGATGGAAACG
CTGGAGCGTCTTGGCCTGCAACGCTTTATTCGCACGAAGCAGGAAATCAACAAGGAAGCGA
TTTTACTGGAACCGAAAGCGGTCGCAGGCGTTGCCGGAATTACAGTTAAATCAGGCATTGAG
GATTTTTCTATTATTCCATTTGAACAGGAAGCCGGTATTTCCGCTGGCTCCGCTGCTGGTTCT
GGCGAATTCATGGTGAGCAAGGGCGAGGAGGATAACATGGCCATCATTAAGGAGTTCATGC
GCTTCAAGGTGCACATGGAGGGGTCCGTGAACGGCCACGTGTTCGAGATCGAGGGCGAGGG
CGAGGGCCGCCCCTACGAGGGCACCCAGACCGCCAAGCTGAAGGTGACCAAGGGTGGCCCC
CTGCCCTTCACCTGGGACATCCTGTCCCCTCAATTCATGTACGGCTCCAATGCCTACGTGAAG
CACCCCGCCGACATCCCCGACTACTTTAAGCTGTCCTTCCCCGAGGGCTTCAAGTGGGAGCG
CGTGATGAAATTCGAGGACGGCGGCGTGGTGACCGTGACCCAGGACTCCTCCCTGCAGGAC
GGTGAGTTCATCTACAAGGTGAAGCTGCGCGGCACCAACTTCCCCTCCGACGGCCCCGTAAT
GCAGAAGAAGACCATGGGCTGGGAGGCCCTCTCCGAGCGGATGTACCCCGAGGACGGCGCC
CTGAAGGGCGAGGTCAAGCCGAGAGTGAAGCTGAAGGACGGCGGCCACTACGACGCTGAG
GTCAAGACCACCTACAAGGCCAAGAAGCCCGTGCAGCTGCCCGGCGCCTACAACGTCAACC
GCAAGTTGGACATCACCTCACACAACGAGGACTACACCATCGTGGAACAGTACGAACGTGC
CGAGGGCCGCCACTCCACCGGCGGCATGGACGAGCTGTACAAGTAAAAGCTTGGGCCCGAA
CAAAAACTCATCTCAGAAGAGGATCTGAATAGCGCCGTCGACCATCATCATCATCATCATTG
AGTTTAAACGGTCTCCAGCTTGGCTGTTTTGGCGGATGAGAGAAGATTTTCAGCCTGATACA
GATTAAATCAGAACGCAGAAGCGGTCTGATAAAACAGAATTTGCCTGGCGGCAGTAGCGCG
GTGGTCCCACCTGACCCCATGCCGAACTCAGAAGTGAAACGCCGTAGCGCCGATGGTAGTGT
GGGGTCTCCCCATGCGAGAGTAGGGAACTGCCAGGCATCAAATAAAACGAAAGGCTCAGTC
GAAAGACTGGGCCTTTCGTTTTATCTGTTGTTTGTCGGTGAACGCTCTCCTGAGTAGGACAAA
TCCGCCGGGAGCGGATTTGAACGTTGCGAAGCAACGGCCCGGAGGGTGGCGGGCAGGACGC
CCGCCATAAACTGCCAGGCATCAAATTAAGCAGAAGGCCATCCTGACGGATGGCCTTTTTGC
GTTTCTACAAACTCTTTTGTTTATTTTTCTAAATACATTCAAATATGTATCCGCTCATGAGAC
AATAACCCTGATAAATGCTTCAATAATATTGAAAAAGGAAGAGTATGAGTATTCAACATTTC
CGTGTCGCCCTTATTCCCTTTTTTGCGGCATTTTGCCTTCCTGTTTTTGCTCACCCAGAAACGC
TGGTGAAAGTAAAAGATGCTGAAGATCAGTTGGGTGCACGAGTGGGTTACATCGAACTGGA
TCTCAACAGCGGTAAGATCCTTGAGAGTTTTCGCCCCGAAGAACGTTTTCCAATGATGAGCA
CTTTTAAAGTTCTGCTATGTGGCGCGGTATTATCCCGTGTTGACGCCGGGCAAGAGCAACTC
GGTCGCCGCATACACTATTCTCAGAATGACTTGGTTGAGTACTCACCAGTCACAGAAAAGCA
TCTTACGGATGGCATGACAGTAAGAGAATTATGCAGTGCTGCCATAACCATGAGTGATAACA
CTGCGGCCAACTTACTTCTGACAACGATCGGAGGACCGAAGGAGCTAACCGCTTTTTTGCAC
AACATGGGGGATCATGTAACTCGCCTTGATCGTTGGGAACCGGAGCTGAATGAAGCCATAC
CAAACGACGAGCGTGACACCACGATGCCTGTAGCAATGGCAACAACGTTGCGCAAACTATT
AACTGGCGAACTACTTACTCTAGCTTCCCGGCAACAATTAATAGACTGGATGGAGGCGGATA
AAGTTGCAGGACCACTTCTGCGCTCGGCCCTTCCGGCTGGCTGGTTTATTGCTGATAAATCTG
GAGCCGGTGAGCGTGGGTCTCGCGGTATCATTGCAGCACTGGGGCCAGATGGTAAGCCCTCC
CGTATCGTAGTTATCTACACGACGGGGAGTCAGGCAACTATGGATGAACGAAATAGACAGA
TCGCTGAGATAGGTGCCTCACTGATTAAGCATTGGTAACTGTCAGACCAAGTTTACTCATAT
ATACTTTAGATTGATTTAAAACTTCATTTTTAATTTAAAAGGATCTAGGTGAAGATCCTTTTT
GATAATCTCATGACCAAAATCCCTTAACGTGAGTTTTCGTTCCACTGAGCGTCAGACCCCGT
AGAAAAGATCAAAGGATCTTCTTGAGATCCTTTTTTTCTGCGCGTAATCTGCTGCTTGCAAAC
AAAAAAACCACCGCTACCAGCGGTGGTTTGTTTGCCGGATCAAGAGCTACCAACTCTTTTTC

CGAAGGTAACTGGCTTCAGCAGAGCGCAGATACCAAATACTGTCCTTCTAGTGTAGCCGTAG
TTAGGCCACCACTTCAAGAACTCTGTAGCACCGCCTACATACCTCGCTCTGCTAATCCTGTTA
CCAGTGGCTGCTGCCAGTGGCGATAAGTCGTGTCTTACCGGGTTGGACTCAAGACGATAGTT
ACCGGATAAGGCGCAGCGGTCGGGCTGAACGGGGGGTTCGTGCACACAGCCCAGCTTGGAG
CGAACGACCTACACCGAACTGAGATACCTACAGCGTGAGCTATGAGAAAGCGCCACGCTTC
CCGAAGGGAGAAAGGCGGACAGGTATCCGGTAAGCGGCAGGGTCGGAACAGGAGAGCGCA
CGAGGGAGCTTCCAGGGGGAAACGCCTGGTATCTTTATAGTCCTGTCGGGTTTCGCCACCTC
TGACTTGAGCGTCGATTTTTGTGATGCTCGTCAGGGGGGCGGAGCCTATGGAAAAACGCCAG
CAACGCGGCCTTTTTACGGTTCCTGGCCTTTTGCTGGCCTTTTGCTCACATGTTCTTTCCTGCG
TTATCCCCTGATTCTGTGGATAACCGTATTACCGCCTTTGAGTGAGCTGATACCGCTCGCCGC
AGCCGAACGACCGAGCGCAGCGAGTCAGTGAGCGAGGAAGCGGAAGAGCGCCTGATGCGG
TATTTTCTCCTTACGCATCTGTGCGGTATTTCACACCGCATAtaTGGTGCACTCTCAGTACAAT
CTGCTCTGATGCCGCATAGTTAAGCCAGTATACACTCCGCTATCGCTACGTGACTGGGTCAT
GGCTGCGCCCCGACACCCGCCAACACCCGCTGACGCGCCCTGACGGGCTTGTCTGCTCCCGG
CATCCGCTTACAGACAAGCTGTGACCGTCTCCGGGAGCTGCATGTGTCAGAGGTTTTCACCG
TCATCACCGAAACGCGCGAGGCAGCAGATCAATTCGCGCGCGAAGGCGAAGCGGCATGCAT
AATGTGCCTGTCAAATGGACGAAGCAGGGATTCTGCAAACCCTATGCTACTCCGTCAAGCCG
TCAATTGTCTGATTCGTTACCAATTATGACAACTTGACGGCTACATCATTCACTTTTTCTTCA
CAACCGGCACGGAACTCGCTCGGGCTGGCCCCGGTGCATTTTTTAAATACCCGCGAGAAATA
GAGTTGATCGTCAAAACCAACATTGCGACCGACGGTGGCGATAGGCATCCGGGTGGTGCTC
AAAAGCAGCTTCGCCTGGCTGATACGTTGGTCCTCGCGCCAGCTTAAGACGCTAATCCCTAA
CTGCTGGCGGAAAAGATGTGACAGACGCGACGGCGACAAGCAAACATGCTGTGCGACGCTG
GCGATATCAAAATTGCTGTCTGCCAGGTGATCGCTGATGTACTGACAAGCCTCGCGTACCCG
ATTATCCATCGGTGGATGGAGCGACTCGTTAATCGCTTCCATGCGCCGCAGTAACAATTGCT
CAAGCAGATTTATCGCCAGCAGCTCCGAATAGCGCCCTTCCCCTTGCCCGGCGTTAATGATT
TGCCCAAACAGGTCGCTGAAATGCGGCTGGTGCGCTTCATCCGGGCGAAAGAACCCCGTATT
GGCAAATATTGACGGCCAGTTAAGCCATTCATGCCAGTAGGCGCGCGGACGAAAGTAAACC
CACTGGTGATACCATTCGCGAGCCTCCGGATGACGACCGTAGTGATGAATCTCTCCTGGCGG
GAACAGCAAAATATCACCCGGTCGGCAAACAAATTCTCGTCCCTGATTTTTCACCACCCCCT
GACCGCGAATGGTGAGATTGAGAATATAACCTTTCATTCCCAGCGGTCGGTCGATAAAAAA
ATCGAGATAACCGTTGGCCTCAATCGGCGTTAAACCCGCCACCAGATGGGCATTAAACGAGT
ATCCCGGCAGCAGGGGATCATTTTGCGCTTCAGCCATACTTTTCATACTCCCGCCATTCAGAG

SI Appendix Figure 1

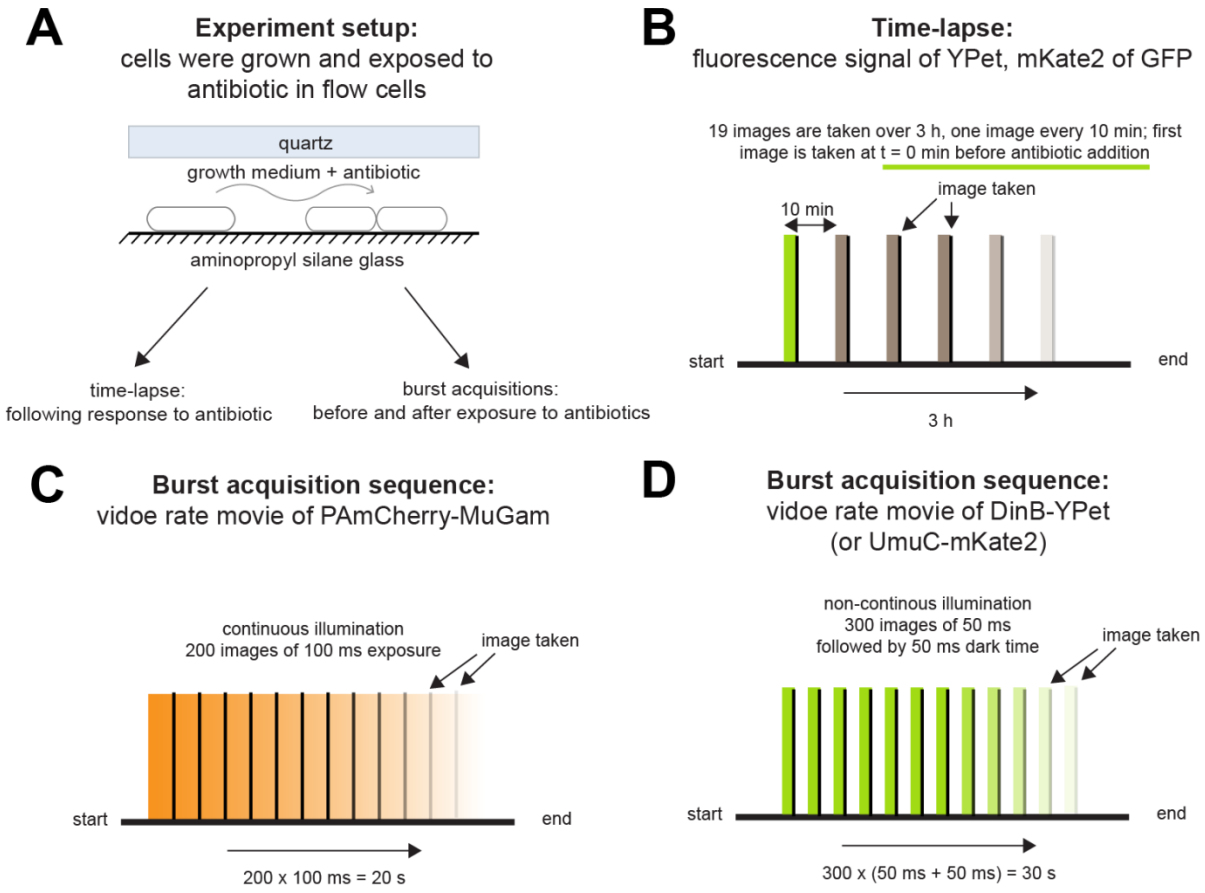

Fig. S1. Experimental design. (*A*) Experimental setup. Cells are loaded in a flow-cell and immobilized on a positively charged aminopropyl silane glass surface. Cells were imaged before and after antibiotic exposure ± ROS mitigator. Time-lapse movies were recorded to follow the cellular response. Burst acquisitions were recorded to follow the dynamic behavior of fluorescent protein fusion constructs in cells. (*B*) Time-lapse movies were recorded over 3 h following the cellular response to antibiotic exposure. An image was taken every 10 min. At t = 0 min, the first image was taken and subsequently antibiotic-containing media was flowed into the flow cell. A total number of 19 frames were recorded. (*C*) Burst acquisition videos were recorded at specific time-points before or after antibiotic addition. Movies of MuGam- PAmCherry were recorded using continuous excitation, containing 200 frames at 100 ms exposure. (*D*) Burst acquisition movies of DinB-YPet or UmuC-mKate2 were recorded using non-continuous excitation, containing 300 frames at 50 ms exposure followed by 50 ms dark time.

SI Appendix Figure 2

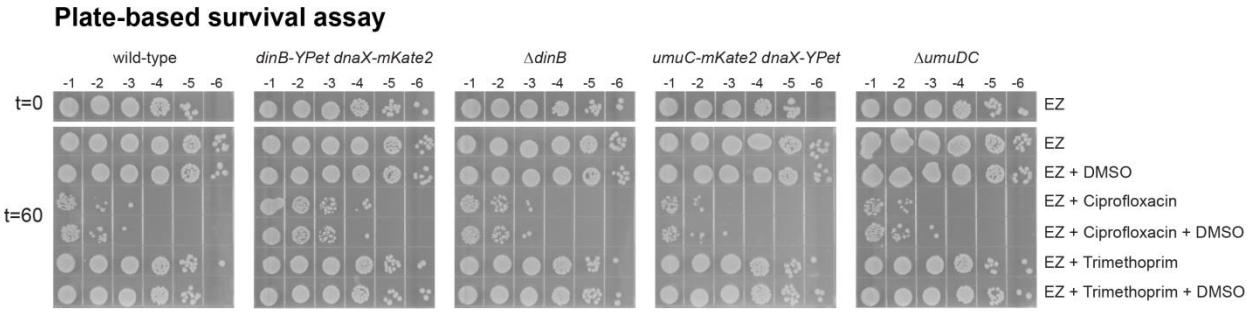

Fig. S2. Survival of strains to ciprofloxacin and trimethoprim in EZ medium. Survival assays using ciprofloxacin or trimethoprim normal or ROS-mitigating condition (+ DMSO). Cell cultures (MG1655 [wild-type], *dinB-YPet dnaX-mKate2*, Δ*dinB*, *umuC-mKate2 dnaX-YPet* and Δ*umuDC*) were grown in EZ glucose medium to exponential growth phase (OD_{600} = 0.2-0.3). Then, culture were split in 6 before, one sample was used as control, 2% DMSO, 30 ng/mL ciprofloxacin, 30 ng/mL ciprofloxacin + DMSO, 1 μg/mL trimethoprim or or 1 μg/mL trimethoprim + 2% DMSO were added in the others and grown for 60 min. Before the treatment and after 60 min samples were taken and serial diluted by factor ten down to 10^{-6}. Dilutions 10^{-1} to 10^{-6} of each culture were spotted on fresh LB plates, incubated in the dark overnight at 37ºC before the image were captured. Images selected are resentative of a biological triplicate. Cells constructs used in this study (*dinB-YPet dnaX-mKate2* and *umuC-mKate2 dnaX-YPet*) exhibit a similar phenotype to MG1655.

SI Appendix Figure 3

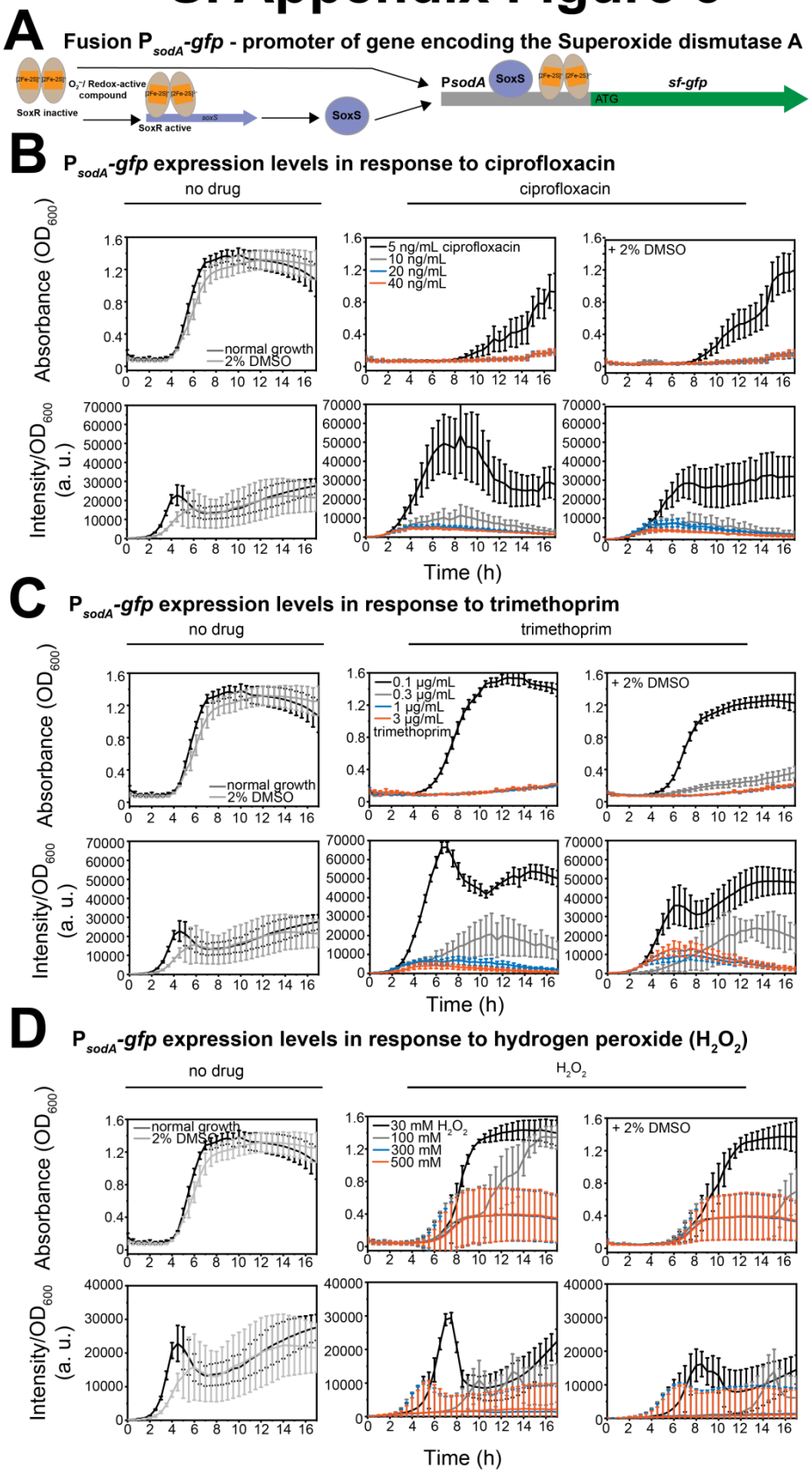

Fig. S3. P_{sodA}-*gfp* expression levels wild-type cells. For each strain, 10^4 – 10^6 cells were added to each well at the beginning of the experiment. Measurements of absorbance (OD_{600}) and fluorescence intensity (a.u.) were carried out every 30 min over 17 h. For (A)-(C): upper row shows absorbance (OD_{600}) and bottom row illustrates intensity values/ OD_{600}, consistent with expression levels. Error bars represent standard error of the mean over three independent biological replicates. (*A*) *sodA* is regulated by SoxRS. Superoxides oxidize the Fe-S clusters of the SoxR transcription factor, promoting transcription of *soxS* and *sodA*. Then, SoxS also acts as a transcription factor for *sodA*. For cells carrying P_{sodA}-*gfp*, superoxides then trigger the expression of GFP from the *sodA* promotor. (*B*) Comparison of normal growth condition with ciprofloxacin treatment ± ROS mitigator for wild-type cells. First column: normal growth conditions (wild-type: dark grey; Δ*recB*: orange) or + 2% DMSO (wild-type: grey); second column: ciprofloxacin treatment of wild-type cells (5 ng/mL: black; 10 ng/mL: grey; 20 ng/mL: blue; 40 ng/mL: orange); third column: ciprofloxacin + 2% DMSO treatment of wild-type cells (same color coding as second column). (*C*) Comparison of normal growth condition with trimethoprim treatment ± ROS mitigator for wild-type cells. First column: as (A) first column; second column: trimethoprim treatment of wild-type cells (0.1 μg/mL: black; 0.3 μg/mL: grey; 1 μg/mL: blue; 3 μg/mL: orange); third column: trimethoprim + 2% DMSO treatment of wild-type cells (same color coding as second column). (*D*) Comparison of normal growth condition with hydrogen peroxide (H_2O_2) treatment ± ROS mitigator for wild-type cells. First column: as (A) first column; second column: H_2O_2 treatment of wild-type cells (30 mM: black; 100 mM: grey; 300 mM: blue; 500 mM: orange); third column: H_2O_2 + 2% DMSO treatment of wild-type cells (same color coding as second column).

SI Appendix Figure 4

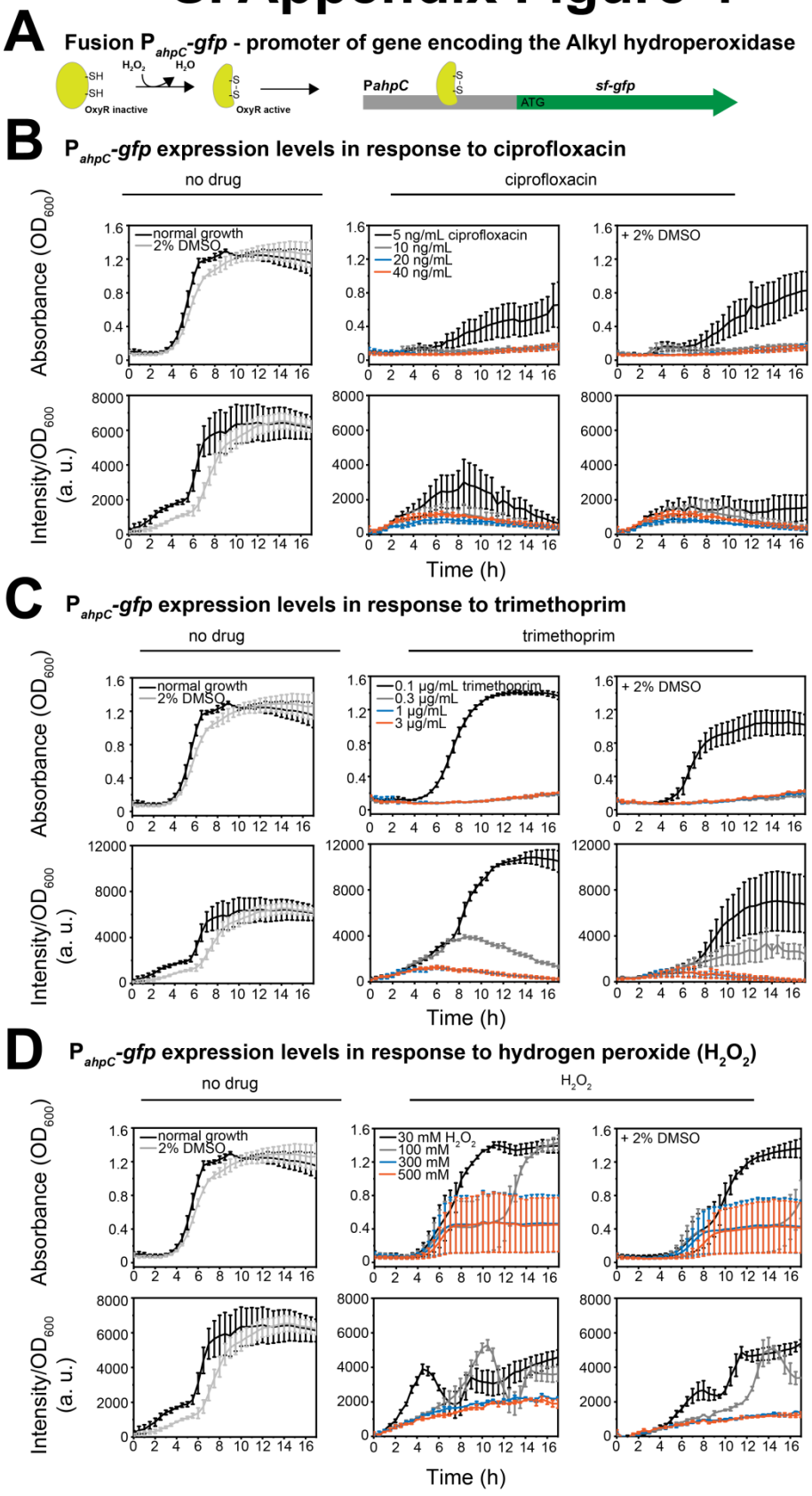

Fig. S4. P_{ahpC}-*gfp* expression levels wild-type cells. For each strain, 10^4 – 10^6 cells were added to each well at the beginning of the experiment. Measurements of absorbance (OD_{600}) and fluorescence intensity

(a.u.) were carried out every 30 min over 17 h. For (A)-(C): upper row shows absorbance (OD_{600}) and bottom row illustrates intensity values/ OD_{600}, consistent with expression levels. Error bars represent standard error of the mean over three independent biological replicates. (*A*) *ahcP* is transcriptionally regulated by OxyR. Oxidation of OxyR cysteines induces transcription and expression of *ahcPC*. For cells carrying P_{ahcP}-*gfp*, oxidative stress triggers the expression of GFP from the *ahcP* promotor. (*B*) Comparison of normal growth condition with ciprofloxacin treatment ± ROS mitigator for wild-type cells. First column: normal growth conditions (wild-type: dark grey; Δ*recB*: orange) or + 2% DMSO (wild-type: grey); second column: ciprofloxacin treatment of wild-type cells (5 ng/mL: black; 10 ng/mL: grey; 20 ng/mL: blue; 40 ng/mL: orange); third column: ciprofloxacin + 2% DMSO treatment of wild-type cells (same color coding as second column). (*C*) Comparison of normal growth condition with trimethoprim treatment ± ROS mitigator for wild-type cells. First column: as (A) first column; second column: trimethoprim treatment of wild-type cells (0.1 µg/mL: black; 0.3 µg/mL: grey; 1 µg/mL: blue; 3 µg/mL: orange); third column: trimethoprim + 2% DMSO treatment of wild-type cells (same color coding as second column). (*D*) Comparison of normal growth condition with hydrogen peroxide (H_2O_2) treatment ± ROS mitigator for wild-type cells. First column: as (A) first column; second column: H_2O_2 treatment of wild-type cells (30 mM: black; 100 mM: grey; 300 mM: blue; 500 mM: orange); third column: H_2O_2 + 2% DMSO treatment of wild-type cells (same color coding as second column).

SI Appendix Figure 5

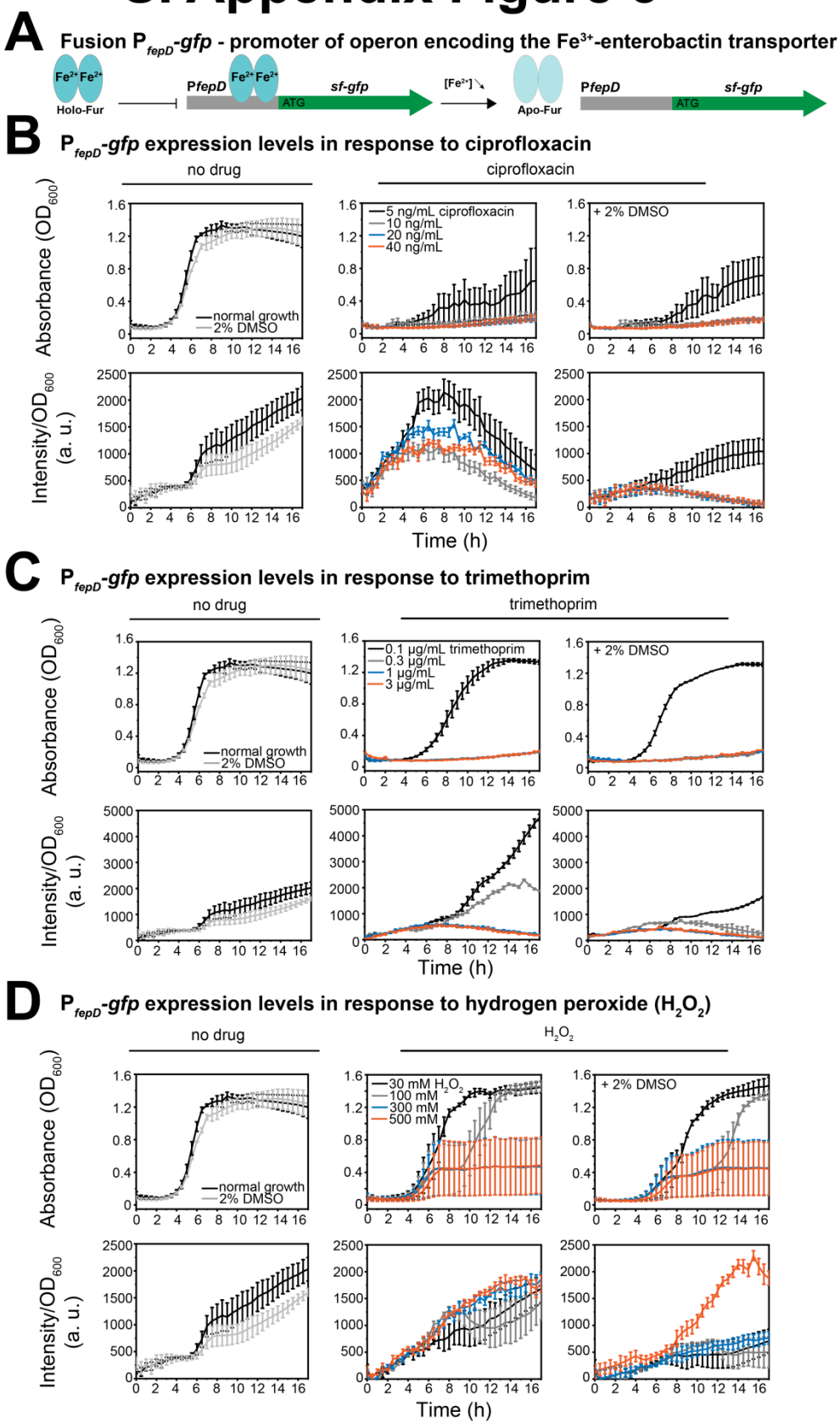

Fig. S5. P_{fepD}-*gfp* expression levels wild-type cells. For each strain, 10^4 – 10^6 cells were added to each well at the beginning of the experiment. Measurements of absorbance (OD_{600}) and fluorescence intensity

(a.u.) were carried out every 30 min over 17 h. For (A)-(C): upper row shows absorbance (OD_{600}) and bottom row illustrates intensity values/ OD_{600}, consistent with expression levels. Error bars represent standard error of the mean over three independent biological replicates. (*A*) *fepD* is regulated by Fur. Under high iron conditions, transcriptional repressor Fur inhibits of *fepD* transcription. Under low iron conditions, in the presence of oxidative damage, Fur is de-repressed and *fepD* is transcribed. For cells carrying P_{fepD}-*gfp*, oxidative stress triggers the expression of GFP from the *fepD* promotor. (*B*) Comparison of normal growth condition with ciprofloxacin treatment ± ROS mitigator for wild-type cells. First column: normal growth conditions (wild-type: dark grey; Δ*recB*: orange) or + 2% DMSO (wild-type: grey); second column: ciprofloxacin treatment of wild-type cells (5 ng/mL: black; 10 ng/mL: grey; 20 ng/mL: blue; 40 ng/mL: orange); third column: ciprofloxacin + 2% DMSO treatment of wild-type cells (same color coding as second column). (*C*) Comparison of normal growth condition with trimethoprim treatment ± ROS mitigator for wild-type cells. First column: as (A) first column; second column: trimethoprim treatment of wild-type cells (0.1 μg/mL: black; 0.3 μg/mL: grey; 1 μg/mL: blue; 3 μg/mL: orange); third column: trimethoprim + 2% DMSO treatment of wild-type cells (same color coding as second column). (*D*) Comparison of normal growth condition with hydrogen peroxide (H_2O_2) treatment ± ROS mitigator for wild-type cells. First column: as (A) first column; second column: H_2O_2 treatment of wild-type cells (30 mM: black; 100 mM: grey; 300 mM: blue; 500 mM: orange); third column: H_2O_2 + 2% DMSO treatment of wild-type cells (same color coding as second column).

SI Appendix Figure 6

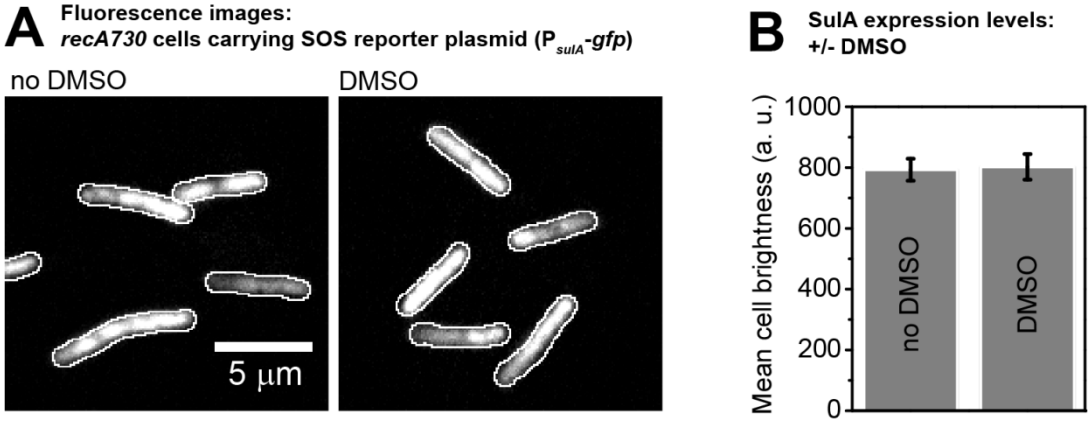

Fig. S6. DMSO has no effect on GFP fluorescence *in vivo*. (*A*) Fluorescence images of *recA730* cells carrying the SOS reporter plasmid (P_{sulA}-*gfp*) in the absence of DMSO (left) and in the presence of DMSO (right). Scale bar represents 5 μm. (*B*) SulA expression levels. Mean cell brightness is plotted for *recA730* cells grown in the absence and presence of DMSO. Error bars represent standard error of the mean from $n > 100$ cells.

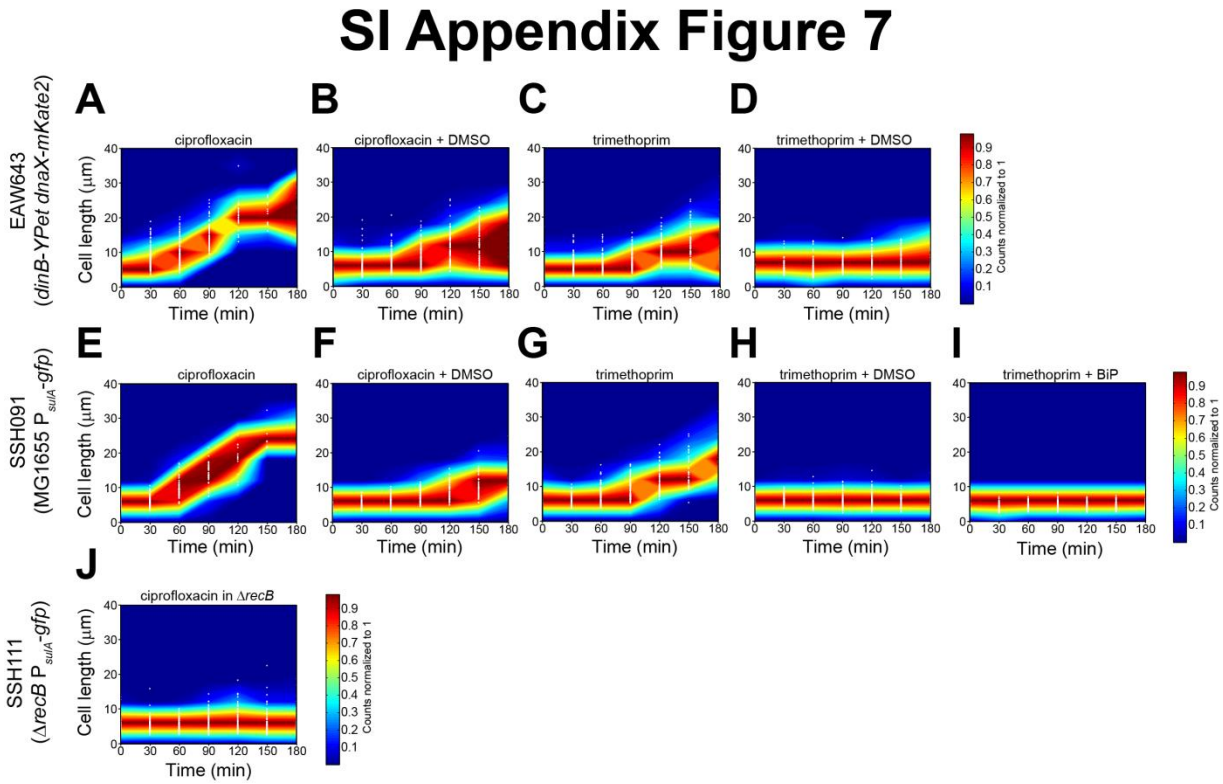

Fig. S7. Scatter plots of cell-size from time-lapse imaging. White points indicate individual data-points, while blue-to-red contours indicate frequencies of observations. Blue areas indicate regions of the plot containing few data points; red areas indicate regions containing a large number of data points. Frequencies were normalized at each time-point to the maximum value at that time-point with dark blue = 0 and dark red = 1. We conservatively estimate that >100 cells were used in each measurement. (*A*) EAW643 cells (*dinB-YPet dnaX-mKate2*) treated with ciprofloxacin-alone. (*B*) EAW643 cells (*dinB-YPet dnaX-mKate2*) treated with ciprofloxacin-DMSO. (*C*) EAW643 cells (*dinB-YPet dnaX-mKate2*) treated with trimethoprim-alone. (*D*) EAW643 cells (*dinB-YPet dnaX-mKate2*) treated with trimethoprim-DMSO. (*E*) SSH091 cells (MG1655 P_{sulA}-*gfp*) treated with ciprofloxacin-alone. (*F*) SSH091 cells (MG1655 P_{sulA}-*gfp*) treated with ciprofloxacin-DMSO. (*G*) SSH091 cells (MG1655 P_{sulA}-*gfp*) treated with trimethoprim-alone. (*H*) SSH091 cells (MG1655 P_{sulA}-*gfp*) treated with trimethoprim-DMSO. (*I*) SSH091 cells (MG1655 P_{sulA}-*gfp*) treated with trimethoprim-BiP. (*J*) SSH111 cells (Δ*recB* P_{sulA}-*gfp*) treated with ciprofloxacin.

SI Appendix Figure 8

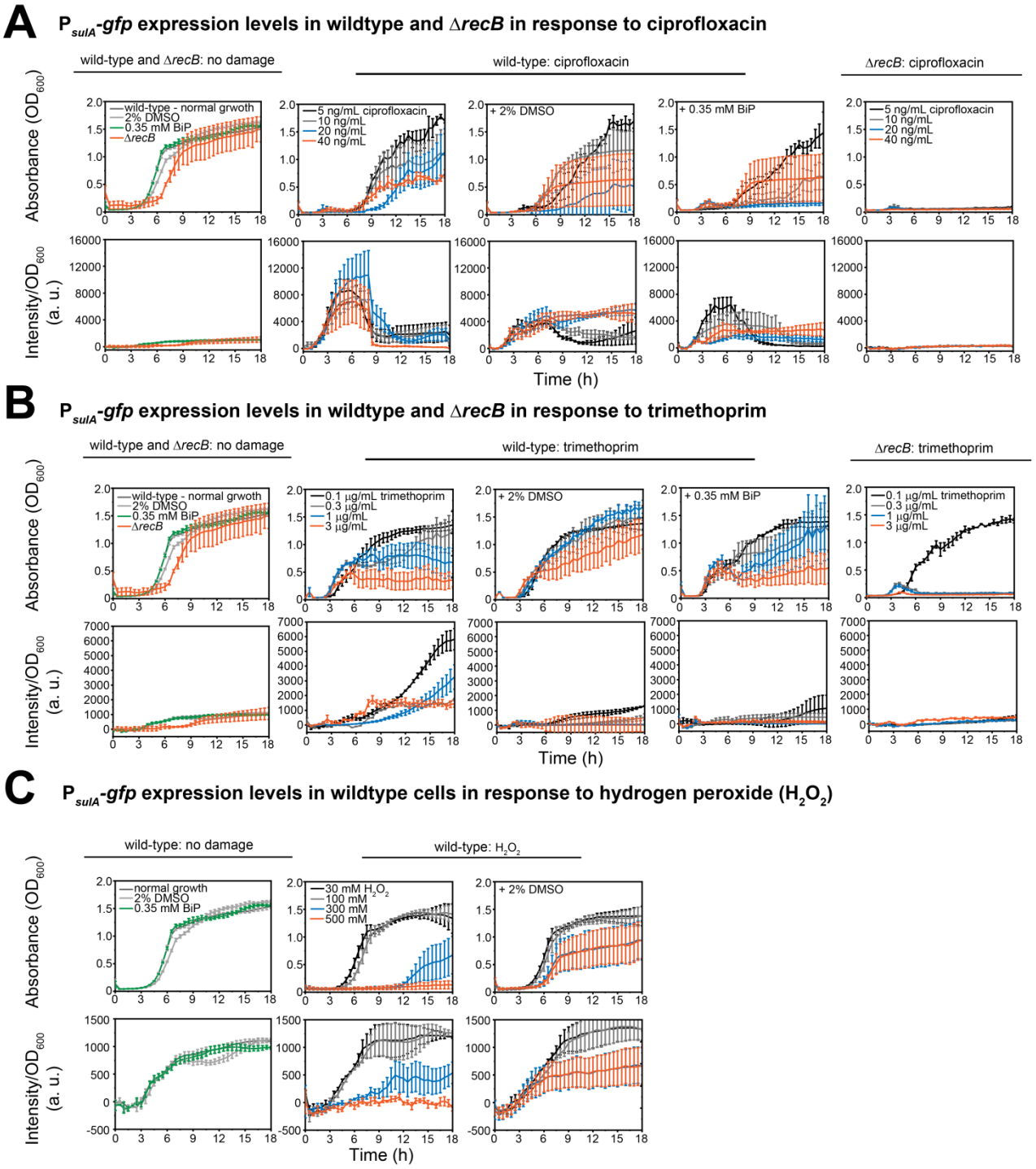

Fig. S8. P_{sulA}-*gfp* expression levels in wild-type and Δ*recB* cells. For each strain, 10^4 – 10^6 cells were added to each well at the beginning of the experiment. Measurements of absorbance (OD_{600}) and fluorescence intensity (a.u.) were carried out every 30 min over 18 h. For (A)-(C): upper row shows absorbance (OD_{600}) and bottom row illustrates intensity values/ OD_{600}, consistent with expression levels. Error bars represent standard error of the mean over three independent biological replicates. (*A*) Comparison of normal growth condition with ciprofloxacin treatment ± ROS mitigator for wild-type cells

or Δ*recB*. First column: normal growth conditions (wild-type: dark grey; Δ*recB*: orange), + 2% DMSO (wild-type: grey) or 0.35 mM BiP (wild-type: green); second column: ciprofloxacin treatment of wild-type cells (5 ng/mL: black; 10 ng/mL: grey; 20 ng/mL: blue; 40 ng/mL: orange); third column: ciprofloxacin + 2% DMSO treatment of wild-type cells (same color coding as second column); forth column: ciprofloxacin + 0.35 mM BiP treatment of wild-type cells (same color coding as second column); fifth column: ciprofloxacin treatment of Δ*recB* cells (same color coding as second column). (*B*) Comparison of normal growth condition with trimethoprim treatment ± ROS mitigator for wild-type cells or Δ*recB*. First column: as (A) first column; second column: trimethoprim treatment of wild-type cells (0.1 μg/mL: black; 0.3 μg/mL: grey; 1 μg/mL: blue; 3 μg/mL: orange); third column: trimethoprim + 2% DMSO treatment of wild-type cells (same color coding as second column); forth column: trimethoprim + 0.35 mM BiP treatment of wild-type cells (same color coding as second column); fifth column: trimethoprim treatment of Δ*recB* cells (same color coding as second column). (*C*) Comparison of normal growth condition with hydrogen peroxide (H_2O_2) treatment ± ROS mitigator for wild-type cells. First column: as (A) first column; second column: H_2O_2 treatment of wild-type cells (30 mM: black; 100 mM: grey; 300 mM: blue; 500 mM: orange); third column: H_2O_2 + 2% DMSO treatment of wild-type cells (same color coding as second column).

SI Appendix Figure 9

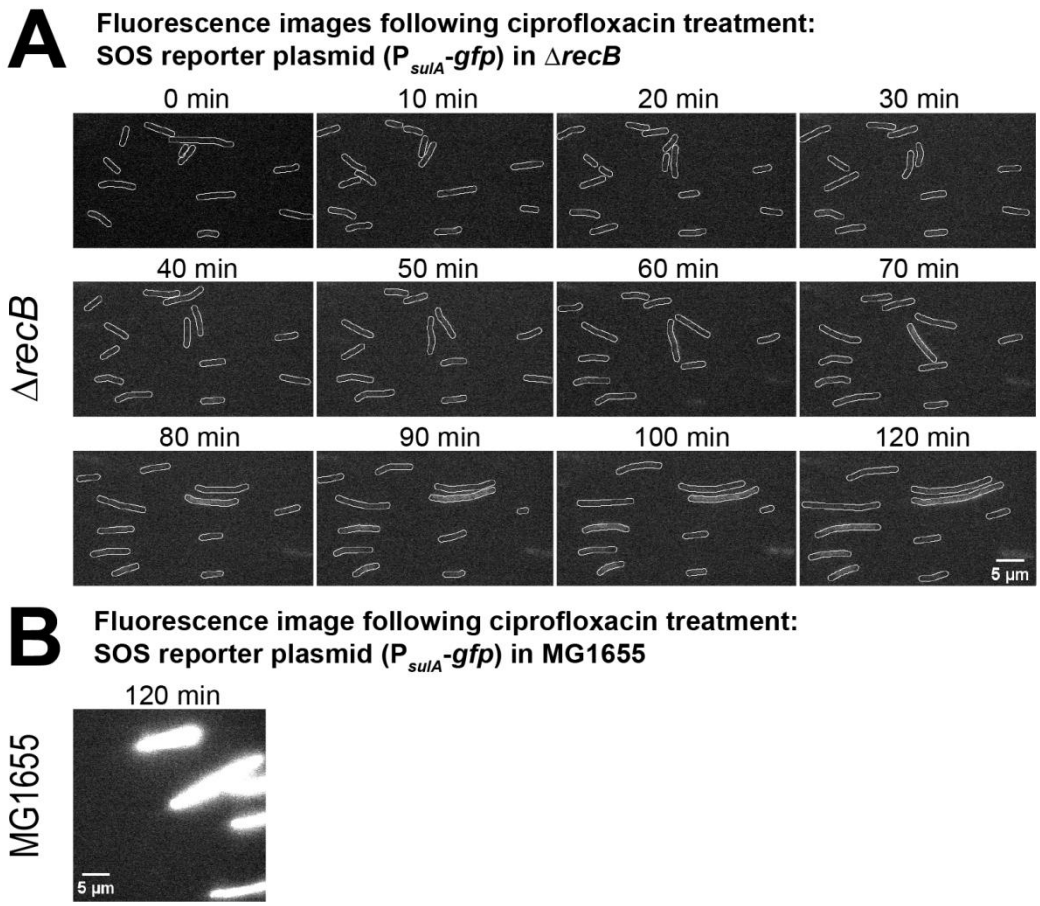

Fig. S9. P$_{sulA}$-*gfp* expression levels following ciprofloxacin-alone treatment in ΔrecB vs. MG1655 (wild-type). (*A*) Fluorescence images showing the expression of GFP from a SOS reporter plasmid (P*sulA*-GFP) from 0-110 min at intervals of 10 min and 120 min after ciprofloxacin addition in Δ*recB*. Scale bar represents 5 μm. (*B*) Fluorescence images showing the expression of GFP from a SOS reporter plasmid (P*sulA*-GFP) at 120 min after ciprofloxacin addition in wild-type cells, MG1655. Scale bar represents 5 μm.

SI Appendix Figure 10

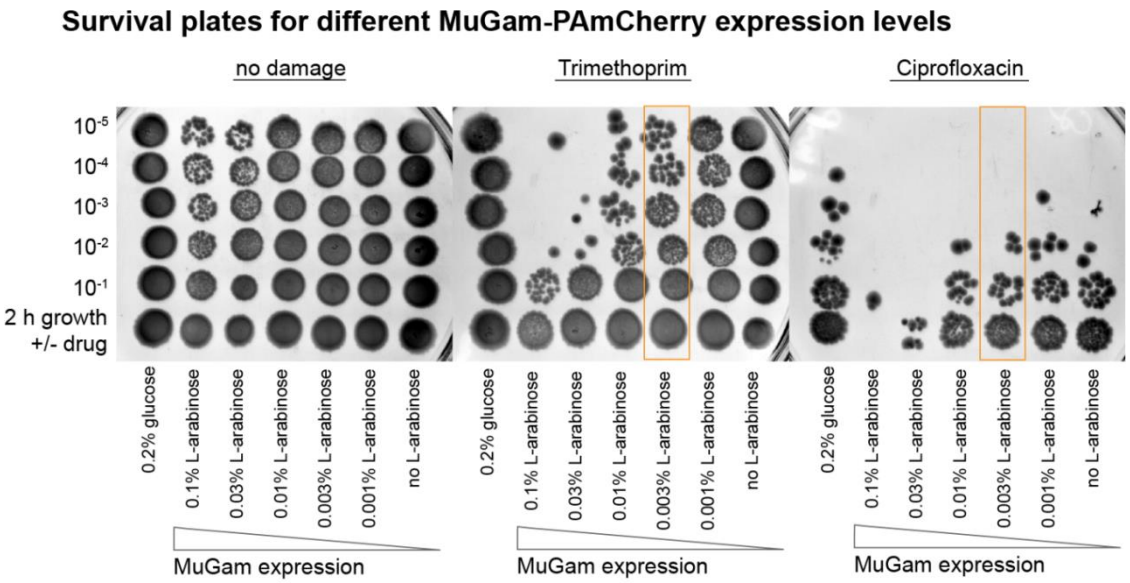

Fig. S10. Plate-based survival assays using ciprofloxacin or trimethoprim at different MuGam-PAmCherry expression levels. Cells carrying a pBAD plasmid for MuGam-PAmCherry expression were grown in EZ glycerol in the presence of ampicillin at different L-arabinose concentrations (0, 0.001, 0.003, 0.01, 0.03, 0.1% wt/vol) or in EZ glucose in order to inhibit expression from the pBAD plasmid. These cultures were split in three to perform two survival assays and a 'no damage' control. For the survival assays, antibiotic was added to these cultures (30 ng/mL ciprofloxacin or 1 μg/mL trimethoprim), then, cell cultures were grown for 2 h. For the control, cells were grown in the absence of antibiotic for 2 h. After 2 h of growth, cultures were centrifuged and resuspended in glucose or glycerol containing media (x 3) to remove the antibiotic. These cultures were serial diluted in PBS by factor ten down to 10^{-5} and spotted onto LB agar plates containing 100 μg/mL ampicillin. At an L-arabinose concentration of 0.003% (orange box), no drastic decrease in survival was observed in comparison to the sample grown in EZ glucose.

SI Appendix Figure 11

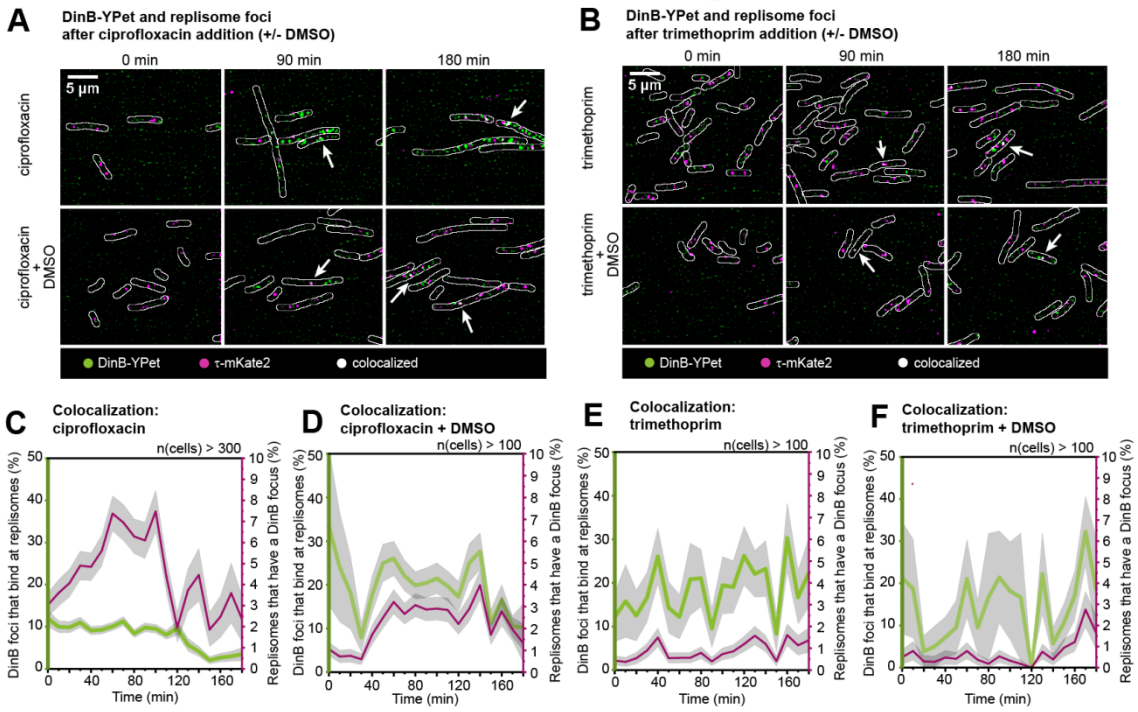

Fig. S11. Measuring colocalization of pol IV with replisomes following ciprofloxacin or trimethoprim treatment in the absence or presence of ROS mitigators. (*A*) Merged images showing DinB-YPet (pol IV) foci in green and τ-mKate2 (replisome) foci in magenta at 0, 90 and 180 min (left to right) for ciprofloxacin-alone or ciprofloxacin-DMSO treatment (top to bottom). White arrows indicate colocalization events (white foci). Scale bar represents 5 µm. (*B*) Merged images showing DinB-YPet (pol IV) foci in green and τ-mKate2 (replisome) foci in magenta at 0, 90 and 180 min (left to right) for trimethoprim-alone or trimethoprim-DMSO treatment (top to bottom). White arrows indicate colocalization events (white foci). Scale bar represents 5 µm. (*C*) Colocalization measurements following ciprofloxacin-alone treatment over 180 min: percentage of pol IV foci that are bound at replisomes (green line), percentage of replisomes that contain a pol IV focus (magenta line). Grey shaded error bands represent the standard error of the mean from six biological replicates together. Measurements are from >300 cells per time point. (*D*) Colocalization measurements following ciprofloxacin-DMSO treatment over 180 min: percentage of pol IV foci that are bound at replisomes (green line), percentage of replisomes that contain a pol IV focus (magenta line). Grey shaded error bands represent the standard error of the mean from four biological replicates together. Measurements are from >100 cells per time point. (*E*) Colocalization measurements following trimethoprim-alone treatment over 180 min: percentage of pol IV foci that are bound at replisomes (green line), percentage of replisomes that contain a pol IV focus (magenta line). Grey shaded error bands represent the standard error of the mean from three biological replicates together. Measurements are from >100 cells per time point. (*F*) Colocalization measurements following trimethoprim-DMSO treatment over 180 min: percentage of pol IV foci that are bound at replisomes (green line), percentage of replisomes that contain a pol IV focus (magenta line). Grey shaded error bands represent the standard error of the mean from three biological replicates together. Measurements are from >100 cells per time point.

SI Appendix Figure 12

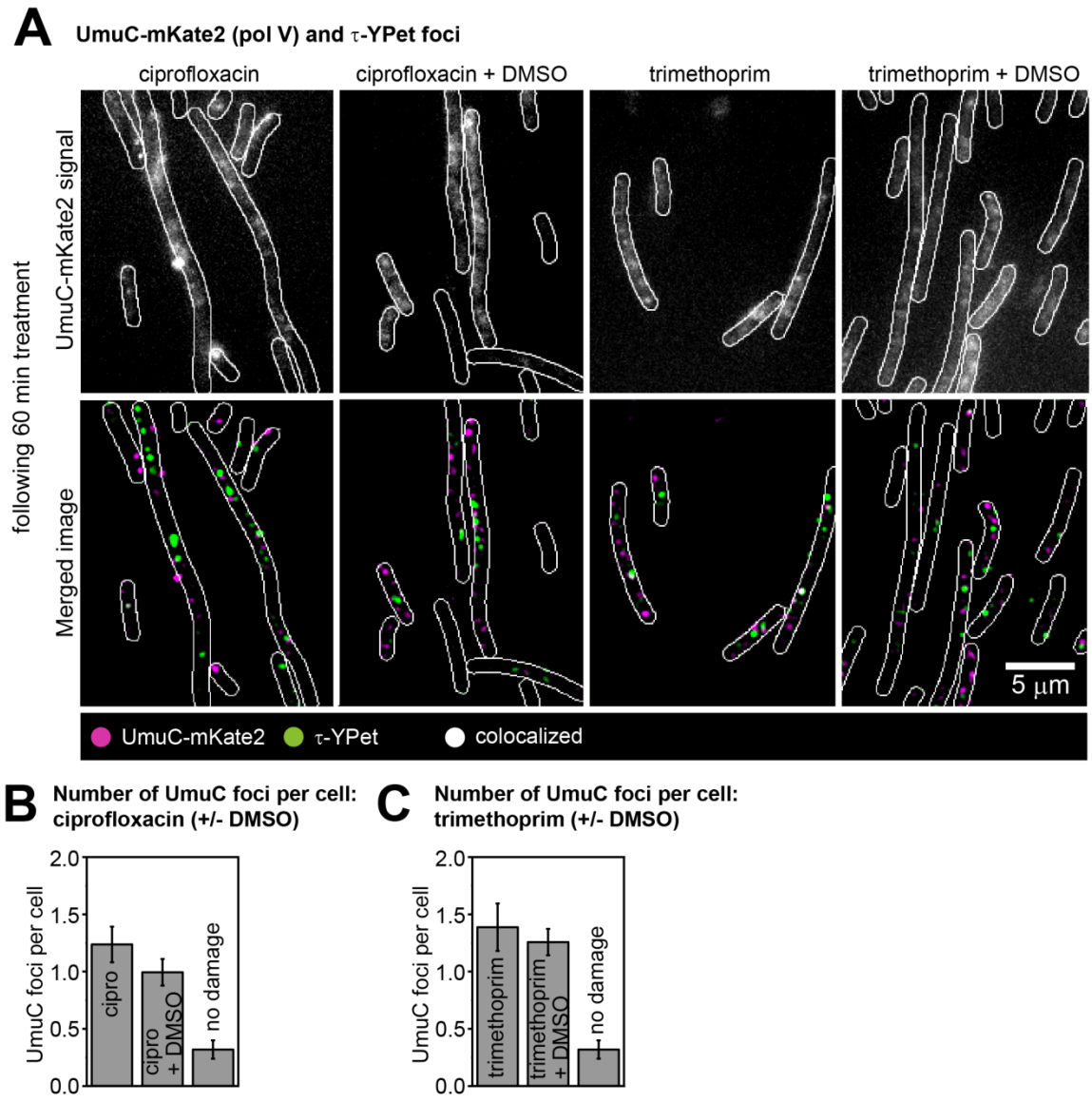

Fig. S12. Measuring the number of pol V foci per cell following ciprofloxacin or trimethoprim treatment under normal conditions or ROS-scavenging conditions in *lexA*(Def) cells. (*A*) UmuC-mKate2 activity at replisomes in *lexA*(Def) cells. Cells were treated for 60 min prior to imaging. Upper row: unfiltered image of an average projection showing UmuC-mKate2 foci that last >1 s (from left to right: ciprofloxacin, ciprofloxacin-DMSO, trimethoprim, trimethoprim-DMSO). Bottom row: merged image showing UmuC-mKate2 foci in magenta and τ-YPet foci in green (from left to right: ciprofloxacin, ciprofloxacin-DMSO, trimethoprim, trimethoprim-DMSO). Scale bar represents 5 μm. (*B*) Number of UmuC-mKate2 foci per cell of foci that last > 1 s. Error bars represent standard error of the mean. Number of cells included in analysis: *n*(ciprofloxacin) = 97, *n*(ciprofloxacin-DMSO) = 109, *n*(untreated) = 87. (*C*) Binding behavior of UmuC-mKate2 at replisomes after ciprofloxacin-alone or ciprofloxacin-DMSO treatment. Mean average autocorrelation function (ciprofloxacin-alone: dark grey line, ciprofloxacin-DMSO: light grey line). Error bar represents standard error of the mean. We conservatively estimate that >400 trajectories from >400 replisomes were used in each measurement. (*D*) Number of UmuC-mKate2 foci per cell. Error bars represent standard error of the mean. Number of cells included in analysis: *n*(trimethoprim) = 102, *n*(trimethoprim-DMSO) = 120, *n*(untreated) = 87. (*E*) Binding behavior of UmuC-mKate2 at replisomes

after trimethoprim-alone or trimethoprim-DMSO treatment. Mean average autocorrelation function (trimethoprim-alone: magenta line, trimethoprim-DMSO: light magenta line). Error bar represents standard error of the mean. We conservatively estimate that >550 trajectories from >550 replisomes were used in each measurement.

SI Appendix Figure 13

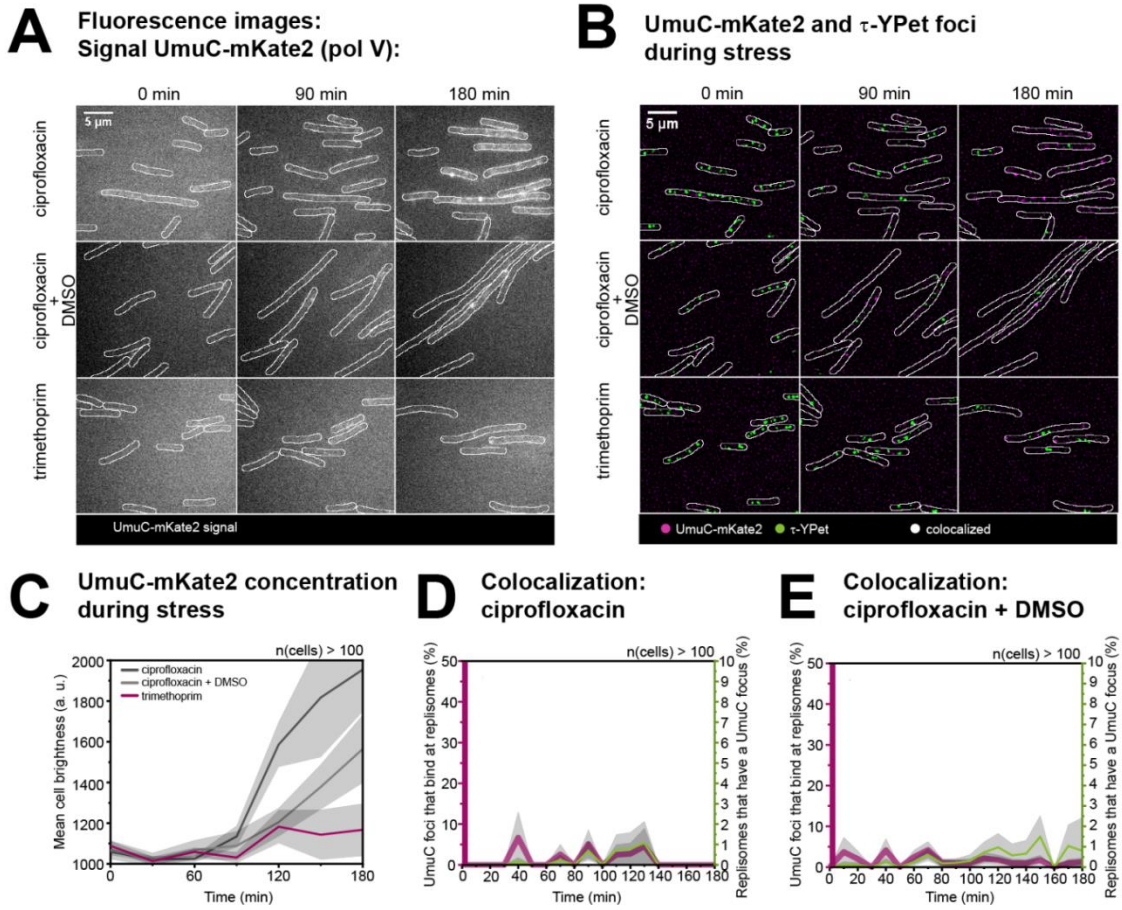

Fig. S13. UmuC concentration and activity following ciprofloxacin or trimethoprim treatment under normal conditions or ROS-scavenging conditions. (*A*) Images showing UmuC-mKate2 (pol V) signal at 0, 90 and 180 min (left to right) for ciprofloxacin-alone, ciprofloxacin-DMSO treatment or trimethoprim-alone treatment (top to bottom). Scale bar represents 5 µm. (*B*) Merged images showing UmuC-mKate2 (pol V) foci in magenta and τ-YPet (replisome) foci in magenta at 0, 90 and 180 min (left to right). Colocalized foci would appear as white foci. Scale bar represents 5 µm. (*C*) Concentration of UmuC-mKate2 during stress. Mean cell brightness is plotted against time (ciprofloxacin-alone: dark grey line, ciprofloxacin-DMSO: light grey line, trimethoprim-alone: magenta line). At each time-point, data are derived from >100 cells. Grey shaded error bands represent standard error of the mean. (*D*) Colocalization measurements following ciprofloxacin-alone treatment over 180 min: percentage of UmuC foci that are bound at replisomes (magenta line), percentage of replisomes that contain a UmuC focus (green line). Grey shaded error bands represent the standard error of the mean from three biological replicates together. Measurements are from >100 cells per time point. (*E*) Colocalization measurements following ciprofloxacin-DMSO treatment over 180 min: percentage of UmuC foci that are bound at replisomes (magenta line), percentage of replisomes that contain a UmuC focus (green line). Grey shaded error bands represent the standard error of the mean from three biological replicates together. Measurements are from >100 cells per time point.

SI Appendix Figure 14

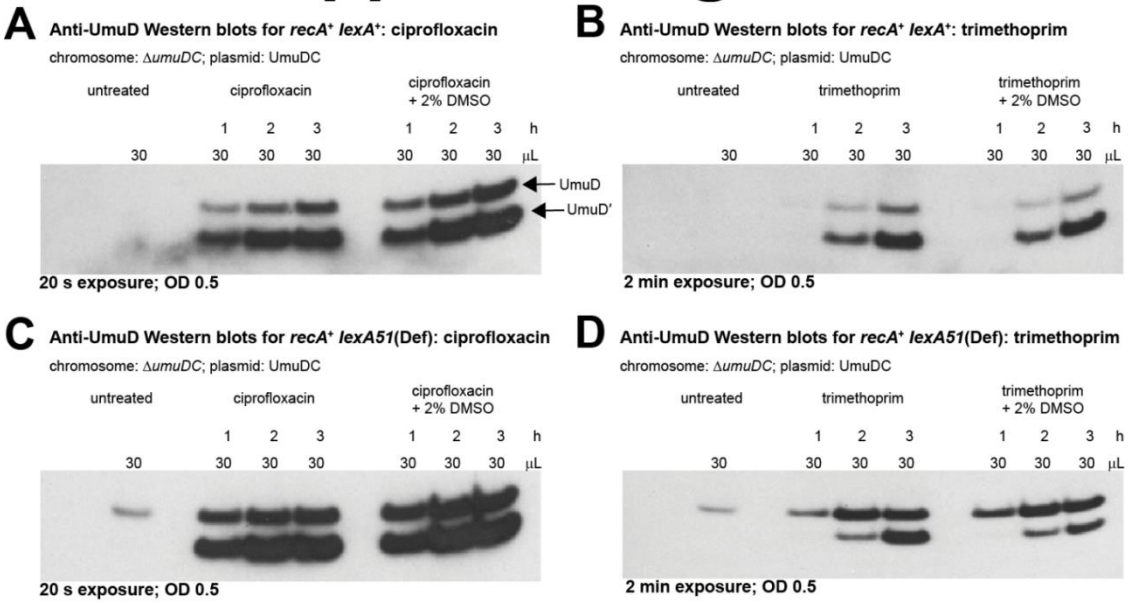

Fig. S14. Western blots with anti-UmuD antibodies measuring levels of UmuD′. For each lane, 30 μL of lysate were loaded from cultures at OD_{600} 0.5. All strains used are Δ*umuDC* expressing UmuDC from a low-copy number plasmid (pRW154). After treatment, time points were taken at 1, 2, 3 h. (*A*) Western blot of *recA*$^+$ *lexA*$^+$ cells (RW120): untreated, treated with ciprofloxacin or ciprofloxacin + 2% DMSO. (*B*) Western blot of *recA*$^+$ *lexA*$^+$ cells: untreated, treated with trimethoprim or trimethoprim + 2% DMSO. (*C*) Western blot of *recA*$^+$ *lexA51*(Def) cells (RW546): untreated, treated with ciprofloxacin or ciprofloxacin + 2% DMSO. (*D*) Western blot of *recA*$^+$ *lexA51*(Def) cells: untreated, treated with trimethoprim or trimethoprim + 2% DMSO.

4.7 References

1. Zhao X, Drlica K. Reactive oxygen species and the bacterial response to lethal stress. *Curr Opin Microbiol*. 2014;21:1–6.

2. van Acker H, Coenye T. The role of reactive oxygen species in antibiotic-mediated killing of bacteria. *Trends Microbiol.* 2017;25:456–466.

3. Imlay JA. The molecular mechanisms and physiological consequences of oxidative stress: lessons from a model bacterium. *Nat Rev Microbiol*. 2013;11:443–454.

4. Imlay JA. Where in the world do bacteria experience oxidative stress? *Environ Microbiol*. 2019;21:521–530.

5. Hong Y, Li L, Luan G, Drlica K, Zhao X. Contribution of reactive oxygen species to thymineless death in *Escherichia coli. Nat Microbiol.* 2017;2:1667–1675.

6. Liu A, Tran L, Becket E, Lee K, Chinn L, Park E, et al. Antibiotic sensitivity profiles determined with an *Escherichia coli* gene knockout collection: Generating an antibiotic bar code. *Antimicrob Agents Chemother*. 2010;54:1393–1403.

7. Foti JJ, Devadoss B, Winkler JA, Collins JJ, Walker GC. Oxidation of the guinine nucleotide pool underlies cell death by bactericidial antibiotics. *Science*. 2012;336:315–319.

8. Dwyer DJ, Kohanski MA, Collins JJ. Role of reactive oxygen species in mechanisms of antimicrobial resistance in bacteria. *Curr Opin Microbiol*. 2009;12:482–489.

9. Drlica K, Zhao X. DNA gyrase, topoisomerase IV, and the 4-quinolones. *Microbiol Mol Biol Rev*. 1997;61:377–392.

10. Champoux JJ. DNA topoisomerases: structure, function, and mechanism. *Annu Rev Biochem*. 2001;70:369–413.

11. Zhao X, Xu C, Domagala J, Drlica K. DNA topoisomerase targets of the fluoroquinolones: a strategy for avoiding bacterial resistance. *Proc Natl Acad Sci USA*. 1997;94:13991–6.

12. Goswami M, Mangoli SH, Jawali N. Involvement of reactive oxygen species in the action of ciprofloxacin against *Escherichia coli*. *Future Microbiol*. 2014;6:949–954.

13. Giroux X, Su W-L, Bredeche M-F, Matic I. Maladaptive DNA repair is the ultimate

contributor to the death of trimethoprim-treated cells under aerobic and anaerobic conditions. *Proc Natl Acad Sci USA*. 2017;114:11512–11517.

14. Kohanski MA, Dwyer DJ, Hayete B, Lawrence CA, Collins JJ. A common mechanism of cellular death induced by bactericidal antibiotics. *Cell*. 2007;130:797–810.

15. Dwyer DJ, Collins JJ, Walker GC. Unraveling the physiological complexities of antibiotic lethality. *Annu Rev Pharmacol Toxicol*. 2015;55:313–332.

16. Gruber CC, Walker GC. Incomplete base excision repair contributes to cell death from antibiotics and other stresses. *DNA Repair*. 2018;71:108–117.

17. Mi H, Wang D, Xue Y, Zhang Z, Niu J, Hong Y, et al. Dimethyl sulfoxide protects *Escherichia coli* from rapid antimicrobial-mediated killing. *Antimicrob Agents Chemother*. 2016;60:5054–5058.

18. Drlica K, Malik M, Kerns RJ, Zhao X. Quinolone-mediated bacterial death. *Antimicrob Agents Chemother*. 2008;52:385–392.

19. Yamada M, Nunoshiba T, Shimizu M, Gruz P, Kamiya H, Harashima H, et al. Involvement of Y-family DNA polymerases in mutagenesis caused by oxidized nucleotides in *Escherichia coli. J Bacteriol*. 2006;188:4992–4995.

20. Moore JM, Correa R, Rosenberg SM, Hastings PJ. Persistent damaged bases in DNA allow mutagenic break repair in *Escherichia coli. PLoS Genet.* 2017;13:e1006733.

21. Shee C, Gibson JL, Darrow MC, Gonzalez C, Rosenberg SM. Impact of a stress-inducible switch to mutagenic repair of DNA breaks on mutation in *Escherichia coli. Proc Natl Acad Sci USA*. 2011;108:13659–13664.

22. Shee C, Ponder R, Gibson JL, Rosenberg SM. What limits the efficiency of double-strand break-dependent stress-induced mutation in *Escherichia coli*? *J Mol Microbiol Biotechnol*. 2012;21:8–19.

23. Ponder RG, Fonville NC, Rosenberg SM. A switch from high-fidelity to error-prone DNA double-strand break repair underlies stress-induced mutation. *Mol Cell*. 2005;19:791–804.

24. Foster PL. Stress-Induced Mutagenesis in Bacteria. *Crit Rev Biochem Mol Biol*. 2007;42:373–397.

25. Rosenberg SM, Shee C, Frisch RL, Hastings PJ. Stress-induced mutation *via* DNA

breaks in *Escherichia coli*: A molecular mechanism with implications for evolution and medicine. *Bioessays*. 2012;34:885–892.

26. Godoy VG, Jarosz DF, Simon SM, Abyzov A, Walker GC. UmuD and RecA directly modulate the mutagenic potential of the Y-family DNA polymerase DinB. *Mol Cell*. 2007;28:1058–1070.

27. Mallik S, Popodi EM, Hanson AJ, Foster PL. Interactions and localization of *Escherichia coli* error-prone DNA polymerase IV after DNA damage. *J Bacteriol*. 2015;197:2792–2809.

28. Pomerantz RT, Kurth I, Goodman MF, O'Donnell M. Preferential D-loop extension by a translesion DNA polymerase underlies error-prone recombination. *Nat Struct Mol Biol.* 2013;20:748–755.

29. Pomerantz RT, Goodman MF, O'Donnell ME. DNA polymerases are error-prone at RecA-mediated recombination intermediates. *Cell Cycle*. 2013;12:2558–2563.

30. Indiani C, Patel M, Goodman MF, O'Donnell ME. RecA acts as a switch to regulate polymerase occupancy in a moving replication fork. *Proc Natl Acad Sci USA*. 2013;110:5410–5.

31. Cafarelli TM, Rands TJ, Godoy VG. The DinB RecA complex of *Escherichia coli* mediates an efficient and high-fidelity response to ubiquitous alkylation lesions. *Environ Mol Mutagen Mutagen*. 2014;55:92–102.

32. Henrikus SS, McGrath AE, Jergic S, Ritger ML, Pham PT, Wood EA, et al. UmuD and RecA* modulate the DNA-binding activity of DNA polymerase IV in *Escherichia coli*. bioRXiv. 2019; https://doi.org/10.1101/620195.

33. Tashjian TF, Danilowicz C, Molza A-E, Nguyen BH, Prévost C, Prentiss M, et al. Residues in the fingers domain of the translesion DNA polymerase DinB enable its unique participation in error-prone double strand break repair. *J Biol Chem*. 2019;jbc.RA118.006233.

34. Smith GR. Homologous recombination in prokaryotes: enzymes and controlling sites. Genome. 1989;31(2):520–527.

35. Simmons LA, Foti JJ, Cohen SE, Walker GC. The SOS regulatory network. *EcoSal Plus*. 2008;3:doi:10.1128/ecosalplus.5.4.3.

36. McPartland A, Green L, Echols H. Control of recA gene RNA in *E. coli*: Regulatory and

signal genes. *Cell*. 1980;20:731–737.

37. Newmark KG, O'Reilley EK, Pohlhaus JR, Kreuzer KN. Genetic analysis of the requirements for SOS indcution by nalidixic acid in *Escherichia coli*. *Gene*. 2005;356:69–76.

38. Courcelle J, Khodursky A, Peter B, Brown PO, Hanawalt PC. Comparative gene expression profiles following UV exposure in wild-type and SOS-deficient. *Genetics*. 2001;158:41–64.

39. Henrikus SS, Wood EA, McDonald JP, Cox MM, Woodgate R, Goodman MF, et al. DNA polymerase IV primarily operates outside of DNA replication forks in *Escherichia coli*. *PLoS Genet.* 2018;14:e1007161.

40. Imlay JA. Transcription factors that defend bacteria against reactive oxygen species. *Annu Rev Microbiol*. 2015;69:93–108.

41. Seo SW, Kim D, Szubin R, Palsson BO. Genome-wide reconstruction of OxyR and SoxRS transcriptional regulatory networks under oxidative stress in *Escherichia coli* K-12 MG1655. *Cell Rep*. 2015;12:1289–1299.

42. Storz G, Tartaglia LA, Ames BN. The OxyR regulon. *Antonie van Leeuwenhoek, Int J Gen Mol Microbiol*. 1990;58:157–161.

43. Jung IL, Kim IG. Transcription of *ahpC, katG*, and *katE* genes in *Escherichia coli* is regulated by polyamines: Polyamine-deficient mutant sensitive to H_2O_2-induced oxidative damage. *Biochem Biophys Res Commun*. 2003;301:915–922.

44. Lavrrar JL, Christoffersen CA, McIntosh MA. Fur-DNA interactions at the bidirectional *fepDGC-entS* promoter region in *Escherichia coli. J Mol Biol.* 2002;322:983–995.

45. Ronayne EA, Wan YCS, Boudreau BA, Landick R, Cox MM. P1 Ref endonuclease: a molecular mechanism for phage-enhanced antibiotic lethality. *PLoS Genet*. 2016;12:e1005797.

46. Goswami M, Mangoli SH, Jawali N. Involvement of reactive oxygen species in the action of ciprofloxacin against *Escherichia coli. Antimicrob Agents Chemother*. 2006;50:949–954.

47. Robinson A, McDonald JP, Caldas VEA, Patel M, Wood EA, Punter CM, et al. Regulation of mutagenic DNA polymerase V activation in space and time. *PLoS Genet*. 2015;11:e1005482.

48. Li G-W, X. Sunney Xie. Central dogma at the single-molecule level of living cells. *Nature*. 2011;475:308–315.

49. Zaslaver A, Bren A, Ronen M, Itzkovitz S, Kikoin I, Shavit S, et al. A comprehensive library of fluorescent transcriptional reporters for *Escherichia coli. Nat Methods*. 2006;3:623–628.

50. Rodriguez- Rosado A, Valencia EY, Rodriguez- Rojas A, Coloma C, Galhardo RS, Blazquez J, et al. Reactive oxygen species are major contributors to SOS-mediated mutagenesis induced by fluoroquinolones. *bioRχiv*. 2018; http://dx.doi.org/10.1101/428961.

51. Shen LL, Pernet AG. Mechanism of inhibition of DNA gyrase by analogues of nalidixic acid: The target of the drugs is DNA. *Proc Natl Acad Sci USA*. 1985;82:307–311.

52. Dorr T, Lewis K, Vulic M. SOS response induces persistence to fluoroquinolones in *Escherichia coli. PLoS Genet*. 2009;5:e1000760.

53. Shee C, Cox BD, Gu F, Luengas EM, Joshi MC, Chiu L-Y, et al. Engineered proteins detect spontaneous DNA breakage in human and bacterial cells. *Elife*. 2013;2:1–25.

54. Ghodke H, Paudel B, Lewis JS, Jergic S, Gopal K, Romero Z, et al. Spatial and temporal organization of RecA in the *Escherichia coli* DNA-damage response. *Elife*. 2019;8:e42761.

55. Pribis JP, Garcia-Villada L, Zhai Y, Lewin-Epstein O, Wang A, Liu J, et al. Gamblers: an antibiotic-induced evolvable cell subpopulation differentiated by reactive-oxygen-induced general stress response. *Mol Cell*. 2019;74:785-800.

56. Ennis DG, Fisher B, Edmiston S, Mount DW. Dual role for *Escherichia coli* RecA protein in SOS mutagenesis. *Proc Natl Acad Sci USA*. 1985;82:3325–3329.

57. Snyder M, Drlica K. DNA gyrase on the bacterial chromosome: DNA cleavage induced by oxolinic acid. *J Mol Biol*. 1979;131:287–302.

58. Deitz WH, Cook TM, Goss W a. Mechanism of action of nalidixic acid on *Escherichia coli* III. Conditions required for lethality. *J Bacteriol*. 1966;91:768–773.

59. Tang M, Shen X, Frank EG, O'Donnell M, Woodgate R, Goodman MF. UmuD′$_{(2)}$C is an error-prone DNA polymerase, *Escherichia coli* pol V. *Proc Natl Acad Sci USA*. 1999;96:8919–8924.

60. Cirz RT, Chin JK, Andes DR, De Crécy-Lagard V, Craig WA, Romesberg FE. Inhibition of mutation and combating the evolution of antibiotic resistance. *PLoS Biol*. 2005;3:e176.

61. Sakai A, Nakanishi M, Yoshiyama K, Maki H. Impact of reactive oxygen species on spontaneous mutagenesis in *Escherichia coli. Genes to Cells.* 2006;11:767–778.

62. Gleckman R, Blagg N, Joubert DW. Trimethoprim: Mechanisms of action, antimicrobial activity, bacterial resistance, pharmacokinetics, adverse reactions, and therapeutic indications. *Pharmacotherapy*. 1981;1:14–19.

63. Birdsall B, Roberts GC, Feeney J, Dann J, Burgen A. Trimethoprim binding to bacterial and mammalian dihydrofolate reductase: a comparison by proton and carbon-13 nuclear magnetic resonance. *Biochemistry*. 1983;22:5597–5604.

64. Vlašić I, Ivančić-Baće I, Imešek M, Mihaljević B, Brčić-Kostić K. RecJ nuclease is required for SOS induction after introduction of a double-strand break in a RecA loading deficient *recB* mutant of *Escherichia coli. Biochimie*. 2008;90:1347–1355.

65. Vlašić I, Šimatović A, Brčić-Kostić K. Genetic requirements for high constitutive SOS expression in *recA730* mutants of *Escherichia coli. J Bacteriol*. 2011;193:4643–4651.

66. Morimatsu K, Kowalczykowski SC. RecFOR proteins load RecA protein onto gapped DNA to accelerate DNA strand exchange: A universal step of recombinational repair. *Mol Cell*. 2003;11:1337–1347.

67. Sakai A, Cox MM. RecFOR and RecOR as distinct RecA loading pathways. *J Bio*. 2009;284:3264–3272.

68. Lesterlin C, Ball G, Schermelleh L, Sherratt DJ. RecA bundles mediate homology pairing between distant sisters during DNA break repair. *Nature*. 2014;506:249–253.

69. Frank EG, Ennis DG, Gonzalez M, Levine a S, Woodgate R. Regulation of SOS mutagenesis by proteolysis. *Proc Natl Acad Sci USA*. 1996;93:10291–10296.

70. Huang LC, Wood EA, Cox MM. Convenient and reversible site-specific targeting of exogenous DNA into a bacterial chromosome by use of the FLP recombinase: The FLIRT system. *J Bacteriol.* 1997;179:6076–6083.

71. Ennis DG, Amunsden SK, Smith GR. Genetic functions promoting homologous recombination in *Escherichia coli*: A study of inversions in phage λ. *Genetics*. 1987;115:11–24.

72. Frank EG, Hauser J, Levine AS, Woodgate R. Targeting the UmuD, UmuD′, and MucA′ mutagenesis proteins to DNA by RecA protein. *Proc Natl Acad Sci USA*. 1993;90:8169–8173.

73. Harris DR, Etc. Directed evolution of ionizing radiation resistance in *Escherichia coli*. *J Bacteriol*. 2009;191:5240–5252.

74. Blattner FR, Plunkett III G, Bloch CA, Perna NT, Burland V, Riley M, et al. The complete genome sequence of *Escherichia coli* K-12. *Science*. 1997;277:1453–1474.

75. Ho C, Kulaeva OI, Levine AS, Woodgate R. A rapid method for cloning mutagenic DNA repair genes: Isolation of *umu*-complementing genes from multidrug resistance plasmids R391, R446b, and R471a. *J Bacteriol*. 1993;175:5411–5419.

76. Rangarajan S, Woodgate R, Goodman MF. Replication restart in UV-irradiated *Escherichia coli* involving pols II, III, V, PriA, RecA and RecFOR proteins. *Mol Microbiol*. 2002;43:617–628.

77. Schneider CA, Rasband WS, Eliceiri KW. NIH Image to ImageJ: 25 years of image analysis. *Nat Methods*. 2012;9:671–675.

78. Sliusarenko O, Heinritz J, Emonet T, Jacobs-Wagner C. High-throughput, subpixel-precision analysis of bacterial morphogenesis and intracellular spatio-temporal dynamics. *Mol Microbiol*. 2012;80:612–627.

4.8 Additional data

4.8.1 Recombination mediator protein RecF inhibits pol IV binding at replisomes

In cells, TLS and homologous recombination proteins are involved in repairing single-stranded gaps and double-strand breaks (1–5). It has been proposed that, initially following, SOS induction, TLS has preference over homologous recombination due to the time-limiting step of the D-loop formation (1,6). After the formation of recombinant ssDNA strands however, gaps are primarily repaired *via* homologous recombination (1). In agreement, a *recA* mutant with slower kinetics of RecA* filament formation, in comparison to wildtype *recA*, showed increased TLS levels (7). Similarly, cells lacking *recF* exhibited an increase in TLS levels. In addition, RecF often binds at replisomes in response to DNA damage (Chapter 6), suggesting that RecF may decrease TLS levels at the replisome.

In this sub-chapter, the colocalisation percentage of pol IV with replisomes was measured in *recF*$^+$ and Δ*recF* cells, following ciprofloxacin-DMSO treatment. Time-lapse movies were recorded following ciprofloxacin-DMSO treatment (3 h time-lapse movies, an image was taken every 10 min). In *recF*$^+$ cells, a strong dip in colocalisation was observed at 30 min after ciprofloxacin addition (Chapter 4.6, Figure S11); fewer pol IV foci were bound in the vicinity of replisomes. In Δ*recF* cells, colocalisation of pol IV with replisomes did not decline directly after ciprofloxacin addition in comparison to wild-type *recF* cells (Figure 6). No drop in colocalisation was observed. When measuring colocalisation of replisomes with pol IV foci, deleting *recF* leads to an increase in colocalisation directly after damage induction. From 40 min, colocalisation is slightly decrease compared to wild-type *recF* (Figure 6).

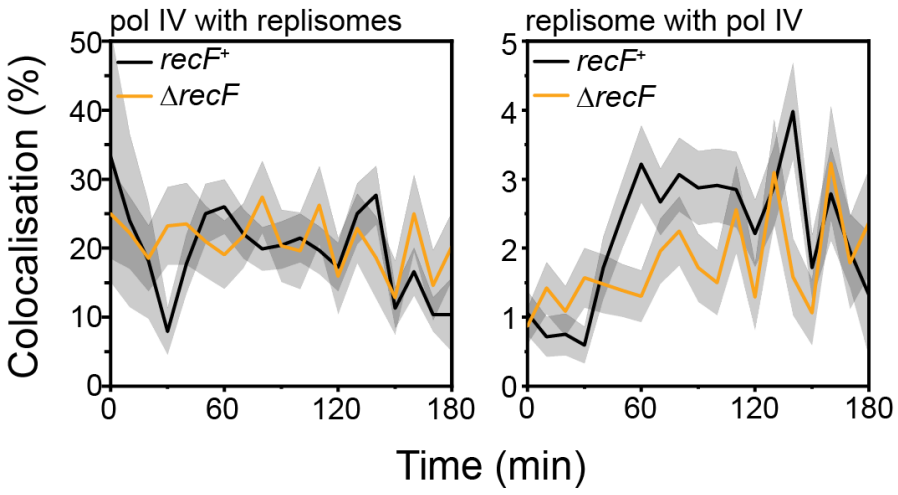

Figure 6. Colocalisation measurement of pol IV with replisomes in *recF*$^+$ (black) and Δ*recF* (orange). Cells were treated with ciprofloxacin-DMSO over 3 h. Left: percentage of pol IV bound at replisomes. Right: percentage of replisomes that contain a pol IV focus. Data points for Δ*recF* experiments are an average over duplicates, data points for *recF*$^+$ experiments are an average over triplicates. Error bars represent the standard deviation of the mean.

In conclusion, the deletion of the recombination mediator protein RecF increases the activity of pol IV at replisomes within the first 30 min after ciprofloxacin addition. These results suggest that during this period RecF activity inhibits replisomal pol IV activity, consistent with RecF having a role at replisomes (Chapter 6). In the future, it would be interesting to conduct similar experiments in an either *recO* or *recR* deletion background.

4.8.2 Materials and Methods

Microscopy, flow cell design and data analysis

All experimental procedures (i.e. imaging in flow cell) were carried out as described in Chapter 4.5 *Materials and Methods.*

Strain construction

Table 4.2. Strains used in this sub-chapter.

Strain	Relevant Genotype	Parent strain	Source/technique
MG1655	*dinB*$^+$ *dnaX*$^+$ *recB*$^+$ *lexA*$^+$	-	published (8)
EAW643	*dinB-YPet*::FRT *dnaX-mKate2*::Kan^R	EAW633	published (9)
SSH102	*dinB-YPet*::FRT *dnaX-mKate2*::FRT Δ*recF*::Kan^R	EAW643	Transduction of EAW643 Kan^S with P1 grown on EAW629 (10)

4.8.3 References

1. Fuchs RP. Tolerance of lesions in E. coli: Chronological competition between translesion synthesis and damage avoidance. *DNA Repair*. 2016;44:51–8.

2. Shee C, Gibson JL, Rosenberg SM. Two mechanisms produce mutation hotspots at DNA breaks in *Escherichia coli. Cell Rep.* 2012;2:714–721.

3. Shee C, Ponder R, Gibson JL, Rosenberg SM. What limits the efficiency of double-strand break-dependent stress-induced mutation in *Escherichia coli*? *J Mol Microbiol Biotechnol*. 2012;21:8–19.

4. Rosenberg SM, Shee C, Frisch RL, Hastings PJ. Stress-induced mutation via DNA breaks in *Escherichia coli*: A molecular mechanism with implications for evolution and medicine. *Bioessays*. 2012;34:885–892.

5. Ponder RG, Fonville NC, Rosenberg SM. A switch from high-fidelity to error-prone DNA double-strand break repair underlies stress-induced mutation. *Mol Cell*. 2005;19:791–804.

6. Naiman K, Philippin G, Fuchs RP, Pages V. Chronology in lesion tolerance gives priority to

genetic variability. *Proc Natl Acad Sci USA*. 2014;111:5526–5531.

7. Naiman K, Pagès V, Fuchs RP. A defect in homologous recombination leads to increased translesion synthesis in *E. coli. Nucleic Acids Res.* 2016;44:7691–7699.

8. Blattner FR, Plunkett III G, Bloch CA, Perna NT, Burland V, Riley M, et al. The complete genome sequence of *Escherichia coli* K-12. *Science*. 1997;277:1453–1474.

9. Henrikus SS, Wood EA, McDonald JP, Cox MM, Woodgate R, Goodman MF, et al. DNA polymerase IV primarily operates outside of DNA replication forks in *Escherichia coli. PLoS Genet.* 2018;14:e1007161.

10. Henrikus SS, Henry C, Ghodke H, Wood EA, Mbele N, Saxena R, et al. RecFOR epistasis group: RecF and RecO have distinct localizations and functions in *Escherichia coli. Nucleic Acids Res*. 2019;47:2946–2965.

5 Modulation of DNA polymerase IV activity by UmuD and RecA* observed by single-molecule time-lapse microscopy

Sarah S. Henrikus, Amy E. McGrath, Slobodan Jergic, Matthew L. Ritger, Phuong T. Pham, Elizabeth A. Wood, Myron F. Goodman, Michael M. Cox, Antoine M. van Oijen, Harshad Ghodke, Andrew Robinson

bioRχiv, 2019, https://doi.org/10.1101/620195.

DNA polymerase IV (pol IV) is expressed at increased levels in *Escherichia coli* cells suffering high levels of DNA damage. In a recent single-molecule imaging study, we demonstrated that elevating the pol IV concentration is not sufficient to provide access to binding sites on the nucleoid, suggesting that other factors may recruit pol IV to its substrates once the DNA becomes damaged. Here we extend this work, investigating the proteins UmuD and RecA as potential modulators of pol IV activity. UmuD promotes long-lived association of pol IV with the nucleoid, whereas its cleaved form, UmuD′, which accumulates in DNA-damaged cells, inhibits binding. In agreement with proposed roles for pol IV in homologous recombination, up to 40% of pol IV foci colocalise with a probe for RecA* nucleoprotein filaments in ciprofloxacin-treated cells. A hyperactive RecA mutant, *recA*(E38K), allows pol IV to bind the nucleoid even in the absence of exogenous DNA damage. *In vitro,* RecA(E38K) forms RecA*-like structures that can recruit pol IV, even on double-stranded DNA, consistent with a physical interaction between RecA and pol IV. Together, the results indicate that UmuD and RecA modulate the binding of pol IV to its DNA substrates, which frequently coincide with RecA* structures.

I carried out and analysed all in vivo single-molecule experiments and plate reader assays. I was involved in strain construction, SPR experiments and the preparation of the manuscript.

5.1 Introduction

DNA polymerase IV (pol IV), encoded by *dinB*, is one of three specialised DNA polymerases that are produced at increased levels in *Escherichia coli* cells suffering DNA damage (1). *In vitro*, DNA polymerase IV is capable of translesion synthesis (TLS) on a variety of different lesion-containing DNA substrates (2–9). The most commonly proposed function for pol IV within cells is TLS at stalled replication forks, which may help to maintain chromosomal replication in cells experiencing DNA damage (10,11). However, in the cell, the majority of binding sites for pol IV on the nucleoid appear distal to replisome markers (12). There is significant evidence that pol IV participates in other pathways, including recombinational repair (13–19) and transcription-coupled TLS (20–23).

Single-molecule time-lapse imaging of fluorescently tagged pol IV in live *Escherichia coli* cells revealed that various DNA-damaging agents (ciprofloxacin, UV light and methyl methanesulfonate [MMS]) up-regulate the production of pol IV and create binding sites for pol IV on the nucleoid (12). Only 10% of the pol IV binding events (pol IV foci) occurred in the vicinity of replisomes. At late time points during the SOS response (90–100 min after damage induction) pol IV continued to form foci but no longer colocalised with replisomes, even at low levels. This led to the hypothesis that replisome access might be controlled by protein–protein interactions that change around 90–100 min after the induction of SOS. The results also suggest that pol IV function is focused primarily on events that occur away from the replication fork. The recruitment of pol IV to the processivity factor β strongly depends on the source of DNA damage (24), indicating that the type of DNA lesion and changes in metabolism may affect which repair pathway(s) pol IV participates in (9).

The UmuD protein and its cleaved form UmuD′ have a potential role in regulating pol IV activity in cells (25). The auto-cleavage of UmuD to the shorter form UmuD′ is induced by the cellular recombinase RecA, in particular RecA nucleoprotein filaments (denoted RecA*). UmuD cleavage (26–28) has long been understood to be a key step in the activation of the highly mutagenic enzyme DNA polymerase V (pol V) Mut (UmuD′$_2$C-RecA-ATP; (29)). Several lines of evidence suggest that the conversion of UmuD to UmuD′ might also regulate the activity of pol IV in *E. coli* (25). Far-Western blots and co-purification experiments indicate that pol IV interacts with UmuD$_2$ and UmuD′$_2$, but not the heterodimer UmuDD′ (25). Overexpression of pol IV induces high rates of –1 frameshift mutations in cells, that can be supressed by co-overexpression of UmuD, but not co-overexpression of UmuD′ (25). Furthermore, UmuD and UmuD′ overexpression reduced frequencies in an adaptive mutagenesis assay compared to an empty vector; overproduction of UmuD even lowered frequencies to equivalent levels of a catalytically dead *dinB* mutant (25). These observations have led to the proposal that UmuD status regulates the mutagenic activity of pol IV-dependent DNA synthesis. Despite these advances, it remains unclear if UmuD or UmuD′ solely affects the fidelity of pol IV, or if UmuD and UmuD′ might also regulate the DNA-binding activity of pol IV as a means to modulate pol IV-dependent mutagenesis.

A series of live-cell studies indicate that pol IV operates in the repair of double-strand breaks (DSBs) (15,19,30–34). Reducing DSB formation (by mitigating the destructive effects of reactive oxygen species) or introducing defects in the end-resection of double-strand breaks (Δ*recB* mutation) greatly reduces the number of pol IV foci formed in cells treated with ciprofloxacin or trimethoprim (35). At end-

resected DSBs, RecA nucleoprotein filaments facilitate repair through homologous recombination (36), suggesting that pol IV should colocalise with RecA* structures in cells engaged in DSB repair. A series of observations support this notion. Pol IV forms a physical interaction with RecA *in vitro* and this interaction modulates the fidelity of pol IV-dependent DNA synthesis (5,25,37). This interaction is proposed to provide pol IV with the ability to participate in DNA synthesis during RecA-dependent strand exchange reactions (38). In a fluorescence microscopy study (34), pol IV was shown to colocalise with RecA structures *in vivo*. However, the RecA-GFP probe that was used to observe RecA localisation does not differentiate between active forms of RecA (i.e. RecA*) and inactive forms, such as storage structures (39). Furthermore, this RecA-GFP (*recA4155-gfp*) probe is deficient in recombination, SOS induction and UV survival (40). It therefore remains unclear whether RecA* structures, such as those that form as intermediates of recombination, represent major or minor substrates for pol IV in cells. With the recent development of a RecA*-specific probe, PAmCherry-mCI (39), we are now in a position to measure pol IV–RecA* colocalisation directly in a time-resolved manner.

In this work, we set out to test the following: 1. whether the UmuD cleavage status affects the extent of pol IV focus formation and pol IV colocalisation with a replisome marker and/or the lifetimes of pol IV molecules binding to its substrates, and 2. whether pol IV predominantly binds at RecA* structures. We use the drug ciprofloxacin, a DNA gyrase inhibitor, that induces DSBs upon treatment (41). Using single-molecule live-cell imaging, we demonstrated that the binding of pol IV to the nucleoid is promoted by full-length UmuD in cells treated with the DNA damaging antibiotic ciprofloxacin. In contrast, UmuD′ diminishes pol IV binding. We observed that a large proportion of pol IV foci (up to 40%) colocalise with a RecA* marker in ciprofloxacin-treated cells. The *recA*(E38K) mutation (also known as *recA730*), which constitutively produces RecA*-like activity (42–44), promotes the binding activity of pol IV to the nucleoid, even in the absence of DNA damage. We further showed that pol IV physically interacts with RecA(E38K), which forms RecA*-like structures on single-stranded as well as double-stranded DNA, suggesting that pol IV might also associate with these RecA*-like structures in cells. These findings provide evidence for regulatory roles for both UmuD and RecA in modulating the binding activity of pol IV in *E. coli* cells. RecA* structures that likely mark sites of on-going DSB repair appear to serve as major binding sites for pol IV in live cells treated with ciprofloxacin.

5.2 Results

5.2.1 Deletion of *umuDC* increases pol IV-τ colocalisation

In a previous study, we carried out time-lapse measurements on *E. coli* cells treated with DNA damaging agents (12). We found that the colocalisation of pol IV foci with replisome markers started at ~10% prior to treatment, and dropped to < 5% (i.e. baseline levels) at a time-point 90–100 after the onset of treatment. In a separate study, we observed that pol V (UmuC-mKate2) enters the cytosol and forms foci on the nucleoid at this same 90 min time-point (45). This spatial re-distribution of the UmuC-mKate2 marker required cleavage of UmuD to UmuD′. The similar timing of the changes in pol IV and pol V localisation, together with established links between pol IV activity and UmuD/UmuD′ status described

above, led us to hypothesise that UmuD cleavage and/or formation of pol V at the 90 min time-point alters the colocalisation of pol IV with replisome markers.

To investigate the effect of pol V and/or its precursors (UmuD and UmuC) on the extent of pol IV focus formation and colocalisation with a replisome marker, we constructed two strains: i) *dinB-YPet dnaX-mKate2 umuDC*$^{+}$ (EAW643, (12)) and ii) *dinB-YPet dnaX-mKate2* Δ*umuDC* (SSH007). The *dnaX-mKate2* allele encodes for a fluorescent fusion of the τ clamp loader protein, serving as a marker for the replisome, τ-mKate2. We previously showed that the fluorescent protein fusion of DinB-YPet is fully functional, yielding pol IV-dependent mutagenesis activity upon ciprofloxacin treatment in both *dnaX*$^{+}$ and *dnaX-mKate2* cells (12,35).

Time-lapse movies were recorded for each strain after treatment with ciprofloxacin (30 ng mL^{-1}). At t = 0 min, images of the DinB-YPet signal and τ-mKate2 signal (replisome marker) were recorded for untreated cells. Directly after t = 0, ciprofloxacin was introduced to the flow cell and a time-lapse was recorded over a period of 3 h. We previously showed that a catalytically dead mutant DinB(D103N)-YPet does not form foci under these imaging conditions (12). This suggests that the DinB-YPet foci we normally detect are formed as DinB-YPet binds to the nucleoid and carries out DNA synthesis, at which point its diffusion is slowed sufficiently to produce a single-molecule focus. From the time-lapse movies, the numbers of DinB-YPet foci per cell, reflective of pol IV binding to the nucleoid (12), were determined at 0, 30, 60, 90 and 120 min time points (**Fig 1**). Colocalisation between DinB-YPet foci and τ-mKate2 foci was also monitored. In order to enhance diffusional contrast in our images we used longer exposure times when capturing DinB-YPet signal (300 ms) than in our previous study (50 ms; (12). We nonetheless recorded a complementary set of colocalisation measurements with the shorter exposure time of 50 ms in order to better capture transient foci and allow for more direct comparison with our previous results (**Fig S1**).

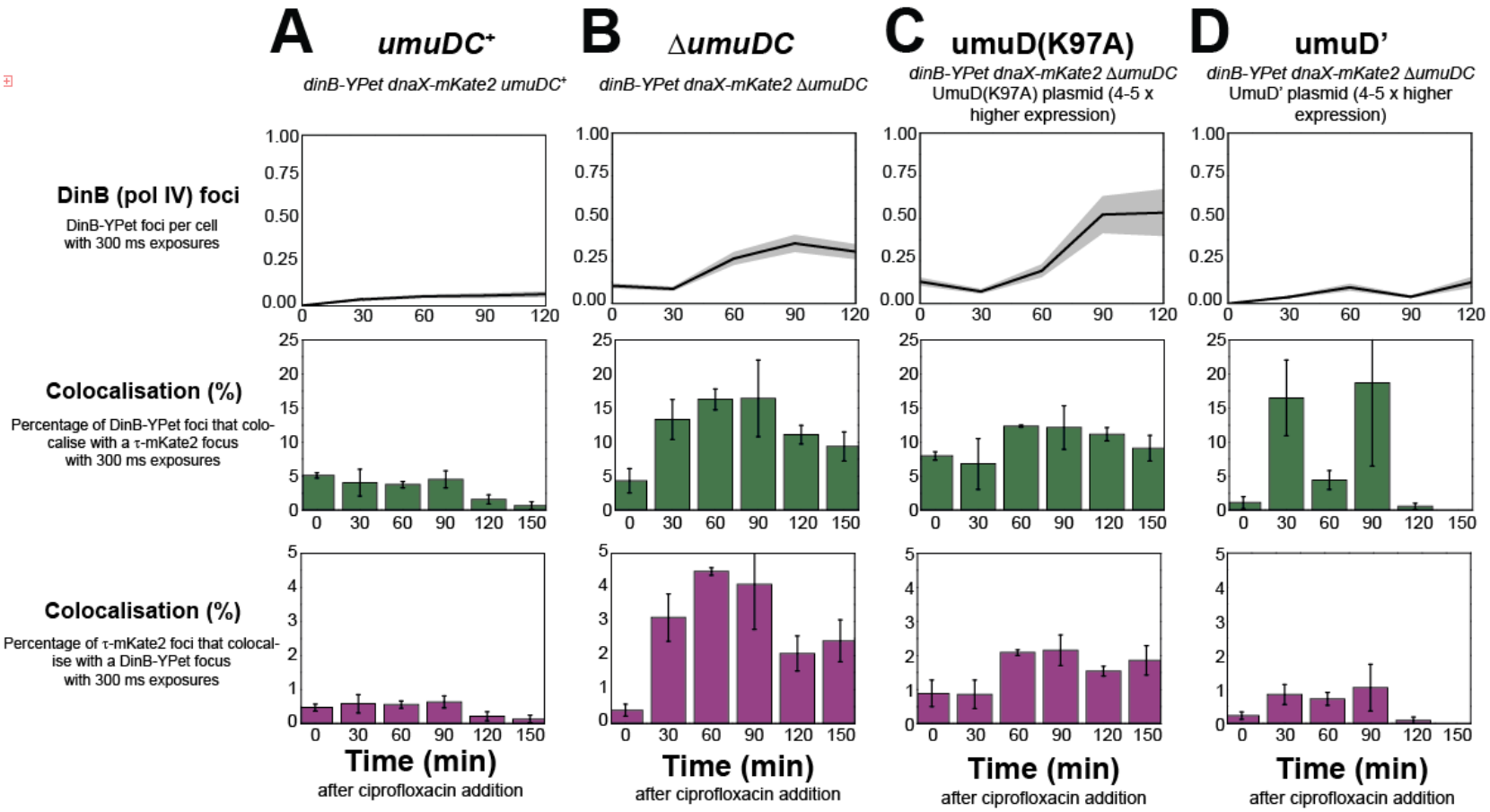

Figure 1. Number of DinB foci per cell and colocalisation measurements between DinB and τ in different *umuDC* mutants following ciprofloxacin treatment. (A) Upper panel: Number of DinB foci per cell in *umuDC*$^+$ at 300 ms exposures. Error bar represents standard error of the mean for $n > 100$ cells. Middle panel: Colocalisation percentage of DinB with DnaX (green bars) in *umuDC*$^+$. Time points are binned over 30 min. Error bar represents standard error of the mean between biological triplicates. Lower panel: Colocalisation percentage of DnaX with DinB (magenta bars) in *umuDC*$^+$. Time points are binned over 30 min. The other columns represent the same measurements as in (A), except from the cell strains (B) Δ*umuDC*, (C) Δ*umuDC* + UmuD(K97A) expressed from a plasmid, and (D) Δ*umuDC* + UmuD′ expressed from a plasmid.

We first monitored pol IV behaviour in cells expressing wild-type levels of UmuD and UmuC (EAW643, **Table 1**). Cells exhibited very few pol IV foci prior to ciprofloxacin treatment (**Fig 1A**, upper panel), as observed previously (12). After ciprofloxacin addition, the number of pol IV foci per cell increased to an average of 0.1 foci per cell from 60 min, i.e. one in ten cells exhibited a pol IV focus. Consistent with our previous observations (12), the percentage of pol IV foci that colocalised with τ-mKate2 dropped markedly between the 90 min and 120 min time-points (**Fig 1A**, middle panel). From 0–90 min after ciprofloxacin addition, 5% of pol IV foci colocalised with the replisome marker τ. From 120–150 min this decreased to < 2%. These values are somewhat lower than those we reported previously (10% dropping to < 5%) and is attributable to the longer image exposure times used in the current study (**Fig S1**). The percentage of τ foci that contained a pol IV focus followed a similar trend (**Fig 1A**, lower panel); from 0–90 min after ciprofloxacin addition, 0.5% of τ foci contained a pol IV focus, dropping to ~0.1% (indistinguishable from chance colocalisation) from 120–150 min.

We next examined the effect of deleting the *umuDC* operon (and thus eliminating UmuD and UmuC) on the number of pol IV foci and the extent of colocalisation with τ foci (SSH007, **Table 1**). From 30 min, 10–15% of pol IV foci colocalised with replisomes. Compared to *umuDC*$^+$ cells, Δ*umuDC* cells exhibited a three-fold increase in the number pol IV foci per cell with ~0.3 foci per cell from 60 min after ciprofloxacin addition (**Fig 1B**, upper panel). Moreover, deletion of *umuDC* led to a three-fold increase in the percentage of pol IV foci that colocalise with a τ focus (**Fig 1B**, middle panel). Interestingly, pol IV-τ colocalisation now persisted above 10% for the 90, 120 and 150 min time points. The percentage of τ foci that contained a pol IV focus was also elevated in the Δ*umuDC* background (**Fig 1B**, lower panel). From 30 min, 2–4% of τ foci contained a pol IV focus. Compared to *umuDC*$^+$ cells, this represents a six- to eight-fold increase in colocalisation.

Taken together, the time-lapse imaging results show that cells lacking *umuDC* exhibit an increase in the number of pol IV foci per cell, accompanied by enhanced pol IV-τ colocalisation during the late SOS response (90–120 min). In cells lacking *umuDC*, the maximum extent of pol IV-τ colocalisation is 15%. This suggests that in cells lacking UmuD and UmuC, replisomes still do not represent the major binding substrate for pol IV.

5.2.2 Cleavage state of UmuD affects the binding behaviour of pol IV

The increased numbers of pol IV foci and increased pol IV-τ colocalisation in Δ*umuDC* than in *umuDC*$^+$ cells could manifest through two scenarios: 1. the deletion of the *umuDC* operon, which encodes for pol V, eliminates competition between pol IV and pol V for binding sites on the nucleoid. 2. a subunit of pol V has a regulatory effect on pol IV focus formation and pol IV-τ colocalisation. It has been shown previously that $UmuD_2$ and $UmuD'_2$ physically interact with pol IV and modulate its mutagenic activity (25). To that end, we tested if UmuD or UmuD′ affect the extent of pol IV focus formation and the colocalisation between pol IV with τ, in the absence of UmuC (and thus pol V).

We constructed two strains, both of which include the *dinB-YPet* and *dnaX-mKate2* alleles: i) Δ*umuDC* (SSH007) expressing the non-cleavable UmuD(K97A) protein from a low-copy plasmid (SSH007 + pJM1243), and ii) SSH007 expressing the ‘cleaved’ UmuD′ protein from a low-copy plasmid

(SSH007 + pRW66). The amount of UmuD(K97A) and UmuD′ produced from each plasmid is 4–5-fold higher than UmuD expressed from its native chromosomal locus (39,46). Time-lapse analysis was repeated as described above.

We first explored the effects of expressing the non-cleavable UmuD(K97A) mutant in *dinB-YPet dnaX-mKate2* Δ*umuDC* cells (SSH007 + pJM1243, **Table 1**). At the 90 min time point, cells contained on average 0.6 pol IV foci per cell — a six-fold increase over *umuDC*$^{+}$ cells (**Fig 1C**, upper panel). This sixfold increase in pol IV foci per cell was accompanied by a three-fold increase in colocalisation with the replisome marker τ-mKate2 (**Fig 1C**, middle panel). From 30 min after damage induction, 13% of pol IV foci overlapped with a τ focus. This colocalisation remained relatively constant during the later stages of the SOS response; colocalisation did not drop below 9% from 90–120 min as observed in *umuDC*$^{+}$ cells. These observations reveal that UmuD(K97A), and by inference uncleaved UmuD, promote the binding of pol IV to DNA and do not limit pol IV-τ colocalisation beyond 90 min.

During the later stages of the SOS response (90 min after SOS induction), UmuD is cleaved to UmuD′ (47). To explore the effects of UmuD′ on pol IV behaviour, we imaged Δ*umuDC* cells expressing UmuD′ directly from a plasmid (SSH007 + pRW66, **Table 1**). These cells produced ~0.1 DinB-YPet foci per cell at 60 min (**Fig 1D**, upper panel), similar to *umuDC*$^{+}$ cells. In the cells expressing UmuD′, colocalisation of pol IV with τ was generally low, but highly variable (**Fig 1D**, middle panel). Two large spikes in colocalisation were apparent at the 30 and 90 min time points. However, due to the low number of foci available for analysis at these time-points, there was very large error associated with these values. No spikes in colocalisation were observed when measuring the proportion of τ foci that contained a pol IV focus (**Fig 1D**, lower panel). Importantly, the colocalisation of pol IV with τ decreased to < 1% after 90 min (**Fig 1D**, middle panel). Similarly, the percentage of τ foci that contained a pol IV focus drops between the 90 and 120 min time points (**Fig 1D**, lower panel). From 30–90 min, ~1% of τ foci contained a pol IV focus. By 120 min < 0.1% of τ foci contained a pol IV focus. Overall, the introduction of UmuD′ into Δ*umuDC* cells restores rates of focus formation and colocalisation with the replisome marker τ to near wild-type (*umuDC*$^{+}$) levels.

Taken together, the time-lapse imaging results show that the presence of non-cleavable UmuD results in an increase in nucleoid binding by pol IV, accompanied by increased pol IV-τ colocalisation during the late SOS response (90–120 min). Strikingly, UmuD′ suppresses the formation of pol IV foci, also limiting pol IV-τ colocalisation. These results suggest that UmuD cleavage represents a biochemical switch that alters aspects of pol IV activity. Importantly, these effects were apparent in the absence of UmuC, ruling out the possibility that the drop in pol IV colocalization with replisomes at 90 min occurs because of competition for substrates between pols IV and V.

5.2.3 UmuD(K97A) but not UmuD′ promotes long-lived pol IV binding events

Time-lapse imaging revealed differences in pol IV activity in *umuDC* variants with respect to the number of foci per cell and pol IV-τ colocalisation. We noted that in the various DinB-YPet images the foci formed in different strains appeared to exhibit differences in both intensity and shape (**Figs 2A–D**, first row; 300 ms exposures). For the *umuDC*$^{+}$ (**Fig 2A**), Δ*umuDC* (**Fig 2B**) and UmuD′-expressing cells

(**Fig 2D**), most foci were relatively faint and diffuse. In contrast, cells expressing UmuD(K97A) produced brighter, and much more distinct, pol IV foci. Reasoning that these differences might reflect differences in the nature of pol IV interactions with the substrates, we next measured the binding lifetime of pol IV at these sites. Image sets were recorded during three periods following the addition of ciprofloxacin: 20–45 min, 55–85 min and 120–180 min. For each time interval and each strain (EAW643, SSH007, SSH007 + pJM1243, SSH007 + pRW66; **Table 1**), burst acquisitions of the DinB-YPet signal were recorded (300 images of 34 ms exposure time, total length of 10.2 s). Subsequently, a corresponding image of the replisome marker τ-mKate2 was collected (see **Fig S2B** for imaging sequence).

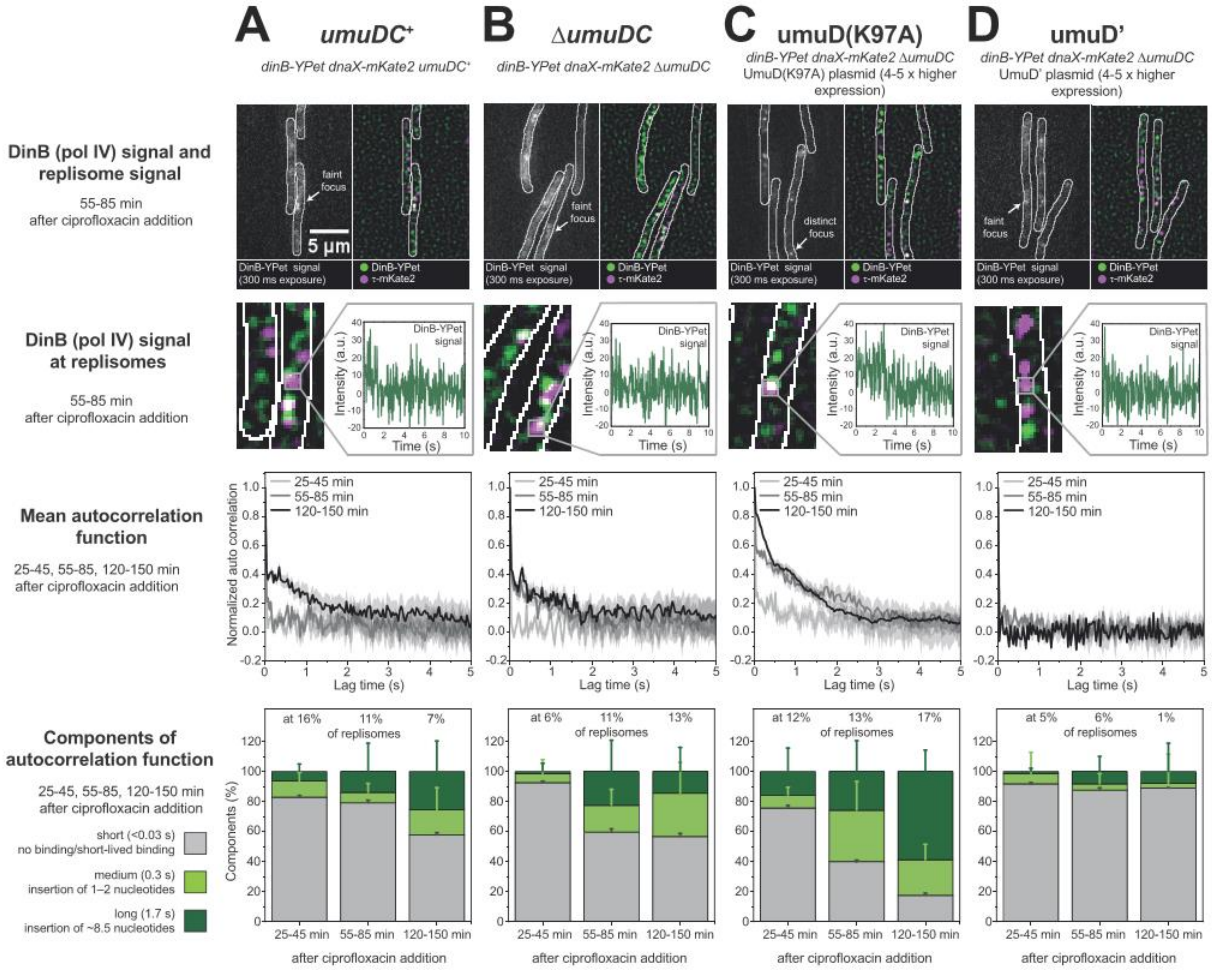

Figure 2. Binding activity of DinB at and away from replisomes in different *umuDC* mutants. (A) **Upper panel**: Images of DinB and DnaX signal in *umuDC*$^+$. Left: Projection of DinB signal consistent with 300 ms exposure times. Right: Merged images of discoidal filtered DinB (green) and DnaX signal (magenta). **Second panel from the top**: Exemplary trajectory showing DinB activity at replisomes in *umuDC*$^+$. **Third panel from the top**: Mean autocorrelation function showing DinB activity at replisomes in *umuDC*$^+$ at 25–45 (light grey line), 55–85 (grey line) and 120–150 min (black line). Error bars represent standard error of the mean over > 100 trajectories. **Bottom panel**: Components of the autocorrelation function for DinB at replisomes in *umuDC*$^+$ showing short (< 0.03 s, grey), medium (0.3 s, light green) and long components (1.7 s, dark green). The error bars for long and medium components were extracted from the fit error using the two-exponential fit (**Suppl. Fig 1G, H**). The error bar from the short components is equivalent to the standard error of the mean from the mean autocorrelation function at lag time 0s. (B) similar to (A), however in Δ*umuDC*. (C) similar to (A), however in Δ*umuDC* +

UmuD(K97A) expressed from a plasmid. (D) similar to (A), however in Δ*umuDC* + UmuD′ expressed from a plasmid.

For the *umuDC*$^+$, Δ*umuDC* and UmuD′-expressing cells, intensity trajectories collected at the positions of τ foci predominantly exhibited short-lived binding events (**Fig 2**, second row). Cells expressing UmuD(K97A), on the other hand, often produced long-lived pol IV binding events. To comprehensively assess the binding lifetimes of pol IV with respect to the UmuD status at sites of the replisome marker, mean autocorrelation functions were calculated for foci within each strain (**Fig 2**, third row; **Fig S2**). This approach allows us to extract characteristic timescales of signal fluctuations within intensity trajectories, which reflect the lifetimes of binding and dissociation events. Exponential fitting of each mean autocorrelation function gave time constants of τ = < 0.03, 0.3 and 3.3 s, reflecting short-, medium-, and long-lived binding events (**Fig S2**). For each strain and time interval after ciprofloxacin addition, the relative proportions of these binding events are plotted in **Fig 2** (fourth row).

For both *umuDC*$^+$ and Δ*umuDC* cells, most pol IV binding at τ positions appeared to be short-lived (**Figs 2A, B**). In the early stages of ciprofloxacin exposure (25–45 min) the components of the autocorrelation function were 80% short-lived (< 0.03 s, shorter than a frame of 34 ms), 10% medium (0.3 s) and 10% long-lived (3.3 s). In the later stages, (120–150 min), the proportion of medium-long lived events increased to 40%. In cells expressing UmuD(K97A) long-lived events were much more common: by the 120–150 min period medium and long-lived events comprised 80% of the autocorrelation function (**Fig 2C**). In stark contrast, cells expressing UmuD′ produced almost exclusively short-lived events (**Fig 2D**). UmuD′ appeared to supress the medium and long-lived pol IV binding events that occur in wild-type *umuDC*$^+$ background following ciprofloxacin treatment.

Taken together, the results indicate that UmuD(K97A) promotes long-lived DNA binding by pol IV, whereas UmuD′ inhibits binding. The deletion of *umuDC* only marginally increases the binding lifetime of pol IV compared to *umuDC*$^+$. The results demonstrate that the binding of pol IV to its substrates on the nucleoid is modulated by UmuD and UmuD′ in cells, independently of pol V formation (i.e. in cells lacking UmuC).

5.2.4 Pol IV binds frequently at RecA* structures

Like UmuD and UmuD′, the RecA recombinase modulates the mutagenic activity of pol IV (14,17). *In vitro*, DNA synthesis by pol IV is error-prone when operating on D-loop substrates that mimic recombination intermediates (14,17). Pol IV is known to participate in error-prone DSB repair under a variety of circumstances (13–19,31,33). *In vitro*, RecA also facilitates DNA synthesis by pol IV in replisomes (37). However, it remains to be determined whether pol IV binds at RecA* *in vivo*.

We determined whether pol IV colocalises with RecA* structures by visualising the localisations of fluorescent pol IV (DinB-YPet) and a RecA* marker PAmCherry-mCI; a red fluorescent protein fusion of a monomeric C-terminal fragment of the λ repressor that retains the ability to bind RecA* in cells (39). We carried out this analysis in SSH092 cells treated with ciprofloxacin — a potent inducer of DSBs (41,48) through reactive oxygen species-dependent and -independent pathways (49). Live-cell photoactivatable localisation microscopy (PALM) of SSH092 cells treated with ciprofloxacin was

performed by collecting images in both channels every 5 min over a period of 3 h following introduction of ciprofloxacin at time point t = 0 min. At each time point, a new field-of-view was recorded.

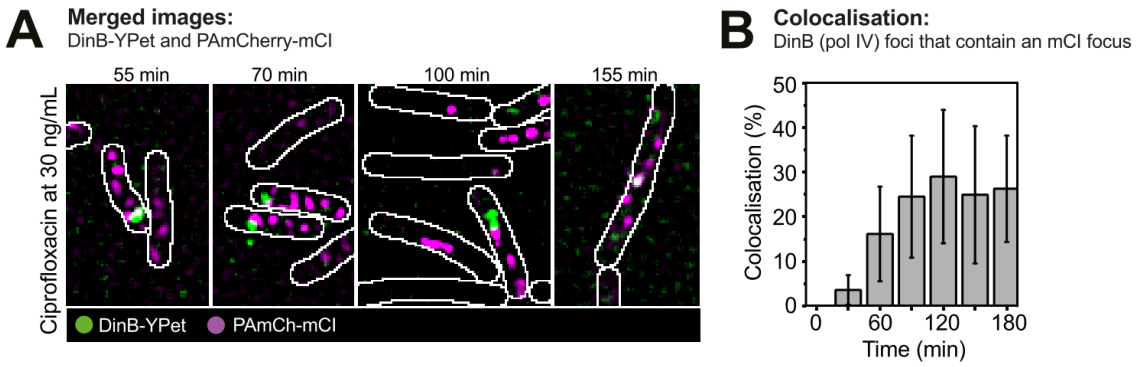

Figure 3. Colocalisation measurement between DinB and mCI after ciprofloxacin treatment. (A) Merged images of discoidal filtered DinB-YPet (green) and PAmCherry-mCI (magenta) at 55, 70, 100 and 155 min after ciprofloxacin addition. (B) Colocalisation percentage of DinB with mCI. Time points are binned over 30 min. Error bar represents standard deviation of biological quadruplicates.

Following ciprofloxacin treatment, cells typically contained multiple mCI foci (**Fig 3A**). At later time points, some cells contained more elongated "bundle" structures as described previously (39). We next determined the percentage of DinB-YPet foci that colocalised with mCI foci and bundle-like structures (**Fig 3B**). Prior to the introduction of ciprofloxacin, mCI foci were rarely formed in cells during normal metabolism (< 0.1 mCI foci per cell) consistent with our previous study (39). Unsurprisingly, we did not detect colocalisation of pol IV with the RecA* probe in untreated cells. Upon introduction of ciprofloxacin to the flow chamber, colocalisation remained low during the early phase of the SOS response (i.e., between 0–45 min after treatment). From 45 min after the introduction of ciprofloxacin, pol IV exhibited extensive colocalisation (10–40%) with mCI in cells. This extensive colocalisation persisted into the late stages of SOS (up to 180 min after treatment). We have previously noted that most of the mCI foci form at locations distal to the replisome in UV-irradiated cells (39). Notably, pol IV foci also mainly form at sites distinct from replisome markers.

5.2.5 RecA* promotes the binding of pol IV to the nucleoid

Having observed that a large proportion of pol IV colocalises with the RecA* probe mCI, we next set out to determine whether RecA* structures could recruit pol IV to the DNA. To isolate the effects of RecA* formation from other effects introduced by exogenous DNA damage, we utilised a RecA mutant, RecA(E38K), which is able to constitutively induce SOS and high rates of pol V-dependent mutagenesis in cells (42–44,50), suggestive of RecA* structures being formed in the absence of endogenous DNA damage.

Using surface plasmon resonance (SPR) as previously described (39), we observed that RecA(E38K) forms filaments on ssDNA *in vitro* (**Figs S3A, B**). Stable association of RecA(E38K) required the presence of ATPγS suggesting that RecA(E38K) forms filaments (**Fig S3B**). Additionally, RecA(E38K) filaments on ssDNA are competent to cleave LexA (**Fig S4**), suggesting that RecA(E38K)

forms RecA*-like structures on ssDNA (28,51). However, in the absence of DNA damage, we expect exposed ssDNA substrates for RecA(E38K) binding to occur infrequently. Therefore, we additionally tested whether constitutive SOS signalling may occur due to constitutive RecA(E38K)-dsDNA filament formation. To that end, we tested the ability of RecA(E38K) to form filaments on a 60-mer dsDNA substrate. We found that RecA(E38K) binds readily to dsDNA (**Figs S3C, D**) and that incubation of dsDNA plasmid substrates with RecA(E38K) promoted LexA cleavage (**Fig S4**), indicating that RecA(E38K) also forms RecA*-like structures on dsDNA (28,51).

Together, these results allowed us to establish conditions where we could now probe the binding of pol IV to constitutive RecA filaments, even in the absence of exogenous DNA damage, in live cells. We carried out single-molecule imaging of *dinB-YPet dnaX-mKate2* cells carrying wild-type or mutant alleles of *lexA* (encoding the SOS-response repressor LexA) and *recA* (encoding the recombinase RecA). Three strains were examined: i) cells with wild-type *lexA* and *recA* alleles (EAW643, *dinB-YPet dnaX-mKate2 lexA*$^{+}$ *recA*$^{+}$, **Table 1**), ii) cells that constitutively express high levels of DinB-YPet (and all other SOS-induced proteins) even in the absence of exogenous DNA damage (51); RW1594, *dinB-YPet dnaX-mKate2 lexA*[Def] *recA*$^{+}$, **Table 1**) and iii) cells that both produce high levels of DinB-YPet and constitutively formed RecA*-like structures (RW1598, *dinB-YPet dnaX-mKate2 lexA*[Def] *recA*[E38K], **Table 1**) (42–44,50). Although cells carrying the *recA*(E38K) allele are constitutive for SOS induction, our previous study of UmuC-mKate2 cells suggested that this induction only operates at ~50% of maximum – expression of UmuC-mKate2 could be further induced by UV irradiation, whereas this was not the case for *lexA*(Def) cells (45) We therefore included the additional *lexA*(Def) allele in RW1598 so that the intracellular concentration of pol IV would match that of RW1594 cells.

We set out to determine if the presence of RecA*-like structures formed by RecA(E38K) is sufficient to recruit pol IV to the nucleoid in cells. We recorded burst acquisitions of DinB-YPet motions in the three strains (300 images of 34 ms exposure time, total length of 10.2 s). For each movie, a corresponding image of the replisome marker τ-mKate2 was also captured (see **Figs S2A, B** for imaging sequence). As expected, cells with wild-type *lexA* and *recA* alleles produced few pol IV foci (**Fig 4A**) (12). Cells that carried the SOS-constitutive *lexA*(Def) allele and the wild-type *recA* allele produced a relatively high level of DinB-YPet signal, but produced few foci (**Fig 4B**) (12). This result is consistent with our previous study in which we concluded that binding is triggered by the presence of damage on the DNA, as opposed to mass action-driven exchange brought on by increased intracellular concentrations of pol IV (12). In contrast to both *recA*$^{+}$ strains, cells carrying both the *lexA*(Def) allele and the RecA*-constitutive *recA*(E38K) allele produced both high DinB-YPet signal and readily visible foci (**Fig 4C**). These results suggest two possibilities. First, in the absence of ciprofloxacin-induced double strand breaks, *lexA*(Def) *recA*(E38K) cells might produce some kind of DNA structures that serve as substrates for pol IV (and are not present in *lexA*(Def) cells carrying wild-type RecA). Second, nucleoid-associated RecA(E38K) assemblies might themselves acts as binding sites for pol IV in *recA*(E38K) cells.

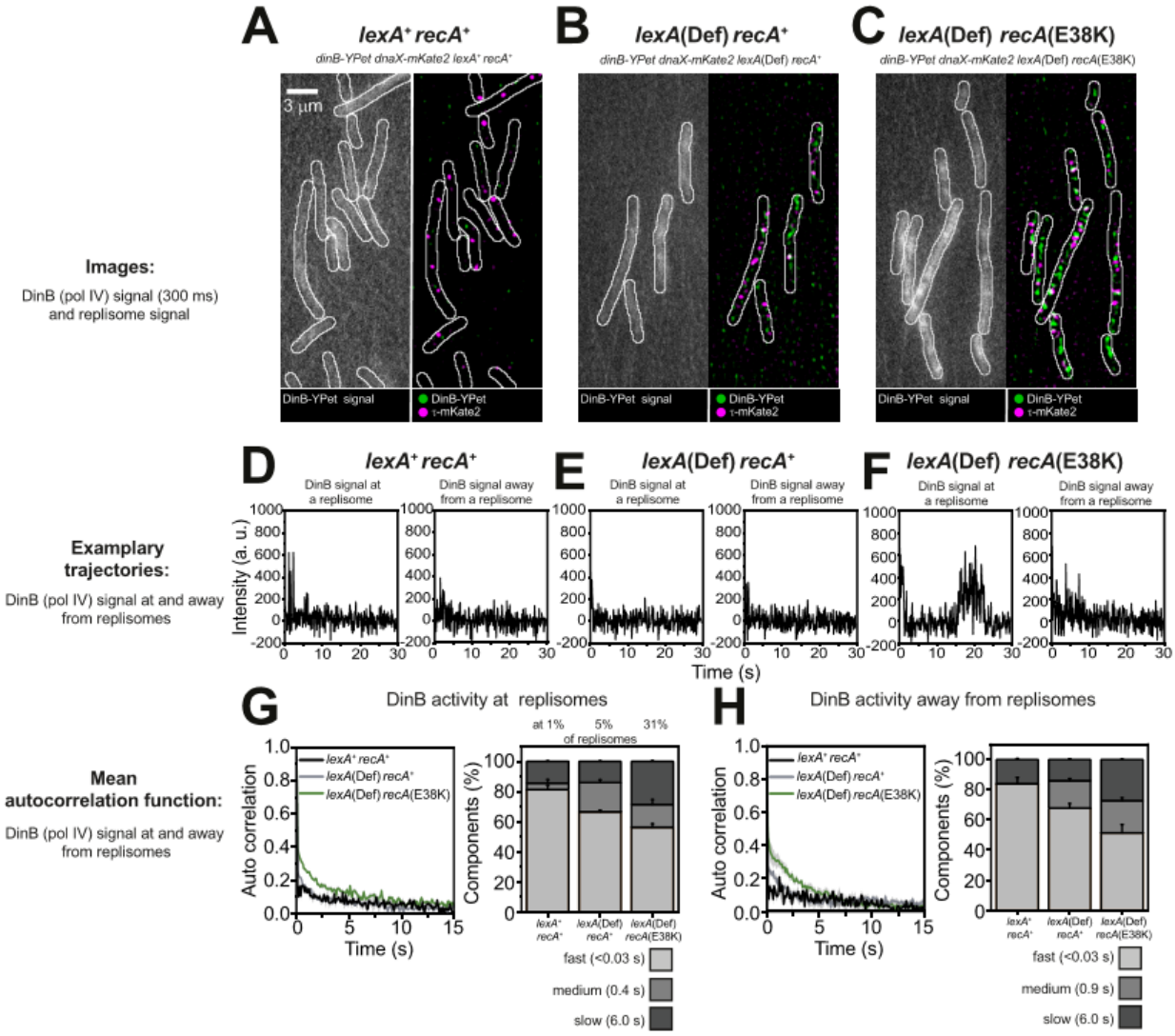

Figure 4. Binding activity of DinB at and away from replisomes in different *lexA* and *recA* mutants. (A) Images of DinB and DnaX signal in *lexA*$^+$ *recA*$^+$. Left: Projection of DinB signal consistent with 300 ms exposure times. Right: Merged images of discoidal filtered DinB (green) and DnaX signal (magenta). (B) similar to (A), however in *lexA*(Def) *recA*$^+$. (C) similar to (A), however in *lexA*(Def) *recA*(E38K). (D) Left: DinB signal at a replisome in *lexA*$^+$ *recA*$^+$. Right: DinB signal away from replisome in *lexA*$^+$ *recA*$^+$. (E) Left: DinB signal at a replisome in *lexA*(Def) *recA*$^+$. Right: DinB signal away from replisome in *lexA*(Def) *recA*$^+$. (F) Left: DinB signal at a replisome in *lexA*(Def) *recA*(E38K). Right: DinB signal away from replisome in *lexA*(Def) *recA*(E38K). (G) Mean autocorrelation function showing DinB activity at replisomes in *lexA*$^+$ *recA*$^+$ (black line), *lexA*(Def) *recA*$^+$ (grey line) and *lexA*(Def) *recA*(E38K) (green line). Error bars represent standard error of the mean over > 100 trajectories. (H) Mean autocorrelation function showing DinB activity away from replisomes in *lexA*$^+$ *recA*$^+$ (black line), *lexA*(Def) *recA*$^+$ (grey line) and *lexA*(Def) *recA*(E38K) (green line). Error bars represent standard error of the mean > 100 trajectories.

We therefore directly tested whether RecA(E38K) interacts with pol IV on filaments assembled dsDNA *in vitro*. Using an identical SPR experimental setup as described above, we assembled RecA(E38K) on a 60-mer dsDNA substrate (**Figs S3C, D**). We found that pol IV associates with RecA(E38K)-ATPγS filaments formed on dsDNA (**Fig S3E**), producing a much stronger response than measurements in which pol IV was exposed to dsDNA in the absence of RecA(E38K) (**Fig S3F**). Unfortunately, despite our attempts to further optimise the assay, non-specific binding of pol IV to the

chip surface hampered our attempts to extract binding parameters from the sensorgrams. Nevertheless, these results clearly demonstrate that the association of pol IV with the nucleoid is promoted by the presence of RecA*-like structures.

Returning to the live-cell single-molecule data, we next examined fluctuations in the DinB-YPet signals that occur as pol IV binds to, or dissociates from, binding sites on the nucleoid. We monitored pol IV binding events within cells, both close to and away from τ foci. Intensity trajectories for DinB-YPet in *lexA*$^+$ *recA*$^+$ cells and *lexA*(Def) *recA*$^+$ cells predominantly showed short-lived spikes (< 1s; **Figs 4D, E**), indicative of transient pol IV binding events (milliseconds timescale). In contrast, trajectories for DinB-YPet in *lexA*(Def) *recA*(E38K) cells often included binding events that were much longer lived (1–10 s, **Fig 4F**), indicative of pol IV binding to its target for longer periods (seconds timescale).

To comprehensively assess pol IV binding lifetimes across all intensity trajectories, mean autocorrelation functions were calculated for each set of trajectories (**Figs S2D–F**). Fitting of each autocorrelation function give time constants τ = < 0.03, 0.4 and 6.0 s, reflecting short-, medium-, and long-lived binding events (**Figs 4G, H; S2G, H**). For *lexA*$^+$ *recA*$^+$ cells in the absence of ciprofloxacin, only 1% of τ positions showed evidence of pol IV binding events (**Fig 4G**, right panel). The normalised mean autocorrelation function for *lexA*$^+$ *recA*$^+$ cells was of low amplitude (0.16 at Δt = 1 frame, **Fig 4G**, black line), indicative of there being relatively few long-lived binding events at replisomes across the different trajectories (12). The *lexA*(Def) *recA*$^+$ background marginally increased pol IV binding activity with 5% of τ foci showing by DinB-YPet binding (**Fig 4G**, right panel) (12). The autocorrelation function remained of low amplitude (0.3 at Δt = 1 frame, **Fig 4G**, grey line), indicating that few long-lived pol IV binding events occurred at τ positions in the *lexA*(Def) *recA*$^+$ background. In contrast, *lexA*(Def) *recA*(E38K) cells exhibited a strong increase in pol IV binding activity, both close to and away from τ foci; 31% of τ positions had a pol IV binding event (**Fig 4G**, right panel). The amplitude of the autocorrelation function was also increased (0.4 at Δt = 1 frame, **Fig 4G**, green line), indicating that long-lived binding events occurred close to replisome markers much more frequently. The decay rate of the autocorrelation function had two longer timescale components (**Fig 4G**, right panel: τ_m = 0.4 s with an amplitude of 15% and τ_l = 6.0 s with an amplitude of 29%), suggesting that pol IV typically binds near τ foci for periods of a few seconds in the *recA*(E38K) background. When analysing the binding behaviour of pol IV away from τ positions in these three backgrounds, similar results were obtained (**Fig 4H**).

5.3 Discussion

In this study, we arrived at four conclusions: i) UmuD promotes the binding of pol IV to the nucleoid, at replisomal and non-replisomal sites; ii) UmuD′ inhibits the binding of pol IV to the nucleoid, at both replisomal and non-replisomal sites; iii) pol IV frequently colocalises with the RecA* probe mCI; iv) RecA*-like structures strongly promote the binding of pol IV to the DNA. These results lead us to infer that RecA*-like structures can recruit pol IV to the nucleoid, where pol IV might associate with the RecA* filaments. Following ciprofloxacin treatment, this pol IV-RecA* interaction might recruit pol IV to carry out repair synthesis at DSB repair intermediates. Furthermore, the RecA* mediated cleavage of UmuD, a biochemical switch that has long been known to regulate pol V activation, also regulates the

binding of pol IV to the nucleoid. The results provide direct evidence for both RecA and UmuD acting as regulatory factors for pol IV *in vivo*, as proposed previously (5,14,17,25,37).

5.3.1 $UmuD_2$ and $UmuD'_2$ as regulators of pol IV

A previous study suggested that both $UmuD_2$ and $UmuD'_2$ bind to pol IV and modulate its mutagenic activity (25). Moreover, *in vitro* experiments have suggested that full-length UmuD binds to the replicative polymerase, α, and destabilises its interaction with the sliding clamp, β, thus facilitating other polymerases, such as pol IV, to access the replisome (52,53).

Here we show that UmuD(K97A) increases the number of pol IV foci and increases the binding time of pol IV at the nucleoid. The increased binding time of pol IV in the presence of umuD(K97A) could be caused by a pol IV-UmuD(K97A) complex binding to the nucleoid; the existence of a pol IV-UmuD(K97A) complex needs to be further tested in the future. In contrast, UmuD′ inhibits nucleoid binding by pol IV. Reasons for this inhibition of binding could be UmuD′ binding to pol IV sites or the formation of a pol IV- UmuD′ complex might impact pol IV binding to the nucleoid. During the first stage of the SOS response, most UmuD is present as full-length $UmuD_2$ (45). This would promote long-lived binding of pol IV to DNA and support high-fidelity DNA synthesis. Based on rates of pol IV-dependent DNA synthesis measured *in vitro* (3–5 nt s^{-1}; (54)), binding events lasting a few seconds, such as those observed during this study, could permit the incorporation of tens of nucleotides. In cells lacking *umuDC*, the operon encoding for pol V, we observed increased colocalisation between pol IV and the replisome marker, however nucleoid-binding was shorter-lived than in cells expressing UmuD(K97A). These effects of UmuD and UmuD′ were observed in strains lacking UmuC, indicating that the changes in replisome colocalization and nucleoid-binding lifetime did not arise from differences in competition for binding sites with pol V. Effects observed might be exaggerated in the backgrounds used because UmuD(K97A) and UmuD′ were produced from plasmids at 4–5-fold higher levels than being expressed from the chromosome (39,46).

This work allows us to propose the following model for pol IV activity in the context of the SOS response. Cells experiencing extensive DNA damage trigger the full extent of the SOS response, leading to the formation of UmuD′ at late time points after DNA damage. At this point, the cell enters a mutagenic phase. The highly error-prone polymerase pol V Mut becomes active and pol IV, now in the absence of UmuD, introduces –1 frameshift mutations. At the same time pol IV binding becomes infrequent and short-lived in the presence of UmuD′, consistent with an earlier observation that UmuD′ reduces the frequency of adaptive mutagenesis (25). Thus, while pol IV is error-prone in the presence of UmuD′, mutagenesis would be kept in check by pol IV having reduced access to substrates. This mechanism of UmuD cleavage restricting mutagenesis is in line with the multiple mechanisms that have evolved to restrict the mutagenic activity of pol V (55). Interestingly, colocalization between pol IV and τ is highest in cells that lack UmuD and UmuC altogether (Δ*umuDC*). One possibility is that in wild-type *umuDC*$^+$ cells pol V competes with pol IV for binding to replisome-proximal binding sites, however this explanation seems unlikely for two reasons: 1. pol IV-τ colocalization is low in cells that express UmuD′, but lack UmuC and therefore cannot produce pol V (**Fig 1D**); 2. fluorescently labelled pol V colocalises

with replisomes even less frequently than pol IV does (45). Another explanation, which is more consistent with the data, is that the accumulation of UmuD′ in response to treatment with DNA damaging agents inhibits the binding of pol IV at replisome-proximal sites in wild-type (*umuDC*$^{+}$) cells.

5.3.2 Pol IV binds to RecA* structures

The high degree of colocalisation we observed between pol IV and the RecA* probe when treating with ciprofloxacin, together with the binding of pol IV to RecA*-like structures *in vitro* and *in vivo*, adds to a growing body of evidence supporting the participation of pol IV in homologous recombination (13–19,30,31,33). In ciprofloxacin-treated cells, pol IV colocalises with the RecA* probe (this study) far more frequently than it colocalises with the replisome marker τ (12). Ciprofloxacin is a DNA gyrase inhibitor, which generates DSBs (41) and rapidly halts DNA synthesis (56,57). Defects in DSB processing strongly suppress both pol IV up-regulation and focus formation (35). Interestingly, *in vitro*, pol IV is capable of associating with RecA(E38K)-ATPγS filaments formed on dsDNA. These filaments are competent of LexA cleavage, indicative of RecA*-like activity. *In vivo* in the absence of DNA damage, pol IV forms foci in a *recA*(E38K) mutant background, suggestive of pol IV binding to RecA(E38K) filaments, which presumably form predominantly on dsDNA. In wild-type cells, an interaction between pol IV and RecA* may well facilitate the recruitment of pol IV to homologous recombination intermediates, or indeed any substrates where amenable RecA* structures form.

The results presented here indicate that in ciprofloxacin-treated cells pol IV primarily forms foci at sites of RecA* structures. Together with the observation that inhibition of DSB resection almost completely eliminates pol IV focus formation in ciprofloxacin-treated cells (35), this suggests that pol IV predominantly acts at double-strand break repair intermediates in ciprofloxacin-treated cells, where its most likely role is the extension of D-loops during repair synthesis (14,17,37). The association of pol IV with RecA has also been observed outside the context of RecA* structures (25) and is proposed to stimulate pol IV-dependent TLS *in vitro* (5). Further research is required to determine whether the pol IV-RecA* interaction plays a role in modulating pol IV activities within pathways other than double-strand break repair.

5.4 Experimental procedures

5.4.1 Strain construction, plasmid construction and transformations

SSH007 is a two-colour strain (*dinB-YPet dnaX-mKate2* Δ*umuDC*) derived from EAW643 (*dinB-YPet dnaX-mKate2*). It was made by replacing the wild-type *umuDC*$^{+}$ gene of EAW643 with Δ*umuDC*::Cm^{R} from RW880 *via* P1 transduction. Colonies were selected by testing for chloramphenicol resistance.

To investigate the influence of UmuD mutants on pol IV activity, SSH007 was complemented with plasmids that express UmuD(K97A) (pJM1243) or UmuD′ (pRW66).

SSH092 was made by transformation; EAW633 (*dinB-YPet*) carries the pJMuvrA-PAmCherry-mCI vector (see **Supplementary Notes** for sequence). The PAmCherry-mCI gene block was commercially synthesised and the sequence was verified (IDT gene block). The gene block was introduced into pSC101 (46) using the *Apa*I and *Sac*II restriction sites.

RW1598 was made by P1 transduction of *recA730 srlD300*::Tn*10* from RW244 into RW1594, selecting for TetR. Colonies were then screened for constitutive UmuD cleavage using Western blotting. *recA* and *srlD* are about 90% linked.

pJM1243 was made by chemically synthesizing an *E.coli* codon optimised *umuD*(K97A) gene that was cloned into the low-copy spectinomycin resistant vector, pSC101 (46), as *Hin*dIII-*Eco*RI fragment. UmuD(K97A) expression is LexA-regulated. Similarly, pRW66 was made by introducing the *umuD′* gene into pSC101 (46).

Table 1. Strains used in this study.

Strain	Relevant Genotype	Parent strain	Source/technique
MG1655	*dinB*$^{+}$ *umuDC*$^{+}$ *lexA*$^{+}$*recA*$^{+}$	-	(58)
RW1594	*dinB-YPet dnaX-mKate2 sulA::kan*^{R} *lexA*(Def) Cm^{R}	RW1588	(12)
RW244	*recA*(E38K) *srlD300*::Tn10	-	(59)
RW1598	*dinB-YPet dnaX-mKate2 sulA*::kan^{R} *lexA*(Def)::Cm^{R} *recA*(E38K) *srlD300*::Tn*10*	RW1594	Transduction of RW1594 with P1 grown on RW244
EAW633	*dinB-YPet*::kan^{R}	MG1655	(12)
EAW643	*dinB-YPet*::FRT *dnaX-mKate2*::kan^{R} *lexA*$^{+}$	EAW633	(12)
RW880	Δ*umuDC*::Cm^{R}	MG1655	(35)
SSH007	*dinB-YPet*::FRT *dnaX-mKate2*::kan^{R} *lexA*$^{+}$ Δ*umuDC*::Cm^{R}	EAW643	Transduction of EAW643 with P1 grown on RW880
SSH007 + pJM1243	*dinB-YPet*::FRT *dnaX-mKate2*::kan^{R} *lexA*$^{+}$	SSH007	Transformation of SSH007 with pJM1243

	Δ*umuDC*::Cm^R (chr) + UmuD(K97A) (pl)		
SSH007+ pRW66	*dinB-YPet*::FRT *dnaX-mKate2*::kan^R *lexA*$^+$ Δ*umuDC*::Cm^R (chr) + UmuD′ (pl)	SSH007	Transformation of SSH007 with pRW66
SSH092	*dinB-YPet*::kan^R (chr) + PAmCherry-mCI (pl)	EAW633	Transformation of EAW633 with pJMuvrA-PAmCherry-mCI (39)

5.4.2 Fluorescence microscopy and imaging protocols

For all experiments except for experiments including imaging of PAmCherry-mCI, wide-field fluorescence imaging was performed on an inverted microscope (IX-81, Olympus with a 1.49 NA 100× objective) in an epifluorescence configuration, as described previously (45). Continuous excitation is provided using semidiode lasers (Sapphire LP, Coherent) of the wavelength 514 nm (150 mW max. output) and 568 nm (200 mW max. output). τ-mKate2 was imaged using yellow excitation light (λ = 568 nm) at high intensity (2750 W cm^{-2}), collecting emitted light between 610–680 nm (ET 645/75m filter, Chroma) on a 512 × 512 pixel^2 EM-CCD camera (C9100-13, Hamamatsu). For DinB-YPet time-lapse imaging, we used green excitation (λ = 514 nm) at lower power (240 W cm^{-2}), collecting light emitted between 525–555 nm (ET540/30m filter, Chroma).

For experiments including imaging of PAmCherry-mCI, imaging was conducted on an inverted microscope (Nikon Eclipse-Ti), equipped with a 1.49 NA 100× objective and a 512 × 512 pixel^2 Photometrics Evolve CCD camera (Photometrics, Arizona, US). NIS-Elements equipped with JOBS module was used to operate the microscope (Nikon, Japan). Continuous excitation is provided using semidiode lasers of the wavelength 405 nm (OBIS, Coherent, 200 mW max. output), 514 nm (Sapphire LP, Coherent, 150 mW max. output) and 568 nm (Sapphire LP, Coherent, 200 mW max. output). DinB-YPet was imaged using green excitation (λ = 514 nm) at lower power (~2200 W cm^{-2}), collecting light emitted between 535–550 nm (ET535/30m filter, Chroma). PAmCherry-mCI was imaged by simultaneous illumination with the activation laser 405 nm (1–5 W cm^{-2}) and 568 nm readout laser (540 W cm^{-2}), a PALM (photoactivation localisation microscopy) acquisition protocol, collecting emitted light from 590 nm (ET590LP, Chroma).

Burst acquisitions (movies of 300 × 34 ms frames, continuous excitation with 514 nm light; each frame at 80 W cm^{-2}) were collected to characterise DinB-YPet binding kinetics; followed by a set of two images (bright-field [34 ms exposure]; mKate2 fluorescence [100 ms exposure]). Data were recorded from 20–45 min, from 55–85 min and from 120–180 min after ciprofloxacin treatment (30 ng mL^{-1}). Time-lapse movies were recorded to visualise changes in DinB-YPet binding activity and measure colocalisation with the replisome marker. Sets of three images were recorded (bright-field [34 ms exposure], YPet fluorescence [50 ms exposure]; mKate2 fluorescence [100 ms exposure]) at an interval of 10 min for 3 h. All images were analysed with ImageJ (60).

Time-sampling of DinB-YPet and PAmCherry-mCI expressing cells were performed as follows: First, the bright-field image was taken with 100 ms exposure time. Then, a PALM acquisition protocol (simultaneous illumination with the activation laser 405 [1–5 W cm^{-2}] and 568 nm readout laser [540 W cm^{-2}] for 200 frames taken every 100 ms) was used to image PAmCherry-mCI. Third, DinB-YPet was detected using 512 nm laser (50 ms exposure time at ~2200 W cm^{-2}). The experiment was performed over 3 h, time points were sampled at an interval of 5 min. At each time point, a new field-of-view was sampled to minimise laser-induced damage.

To image DinB-YPet and PAmCherry-mCI, sets of three acquisitions were recorded (bright-field [100 ms exposure], YPet fluorescence [50 ms exposure]; PAmCherry fluorescence [simultaneous illumination with the activation laser 405 and 568 nm readout laser for 200 frames each with 100 ms exposure]). This protocol was only executed once for a field-of-view to minimise laser damage. Consequently, each time point shows a new set of cells. The experiment was conducted over 3 h, an image was taken every 5 min.

5.4.3 Flow cell design

All imaging was carried out on cultures growing in home-built flow cells. Imaging was carried out in quartz-based flow cells, similar to those used in our previous study (12). These flow cells were assembled from a no. 1.5 coverslip (Marienfeld, reference number 0102222 or 0107222), a quartz top piece (45 × 20 × 1 mm^3) and PE-60 tubing (Instech Laboratories, Inc.). Prior to flow cell assembly, coverslips were silanized with aminopropyltriethoxy silane (APTES; Alfa Aeser). First, coverslips were sonicated for 30 min in a 5 M KOH solution to clean and activate the surface. The cleaned coverslips were rinsed thoroughly with MilliQ water, then treated with a 5% (v/v) solution of APTES in MilliQ water. The coverslips were subsequently rinsed with ethanol and sonicated in ethanol for 20 s. Afterwards, the coverslips were rinsed with MilliQ water and dried in a jet of N_2. Silanised slides were stored under vacuum prior to use.

To assemble each flow cell, polyethylene tubing (BTPE-60, Instech Laboratories, Inc.) was glued (BONDiT B-482, Reltek LLC) into two holes that were drilled into a quartz piece. After the glue solidified overnight, double-sided adhesive tape was stuck on two opposite sides of the quartz piece to create a channel. Then, the quartz piece was stuck to an APTES-treated coverslip. The edges were sealed with epoxy glue (5 Minute Epoxy, DEVCON home and Epoxy Adhesive, 5 Minute Everyday, PARFIX). Each flow cell was stored in a desiccator under mild vacuum while the glue dried. Typical channel dimensions were 45 × 5 × 0.1 mm.

5.4.4 Setup of flow cell experiments

For all imaging experiments, cells were grown at 37 °C in EZ rich defined medium (Teknova) that contained 0.2% (w/v) glucose. EAW643, RW1594 and RW1598 cells were grown in the presence of kanamycin (25 μg mL^{-1}), SH001 cells were grown in the presence of chloramphenicol (25 μg mL^{-1}), SSH007 cells carrying pJM1243 or pRW66 were grown in the presence of spectinomycin (50 μg mL^{-1}).

Cells carrying PAmCherry-mCI were also grown in the presence of spectinomycin (50 μg mL^{-1}). Cells were loaded into flow cells, allowed a few minutes to associate with the APTES surface, then, loosely associated cells were removed by pulling through fresh medium. The experiment was then initiated by switching the medium to a medium that contains 30 ng mL^{-1} ciprofloxacin (for cells carrying plasmids: 50 μg mL^{-1} spectinomycin was added). A flow rate of 50 μL min^{-1} was applied during the experiment to allow a constant nutrient and oxygen supply by using a syringe pump.

5.4.5 Proteins

The wild-type *E. coli* RecA protein was purified as described (61). The RecA concentration was determined using the extinction coefficient $\varepsilon_{280} = 2.23 \times 10^4\ M^{-1}\ cm^{-1}$ (61).

The *E. coli* RecA(E38K) protein was purified as previously described (62) with the following modifications. After washing the protein pellet with R buffer plus 2.1 M ammonium sulfate, the pellet was resuspended in R buffer plus 1 M ammonium sulfate. The sample was loaded onto a butyl-Sepharose column and washed with 1.5 column volumes of R buffer plus 1 M ammonium sulfate. It was then eluted with a linear gradient from R buffer plus 1 M ammonium sulfate to R buffer, carried out over 5 column volumes. Peak fractions were identified by SDS-PAGE analysis and pooled. The protein was loaded onto a hydroxyapatite column as done previously, but with the linear gradient from 10–500 mM P buffer. The fractions were dialyzed against R buffer plus 50 mM KCL and 1 mM dithiothreitol three times. The fractions were loaded onto a Source 15S column and washed with R buffer plus 50 mM KCl and 1 mM dithiothreitol until the UV trace receded from peak. Next, the pool was loaded onto a Source 15Q column and eluted with a linear gradient from 0.05–1 M KCl over 25 column volumes. Peak fractions were identified as above and pooled. A DEAE-Sepharose column was not used. Protein in this pool was precipitated by the addition of equal volume of 90% saturated ammonium sulfate. The precipitate was stirred and then spun down at 13,000 rpm for 30 min. The pellet was resuspended in R buffer plus 1 M ammonium sulfate, stirred for an hour, and then spun down again. This protein was loaded onto a butyl-Sepharose column and eluted in a gradient from R buffer and 1 M ammonium sulfate to R buffer. The fractions were identified, pooled, and concentrated using GE Vivispin 20 10K MWCO centrifuge filter concentrating units. The protein was flash frozen in liquid nitrogen and stored at –80 °C. The concentration was determined as above. No exonuclease or other endonuclease activities were detected.

Pol IV (*dinB*) coding sequence was cloned into NcoI and BamHI sites of pET16b to generate a native pol IV expression construct. *E. coli* strain Turner/pLysS (Novagen) carrying the expression construct was grown in LB medium supplemented with 20 μg/ml chloramphenicol and 100 μg ml^{-1} ampicillin. Expression of pol IV was induced by adding IPTG to 1 mM and growing for 3-4 h at 30ºC. Collected cells (~20 g) were resuspended in 50 mL of lysis buffer (50 mM Tris-HCl, pH 7.5, 1 M NaCl, 10% sucrose, 2 mM DITHIOTHREITOL, 1 mM EDTA and protease inhibitor cocktail). Cells were lysed by lysozyme (2 mg/mL) and the clarified extract was collected following centrifugation at 15000 x g for 30 min. Pol IV was then precipitated by ammonium sulfate added to 30% saturation and stirring for 10 min. The precipitate was subjected to gel-filtration in GF-buffer (20 mM Tris-HCl, pH 7.5, 1 M NaCl, 0.1 mM EDTA, 1 mM DITHIOTHREITOL) using a GE Healthcare Superdex-75 XK-26/60 gel filtration column. Pol IV fractions were pooled, dialyzed overnight in PC-buffer (20 mM Tris-HCl, pH 7.5, 0.1

mM EDTA 1 mM DITHIOTHREITOL, 10% glycerol), containing 200 mM NaCl and then subjected to phosphocellulose chromatography (P-11, Whatman). After washing extensively with PC-buffer + 200 mM NaCl, pol IV was eluted with a linear gradient of 200–500 mM NaCl. Fractions containing native pol IV (> 99% pure) were pooled and stored at –70 °C.

5.4.6 Surface Plasmon Resonance (SPR) experiments

SPR experiments were conducted on BIAcore T200 istrument (GE Healthcare) using streptavidin (SA) coated sensor chips, probing the formation of RecA structures (assembled from RecA[E38K]) on ssDNA and dsDNA. Experiments were carried out at 20 °C at a flow rate of 5 μL min^{-1}. As described previously (39), SA chips were activated and stabilised, single-stranded biotinylated 71-mer poly-dT oligonucleotide bio-$(dT)_{71}$ was immobilised, followed by RecA(E38K) filament assembly (**Figs S3A, B**). RecA(E38K) filaments were assembled on bio-$(dT)_{71}$ by injecting 1 μM RecA(E38K) in $SPR^{RecA(E38K)}$ buffer (20mM Tris-HCl, pH 8.0, 10 mM KCl, 10 mM $MgCl_2$, 0.005% surfactant P20 and 0.5 mM dithiothreitol) supplemented with 1 mM adenosine 5'-(γ-thio) triphosphate (ATPγS) at 10 μL min^{-1} for 400 s. Similarly, biotinylated dsDNA was immobilised (as previously described (39)), followed by RecA(E38K) filament assembly (**Figs S3C, D**). RecA(E38K) filaments were assembled on dsDNA (sequence: 5'-TCC TTT CGT CTT CAA AGT TCT AGA CTC GAG GAA TTC TAA AGA TCT TTG ACA GCT AGC CAG-3', 5' end is biotinylated) by injecting 1 μM RecA(E38K) in $SPR^{RecA(E38K)}$ buffer (20mM Tris-HCl, pH 8.0, 10 mM KCl, 10 mM $MgCl_2$, 0.005% surfactant P20 and 0.5 mM dithiothreitol) supplemented with 0.5 mM ATPγS at 5 μL min^{-1} for 500 s. Then, $SPR^{RecA(E38K)}$ supplemented with 0.5 or 1 mM ATPγS buffer was flowed in at 5 μL min^{-1} for 2,500 s, in order to stabilise the formed filaments. From 3,000 s, 1 μM RecA(E38K) in $SPR^{RecA(E38K)}$ buffer supplemented with 0.5 mM ATPγS was injected at a flow rate of 5 μL min^{-1} for 4,200 s.

Pol IV association with RecA(E38K)-dsDNA filaments was observed by injecting 0.65 μM pol IV in $SPR^{RecA(E38K)}$ buffer supplemented with 0.5 mM ATPγS for 220 s at 5 μL min^{-1}, monitoring pol IV association (**Fig S3E**). From 220 s, buffer containing 0.5 mM ATPγS was flowed in at 5 μL min^{-1} and fast dissociation of pol IV was observed. Similarly, pol IV association with dsDNA was monitored, giving a lower response curve (**Fig S3F**). We also observed non-specific binding of pol IV to the chip surface, making it impossible to measure binding kinetics of pol IV.

The surface was regenerated as previously reported (39). Furthermore, the SPR signal were corrected using a flow cell without immobilised bio-$(dT)_{71}$ or dsDNA and corrected for the amount of immobilised RecA(E38K) (39). Ghodke *et al.* utilised this assay to monitor the binding kinetics of mCI at RecA-ssDNA filament (39).

5.4.7 DNA substrates for ATPase and LexA cleavage assay

M13mp18 cssDNA was purified as previously described (63), and M13mp18 cdsDNA was prepared as previously described (63–65). The M13mp18 nicked dsDNA (from here onward called pEAW951) was prepared by nicking with DNaseI according to manufacturer's recommendations. All DNA concentrations are given in terms of total nucleotides.

5.4.8 ATPase assay

ATP hydrolysis of wild-type RecA and RecA(E38K) on nicked cdsDNA was measured using a spectrophotometric enzyme assay (66,67). ATP regeneration from phosphoenolpyruvate and ADP was coupled to the oxidation of NADH, which was monitored by the decrease in absorbance of NADH at 380 nm. 380-nm light was used so that the signal remained within the linear range of the spectrophotometer during the experiment. The assays were carried out on a Varian Cary 300 dual beam spectrophotometer equipped with a temperature controller and a 12-position cell changer. The cell path length and band pass were 0.5 cm and 2 nm, respectively. The NADH extinction coefficient at 380 nm of 1.21 mM^{-1} cm^{-1} was used to calculate the rate of ATP hydrolysis.

The reactions were carried out at 37 °C in a buffer containing 25mM Tris-Ac (80% cation, pH 7.5), 3 mM potassium glutamate, 10 mM magnesium acetate, 5% (w/v) glycerol, 1mM dithiothreitol, an ATP regeneration system (10 units ml^{-1} pyruvate kinase, 3 mM phosphoenolpyruvate), and a coupling system (2 mM NADH and 10 units ml^{-1} lactate dehydrogenase). The concentration of DNA (pEAW951 nicked cdsDNA) was 5 µM. One cuvette was a blank control that contained everything except the DNA (volume compensated with TE). The nicked cdsDNA, buffer, and ATP regeneration system were preincubated at 37 °C for 10 min before addition of 3 mM ATP and 3 µM wild-type RecA or RecA(E38K). Data collection was then begun.

5.4.9 LexA cleavage assay

The cleavage of LexA was performed essentially as previously described (28). Reaction mixtures (125µl) contained 40 mM Tris-HCl, pH 8.0, 10 mM $MgCl_2$, 30 mM NaCl, 2 mM dithiothreitol, 3 µM of M13mp18 circular single-stranded DNA or pEAW951 nicked circular double-stranded DNA, 3 mM ATPγS, LexA, and RecA as noted. Reactions were incubated at 37 °C for 10 min before addition of LexA. The reaction products were separated and visualized by 15% SDS-PAGE stained with Coomassie blue.

5.4.10 Analysis of colocalisation events of pol IV with replisomes

Foci were classed as colocalised if their centroid positions (determined using our peak fitter tool) fell within 2.18 pixels (218 nm) of each other (68). For colocalisation analysis, we binned the data in 30 min intervals for a larger sample size per time point due to low numbers of pol IV foci per cell at exposures of 300 ms. We determined that for DinB-YPet–τ-mKate2 localisation the background of pol IV foci expected to colocalise with replisomes purely by chance is ~4%. This was calculated by taking the area of each cell occupied by replisome foci (including the colocalisation search radius) and dividing by the total area of the cell. The value of 4% corresponds to the mean of measurements made over > 300 cells. As the number of pol IV foci changes in time, the proportion of replisome foci expected to colocalise with pol IV foci by chance also changes in time. At an exposure time of 50 ms, there are almost zero pol IV foci at the beginning of the measurement, thus there is close to zero probability that a

replisome focus will colocalise with a pol IV focus by chance. At t = 30 min, chance colocalisation is expected to be 5% and at t = 120 min, the chance colocalisation is expected to be 3%. At an exposure time of 300 ms, the number of pol IV foci per cell never exceeds ~0.6 foci per cell, thus the level of colocalisation expected to occur by chance is close to zero.

5.4.11 Analysis of pol IV binding kinetics

Replisome localisations were determined by identifying and fitting peaks from τ-mKate2 images. From the corresponding burst acquisition movie, the DinB-YPet signal at replisomes was plotted against time (trajectories of DinB-YPet activity at replisomes) from 20–45 min, from 55–85 min and from 120–180 min after ciprofloxacin treatment (**Fig S2C**). These were divided into trajectories that give and not give pol IV binding events (**Figs S2D, E**). From this, the percentage of replisomes (τ-mKate2 foci) that are visited by DinB-YPet molecules (**Fig 4G**, right panel) is calculated.

Only trajectories that have pol IV binding events were then used to separate pol IV binding kinetics. The autocorrelation function was applied to each of these trajectories giving signal similarities as a function of the lag time, a method that identifies time-dependent fluctuations in signal dependent on binding and dissociation of molecules. When applying the autocorrelation function to a DinB-YPet trajectory, the correlation of this trajectory with its time delayed copy is generated for various lag times. With zero lag time, the normalised correlation of a trajectory with itself is 1. The correlation of a trajectory with its time delayed copy, however, gives autocorrelation values that range from 0–1 depending on signal fluctuations. DinB-YPet molecules that are statically bound show no fluctuations in the DinB-YPet fluorescence signal over time, consistent with the signal being correlated in time. Consequently, the autocorrelation is between 0–1 for lag times after zero. In contrast, DinB-YPet molecules that are transiently associated show many fluctuations in the DinB-YPet fluorescence signal over time. The signal is not correlated in time and results in zero autocorrelation for lag times after zero.

For each time window (20–45 min, 55–85 min and 120–180 min), the mean autocorrelation function output was calculated to determine the average of DinB-YPet binding kinetics. The fast decay at t = 0 s corresponds to short components. From t > 0 s, the curve was fitted with a two-exponential function where medium or short components were identified ($y=y_0+A_1\cdot e^{-x\cdot\tau 1}+A_2\cdot e^{-x\cdot\tau 2}$). Using the *in vitro* experimentally determined rate of nucleotide incorporation of pol IV as a guide (3–5 nt s^{-1} (54)), the short, medium and long components are translated to no binding/short-lived binding (unproductive binding), binding events that are sufficient for the insertion of 1–2 nucleotides or ~8.5 nucleotides, respectively.

Pol IV binding activity away from replisomes was determined as described above. Pol IV trajectories were, however sampled, from average projections of pol IV burst acquisitions in time (average projection over 100 frames, exposure time for each frame was 34 ms; total exposure 3.4 s; see **Fig 2**, upper row).

5.4.12 Analysis of colocalisation events of pol IV with mCI

To measure colocalisation between pol IV and mCI, we first created a maximum projection of each PAmCherry-mCI movie. Similar to the colocalisation analysis performed for pol IV with replisomes, foci were classed as colocalised if their centroid positions fell within 218 nm of each other. Chance colocalisation of pol IV with mCI is close to zero at 0 min. Chance colocalisation is increased from 50 min with ~4%. At 100 min, the chance colocalisation is ~15%.

5.5 Supplementary Notes and Figures

Sequence of pJMuvrA-PAmCherry-mCI vector:

AAGCTGGAAGATCTTCCCTGGCACGACAGGTTTCCCGACTGGAAAGCGGGCAGTGAGCGCA
ACGCAATTAATGTGAGTTAGCTCACTCATTAGGCACCCCAGGCTTTACACTTTATGCTTCCGGC
TCGTATGTTGTGTGGAATTGTGAGCGGATAACAATTTCACACAGGAAACAGCTATGACCATGA
TTACGCCAAGCGCGCAATTAACCCTCACTAAAGGGAACAAAAGCTGGGTACCGGGCCCCCCC
TCGAGGTCGACTTCCGGGAAACAAACCTGGCCAGACATTGTTACACAACACTCCGGGTAATG
CATTCCAATACTGTATATTCATTCAGGTCAATTTGTGTCATAATTAACCGTTTGTGATCGGATCC
AGCACCATGCCACCGGGCAAAAAAGCGTTTAATCCGGGAAAGCATATGGTGAGCAAGGGCGA
GGAGGATAACATGGCCATCATTAAGGAGTTCATGCGCTTCAAGGTGCACATGGAGGGGTCCGT
GAACGGCCACGTGTTCGAGATCGAGGGCGAGGGCGAGGGCCGCCCCTACGAGGGCACCCAG
ACCGCCAAGCTGAAGGTGACCAAGGGTGGCCCCCTGCCCTTCACCTGGGACATCCTGTCCCC
TCAATTCATGTACGGCTCCAATGCCTACGTGAAGCACCCCGCCGACATCCCCGACTACTTTAA
GCTGTCCTTCCCCGAGGGCTTCAAGTGGGAGCGCGTGATGAAATTCGAGGACGGCGGCGTGG
TGACCGTGACCCAGGACTCCTCCCTGCAAGACGGTGAGTTCATCTACAAGGTGAAGCTGCGC
GGCACCAACTTCCCCTCCGACGGCCCCGTAATGCAGAAGAAGACCATGGGCTGGGAGGCCCT
CTCCGAGCGGATGTACCCCGAGGACGGCGCCCTGAAGGGCGAGGTCAAGCCGCGCGTGAAG
CTGAAGGACGGCGGCCACTACGACGCTGAGGTCAAGACCACCTACAAGGCCAAGAAGCCCG
TGCAGCTGCCCGGCGCCTACAACGTCAACCGCAAGTTGGACATCACCTCACACAACGAGGAC
TACACCATCGTGGAACAGTACGAACGTGCCGAGGGCCGCCACTCCACCGGCGGCATGGACGA
GCTGTACAAGGAGCTCGCTGCAGGTGGCGGCGGCGGCTCCGGCAGCCATATGTATGAGTACC
CTGTTTTTTCTCATGTTCAGGCAGGGATGTTCTCACCTGAGCTTCGCACCTTTACCAAAGGTGA
TGCGGAGCGCTGGGTAAGCACAACCAAAAAAGCCAGTGATTCTGCATTCTGGCTTGAGGTTG
AAGGTAATTCCATGACCACACCAACAGGCTCCAAGACAAGCTTTCCTGACGGAATGTTAATTC
TCGTTGACCCTGAGCAGGCTGTTGAGCCAGGTGATTTCTGCATTGCCCGCCTTGGGGGTGATG
AGTTTACCTTCGCGAAACTGATCCGCGATAGCGGTCAGGTGTTTTTACAACCACTGAACCCAC
AGTACCCAATGATCCCATGCAATGAGAGTTGTTCCGTTGTGGGGAAAGTTATCGCTAGTCAGT
GAGCGGCCGCGAATTCGAAGTTCCTATAGTTTCTAGAGAATAGGAACTTCGATCTTTAGAAAA
ACTCATCGAGCATCAAATGAAACTGCAATTTATTCATATCAGGATTATCAATACCATATTTTTGA
AAAAGCCGTTTCTGTAATGAAGGAGAAAACTCACCGAGGCAGTTCCATAGGATGGCAAGATC
CTGGTATCGGTCTGCGATTCCGACTCGTCCAACATCAATACAACCTATTAATTTCCCCTCGTCA
AAAATAAGGTTATCAAGTGAGAAATCACCATGAGTGACGACTGAATCCGGTGAGAATGGCAA
AAGCTTATGCATTTCTTTCCAGACTTGTTCAACAGGCCAGCCATTACGCTCGTCATCAAAATCA
CTCGCATCAACCAAACCGTTATTCATTCGTGATTGCGCCTGAGCGAGACGAAATACACGATCG
CTGTTAAAAGGACAATTACAAACAGGAATCGAATGCAACCGGCGCAGGAACACTGCCAGCGC
ATCAACAATATTTTCACCTGAATCAGGATATTCTTCTAATACCTGGAATGCTGTTTTCCCGGGGA
TCGCAGTGGTGAGTAACCATGCATCATCAGGAGTACGGATAAAATGCTTGATGGTCGGAAGAG
GCATAAATTCCGTCAGCCAGTTTAGTCTGACCATCTCATCTGTAACATCATTGGCAACGCTACC

TTTGCCATGTTTCAGAAACAACTCTGGCGCATCGGGCTTCCCATACAATCGATAGATTGTCGCA
CCTGATTGCCCGACATTATCGCGAGCCCATTTATACCCATATAAATCAGCATCCATGTTGGAATT
TAATCGCGGGCGCGAGCAAGACGTTTCCCGTTGAATATGGCTCATAACACCCCTTGTATTACTG
TTTATGTAAGCAGACAGTTTTATTGTTCATGATGATATATTTTTATCTTGTGCAATGTAACATCAG
AGATTTTGAGACACAACGTGGCTTTCCCCGCCCGCCCGATCCCCGGGTACCGAGCTCGAATTT
CGACCAATTCGAAGTTCCTATACTTTCTAGAGAATAGGAACTTCCCGCGGTGGAGCTCCAATT
CGCCCTATAGTGAGTCGTATTACGCGCGCTCACTGGCCGTCGTTTTACAACGTCGTGACTGGG
AAAACCCTGGCGTTACCCAACTTAATCGCCTTGCAGCACATCCCCCTTTCGCCAGCTGGCGTA
ATAGCGAAGAGGCCCGCACCGATCGCCCTTCCCAACAGTTGCGCAGCCTGAATGGCGAATGG
GACGCGCCCTGTAGCGGCGCATTAAGCGCGGCGGGTGTGGTGGTTACGCGCAGCGTGACCGC
TACACTTGCCAGCGCCCTAGCGCCCGCTCCTTTCGCTTTCTTCCCTTCCTTTCTCGCCACGTTC
GCCGGAAGATCTTCCAATTCCCGACAGTAAGACGGGTAAGCCTGTTGATGATACCGCTGCCTT
ACTGGGTGCATTAGCCAGTCTGAATGACCTGTCACGGGATAATCCGAAGTGGTCAGACTGGA
AAATCAGAGGGCAGGAACTGCTGAACAGCAAAAAGTCAGATAGCACCACATAGCAGACCCG
CCATAAAACGCCCTGAGAAGCCCGTGACGGGCTTTTCTTGTATTATGGGTAGTTTCCTTGCATG
AATCCATAAAAGGCGCCTGTAGTGCCATTTACCCCCATTCACTGCCAGAGCCGTGAGCGCAGC
GAACTGAATGTCACGAAAAAGACAGCGACTCAGGTGCCTGATGGTCGGAGACAAAAGGAAT
ATTCAGCGATTTGCCCGAGCTTGCGAGGGTGCTACTTAAGCCTTTAGGGTTTTAAGGTCTGTTT
TGTAGAGGAGCAAACAGCGTTTGCGACATCCTTTTGTAATACTGCGGAACTGACTAAAGTAGT
GAGTTATACACAGGGCTGGGATCTATTCTTTTTATCTTTTTTTATTCTTTCTTTATTCTATAAATTA
TAACCACTTGAATATAAACAAAAAAAACACACAAAGGTCTAGCGGAATTTACAGAGGGTCTA
GCAGAATTTACAAGTTTTCCAGCAAAGGTCTAGCAGAATTTACAGATACCCACAACTCAAAGG
AAAAGGACTAGTAATTATCATTGACTAGCCCATCTCAATTGGTATAGTGATTAAAATCACCTAG
ACCAATTGAGATGTATGTCTGAATTAGTTGTTTTCAAAGCAAATGAACTAGCGATTAGTCGCTA
TGACTTAACGGAGCATGAAACCAAGCTAATTTTATGCTGTGTGGCACTACTCAACCCCACGAT
TGAAAACCCTACAAGGAAAGAACGGACGGTATCGTTCACTTATAACCAATACGCTCAGATGAT
GAACATCAGTAGGGAAAATGCTTATGGTGTATTAGCTAAAGCAACCAGAGAGCTGATGACGA
GAACTGTGGAAATCAGGAATCCTTTGGTTAAAGGCTTTGAGATTTTCCAGTGGACAAACTATG
CCAAGTTCTCAAGCGAAAAATTAGAATTAGTTTTTAGTGAAGAGATATTGCCTTATCTTTTCCA
GTTAAAAAAATTCATAAAATATAATCTGGAACATGTTAAGTCTTTTGAAAACAAATACTCTATG
AGGATTTATGAGTGGTTATTAAAAGAACTAACACAAAAGAAAACTCACAAGGCAAATATAGA
GATTAGCCTTGATGAATTTAAGTTCATGTTAATGCTTGAAAATAACTACCATGAGTTTAAAAGG
CTTAACCAATGGGTTTTGAAACCAATAAGTAAAGATTTAAACACTTACAGCAATATGAAATTG
GTGGTTGATAAGCGAGGCCGCCCGACTGATACGTTGATTTTCCAAGTTGAACTAGATAGACAA
ATGGATCTCGTAACCGAACTTGAGAACAACCAGATAAAAATGAATGGTGACAAAATACCAAC
AACCATTACATCAGATTCCTACCTACATAACGGACTAAGAAAAACACTACACGATGCTTTAACT
GCAAAAATTCAGCTCACCAGTTTTGAGGCAAAATTTTTGAGTGACATGCAAAGTAAGTATGAT
CTCAATGGTTCGTTCTCATGGCTCACGCAAAAACAACGAACCACACTAGAGAACATACTGGCT
AAATACGGAAGGATCTGAGGTTCTTATGGCTCTTGTATCTATCAGTGAAGCATCAAGACTAAC
AAACAAAAGTAGAACAACTGTTCACCGTTACATATCAAAGGGAAAACTGTCCATATATGCACA

GATGAAAACGGTGTAAAAAAGATAGATACATCAGAGCTTTTACGAGTTTTTGGTGCATTCAAA
GCTGTTCACCATGAACAGATCGACAATGTAACAGATGAACAGCATGTAACACCTAATAGAACA
GGTGAAACCAGTAAAACAAAGCAACTAGAACATGAAATTGAACACCTGAGACAACTTGTTAC
AGCTCAACAGTCACACATAGACAGCCTGAAACAGGCGATGCTGCTTATCGAATCAAAGCTGC
CGACAACACGGGAGCCAGTGACGCCTCCCGTGGGGAAAAAATCATGGCAATTCTGGAAGAA
ATAGCGCTTTCAGCCGGCAAACCTGAAGCCGGATCTGCGATTCTGATAACAAACTAGCAACAC
CAGAACAGCCCGTTTGCGGGCAGCAAAACCCGTGGGAATTAATTCCCCTGCTCGCGCAGGCT
GGGTGCCAAGCTCTCGGGTAACATCAAGGCCCGATCCTTGGAGCCCTTGCCCTCCCGCACGAT
GATCGTGCCGTGATCGAAATCCAGATCCTTGACCCGCAGTTGCAAACCCTCACTGATCCGCAT
GCCCGTTCCATACAGAAGCTGGGCGAACAAACGATGCTCGCCTTCCAGAAAACCGAGGATGC
GAACCACTTCATCCGGGGTCAGCACCACCGGCAAGCGCCGCGACGGCCGAGGTCTTCCGATC
TCCTGAAGCCAGGGCAGATCCGTGCACAGCACCTTGCCGTAGAAGAACAGCAAGGCCGCCA
ATGCCTGACGATGCGTGGAGACCGAAACCTTGCGCTCGTTCGCCAGCCAGGACAGAAATGCC
TCGACTTCGCTGCTGCCCAAGGTTGCCGGGTGACGCACACCGTGGAAACGGATGAAGGCAC
GAACCCAGTGGACATAAGCCTGTTCGGTTCGTAAGCTGTAATGCAAGTAGCGTATGCGCTCAC
GCAACTGGTCCAGAACCTTGACCGAACGCAGCGGTGGTAACGGCGCAGTGGCGGTTTTCATG
GCTTGTTATGACTGTTTTTTTGGGGTACAGTCTATGCCTCGGGCATCCAAGCAGCAAGCGCGTT
ACGCCGTGGGTCGATGTTTGATGTTATGGAGCAGCAACGATGTTACGCAGCAGGGCAGTCGC
CCTAAAACAAAGTTAAACATCATGAGGGAAGCGGTGATCGCCGAAGTATCGACTCAACTATCA
GAGGTAGTTGGCGTCATCGAGCGCCATCTCGAACCGACGTTGCTGGCCGTACATTTGTACGGC
TCCGCAGTGGATGGCGGCCTGAAGCCACACAGTGATATTGATTTGCTGGTTACGGTGACCGTA
AGGCTTGATGAAACAACGCGGCGAGCTTTGATCAACGACCTTTTGGAAACTTCGGCTTCCCC
TGGAGAGAGCGAGATTCTCCGCGCTGTAGAAGTCACCATTGTTGTGCACGACGACATCATTCC
GTGGCGTTATCCAGCTAAGCGCGAACTGCAATTTGGAGAATGGCAGCGCAATGACATTCTTGC
AGGTATCTTCGAGCCAGCCACGATCGACATTGATCTGGCTATCTTGCTGACAAAAGCAAGAGA
ACATAGCGTTGCCTTGGTAGGTCCAGCGGCGGAGGAACTCTTTGATCCGGTTCCTGAACAGGA
TCTATTTGAGGCGCTAAATGAAACCTTAACGCTATGGAACTCGCCGCCCGACTGGGCTGGCGA
TGAGCGAAATGTAGTGCTTACGTTGTCCCGCATTTGGTACAGCGCAGTAACCGGCAAAATCGC
GCCGAAGGATGTCGCTGCCGACTGGGCAATGGAGCGCCTGCCGGCCCAGTATCAGCCCGTCA
TACTTGAAGCTAGACAGGCTTATCTTGGACAAGAAGAAGATCGCTTGGCCTCGCGCGCAGAT
CAGTTGGAAGAATTTGTCCACTACGTGAAAGGCGAGATCACCAAGGTAGTCGGCAAATAATG
TCTAACAATTCGTTCAAGCCGACGCCGCTTCGCGGCGCGGCTTAACTCAAGCGTTAGATGCAC
TAAGCACATAATTGCTCACAGCCAAACTATCAGGTCAAGTCTGCTTTTATTATTTTTAAGCGTG
CATAATAAGCCCTACACAAATTGGGAGATATATCATGAAAGGCTGGCTTTTTCTTGTTATCGCA
ATAGTTGGCGAAGTAATCGCAACATCCGCATTAAAATCTAGCGAGGGCTTTACT

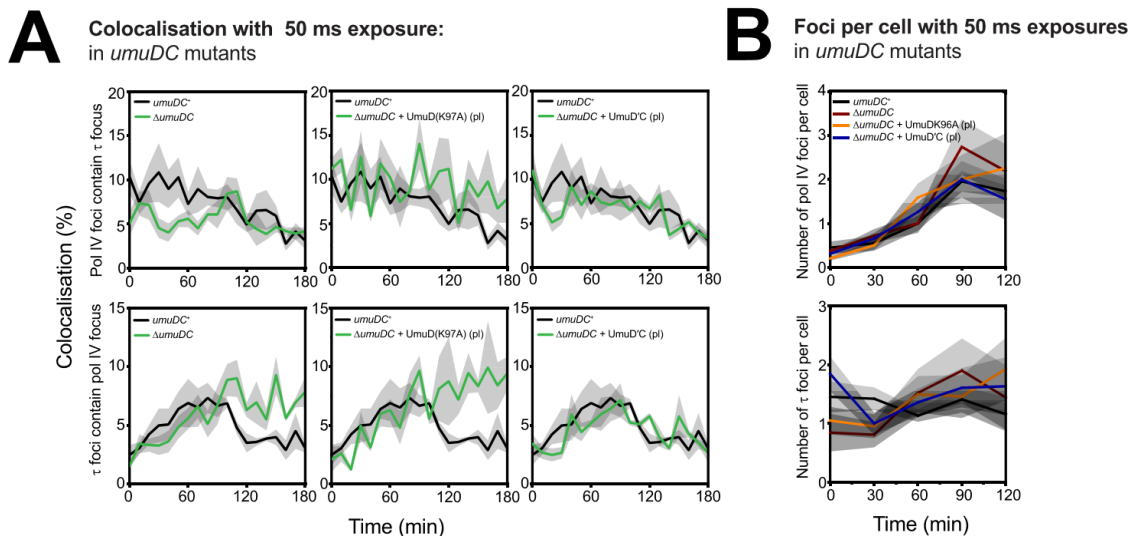

Supplementary Figure S1. Colocalisation analysis using 50 ms exposures for DinB-YPet and number of DinB-YPet and τ-mKate2 foci per cell. (A) Upper row: colocalisation of DinB with DnaX. Left plot compares *umuDC*$^+$ (black line) with Δ*umuDC* (green line). Middle plot compares *umuDC*$^+$ (black line) with Δ*umuDC* + UmuD(K97A) expressed from plasmid (green line). Right plot compares *umuDC*$^+$ (black line) with Δ*umuDC* + UmuD′ expressed from plasmid (green line). Bottom row: colocalisation of DnaX with DinB. Left plot compares *umuDC*$^+$ (black line) with Δ*umuDC* (green line). Middle plot compares *umuDC*$^+$ (black line) with Δ*umuDC* + UmuD(K97A) expressed from plasmid (green line). Right plot compares *umuDC*$^+$ (black line) with Δ*umuDC* + UmuD′ expressed from plasmid (green line). Error bars represent standard error of the mean between at least biological triplicates. (B) Number of DinB (upper plot) and DnaX foci per cell (bottom plot) in *umuDC*$^+$ (black line), Δ*umuDC* (red line), Δ*umuDC* + UmuD(K97A) (yellow line) and Δ*umuDC* + UmuD′ (blue line) after ciprofloxacin treatment. Error bars represent standard error of the mean for $n > 100$ cells.

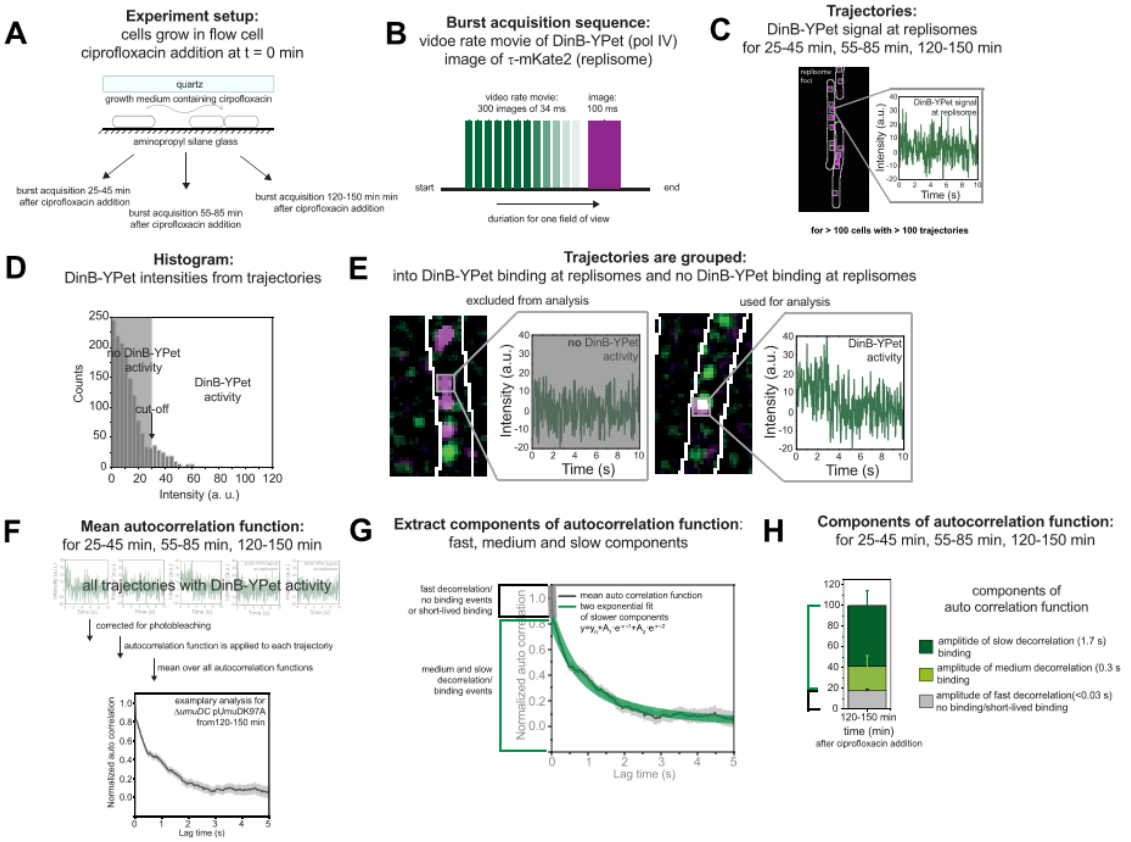

Supplementary Figure S2. Burst acquisitions and analysis. (A) Experimental setup. Cells are loaded in a flow cell and immobilised on a positively charged APTES glass surface. Cells were imaged before addition of ciprofloxacin and 25–45, 55–85 and 120–150 min after addition. (B) Burst acquisition sequence. Movies of DinB-YPet were recorded. The movies contain 300 frames at an exposure of 50 ms taken every 100 ms. Subsequently, an image of the τ-mKate2 channel is taken at an exposure time of 100 ms. (C) Exemplary intensity trajectories showing DinB-YPet binding at replisomes. (D) Histogram of DinB-YPet intensities at replisomes. From cut-off to 0: replisomes with no DinB-YPet binding. From cut-off to higher intensities: replisomes with DinB-YPet binding. (E) Grouping of trajectories. Trajectories that show no DinB-YPet binding at replisomes are excluded from the analysis. Trajectories that show DinB-YPet binding at replisomes are used for the analysis. (F), The mean autocorrelation function is obtained from single autocorrelation function. Each autocorrelation function stems from single intensity trajectories of a DinB-YPet binding event at replisomes. (G), Determining components of autocorrelation functions. The mean autocorrelation function is plotted in black. The autocorrelation function has short-lived components which consist of noise, short-lived and transient binding events (light grey line). Slower components retrieved from longer-lived events are fitted with a two-exponential fit (green line) which consist of medium and slow decorrelation events consistent with binding events. (H), Components of the autocorrelation function are plotted in a bar graph. Long, medium and short components are indicated by different colours: long (dark green), medium (light green), short (light grey). The error bars for long and medium components were extracted from the fit error using the two-exponential fit. The error bar from the short-lived components is equivalent to the standard error of the mean from the mean autocorrelation function at lag time 0 s.

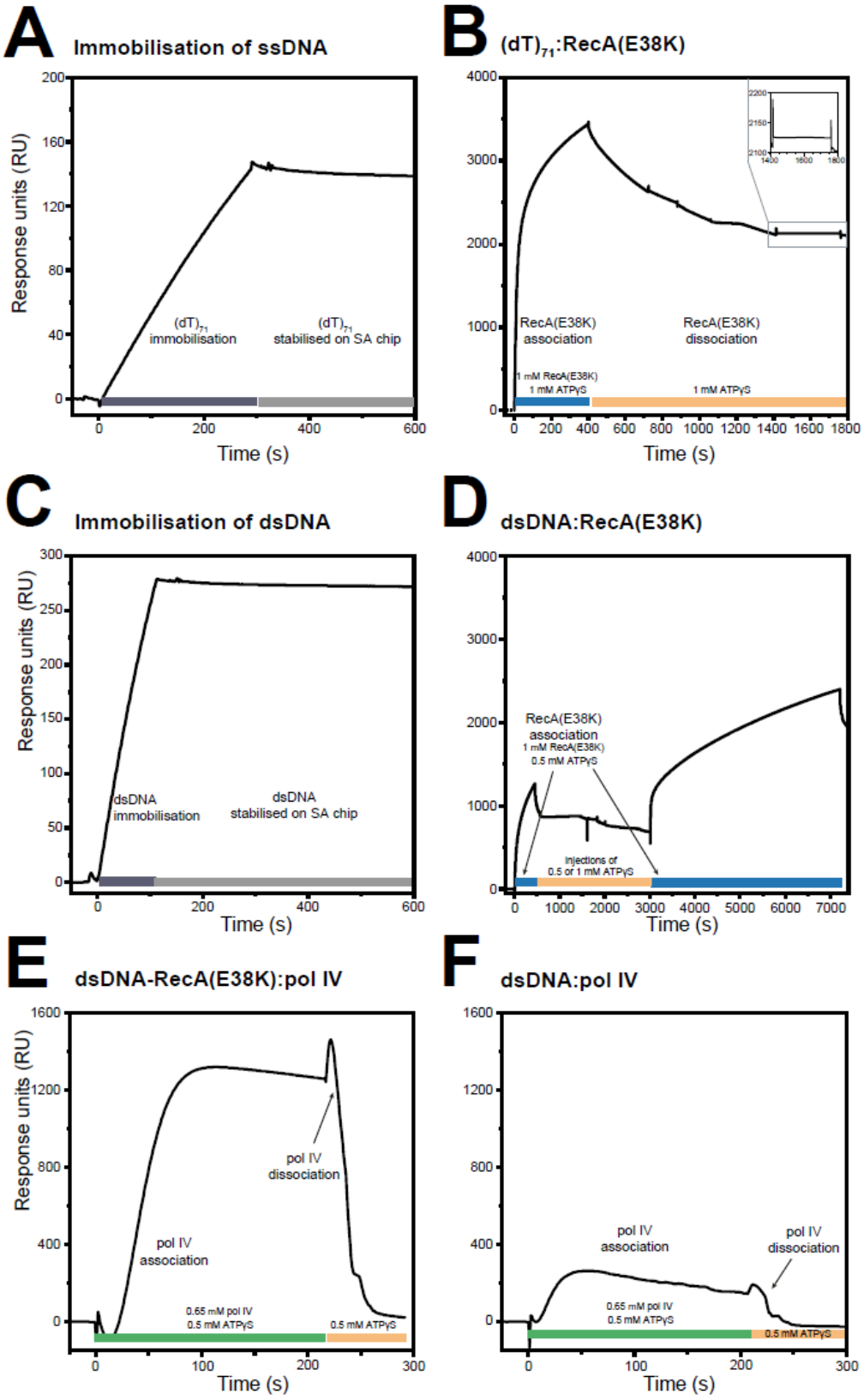

Supplementary Figure S3. Sensorgram showing RecA(E38K) filament assembly on ssDNA and dsDNA in order to probe interactions with pol IV. (A) Sensorgram showing the immobilisation of ssDNA, $(dT)_{71}$, on the SA chip surface (association: dark grey phase; immobilised ssDNA: light grey phase). (B) Following ssDNA immobilisation, buffer containing 1 μM RecA(E38K) (+ 1 mM ATPγS) was flowed into the flow cell, at t = 0 min for 400 s. During this period, RecA(E38K) associated with

ssDNA (blue phase), forming a RecA(E38K) filament. At 400 s, buffer containing 1 mM ATPγS was flowed into the flow cell. RecA(E38K) dissociates from the surface (yellow phase). From 1,400 s, RU units are constant, consistent with stabilised RecA(E38K) filaments. (C) Sensorgram showing the immobilisation of dsDNA on the SA chip surface (association: dark grey phase; immobilised dsDNA: light grey phase). (D) Following dsDNA immobilisation, buffer containing 1 μM RecA(E38K) (+ 0.5 mM ATPγS) was flowed into the flow cell, at t = 0 min for 500 s. During this period, RecA(E38K) associated with ssDNA (blue phase), forming a RecA(E38K) filament. From 500 – 3,000 s, buffer containing 0.5 or 1 mM ATPγS was flowed into the flow cell (yellow phase). From 3,000 – 7,200 s, buffer containing 1 μM RecA(E38K) (+ 0.5 mM ATPγS) was flowed into the flow cell to allow for more RecA(E38K) to associate with the dsDNA. (E) Sensorgram showing the association of pol IV with RecA(E38K) structures formed on dsDNA. At t = 0 s, 0.65 uM pol IV (+ 0.5 mM ATPγS) was flowed into the flow cell for 220 s and association of pol IV was observed (green phase). At t = 220 s, buffer containing 0.5 mM ATPγS was flowed into the flow cell (yellow phase). (F) Sensorgram showing the association of pol IV with dsDNA. At t = 0 s, 0.65 uM pol IV (+ 0.5 mM ATPγS) was flowed into the flow cell for 220 s and association of pol IV was observed (green phase). At t = 220 s, buffer containing 0.5 mM ATPγS was flowed into the flow cell (yellow phase). Lower response units are recorded than for the association of pol IV with RecA(E38K) structures on dsDNA.

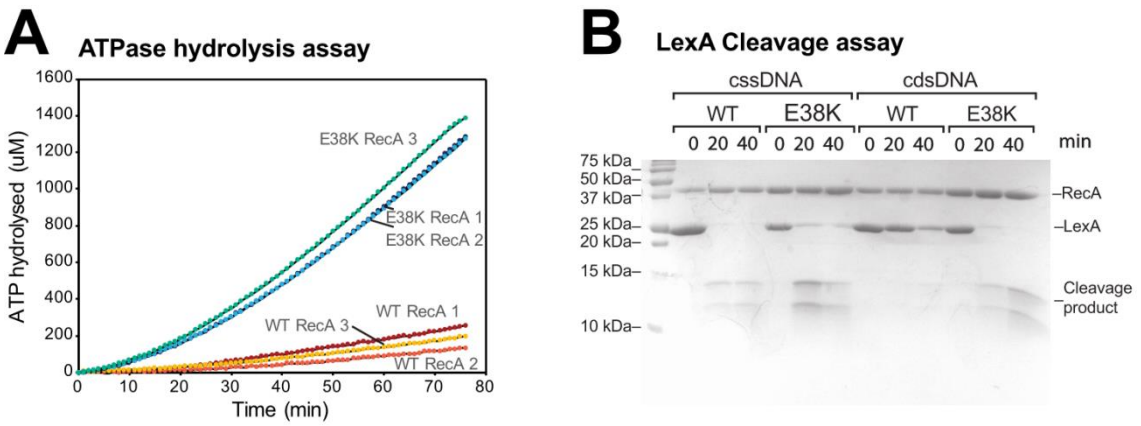

Supplementary Figure S4. RecA(E38K) forms RecA*-like structures on circular dsDNA. (A) RecA(E38K) readily binds to dsDNA. In six separate reactions, either RecA(E38K) or wild-type RecA was incubated at 37 ˚C with nicked circular dsDNA (cdsDNA), ATP, and an ATP regeneration system. (B) LexA Cleavage Assays. Reaction mixtures contained 40 mM Tris-HCl at pH 8.0, 10 mM $MgCl_2$, 30 mM NaCl, 2 mM dithiothreitol, 3 μM circular single-stranded DNA (cssDNA) or nicked circular double-stranded DNA (cdsDNA), 3 mM ATPγS, LexA, and RecA as noted. Reactions were incubated at 37˚C for 10 minutes before addition of UmuD or LexA. The reaction products were separated and visualized by 15% SDS-PAGE stained with Coomassie blue. Lane 1 contains a protein ladder while subsequent groups of three lanes contain the same reaction mixture sampled at 0, 20, and 40 minutes. On cssDNA, RecA(E38K) and wild-type RecA form RecA* structures. On cdsDNA however, RecA(E38K) forms RecA*-like structures in contrast to wildtype RecA.

5.6 References

1. Napolitano R, Janel-Bintz R, Wagner J, Fuchs RPP. All three SOS-inducible DNA polymerases (Pol II, Pol IV and Pol V) are involved in induced mutagenesis. *EMBO J.* 2000;19:6259–6265.

2. Kumari A, Minko IG, Harbut MB, Finkel SE, Goodman MF, Lloyd RS. Replication bypass of interstrand cross-link intermediates by *Escherichia coli* DNA polymerase IV. *J Biol Chem*. 2008;283:27433–27437.

3. Ikeda M, Furukohri A, Philippin G, Loechler E, Akiyama MT, Katayama T, et al. DNA polymerase IV mediates efficient and quick recovery of replication forks stalled at N^2-dG adducts. *Nucleic Acids Res*. 2014;42:8461–8472.

4. Yuan B, Cao H, Jiang Y, Hong H, Wang Y. Efficient and accurate bypass of N^2-(1-carboxyethyl)-2'-deoxyguanosine by DinB DNA polymerase *in vitro* and *in vivo*. *Proc Natl Acad Sci USA*. 2008;105:8679–9684.

5. Cafarelli TM, Rands TJ, Godoy VG. The DinB·RecA complex of *Escherichia coli* mediates an efficient and high-fidelity response to ubiquitous alkylation lesions. *Environ Mol Mutagen Mutagen*. 2014;55:92–102.

6. Jarosz DF, Godoy VG, Delaney JC, Essigmann JM, Walker GC. A single amino acid governs enhanced activity of DinB DNA polymerases on damaged templates. *Nature*. 2006;439:225–228.

7. Kim SR, Maenhaut-Michel G, Yamada M, Yamamoto Y, Matsui K, Sofuni T, et al. Multiple pathways for SOS-induced mutagenesis in *Escherichia coli*: an overexpression of *dinB*/*dinP* results in strongly enhancing mutagenesis in the absence of any exogenous treatment to damage DNA. *Proc Natl Acad Sci USA*. 1997;94:13792–13797.

8. Fuchs RP. Tolerance of lesions in E. coli: Chronological competition between translesion synthesis and damage avoidance. *DNA Repair*. 2016;44:51–58.

9. Henrikus SS, van Oijen AM, Robinson A. Specialised DNA polymerases in *Escherichia coli*: roles within multiple pathways. *Curr Genet*. 2018;64:1189–1196.

10. Fuchs RP, Fujii S. Translesion DNA synthesis and mutagenesis in prokaryotes. *Cold Spring Harb Perspect Biol*. 2013;5:a012682.

11. Kath JE, Jergic S, Heltzel JMH, Jacob DT, Dixon NE, Sutton MD, et al. Polymerase exchange on single DNA molecules reveals processivity clamp control of translesion synthesis. *Proc Natl Acad Sci USA*. 2014;111:7647–7652.

12. Henrikus SS, Wood EA, McDonald JP, Cox MM, Woodgate R, Goodman MF, et al. DNA polymerase IV primarily operates outside of DNA replication forks in *Escherichia coli. PLoS*

Genet. 2018;14:e1007161.

13. Lovett ST. Replication arrest-stimulated recombination: Dependence on the RecA paralog, RadA/Sms and translesion polymerase, DinB. *DNA Repair*. 2006;5:1421–1427.

14. Pomerantz RT, Goodman MF, O'Donnell ME. DNA polymerases are error-prone at RecA-mediated recombination intermediates. *Cell Cycle*. 2013;12:2558–2563.

15. Shee C, Ponder R, Gibson JL, Rosenberg SM. What limits the efficiency of double-strand break-dependent stress-induced mutation in *Escherichia coli*? *J Mol Microbiol Biotechnol*. 2012;21:8–19.

16. Williams AB, Hetrick KM, Foster PL. Interplay of DNA repair, homologous recombination, and DNA polymerases in resistance to the DNA damaging agent 4-nitroquinoline-1-oxide in *Escherichia coli. DNA Repair*. 2010;9:1090–1097.

17. Pomerantz RT, Kurth I, Goodman MF, O'Donnell M. Preferential D-loop extension by a translesion DNA polymerase underlies error-prone recombination. *Nat Struct Mol Biol*. 2013;20:748–755.

18. Shee C, Gibson JL, Rosenberg SM. Two mechanisms produce mutation hotspots at DNA breaks in *Escherichia coli. Cell Rep.* 2012;2:714–721.

19. Shee C, Gibson JL, Darrow MC, Gonzalez C, Rosenberg SM. Impact of a stress-inducible switch to mutagenic repair of DNA breaks on mutation in *Escherichia coli. Proc Natl Acad Sci USA.* 2011;108:13659–13664.

20. Cohen SE, Godoy VG, Walker GC. Transcriptional modulator NusA interacts with translesion DNA polymerases in *Escherichia coli. J Bacteriol.* 2009;191:665–672.

21. Kang P, Liao M, Wester MR, Leeder JS, Pearce RE. The transcription elongation factor NusA is required for stress-induced mutagenesis in *Escherichia coli. Curr Biol.* 2010;20:80–85.

22. Cohen SE, Lewis CA, Mooney RA, Kohanski MA, Collins JJ, Landick R, et al. Roles for the transcription elongation factor NusA in both DNA repair and damage tolerance pathways in *Escherichia coli. Proc Natl Acad Sci USA.* 2010;107:15517–15522.

23. Cohen SE, Walker GC. New discoveries linking transcription to DNA repair and damage tolerance pathways. *Transcription.* 2011;2:37–40.

24. Thrall ES, Kath JE, Chang S, Loparo JJ. Single-molecule imaging reveals multiple pathways for the recruitment of translesion polymerases after DNA damage. *Nat Commun*. 2017;8:2170.

25. Godoy VG, Jarosz DF, Simon SM, Abyzov A, Walker GC. UmuD and RecA directly modulate the mutagenic potential of the Y-family DNA polymerase DinB. Mol Cell. 2007;28:1058–1070.

26. Frank EG, Ennis DG, Gonzalez M, Levine a S, Woodgate R. Regulation of SOS mutagenesis by proteolysis. *Proc Natl Acad Sci USA*. 1996;93:10291–10296.

27. Woodgate R, Ennis DG. Levels of chromosomally encoded Umu proteins and requirements for *in vivo* UmuD cleavage. *Mol Genet Genomics.* 1991;229:10–16.

28. Burckhardt SE, Woodgate R, Scheuermann RH, Echols H, Battista JR, Ohta T, et al. UmuD mutagenesis protein of *Escherichia coli*: overproduction, purification, and cleavage by RecA. *Proc Natl Acad Sci USA*. 1988;85:1811–1815.

29. Jiang Q, Karata K, Woodgate R, Cox MM, Goodman MF. The active form of DNA polymerase V is UmuD′2C–RecA–ATP. *Nature*. 2009;460:359–363.

30. Moore JM, Correa R, Rosenberg SM, Hastings PJ. Persistent damaged bases in DNA allow mutagenic break repair in *Escherichia coli. PLoS Genet*. 2017;13:e1006733.

31. Ponder RG, Fonville NC, Rosenberg SM. A switch from high-fidelity to error-prone DNA double-strand break repair underlies stress-induced mutation. *Mol Cell*. 2005;19:791–804.

32. Foster PL. Stress-Induced Mutagenesis in Bacteria. *Crit Rev Biochem Mol Biol*. 2007;42:373–397.

33. Rosenberg SM, Shee C, Frisch RL, Hastings PJ. Stress-induced mutation via DNA breaks in *Escherichia coli*: A molecular mechanism with implications for evolution and medicine. *Bioessays*. 2012;34:885–892.

34. Mallik S, Popodi EM, Hanson AJ, Foster PL. Interactions and localization of *Escherichia coli* error-prone DNA Polymerase IV after DNA damage. *J Bacteriol*. 2015;197:2792–2809.

35. Henrikus SS, Henry C, Mcdonald JP, Hellmich Y, Wood EA, Woodgate R, et al. DNA double-strand breaks induced by reactive oxygen species promote DNA polymerase IV activity in *Escherichia coli*. *bioRχiv* 2019; https://doi.org/10.1101/533422.

36. Cox MM. Regulation of bacterial RecA protein function. *Crit Rev Biochem Mol Biol*. 2007;42:41–63.

37. Indiani C, Patel M, Goodman MF, O'Donnell ME. RecA acts as a switch to regulate polymerase occupancy in a moving replication fork. *Proc Natl Acad Sci USA*. 2013;110:5410–5415.

38. Tashjian TF, Danilowicz C, Molza A-E, Nguyen BH, Prévost C, Prentiss M, et al. Residues in the fingers domain of the translesion DNA polymerase DinB enable its unique participation in error-prone double strand break repair. *J Biol Chem*. 2019;jbc.RA118.006233.

39. Ghodke H, Paudel B, Lewis JS, Jergic S, Gopal K, Romero Z, et al. Spatial and temporal organization of RecA in the *Escherichia coli* DNA-damage response. *Elife*. 2019;8:e42761.

40. Renzette N, Gumlaw N, Nordman JT, Krieger M, Yeh S-P, Long E, et al. Localization of RecA in *Escherichia coli* K-12 using RecA-GFP. *Mol Microbiol*. 2005;57:1074–1085.

41. Zhao X, Xu C, Domagala J, Drlica K. DNA topoisomerase targets of the fluoroquinolones: a strategy for avoiding bacterial resistance. *Proc Natl Acad Sci USA*. 1997;94:13991–13996.

42. Wang TC, Chang HY, Hung JL. Cosuppression of *recF*, *recR* and *recO* mutations by mutant *recA* alleles in *Escherichia coli* cells. *Mutagen Res*. 1993;294:157–166.

43. Cazaux C, Mazard AM, Defais M. Inducibility of the SOS response in a *recA730* or *recA441* strain is restored by transformation with a new *recA* allele. *Mol Genet Genomics.* 1993;240:296–301.

44. Ennis DG, Levine AS, Koch WH, Woodgate R. Analysis of recA mutants with altered SOS functions. *Mutat Res*. 1995;336:39–48.

45. Robinson A, McDonald JP, Caldas VEA, Patel M, Wood EA, Punter CM, et al. Regulation of mutagenic DNA polymerase V activation in space and time. *PLoS Genet*. 2015;11:e1005482.

46. Churchward G, Belin D, Nagamine Y. A pSC101-derived plasmid which shows no sequence homology to other commonly used cloning vectors. *Gene*. 1984;31:165–171.

47. Woodgate R, Rajagopalan M, Lu C, Echols H. UmuC mutagenesis protein of *Escherichia coli*: Purification and interaction with UmuD and UmuD′. *Proc Natl Acad Sci USA*. 1989;86:7301–7305.

48. Drlica K, Zhao X. DNA gyrase, topoisomerase IV, and the 4-quinolones. *Microbiol Mol Biol Rev*. 1997;61:377–392.

49. Goswami M, Mangoli SH, Jawali N. Involvement of reactive oxygen species in the action of ciprofloxacin against *Escherichia coli*. *Future Microbiol*. 2014;6:949–954.

50. Gruenig MC, Renzette N, Long E, Chitteni-Pattu S, Inman RB, Cox MM, et al. RecA-mediated SOS induction requires an extended filament conformation but no ATP hydrolysis. *Mol Microbiol*. 2008;69:1165–1179.

51. Simmons LA, Foti JJ, Cohen SE, Walker GC. The SOS regulatory network. *EcoSal Plus*. 2008;3:doi:10.1128/ecosalplus.5.4.3.

52. Silva MC, Nevin P, Ronayne EA, Beuning PJ. Selective disruption of the DNA polymerase III α-β complex by the *umuD* gene products. *Nucleic Acids Res*. 2012;40:5511–5522.

53. Sutton MD, Opperman T, Walker GC. The *Escherichia coli* SOS mutagenesis proteins UmuD and UmuD′ interact physically with the replicative DNA polymerase. *Proc Natl Acad Sci USA*. 1999;96:12373–12378.

54. Wagner J, Fujii S, Gruz P, Nohmi T, Fuchs RPP. The beta clamp targets DNA polymerase IV to DNA and strongly increases its processivity. *EMBO Rep*. 2000;1:484–488.

55. Jaszczur MM, Bertram JG, Robinson A, van Oijen AM, Woodgate R, Cox MM, et al. Mutations for worse or better: Low fidelity DNA synthesis by SOS DNA polymerase V is a tightly-regulated double-edged sword. *Biochemistry*. 2016;2:2309–2318.

56. Snyder M, Drlica K. DNA gyrase on the bacterial chromosome: DNA cleavage induced by oxolinic acid. *J Mol Biol*. 1979;131:287–302.

57. Deitz WH, Cook TM, Goss W a. Mechanism of action of nalidixic acid on *Escherichia coli* III. Conditions required for lethality. *J Bacteriol*. 1966;91:768–773.

58. Blattner FR, Plunkett III G, Bloch CA, Perna NT, Burland V, Riley M, et al. The complete genome sequence of *Escherichia coli* K-12. *Science*. 1997;277:1453–1474.

59. McDonald JP, Frank EG, Levine AS, Woodgate R. Intermolecular cleavage by UmuD-like mutagenesis proteins. *Proc Natl Acad Sci USA*. 1998;95:1478–1483.

60. Schneider CA, Rasband WS, Eliceiri KW. NIH Image to ImageJ: 25 years of image analysis. *Nat Methods*. 2012;9:671–675.

61. Craig NL, Roberts JW. Function of nucleoside triphosphate and polynucleotide in *Escherichia coli recA* protein-directed cleavage of phage λ repressor. *J Biol Chem*. 1981;256:8039–8044.

62. Cox MM, Lusetti SL, Korth J, Modica MJ, Roca AI, Inman RB, et al. C-terminal deletions of the *Escherichia coli* RecA protein . *J Biol Chem*. 2003;278:16372–16380.

63. Neuendorf SK, Cox MM. Exchange of RecA protein between adjacent RecA protein-single-stranded DNA complexes. *J Biol Chem*. 1986;261:8276–8282.

64. Messing J. New M13 vectors for cloning. *Methods Enzymol*. 1983;101:20–78.

65. Haruta N, Yu X, Yang S, Egelman EH, Cox MM. A DNA Pairing-enhanced conformation of bacterial RecA proteins. *J Biol Chem*. 2003;278:52710–52723.

66. Lindsleys E, Cox MM. Assembly and disassembly of RecA protein filaments opposite filament ends occur at opposite filament ends. *J Biol Chem.* 1990;265:9043–9054.

67. Morrical SW, Cox MM. Stabilization of recA Protein-ssDNA Complexes by the single-stranded DNA binding protein of *Escherichia coli. Biochemistry.* 1990;29:837–843.

68. Henrikus SS, Henry C, Ghodke H, Wood EA, Mbele N, Saxena R, et al. RecFOR epistasis group: RecF and RecO have distinct localizations and functions in *Escherichia coli. Nucleic Acids Res*. 2019;47:2946–65.

6 RecFOR epistasis group:

RecF and RecO have distinct localizations and functions in *Escherichia coli*

Sarah S. Henrikus, Camille Henry, Harshad Ghodke, Elizabeth A. Wood, Neema Mbele, Roopashi Saxena, Upasana Basu, Antoine M. van Oijen, Michael M. Cox, and Andrew Robinson

Published in *Nucleic Acid Research*, **47**, 2946-2965 (2019).

In bacteria, genetic recombination is a major mechanism for DNA repair. The RecF, RecO and RecR proteins are proposed to initiate recombination by loading the RecA recombinase onto DNA. However, the biophysical mechanisms underlying this process remain poorly understood. Here we used genetics and single-molecule fluorescence microscopy to investigate whether RecF and RecO function together, or separately, in live *Escherichia coli* cells. We identified conditions in which RecF and RecO functions are genetically separable. Single-molecule imaging revealed key differences in the spatiotemporal behaviours of RecF and RecO. RecF foci frequently colocalize with replisome markers. In response to DNA damage, colocalization increases and RecF dimerizes. The majority of RecF foci are dependent on RecR. Conversely, RecO foci occur infrequently, rarely colocalize with replisomes or RecF and are largely independent of RecR. In response to DNA damage, RecO foci appeared to spatially redistribute, occupying a region close to the cell membrane. These observations indicate that RecF and RecO have distinct functions in the DNA damage response. The observed localization of RecF to the replisome supports the notion that RecF helps to maintain active DNA replication in cells carrying DNA damage.

I carried out and analysed all in vivo single-molecule experiments. I was involved in strain construction and the preparation of the manuscript and, reviewer responses.

6.1 Introduction

DNA damage and nucleotide depletion impede DNA replication and occasionally cause single-strand gaps to be left in the wake of the replisome. These postreplicative gaps meet one of several fates: 1. Gap filling by polymerases (1) 2. Homology directed repair synthesis involving template switching (2–5) or 3. Conversion to potentially lethal double strand breaks that may be resolved by DNA recombination (4,6). In bacteria, the majority of postreplicative gaps are thought to be resolved by recombinational DNA repair via the RecFOR pathway (7,8).

The RecFOR pathway is mediated by the recombination mediator proteins - RecF, RecO and RecR. Their proposed function is to facilitate the loading of RecA onto single stranded DNA (ssDNA) by displacing the single-stranded DNA binding protein SSB (9–12). The *recF*, *recO* and *recR* genes form a putative epistasis group (5,13–21). This grouping is supported by several findings: 1. an identical level of increased sensitivity to UV irradiation when one of these functions is absent (22) 2. almost identical deficiencies in DNA repair and recombination (23) 3. the joint suppression of mutant alleles of all three genes by certain mutations in the *recA* gene (14,24); and 4. the existence of a gene in bacteriophage λ that eliminates the requirement for all three genes in λ recombination (17,18). These observations have helped to perpetuate a misconception that the RecFOR pathway features a RecFOR complex (7,25). However, despite extensive examination, evidence for a RecFOR complex – even one formed transiently – is lacking.

The cohesiveness of a putative *recFOR* epistasis group begins to fray further upon closer examination of *in vivo* observations. First, many bacterial species lack a gene for RecF, but virtually all bacteria appear to have genes encoding RecR and one of two variants of RecO (25,26). Second, there are clear instances where the phenotype of a mutation in one of the *recFOR* genes diverges from the others (27–32). In *B. subtilis*, RecF protein recruitment to repair foci is preceded by the appearance of RecO protein by several minutes (33). RecF is not essential, although its absence leads to a delayed increase in RecA foci formation when DNA is damaged (34).

The RecO and RecR proteins function together and are both necessary and sufficient for the nucleation of RecA on SSB-coated ssDNA *in vitro* (11,35). Further, RecO and RecR are essential for the formation of RecA foci *in vivo* (34). The RecO protein contains an oligonucleotide-binding fold (OB-fold) in its N-terminal domain and binds both ssDNA and dsDNA (36,37). In a RecA independent manner, RecO catalyses the annealing of complementary oligonucleotides and can also catalyse invasion of duplex DNA by a complementary ssDNA (37,38). The RecR protein has no known intrinsic enzymatic activities and exhibits poor functional conservation across bacteria. *Ec*RecR does not bind DNA, whereas the RecR homologs in *Deinococcus radiodurans* and *B. subtilis* both bind to DNA (39,40). In *E. coli*, there is an apparent competition between RecF and RecO for RecR binding that may involve an interaction of both RecF and RecO with the C-terminal TOPRIM domain of RecR (41,42). RecR increases the apparent affinity of both RecO and RecF for DNA (11,43,44). Stimulation of RecA loading onto SSB-bound ssDNA does not occur in the presence of either RecO or RecR protein alone; it requires the formation of the RecOR complex (7,11,35). The RecOR-facilitated nucleation of RecA filaments onto SSB-coated ssDNA (RecAOR nucleation) is limited by access of RecOR to ssDNA, and requires an interaction of RecO with the C-terminus of SSB (45). The *Ec*RecR protein also forms a complex with

RecF *in vitro* (11,43,44). As in the case of RecO, RecR increases the apparent affinity of RecF for DNA (11,43,44).

RecF is an SMC-like protein, exhibiting structural similarity with the head domain of the eukaryotic Rad50 protein, as well as sequence similarity to the head domains of the eukaryotic SMC proteins (46). However, RecF lacks the long coiled-coil domains of Rad50. RecF belongs to the ATP-binding cassette (ABC) ATPase family of proteins, and it has the Walker A, Walker B, and signature motifs characteristic of that family. ATP binding triggers RecF dimerization (46). The RecF protein (functioning in complex with RecR) cannot serve as a RecA loader (44). *In vitro*, RecFR binds randomly to dsDNA and can act as a barrier to RecA filament extension (44). RecF can also facilitate RecA filament extension on ssDNA by antagonizing the activity of the RecX inhibitor (47). Addition of RecF protein has a neutral or inhibitory effect on RecOR function (11,35,41,45,47), consistent with competition between RecF and RecO for RecR binding that may involve an interaction with the C-terminal TOPRIM domain of RecR (41,42). A RecF enhancement to RecOR-mediated loading has been observed when SSB is present in large excess (7). RecF can also have a positive effect on RecOR-mediated RecA loading when the interaction between RecO and SSB is abolished by utilizing an SSB mutant lacking the RecO interaction site in the SSB C-terminal tail (8). However, the latter two situations are unlikely to be physiologically relevant and the RecFR complex may well possess a function distinct from RecOR.

Given the complex and overlapping phenotypes, we set out to document the spatial and temporal behaviours of fluorescently tagged RecF and RecO proteins in live *E. coli* cells in response to DNA damage. RecR fusions caused a complete loss of RecR function and were not further perused. Our observations provide insights into the intracellular localizations of RecF and RecO and reveal that the two proteins rarely interact with each other in cells during the DNA damage response.

6.2 Materials and Methods

6.2.1 Strain construction

EAW670 is *E. coli* K-12 MG1655 *recF-YPet*. The 3′ end of the *recF* gene includes the promotor sequence for the *gyrB* gene downstream. We thus preserved the last 129 bp of *recF* and inserted an altered *recF* gene fused to sequences encoding *YPet* upstream (including mutant FRT-Kanamycin resistance-wt FRT cassette) using λ_{RED} recombineering. Positive colonies were selected for kanamycin resistance. The fusion gene *recF-YPet* encodes RecF, a C-terminal twelve amino acid spacer, followed by YPet. We similarly constructed EAW779, *E. coli* K-12 MG1655 *recF-mKate2.*

EAW814 is *E. coli* K-12 MG1655 *recO-YPet.* This construct was also made by λ_{RED} recombineering and contains a 3′ end duplication of *recO* gene (last 124 bp). This gene duplication is downstream of an altered *recO* gene fused to sequences encoding *YPet* (including mutant FRT-Kanamycin resistance-wt FRT cassette). EAW672 (*E.coli* K-12 MG1655 *recO-mKate2)* was constructed similarly.

EAW673 is *E. coli* K-12 MG1655 *recR-mKate2*$_{(SL)}$. The fusion gene *recR-mKate2*$_{(SL)}$ encodes RecR, a C-terminal eleven amino acid spacer, followed by mKate2 (including mutant FRT-Kanamycin resistance-wt FRT cassette). This construct was also made by λ_{RED} recombineering and contains a 3′ end

duplication of *recR* gene (last 247 bp). EAW897 (*E. coli* K-12 MG1655 *recR-mKate2*$_{(LL)}$) and EAW898 (*E. coli* K-12 MG1655 *recR-YPet*$_{(LL)}$) were constructed similarly except that they contain a twenty amino acid spacers.

EAW642 is *E. coli* K-12 MG1655 *dnaX-mKate2.* The fusion gene *dnaX-mKate2* encodes DnaX, a C-terminal eleven amino acid spacer, followed by mKate2 (including mutant FRT-Kanamycin resistance-wt FRT cassette).

EAW676 (*recF-YPet recO-mKate2*) is a two-colour strain derived from EAW672 (*recO-mKate2*). The kanamycin resistance marker in EAW672 was removed via FLP-FRT recombination using the plasmid pLH29 (48) to obtain kanamycin sensitive EAW672. EAW676 was then constructed by replacing the *recF* gene of EAW672 with *recF-YPet*, a FRT-Kanamycin resistance-wt FRT cassette and the 3' end duplication of *recF* using λ_{RED} recombineering. Colonies were selected for kanamycin resistance.

EAW762 (*recO-mKate2 dnaX-YPet*) is derived from the kanamycin sensitive parent strain EAW672 (*recO-mKate2*). To construct EAW762, λ_{RED} recombination was used to replace the *dnaX* gene of EAW672 with *dnaX-YPet* and a mutant FRT-kanamycin resistance-wt FRT cassette. Colonies were selected for kanamycin resistance. CJH0015 (*recF-mKate2 dnaX-YPet*) was constructed just as EAW762; the kanamycin sensitive EAW670 was infected with the P1 phage grown on JJC5945 (*dnaX-YPet*). We selected colonies for kanamycin resistance.

Deletion strains were constructed using λ_{RED} recombination, pKD46 was used for the λ_{RED} recombinase production and then removed from the strains (49). We created the following strains: EAW629 (Δ*recF*), EAW114 (Δ*recO*) and EAW669 (Δ*recR*). EAW788 was constructed using λ_{RED} recombination. We used pBLW24 (43) as a template to fuse the region encoding for *recF*(K36R) to the RT-Kanamycin resistance-wt FRT cassette. In all cases, deletion mutants and the *recF*(K36R) mutant maintain 3′ portions of each gene in order to preserve promoter sequences for genes downstream. Colonies were selected for kanamycin resistance. EAW214 (Δ*araBAD*) and HH020 (Δ*recA*) were used in previous studies (50,51).

Using λ_{RED} recombineering, we deleted *recF*, *recR* and *recA* in kanamycin sensitive EAW670 (*recF-YPet*). We produced EAW824 (*recF-YPet* Δ*recO*), SSH068 (*recF-YPet* Δ*recR*) and SSH070 (*recF-YPet* Δ*recA*). By analogy, deletion strains expressing RecO-mKate2 were constructed: EAW822 (*recO-mKate2* Δ*recF*), EAW697 (*recO-mKate2* Δ*recR*) and SSH067 (*recO-mKate2* Δ*recA*). We selected for kanamycin resistance.

To investigate the dependency of RecF on RecO, we created the two-colour strain EAW828 (*recO-mKate2 dnaX-YPet* Δ*recF*). The kanamycin sensitive parent strain EAW762 was transduced with a P1 phage lysate grown on EAW629. Colonies were selected for kanamycin resistance. EAW826 (*recF-mKate2 dnaX-YPet* Δ*recO*) was constructed in a similar manner, transducing CJH0015 with a P1 phage lysate grown on EAW114.

We further constructed a pair of two-colour strains (SSH114: *recF-mKate2 dnaX-YPet dnaB8*[Ts], SSH115: *recO-mKate2 dnaX-YPet dnaB8*[Ts]) that have a temperature-sensitive *dnaB* allele (52,53). The *dnaB8* allele encodes DnaB A130V (53). These strains were used to monitor the behaviours of RecF, DnaX, and RecO under conditions where DNA replication is blocked (by shifting to the non-

permissive temperature, 42°C) soon after inducing UV damage. SSH114 constructed by transducing the parent strain, CJH0015 (*recF-mKate2 dnaX-YPet dnaB*$^{+}$), with a P1 phage lysate grown on WX31. Similarly, SSH115 was made by transducing EAW762 (*recO-mKate2 dnaX-YPet dnaB*$^{+}$) with a P1 phage lysate grown on WX31. We also transduced the *dnaB8*(Ts) allele into MG1655 to produce HG362. HG362 was used to confirm the temperature sensitivity of all constructs in the MG1655 background (**Supplementary Figure S14**).

The two strains expressing either the fluorescent protein mKate2 (HG012) or YPet (HG013) were used to investigate if the fluorescent proteins themselves form foci after UV irradiation (**Supplementary Figure S16**). These two strains were produced by transforming either pBAD-Linker-mKate2 (for HG012) or pBAD-Linker-YPet (for HG013) into *E. coli* K-12 MG1655. The construction of these fluorescent proteins fused to a linker was previously published (54).

All constructs were confirmed by PCR and sequencing as required.

Table 6.1. Strains used in this study.

Strain	Relevant Genotype	Parent strain	Source/technique
MG1655	*recF+ recO+ dnaX+*	-	(55)
EAW629	Δ*recF::kan*	MG1655	Lambda Red recombination
EAW114	Δ*recO::kan*	MG1655	Lambda Red recombination
EAW669	Δ*recR::kan*	MG1655	Lambda Red recombination
EAW20	Δ*recA::kan*	MG1655	Lambda Red recombination
EAW788	*recF(K36R)::kan*	EAW629	Lambda Red recombination
HH020	Δ*recA::kan*	MG1655	(50)
EAW670	*recF-YPet::kan*	EAW629	Lambda Red recombination
EAW779	*recF-mKate2::kan*	EAW629	Lambda Red recombination
EAW814	*recO-YPet::kan*	EAW114	Lambda Red recombination
EAW672	*recO-mKate2::kan*	EAW114	Lambda Red recombination
EAW676	*recF-YPet::FRT recO-mKate2::kan*	EAW672	Transduction of EAW672 with P1 grown on EAW670
EAW824	*recF-YPet::FRT* Δ*recO::kan*	EAW114	Transduction of EAW114 with P1 grown on EAW670
SSH068	*recF-YPet::FRT* Δ*recR::kan*	EAW670	Transduction of EAW672 with P1 grown on EAW669
SSH070	*recF-YPet::kan* Δ*recA::kan*	EAW670	Transduction of EAW672 with P1 grown on HH020
EAW822	*recO-mKate2::FRT* Δ*recF::kan*	EAW629	Transduction of EAW629 with P1 grown on EAW672
EAW697	*recO-mKate2::FRT* Δ*recR::kan*	EAW672	Transduction of EAW672 with P1 grown on EAW669
SSH067	*recO-mKate2::FRT* Δ*recA::kan*	EAW672	Transduction of EAW672 with P1 grown on HH020
JJC5945	*dnaX-YPet::kan*	MG1655	from Bénédicte Michel
CJH0015	*recF-mKate2::FRT dnaX-YPet::kan*	EAW672	Transduction of EAW672 with P1 grown on JJC5945
EAW762	*recO-mKate2::FRT dnaX-YPet::kan*	EAW672	Transduction of EAW672 with P1 grown on JJC5945
EAW826	*recF-mKate2::FRT dnaX-YPet::FRT* Δ*recO::kan*	CJH0015	Transduction of CJH0015 with P1 grown on EAW669
EAW828	*recO-mKate2::FRT dnaX-YPet::FRT* Δ*recF::kan*	EAW762	Transduction of EAW672 with P1 grown on EAW629
EAW673	*recR-mKate2::kan (Short Linker, 11 a.a.)*	EAW669	Lambda Red recombination
EAW897	*recR-mKate2::kan (Long Linker,20*	EAW669	Lambda Red recombination

	a.a.)		
EAW898	*recR-YPet::kan (Long Linker,20 a.a.)*	EAW669	Lambda Red recombination
EAW642	*dnaX-mKate2::kan*	MG1655	Lambda Red recombination
EAW214	*ΔaraBAD*	MG1655	(51)
CJH0004	*dnaX-YPet::FRT ΔaraBAD::kan*	JJC5945	Transduction of JJC5945 with P1 grown on EAW214
CJH0014	*recF-mKate2::FRT ΔaraBAD::kan*	EAW779	Transduction of EAW779 with P1 grown on EAW214
CJH0010	*recF-YPet::FRT ΔaraBAD::kan*	EAW670	Transduction of EAW770 with P1 grown on EAW214
UB2	*recO-mKate2::FRT ΔaraBAD::kan*	EAW672	Transduction of EAW672 with P1 grown on EAW214
CJH0072	*recO-YPet::FRT ΔaraBAD::kan*	EAW814	Transduction of EAW814 with P1 grown on EAW214
EAW1116	*recF-YPet::FRT recO-mKate2::FRT ΔaraBAD::kan*	EAW676	Transduction of EAW676 with P1 grown on EAW214
WX31	*dnaB8*(Ts)*::kan*	AB1157	(52)
SSH114	*recF-mKate2::FRT dnaX-YPet::FRT dnaB8*(Ts)*::kan*	CJH0015	Transduction of CJH0015 with P1 grown on WX31
SSH115	*recO-mKate2::FRT dnaX-YPet::FRT dnaB8*(Ts)*::kan*	EAW762	Transduction of EAW762 with P1 grown on WX31
HG012	*Linker-mKate2* (plasmid)	MG1655	Transformation of MG1655 with pBAD-Linker-mKate2 (54)
HG013	*Linker-YPet* (plasmid)	MG1655	Transformation of MG1655 with pBAD-Linker-YPet (54)
HG362	*dnaB8*(Ts)*::kan*	MG1655	Transduction of MG1655 with P1 grown on WX31

6.2.2 Growth curves

Wild-type cells, deletion mutants and protein fusion constructs were grown in LB at 37ºC in a microplate reader at a medium shaking rate (Biotek model Synergy2). Growth was monitored by measuring the optical density at a wavelength of 600 nm (OD_{600}) over 10h. For each strain, a biological quadruplet was recorded. To determine the growth of each strain, the average OD_{600} of the quadruplets and the corresponding standard deviation were plotted over time.

6.2.3 Fitness of fusion strain constructs

Cell fitness was determined for each fusion strain using a modified growth competition assays described by Lenski *et al.* (56). In general, this two-colour colony assay is based on the colour difference of Ara^+ and Ara^- colonies on tetrazolium arabinose indicator plates (TA plates). Ara^- colonies typically are red coloured, while Ara^+ colonies are white. Ara^+ and Ara^- cells can be counted and thus fitness in a mixed population of two strains can be assessed. Using this two-colour colony assay, the fitness of each fusion protein construct was measured in comparison to the parental strain that has the native gene instead of the fusion construct.

In preparation for the assay, individual overnight cultures of Ara^- and Ara^+ cells were grown in 3 mL LB at 37ºC. The next day, a mixed culture of Ara^- and Ara^+ cells was set up at a 1:1 ratio by volume. To start the experiment, 3 mL of medium was inoculated with 30 μL of the mixed culture and grown at 37ºC. Fitness was assessed over the period of 72 h; cells were serial diluted in PBS at 0, 24, 48 and 72 h. The dilutions were spread on plates containing TA plates and incubated at 37ºC for 16h before counting.

We performed this assay competing Ara^+ cells of each fusion protein construct with Ara^- cells of the corresponding parental strain and vice versa. We carried out triplicate measurements for each combination to determine the red and white percentage of the total population.

6.2.4 UV survival assay

Cells were grown in LB overnight at 37ºC. The next day, a 1/100 dilution of each culture was grown in LB medium (at 37ºC, 150 rpm) until reaching mid-log phase (OD_{600} = 0.2). Cell cultures were then serial diluted in PBS by factors of ten down to 10^{-5} and 10 μL of each dilution was spotted in duplicates onto two LB plates. One of the plates was exposed to 60 J/m^2 UV light using a cross linker (Spectrolinker model XL1000 UV). The other was used as a no-exposure control. Unexposed and exposed plates were incubated at 37ºC in the dark for 16h. Images of plates were acquired with LAS4000 imager in digitalization mode (GE healthcare).

6.2.5 SOS induction using mytomycin C

To investigate the levels of SOS induction in each fusion strain, we performed the β-galactosidase assay (Miller assay (57)) using a plasmid that expresses β-galactosidase from the SOS-inducible promoter for the *recN* gene (pEAW362)(58). Cells were grown in LB_{Amp} media (100 μg/mL ampicillin) overnight at 37ºC and 150 rpm. The next day, a 1/100 dilution of the overnight cultures (total volume = 10 mL) was grown in LB_{Amp} medium (at 37ºC, 150 rpm) until reaching an OD_{600} of 0.2-0.4. Two aliquots of 3mL culture were taken. Mitomycin C was added to one 3mL culture (to 0.2 μg/ml) and the other 3 mL culture was used as a control. The MMC-treated and untreated cells were grown for 2h, then 1 mL of each culture was centrifuged and the pellet resuspended in Z buffer (0.06M sodium phosphate dibasic heptahydrate, 0.04M sodium phosphate monobasic, 0.01M potassium chloride, 0.001M magnesium sulfate, pH 7.0). Levels of SOS induction were determined by β-galactosidase assay (Miller) and were expressed as fold induction. Fold induction was determined by dividing the β-galactosidase activity of cells exposed to mitomycin C by the activity of the untreated cells.

6.2.6 DNA damaging agent sensitivity assay

Cells were grown in LB overnight at 37ºC. The next day, a 1/100 dilution of each culture was grown in LB medium (at 37ºC, 150 rpm) until reaching mid log phase (OD_{600} = 0.2). Cell cultures were then serially diluted in PBS by factors of ten down to 10^{-5}. Serial dilutions were spotted (spot volume 10 μL) on fresh LB plates and LB plates containing DNA damaging agent (which were protected from light). DNA damaging agents were added at the following concentrations: 5 μM NFZ, 3 μg/mL MMC, 0.3 μM bleomycin, 0.1 μg/mL trimethoprim, 7.5 ng/mL ciprofloxacin or 5 mM hydroxyurea. Plates were incubated at 37ºC for 16h in the dark. Images of plates are acquired with LAS4000 imager in digitalization mode (GE healthcare).

6.2.7 Temperature sensitivity assay

Cells were grown in LB overnight at 37ºC. The next day, a 1/100 dilution of each culture was grown in LB medium (at 37ºC, 150 rpm) until reaching mid log phase (OD_{600} = 0.2). Cell cultures were then serially diluted in PBS by factors of ten down to 10^{-5}. Serial dilutions were spotted (spot volume 10 μL) on fresh LB plates. Plates were incubated at either 37ºC or 42ºC for 16h in the dark.

6.2.8 SOS induction using DNA damaging agents

To compare the levels of SOS induction in deletion mutants with wild-type cells, we used cells that carry a vector for GFP expression from the SOS-inducible promoter of *recN* (pEAW903). Cells carrying the empty vector pET21A were used as a control. Cultures were grown in LB Amp medium at 37ºC while shaking at 150 rpm until reaching mid log phase (OD_{600} = 0.2). For each strain, 200 μL of cultures were transferred into a 96 well microplate (Corning model black plate Costar). One culture was left untreated; the other culture was incubated with 0.5 μg/mL mitomycin C, 10 μM nitrofurazone, 0.4 μM bleomycin, 15 μg/mL trimethoprim, 10 ng/mL ciprofloxacin, or 200 mM hydroxyurea. The 96 well microplate containing the untreated and treated cells was kept at 37ºC for 10h while medium shaking using a microplate reader (Biotek model Synergy2). The optical density (absorbance at 600 nm) and the fluorescence intensity (excitation 485 nm – emission 510 nm) were measured every 10min. Cells carrying the empty vector and also untreated cells were expected to emit a low intensity fluorescence signal. Cells treated with DNA damaging agents that were carrying the SOS reporter plasmid were expected to emit a high intensity fluorescence signal due to the expression of GFP. For each strain and condition (treated or untreated), the expression level of the P*recN-GFP* was calculated at each time point as followed. We divided the fluorescence signal gained from cells carrying the SOS reporter plasmid by their optical density and subtracted the fluorescence signal gained from cells carrying the empty vector by their optical density. We recorded triplicates for each condition. From these triplicates, two plots were generated. The average level of SOS induction and standard deviation were calculated and plotted as a function of time. The global SOS response over 10h was illustrated as violin plots with identical max width using R software. Data are compiled from triplicate measurements. The median value is represented with a black dot along the vertical axis of each violin plot.

6.2.9 Fluorescence microscopy

For all microscopy data except for those comparing *dnaB* alleles and some controls (Supplementary Figure S13, S15-S17), wide-field fluorescence imaging was conducted on an inverted microscope (IX-81, Olympus with a 1.49 NA 100x objective) in an epifluorescence configuration. Continuous excitation is provided using semidiode lasers (Sapphire LP, Coherent) of the wavelength 514 nm (150 mW max. output) and 568 nm (200 mW max. output). RecF-mKate2 and RecO-mKate2 (CJH0015, EAW672, EAW676, EAW697, EAW762, EAW822, EAW826, EAW828, SSH067) were imaged using yellow excitation light (λ = 568 nm) at high intensity (2750 Wcm^{-2} at EM gain 300), collecting emitted light between 610–680 nm (ET 645/75m filter, Chroma) on a 512 × 512 pixel EM-CCD camera (C9100-13, Hamamatsu). For RecF-YPet, RecO-YPet and DnaX-YPet imaging, we used

green excitation (λ = 514 nm) at either lower (16 Wcm^{-2} at EM gain 300) or higher laser power (160 Wcm^{-2} at EM gain 300) for RecF-YPet and RecO-YPet strains (EAW670, EAW676, EAW814, EAW824, SSH068, SSH070) and 60 Wcm^{-2} for the DnaX-YPet strains (CJH0015, EAW762, EAW826, EAW828), collecting light emitted between 525–555 nm (ET540/30m filter, Chroma).

For the comparison of *dnaB* alleles, data were recorded on a Nikon Ti2-E microscope with a heated stage insert. Continuous excitation was provided by the same setup as described above. In all experiments including a temperature shift from 30^0C to 42^0C, RecF-mKate2 and RecO-mKate2(CJH0015, EAW762, SSH114, SSH115) were also imaged using yellow excitation light (λ = 568 nm) at high intensity (2750 Wcm^{-2} at EM gain 100), collecting emitted light between 610–680 nm, (ET654/75m filter, Chroma) on a 512 × 512 pixel EM-CCD camera (C9100-13, Hamamatsu). DnaX-YPet (CJH0015, EAW762, SSH114, SSH115) was imaged using green excitation (λ = 514 nm) at lower (60 Wcm^{-2} at EM gain 255), collecting light emitted between 525–555 nm (ET540/30m filter mounted in Nikon Ti2 Filter Cubes, Chroma).

Burst acquisitions (movies of 300 × 34ms frames, continuous excitation with 514 nm light) were collected to characterise the motions of RecF-YPet and RecO-YPet molecules, and to determine the number of RecF-YPet and RecO-YPet molecules per cell. Single-colour time-lapse movies were recorded to visualise RecF-YPet or RecO-mKate2 binding to DNA (EAW670, EAW672, EAW697, EAW779, EAW814, EAW822, EAW824, SSH067, SSH068, SSH070). A set of two-images was recorded at an interval of 10min for 3h, UV irradiating just after the first image was taken (bright-field [34ms exposure], YPet fluorescence [100ms exposure] or bright-field [34ms exposure], mKate2 fluorescence [100ms exposure]). Two-colour time-lapse movies were recorded to visualise if RecF-YPet and RecO-mKate2 (EAW676) bind to DNA as a complex. Sets of three images were recorded (bright-field [34ms exposure], mKate2 fluorescence [100ms exposure], YPet fluorescence [100ms exposure]) at an interval of 10min for 3h. To measure colocalization between RecF-mKate2 or RecO-mKate2 with the replisome marker (CJH0015, EAW762, EAW826, EAW828, SSH114, SSH115), we recorded time-lapse movies at the same intervals but different exposures for the replisome marker (bright-field [34ms exposure], mKate2 fluorescence [100ms exposure], YPet fluorescence [500ms exposure]). All images were analysed with ImageJ (59).

6.2.10 Flow cell designs

All imaging experiments were carried out in home-built quartz-based flow cells (62). These flow cells were assembled from a no. 1.5 coverslip (Marienfeld, REF 0102222), a quartz top piece (45x20x1 mm) and PE-60 tubing (Instech Laboratories, Inc.). Prior to flow-cell assembly, coverslips were silanised with aminopropyltriethoxy silane (Alfa Aeser). First, coverslips were sonicated for 30min in a 5M KOH solution to clean and activate the surface. The cleaned coverslips were rinsed thoroughly with MilliQ water and then treated with a 5% (v/v) solution of amino-propyl-triethoxysilane (APTES) in MilliQ water. The coverslips were subsequently rinsed with ethanol and sonicated in ethanol for 20 seconds. Afterwards, the coverslips were rinsed with MilliQ water and dried in a jet of N_2. Silanised slides were stored under vacuum prior to use.

To assemble each flow cell, polyethylene tubing (BTPE-60, Instech Laboratories, Inc.) was glued (BONDiT B-482, Reltek LLC) into two holes that were drilled into a quartz piece. After the glue solidified overnight, double-sided adhesive tape was stuck on two opposite sides of the quartz piece to create a channel. Then, the quartz piece was stuck to an APTES-treated coverslip. The edges were sealed with epoxy glue (5 Minute Epoxy, PARFIX). Each flow cell was stored in a desiccator under mild vacuum while the glue dried. Typical channel dimensions were 45 mm × 5 mm × 0.1 mm (length × width × height).

6.2.11 Imaging in flow cells

For imaging experiments in a *dnaB*$^{+}$ background, cells were grown at 37^{0}C in EZ rich defined medium (Teknova) that contained 0.2% (w/v) glucose (62). All strains that have a *kanR* cassette were grown in the presence of kanamycin (20 μg/mL). Cells were loaded into flow cells, allowed a few minutes to associate with the APTES surface, then loosely associated cells were removed by pulling through fresh medium. The experiment was then initiated by irradiating cells *in situ* with 254 nm UV light from a mercury lamp (UVP) at a fluence of 10 J·m^{-2}. Throughout the experiment, medium was pulled through the flow cell using a syringe pump, at a rate of 50 μL/min.

For imaging experiments conducted at the *dnaB8*(Ts) non-permissive temperature, cells were grown at 30^{0}C in EZ rich defined medium (Teknova) that contained 0.2% (w/v) glucose (62). All strains have a *kanR* cassette, and thus, were grown in the presence of kanamycin (20 μg/mL). Cells were loaded into flow cells as described above, at 30^{0}C. Following acquisition of data at the first time point (t = 0 min), the temperature was rapidly ramped up to 42^{0}C. After 3 min, the stage reached a temperature of 39-41^{0}C. Following this, cells were irradiated *in situ* with a brief pulse of 254 nm light (10 J·m^{-2}) through a quartz window in the flow cell. The temperature of the stage stabilized at 42^{0}C within 5 minutes following the first acquisition, and was maintained constant at this value for the rest of the experimental time line. Throughout the experiment, medium was pulled through the flow cell using a syringe pump, at a rate of 50 μL/min.

6.2.12 Analysis of cell filamentation, RecF and RecO levels and foci per cell

We selected single cells to obtain information about RecF and RecO levels upon UV irradiation (>100 cells for every time point). MicrobeTracker 0.937 (60), a MATLAB script, was used to create cell outlines as regions of interest (ROI). We manually curated cell outlines designated by MicrobeTracker before UV irradiation and at intervals of 30min up to 120min after UV irradiation. By obtaining cell outlines manually, we ensure accuracy and purely select non-overlapping, in-focus cells for analysis. These ROI were imported in ImageJ 1.50i. The cell outlines were then used to measure mean cell intensities, cell lengths and the number of foci per cell. Parameters describing foci (number, positions and intensities) were obtained using a Peak Fitter plug-in, described previously (61,62).

6.2.13 Analysis of colocalization events

It has been shown that freely moving molecules diffuse quickly ($D \approx 10$ μm^2/s), whereas, DNA-bound molecules diffuse much slower ($D \approx 10^{-5}$ μm^2/s) (63,64). The imaging conditions (34ms or 100ms exposures) used here separate freely diffusing molecules from bound molecules due to the difference in their diffusion behaviour; a focus represents a DNA bound molecule, diffusive molecules increase the background signal.

Foci were classed as colocalized if their centroid positions (determined using our peak fitter tool) fell within 2.18 px (218 nm) of each other. We determined that for RecF-mKate2–DnaX-Pet localization the background of RecF foci expected to colocalize with replisomes purely by chance is ~4% when imaging at 37^{0}C. This was calculated by taking the area of each cell occupied by replisome foci (including the colocalization search radius) and dividing by the total area of the cell. The value of 4% corresponds to the mean of measurements made over >200 cells. Since the foci density of replisomes stays fairly constant after UV irradiation, the chance colocalization of RecF-mKate2 foci with DnaX-YPet is ~4%. Similarly, the chance colocalization of RecO-mKate2 with DnaX-YPet is ~4% before and after UV irradiation. Similarly, chance colocalization is ~4% for RecF with DnaX and RecO with DnaX in *dnaB8*(Ts) and *dnaB*$^+$ at 30^{0}C. After UV irradiation, at 42^{0}C, in *dnaB*$^+$, chance colocalization of RecF with DnaX and RecO with DnaX is also ~4%. In contrast, chance colocalization of RecF with DnaX and RecO with DnaX decreases in *dnaB8*(Ts) at the non-permissive temperature (42^{0}C) after UV irradiation. Chance colocalization is ~0.5% at 90min.

At 37^{0}C, in *dnaB*$^+$ cells, the chance colocalization of DnaX-YPet with RecF-mKate2 is similar to chance colocalization with replisomes due to a similar foci density before and after UV irradiation (chance colocalization ~4%, >100 cells). The chance colocalization of RecO-mKate2 with RecF-YPet is ~4% following UV irradiation. At 30^{0}C, in *dnaB*$^+$ and *dnaB8*(Ts), chance colocalization of DnaX-YPet with RecF-mKate2 is ~2% because half the number of RecF foci per cell are detected. In *dnaB*$^+$, chance colocalization is also ~2% after UV irradiation at 42^{0}C. In *dnaB8*(Ts), chance colocalization however drops after UV irradiation at the non-permissive temperature as the number of RecF foci per cell declines. At 90 min, chance colocalization is ~0.5%.

In *dnaB*$^+$ and *dnaB8*(Ts) under all conditions, there are <0.3 RecO foci per cell before UV irradiation, thus there is close to zero chance that a replisome focus or RecF focus will colocalize with a RecO focus by chance. At 30min, in *dnaB*$^+$ at 37^{0}C and 42^{0}C, chance colocalization is expected to be <1% and at 120min, the chance for co-localization 1%. In *dnaB8*(Ts), chance colocalization is close to zero when imaging at 30^{0}C as well as after UV irradiation at the non-permissive temperature because <0.3 foci per cell are detected.

6.2.14 Analysis of RecF and RecO copy numbers per cell

The number of RecF-YPet and RecO-YPet molecules and thus the physiological concentration of RecF and RecO are extracted from the integrated fluorescence signal under each cell outline during time series experiments. Each cell exhibits an intensity decay which is composed of YPet bleaching, cellular auto-fluorescence and background fluorescence (62). Exciting with a higher laser power (160

Wcm^{-2}), *Escherichia coli* MG1655 cells, expressing no YPet, exhibit auto fluorescence equivalent to ~2.5 YPet molecules which we corrected for. The background fluorescence was negligible (equivalent to < 1 YPet molecule). After correcting for auto-fluorescence, the integrated fluorescence signal under each cell outline corresponds to the fluorescence signal of intracellular YPet molecules.

Images were corrected for the electronic offset and flattened to correct for inhomogeneity of the excitation beam (inhomogeneity was small at a laser power of 160 Wcm^{-2}; the brightest part at the centre of the image was 12% more intense than at the corners). For each cell, the mean YPet signal per pixel of the first frame from the time series experiments was extracted. The mean YPet signal multiplied by the cell area gives the integrated YPet intensity, which was used to determine the number of YPet molecules per cell.

The mean intensity of individual YPet molecules was determined by analysing single-molecule return events (**Supplementary Figure S5**), as previously described (62). For each cell, the number of RecF-YPet or RecO-YPet molecules was then calculated by dividing the mean YPet signal of the first frame from the burst acquisition experiments by the mean single-molecule intensity. The cellular concentration was calculated using the cell volume of each cell, determined during cell outline assignation in MicrobeTracker.

6.2.15 Autocorrelation analysis and simulation of intensity versus time trajectories

Within the rapid acquisition movies, intensity fluctuations within regions of cells corresponding to RecF or RecO foci were monitored as a function of time. The resulting intensity versus time trajectories contain information on the binding and dissociation behaviours of RecF and RecO, convoluted with photobleaching effects (which cause an exponential loss of signal as a function of time) and noise (which by definition is not correlated in time). To gain information on the binding and dissociation behaviours of RecF and RecO we calculated the autocorrelation functions for all trajectories recorded and determined the mean autocorrelation for each particular set of conditions. The averaged autocorrelation function contained three major components. Fast decorrelation occurred on the time scale of the integration time due to noise and transient binding event (τ_s < 0.034s). The exponential decay in the autocorrelation curve was fitted starting from lag time 0.034s (after the initial fast decorrelation) with single and double exponential-decay functions. Two major component timescales were present in the remainder of the autocorrelation curve (τ_m = 0.3s for RecF-YPet and RecO-YPet**,** τ_l = 1.5s for RecF-YPet and 2.2s for recO-YPet, **Supplementary Figure S4**). The amplitude of each component (a_s, a_m, a_l) represents the weight for each autocorrelation components. Error bars for a_s were derived from the standard deviation of the error mean for each average autocorrelation function at lag time 0.034s. Error bars for a_m and a_l were derived from the fit error.

An increase in signal intensity within foci, such as that observed upon dimerization of RecF, will cause an increase in the signal-to-noise ratio within trajectories. When the autocorrelation curve is determined, this will manifest as a reduction in the fast-decorrelating component. To determine what effect a two-fold increase in focus intensity would have during autocorrelation analysis, we produced

simulated trajectories in which complexes containing either one or two fluorescent molecules photobleached, bound to DNA, and dissociated from DNA. Simulations were run in Matlab 2012a using custom-written code (**Appendix PDF**). The simulator is comprised of three sub-routines. In the first sub-routine, binding/dissociation trajectories are generated for a complex (representing RecF or $RecF_2$ binding to DNA). When bound, the complex produces signal (I = 1). When unbound it produces none (I = 0). Binding and dissociation times are determined by randomly sampling user-defined distributions of k_{on} *and* k_{off}. In the second sub-routine, similar trajectories are produced for individual molecules binding to each complex. In the third sub-routine, photobleaching trajectories are produced for each molecule in the simulation, by drawing randomly from a user-defined distribution of bleaching rates τ_{bleach}. The three signals are then combined such that a molecule only produces signal when it is bound to the complex, the complex is bound to DNA and the molecule has not yet photobleached. Poissonian noise is added to the signal for each molecule according to a user-defined signal-to-noise parameter. Averaging is used to appropriately reduce noise when multiple molecules are bound. The key input parameters for simulation are: $N_{mol/comp}$, the maximum number of molecules that can bind to each complex; k_{on}*(complex)*, the on-rate for complex binding to DNA; k_{off}*(complex)*, off-rate for complex dissociation from DNA; k_{on}*(molecule)*, on-rate for molecule binding to complex; k_{off}*(molecule)*, off-rate for molecules dissociating from complex; τ_{bleach}, the mean photobleaching rate for molecules. Using this code, simulations were run for complexes that permanently contained either one or two molecules (of RecF), keeping all other parameters constant. The autocorrelation functions for one-molecule and two-molecule trajectories were compared.

6.3 Results

6.3.1 *recF* and *recO* mutant phenotypes diverge depending upon DNA damaging agent

The *recF* and *recO* genes (along with *recR*) have been grouped to reflect the very similar phenotypes displayed by mutants lacking the function of the encoded proteins. We set out to systematically investigate the phenotype of mutations in these two genes, exploring a range of DNA damaging agents with different modes of action. To generate DNA damage, we treated cell cultures separately with nitrofurazone (NFZ), mitomycin C (MMC), bleomycin (bleo), ciprofloxacin (cipro), hydroxyurea (HU) and trimethoprim (TMP). We did not further explore the effects of ultraviolet light exposure, as the original observation of phenotypic equivalence with this stressor (22) has been repeatedly reproduced in our laboratories and many others. The sensitivity of the mutant strains EAW629 (Δ*recF*), EAW114 (Δ*recO*), EAW669 (Δ*recR*), and EAW788 (*recF*[K36R]) to each DNA damaging agent was tested using a spot plate dilution assay. The mutants were compared to the wild type strain MG1655 (wild-type), which is the genetic background into which all gene mutations were introduced.

In these trials, three patterns emerged. First, in some cases, there was no evident difference between the Δ*recF* and Δ*recO* phenotype, congruent with previous reports on UV-induced damage. When cells were challenged with NFZ or MMC, the strains carrying deletions in any of the three genes displayed an approximately equal degree of sensitivity (**Figure 1A**). In the second pattern, Δ*recO*

produced results that diverged from wild-type, while Δ*recF* did not. When cells were exposed to bleomycin or trimethoprim, the strains Δ*recO* and Δ*recR* were approximately 10-fold more sensitive than the wild-type cells or a strain lacking *recF* (**Figure 1B**). Third and finally, strains with a *recF* deletion uniquely diverged from the wild-type phenotype in some cases. When cells were exposed to ciprofloxacin or HU, the Δ*recF* strain was more resistant (up to 2 logs for ciprofloxacin and about 1 log for HU, depending on the concentration of stressor) (**Figure 1C**). We also investigated the contribution of the RecF ATPase activity to the *recF* phenotype, using the RecF ATPase deficient mutant (*recF*[K36R]). Interestingly, cells with the *recF*(K36R) mutation were more resistant to ciprofloxacin but not to HU (**Figure 1C**). Altogether, the results reveal several DNA damaging conditions in which the Δ*recO* and Δ*recF* mutations produce quite different phenotypes.

We set out to determine if the difference between the Δ*recF* and Δ*recO* phenotypes to the different DNA damaging agents was also reflected in a difference in SOS induction. We used a plasmid expressing GFP from the SOS-inducible promoter for the *recN* gene, pEAW903 (p*PrecN-gfp*)(65). Deletion strains of *recF* and *recO* carrying p*PrecN-gfp* were grown to exponential phase and treated with the various DNA damaging agents (NFZ, MMC, bleo, cipro, HU or TMP). We then monitored GFP expression for 10 hours. Exposure to NFZ induced little or no *PrecN-gfp* expression in the wild-type cells and moderate expression (~18 000 R.F.U.) in Δ*recF* and Δ*recO* cells (**Figure 1D**). Exposure to bleo, cipro or TMP triggered similar SOS induction profiles for all three strains (~ 40,000 R.F.U with bleo or cipro and ~12,000 R.F.U with TMP). Exposure to HU or MMC showed a slight reduction in *PrecN-gfp* expression in Δ*recF* or Δ*recO* mutants relative to wild-type cells (~12 000 R.F.U vs ~20 000 R.F.U. for HU; ~45 000 R.F.U vs ~ 58 000 R.F.U for MMC). Overall, we found differences in *recF* and *recO* phenotypes suggesting that RecF and RecO might have distinct functions. We thus chose to further investigate RecF and RecO behaviour on the single-molecule level in live *Escherichia coli* cells.

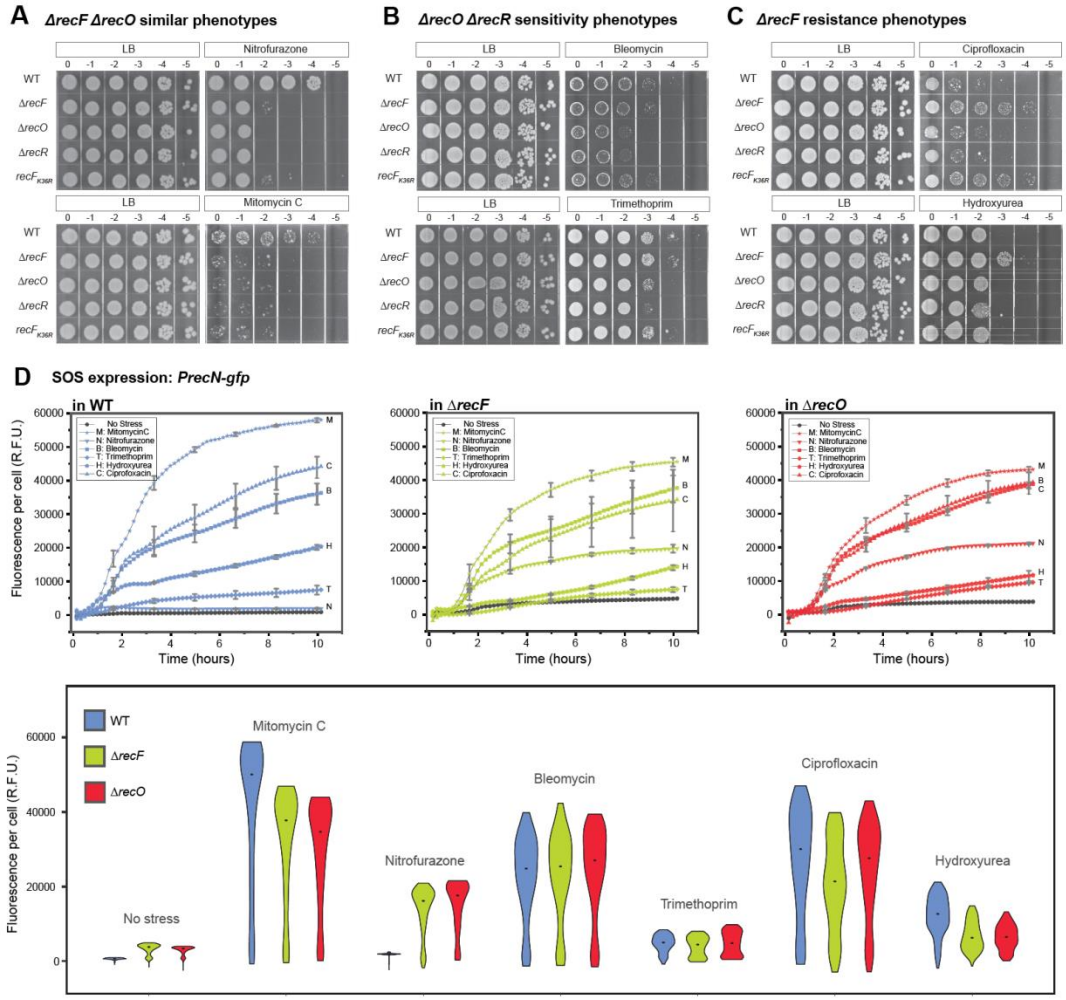

Figure 1. Cells lacking *recF* and *recO* present differences in sensitivity to DNA damaging agents. (A), (B) and (C) Spot plate dilution assays of MG1655 (wild-type), EAW629 (Δ*recF*), EAW114 (Δ*recO*), EAW669 (Δ*recR*), EAW788 (*recF*[K36R]). Cells grown to exponential phase (OD_{600} ~0.2) were serial diluted to the dilution 10^{-5}. Serial dilutions were spotted on LB agar and LB agar supplemented with the indicated DNA damaging agent. Plates were incubated overnight at 37°C. Images show a representative experiment of independent triplicates. (A) Sensitivity of cells exposed to 5 μM NFZ or 3 μg/mL MMC. The sensitivities to NFZ and MMC are almost identical for Δ*recF*, Δ*recO*, Δ*recR* and *recF*(K36R) strains (Δ*recF* and *recF*(K36R) are slightly more resistant than Δ*recO*, Δ*recR* to NFZ). (B) Sensitivity of cells exposed to 0.3 μM bleo or 0.10 μg/mL TMP. Δ*recO*, Δ*recR* are ~10 times more sensitive to bleo in comparison to wild-type, Δ*recF* and *recF*(K36R) mutants. (C) Sensitivity of cells exposed to 7.5 ng/mL cipro or 5 mM HU. Deletion of *recF* confers resistance to cipro and HU. The ATPase deficient *recF* mutant (*recF*[K36R]) confers resistance to cipro. (D) Expression of the SOS reporter fusion *PrecN-gfp* over a period of 10h in wild-type (blue), Δ*recF* (green) and Δ*recO* strains (red). Cells grown to exponential phase (OD_{600} ~0.2) were exposed to 10 μM NFZ (downwards facing triangle), 0.5 μg/mL MMC (star-shaped), 0.4 μM bleo (square), 15 μg/mL TMP (diamond), 10 ng/mL cip (pentagon) or 200 mM HU (upwards facing triangle). Untreated cells (grey circle) were used as a control. The expression of *PrecN-gfp* per cell is expressed in relative fluorescent units (R.F.U). Upper three panels show the *PrecN-gfp* average expression as function of time for wt (left, blue), Δ*recF* (middle, green) and Δ*recO* (right, red). Error bars represent the standard deviation of biological triplicates. Lower panel, violin plot representing the global expression of *PrecN-gfp*, the central dot indicates the median value.

6.3.2 RecF and RecO have different DNA binding behaviours and respond differently to UV irradiation

To characterise the spatiotemporal behaviour of the RecF and RecO proteins in live *E. coli* cells, we constructed functional fluorescent protein fusions of the RecF and RecO proteins to the yellow fluorescent protein (YPet) and the red fluorescent protein (mKate2) (**Figure 2A, Materials and methods, Table 1**). The activity of the RecO and RecF fusion proteins, as well as the DnaX-YPet fusion used in this work, was validated *in vivo* in several ways (**Supplementary Figure S1**). Briefly, all constructs used in the present study harbour similar growth, fitness, UV sensitivity and SOS induction level compared to the WT. A number of RecR fusion proteins were also constructed (**Table 1**). However, the fusions caused a complete loss of RecR function upon UV exposure (**Supplementary Figure S1**), and further work on them was not pursued.

The functional fusion constructs of the RecF and RecO proteins allowed us to generate a series of two colour strains to examine RecF and RecO within the same cell, or to examine either of these proteins in concert with the replisome. We also constructed a series of strains in which single deletions of *recO*, *recF*, *recR* or *recA*, as appropriate, were transduced into the strains encoding various fusion proteins and combinations of fusion proteins (**Table 1**). This was done to allow examination of the effects of such deletions on fusion protein behaviour and colocalization.

To investigate the spatiotemporal regulation of RecF and RecO proteins, we imaged single-colour strains (encoding *recF-mKate2*, *recF-YPet*, *recO-mKate2* or *recO-YPet*) in home-built flow-cells under continuous flow of oxygenated media throughout the experiment at 37˚C using a custom-built single molecule fluorescence microscope (62). Cells were irradiated with a pulse of UV light (10 J/m^2) immediately after t = 0min and imaged for 3h after UV irradiation. In these experiments, we set out to measure three properties: 1. Stoichiometry; 2. Binding lifetime and 3. Intracellular localization. We used two different single-molecule imaging modes to extract these measurements. First, burst acquisitions (movies of 300 x 34ms, continuous excitation) enabled us to extract information on binding lifetimes, and perform photobleaching experiments used to measure stoichiometry. To measure changes in intracellular localization, we performed time-lapse imaging by collecting a snapshot of the cells every 10min for three hours after UV-irradiation. We also recorded a bright-field image at each time-point. All fluorescence images were recorded with single-molecule sensitivity, allowing us to observe RecF and RecO fusions binding to DNA (**Figure 2B**).

When recording time-lapse data in the absence of DNA damage, we observed punctate foci of RecF-YPet, consistent with RecF-YPet molecules binding to DNA (**Figure 2C**). On average, cells contained 2.2 ± 0.2 RecF-YPet foci (**Figure 2D**). Similarly, RecF-mKate2 cells contain 1.7 ± 0.1 foci per cell (**Supplementary Figure S2**). We then investigated the binding behaviour of RecF-YPet more closely. Using burst acquisition measurements, we observed RecF-YPet molecules binding to DNA while others were freely diffusing (**Figure 3A**). We extracted fluorescence intensity trajectories from binding events that lasted several hundreds of milliseconds (>150 trajectories) (**Supplementary Figure S3**). Trajectories featured prominent bleaching steps due to the continuous exposure to excitation light, each step representing a single YPet molecule that has bleached. The distribution of intensity steps was used to determine the intensity equivalent to one RecF-YPet molecule (**Supplementary Figure S3**). Knowing the

intensity of a single RecF-YPet molecule, we determined that RecF foci predominantly contain one molecule per focus in undamaged cells (**Figure 3C**). Brighter foci could correspond to oligomers of RecF (i.e. dimers, trimers…) or multiple RecF monomers producing overlapping foci.

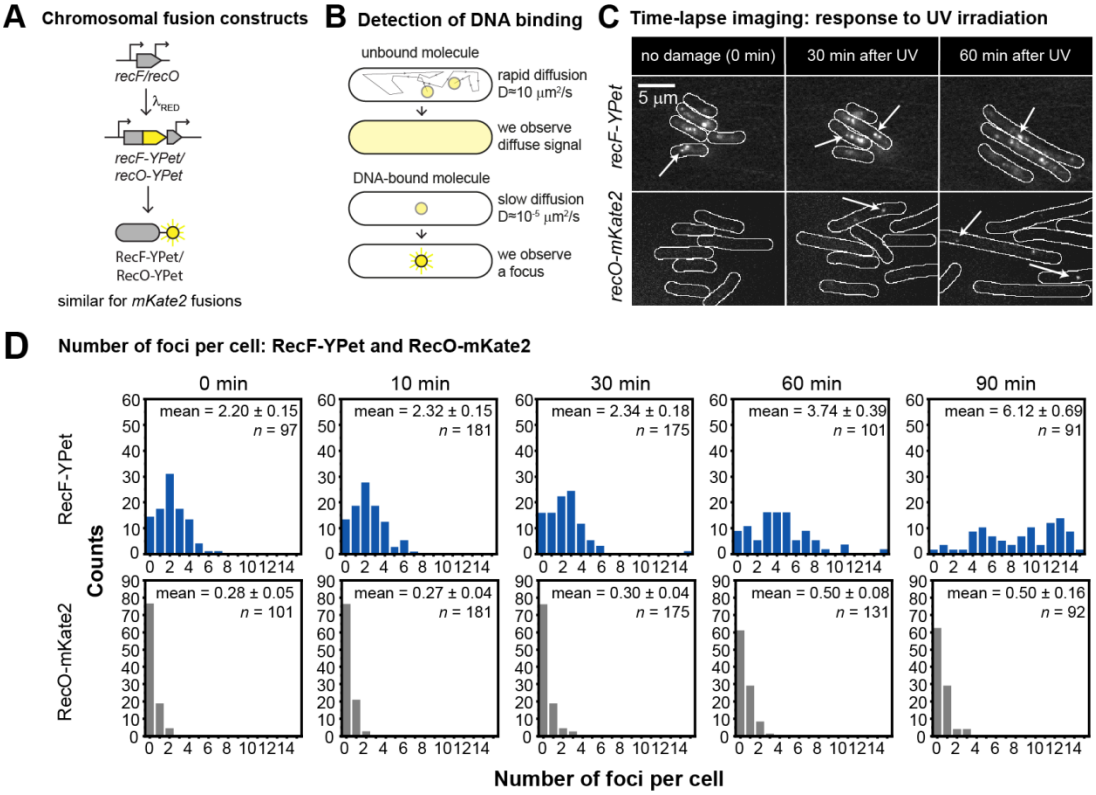

Figure 2. Construction and single-molecule imaging of RecF and RecO fusion constructs. (A) Construction of EAW670 (*recF-YPet*) and EAW814 (*recO-YPet*) as well as EAW779 (*recF-mKate2*) and EAW672 (*recO-mKate2*). The *recF* or *recO* gene of *E. coli* K12 MG1655 was modified using λ_{RED} recombineering so that RecF or RecO is expressed as a fusion with a fluorescent protein YPet or mKate2. (B) Detection of DNA-bound molecules in single-molecule fluorescence images. Molecules of fusion proteins that are not bound to DNA will diffuse quickly ($D \approx 10\ \mu m^2/s$ for a typical cytosolic protein) and thus signals from individual molecules will blur over the entire cell in our images (34ms or 100ms exposures). Molecules of fusion proteins that are bound to DNA, however, experience greatly reduced motion and thus appear as punctate foci. Because of this diffusional contrast, it is possible to detect individual molecules of RecF and RecO fusion proteins when bound to DNA. (C) Time-lapse imaging of RecF-YPet and RecO-mKate2 in response to UV irradiation. Cells were UV irradiated in a flow cell directly after t = 0min. Images were taken from time-lapse experiments before UV irradiation (0min) and after UV irradiation (30min, 60min time-points). Scale bar: 5 μm. (D) Histograms showing the number of RecF-YPet and RecO-mKate2 foci per cell in response to UV irradiation. Bright-field images were used to determine the position of cells within different fields of view. The number of foci per cell were counted for each cell and plotted in a histogram. We plotted these histograms for the time-point before UV irradiation (0min) and several time-points following UV irradiation (10, 30, 60 and 90min). The mean over the number of foci per cell is depicted in each histogram for each time-point. The number of cells that went into each histogram is indicated as *n*.

Intensity traces were further used to investigate the time scale on which RecF-YPet molecules are bound to DNA (**Supplementary Figure S4**). To investigate the time scale of binding events, we utilised autocorrelation analysis, a method that identifies time-dependent fluctuations in signal which are also dependent on binding and dissociation of molecules. When applying the autocorrelation function to a

RecF-YPet trajectory, the correlation of this trajectory with its time delayed copy is generated for various lag times. With zero lag time, the normalized correlation of a trajectory with itself is one. After zero lag time, RecF-YPet molecules that are statically bound would give autocorrelation values between zero and one depending on the signal-to-noise. However, RecF-YPet molecules that are transiently associated show zero autocorrelation. Autocorrelation analysis can thus be used to identify major components of binding events. We generated an average over all autocorrelation functions for each condition (before and after UV irradiation) which was then used to extract information on the overall binding behaviour (**Figure 3D, Supplementary Figure S4**). The averaged autocorrelation function contained three major components reflecting multiple time-dependent processes present in the signal. The first was a fast decorrelation occurring on the time scale of the integration time (an individual camera frame exposure, one frame of the burst acquisition) attributable to noise as well as, transient binding events that occur within the time resolution of imaging. This fast decorrelation component is hereafter referred to as the short component ($\tau_s < 0.034$s). Fitting the averaged autocorrelation curve starting from lag time 0.034s (after the initial fast decorrelation) with single and double exponential-decay functions indicated that there were two major component timescales present in the remainder of the autocorrelation curve (**Supplementary Figure S4** shows two-exponential fit). In both undamaged as well as damaged cells (30 – 60min after UV), the fluorescence signal decayed according to two timescales: medium corresponding to 0.3s (τ_m) and long corresponding to 1.5s (τ_l) reflecting longer-lived binding events. The amplitudes of these decay functions in the autocorrelation function for RecF-YPet are 53% short (a_s), 12% medium (a_m) and 35% long (a_l).

Our experiments also enabled us to further determine the cellular concentration of RecF-YPet. Knowing the intensity of a single YPet molecule from our trajectories, we calculated that there were 18.1 ± 0.7 molecules of RecF-YPet per cell (standard deviation STD = 5.5; *n* = 71 cells) (**Supplementary Figure S5**), equivalent to a RecF-YPet concentration of 5.4 ± 0.2 nM (**Materials and methods**). From the above measurements (18 molecules per cell, two foci, one molecule per focus), we concluded that ~11% of RecF-YPet molecules were bound to DNA at any given moment in the absence of DNA damage.

We undertook the same measurements for EAW814 (*recO-YPet)* and EAW672 (*recO-mKate2*). RecO foci were much less common than RecF foci. Using time-lapse measurements (100ms exposure), we determined that only three in ten cells have a RecO-mKate2 focus (**Figure 2D**). Consistent with these measurements, cells expressing a RecO-YPet fusion (EAW814) contain on average 0.4 ± 0.04 foci per cell (**Supplementary Figure S2**). Burst acquisition measurements showed that most RecO-YPet molecules are diffusive and a RecO-YPet molecule binds to DNA only occasionally (**Figure 3B**). These RecO-YPet foci contain one molecule per focus (**Figure 3C, Supplementary Figure S3**). RecO-YPet binding events were then analysed using autocorrelation analysis. The components of the autocorrelation function were 75% short (a_s, $\tau_s < 0.034$s), 13% medium (a_m, $\tau_m = 0.3$s) and 12% long (a_l, $\tau_l = 2.2$s) (**Figure 3E and F, Supplementary Figure S4**). We further determined that cells have 12.2 ± 0.6 RecO-YPet molecules per cell (STD = 5.9; *n* = 98 cells), corresponding to a RecO-YPet concentration of 3.7 ± 0.2 nM (**Supplementary Figure S5**). With only 0.3 foci per cell and 12 RecO-YPet molecules per cell, only ~2% of RecO molecules are DNA bound at any given moment in the absence of any cellular stress.

Next, we investigated the behaviour of RecF and RecO fusions in cells damaged with $10Jm^{-2}$ of UV light. Using time-lapse measurements, we observed that cells filament after acquiring UV induced DNA damage, beginning approximately 30min after UV irradiation (**Supplementary Figure S6A**). We further determined the mean pixel intensities within cell boundaries (mean cell intensity) to identify possible changes in the concentration of RecF-YPet upon DNA damage induction. We found that the mean cell intensity is constant during the experiment, indicating that the concentration of RecF-YPet remains constant throughout the experiment (**Supplementary Figure S6B**). As cells grow into filaments, more RecF-YPet molecules bind to DNA (**Figure 2C and D**), for instance, cells have approximately six RecF-YPet foci per cell at 90min. We calculated the focus density (foci per cell area) using the time-lapse data. Even though the number of binding sites increases for RecF-YPet, the focus density is constant before and after UV irradiation as the number of binding sites increases proportionally with the increase in cell length (**Supplementary Figure S6C)**. In contrast to untreated cells however, RecF-YPet foci contain approximately two molecules per focus starting 30min after UV irradiation (**Figure 3A and C**). This suggests that RecF forms a dimer, a molecular form previously characterized (46,66–68), in response to UV irradiation. From autocorrelation analysis, we identified that more RecF molecules seem to bind slightly longer to DNA 30-60min after UV irradiation. The components of the autocorrelation function are 38% short (a_s, $\tau_s < 0.034s$), 12% (a_m, $\tau_m = 0.3s$) medium and 50% long (a_l, $\tau_l = 1.5s$) (**Figure 3D and F**). There are (at least) two possible explanations for the difference in RecF binding behaviour between untreated and UV-irradiated cells. More RecF molecules may bind on the longer timescale to DNA after UV-irradiation. Alternatively, the formation of RecF-YPet dimers observed after UV is associated with an increase in focus intensity. This increase in intensity causes an increase in the signal-to-noise ratio for RecF foci which then decreases the rapid (short) component of the autocorrelation curve. Analysis of simulated data suggests that the second case is likely (**Supplementary Figure S7**, **Materials and methods**). With RecF forming a dimer and cells exhibiting a constant focus density and mean cell intensity, ~22% of RecF-YPet molecules are DNA bound after damage induction. This is a two-fold increase compared to untreated cells and is driven primarily by dimerization of RecF rather than an increase in the density of binding sites on the DNA.

As observed for cells expressing RecF fusion proteins, cells carrying RecO fusion constructs grow into filaments upon UV irradiation (**Figure 2C, Supplementary Figure S6A**). The mean cell intensity derived from the fusion proteins stays constant over time (**Supplementary Figure S6B**) suggesting no change in the cellular concentration of RecO. As cells grow into filaments upon UV irradiation, cells contain more RecO foci (**Figure 2C and D, Supplementary Figure S2**) while the focus density remains constant over time (**Supplementary Figure S6C**). In contrast to RecF-YPet foci, RecO-YPet foci consist of only one molecule per focus and thus are monomeric before and after UV damage (**Figure 3B and C**). UV irradiation results in a small increase in the number of long-lived RecO foci; the components of the autocorrelation function were 62% short (a_s, $\tau_s < 0.034s$), 20% (a_m, $\tau_m = 0.3s$) medium and 18% long (a_l, $\tau_l = 2.2s$) (**Figure 3E and F**). Since the focus density and mean cell brightness are constant and RecO foci are still monomeric after UV irradiation, ~2% of RecO-YPet molecules are DNA bound both before and after DNA damage induction.

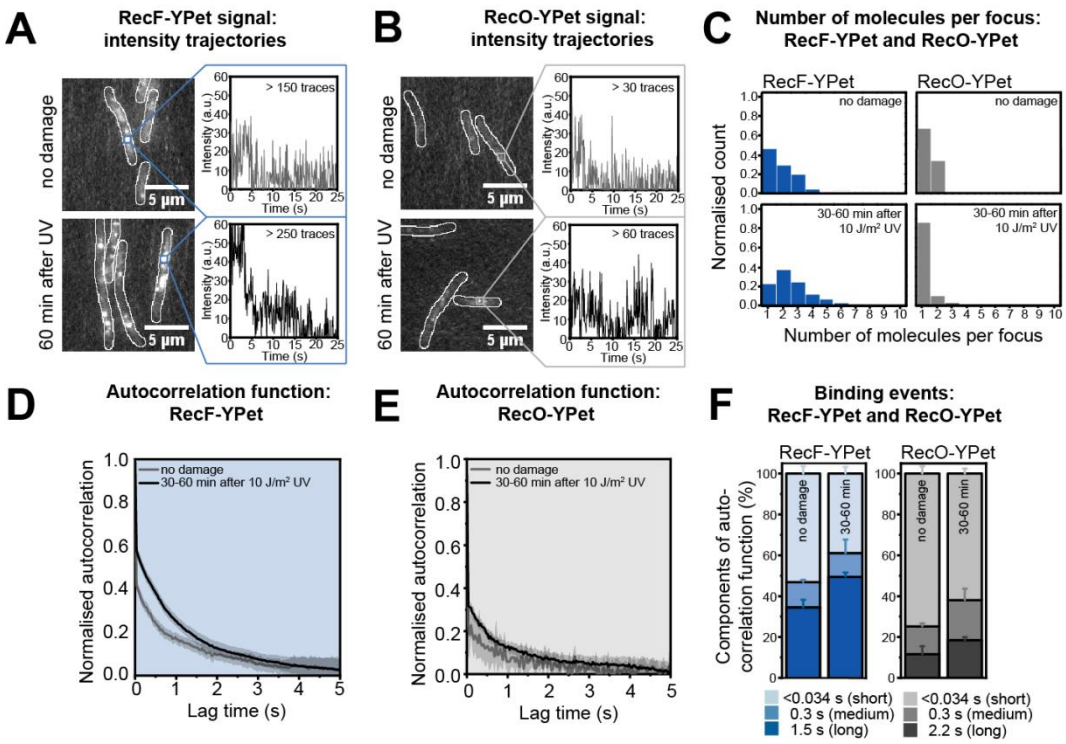

Figure 3. Binding behaviour of RecF-YPet and RecO-YPet to chromosomal DNA. (A) Average projection over time of RecF-YPet signal and representative time traces for RecF-YPet binding to DNA (continuous illumination with 34ms exposure times over 300 frames). Average projections stem from burst acquisition movies before UV exposure and 60min after UV exposure. The projection was made over 10 x 34ms. Scale bar: 5 µm. (B) Average projection over time of RecO-YPet signal and representative time traces for RecO-YPet binding to DNA (continuous illumination with 34ms exposure times over 300 frames). Average projections stem from burst acquisition movies before UV exposure and 60min after UV exposure. The projection was made over 10 x 34ms. Scale bar: 5 µm. (C) Histogram showing the number of RecF-YPet and RecO-YPet molecules per focus before UV exposure and 30-60min after UV exposure. For the number of RecF-YPet molecules per focus before UV irradiation, 161 trajectories were samples. For the number of RecF-YPet molecules per focus upon UV irradiation, 285 trajectories were samples. To determine the number of RecO-YPet molecules per focus, 32 trajectories were sampled before UV exposure and 61 trajectories after UV exposure. For further explanation see **Supplementary Figure S3**. (D) Autocorrelation function obtained for RecF-YPet binding events before and after UV exposure. For further explanation see **Supplementary Figure S4**. (E) Autocorrelation function obtained for RecO-YPet binding events before and after UV exposure. For further explanation see **Supplementary Figure S4**. (F) Components of the autocorrelation for RecF-YPet and RecO-YPet binding to DNA. Components of the autocorrelation function for RecF-YPet before and after UV exposure are long (1.5s), medium (0.3s) and short (<0.034s). For RecO-YPet, components are split in long (2.2s), medium (0.3s) and short (<0.034s). Error bars for long and medium components are derived from the exponential fit (**Supplementary Figure S4**), error bars for short events stem from the standard error of the mean at lag time 0s.

6.3.3 RecF and RecO exhibit different spatiotemporal behaviour

We further defined the spatiotemporal behaviour of RecF and RecO in response to UV damage. This was achieved through two-colour time-lapse imaging of EAW676 (*recF-YPet recO-mKate2*). Cells were irradiated with a UV dose of 10J/m^2 directly after t = 0min and imaged for a period of 3h after UV irradiation. Images were recorded once every 10min (**Figure 4A and D**).

When analysing the spatial localization of RecF in response to DNA damage, we examined whether foci localize within the inner part of the cell or closer to the membrane (focus position along the cellular width). We plotted histograms of the RecF foci position with respect to the short axis of the cell (i.e. width) prior to damage induction, as well as 30min and 90min after UV irradiation (**Figure 4B**). The centre spline of the cell (a line drawn down the long axis) is at 0 μm, the cell membrane is at 0.5 μm and -0.5 μm. We found that RecF foci localize predominantly within the inner part of the cell before and after UV irradiation. The vast majority of the RecF foci were located within 0.2 μm of the cell centre. To further characterize the spatiotemporal localization of RecF throughout the experiment, we used a tool that yields information on the distributions of sparse fluorescence signals by averaging signals across cross-sections of many cells (69). The resulting data are referred to as line scans and represent the average fluorescence intensity across the short axis of the cell. Prior to analysis, we enhanced the focus intensity and reduced the background signal using digital filters (61). High intensity areas within cells thus represent foci and other high-spatial frequency features. Using our time-lapse data, this tool plots a 2D contour plot showing the spatiotemporal behaviour of RecF-YPet following the SOS response (**Figure 4C**). The cell width is given in micrometres, whereas, the mid-cell position is at 0 μm and the dashed red line indicates the signal of a membrane binding protein, LacY (61). High focus abundance is shown by red coloured areas in the localization map; low focus abundance is illustrated by blue coloured areas. We found that RecF foci are localized to the inner part of the cell before and after damage induction. This localization behaviour has previously been found for replisome markers following UV irradiation (69).

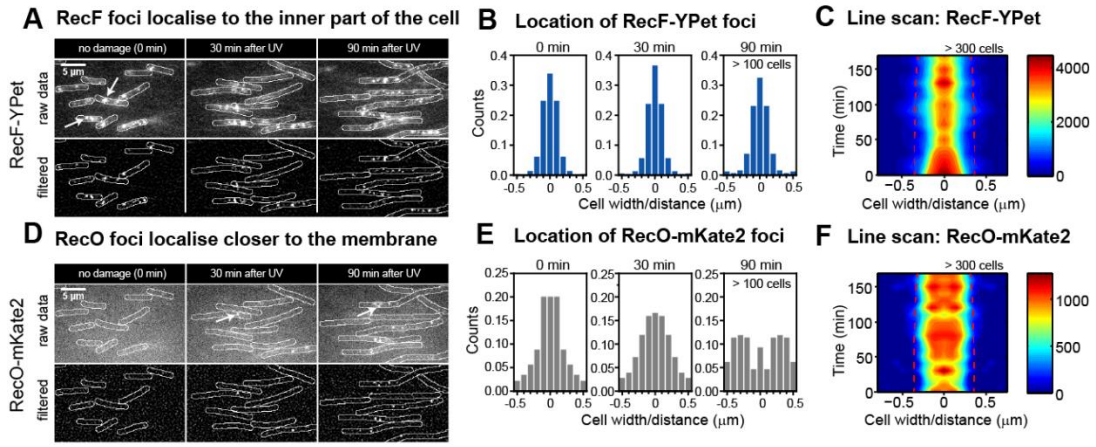

Figure 4. Spatiotemporal behaviour of RecF-YPet and RecO-mKate2 following UV treatment. (A) Time-lapse imaging of RecF-YPet in response to UV irradiation. Cells were UV irradiated in a flow cell directly after t = 0min. Images were taken from time-lapse experiments before UV irradiation (0min) and after UV irradiation (30min, 90min time-points). Scale bar: 5 μm. (B) Histogram showing the localization of RecF foci along the short axis of the cell. Histograms are derived from ~100 cells at each time point (for exact numbers see **Figure 2**). The centre spline of the cell (a line drawn down the long axis) is at 0 μm, the cell membrane is at 0.5 μm and -0.5 μm. (C) 2D contour plot showing the spatiotemporal behaviour of RecF-YPet following the SOS response. The cell width is given in micrometres, the mid-cell position is at 0 μm and the dashed red line indicates the signal of a membrane binding protein, LacY. High focus abundance and other high-spatial frequency features are shown by red coloured areas in the localization map; low focus abundance is illustrated by blue coloured areas. (D) Time-lapse imaging of RecO-mKate2 in response to UV irradiation. For further description see (A). Scale bar: 5 μm. (E) Histogram showing the localization of RecO foci along the short axis of the cell. For further description

see (B). (F) 2D contour plot showing the spatiotemporal behaviour of RecO-mKate2 following the SOS response. For further description see (C).

We also investigated the spatiotemporal behaviour of RecO. In comparison with RecF, RecO produces a broader distribution around 0 μm prior to UV irradiation (**Figure 4E**). After UV irradiation, the distribution broadened further. At 30min, more foci were localized closer to the membrane. At 90min, most RecO foci were localized in proximity to the membrane. Two broader peaks appeared at the -0.3 μm and 0.3 μm position, with relatively few foci found at the 0 μm position. When plotting the 2D contour plot showing the spatiotemporal behaviour of RecO-mKate2, we observed that the distribution broadened 30-50min after damage induction, corresponding closely to the time when cells begin to grow into filaments (**Figure 4F**). This reveals that RecO usually binds at positions closer to the membrane following the SOS response, likely excluded from the nucleoid.

6.3.4 RecF and RecO foci localize differently with respect to replisome markers

Due to strong differences in the spatiotemporal behaviour of RecF and RecO, we wished to determine if there was any indication that RecF and RecO formed a complex in vivo, as indicated by a sharing of chromosomal binding sites. We determined the percentage of RecF foci that colocalized with RecO foci and the percentage of RecO foci that colocalized with RecF foci following the SOS response. For colocalization analysis, we selected foci for each of the proteins that are each labelled with a different fluorescent protein (i.e. RecF-YPet and RecO-mKate2, **Figure 5A**). We defined two foci (i.e. a RecF and a RecO focus) as colocalized if their centroid positions were within 218 nm of each other (**Figure 5B and C**). This distance corresponds to the maximum colocalization distance observed between two replisome probes, which are expected to be highly colocalized (62). To conduct colocalization analysis of RecF and RecO, we used the two-colour time-lapse data of EAW676 (*recF-YPet recO-mKate2*) inducing UV damage directly after t = 0min.

In undamaged cells, only 0.5% of RecF foci also contained a RecO focus (chance colocalization <1%, **Materials and methods**) while 5% of RecO foci had a coincident RecF focus (chance colocalization ~4%, **Materials and methods**) (**Figure 5D**). Note that the calculated frequency of chance colocalization takes into account the fact that many cells do not have RecO foci, but most have RecF foci. After exposure to 10 J/m^2 UV, the percentage of RecF foci that are coincident with a RecO focus slightly increased to ~2% at 40min after damage induction. The colocalization of RecO with RecF increased to 12% at 30-40min followed by a gradual drop in colocalization to 5% at 50min. Following the SOS response, the colocalization of RecF with RecO was just above the level calculated for chance colocalization, whereas colocalization of RecO with RecF is slightly above chance in the 10-50min time interval. Our data clearly suggest that RecF and RecO have predominantly distinct binding sites both before and after exposure to UV, and provide no evidence for a RecFOR complex.

We further examined if RecF and RecO localized to the replisome. We performed two-colour time-lapse experiments and colocalization analysis by imaging CJH0015 (*recF-mKate2 dnaX-YPet*) and EAW762 (*recO-mKate2 dnaX-YPet*) as described above (UV dose: 10 J/m^2 just after t = 0min; images were taken every 10min for 3h after UV, experiments were conducted at 37˚C).

We observed that the colocalization of RecF with the replisome marker DnaX-YPet was quite significant, both before and after UV irradiation (**Figure 5E**). Before damage induction, colocalization of RecF with the replisome marker was 22% (chance colocalization ~4%, **Materials and methods**). Similarly, 20% of replisome foci contained a RecF focus (chance colocalization ~4%, **Materials and methods**). After UV irradiation, the percentage of RecF foci that contained a replisome focus peaked at 30% at 30min. This peak was followed by a gradual decline in colocalization, and at 120min after UV irradiation only 15% of RecF foci overlapped with a replisome focus. The colocalization of replisomes with RecF followed the same trend upon UV irradiation. At 30min, 27% of replisome foci contained a RecF focus. At 120min, 13% of replisome foci had a RecF focus. RecF appeared to be recruited to replisomes directly after UV exposure. In general, RecF displayed relatively high colocalization with replisome markers, suggesting that RecF function often involves action at, or near, replisomes.

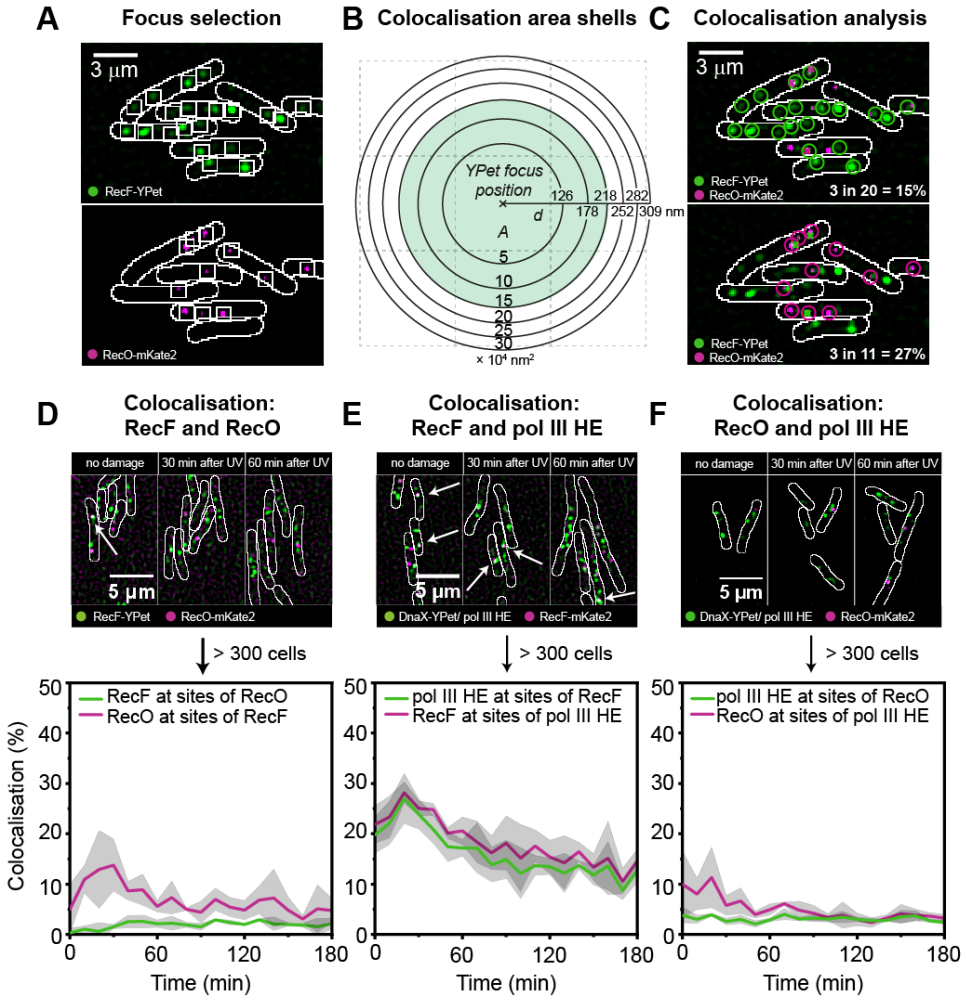

Figure 5. Colocalization measurements of RecF/RecO, RecF/replisomes and RecO/replisomes. (A) Exemplary selection of RecF-YPet and RecO-mKate2 foci. Selection boxes indicate selected foci for recF-YPet and RecO-mKate2. Scale bar: 3 µm. (B) Diagram of area shells used for colocalization analysis. As colocalization is a radial measurement, histograms of colocalization distances are constructed using bins of linearly increasing area rather than distance. A colocalization radius of 218 nm was used for all measurements since two replisome components colocalize within this colcoalisation radius. (C) Montage of two-colour images shown in (A). RecF-YPet foci appear in green and RecO-mKate2 foci appear in magenta. Upper panel: Colocalization percentages for RecF-YPet with RecO-mKate2 are

determined from selected foci in the RecF-YPet channel (green circles) that colocalize to the same position with RecO-mKate2 foci from the other channel (magenta crosses). Lower panel: The opposite is shown to determine colcoalisation percentages of RecO-mKate2 (magenta circles) with RecF-YPet (green crosses). Scale bar: 3 μm. (D) Colocalization measurements of RecF-YPet with RecO-mKate2 in response to 10 J/m^2 UV. Merged images of RecF-YPet (green signal) and RecO-mkate2 (magenta signal) are shown before UV irradiation and after UV irradiation (30min and 60min). Colocalization was measured over >300 cells. The percentage of RecF-YPet foci that contain a RecO-mKate2 focus is plotted as a green line plot over 180min at intervals of 10min. Similarly, the colocalization of RecO-mkate2 with RecF-YPet is plotted as a magenta line plot. Scale bar: 5 μm. (E) Colocalization measurements of RecF-mKate2 with DnaX-YPet (replisomes) in response to 10 J/m^2 UV. Merged images of RecF-mKate2 (magenta signal) and DnaX-YPet (green signal) are shown before UV irradiation and after UV irradiation (30min and 60min). The percentage of RecF-mKate2 foci that contain a DnaX-YPet focus is plotted in green, the percentage of DnaX-YPet that colocalize with RecF-mKate2 is depicted with a magenta line plot (n > 300 cells). Scale bar: 5 □m. (F) Colocalization measurements of RecO-mKate2 with DnaX-YPet (replisomes) in response to 10 J/m^2 UV. Merged images of RecO-mkate2 (magenta signal) and DnaX-YPet (green signal) are shown before UV irradiation and after UV irradiation (30min and 60min). Colocalization of RecF-mKate2 with DnaX-YPet is illustrated by a green line plot; colocalization of DnaX-YPet with RecO-mKate2 is presented by a magenta line plot (n > 300 cells). Scale bar: 5 μm.

In contrast to colocalization measurements between RecF and replisomes, RecO rarely bound at sites of replisomes (**Figure 5F**). In undamaged cells, 10% of RecO foci colocalized with replisomes (chance colocalization ~4%, **Materials and methods**); 4% of replisome foci contained a RecO focus (chance colocalization ~1%, **Materials and methods**). Colocalization between RecO and replisomes progressively decreased after UV irradiation; only 3% of RecO foci contained a replisome focus at 120min, a level below that expected by chance. Thus, the vast majority of RecO foci (97%) are spatially distinct from replisomes. The percentage of replisomes containing a RecO molecule remained at 3-4% throughout the experiment, constantly just above the level calculated for chance colocalization. This suggests that RecO binding sites, and sites of action, rarely correspond with replisomes in cells.

6.3.5 RecF and RecO function independently of each other

To investigate if RecF and RecO act independently, we first determined the number of RecF foci in Δ*recO* cells and the number RecO foci in Δ*recF* cells at 37˚C. A slower cell filamentation rate is associated with a slower increase in the number of foci. In these experiments, we used cell filamentation as a proxy for SOS induction.

In the absence of DNA damage, we found that the deletion of *recO* did not affect the number of RecF foci (**Figure 6A, Supplementary Figure S8**). After damage induction, cells lacking *recO* filamented slower than wild-type cells. A subset of cells within the population were static and did not grow into filaments (**Supplementary Figure S10**). The mixed population of slowly filamenting cells and static cells produced a broad distribution in cell length beginning about 30min after UV irradiation. We further observed that the number of RecF-YPet foci in Δ*recO* cells increased slower than in *recO*$^+$ cells (**Supplementary Figure S11**). This result agrees with our previous observation that the increase in cell length is associated with an increase in number of foci (i.e. the focus density is constant, **Supplementary Figure S6**).

The deletion of *recF* marginally lowered the number of RecO foci before UV irradiation (**Supplementary Figure S9**). Cells lacking *recF* also filamented slower than wild-type cells upon UV

treatment. However, we did not detect a static population that does not grow into filaments as seen for cells lacking *recO* (**Supplementary Figure S10**). The number of RecO foci in Δ*recF* increases steadily as cells grow into filaments, remaining just slightly lower than in wild-type cells (**Supplementary Figure S12**).

To determine if the activity of RecF at replisomes is independent of RecO and *vice versa*, we conducted colocalization measurements for RecF and replisomes in the Δ*recO* background as well as RecO and replisomes in the Δ*recF* background. Time-lapse experiments (10 J/m^2 directly after 0min, at 37˚C) and colocalization measurements were conducted as described above.

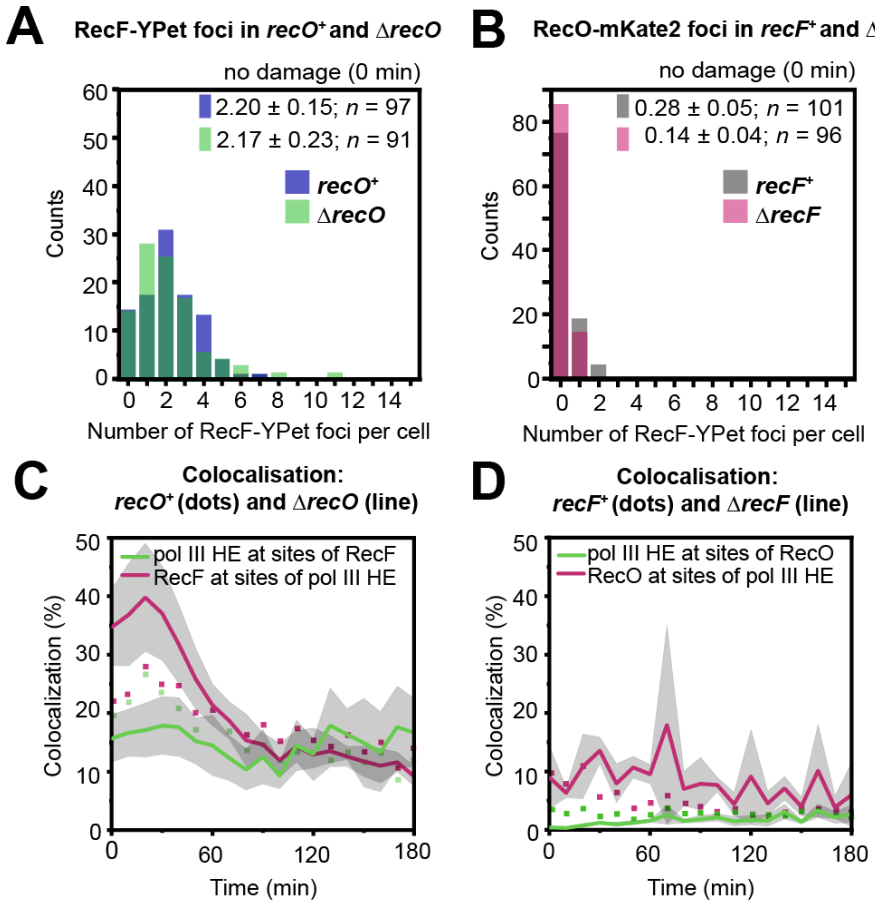

Figure 6. Colocalization measurements of RecF with replisomes in Δ*recO* and RecO with replisomes in Δ*recF*. (A) Histograms showing the number of RecF-YPet foci per cell in Δ*recO* (green) and *recO*$^+$ (blue) under normal growth conditions. Bright-field images were used to determine the position of cells within different fields of view. The number of foci per cell were counted for each cell and plotted in a histogram. The mean over the number of foci per cell is given in each histogram. The number of cells included in each histogram is also indicated as *n*. (B) Histograms showing the number of RecO-mKate2 foci per cell in Δ*recF* (pink) and *recF*$^+$ (grey) under normal growth conditions. Bright-field images were used to determine the position of cells within different fields of view. The number of foci per cell were counted for each cell and plotted in a histogram. The mean over the number of foci per cell is given in each histogram. The number of cells included in each histogram is also indicated as *n*. (C) Colocalization measurements of RecF-mKate2 with DnaX-YPet (replisomes) in Δ*recO* following 10 J/m^2 UV. The

percentage of RecF-mKate2 foci that contain a DnaX-YPet focus is plotted in green, the percentage of DnaX-YPet that colocalize with RecF-mKate2 is depicted with a magenta line plot (n > 100 cells). The colocalization of RecF-mKate2 with DnaX-YPet in *recO*$^+$ (magenta scatter plot) and the colocalization of DnaX-YPet with RecF-mKate2 in *recO*$^+$ (green scatter plot) is also plotted for each time-point as in **Figure 5E**. (D) Colocalization measurements of RecO-mKate2 with DnaX-YPet (replisomes) in Δ*recF* following 10 J/m^2 UV. The percentage of RecO-mKate2 foci that contain a DnaX-YPet focus is plotted in green, the percentage of DnaX-YPet that colocalize with RecO-mKate2 is depicted with a magenta line plot (n > 100 cells). The colocalization of RecO-mKate2 with DnaX-YPet in *recF*$^+$ (magenta scatter plot) and the colocalization of DnaX-YPet with RecO-mKate2 in *recF*$^+$ (green scatter plot) is also plotted for each time-point as in **Figure 5F**.

Colocalization measurements of RecF with the replisome in Δ*recO* cells returned higher extents of colocalization while retaining the trend observed for wild-type cells (**Figure 6C**). In the absence of damage, 35% of RecF foci were colocalized with a replisome. At 30min, colocalization peaked at 40% followed by a slow decrease in colocalization (chance colocalization ~4%). From 90min, 14% of RecF foci were coincident with a replisome focus. When measuring colocalization between the replisome and RecF in Δ*recO*, 16% of replisomes had a RecF focus bound before UV irradiation, which is slightly lower than in wild-type cells (chance colocalization ~4%). After UV irradiation, colocalization marginally increased to 18% at 30min, followed by a slight drop to 13% at 90min.

The deletion of *recF* only marginally changed the colocalization behaviour of RecO with replisomes. In the absence of damage, 9% of RecO foci contained a replisome focus (**Figure 6D**) as seen for wild-type cells. During the experiment, the percentage of RecO foci that contained a replisome stays on average at ~8% which was just above chance (chance colocalization ~4%). In the *recF*$^+$ background, the small degree of RecO-replisome colocalization present in the absence of damage dropped below chance after UV irradiation. This drop did not appear to occur in the Δ*recF* background. We then measured the colocalization of replisomes with RecO foci; 0.5% of replisomes contained a RecO focus in the absence of damage. The colocalization percentage stayed low following the SOS response. From 60min, only 2% of replisomes contained a RecO focus (chance colocalization <1%).

Thus, independently of RecO, RecF is recruited to replisomes directly after UV irradiation while the number of RecF foci per cell slowly increases. Similarly, the number of RecO foci per cell increases upon UV irradiation independently of RecF. In *recF*$^+$ and Δ*recF*, RecO predominantly binds at sites that are spatially distinct from replisomes, in both untreated and UV-irradiated cells.

6.3.6 RecF and RecO form foci only under conditions of active DNA replication

Recombination via the RecFOR pathway is thought to be the major mechanism for the resolution of post-replicative ssDNA gaps in bacteria. We reasoned that if the majority of RecF and RecO foci observed in our experiments represent proteins engaged in post-replicative gap repair, then blocking DNA replication should reduce the number of RecF and RecO foci. To test this hypothesis, we first constructed strains that carry a temperature sensitive *dnaB* allele in place of the wild-type allele (52,53): SSH114 (*recF-mKate2 dnaX-YPet dnaB8*[Ts]) and SSH115 (*recO-mKate2 dnaX-YPet dnaB8*[Ts]). Next, we conducted two-colour time-lapse experiments in which we observed the ability of tagged RecF and RecO

proteins to form foci in UV-irradiated cells following a rapid jump from the permissive to the non-permissive temperature (**Figure 7**; **Supplementary Figure S13, S14**). To that end, we first collected data at the permissive temperature at the first time point (t = 0 min, T = 30˚C). Following this acquisition, cells were irradiated with a UV-dose of 10 $J \cdot m^{-2}$ and imaged every 10 minutes for 2 hours. In these experiments, the stage temperature changed from 30 to 42^0C within 5 minutes, such that the temperature of the flow cell was maintained at 42^0C for all time points but the first (**Figure 7A**). Additionally, we repeated these experiments with cells carrying the wild-type *dnaB* allele.

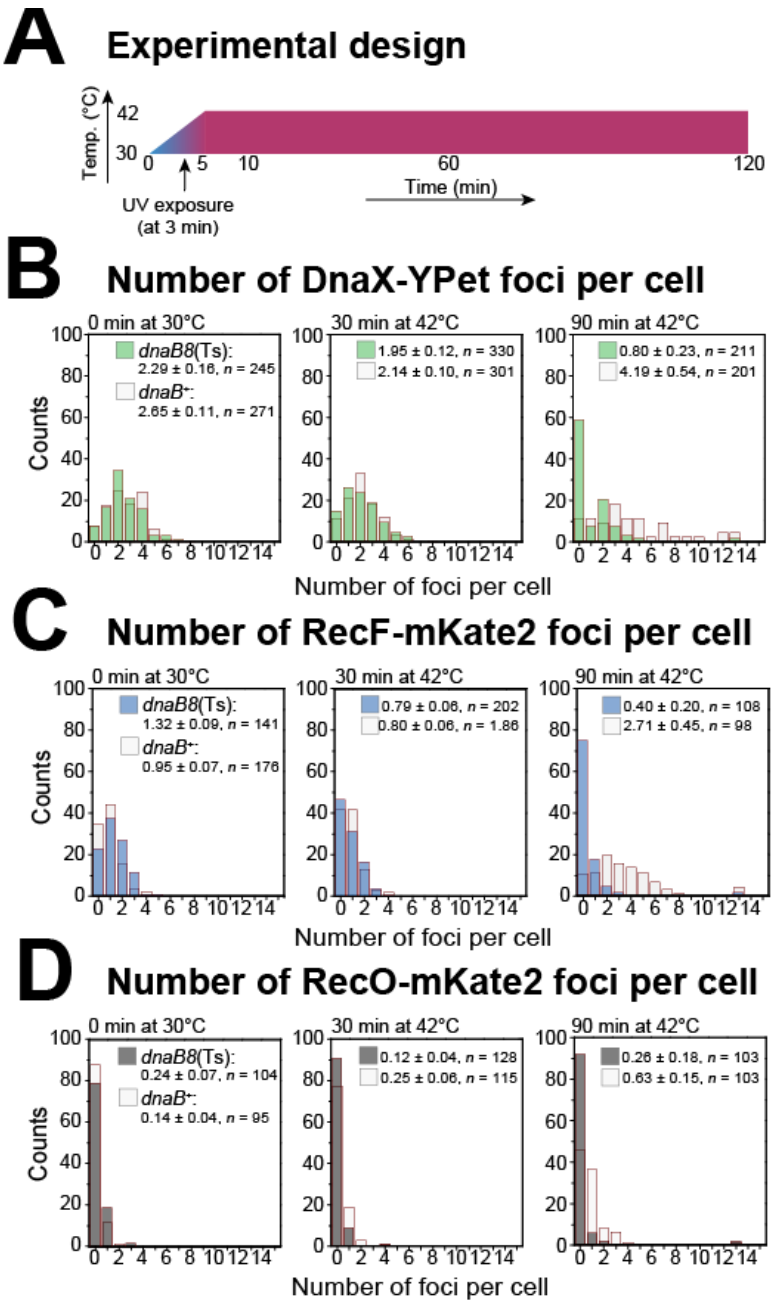

Figure 7. Number of DnaX-YPet, RecF-mKate2 and RecO-mKate2 foci per cell in replicating cells (*dnaB*$^+$) and cells experiencing replication blocking (*dnaB8*[Ts]). (A) Experimental design. First image is taken at 30˚C (0min) when no UV image is yet induced. Then, the temperature is ramped up to 42˚C. UV damage is induced at 3-4min. 42˚C are reached at 5min and hold until the end of the experiment, at

120min. (B) Histograms showing the number of DnaX-YPet foci per cell in *dnaB*$^+$ (light grey) and *dnaB8*(Ts) (green) before UV exposure, at 30˚C (0min) and after UV exposure at 42˚C (30min and 90min). Bright-field images were used to determine the position of cells within different fields of view. The number of foci per cell were counted for each cell and plotted in a histogram. The mean over the number of foci per cell is given in each histogram. The number of cells included in each histogram is also indicated as *n*. (C) Histograms showing the number of RecF-mKate2 foci per cell in *dnaB*$^+$ (light grey) and *dnaB8*(Ts) (blue) before UV exposure, at 30˚C (0min) and after UV exposure at 42˚C (30min and 90min). Bright-field images were used to determine the position of cells within different fields of view. The number of foci per cell were counted for each cell and plotted in a histogram. The mean over the number of foci per cell is given in each histogram. The number of cells included in each histogram is also indicated as *n*. (D) Histograms showing the number of RecO-mKate2 foci per cell in *dnaB*$^+$ (light grey) and *dnaB8*(Ts) (dark grey) before UV exposure, at 30˚C (0min) and after UV exposure at 42˚C (30min and 90min). Bright-field images were used to determine the position of cells within different fields of view. The number of foci per cell were counted for each cell and plotted in a histogram. The mean over the number of foci per cell is given in each histogram. The number of cells included in each histogram is also indicated as *n*.

From the time-lapse images we then measured the number of DnaX foci per cell as a proxy for active DNA replication forks. As expected, both wild-type and temperature sensitive cells exhibited identical number of DnaX-YPet foci (*dnaB*$^+$: 2.65 ± 0.11, *dnaB8*(Ts): 2.29 ± 0.16) prior to UV irradiation at the permissive temperature (**Figure 7B**). Following UV damage, whereas both *dnaB8*(Ts) and *dnaB*$^+$ cells exhibited classic cell filamentation that accompanies the triggering of the SOS response (**Supplementary Figure S13**). The number of DnaX foci per cell decreased in *dnaB8(Ts)* while the number of DnaX foci increased in *dnaB*$^+$ cells (**Figure 7B**, **Supplementary Figure S13**). At 90min after irradiation, cells contain on average 0.80 ± 0.23 DnaX foci in the *dnaB8*(Ts) background and 4.19 ± 0.54 DnaX foci in the *dnaB*$^+$ background. The loss of replisomes detected in the *dnaB8*(Ts) cells at the non-permissive temperature is consistent with the inability of this DnaB mutant to maintain processive replication at the non-permissive temperature.

The number of RecF and RecO foci per cell was comparable between the two *dnaB* backgrounds (RecF: 0.95 ± 0.07 in *dnaB*$^+$, 1.32 ± 0.09 in *dnaB8*[Ts]; RecO: 0.14 ± 0.04 in *dnaB*$^+$, 0.24 ± 0.07 in *dnaB8*[Ts], **Figure 7C, D**). Notably, the colocalization of RecF with replisomes was 1.5 fold higher in *dnaB8*(Ts) cells (36%) compared to *dnaB*$^+$ cells (24%) (**Supplementary Figure S15**; chance colocalization ~4% in both cases, see **Materials and methods**). Strikingly, the colocalization of RecO with replisomes increased from 5% in *dnaB8*(Ts) cells to 20% in *dnaB8*(Ts) cells (chance colocalization ~4% in both cases, see **Materials and methods**). The enhanced co-localization of RecF and RecO with the replication forks may reflect the weaker helicase activity of DnaB8 compared to DnaB (53).

Irradiating with UV and increasing the temperature led to a reduction of RecF foci in *dnaB8*(Ts) cells (**Figure 7C**, **Supplementary Figure S13**) mirroring the previously observed reduction in DnaX foci (**Figure 7B**). By the 90 min time-point, *dnaB8*(Ts) cells contained on average only 0.40 ± 0.20 RecF foci per cell, compared with 2.71 ± 0.45 foci for *dnaB*$^+$ cells under the same conditions. A similar trend was observed for RecO foci (**Figure 7D**). By the 90 min time-point, *dnaB8*(Ts) cells contained on average only 0.26 ± 0.18 RecO foci per cell, compared with 0.6 ± 0.2 foci for *dnaB*$^+$ cells under the same conditions.

Our data demonstrate that UV irradiation leads to an increase in DnaX, RecF and RecO foci per cell in *dnaB*$^{+}$ cells. Whereas RecF is often found at replisomes, most RecO molecules reside at sites away from the replisome. Loss of replisomes is accompanied by an overall loss of RecF and RecO binding sites in cells. These findings lead us to suggest that whereas RecF may play a role at the replisome, RecO instead acts on substrates that are generated and left behind in the wake of the replisome - consistent with its proposed role in post-replicative gap repair.

6.4 Discussion

The epistatic relationship of the *recF*, *recO*, and *recR* genes has led to the expectation that the proteins function together, perhaps forming a complex or forming multiple complexes in a temporal order at one location. Here, we examined this hypothesis by obtaining a high-resolution description of the spatial and temporal organisation of RecF and RecO in cells following DNA damage. The evidence points to several key differences in the behaviour of RecF and RecO in cells. We found that the RecF protein spends most of its time near the centre of the nucleoid, often colocalizing with the replisome. This is true both before and after exposure to a UV challenge. The formation of RecF foci is strikingly dependent on DNA replication. In contrast, the RecO protein is usually found closer to the nucleoid/cell periphery, and RecO foci are rarely coincident with replisomes. The formation of RecO foci, however, is also dependent on DNA replication. In all of our experiments, RecF and RecO rarely colocalized with each other. The spatial and temporal properties of RecF and RecO foci imply differences in function. A distinction in function is also brought forward in phenotypic differences observed when cells are challenged with a broad range of DNA damaging agents. The results indicate that, irrespective of phenotypic similarities documented in earlier work, the RecF and RecO proteins have distinct functions in recombinational repair.

The RecOR complex is both necessary and sufficient for facilitating the nucleation of RecA filaments on SSB-coated ssDNA (7,11,35,45). The observation that RecO foci are usually found at some distance from replisomes might be consistent with a role in loading RecA protein at DNA post-replicative gaps and/or double-strand breaks spatially separated from replisomes. Additional support for a role in post-replicative gap repair comes from the observation that DNA replication is required for the UV-induced increase in the number of RecO foci. It is interesting to note that this same region of the cell in which RecO foci form plays host to large bundles of RecA, which are proposed to mediate double-strand break repair (6,70,71). The RecO localizations detected in our work may reflect intermediates formed during RecA loading during the DNA damage response. Unfortunately it is not yet possible to simultaneously image fluorescently tagged RecO and RecA due to technical limitations; RecA is present at 10^{5}–10^{6} molecules per cell (72–75) and thus bleed-through from fluorescently tagged RecA floods the RecO channel. Alternative probes for RecA may alleviate this limitation in the future.

RecF can enhance RecOR-mediated RecA loading under certain (non-physiological) conditions *in vitro* (7,8), a clear role in this process *in vivo* has however not been demonstrated. We found no evidence supporting these observations under physiological conditions in live cells. RecF foci did not colocalize with RecO foci. Instead RecF frequently localized to replisomes, suggesting a potential RecF function at or near the replisome. Indeed, RecF foci are strongly dependent on the presence of active

replication forks. A replisome-associated role for RecF is not an entirely new concept (76). RecF and RecR are required *in vivo* to recover replication after fork stalling, to prevent DNA degradation at stalled forks, and to complete ongoing replication (76). We also detected dimerization of RecF upon UV irradiation. RecF dimerization is required for fork recovery after UV irradiation in *E. coli* (67). The present results more directly tie RecF to a possible role at the replisome and are in line with the proposal that the effects of *recF* deletion on recombination may well stem from problems that arise at the replication fork (76).

6.5 Supplementary data

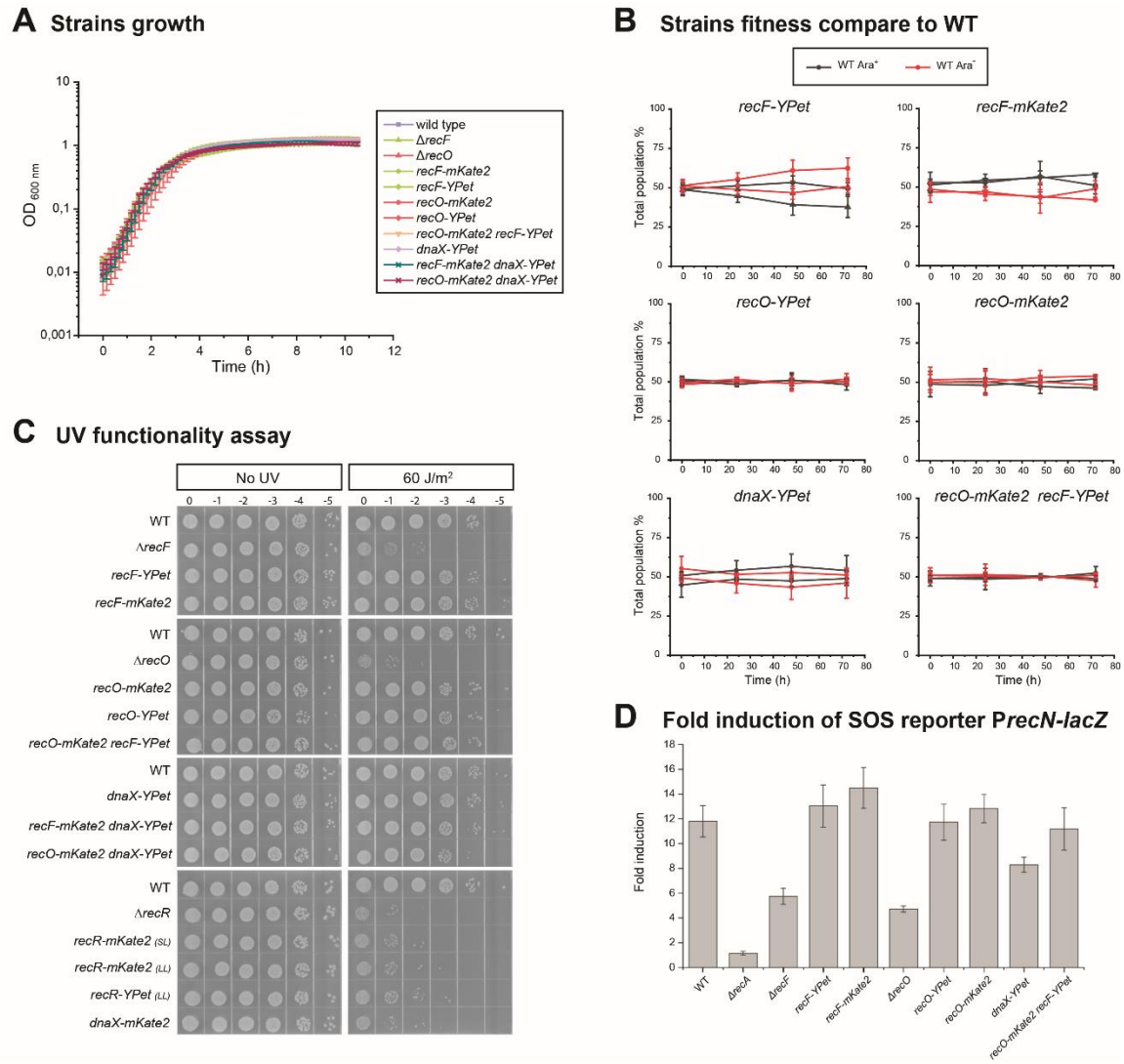

Supplementary Figure S1. Functionality assays for fusion protein constructs. (A) Growth curves of single-colour strains carrying the protein fusions RecF-YPet, RecF-mKate2, RecO-YPet, RecO-mKate2 or DnaX-YPet, as well as two-colour strains expressing RecO-mKate2 RecF-YPet, RecF-mKate2 DnaX-YPet or RecO-mKate2 DnaX-YPet. wild-type, Δ*recF* and Δ*recO* strains were used as controls. Cells were grown in LB at 37°C over a period of 10h. Growth curves are averaged over biological quadruplets while error bars represent the standard deviation. No growth defects were observed. (B) Fitness of single protein fusion constructs (RecF-YPet, RecF-mKate2, RecO-YPet, RecO-mKate2 or DnaX-YPet) and two-colour protein fusion construct (RecO-mKate2 RecF-YPet). For each construction, two growth competition assays were performed. First, the strain Ara+ of each protein fusion construct was compared to wild-type Ara- (EAW214). Second, the strain Ara- of each fusion protein construct was compare to the wild-type Ara+ (MG1655). The assay was started with 50% of each of the two strains in the population mixture. For each of the two competing strains, the percentage cell population was determined at t = 0, 24, 48 and 72h. Black lines represent Ara+ strains, red lines represent Ara- strains. Strains were indicated by symbol shape (wild-type: circle, RecF-YPet: upwards facing triangle, RecF-mKate2: downwards facing triangle, RecO-YPet: cross, RecO-mKate2: square, DnaX-YPet: diamond, RecO-mKate2 RecF-YPet: pentagone). Fusion protein constructs exhibit similar fitness to wild-type cells. (C) UV survival assays. Cells grown in LB to exponential phase were serial diluted and spotted on two LB plates. One plate was exposed to 60 J/m^2 the other was used as a control for unexposed cells. Plates were incubated overnight at 37°C. Images show a representative experiment of independent triplicates. Strains expressing RecF-YPet, RecF-

mKate2, RecO-YPet, RecO-mKate2, DnaX-YPet exhibit similar sensitivity to UV like wild-type. RecR fusions and DnaX-mKate2 fusion constructs were sensitised and showed similar sensitivity to Δ*recR* upon UV exposure. (D) Bar graphs showing the fold induction of the SOS reporter fusion P*recN-lacZ* (pEAW362) in MG1655 (wild-type), EAW20 (Δ*recA*), EAW629 (Δ*recF*), EAW670 (*recF-YPet*), EAW779 (*recF-mKate2*), EAW114 (Δ*recO*), EAW814 (*recO-YPet*), EAW672 (*recO-mKate2*), JJC5945 (*dnaX-YPet*) and EAW676 (*recO-mKate2 recF-YPet*). Cells carrying P*recN-lacZ* were grown in LB_{Amp} at 37°C until reaching exponential phase. Cultures were split; one subculture was treated with 0.25 μg/mL mitomycin C inducing the SOS reponse, the other was used as a control. After 2h of growth at 37°C, expression of P*recN-lacZ* was measured by the β-galactosidase assay. The SOS induction level (fold induction) was determined by dividing the β-galactosidase activity from the MMC treated culture by the β-galactosidase activity from the untreated control. The standard deviations across biological triplicates are indicated with error bars.

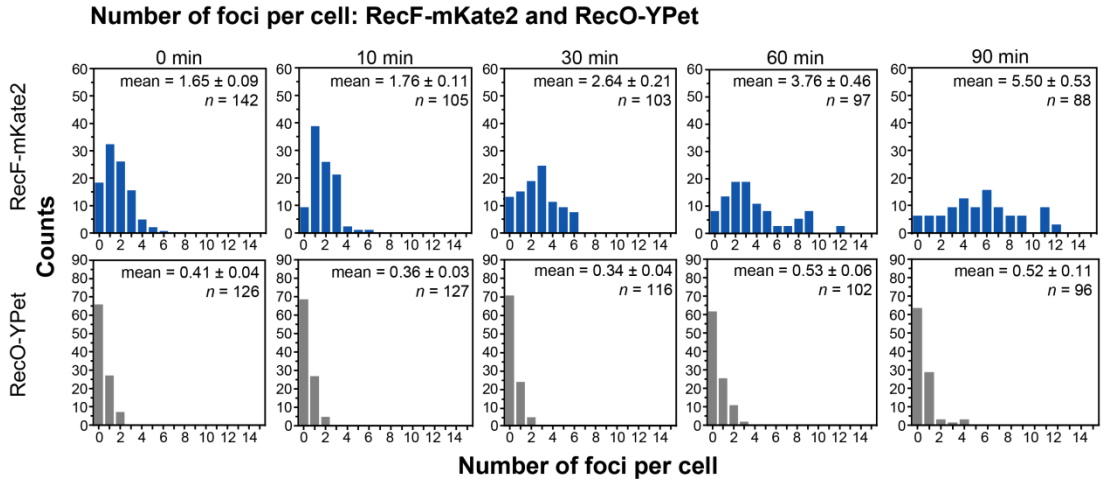

Supplementary Figure S2. Single-molecule imaging of RecF-mKate2 and RecO-YPet fusion constructs. Histograms showing the number of RecF-mKate2 and RecO-YPet foci per cell in response to UV irradiation. Bright-field images were used to determine the position of cells within different fields of view. The number of foci per cell were counted for each cell and plotted in a histogram. We plotted these histograms for the time-point before UV irradiation (0min) and several time-points following UV irradiation (10, 30, 60 and 90min). The mean over the number of foci per cell is depicted in each histogram for each time-point. The number of cells included in each histogram is also indicated as *n*.

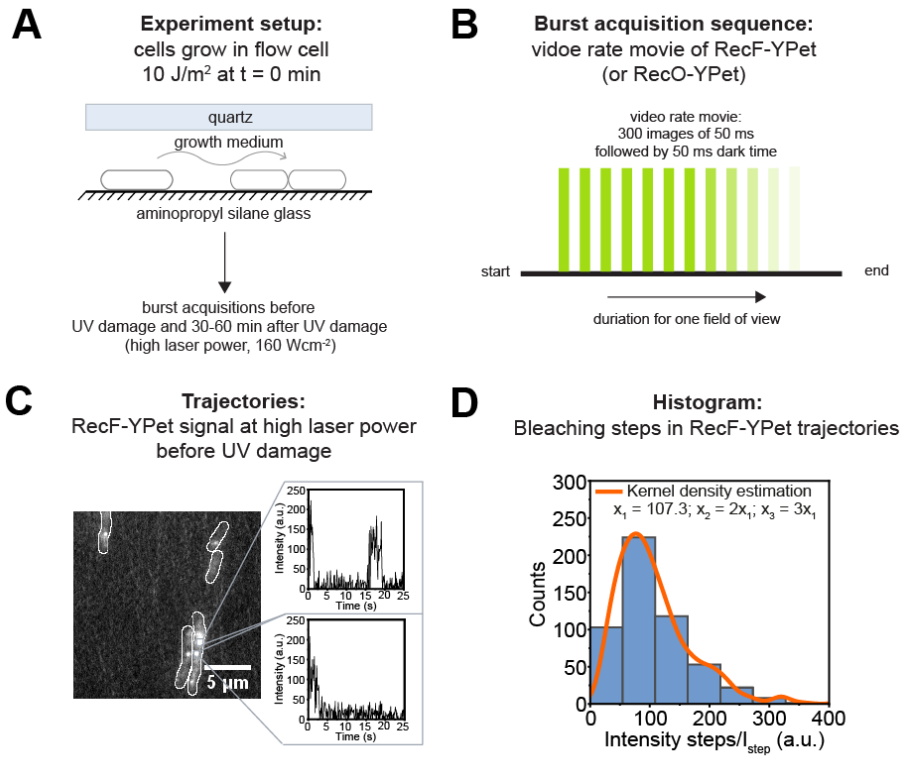

Supplementary Figure S3. Burst acquisitions and analysis at 160 Wcm^{-2}. (A) Experimental setup. Cells are loaded in a flow-cell and immobilised on a positively charged aminopropyl silane glass surface. Cells were images before UV exposure and 30-60min after UV exposure. UV exposure was conducted in flow-cells. (B) Burst acquisition sequence. Movies of RecF-YPet or RecO-YPet were recorded. The movies contain 300 frames at 34ms recorded at continuous excitation. (C) Exemplary average projection of one RecF-YPet movie. The average projection originates from one burst acquisition movie before UV exposure. The projection was made over 10 x 34ms. Two exemplary intensity trajectories are plotted showing RecF-YPet binding to DNA. Scale bar: 5 µm. (D) Histrogram of bleaching step intensities. The histogram was fit with the Kernel density estimation function (orange line) to determine the bleaching step of a single YPet molecule with $x_1 = 107.3$, $x_2 = 2x_1$ and $x_3 = 3x_1$. The intensity of a single YPet molecule was used to determine the number of RecF-YPet and RecO-YPet molecules per focus in **Figure 3C**.

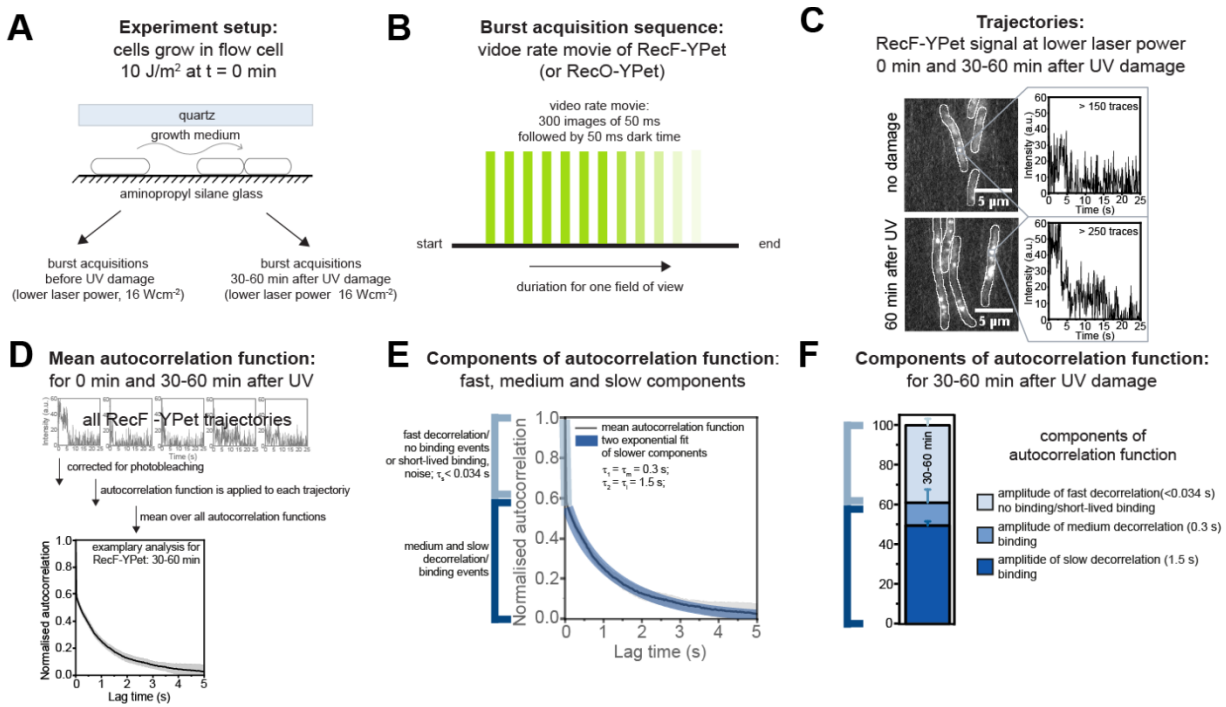

Supplementary Figure S4. Burst acquisitions and analysis at 16 Wcm^{-2}. (A) Experimental setup. Cells are loaded in a flow-cell and immobilised on a positively charged aminopropyl silane glass surface. Cells were images before UV exposure and 30-60min after UV exposure. UV exposure was conducted in flow-cells. (B) Burst acquisition sequence. Movies of RecF-YPet or RecO-YPet were recorded. The movies contain 300 frames at an exposure of 34ms. (C) Exemplary average projections of one RecF-YPet movie before UV exposure and one movie after UV exposure. The average projection was made over 10 x 34ms. One exemplary intensity trajectories is plotted showing RecF-YPet binding to DNA before UV exposure and one trajectory that stems from a burst acquisition post UV exposure. Scale bar: 5 µm. (D) Mean autocorrelation function is obtained from single autocorrelation function. Each autocorrelation function stems from single intensity trajectories of binding events. (E) Determining components of autocorrelation functions. The autocorrelation function is plotted in black. The autocorrelation function has fast components which consist of noise, short-lived and transient binding events (light blue line). Slower components are fitted with a two exponential fit (dark blue line) which consist of medium and slow decorrelation events consistent with binding events. (F) Components of the autocorrelation function are plotted in a bar graph. Slow, medium and fast components are indicated by shades of blue: slow (dark blue), medium (blue), fast (light blue). The error bars for slow and medium components were extracted from the fit error using the two exponential fit. The error bar from the fast components is equivalent to the standard error of the mean from the mean autocorrelation function at lag time 0s.

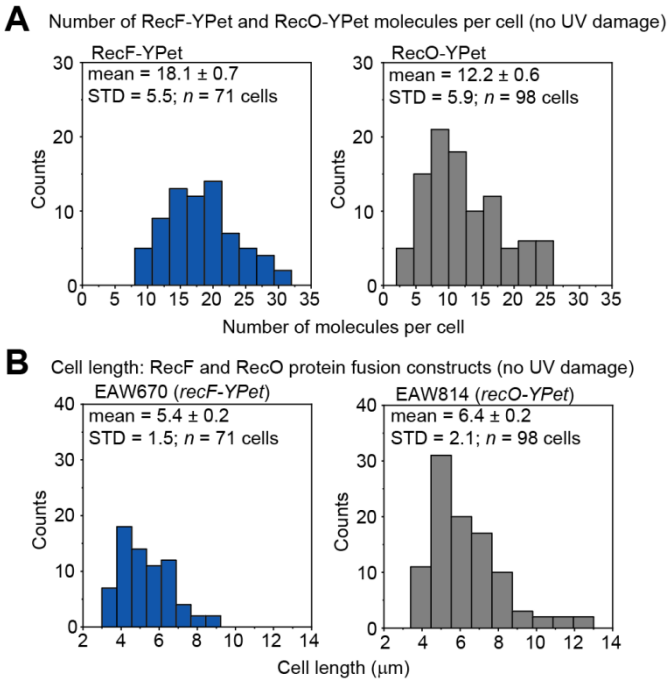

Supplementary Figure S5. RecF-YPet and RecO-YPet molecules per cell. (A) Histogram of the number of RecF-YPet molecules per cell (blue) and RecO-YPet molecules per cell (grey) under normal growth conditions. The mean, standard error of the mean, standard deviation and number of cells (n = 71 for RecF-YPet; n = 98 for RecO-YPet) are depicted in each histogram. (B) Histogram of the cell length for EAW670 (*recF-YPet*, blue) and EAW814 (*recO-YPet*, grey) under normal growth conditions. The mean, standard error of the mean, standard deviation and number of cells (n = 71 for RecF-YPet; n = 98 for RecO-YPet) are depicted in each histogram.

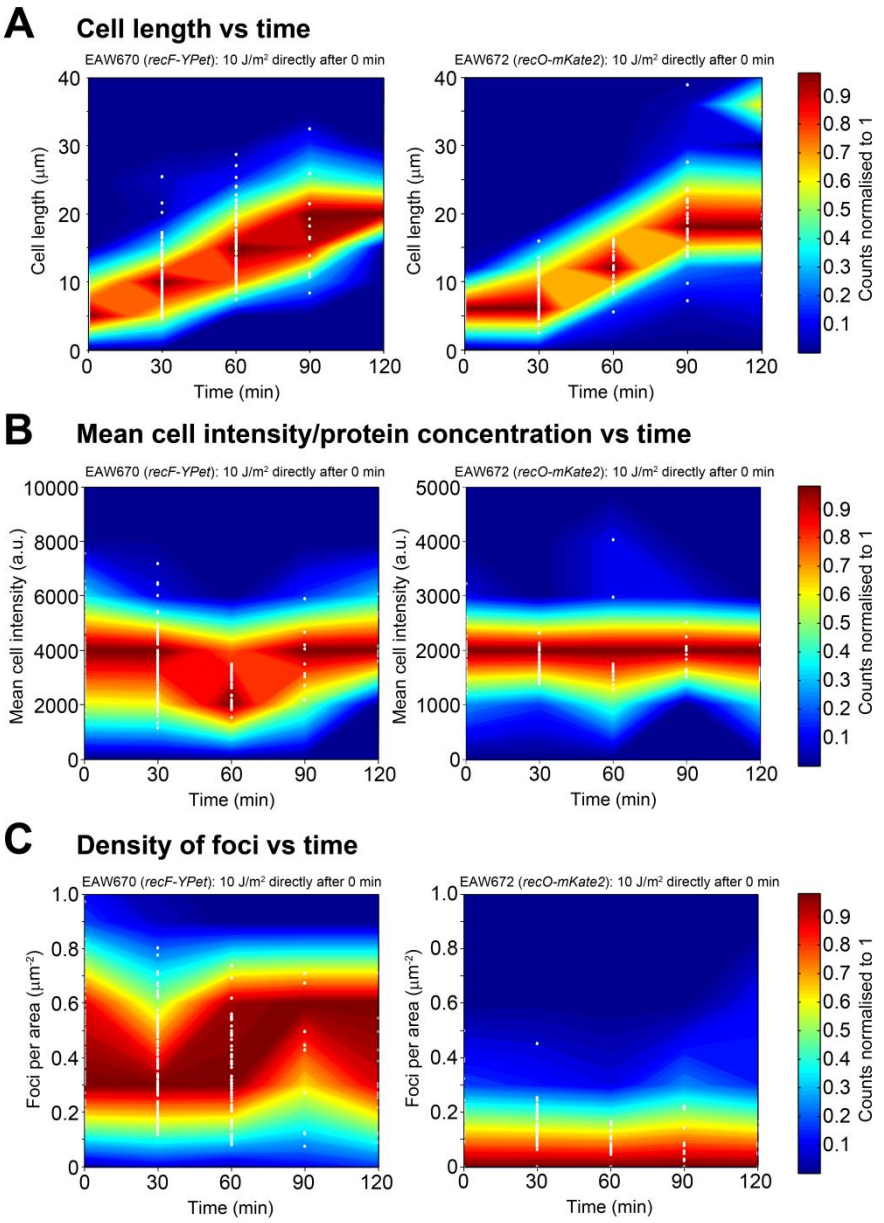

Supplementary Figure S6. Scatter plots of cell-size and fluorescence signal parameters from time-lapse imaging of cells expressing RecF-YPet (EAW670) or RecO-mKate2 (EAW672).White points indicate individual data-points, while blue-to-red contours indicate frequencies of observations. Blue regions indicate regions with few data points and red regions indicate regions with a large number of data points. Frequencies were normalised at each sampled time-point to the maximum at each time-point. (A) Distribution of cell length over time following UV irradiation directly after t = 0min. Fusion constructs grow into filaments at the same filamentation rate when exposed to UV light. (B) Mean pixel intensity within cell boundaries. Changes in the mean cell intensity over time would indicate changes in the concentration of either RecF-YPet or RecO-mKate2. After UV exposure, mean cell intensities for cells expressing RecF-YPet or RecO-mKate2 stays constant indicating that the concentration of each protein stays constant as cells grow into filaments. (C) Density of RecF-YPet and RecO-mKate2 foci per cell, measured as the number of foci per cell area in $\square m^2$. The foci density for RecF-YPet and RecO-mKate2 stays relatively constant in response to UV damage. The density of RecF-YPet foci has a slight dip at 30min after UV irradiation exactly when nucleoids compact and colocalisation with replisomes is increased. The foci density of RecF-YPet foci is overall higher than the density of RecO-mKate2 foci since cells contain more RecF-YPet foci per cell then RecO-mKate2 foci (**Figure 2D**).

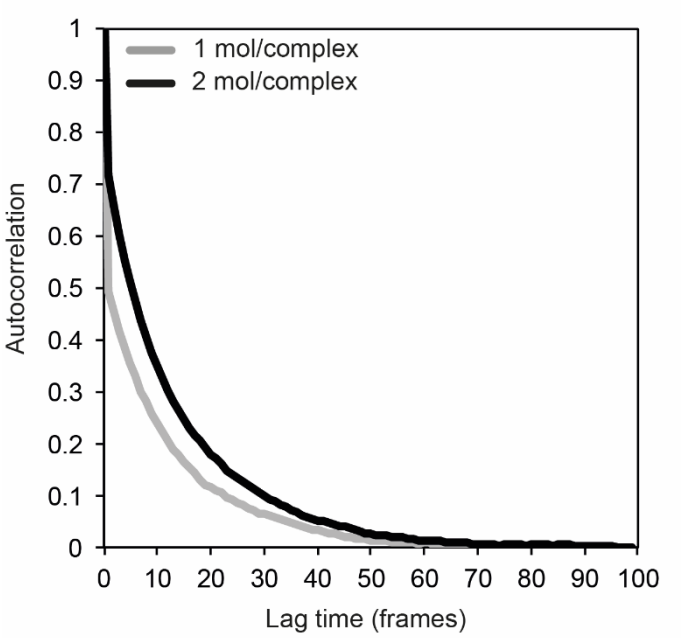

Supplementary Figure S7. Autocorrelation analysis of simulated rapid-acquisition data. To determine what effect the dimerization of a protein would have on the autocorrelation analysis of rapid-acquisition movies, simulated data were generated. Intensity versus time trajectories were generated for two types of complexes: one containing one molecule per complex (representing RecF-YPet), and one containing two molecules per complex (representing $[RecF\text{-}YPet]_2$). Custom Matlab code (**Appendix PDF**) was used to simulate a scenario in which each complex binds to and dissociates from DNA, while the pool of available fluorescent proteins photobleaches. Signal is only generated when a complex is bound, the complex contains a molecule, and the molecule has not yet photobleached, analogous to focus formation in the experimental data. User-defined parameters are described within the code. For the displayed simulation the parameters were set as follows: *frames* = 100; *signal* = 1; *bkg* = 3; *max_sites_mol1* = 1; *max_sites_mol2* = 2; *complexes* = 1000; *mol_per_complex* = 10; *fracunbndt0* = 0; *Kon_complex* = 0.00001; *Koff_complex* = 0.03; *StoN_mol1* = 3; *Tbleach_mol1* = 50; *Kon_mol1 = 0.00001*; *Koff_mol1 = 0.00001*; *StoN_mol2* = 3; *Tbleach_mol2* = 50; *Kon_mol2* = 0.00001; *Koff_mol2* = 0.00001. Autocorrelation functions were calculated as for the experimental data (**Materials and Methods**). Comparing the autocorrelation function for the simulated data (above) against that for the experimental data (**Figure 3D**) it is clear that dimerization of RecF (**Figure 3C**) would be sufficient to explain the increase in autocorrelation observed after UV-irradiation of cells.

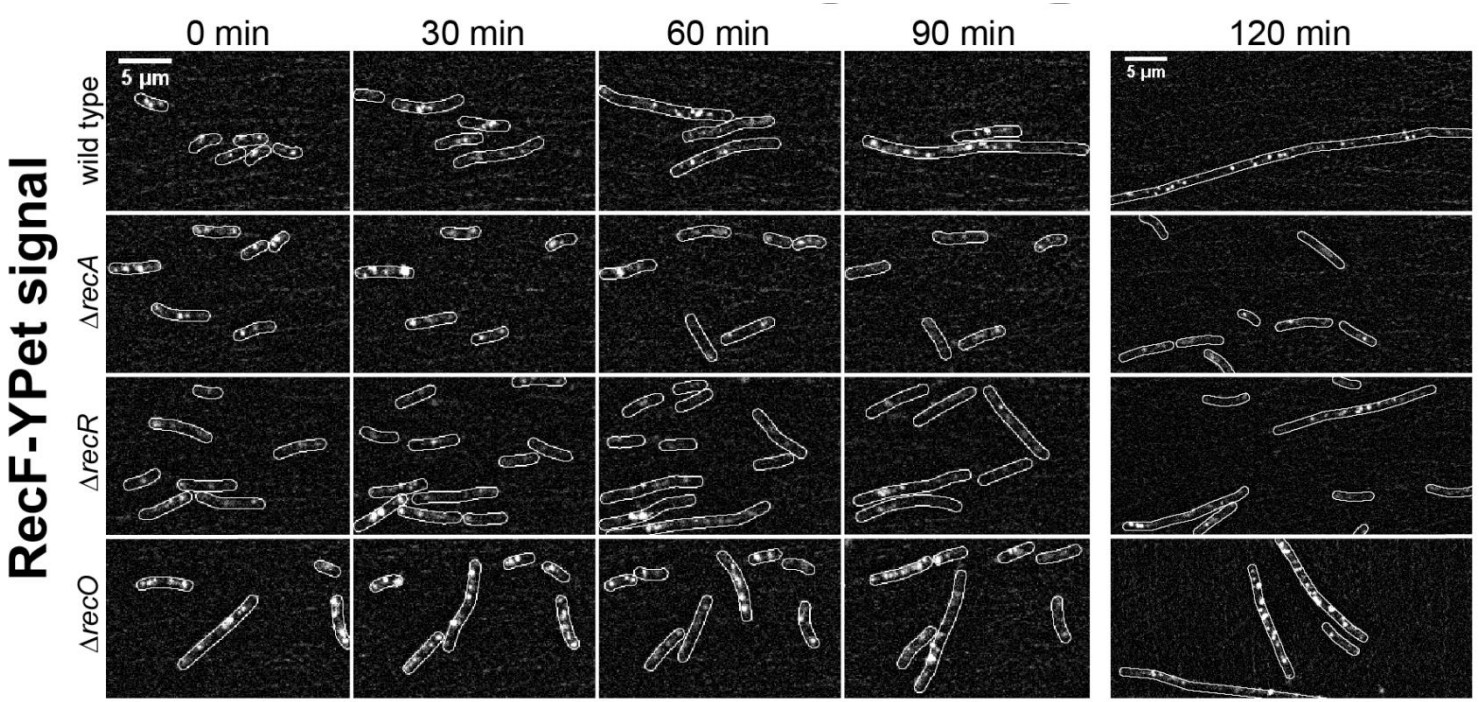

Supplementary Figure S8. Time-lapse images of RecF-YPet in wild type, Δ*recA*, Δ*recR* and Δ*recO*. Time-lapse images are shown at 0, 30, 60, 90 and 120min after UV irradiation. Cell outlines indicate the boundaries of single cells. In wild type cells, the number of RecF-YPet foci increases as cells filament. In a Δ*recA* background, cells do not grow into filaments and lose their RecF-YPet foci in response to UV damage. In a Δ*recR* background, cells either do not grow into filaments or filament slower than wild type cells. Cells that do not filament lose their RecF-YPet foci, whereas, cells that slowly filament have some foci. In a Δ*recO* background, cells either do not grow into filaments or filament slower than wild type cells. All Δ*recO* cells contain RecF-YPet foci. Scale bar: 5 µm.

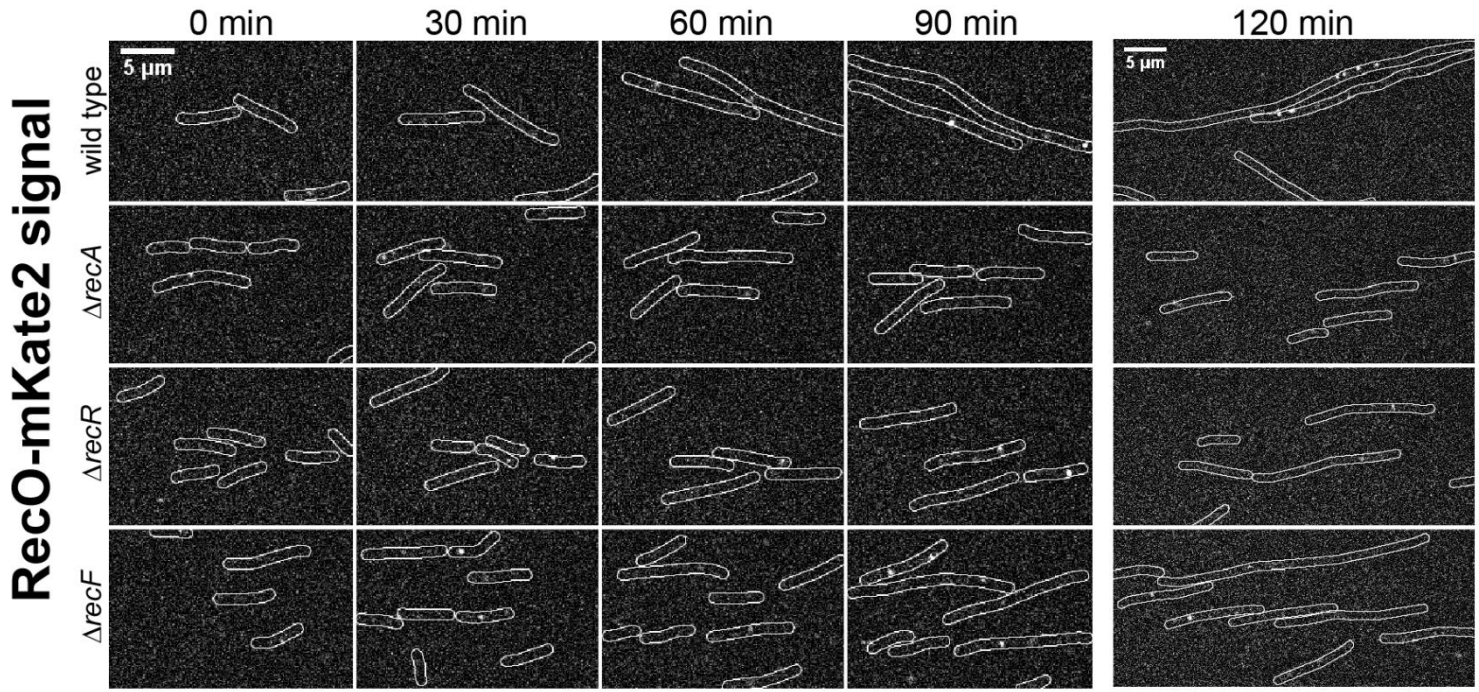

Supplementary Figure S9. Time-lapse images of RecO-mKate2 in wild type, Δ*recA*, Δ*recR* and Δ*recF*. Time-lapse images are shown at 0, 30, 60, 90 and 120min after UV irradiation. Cell outlines indicate the boundaries of single cells. In wild type cells, the number of RecO-mKate2 foci increases as cells filament. In a Δ*recA* background, cells do not grow into filaments and lose their RecO-mKate2 foci in response to UV damage. In a Δ*recR* background, cells either do not grow into filaments or filament slower than wild type cells. All Δ*recR* cells contain RecO-mKate2 foci. In a Δ*recF* background, cells either do not grow into filaments or filament slower than wild type cells. All Δ*recF* cells contain RecO-mKate2 foci. Scale bar: 5 µm.

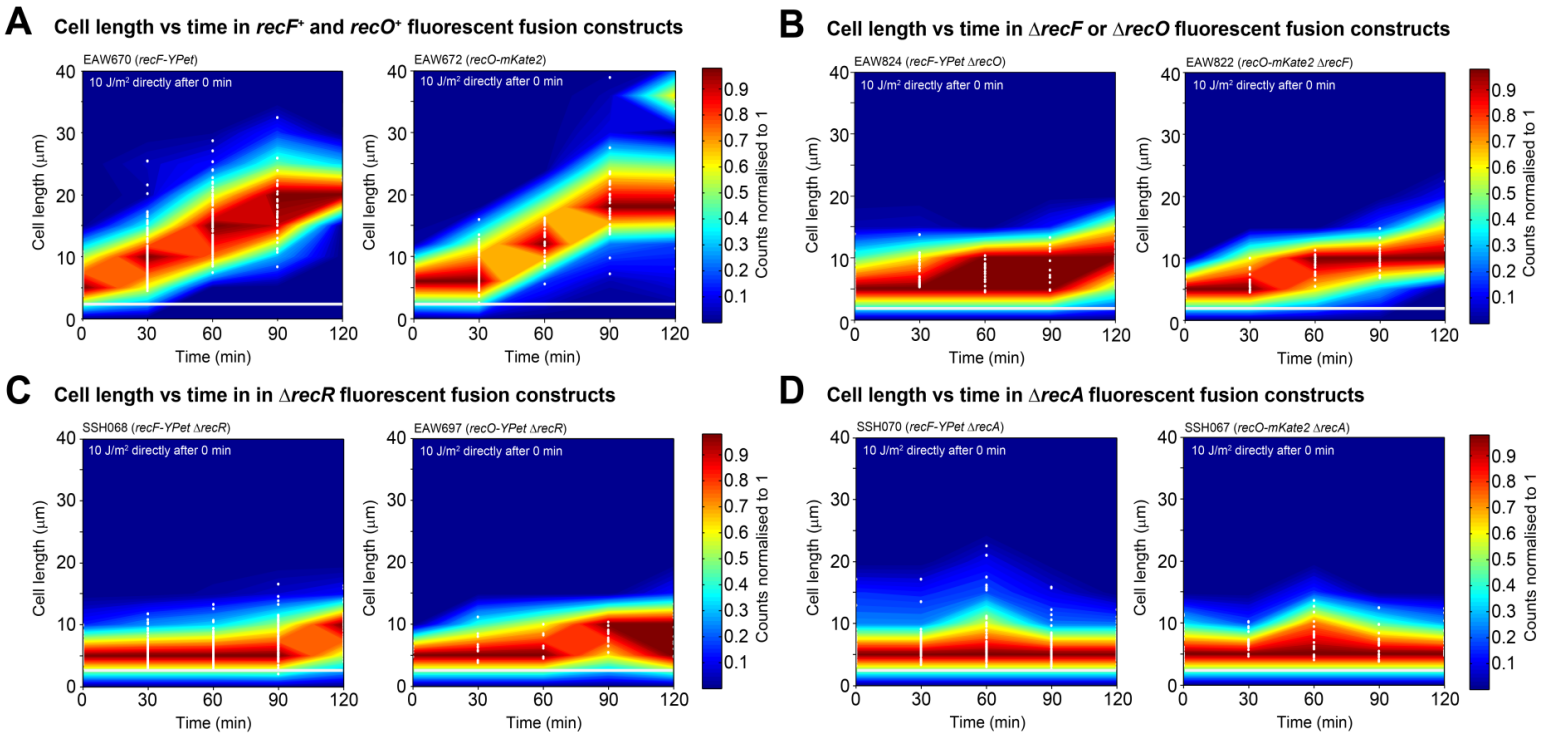

Supplementary Figure S10. Scatter plots of cell length over time from time-lapse imaging of cells expressing RecF-YPet (EAW670) or RecO-mKate2 (EAW672) in comparison to fusion constructs lacking *recR* (SSH068, EAW697), *recA* (SSH070, SSH067) and either *recO* (EAW824) or *recF* (EAW822). Cells were exposed to a single UV dose directly after t = 0min. All contour plots have white points indicating individual data-points, while blue-to-red contours illustrate frequencies of observations. Blue regions indicate regions with few data points and red regions indicate regions with a large number of data points. Frequencies were normalised at each sampled time-point to the maximum at each time-point. (A) Fusion constructs that do have no deletion background grow into filaments at the same filamentation rate when exposed to UV light. Same figure as **Supplementary Figure S6**. (B) Cells expressing RecF-YPet while lacking *recO* have two populations of cells post UV exposure, one does not grow while the other slowly filaments. In contrast, cells expressing RecO-mKate2 mostly grow into filaments at a slower rate than wild type cells. (C) Cells lacking *recR* and expressing either RecF-YPet or RecO-mKate2 have two populations of cells post UV exposure, one does not grow while the other slowly filaments. This behaviour is similar to cells lacking *recO* (**Supplementary Figure S10B**). (D) Cells lacking *recA* and expressing either RecF-YPet or RecO-mKate2 either divide once and then do not grow or do not grow at all post UV treatment.

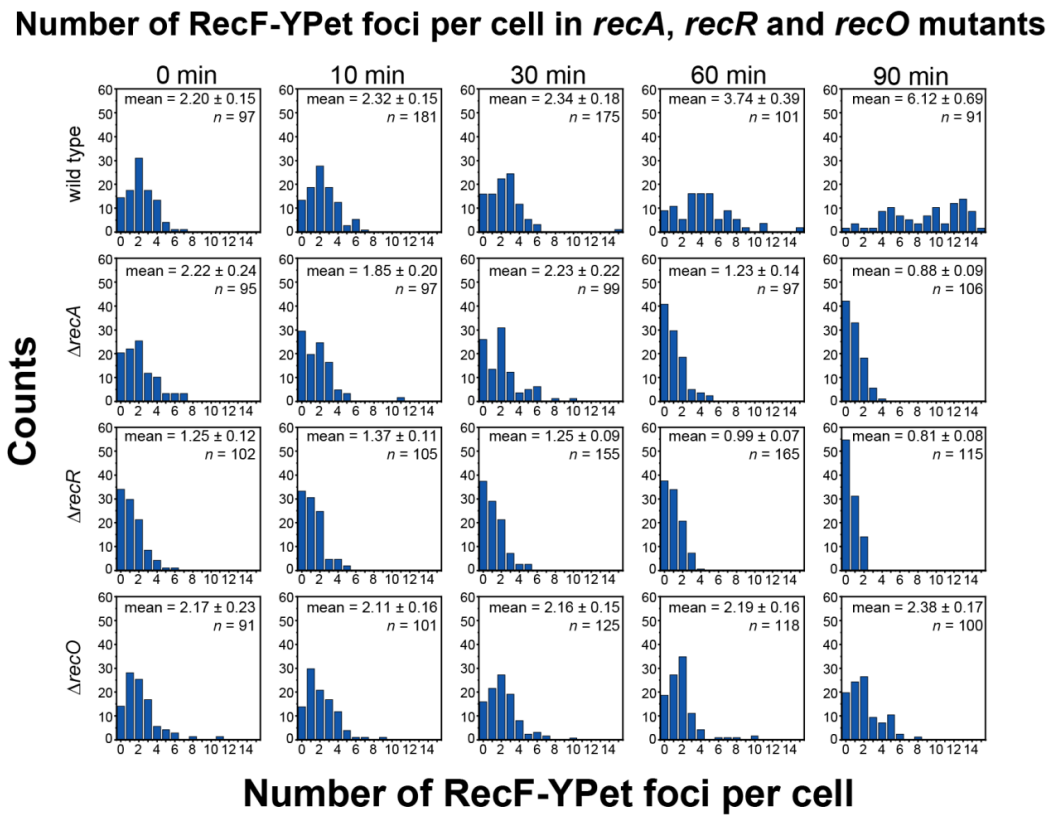

Supplementary Figure S11. Histograms of the number of RecF-YPet foci in wild type cells and cells lacking *recA*, *recR* or *recO*. Bright-field images were used to determine the position of cells within different fields of view. The number of foci per cell were counted for each cell and plotted in a histogram. We plotted these histograms for the time-point before UV irradiation (0min) and several time-points following UV irradiation (10, 30, 60 and 90min). The mean over the number of foci per cell is depicted in each histogram for each time-point. The number of cells included in each histogram is also indicated as *n*. Wild-type cells contain more foci per cell as cells grow into filaments. Cells lacking *recA* lose their RecF-YPet foci post UV exposure. Cells lacking *recR* contain less RecF-YPet foci under normal growth conditions (see **Supplementary Figure S8** for time-lapse images). Post UV, cells either lose their RecF foci or have some RecF foci. Cells lacking *recO* however slightly increase the number of RecF foci until 90min after UV exposure.

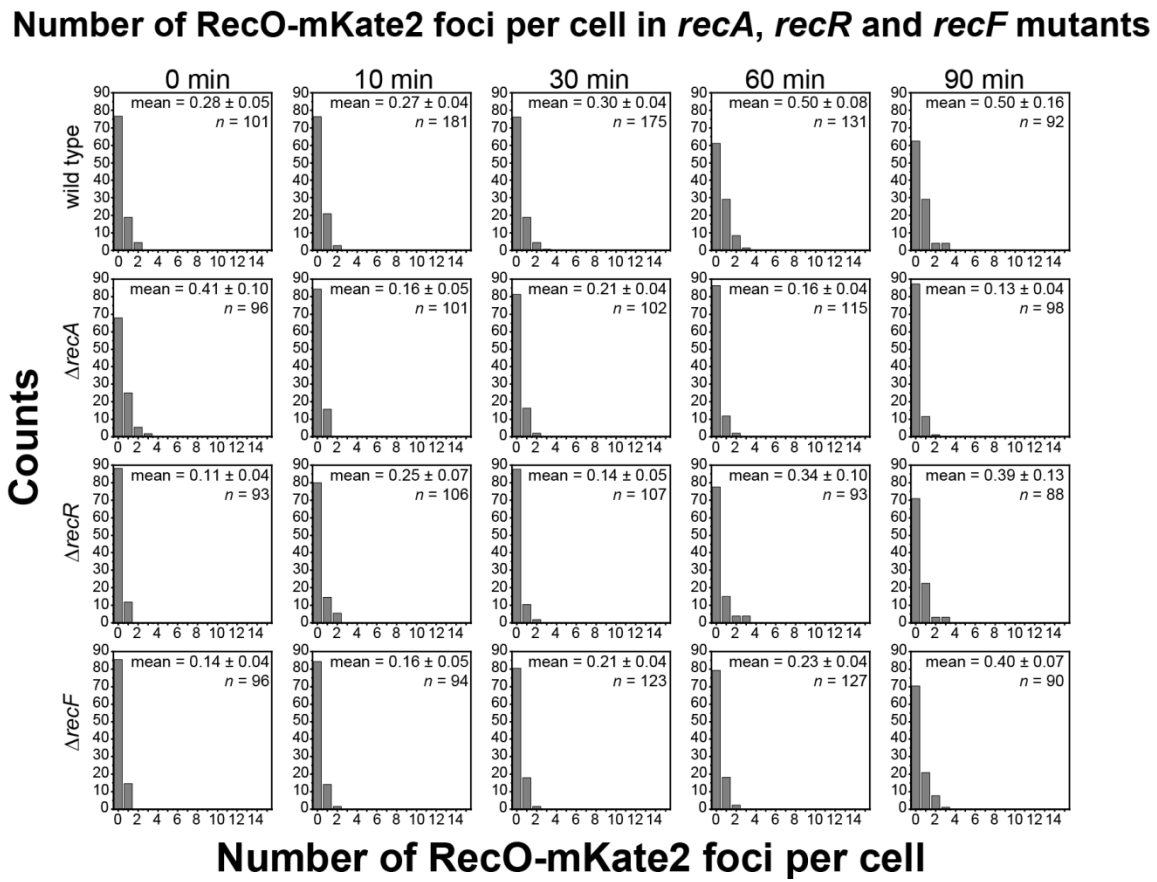

Supplementary Figure S12. Histograms of the number of RecO-mkate foci in wild type cells and cells lacking *recA*, *recR* or *recF*. Bright-field images were used to determine the position of cells within different fields of view. The number of foci per cell were counted for each cell and plotted in a histogram. We plotted these histograms for the time-point before UV irradiation (0min) and several time-points following UV irradiation (10, 30, 60 and 90min). The mean over the number of foci per cell is depicted in each histogram for each time-point. The number of cells included in each histogram is also indicated as *n*. Corresponding time-lapse images are shown in **Supplementary Figure S9**. Upon UV exposure, more wild type cells contain RecO-mKate2 foci while some still have zero foci. Most cells lacking *recA* contain no foci after UV exposure. Cells lacking *recR* or *recF* however have more RecO foci after a single UV dose.

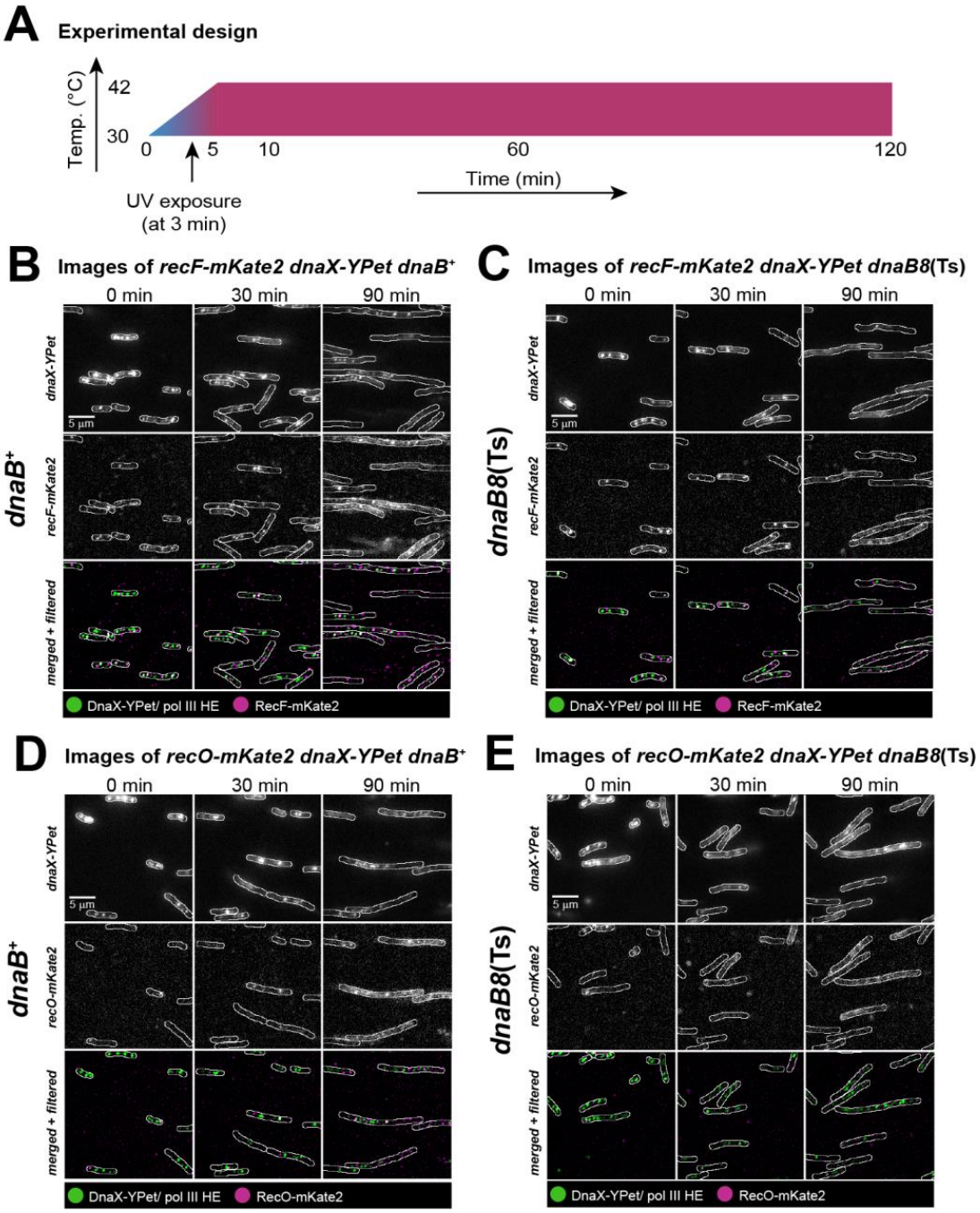

Supplementary Figure S13. Experimental design and images (unfiltered and filtered) of CJH0015 (*recF-mKate2 dnaX-YPet dnaB*$^+$), EAW762 (*recO-mKate2 dnaX-YPet dnaB*$^+$), SSH114 (*recF-mKate2 dnaX-YPet dnaB8*(Ts)) and SSH115 (*recO-mKate2 dnaX-YPet dnaB8*(Ts)) at 0, 30 and 90min. (A) Experimental design. First image is taken at 30˚C (0min) when no UV image is yet induced. Then, the temperature is ramped up to 42˚C. UV damage is induced at 3-4min. 42˚C are reached at 5min and hold until the end of the experiment, at 120min. (B) Images of *recF-mKate2 dnaX-YPet dnaB*$^+$. Upper panel: DnaX-YPet signal, raw images. Middle panel: RecF-mKate2 signal, raw images. Lower panel: Merged images of RecF-mKate2 (magenta signal) and DnaX-YPet (green signal) are shown before UV irradiation, at 30˚C, and after UV irradiation, at 42˚C (30min and 90min). Scale bar: 5 µm. (C) Images of *recF-mKate2 dnaX-YPet dnaB8*(Ts). Upper panel: DnaX-YPet signal, raw images. Middle panel: RecF-mKate2 signal, raw images. Lower panel: Merged images of RecF-mKate2 (magenta signal) and DnaX-YPet (green signal) are shown before UV irradiation, at 30˚C, and after UV irradiation, at 42˚C (30min and 90min). Scale bar: 5 µm. (D) Images of *recO-mKate2 dnaX-YPet dnaB*$^+$. Upper panel: DnaX-YPet

signal, raw images. Middle panel: RecF-mKate2 signal, raw images. Lower panel: Merged images of RecF-mKate2 (magenta signal) and DnaX-YPet (green signal) are shown before UV irradiation, at 30˚C, and after UV irradiation, at 42˚C (30min and 90min). Scale bar: 5 μm. (E) Images of *recO-mKate2 dnaX-YPet dnaB8*(Ts). Upper panel: DnaX-YPet signal, raw images. Middle panel: RecF-mKate2 signal, raw images. Lower panel: Merged images of RecF-mKate2 (magenta signal) and DnaX-YPet (green signal) are shown before UV irradiation, at 30˚C, and after UV irradiation, at 42˚C (30min and 90min). Scale bar: 5 μm.

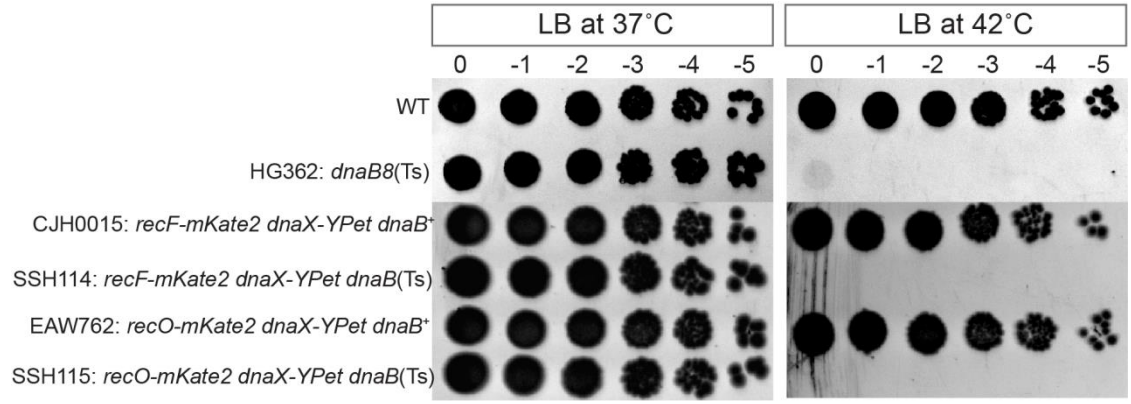

Supplementary Figure S14. The non-permissive temperature of cells carrying the dnaB8(Ts) allele is 42°C. Spot plate dilution assays of MG1655 (wild-type), HG362 (*dnaB8*[Ts]), CJH0015 (*recF-mKate2 dnaX-YPet dnaB*$^{+}$), SSH114 (*recF-mKate2 dnaX-YPet dnaB8*[Ts]), EAW762 (*recO-mKate2 dnaX-YPet dnaB*$^{+}$) and SSH115 (*recO-mKate2 dnaX-YPet dnaB8*[Ts]). Cells grown to exponential phase (OD_{600} ~0.2) were serial diluted to the dilution 10^{-5}. Serial dilutions were spotted on LB agar. Plates were incubated overnight either at 37°C or 42°C. Images show a representative experiment of independent duplicates.

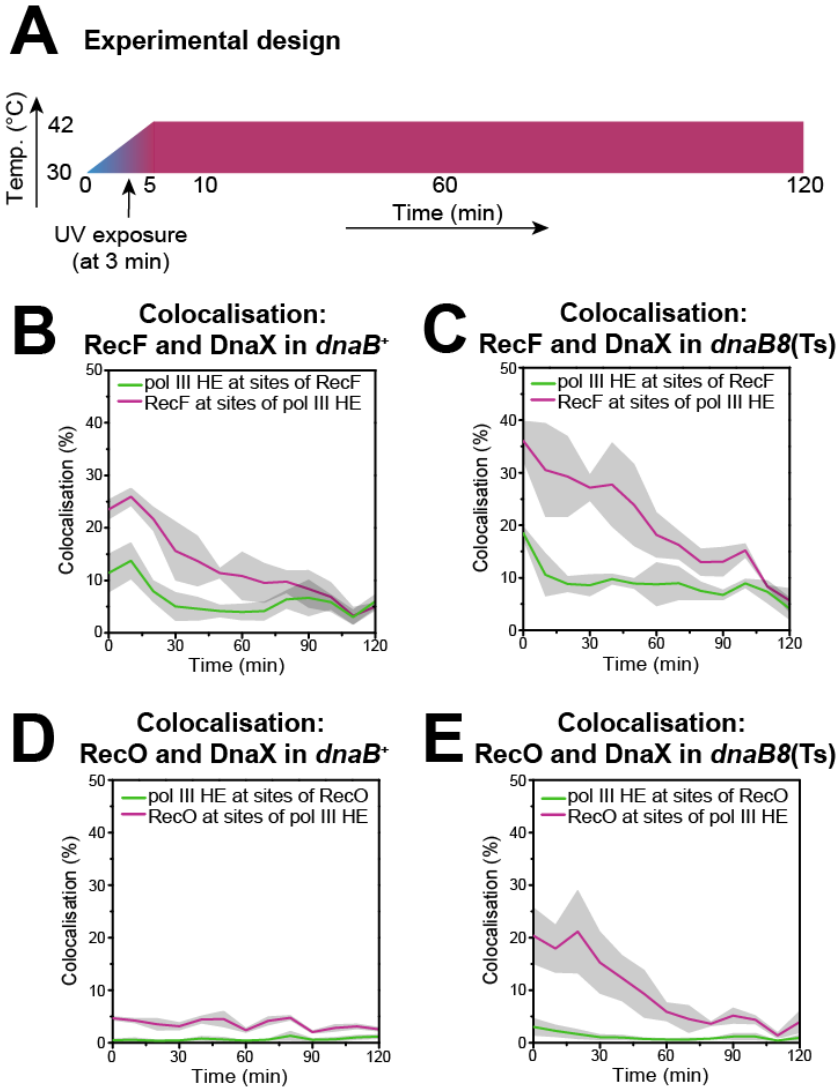

Supplementary Figure S15. Experimental design and colocalisation measurements of CJH0015 (*recF-mKate2 dnaX-YPet dnaB*$^{+}$), EAW762 (*recO-mKate2 dnaX-YPet dnaB*$^{+}$), SSH114 (*recF-mKate2 dnaX-YPet dnaB8*(Ts)) and SSH115 (*recO-mKate2 dnaX-YPet dnaB8*(Ts)) at 0, 30 and 90min. Colocalisation was measured over >300 cells. (A) Experimental design. First image is taken at 30˚C (0min) when no UV image is yet induced. Then, the temperature is ramped up to 42˚C. UV damage is induced at 3-4min. 42˚C are reached at 5min and hold until the end of the experiment, at 120min. (B) Colocalisation measurement of RecF-mKate2 with DnaX-YPet in *dnaB*$^{+}$. The percentage of RecF-mKate2 foci that contain a DnaX-YPet focus is plotted as a magenta line plot over 120min at intervals of 10min. Similarly, the colocalisation of DnaX-YPet with RecF-mKate2 is plotted as a green line plot. (C) Colocalisation measurement of RecF-mKate2 with DnaX-YPet in *dnaB8*(Ts). The percentage of RecF-mKate2 foci that contain a DnaX-YPet focus is plotted as a magenta line plot over 120min at intervals of 10min. Similarly, the colocalisation of DnaX-YPet with RecF-mKate2 is plotted as a green line plot. (D) Colocalisation measurement of RecO-mKate2 with DnaX-YPet in *dnaB*$^{+}$. The percentage of RecO-mKate2 foci that contain a DnaX-YPet focus is plotted as a magenta line plot over 120min at intervals of 10min. Similarly, the colocalisation of DnaX-YPet with RecO-mKate2 is plotted as a green line plot. (E) Colocalisation measurement of RecO-mKate2 with DnaX-YPet in *dnaB8*(Ts). The percentage of RecO-mKate2 foci that contain a DnaX-YPet focus is plotted as a magenta line plot over 120min at intervals of 10min. Similarly, the colocalisation of DnaX-YPet with RecO-mKate2 is plotted as a green line plot.

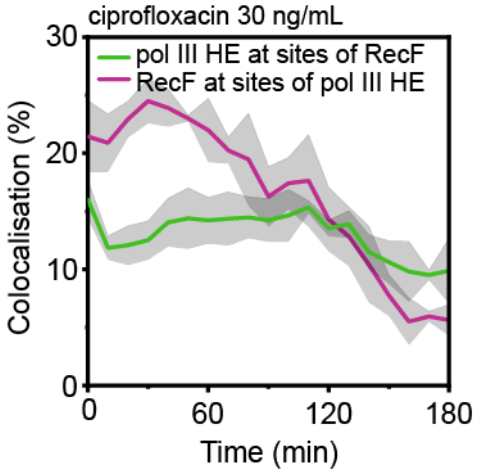

Supplementary Figure S16. Colocalisation measurements of CJH0015 (*recF-mKate2 dnaX-YPet dnaB*$^{+}$) following ciprofloxacin treatment (30 ng/mL). Colocalisation was measured over >300 cells. The percentage of RecF-mKate2 foci that contain a DnaX-YPet focus is plotted as a magenta line plot over 180min at intervals of 10min. Similarly, the colocalisation of DnaX-YPet with RecF-mKate2 is plotted as a green line plot.

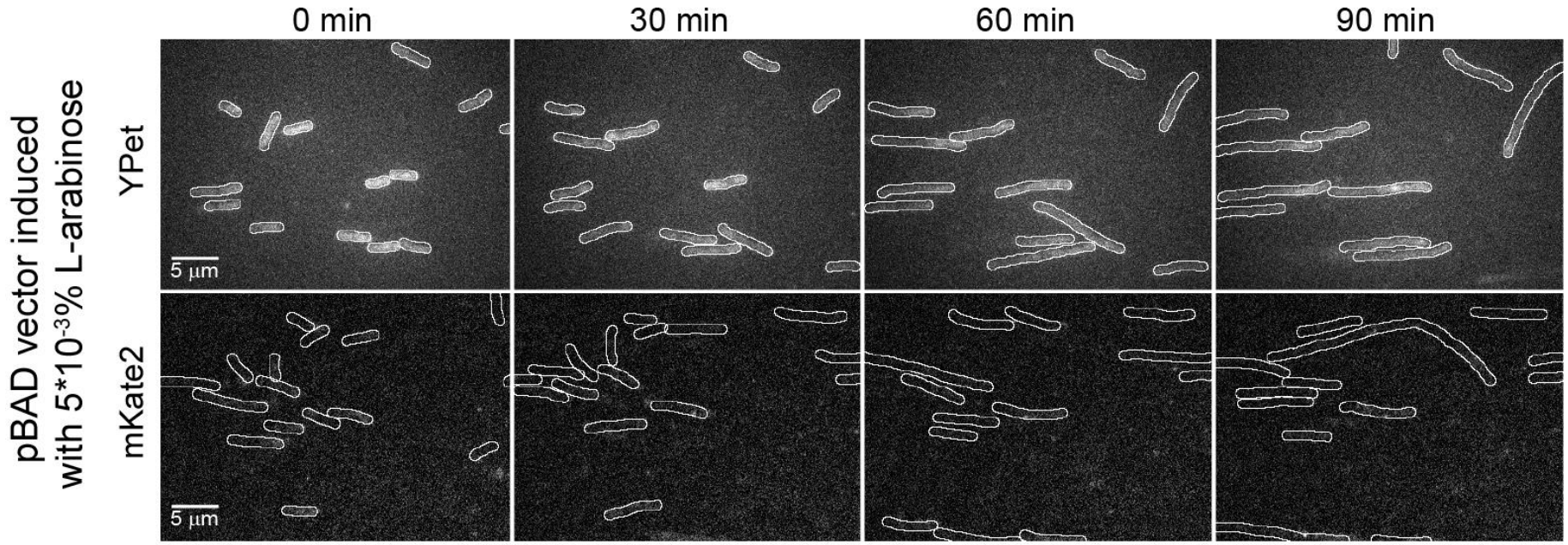

Supplementary Figure S17. Time-lapse data of cells carrying a pBAD plasmid to express either YPet or mKate2. Expression is induced at low levels with $5 \cdot 10^{-3}$% L-arabinose. Cells were exposed to a UV dose of 10 $J \cdot m^{-2}$ directly after t = 0min. Images are shown at 0, 30, 60 and 90min. Upper panel: signal of cells expressing YPet. The fluorescent protein YPet does not form foci after UV exposure. Bottom panel: signal of cells expressing mKate2. The fluorescent protein mKate2 does show some diffusive signal after UV exposure, however, no foci. Scale bar: 5 µm.

Supplementary Materials PDF contains the MATLAB codes used for 'Autocorrelation analysis and simulation of intensity versus time trajectories' (see **Material and methods**).

6.6 References

1. Fuchs R.P. Tolerance of lesions in *E. coli*: Chronological competition between translesion synthesis and damage avoidance. *DNA Repair*. 2016; 44:51–8.

2. Laranjo L.T., Gross S.J., Zeiger D.M., Lovett S.T. SSB recruitment of Exonuclease I aborts template-switching in *Escherichia coli*. *DNA Repair*. 2017; 57:12–6.

3. Lovett S.T. Template-switching during replication fork repair in bacteria. *DNA Repair*. 2017; 56:118–28.

4. Cox M.M., Goodman M.F., Kreuzer K.N., Sherratt D.J., Sandler S.J., Marians K.J. The importance of repairing stalled replication forks. *Nature*. 2000; 404:37–41.

5. Clark A.J., Sandler S.J. Homologous genetic recombination: The pieces begin to fall into place. *Crit. Rev. Microbiol*. 1994; 20:125–142.

6. Lesterlin C., Ball G., Schermelleh L., Sherratt D.J. RecA bundles mediate homology pairing between distant sisters during DNA break repair. *Nature*. 2014; 506:249–253.

7. Morimatsu K., Kowalczykowski S.C. RecFOR proteins load RecA protein onto gapped DNA to accelerate DNA strand exchange: A universal step of recombinational repair. *Mol. Cell*. 2003; 11:1337–1347.

8. Sakai A., Cox M.M. RecFOR and RecOR as distinct RecA loading pathways. *J. Bio.* 2009; 284:3264–3272.

9. Kowalczykowski S.C., Krupp R.A. Effects of *Escherichia coli* SSB protein on the single-stranded DNA-dependent ATPase activity of *Escherichia coli* RecA protein: Evidence that SSB protein facilitates the binding of RecA protein to regions of secondary structure within single-stranded DNA. *J. Mol. Biol*. 1987; 193:97–113.

10. Umezu K., Chi N.W., Kolodner R.D. Biochemical interaction of the *Escherichia coli* RecF, RecO, and RecR proteins with RecA protein and single-stranded DNA binding protein. *Proc. Natl. Acad. Sci. USA*. 1993; 90:3875–3879.

11. Umezu K., Kolodner R.D. Protein interactions in genetic recombination in *Escherichia coli*. *J. Biol. Chem*. 1994; 269:30005–30013.

12. Cox M.M. Regulation of bacterial RecA protein function. *Crit. Rev. Biochem. Mol. Biol.* 2007; 42:41–63.

13. Smith K.C., Wang T.C. RecA-dependent DNA repair processes. *Bioessays*. 1989; 10:12–6.

14. Wang T.C., Chang H.Y., Hung J.L. Cosuppression of *recF*, *recR* and *recO* mutations by mutant *recA* alleles in *Escherichia coli* cells. *Mutagen. Res*. 1993; 294:157–166.

15. Lavery P.E., Kowalczykowski S.C. Biochemical basis of the temperature-inducible constitutive protease activity of the RecA441 protein of *Escherichia coli*. *J. Mol. Biol*. 1988; 203:861–874.

16. Madiraju M.V., Lavery P.E., Kowalczykowski S.C., Clark A.J. Enzymatic properties of the RecA803 protein, a partial suppressor of *recF* mutations. *Biochemistry*. 1992; 31:10529–10535.

17. Sawitzke J.A., Stahl F.W. Phage λ has an analog of *Escherichia coli recO, recR* and *recF* genes. *Genet. Soc. Am*. 1992; 130:7–16.

18. Sawitzke J.A., Stahl F.W. The Phage λ *orf* gene encodes a *trans*-acting factor that suppresses *Escherichia coli recO*, *recR*, and *recF* mutations for recombination of λ but not of *E . coli*. *J. Bacteriol*. 1994; 176:6730–6737.

19. Madiraju M.V.V.S., Templin A., Clark A.J. Properties of a mutant *recA*-encoded protein reveal a possible role for *Escherichia coli recF*-encoded protein in genetic recombination. *Proc. Natl. Acad. Sci. USA*. 1988; 85:6592–6596.

20. Whitby M.C., Lloyd R.G. Altered SOS induction associated with mutations in *recF*, *recO* and *recR*. *Mol. Genet. Genomics*. 1995; 246:174–179.

21. Moreau P.L. Overproduction of single-stranded-DNA-binding protein specifically inhibits recombination of UV-irradiated bacteriophage DNA in *Escherichia coli*. *J. Bacteriol*. 1988; 170:2493–2500.

22. Lloyd R.G., Porton M.C., Buckman C. Effect of *recF*, *recJ*, *recN*, *recO* and *ruv* mutations on ultraviolet survival and genetic recombination in a *recD* strain of *Escherichia coli* K12. *Mol. Genet. Genomics*. 1988; 212:317–324.

23. Lloyd R.G., Buckman C. Genetic analysis of the *recG* locus of *Escherichia coli* K-12 and of its role in recombination and DNA repair. *J. Bacteriol*. 1991; 173:1004–1011.

24. Madiraju M.V.V.S., Clark A.J. Effect of RecF protein on reactions catalyzed by RecA protein. *Nucleic Acids Res*. 1991; 19:6295–6300.

25. Rocha E.P.C., Cornet E., Michel B. Comparative and evolutionary analysis of the bacterial homologous recombination systems. *PLoS Comput. Biol*. 2005; 1:e15.

26. Marsin S, Mathieu A, Kortulewski T, Guerois G, Radicella JP. Unveiling novel RecO distant orthologues involved in homologous recombination. *PLoS Genet*. 2008; 4:e1000146.

27. Grompone G., Ehrlich D., Michel B. Cells defective for replication restart undergo replication fork reversal. *EMBO Rep*. 2004; 5:607–612.

28. Sandler S.J., Samra H.S., Clark A.J. Differential suppression of *priA2*::kan phenotypes in *Escherichia coli* K-12 by mutations in *priA*, *lexA*, and *dnaC*. *Genetics*. 1996; 143:5–13.

29. Sandler S.J., Clark A.J. Use of high and low level overexpression plasmids to test mutant alleles of the *recF* gene of *Escherichia coli* K-12 for partial activity. *Genet. Soc. Am.* 1993; 654:643–654.

30. Sandler S.J. Studies on the mechanism of reduction of UV-inducible *sulAp* expression by *recF* overexpression in *Escherichia coli* K-12. *Mol. Genet. Genomics*. 1994; 245:741–749.

31. Sandler S.J., Clark A.J. RecOR suppression of *recF* mutant phenotypes in *Escherichia coli* K-12. *J. Bacteriol*. 1994; 176:3661–3672.

32. Sangurdekar D.P., Hamann B.L., Smirnov D., Srienc F., Hanawalt P.C., Khodursky A.B. Thymineless death is associated with loss of essential genetic information from the replication origin. *Mol. Microbiol*. 2010; 75:1455–1467.

33. Kidane D., Sanchez H., Alonso J.C., Graumann P.L. Visualization of DNA double-strand break repair in live bacteria reveals dynamic recruitment of *Bacillus subtilis* RecF, RecO and RecN proteins to distinct sites on the nucleoids. *Mol. Microbiol*. 2004; 52:1627–1639.

34. Lenhart J.S., Brandes E.R., Schroeder J.W., Sorenson R.J., Showalter H.D., Simmons L.A. RecO and RecR are necessary for RecA loading in response to DNA damage and replication fork stress. *J. Bacteriol*. 2014; 196:2851–2860.

35. Shan Q., Bork J.M., Webb B.L., Inman R.B., Cox M.M. RecA protein filaments: End-dependent dissociation from ssDNA and stabilization by RecO and RecR proteins. *J. Mol. Biol.* 1997; 265:519–540.

36. Leiros I., Timmins J., Hall D.R., McSweeney S. Crystal structure and DNA-binding analysis of RecO from *Deinococcus radiodurans*. *EMBO J*. 2005; 24:906–918.

37. Luisi-DeLuca C., Kolodner R. Purification and characterization of the *Escherichia coli* RecO protein. Renaturation of complementary single-stranded DNA molecules catalyzed by the RecO protein. *J. Mol. Biol*. 1994; 236:124–138.

38. Kantake N., Madiraju M.V.V.M., Sugiyama T., Kowalczykowski S.C. *Escherichia coli* RecO protein anneals ssDNA complexed with its cognate ssDNA-binding protein: A common step in genetic recombination. *Proc. Natl. Acad. Sci. USA*. 2002; 99:15327–15332.

39. Alonso J.C., Stiege A.C., Dobrinski B., Lurz R. Purification and properties of the RecR protein from *Bacillus subtilis*. *J. Biol. Chem*. 1993; 268:1424–1429.

40. Lee B. Il, Kim K.H., Park S.J., Eom S.H., Song H.K., Suh S.W. Ring-shaped architecture of RecR: implications for its role in homologous recombinational DNA repair. *EMBO J*. 2004; 23:2029–2038.

41. Bork J.M., Cox M.M., Inman R.B. The RecOR proteins modulate RecA protein function at 5′

ends of single-stranded DNA. *EMBO J*. 2001; 20:7313–7322.

42. Honda M., Inoue J., Yoshimasu M., Itp Y., Shibata T., Mikawa T. Identification of the RecR TOPRIM domain as the binding site for both RecF and RecO. *J. Biol. Chem*. 2006; 281:18549–18559.

43. Webb B.L., Cox M.M., Inman R.B. An interaction between the *Escherichia coli* RecF and RecR proteins dependent on ATP and double-stranded DNA. *J. Biol. Chem*. 1995; 270:31397–31404.

44. Webb B.L., Cox M.M., Inman R.B. Recombinational DNA repair: The RecF and RecR proteins limit the extension of RecA filaments beyond single-strand DNA gaps. *Cell*. 1997; 91:347–356.

45. Hobbs M.D., Sakai A., Cox M.M. SSB protein limits RecOR binding onto single-stranded DNA. *J. Biol. Chem*. 2007; 282:11058–11067.

46. Koroleva O., Makharashvili N., Courcelle C.T., Courcelle J., Korolev S. Structural conservation of RecF and Rad50: implications for DNA recognition and RecF function. *EMBO J*. 2007; 26:867–877.

47. Lusetti S.L., Hobbs M.D., Stohl E.A., Chitteni-Pattu S., Inman R.B., Seifert H.S., Cox M.M. The RecF protein antagonizes RecX function via direct interaction. *Mol. Cell*. 2014; 21:41–50.

48. Huang L.C., Wood E.A., Cox M.M. Convenient and reversible site-specific targeting of exogenous DNA into a bacterial chromosome by use of the FLP recombinase: The FLIRT system. *J. Bacteriol*. 1997; 179:6076–6083.

49. Datsenko K.A., Wanner B.L. One-step inactivation of chromosomal genes in *Escherichia coli* K-12 using PCR products. *Proc. Natl. Acad. Sci. USA*. 2000; 97:6640–6645.

50. Ho H.N., van Oijen A.M., Ghodke H. The transcription-repair coupling factor Mfd associates with RNA polymerase in the absence of exogenous damage. *Nat. Commun*. 2018; 9:1570.

51. Kim T., Chitteni-Pattu S., Cox B.L., Wood E.A., Sandler S.J., Cox M.M. Directed evolution of RecA variants with enhanced capacity for conjugational recombination. *PLoS Genet*. 2015; 11:e1005278.

52. Mettrick K.A., Grainge I. Stability of blocked replication forks *in vivo*. *Nucleic Acids Res*. 2015; 44:657–668.

53. Saluja D., Godson G.N. Biochemical characterization of *Escherichia coli* temperature-sensitive *dnaB* mutants *dnaB8*, *dnaB252*, *dnaB70*, *dnaB43*, and *dnaB454*. *J. Bacteriol*. 1995; 177:1104–1111.

54. Ghodke H., Caldas V.E.A., Punter C.M., van Oijen A.M., Robinson A. Single-molecule specific mislocalization of red fluorescent proteins in live *Escherichia coli*. *Biophys. J*. 2016; 111:25–27.

55. Blattner F.R., Plunkett III G., Bloch C.A., Perna N.T., Burland V., Riley M., Collado-Vides J., Gaslner J.D., Rode C.K., Mayhew G.F. *et al*. The complete genome sequence of *Escherichia coli* K-12. *Science*. 1997; 277:1453–1474.

56. Lenski R.E., Rose M.R., Simpson S.C., Tadler S.C. Long-term experimental evolution in *Escherichia coli*. I. Adaptation and divergence during 2,000 generations. *Am. Nat*. 1991; 138:1315–1341.

57. Miller J.H. Experiments in Molecular Genetics. *Cold Spring Harbor Laboratory*. 1972.

58. Gruber A.J., Erdem A.L., Sabat G., Karata K., Jaszczur M.M., Vo D.D., Olsen T.M., Woodgate, R., Goodman M.F., Cox M.M. A RecA protein surface required for activation of DNA polymerase V. *PLoS Genet*. 2015; 11:e1005066.

59. Schneider C.A., Rasband W.S., Eliceiri K.W. NIH Image to ImageJ: 25 years of image analysis. *Nat. Methods*. 2012; 9:671–675.

60. Sliusarenko O., Heinritz J., Emonet T., Jacobs-Wagner C.. High-throughput, subpixel-precision analysis of bacterial morphogenesis and intracellular spatio-temporal dynamics. *Mol. Microbiol*. 2012; 80:612–627.

61. Robinson A., McDonald J.P., Caldas V.E.A., Patel M., Wood E.A., Punter C.M., Ghodke H., Cox M.M., Woodgate R., Goodman M.F., van Oijen A.M. Regulation of mutagenic DNA polymerase V activation in space and time. *PLoS Genet*. 2015; 11:e1005482.

62. Henrikus S.S., Wood E.A., McDonald J.P., Cox M.M., Woodgate R., Goodman M.F., van Oijen A.M., Robinson, A. DNA polymerase IV primarily operates outside of DNA replication forks in *Escherichia coli*. *PLoS Genet*. 2018; 14:e1007161.

63. Reyes-Lamothe R., Possoz C., Danilova O., Sherratt D.J. Independent positioning and action of *Escherichia coli* replisomes in live cells. *Cell*. 2008; 133:90–102.

64. Ritchie K., Lill Y., Sood C., Lee H., Zhang S. Single-molecule imaging in live bacteria cells. *Phil. Trans. R. Soc. B*. 2013; 368:1–8.

65. Ronayne E.A., Wan Y.C.S., Boudreau B.A., Landick R., Cox M.M. P1 Ref endonuclease: a molecular mechanism for phage-enhanced antibiotic lethality. *PLoS Genet*. 2016; 12:e1005797.

66. Makharashvili N., Mi T., Koroleva O., Korolev S. RecR-mediated modulation of RecF dimer specificity for single- and double-stranded DNA. *J. Biol. Chem*. 2009; 284:1425–1434.

67. Michel-Marks E., Courcelle C.T., Korolev S., Courcelle J. ATP binding, ATP hydrolysis, and protein dimerization are required for RecF to catalyze an early step in the processing and recovery of replication forks disrupted by DNA damage. *J. Mol. Biol*. 2010; 401:579–589.

68. Tang Q., Liu Y.P., Shan H.H., Tian L.F., Zhang J.Z., Yan X.X. ATP-dependent conformational

change in ABC-ATPase RecF serves as a switch in DNA repair. *Sci. Rep.* 2018; 8:2127.

69. Goudsmits J.M.H., Van Oijen A.M., Robinson A. A tool for alignment and averaging of sparse fluorescence signals in rod-shaped bacteria. *Biophys. J*. 2016; 110:1708–1715.

70. Rajendram M., Zhang L., Reynolds B.J., Auer G.K., Tuson H.H., Ngo K.V., Cox M.M., Yethiraj A., Cui Q., Weibel D.B. Anionic phospholipids stabilize RecA filament bundles in *Escherichia coli*. *Mol. Cell*. 2016; 60:374–384.

71. Amarh V., White M.A., Leach D.R.F. Dynamics of RecA-mediated repair of replication-dependent DNA breaks. *J. Cell Biol*. 2018.

72. Courcelle J., Khodursky A., Peter B., Brown P.O., Hanawalt P.C. Comparative gene expression profiles following UV exposure in wild-type and SOS-deficient *Escherichia coli*. *Genetics*. 2001; 158:41–64.

73. Renzette N., Gumlaw N., Nordman J.T., Krieger M., Yeh S.P., Long E., Centore R., Boonsombat R., Sandler S.J. Localization of RecA in *Escherichia coli* K-12 using RecA-GFP. *Mol. Microbiol*. 2005; 57:1074–1085.

74. Boudsocq F., Campbell M., Devoret R., Bailone A. Quantitation of the inhibition of Hfr x F- recombination by the mutagenesis complex UmuD′C. *J. Mol. Biol*. 1997; 270:201–211.

75. Stohl E.A., Brockman J.P., Burkle K.L., Morimatsu K., Kowalczykowski S.C., Seifert H.S. *Escherichia coli* RecX inhibits RecA recombinase and coprotease activities *in vitro* and *in vivo*. *J. Biol. Chem*. 2003; 278:2278–2285.

76. Courcelle J., Carswell-Crumpton C., Hanawalt P.C. *recF* and *recR* are required for the resumption of replication at DNA replication forks in *Escherichia coli*. *Proc. Natl. Acad. Sci. USA*. 1997; 94:3714–3719.

6.7 Additional data

6.7.1 RecF and RecO colocalise with the RecA probe mCI

In cells exposed to DNA damaging agents, the number of RecF and RecO binding sites are increased as cells filament, as shown earlier in this chapter. RecF and RecO each have roles in loading of the recombinase RecA. The mechanism of RecA loading is however still poorly understood. RecF has been described to act as a catalyst for RecA loading while RecO seems to be more actively engaged in the loading of RecA onto single-stranded DNA gaps or resected double-strand breaks.

To further investigate the roles of RecF and RecO in loading RecA, two-colour experiments were conducted recording the signal of fluorescent fusions of either RecF or RecO and a RecA-binding probe, mCI. The truncated bacteriophage λ repressor mCI binds to RecA filaments formed on ssDNA regions (1). Two-colour time-sampling experiments were carried out over a period of 3 h (acquisition protocol: 1. bright-field; 100 ms exposure time; 2. PALM acquisition protocol for PAmCherry-mCI: simultaneous illumination with the activation laser 405 [1-5 W/cm^2] and 568 nm readout laser [540 W/cm^2] for 200 frames, image cycle time 100 ms; 3. image of RecF-YPet or RecO-YPet signal: 50 ms exposure time at ~2200 W/cm^2). A new field-of-view was sampled at every 5 min. Cells were irradiated with UV light (fluence =10 J/ m^2), Directly after t = 0 min, cells were irradiated with 10 J/ m^2.

Before UV irradiation, colocalisation of RecF and RecO with mCI is zero (**Figure 8**) because mCI foci start to increasingly form subsequently after irradiation (1). After UV irradiation, the colocalisation of RecF with mCi is increased with 27% colocalisation at 60 min (**Figure 8**). From 90 min, fewer RecF foci localised in the vicinity of mCI foci with 9% at 115 min. In contrast, the colocalisation of RecO with mCI is highly increased from 90 min (26% at 110 min, 42% at 180 min, Figure 8).

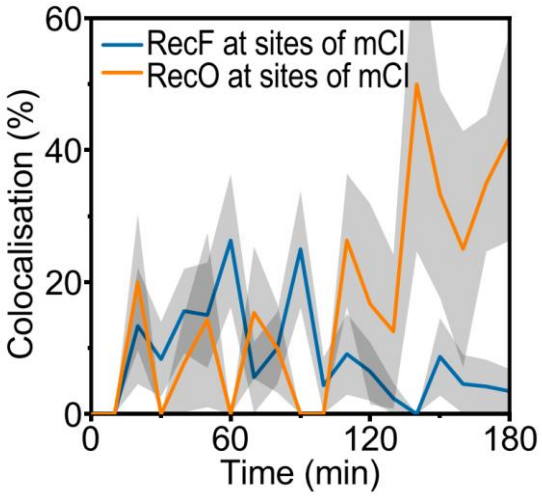

Figure 8. Colocalisation measurement of RecF with mCI (blue) and RecO with mCI (orange). Cells were irradiated with 10 J/m2 directly after t = 0 min. Data points are an average over duplicates. Error bars represent the standard deviation of the mean.

In conclusion, RecF foci colocalised with mCI foci from 10 – 90 min with ~10-25% colocalisation, whereas, RecO foci predominantly overlapped with mCI foci from 90 min after UV

exposure with ~13-42% colocalisation. These results are suggestive of two distinct phases for DNA damage repair after UV irradiation with respect to the recombination mediator proteins RecF and RecO. One possibility is that RecF may play a role in ssDNA gap repair, whereas, RecO might actually participate in DSB repair. It would be of great interest to conduct similar experiments in deletion backgrounds, such as Δ*recF*, Δ*recO*, Δ*recR* etc., to gain further insights into the mechanism of RecA loading.

6.7.2 Materials and Methods

Microscopy, flow cell design and data analysis

All experimental procedures (i.e. imaging in flow cell) were carried out as described in Chapter 6.2 *Materials and Methods*.

Strain construction

The plasmid pJM-mfd-PAmCherry-mCI was commercially synthesised (Aldevron), replacing the *uvrA* promotor in pJM-uvrA-PAmCherry-mCI (Chapter 5) with the *mfd* promotor.

Table 2. Strains used in this sub-chapter.

Strain	Relevant Genotype	Parent strain	Source/technique
MG1655	*dinB*$^+$ *dnaX*$^+$ *recB*$^+$ *lexA*$^+$	-	published (2)
EAW670	*recF-YPet*::Kan^R	MG1655	published (3)
EAW814	*recO-YPet*::Kan^R	MG1655	published (3)
SSH104	*recF-YPet*:: Kan^R (chr) PAmCherry-mCI (pl, spec^R)	EAW670	Transformation of EAW670 with pJM-mfd-PAmCherry-mCI
SSH105	*recO-YPet*:: Kan^R (chr) PAmCherry-mCI (pl, spec^R)	EAW814	Transformation of EAW814 with pJM-mfd-PAmCherry-mCI

6.7.3 References

1. Ghodke H, Paudel B, Lewis JS, Jergic S, Gopal K, Romero Z, et al. Spatial and temporal organization of RecA in the *Escherichia coli* DNA-damage response. *Elife*. 2019;8:e42761.

2. Blattner FR, Plunkett III G, Bloch CA, Perna NT, Burland V, Riley M, et al. The complete genome sequence of *Escherichia coli* K-12. *Science*. 1997;277:1453–1474.

3. Henrikus SS, Henry C, Ghodke H, Wood EA, Mbele N, Saxena R, et al. RecFOR epistasis group: RecF and RecO have distinct localizations and functions in *Escherichia coli*. *Nucleic Acids Res.* 2019;47:2946–2965.

7 Role of RNase H enzymes in maintaining genome stability in *Escherichia coli* expressing a steric-gate mutant of pol V_{ICE391}

Erin Walsh, **Sarah S. Henrikus**, Alexandra Vaisman, Karolina Makiela-Dzbenska, Thomas J. Armstrong, Krystian Łazowski, John P. McDonald, Myron F. Goodman, Antoine M. van Oijen Piotr Jonczyk, Iwona J. Fijalkowska, Andrew Robinson, Roger Woodgate

Accepted in *DNA Repair*.

pol V_{ICE391} (RumA′$_2$B) is a low-fidelity polymerase that promotes considerably higher levels of spontaneous "SOS-induced" mutagenesis than the related *E. coli* pol V (UmuD′$_2$C). The molecular basis for the enhanced mutagenesis was previously unknown. Using single molecule fluorescence microscopy to visualize pol V enzymes, we discovered that the elevated levels of mutagenesis are likely due, in part, to prolonged binding of RumB to genomic DNA leading to its increased levels of DNA synthesis compared to UmuC.

We have generated a steric gate pol V_{ICE391} variant (pol V_{ICE391}_Y13A) that readily misincorporates ribonucleotides into the *E. coli* genome and have used the enzyme to investigate the molecular mechanisms of Ribonucleotide Excision Repair (RER) under conditions of increased ribonucleotide-induced stress. To do so, we compared the extent of spontaneous mutagenesis promoted by pol V and pol V_{ICE391} to that of their respective steric gate variants. Levels of mutagenesis promoted by the steric gate variants that are lower than that of the wild-type enzyme are indicative of active RER that removes misincorporated ribonucleotides, but also misincorporated deoxyribonucleotides from the genome.

Using such an approach, we confirmed that RNase HII plays a pivotal role in RER. In the absence of RNase HII, Nucleotide Excision Repair (NER) proteins help remove misincorporated ribonucleotides. However, significant RER occurs in the absence of RNase HII and NER. Most of the RNase HII and NER-independent RER occurs on the lagging strand during genome duplication. We suggest that this is most likely due to efficient RNase HI-dependent RER which recognizes the polyribonucleotide tracts generated by pol V_{ICE391}_Y13A. These activities are critical for the maintenance of genomic integrity when RNase HII is overwhelmed, or inactivated, as Δ*rnhB* or Δ*rnhB* Δ*uvrA* strains expressing pol V_{ICE391}_Y13A exhibit genome and plasmid instability in the absence of RNase HI.

I carried out and analysed some in vivo single-molecule experiments. I was involved in strain construction and the preparation of the manuscript.

7.1 Introduction

Escherichia coli DNA polymerase V (pol V), a trimeric UmuD´$_2$C complex (1), is a Y-family polymerase (2) that is best characterized for its ability to promote damage-induced "SOS"-mutagenesis (3, 4). The mutagenesis occurs during error-prone translesion synthesis (TLS) across lesions that would otherwise block the cell's replicase, DNA polymerase III (pol III) (5, 6). Because of its error-prone DNA synthesis, pol V is subject to multiple levels of regulation (7). This includes LexA-regulated transcriptional control; activated RecA*-mediated posttranslational modification; Lon- and ClpXP-targeted proteolysis; the need for additional specific protein-protein interactions; as well as spatial regulation inside the cell. As a result, pol V activity is usually kept to a minimum, such that it is utilized only when absolutely required.

However, in a *lexA*(Def) *recA730* genetic background, in which the RecA730 (E38K) protein is in a constitutively activated state (RecA*), virtually all of the regulation normally imposed on pol V activity in a wild-type cell is circumvented, allowing error-prone pol V to replicate undamaged DNA. This leads to a roughly 100-fold increase in so-called "SOS-dependent spontaneous mutagenesis" (8). It is believed that this mutagenesis occurs, in part, due to the higher basal steady state levels of pol V in undamaged *recA730* strains compared to *recA*$^+$ strains (~20 pol V molecules in a *recA730* cell vs. one pol V molecule in a *recA*$^+$ cell (9)) that transiently compete with pol III for access to undamaged DNA (10). Studies with *lacZ* reporter alleles suggest that this occurs primarily on the lagging strand during genome duplication (11).

The intracellular levels of ribonucleotides in a cell are considerably higher (up to 1000-fold) than the concentrations of the corresponding deoxyribonucleotides (12-14). It is now well established that the main line of defense against errant misincorporation of ribonucleotides by DNA polymerases is a so-called "steric gate", which usually comprises a single amino acid residue with a bulky side chain that physically clashes with the 2´-OH of the incoming ribonucleotide to prevent its misincorporation into DNA (15-17). Mutant DNA polymerases in which the bulky side chain of the steric gate amino acid has been replaced with a much smaller moiety have been widely used to increase the levels of errant ribonucleotides misincorporated into DNA and to elucidate the mechanism of their subsequent removal during Ribonucleotide Excision Repair (RER) (18-23). Indeed, we previously utilized a steric gate pol V mutant with a Y11A substitution in the catalytic UmuC subunit of the polymerase to investigate the mechanisms of RER in *E. coli* (24, 25). *In vitro* studies with the pol V_Y11A mutant revealed that the enzyme not only distinguishes poorly between ribo- and deoxyribonucleotides, but also exhibits low base selectivity (24). We therefore expected the pol V_Y11A mutant to promote high levels of SOS-dependent mutagenesis *in vivo*. To our surprise, the level of mutagenesis was a fraction of that promoted by wild-type pol V (24). To explain these observations, we hypothesized that misincorporated deoxyribonucleotides were removed by active RER triggered by the misincorporated ribonucleotides. We further hypothesized that if all RER pathways were inactivated, pol V_Y11A-dependent mutagenesis would be as high as (or even higher than) that promoted by wild-type pol V (26). On the basis of these hypotheses, we discovered that RNase HII encoded by *rnhB*, provides the lead role in RER in *E. coli*, while RNase HI (encoded by *rnhA*) and the Nucleotide Excision Repair proteins (encoded by *uvrA*, *uvrB* and *uvrC*) provide back-up roles in the absence of RNase HII (26).

Although *E. coli* pol V promotes significant levels of SOS-dependent spontaneous mutagenesis, orthologs of pol V, such as polR1 (comprising MucA′$_2$B and encoded by *mucAB* on R46/pKM101, and used to increase the efficacy of mutagen detection in the "Ames-test") (27), or pol V$_{ICE391}$ (comprising RumA′$_2$B and encoded by *rumAB* on R391/ICE391) (28, 29) are much more efficient at promoting SOS-dependent spontaneous mutagenesis (30). Indeed, pol V$_{ICE391}$ is the most potent pol V mutator reported in the literature to date (30).

We were therefore interested in recapitulating our earlier RER studies with the *E. coli* pol V_Y11A using a steric gate mutant of pol V$_{ICE391}$ harboring a Y13A substitution in its catalytic RumB subunit. Our initial studies suggest that pol V$_{ICE391}$ can bind to undamaged DNA more frequently, and for far longer, than *E. coli* pol V. Our expectation was that the more potent pol V$_{ICE391}$_Y13A enzyme would potentially increase the number of errantly misincorporated ribonucleotides into the *E. coli* genome and possibly reveal additional pathways of RER. Our studies suggest that while RNase HII maintains its pivotal role in RER, the increased load of ribonucleotides incorporated into the genome by pol V$_{ICE391}$_Y13A leads to a greater dependency on RNase HI to protect *E. coli* from the deleterious effects of errant ribonucleotide incorporation into its genome.

7.2 Materials and Methods

7.2.1 Bacterial Strains and Plasmids

Bacterial strains used in this study are described in Table 1. New strains were generated via generalized transduction using P1*vir* (31). Where noted, the following antibiotics were used for selection; zeocin (25 μg/ml), kanamycin (50 μg/ml), tetracycline (15 μg/ml), chloramphenicol (20 μg/ml), ampicillin (100 μg/ml) and spectinomycin (50 μg/ml).

The *E. coli* strains used for the leading/lagging strand mutagenesis assay (see section 2.5 below) are derivatives of RW698 (26), but carry a *lacZ* missense allele that allows for scoring of mutagenesis via reversion to Lac$^+$ by an A·T→T·A transversion (32), inserted into the phage λ attachment site in one of the two orientations (Left and Right) with respect to the origin of replication (33). Recipient pairs of *lacZ* integrants were transformed with low-copy-number plasmids expressing either wild-type pol V$_{ICE391}$ (pRW320), the pol V$_{ICE391}$_Y13A variant (pJM1282), or the control vector (pGB2), to measure mutagenesis levels on the leading and lagging DNA strands.

Plasmids used in this study are described in Table 2. A low-copy-number plasmid, pJM1282, expressing a Y13A steric gate variant of *rumB* was generated by synthesizing a *Bam*HI to *Acc*I fragment (Genscript) containing the Y13A allele marked with a *Bss*HII site into the corresponding sites of pRW320 (34). The mKate2-RumB containing plasmid, pJM1324, was constructed by sub-cloning an N-terminal mKate2-RumB chimera (Genscript) into pRW320 from *Ale*I to *Pml*I to generate pJM1324. Subsequently, a fragment carrying the catalytically inactive D103A-E104A double mutation in *rumB* (Genscript) was sub-cloned into pJM1324 from *Pml*I to *Acc*I to generate pJM1347. In addition, a fragment carrying the β-clamp binding site mutant, Q358A-L361A-F364A in *rumB* (Genscript) was sub-cloned into pJM1324

from *Msc*I to *Nar*I to generate pJM1350. A C-terminal *umuC-mKate2* chimera was generated by synthesizing a *Bam*HI fragment containing the desired gene fusion and sub-cloned into the unique *Bam*HI site of pRW134 (34). One clone with *umuC-mKate* in the correct orientation was designated as pJM1334.

pJM1295, which expresses N-terminal His-tagged RumB_Y13A was generated by cloning a synthesized *Xba*I-*Nco*I *rumB* fragment with the Y13A substitution (Genscript) into pHRB1 (35).

7.2.2 Quantitative spontaneous mutagenesis

E. coli cells were transformed with the one of the following plasmids and grown at 37°C overnight in LB media containing spectinomycin: pGB2 (low-copy-number vector), or low-copy plasmids expressing pol V (pRW134), pol V_Y11A steric gate mutant (pJM963), pol V_{ICE391} (pRW320), or pol V_{ICE391}_Y13A steric gate mutant (pJM1282). The following day, cells were isolated by centrifugation and resuspended in an equal volume of SM buffer (31). To determine the number of spontaneously arising histidine revertant (His^+) mutants, (100 µl) cells were seeded upon Davis and Mingioli minimal agar plates (36) containing glucose (0.4% wt/vol); agar (1.0% wt/vol); proline, threonine, valine, leucine and isoleucine (all at 100 µg/ml); thiamine (0.25 µg/ml); and histidine (1 µg/ml). Spontaneously arising His^+ mutants were counted after four days growth at 37°C and are a direct measure of the spontaneous mutagenesis frequency since the number of mutants that arise on each plate is dependent on the limiting amount of histidine present in the media, independent of the number of cells seeded.

7.2.3 Western blotting to detect plasmid encoded UmuC and RumB proteins

Overnight cultures of RW584 harboring pRW134, pRW320, pJM1324, or pJM1334 were grown in LB media containing 50 µg/ml spectinomycin. The next day, the cultures were diluted 1:100 in fresh LB containing spectinomycin and grown to mid-log (~OD 0.5) (~3 hrs). Whole cell extracts were made by centrifuging 1.5 ml of culture and adding 90µl of sterile deionized water and 30 µl of NuPAGE LDS sample buffer (4X) (Novex, Life Technologies) to the cell pellet. Cells were lysed by five cycles of freeze/thaw on dry ice and in a 37°C water bath. Extracts were boiled for 5 minutes prior to loading. Samples were run on NuPAGE 4-12% Bis-Tris gels (Novex Life Technologies) and transferred to Invitrolon PVDF (0.45 µm pore size) membranes (Novex Life Technologies). Membranes were incubated with affinity purified polyclonal rabbit anti-UmuC or rabbit anti-RumB antibodies (1:7,500 dilution) at room temperature overnight. Then the membranes were incubated with goat anti-rabbit IgG (H+L) alkaline phosphatase conjugate (1:10,000 dilution) (BIO-RAD). Subsequently, the membranes were treated with the CDP-Star substrate (Tropix). Membranes were then exposed to BioMax XAR film (Carestream) to visualize UmuC, or RumB protein bands.

7.2.4 Expression and purification of pol V_{ICE391}_Y13A

Pol V_{ICE391}_Y13A was purified from RW644/ pARA1 /pJM1295 following the previously published protocol for wild-type Pol V_{ICE391} (35) as a custom service by scientists at Eurofins (Dundee, United Kingdom).

7.2.5 *In vitro* replication assays

Wild-type *E.coli* pol V (37), wild-type pol V_{ICE391} (35), the steric gate variant pol V_{ICE391}_Y13A (this manuscript), β-clamp, and γ-complex (37) were purified as previously described. All oligonucleotides were synthesized by Lofstrand Laboratories (Gaithersburg, MD) and gel purified prior to use. The primer used for the characterization of (mis)incorporation specificity of pol V variants has the following sequences: 5A17M (5'-GAC AAA CAA CGC GAC A). The 5′-^{32}P labeled primer was hybridized to single stranded circular M13mp18 plasmid at a 1.5:1 molar ratio by heating the DNA mixtures in an annealing buffer [50 mM Tris–HCl (pH 8), 50 μg/ml BSA, 1.42 mM 2-mercaptoethanol] for 10 min at 100°C followed by slow cooling to room temperature.

RecA (4 μM) (New England Biolabs, Ipswich, MA) was incubated with 0.25 μM 48-mer single-stranded oligonucleotide in the presence of 1 mM adenosine 5′[γ-thio]triphosphate (ATPγS, Biolog Life Science Institute, Bremen, Germany) in the 1x reaction buffer [20 mM Tris-HCl pH 7.5, 8 mM $MgCl_2$, 8 mM DTT, 80 μg/ml BSA, 4% glycerol] at 37°C for 5 min to form RecA nucleoprotein filament on ssDNA (RecA*). Purified pol V polymerases (80 nM) were first combined with RecA* to form pol V Mut complexes (37) and then added to the reaction mixture which had been pre-incubated for 3 min at 37°C. The reaction mixture contained 1 mM ATP, 50 μM dNTPs or rNTPs (added individually, or as a mixtures), 2 nM primed ssDNA templates (expressed as primer termini), 100 nM (as tetramer) single-stranded binding protein (SSB, Epicentre Biotechnologies, Madison, WI, USA), 50 nM (as a dimer) β-clamp and 5 nM γ-complex in the 1x reaction buffer. The reactions were incubated at 37°C for 0.5–20 min, split into two and treated with either 0.3 M KCl, or 0.3 M KOH for 2 h at 55°C.

For processivity measurements, primer extension reactions were carried out essentially as described above, except that the reaction mixtures contained primer-templates in sufficient excess (20-fold) over polymerase and that RecA* was pre-formed on biotinylated 48-mer oligomers (UTTA: 5′-TCG ATA CTG GTA CTA ATG ATT AAC GAC **TT**A AGC ACG TCC GTA CCA TCG-3′) linked to streptavidin-coated agarose resin as previously described (38). Pol V Mut complexes were generated by incubation of wild-type pol V and pol V_{ICE391} with RecA* and isolated by centrifugation (37). As we have shown previously (38), because pol V Mut deactivates after every round of primer extension and requires new RecA* for reactivation, addition of a trap has no effect on pol V Mut and consequently, heparin was not used in these experiments. In addition, less than 20% of the radiolabeled primer was utilized in the reactions and therefore represents replication products generated from a single polymerase-primer-template binding event (39).

All reactions were terminated by addition of an equal volume of loading buffer (97% formamide, 10 mM EDTA, 0.1% xylene cyanol, 0.1% bromophenol blue) and after heat-denaturation, the products were immediately resolved by denaturing PAGE (8 M urea, 15% acrylamide), followed by visualization using a Fuji image analyzer FLA-5100.

7.2.6 Measurement of leading vs. lagging strand *lacZ* mutagenesis

Mutant frequencies were determined for 10-30 cultures for each strain (for 2 independent *lacZ* integrants per orientation) inoculated in 2 ml LB containing 50 μg/ml spectinomycin and grown with agitation at 37°C. After overnight incubation the appropriate dilutions of the cultures were plated on minimal-Lac plates to determine the number of Lac^+ mutants and on minimal plates containing glucose to determine the total cell count. Mutant frequencies were calculated by dividing the number of Lac^+ mutants by the total number of cells. Table 3 presents the mean values of frequencies ± 95% confidence intervals obtained from 3 independent experiments. The results for strains harboring control vector pGB2 were excluded from analyses due to negligible mutability in all tested genetic backgrounds.

Solid and liquid media were prepared as described in Fijalkowska and Schaaper (40), supplemented with appropriate amino acids and antibiotics when required.

7.2.7 Fluorescence microscopy

Wide-field fluorescence imaging was conducted on an inverted microscope (IX-81, Olympus with a 1.49 NA 100x objective) in an epifluorescence configuration (9, 41). Continuous excitation is provided using semidiode lasers (Sapphire LP, Coherent) at a wavelength of 514 nm (150 mW max. output) and 568 nm (200 mW max. output). Imaging of strains SSH118 and SSH119 were carried out on a Nikon Ti2-E microscope. Excitation light was provided by the same setup as described above. For all measurements, the sample compartment and objective lens were heated to 37°C.

All mKate2 fusion proteins expressed from plasmids pJM1224, pJM1334, pJM1347, pJM1350 (Table 2), were imaged using yellow excitation light (λ = 568 nm) at 275 Wcm^{-2} (for colocalization measurements, imaging of RumB mutants and molecules per cell measurements), collecting emitted light between 610–680 nm (ET 645/75m filter, Chroma) on a 512 × 512 pixel EM-CCD camera (C9100-13, Hamamatsu). For DnaX-YPet imaging, we used green excitation (λ = 514 nm) at 60 Wcm^{-2} (SSH038, SSH040, SSH073, SSH074, SSH118, SSH119), collecting light emitted between 525–555 nm (ET540/30m filter, Chroma). Burst acquisitions in undamaged *recA730* cells movies of 300 frames, each frame has 100 ms exposures followed by 50 ms dark time using 568 nm light) were collected to characterize the effective binding lifetimes of UmuC-mKate2 (pJM1224) and mKate2-RumB (pJM1334) as a function of foci number per cell.

Burst acquisitions (movies of 300 frames, each frame has 50ms exposures followed by 50ms dark time using 568 nm light) were collected to characterize the motions of UmuC and RumB fused to mKate2 (including RumB mutants), and to determine the number of UmuC-mKate2 and mKate2-RumB molecules per cell. Images of DnaX-YPet were recorded with 500 ms exposures, bright-field images were recorded with 34ms exposures. All images were analyzed with ImageJ (42).

7.2.8 Flow cell designs

All imaging experiments were carried out in home-built quartz-based flow cells (9). These flow cells were assembled from a no. 1.5 coverslip (Marienfeld, REF 0102222), a quartz top piece (45x20x1 mm) and PE-60 tubing (Instech Laboratories, Inc.). Prior to flow-cell assembly, coverslips were silanized with aminopropyltriethoxy silane (Alfa Aesar). First, coverslips were sonicated for 30 min in a 5 M KOH solution to clean and activate the surface. The cleaned coverslips were rinsed thoroughly with MilliQ water and then treated with a 5% (v/v) solution of amino-propyl-triethoxysilane (APTES) in MilliQ water. The coverslips were subsequently rinsed with ethanol and sonicated in ethanol for 20 s. Afterwards, the coverslips were rinsed with MilliQ water and dried in a jet of N_2. Silanized slides were stored under vacuum prior to use.

To assemble each flow cell, polyethylene tubing (BTPE-60, Instech Laboratories, Inc.) was glued (BONDiT B-482, Reltek LLC) into two holes that were drilled into a quartz piece. After the glue solidified overnight, double-sided adhesive tape was adhered on two opposite sides of the quartz piece to create a channel. Then, the quartz piece was affixed to an APTES-treated coverslip. The edges were sealed with epoxy glue (5 Minute Epoxy, PARFIX). Each flow cell was stored in a desiccator under mild vacuum while the glue dried. Typical channel dimensions were 45 mm × 5 mm × 0.1 mm (length × width × height).

7.2.9 Imaging in flow cells

Cells were grown at 37ºC in EZ rich defined medium (Teknova) that contained 0.2% (wt/vol) glucose. All strains were grown in the presence of spectinomycin (50 μg/ml). Cells were loaded into flow cells, allowed a few minutes to associate with the APTES surface, then loosely associated cells were removed by pulling through fresh medium that contained spectinomycin (50 μg/ml). Throughout the experiment, medium was pulled through the flow cell using a syringe pump, at a rate of 50 μl/min.

7.2.10 Analysis of foci number per cell

Single cells were selected to obtain information about the number of UmuC and RumB foci present in undamaged *recA730* cells. MicrobeTracker 0.937 (43), a MATLAB script, was used to manually create cell outlines as regions of interest (ROI). By manually outlining cells, we ensure accuracy and purely select non-overlapping, in-focus cells for analysis. ImageJ 1.50i (42) was used to create average projections of effective exposure times (0.1, 7.5, 15 and 45 s). A Peak Fitter plugin, as described previously (9), was used to describe the position of each foci. The position of each defined foci was then meshed with the previously defined cell ROIs to define the number of foci per cell.

7.2.11 Analysis of UmuC and RumB copy numbers per cell

The number of UmuC-mKate2 and mKate2-RumB molecules and thus their concentration are extracted from the integrated fluorescence signal under each cell outline during burst acquisition experiments. Each cell exhibits an intensity decay which is comprised of mKate2 bleaching, cellular auto-fluorescence and background fluorescence. Exciting with a laser power of 275 Wcm^{-2}, *E. coli* MG1655 cells, expressing no mKate2, exhibit no auto-fluorescence. The background fluorescence was negligible (equivalent to <1 mKate2 molecule). The integrated fluorescence signal under each cell outline corresponds to the fluorescence signal of intracellular mKate2 molecules.

Images were corrected for the electronic offset and flattened to correct for inhomogeneity of the excitation beam (inhomogeneity was small at a laser power of 275 Wcm^{-2}; the brightest part at the center of the image was <10% more intense than at the corners). For each cell, the mean mKate2 signal per pixel of the first frame from the time series experiments was extracted. The mean mKate2 signal multiplied by the cell area gives the integrated mKate2 intensity, which was used to determine the number of mKate2 molecules per cell.

The mean intensity of individual mKate2 molecules was determined by analysing single-molecule return events. For each cell, the number of UmuC-mKate2 and mKate2-RumB molecules was then calculated by dividing the mean mKate2 signal of the first frame from the burst acquisition experiments by the mean single-molecule intensity. The cellular concentration was calculated using the cell volume of each cell, determined during cell outline assignation in MicrobeTracker (43).

7.2.12 Autocorrelation analysis

Intensity vs time trajectories for UmuC-mKate2 and mKate2-RumB were extracted from fluorescence movies using ImageJ (42). Regions of interest were defined based on the positions of DnaX-YPet foci. To capture and locally background correct mKate2 signals at these regions-of-interest, the mean intensity within a 5x5 pixel selection box was measured, subtracting the signal from a two-pixel ring placed around the box. This was repeated for each region-of-interest across each time-point of each movie. The resulting intensity vs time trajectories, measured at each replisomal position, were imported into MATLAB. The autocorrelation function of each trajectory was calculated using the *xcorr* routine. The mean of these functions was determined for each set of data (UmuC-mKate2 or mKate2-RumB). In parallel, a mean intensity trajectory was calculated for each data set, reflecting the photobleaching kinetics. The autocorrelation function of this photobleaching curve was then calculated. To separate the effects of photobleaching from other time-dependent signal fluctuations (protein dynamics), the mean autocorrelation function for individual trajectories was divided by the autocorrelation function of the photobleaching curve. To extract time constants from the signatures detected in the normalized autocorrelation functions, the first 1 s of these signatures were fit with a single exponential decay function.

7.3 Results

7.3.1 pol V and pol V_{ICE391} dependent spontaneous mutagenesis in *dnaE*$^+$ and *dnaE915* strains

pol V_{ICE391} is encoded by the *rumAB* genes, which were first cloned in 1993 from the IncJ plasmid, R391 (28). Due to the fact that R391 spends much of its natural life cycle integrated into its host genome (44), it has subsequently been renamed Integrating Conjugating Element 391 (ICE391). In its native ICE environment, pol V_{ICE391} promotes minimal levels of spontaneous SOS mutagenesis (45, 46). However, when sub-cloned, pol V_{ICE391} is a potent mutator that exhibits 3-5 fold higher levels of SOS-dependent spontaneous mutagenesis compared to *E. coli* pol V (28, 30). The higher levels of mutagenesis could be due to a variety of reasons, such as higher steady-state levels of pol V_{ICE391} compared to *E. coli* pol V within the cell, or reduced fidelity during replication of undamaged DNA. Another possibility that we considered is that pol V_{ICE391} might bind to undamaged DNA more efficiently than pol V, resulting in a greater opportunity to compete with the cell's replicase, pol III. To investigate this hypothesis further, we compared the extent of pol V and pol V_{ICE391}-dependent mutagenesis in strains expressing a *dnaE915* allele. *dnaE915* (an A498T substitution in the α-catalytic subunit of the pol III replicase) was first characterized as a potential "antimutator" allele of *dnaE* (47). It was postulated that the *dnaE915*-encoded mutant α-catalytic subunit of pol III frequently dissociates from DNA allowing any 3′-5′ exonuclease, including the intrinsic proofreading domain of DNA polymerase II, to extrinsically proofread mispaired bases at the abandoned 3′ primer terminus (48). However, the same strains become "mutators" in the presence of SOS-induced error-prone pol V (49) which extends pol III terminal mispairs and participates more efficiently in replication after pol III dissociation. Indeed, the level of pol V-dependent SOS mutagenesis increased roughly 3-fold between *dnaE*$^+$ and *dnaE915* strains (Fig. 1), suggesting that pol V is not necessarily intrinsically less mutagenic than pol V_{ICE391}, but under physiological conditions, it may have limited access to undamaged genomic DNA and/or does not compete well with the wild-type α-catalytic subunit of pol III. Conversely, there was no obvious difference in the high levels of pol V_{ICE391}-dependent mutagenesis in *dnaE*$^+$ and *dnaE915* strains (Fig. 1), supporting the idea that pol V_{ICE391} may have better access to undamaged DNA and/or competes more efficiently with the wild-type α-catalytic subunit of pol III for access to the free 3′ primer termini, so as to promote much higher levels of spontaneous SOS mutagenesis.

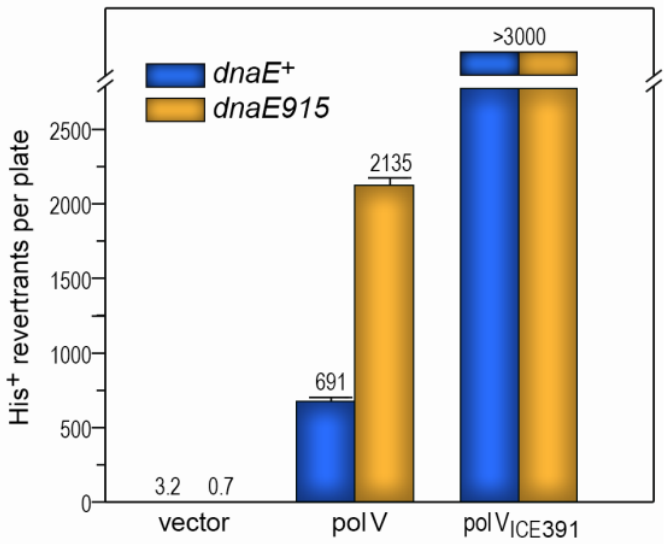

Fig. 1. Comparison of pol V- and pol V_{ICE391}-dependent spontaneous mutagenesis in *recA730 lexA51*(Def) Δ*umuDC dnaE*$^+$ or *dnaE915* strains. Strains were transformed with low copy plasmids pGB2 (vector); pRW134 (*umuD′C*); or pRW320 (*rumA′B*). Cultures were grown overnight in LB plus spectinomycin and processed as described in *Materials and methods* to measure reversion to histidine prototrophy. The revertants were counted after incubation at 37ºC for 4 days. The data reported represent the average number of His$^+$ mutants per plate (with error bars indicating Standard Errors of the Mean [SEM]). The numbers shown above the bars are the mean values calculated from the data obtained using 3 individual cultures per strain each plated on 5 plates, for a total of 15 plates per strain.

7.3.2 Fluorescent protein reporters and cellular concentrations

To test the hypothesis that pol V_{ICE391} may have better access to undamaged DNA where it would compete with the cell's replisome, we used single-molecule time-lapse microscopy to directly visualize fluorescently labelled pol V and pol V_{ICE391} in live cells. We have previously used this technique to visualize the localization of a chromosomally expressed UmuC-mKate2 fusion protein (9) and have now extended these studies with plasmid encoded fluorescent constructs. So as to ensure the fusion constructs were catalytically active, we first generated low-copy number plasmids expressing UmuD′ and mKate2 fused to either the N- or C- terminus of UmuC, along with analogous RumA′ and mKate2-RumB fusions. These plasmids were introduced into *E. coli* RW584 (*recA730 lexA51*(Def) Δ*(umuDC)596*::*ermGT*) and the level of spontaneous mutagenesis assayed (Supplemental Fig. 1). Both N- and C- mKate2-RumB fusions were highly proficient at promoting spontaneous mutagenesis. The N-terminal fusion construct, pJM1324, promoted slightly higher levels of spontaneous mutagenesis than the untagged construct (pRW320) and was accordingly chosen for further analysis. As expected, all pol V constructs gave much lower levels of spontaneous mutagenesis than the pol V_{ICE391} constructs. The highest level of mutagenesis was observed when mKate2 was fused to the C-terminus of UmuC and as a consequence, pJM1334 was used in the fluorescence assays.

Western blots using affinity purified anti-UmuC were initially used to compare steady-state levels of the plasmid encoded untagged- and mKate2-tagged UmuC proteins (Supplemental Fig. 2). The level of UmuC-mKate2 was ~20% of that observed for wild-type UmuC. These observations are consistent with our earlier studies with chromosomally encoded *umuC*-mKate2, which also exhibited lower steady-state

levels than wild-type UmuC protein (9). The lower level of mutagenesis promoted by plasmid encoded UmuC-mKate2 compared to wild-type UmuC therefore equates to the lower steady-state levels of the fusion protein compared to the wild-type UmuC protein, rather than a change in function of the fusion protein compared to the wild-type protein.

Western blotting does not allow for ready comparison of steady-state UmuC-mKate2 and mKate2-RumB concentrations. We therefore used single-molecule fluorescence microscopy to measure these concentrations using an approach that has been described in detail previously (41). Briefly, the integrated fluorescence intensity within each cell is measured within microscope images and normalized by the mean intensity of a single molecule, which is extracted from photobleaching traces. We found that in undamaged *recA730* cells, steady-state levels of UmuC-mKate2 were ~3-fold higher than mKate2-RumB. Specifically, cells that carried pJM1334 ($UmuD'_2$ UmuC-mKate2) contained on average 315 ± 29 molecules of UmuC-mKate2 (STD = 296; n = 80 cells), whereas cells that carried pJM1324 ($RumA'_2$ mKate2-RumB) contained 92 ± 11 molecules of mKate2-RumB (STD = 90; n = 65 cells). Taking account cell volumes, which were measured from bright-field images, these values correspond to intracellular concentrations of 40 ± 3 nM for mKate2-RumB and 101 ± 4 nM for UmuC-mKate2. Together, these results indicate that in the *recA730* background pol V_{ICE391} supports higher levels of spontaneous mutagenesis than pol V, despite its intracellular levels being lower than those of pol V. For the tagged proteins, the intracellular concentration of mKate2-RumB (40 nM) is 2.5-fold lower than for UmuC-mKate2 (101 nM).

7.3.3 Number and longevity of UmuC and RumB foci in undamaged *recA730* cells

As the intracellular concentrations did not explain the higher levels spontaneous mutagenesis observed in pol V_{ICE391}-expressing cells, we next looked for evidence of increased polymerase activity. In single-molecule fluorescence images, we would expect individual polymerase molecules to produce foci as they bind to DNA. This phenomenon is well described and is commonly referred to as detection by localization (50). As the polymerases bind to DNA, their diffusional motion becomes sufficiently slow that they appear as static foci in images recorded on the millisecond timescale.

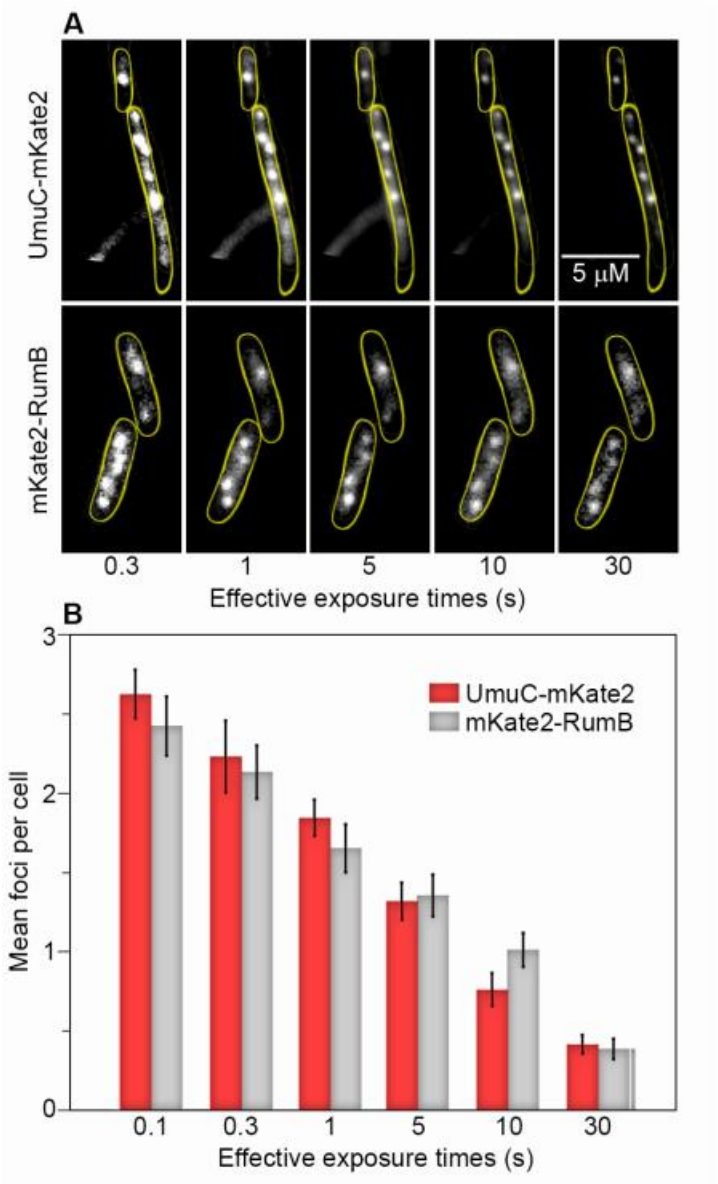

Fig.2. **Effective exposure times and number of UmuC and RumB foci in undamaged *recA730* cells. A,** Top panel: Focus longevity of UmuC-mKate2 foci. Bottom panel: Focus longevity of mKate2-RumB. Scale bar 5 μm. Cells shown are representative of n>100 cells. **B.** Mean foci per cell over longer effective exposure times. Over all projection lengths the mean number of mKate2-RumB foci per cell is similar to the mean number UmuC-mKate2 foci per cell. n>100 cells. Error bars displayed indicate standard error of the mean.

To visualize fluorescently labelled pol V and pol V_{ICE391}, a bright field image was first acquired to define the position of each *recA730* Δ*umuDC* cell. Burst acquisition movies were then collected, capturing fluorescence signals from UmuC-mKate2 or mKate2-RumB signals (300 cycles of 50 ms exposure time followed by 50ms dark time, total length of movie = 30 s). For both UmuC-mKate2 and mKate2-RumB, punctate foci were visible in most cells (Fig. 2). If foci appearing in our single-molecule images correspond to DNA polymerases actively engaged in DNA synthesis, one would predict that mutants that are defective for either DNA synthesis or impaired for substrate binding would fail to produce foci. Indeed, a catalytically inactive mutant of RumB and a mutant of RumB that is defective for binding to the β-sliding clamp, each fused to mKate2 (pJM1347 and pJM1350, respectively) failed to produce foci under conditions where the unaltered mKate2-RumB probe readily produced foci (Supplemental Figure. 3). These observations support the notion that those foci seen in the *recA730* Δ*umuDC* cells represent catalytically functional pol V, or pol V_{ICE391}.

We next set out to quantify the number of UmuC-mKate2 and mKate2-RumB foci per cell as a window into their polymerase activities. Visually comparing the UmuC-mKate2 and mKate2-RumB movies, it appeared that mKate2-RumB foci were longer-lived than the UmuC-mKate2 foci. To gain further insight into focus lifetimes, we quantified foci within average projections that captured different lengths of time. We compared the number of foci that could be detected in the first frame of the movie against projections of frames 1–3, 1–10, 1–50, 1–100, and 1–300 (Fig. 2A). This approach is equivalent to comparing images with exposure times of 0.3, 1, 5, 10 and 30 s respectively. Short effective exposure times capture both short- and long-lived foci, whereas longer effective exposure times capture long-lived foci exclusively, with short-lived foci blurring into the background. We observed similar numbers of UmuC-mKate2 and mKate2-RumB foci present in cells over all effective exposure times (Fig. 2B). For both probes approximately 2.5 foci were detected per cell in images with an effective exposure time of 0.3 s, whereas approximately 0.5 foci per cell (i.e. one focus per two cells) were detected in images with an effective exposure time of 30 s. It is important to note that this approach does not allow for precise determination of focus lifetimes; detection of a focus in an average projection does not necessarily imply that the focus was present for the entire duration of the projection. Nevertheless, the analysis suggests that many UmuC-mKate2 and mKate2-RumB foci persist for at least a few seconds. The ratio of mKate2-RumB foci to UmuC-mKate2 foci increases with exposure time, indicating that a higher proportion of mKate2-RumB foci are longer-lived relative to the UmuC-mKate2 foci. The greater longevity of RumB foci suggests that pol V_{ICE391} may have more prolonged access to DNA than *E. coli* pol V in *recA730* cells. Interestingly, these apparent differences in focus lifetimes were much more pronounced in UV-irradiated *recA*$^{+}$ cells (Supplemental Figure 4), with UmuC-mKate2 foci being rarely visible in projections longer than 10 s, whereas mKate2-RumB foci could be detected in projections of up to 80 s.

7.3.4 UmuC/RumB: replisome colocalization analysis in undamaged *recA730* Δ*umuDC* cells

Having ascertained that *recA730* cells produce similar numbers of UmuC-mKate2 and mKate2-rumB foci, and that mKate2-rumB foci appear to be somewhat longer lived, we next set out to determine where the two polymerases localize within cells. Specifically, we wished to investigate whether pol V and pol V_{ICE391} differ in their colocalization with replication fork markers. To facilitate two-color imaging of pol V and pol V_{ICE391} and replisomes, the strains described above also expressed a yellow fluorescent protein fusion of the pol III HE τ-subunit (encoded by *dnaX*). We have previously used the *dnaX-YPet* fusion to indicate the position of replisomes in cells (9). The *dnaX-YPet* allele used here is fully functional and has no impact on the growth of cells (51). When collecting the movies described in Fig. 2, we also collected an image of the DnaX-YPet signals (500 ms exposure time) to indicate the position of replisomes.

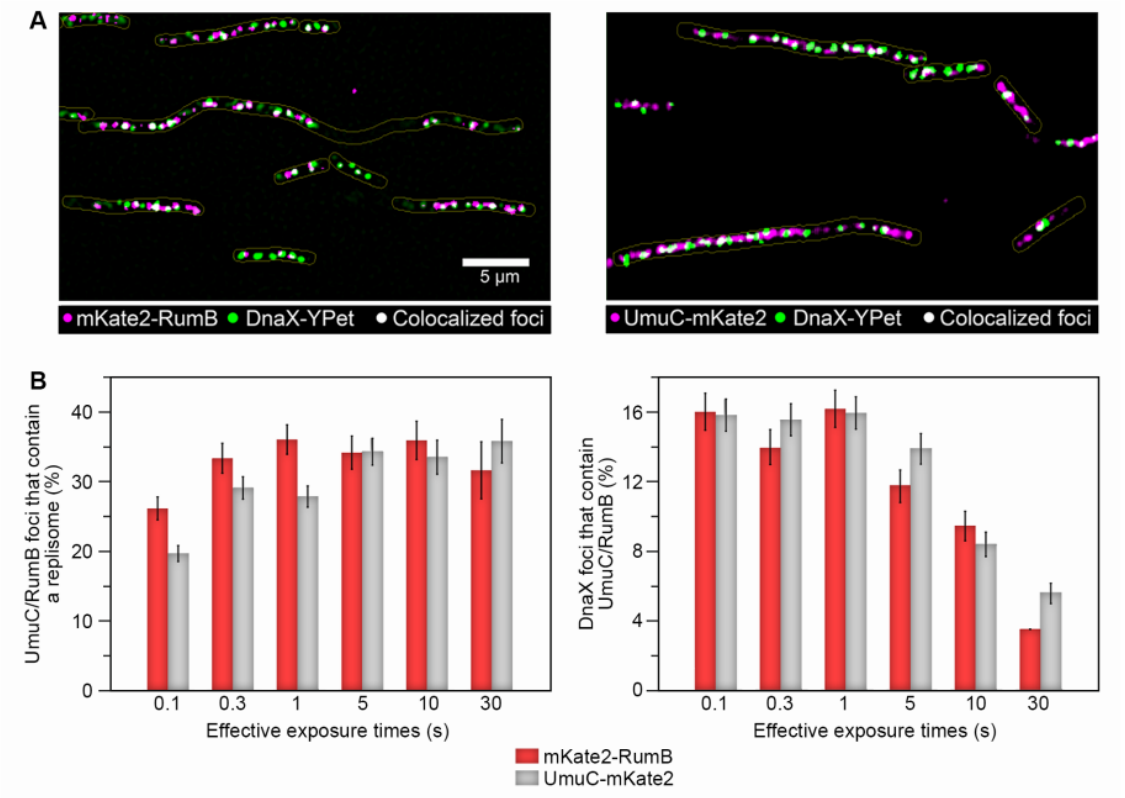

Fig.3. Colocalization measurements of DnaX-YPet with UmuC-mKate2 or mKate2-RumB in a Δ*umuDC recA730* strain. A, Left panel: Merged images of DnaX-YPet (green) and UmuC-mKate2 (magenta, foci bound for 1s). Right panel: Merged images of DnaX-YPet (green) and mKate2-RumB (magenta, foci bound for 1s). Scale bar: 5 µm. **B,** Left panel: percentage of DnaX foci that contain an UmuC (grey) or RumB focus (red) at effective exposure times of 0.1, 0.3, 1, 5, 10 and 30 s. Right panel: percentage of UmuC (grey) or RumB foci (red), that overlap with DnaX foci at effective exposure times of 0.1, 0.3, 1, 5, 10 and 30 s

We measured rates of colocalization between replisome markers and UmuC-mKate2/mKate2-RumB foci as a function of effective exposure time. We determined the percentage of UmuC-mKate2 foci that formed in the vicinity of replisome foci (within 218 nm (41)) and the percentage of replisome foci that contained a UmuC-mKate2 focus. Colocalization between mKate2-RumB and replisomes was determined

similarly. At the shortest exposure time of 0.1s, approximately 20% of UmuC-mKate2 foci we detected were colocalized with replisomes (Fig. 3A), in agreement with our previous measurements for chromosomally expressed UmuC-mKate2 in *recA730* cells (9). For longer effective exposure times (0.3–30 s), the colocalization of UmuC-mKate2 foci with replisomes increased slightly to ~30%, suggesting that longer-lived foci were more likely to form close to replisomes. Similarly, for RumB foci the colocalization increased from 25% for the shortest exposure time (0.1 s) to ~35% for longer exposure times (0.3–30 s). Thus, UmuC-mKate2 and mKate2-RumB foci colocalized with replisomes to a similar extent and exhibited similar behaviors as a function of exposure time.

The proportion of replisomes that contain a UmuC or RumB focus was also determined. Approximately 16% of replisomes had a colocalized UmuC-mKate2 focus detected at the shortest effective exposure time (Fig. 3B). Similar results were observed for mKate2-RumB. In both cases increasing the effective exposure time led to a decrease in colocalization as fewer UmuC-mKate2 or mKate2-RumB foci were detected. The increased colocalization of replisomes containing a UmuC-mKate2 focus over a group size of 30 s may be due to spurious detection of background signals as foci as a consequence of the higher steady-state levels of pol V present in the UmuC-mKate2 cells.

Overall, the results of the colocalization analysis suggest few differences between pol V and pol V_{ICE391} in *recA730* cells. Interestingly, similar analysis carried out for UV-irradiated *recA*$^+$ cells revealed stark differences between pol V and pol V_{ICE391}, with the later forming much more long-lived foci in the vicinity of replication forks (Supplemental Figure 4). Thus, while differences in replisome colocalization and focus lifetimes can occur for pol V and pol V_{ICE391}, the two polymerases behave similarly in untreated *recA730* cells. It is therefore unlikely that the higher mutagenesis observed for pol V_{ICE391} in *recA730* cells (Fig. 1) arises as a result of increased access of pol V_{ICE391} to replication forks.

7.3.5 Repetitive binding of pol V and pol V_{ICE391} at replisomes

Thus far, the single-molecule analysis had revealed differences in pol V and pol V_{ICE391} focus lifetimes in UV-irradiated *recA*$^+$ cells but produced few clues to explain the higher rates of mutagenesis observed for pol V_{ICE391} in untreated *recA730* cells. We reasoned that pol V_{ICE391} could potentially support higher rates of mutagenesis if it simply had more robust polymerase activity than pol V once suitable substrates became available. This would allow pol V_{ICE391} to synthesize more DNA in total and therefore produce a larger number of mutations. Pursuing this idea further, we closely examined fluctuations in mKate2 fluorescence signals in regions corresponding to UmuC-mKate2 or mKate2-RumB foci. Rather than selecting regions-of-interest based on the positions of UmuC-mKate2 or mKate2-RumB foci, we monitored mKate2 signals close to replisomes, so as not to bias our results towards longer-lived (and thus more readily detected) states. Within microscope movies, intensities within 5x5 pixel selection boxes (large enough to capture a single focus) placed at replisomes were monitored as a function of time for both UmuC-mKate2 or mKate2-RumB in *recA730* cells.

Interestingly, the intensity versus time trajectories for both proteins exhibited significant evidence of dynamics occurring on the milliseconds–seconds timescale (Supplemental Figure 5). As expected, all trajectories showed evidence of overall signal loss as a result of photobleaching, which in these measurements occurred with a time constant τ_{bleach} = 1.3 s. More strikingly, the trajectories showed

frequent transitions between high and low fluorescence states, indicative of the rapid formation and loss of mKate2 foci and consistent with repeated cycles of binding and dissociation of UmuC-mKate2 and mKate2-RumB at replisome positions. Interestingly, the duration of the high fluorescence states appeared to be longer for mKate2-RumB than for UmuC-mKate2. To examine these time-dependent fluctuations more systematically, we calculated autocorrelation functions for each trajectory, comparing the mean of these functions for UmuC-mKate2 signals against mKate2-RumB signals. Repeated cycles of focus formation and loss would be expected to produce a characteristic signature in the autocorrelation functions with a lifetime that represents the combined durations of the on (high intensity, bound) and off (low intensity, unbound) states. The photobleaching-corrected autocorrelation function of UmuC-mKate2 signals produced a relatively weak signature (peaks at a value of 0.96) with a time constant τ_{acf_UmuC} = 0.05 s (Fig. 4). The equivalent autocorrelation function for mKate2-RumB signal produced a much stronger signature (peaks at a value of 0.85) with a time constant τ_{acf_RumB} = 0.35 s. The stronger signature observed for mKate2-RumB suggests that it undergoes repeated cycles of binding and dissociation at replisomes more often than UmuC-mKate2, which produces a weaker autocorrelation signature. The time constants indicate that each time mKate2-RumB binds near a replisome, it remains bound approximately seven-fold longer than UmuC-mKate2. This longer binding time may increase the likelihood that the association of the polymerase with DNA substrates would be productive (i.e. leading to the incorporation of nucleotides). Alternatively, longer binding could allow the polymerase to incorporate more nucleotides per binding event (i.e. it would have higher processivity). As these events occur repetitively, this could have a major impact on the total amount of DNA synthesized by the two enzymes and thus the number of mutations they introduce.

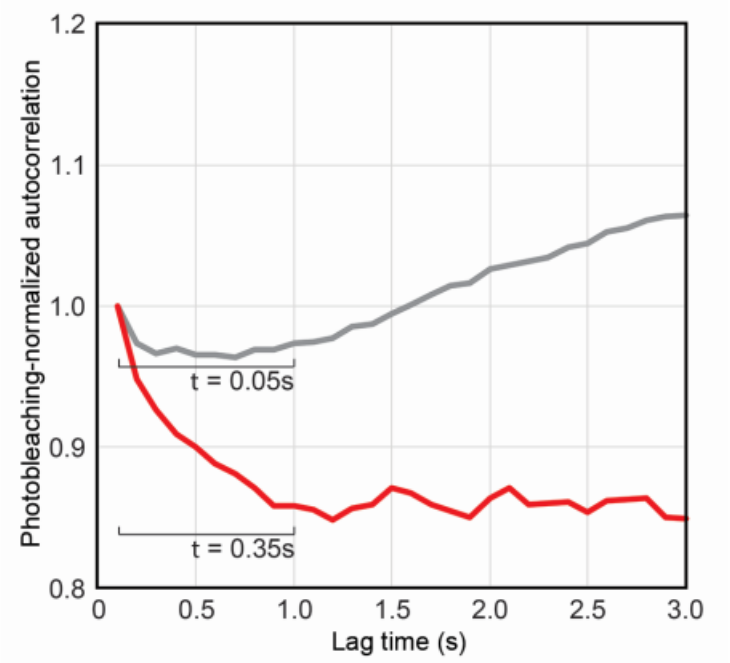

Fig.4. Autocorrelation analysis of mKate2 signal fluctuations at replisomes. Photobleaching-normalized autocorrelation functions for UmuC-mKate2 (gray) and mKate2-RumB (red). Intensities of mKate2 signals within movies were monitored at replisome positions (Supplemental Fig 5). Autocorrelation functions were calculated for each of the resulting intensity vs time trajectories. For each

data set the mean of these functions was divided by the autocorrelation function of the photobleaching curve to separate the effects of photobleaching from the effects of protein dynamics. To determine the characteristic timescale for signal fluctuations within each data set, the initial part of each autocorrelation curve (first 1 s) was fit with an exponential decay function.

7.3.6 Processivity of wild-type pol V and pol V_{ICE391} *in vitro*

We have previously characterized the biochemical properties of *E. coli* pol V and found that it shows optimal activity *in vitro* in the presence of a RecA* filament where it forms a pol V Mut complex ($UmuD'_2C$–RecA–ATP). In the presence of the β/γ-complex and single-strand DNA-binding protein (SSB) pol V Mut readily catalyzes DNA replication on circular DNA templates (37, 38, 52, 53).

To compare the processivity of wild-type pol V and pol V_{ICE391} *in vitro* and ensure that reaction products were generated from a single polymerase-binding event, we (i) used at least 20-fold excess of primer-templates over polymerase and (ii) carried out reactions in the absence of additional RecA* (to prevent pol V Mut re-activation). However, even at the lowest enzyme-to-substrate ratios, i.e., conditions that prevent re-initiation of primer extension on previously used primer-templates, the termination probabilities at most template positions changed depending on incubation time, and therefore, accurate quantification of these values is not feasible. Nevertheless, we can conclude that like pol V, pol V_{ICE391} is moderately processive (Fig. 5), generating replication products of several hundred nucleotides in length per single polymerase-binding event by ~3 minutes after the reaction was initiated. As seen in Fig. 5, both pol V and pol V_{ICE391} synthesized replication products with lengths gradually increasing over the 16-minute incubation period, while the overall primer utilization remained constant at all time points. The presence of strong pause sites along the DNA template, especially opposite the first ~30 bases and the fact that the length of replication products increases over at least 16 minutes, indicate that both polymerases, despite being moderately processive, are very slow. Indeed, we previously reported that the velocity of pol V-catalyzed DNA synthesis was ~0.3–1 nucleotides per second (37). Under the same experimental conditions, pol V_{ICE391} appears to synthesize DNA with a faster velocity than pol V, inserting ~1.75-2 nucleotides per second (Fig. 5). As a result, pol V_{ICE391} synthesizes substantially longer DNA products compared to pol V at the same time point. This is best seen at shorter incubation times (Fig. 5). For example, 20 seconds after initiation of the reactions catalyzed by pol V and pol V_{ICE391}, the primers were extended by up to ~14 and ~30 nucleotides, respectively.

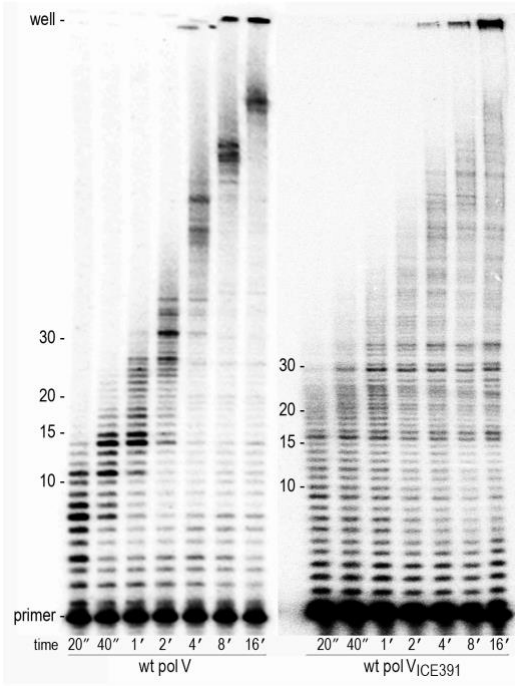

Fig. 5. Processivity and velocity of pol V and pol V_{ICE391}-catalyzed DNA synthesis. RecA was incubated for 3 min at 37°C with biotinylated 48-mer single-stranded oligonucleotide linked to streptavidin-coated agarose resin in the presence of ATPγS to generate RecA* (RecA nucleoprotein filament). Purified wild-type pol V or pol V_{ICE391} were combined with RecA* and the resulting pol V Mut complexes were purified by centrifugation. 100 pM pol V Mut or pol V_{ICE391} Mut were added to the reaction mixtures containing 1 mM ATP, 50 μM dNTPs, 2 nM primed ssDNA templates, 100 nM SSB, 50 nM β-clamp and 5 nM γ-complex. Primer extensions were carried out at 37°C for 20s, 40s, 1, 2, 4, 8, or 16 min and analyzed by PAGE. Position of the bands corresponding to the unextended primers (pr), or primers elongated by 5-30 nucleotides, as well as the position of the wells are indicated on the left side of the gel.

7.3.7 Comparison of wild-type pol V_{ICE391} and pol V_{ICE391}_Y13A *in vitro*

Next, we compared the enzymatic properties of wild-type pol V_{ICE391} to the steric gate variant, pol V_{ICE391}_Y13A *in vitro* (Fig. 6). We have demonstrated previously that pol V exhibits an exceptional ability to misincorporate ribonucleotides into DNA *in vitro* (24). Thus, we initially assumed that pol V_{ICE391} would discriminate against ribonucleotide incorporation as poorly as pol V. To test this hypothesis, we compared primer extension reactions in the presence of dNTPs and rNTPs (Fig. 6A, lanes 1-15). Unexpectedly, the amount and size distribution of reaction products accumulated after incubation with ATP alone, or after addition of all four NTPs, were almost identical (Fig. 6A, lanes 1-5 and 11-15). The efficiency of nucleotide incorporation and rate of the reactions with rNTPs were much lower compared to the reactions with dNTPs. For example, pol V_{ICE391} which was able to incorporate as many as 2 dNTPs every second, synthesized RNA with a rate of ~18 rNTPs per min.

We therefore conclude that pol V_{ICE391} has much more stringent sugar discrimination compared to pol V. This hypothesis can be supported by the comparison of the products of primer elongation reactions carried out in the presence of ribo- or deoxyribonucleotides with and without subsequent alkali treatment under conditions that completely hydrolyze DNA chains at the positions of rNTP insertion (Fig. 6A, lanes

4 & 5, 9 & 10, and 14 & 15). Indeed, although the reactions were carried out in the presence of ATP in 10-fold excess, pol V_{ICE391} preferred to incorporate dNTP, as judged by the negligible alkali sensitivity of reaction products (Fig. 6A, lane 10). Furthermore, products of reactions with ATP alone, or a mixture of four NTPs were only partially sensitive to alkali cleavage as judged by the presence of bands corresponding to primers elongated by 2-5 nucleotides (Fig. 6A, lanes 5, 10, and 15). These data suggest that wild-type pol V_{ICE391} discriminates against nucleotides with the wrong sugar so effectively that it prefers to incorporate dNTPs present in only miniscule amounts within the reactions (as a contaminant of NTPs).

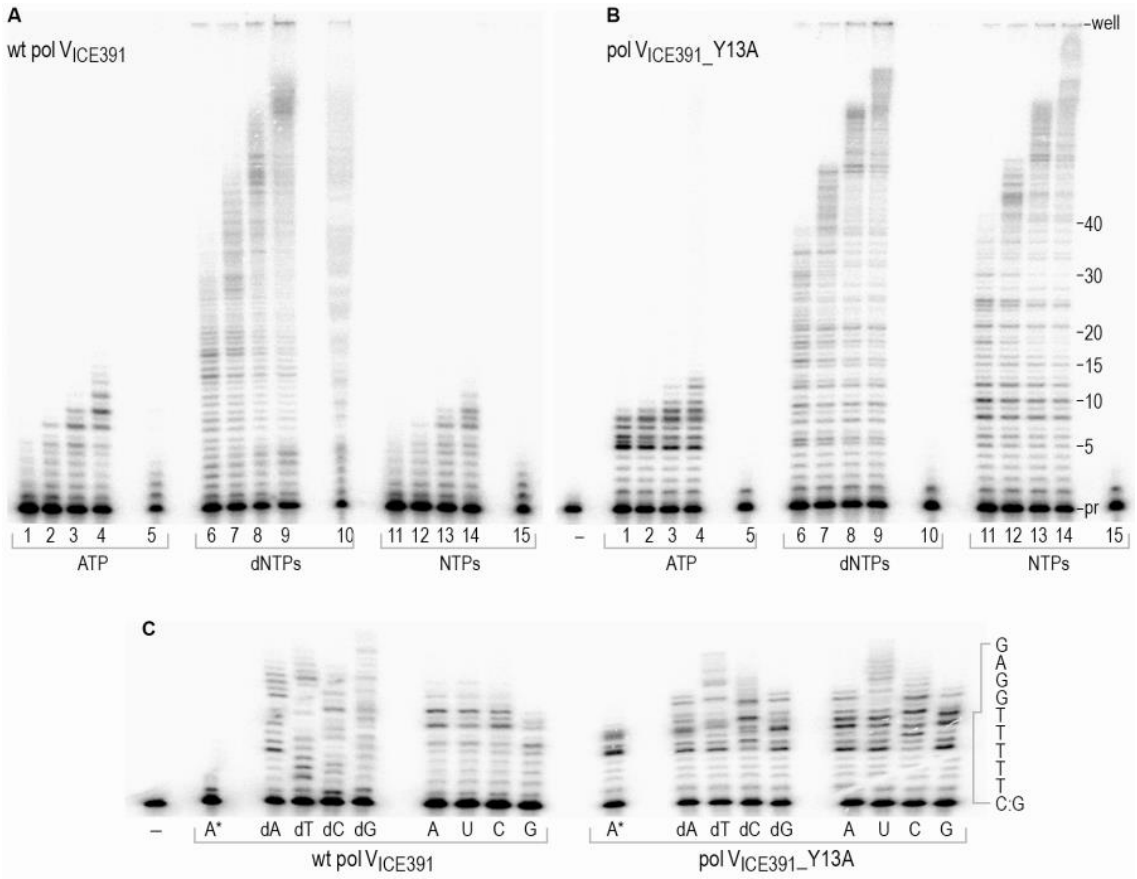

Fig. 6. Effect of a Y13A RumB substitution on the biochemical properties of pol V_{ICE391}. Primer extensions catalyzed by purified wild-type pol V_{ICE391} (**A**) and its Y13A steric gate variant (**B**) were carried out for 20s, 1, 3, or 10 min (lanes 1–4, 6-9, 11-14 respectively) under optimal conditions. Reactions incubated for 10 min were split into two and treated with either 0.3 M KCl (lanes 4, 9, and 14) or 0.3 M KOH (lanes 5, 10, and 15) for 2 h at 55°C. All reactions contained 1 mM ATP and were performed either in the absence of additional nucleotide (lanes 1-5, indicated as "A") or in the presence of 100 μM mixture of four dNTPs (lanes 6-10) or rNTPs (lanes 11-15). Lane with reaction mixture lacking polymerase is indicated by dash (–). Position of the bands corresponding to the unextended primers (pr) or primers elongated by 5-40 nucleotides, as well as position of the wells are indicated on the right side of the gel. (**C**). Specificity of nucleotide incorporation by wild-type pol V_{ICE391} and steric gate mutant pol V_{ICE391}_Y13A. All reactions contained 1 mM ATP. Lane with reaction lacking polymerase is indicated by dash (-) and reactions with no additional nucleotide are indicated as "A*". These reactions were terminated immediately after combining all components. Reactions in the presence of 100 μM of each nucleotide individually were carried out for 5 min. Identity of the nucleotide added to the reaction is shown below each lane. The extended sequence of templates with 5 consecutive Ts adjacent to the 3'

primer end, is indicated to the right of the gel panel. The results presented are representative of several independent experiments.

We then determined the effect of the substitution of the steric gate residue on the *in vitro* properties of pol V_{ICE391}. The wild-type and mutant polymerases had similar overall catalytic parameters of DNA synthesis, i.e., the percent of extended primers reached comparable levels for both polymerases when reactions were performed at equal enzyme/template ratios (Figs. 6A & 6B). However, pol V_{ICE391}_Y13A also had a distinct pattern of size distribution of replication products, i.e. at several positions, reaction products consisted of two bands with slightly different electrophoretic mobility (see for example doublet bands opposite the template T at the position +5, Fig. 6B, lanes 6-9). This pattern suggests that pol V_{ICE391}_Y13A catalyzes a significant degree of misincorporation opposite these sites.

As anticipated, the Y13A substitution compromised the sugar selectivity of the enzyme leading to a dramatically enhanced ability to insert rNTPs (Fig. 6B). An estimate for the time-dependent product accumulation revealed that pol V_{ICE391}_Y13A synthesized RNA with ~7 times faster rates relative to the wild-type enzyme. This is best illustrated by comparison of the products of the reactions terminated immediately after combining all ingredients (Fig. 6C, lanes labeled as "A*"). pol V_{ICE391}_Y13A promptly inserted as many as 7 AMPs, while the wild-type polymerase barely elongated primers by one ribonucleotide. DNA replication by pol V_{ICE391}_Y13A using different nucleotide substrates (NTPs and dNTPs) was not identical. For example, we detected several transient pauses specific for RNA synthesis (such as seen at positions 8 and 10). However, the velocities of DNA and RNA synthesis by pol V_{ICE391}_Y13A, length distribution of reaction products, and the maximum size of synthesized DNA and RNA were similar. In reactions where dNTPs competed with ATP present at 10-fold excess, pol V_{ICE391}_Y13A exclusively incorporated ATPs, at least opposite the first T (the first available template base). As seen in Fig. 6B, all reaction products were digested by alkali hydrolysis independently of nucleotide substrate used (lanes 5, 10, and 15).

The fidelity of the wild-type and steric gate mutant pol V_{ICE391} were compared in reactions containing each nucleotide individually (Fig. 6C). These assays suggest that both enzymes are highly error-prone and are capable of incorporating multiple wrong dNTPs. The main difference is seen in reactions performed in the presence of a single dNTP. In contrast to the wild type enzyme, pol V_{ICE391}_Y13A preferentially selects the correctly-paired ribonucleotide (ATP) rather than incorporating the correct, or incorrect dNTP. Thus, when a single dNTP was added to the reaction mixture containing pol V_{ICE391}_Y13A, ATP and DNA template with five consecutive Ts adjacent to the 3' primer terminus, primers were extended by incorporation of at least five sequential ATPs (Fig. 6C, note similar pattern of product distribution opposite the first five template bases in all reactions with pol V_{ICE391}_Y13A).

We conclude that the major difference between wild-type pol V_{ICE391}, and the pol V_{ICE391}_Y13A mutant is the ability of the steric gate mutant to readily incorporate polyribonucleotides into DNA.

7.3.8 pol V_{ICE391} _Y13A-dependent spontaneous mutagenesis

To investigate ribonucleotide incorporation by pol V_{ICE391} _Y13A in *E. coli*, we measured spontaneous His^+ mutagenesis in a *recA730 lexA*(Def) Δ*dinB* Δ*umuDC* strain. Although *recA730* is thought to be in a constitutively activated state (RecA730*), this activity can be up- or down- regulated, depending upon the genetic background of the strain (54) which leads to different levels of pol V-dependent spontaneous mutagenesis (26). The highest level of pol V-dependent mutagenesis was observed in a Δ*rnhA* strain, which we attribute to a stronger RecA730* activating signal in this background, due to impaired replication in the absence of RNase HI, which is a pre-requisite for SOS induction. Wild-type pol V_{ICE391} exhibited high levels of spontaneous mutagenesis in all strain backgrounds. There was also an indication of the Δ*rnhA*-associated mutagenesis increase, but due to the high (>3000) number of mutants per plate, accurate quantification was unachievable (Table 3, line 3).

As observed previously with the *E. coli* pol V_Y11A mutant (26), the pol V_{ICE391}_Y13A mutant exhibited a significant (~100-fold) reduction in spontaneous mutagenesis compared to wild-type pol V_{ICE391} (Table 3, line 1). This phenotype is attributed to efficient RER targeted to misincorporated ribonucleotides, but also concomitant removal of misincorporated deoxyribonucleotides, so as to lower the overall level of spontaneous mutagenesis. In *E. coli* cells lacking RNase HII (Δ*rnhB*), pol V_{ICE391}_Y13A His^+ mutagenesis was restored from less than 1% to ~10% of wild-type pol V_{ICE391} levels (Table 3, line 2). Inactivation of RNase HI, or NER alone, had minimal effect on the level of mutagenesis promoted by pol V_{ICE391}_Y13A, which is in agreement with a lead role for RNase HII in RER (Table 3, line 2). A concomitant RNase HII-NER deficiency (Δ*rnhB* Δ*uvrA*) restored spontaneous mutagenesis to ~17% of wild-type pol V_{ICE391} (Table 3, line 4), suggesting that NER provides compensatory RER functions when RNase HII is overwhelmed, or inactivated (26). These findings therefore support the idea that errant ribonucleotides misincorporated by pol V_{ICE391}_Y13A stimulate RER mechanisms that also result in the removal of misincorporated deoxyribonucleotides.

Intriguingly, spontaneous mutagenesis promoted by pol V_{ICE391}_Y13A was not restored to the same extent as that observed for pol V_Y11A in the Δ*rnhB* or Δ*rnhB* Δ*uvrA* strains (~10% versus 31%, and ~17% versus 62%, respectively) (Table 3). We interpret these observations to indicate that RER pathways remain active, despite the loss of RNase HII and NER functions. Our previous studies with pol V_Y11A suggest that RNase HI plays a back-up role in RER in *E. coli*, but given that pol V_{ICE391}_Y13A has greater access to DNA than pol V (Figs. 1-4) and is also more likely to misincorporate consecutive ribonucleotides (Fig. 6), we suggest the back-up role of RNase HI is much more critical under these circumstances.

We were unable to stably introduce the pol V_{ICE391}_Y13A plasmid, pJM1282, into Δ*rnhB* Δ*rnhA*, or Δ*rnhB* Δ*rnhA* Δ*uvrA* strains when grown at either 30°C or 37°C. In these instances, the transformation efficiency of pJM1282 was ~1/200 of that of pRW320 (wild-type pol V_{ICE391}) and resulted in only a handful of transformants. These transformants exhibited very slow growth and differing colony morphology. Furthermore, restriction digests of pJM1282 purified from the Δ*rnhB* Δ*rnhA*, or Δ*rnhB* Δ*rnhA* Δ*uvrA* strains did not match that of the parental pRW320 (Supplemental Fig. 2), suggesting increased plasmid instability under these conditions. No such instability was observed when the pol

V_Y11A steric gate mutant was introduced into the Δ*rnhB* Δ*rnhA* Δ*uvrA* strain. The pJM1282 plasmid instability observed in the Δ*rnhB* Δ*rnhA*, or Δ*rnhB* Δ*rnhA* Δ*uvrA* strains is therefore directly attributed to the enhanced ability of pol V_{ICE391}_Y13A to incorporate (poly)ribonucleotides into the *E.coli* genome.

7.3.9 Leading vs lagging strand mutagenesis

To test the efficiency of RER pathways on both DNA strands in strains expressing pol V_{ICE391}_Y13A, we employed a genetic system that allows us to determine the leading- and lagging- DNA strand replication fidelity (33). The system is based on the measurement of mutagenesis in the *lacZ* reporter gene which is integrated into the bacterial chromosome in one of two orientations with respect to the origin of replication. The target sequence is replicated as a leading strand in one orientation and as a lagging strand in the other orientation. The differences in mutant frequencies between the two orientations reflect the replication fidelity of the leading and lagging DNA strand. We assayed a *lacZ* allele that reverts via an A·T→T·A transversion (32), as such substitutions are the predominating pol V-dependent mutagenic events observed in a *recA730 lexA*(Def) background (55, 56).

As shown in Table 4, expression of the wild-type pol V_{ICE391} from a low-copy-number plasmid in the *recA730 lexA*(Def) background resulted in a much stronger mutator effect on the lagging-strand (591.2 x 10^8) than on the leading- strand (28.9 x 10^8). While this observation is consistent with previously published data for wild-type pol V in a *recA730* background (11), we note that the level of mutagenesis on the lagging strand in the presence of pol V_{ICE391} is approximately 10-fold higher than that observed with pol V (unpublished observations) which again emphasizes the enhanced capacity of pol V_{ICE391} to promote SOS-dependent mutagenesis compared to pol V. In contrast, mutagenesis in the presence of the pol V_{ICE391}_Y13A mutant was notably reduced on both DNA strands, down to 3% of that observed for the wild-type on the leading- and to 0.1% on the lagging-strand. As previously proposed for the pol V_Y11A steric gate mutant (25, 26), the reduction in mutagenesis is consistent with ribonucleotide-induced RER that removes misincorporated ribonucleotides, but also deoxyribonucleotides in their vicinity. The analysis of pol V_{ICE391}_Y13A –dependent mutagenesis levels in strains deficient in RNase HII and/or NER support this hypothesis. Importantly, a significant increase in mutagenesis was observed in strains lacking RNase HII (Δ*rnhB*), which is in agreement with the primary role of RNase HII-mediated RER (26). The lack of RNase HII in strains expressing pol V_{ICE391}_Y13A significantly increases the relative mutagenesis compared to wild-type pol V_{ICE391} on the leading strand (up to 50% of that observed for the wild-type pol V_{ICE391}). The relative amount of pol V_{ICE391}_Y13A mutagenesis is also increased on the lagging strand, but only to ~1% of that of the wild-type pol $V_{ICE391.}$ These data suggest that RNase HII plays a major role in RER on the leading strand, whereas pol V_{ICE391}_Y13A –dependent mutagenesis on the lagging strand is kept to a minimum by other ribonucleotide-directed repair pathways (e.g. NER, and RNase HI). Interestingly, upon inactivation of both RNase HII-dependent RER and NER, the amount of relative mutagenesis is increased to 79% on the leading- but only to 4% on the lagging- strand, suggesting that RER is still very efficient on the lagging strand, even in the absence of RNase HII and NER. We hypothesize that this is most likely due to efficient RNase HI-dependent RER that mistakes the polyribonucleotide tracts generated by pol V_{ICE391}_Y13A as primers for Okazaki fragment synthesis generated during normal genome duplication.

7.4 Discussion

pol V_{ICE391} is a pol V ortholog, which when sub-cloned from its native ICE391 environment, becomes a very potent, highly mutagenic DNA polymerase (29, 30). The molecular basis for the enhanced activity leading to 3-5 fold higher levels of SOS-dependent mutagenesis compared to *E. coli* pol V has been of great interest to us for over two decades (29). Since *E. coli* pol V activity is kept to a minimum though a plethora of regulatory steps (7), it is easy to envisage that pol V_{ICE391} activity could be enhanced by its differential regulation compared to *E. coli* pol V at any of these stages. Indeed, we have recently shown that in addition to LexA-controlled transcriptional regulation, pol V_{ICE391} is subject to transcriptional control by the ICE391-encoded SetR protein (57).

Here, we show that the enhanced mutagenesis is likely due to two factors; 1) *in vitro*, pol V_{ICE391} replicates DNA ~2 to 6-fold faster than *E. coli* pol V (Fig. 6); 2) both pol V and pol V_{ICE391} bind repetitively to specific sites on the nucleoid, but with each cycle pol V_{ICE391} resides on the DNA for significantly longer than pol V (Fig. 4). Based upon these observations, low-fidelity pol V_{ICE391} would be expected to duplicate significantly more of the *E. coli* genome, which helps explain why pol V_{ICE391} promotes higher levels of mutagenesis than *E. coli* pol V, despite exhibiting a similar fidelity of DNA synthesis *in vitro*. However, we cannot exclude the possibility of yet-to-be discovered differences in *E. coli* pol V and pol V_{ICE391} activity that may also contribute to the enhanced SOS-dependent mutator activity *in vivo*.

We have previously used a steric gate mutant of pol V to investigate the molecular mechanisms of RER in *E. coli* (25, 26). We suggested that the primary line of defense against ribonucleotides that have been incorporated by steric gate polymerase mutants is RNase HII-mediated RER, with back-up roles provided by RNase HI and NER proteins. Based upon the fact that we restored the level of spontaneous mutagenesis promoted by the pol V_Y11A mutant to that promoted by wild-type pol V, we assumed that we had identified the major participants involved in RER in *E. coli* (26). We were therefore interested in determining if similar phenotypes might be observed with a steric gate variant of pol V_{ICE391}, which as noted above, has greater longevity in replication foci than pol V, and would therefore be expected to dramatically increase the number of errantly misincorporated ribonucleotides into the *E. coli* genome.

Similar to our earlier studies with *E. coli* pol V and a steric gate pol V_Y11A mutant (26), our *in vitro* assays indicate that both pol V_{ICE391} and pol V_{ICE391}_Y13A exhibit low fidelity DNA synthesis (Fig. 6) and both would be expected to promote high levels of spontaneous mutagenesis in a *recA730 lexA*(Def) strain if RER-functions were inactivated. Lower levels of pol V_{ICE391}_Y13A-dependent mutagenesis are therefore indicative of active RER which, during RER-patch re-synthesis, can replace incorrect deoxyribonucleotides located in the vicinity of a target ribonucleotide. Our studies using strains with deletions in *rnhB, rnhA* and *uvrA* alone, confirm that the principal pathway involved in the repair of misincorporated ribonucleotides is RNase HII-mediated RER, since there was an increase in pol V_{ICE391}_Y13A dependent mutagenesis in the Δ*rnhB* strain, but not the Δ*rnhA* or Δ*uvrA* strains (Table 3). However, the level of restoration (10% of that seen with wild-type pol V_{ICE391}) was significantly lower than observed with pol V and its steric gate mutant (Table 3). Further differences were observed in the Δ*rnhB* Δ*uvrA* strain, where pol V_{ICE391}_Y13A mutagenesis was just 17% of the wild-type pol V_{ICE391} compared to 62% for pol V_Y11A vs. wild-type pol V (Table 3), suggesting efficient RER, even in the absence of RNase HII, or NER proteins. The most likely candidate

expected to compensate for the loss of RNase HII-dependent RER is *rnhA* encoded- RNase HI, since Δ*rnhB* strains expressing pol V_{ICE391}_Y13A and lacking *rnhA*-encoded RNase HI exhibit increased genomic/plasmid instability (Supplemental Fig. 2). This is in contrast to pol V_Y11A strains that show no-such instability even in the absence of RNase HII, RNase HI and NER proteins (26). We therefore conclude that under circumstances where there is a significant increase in misincorporated ribonucleotides into the *E.coli* genome and the compromise of primary RNase HII-mediated RER pathway, RNase HI may play an essential role in protecting *E. coli* from the genomic instability caused by errant misincorporation of ribonucleotides. We have tacitly assumed that it reflects a simple threshold for the level of misincorporated ribonucleotides in its genome, but we cannot formally exclude the possibility that it is also the type of ribonucleotide (mono- vs. poly-), or the location (such as better access to the lagging strand, or at alternate origins) that leads to a greater dependency on RNase HI for genome stability in the absence of RNase HII.

7.5 Tables and legends

Table 1. *E. coli* strains used in this study

Strain	Relevant Genotype	Source or Reference
MG1655	F- λ^- *rph*-	*E. coli* Genetic Stock Center
JJC5945	F- λ^- *rph- dnaX-YPet*::kan	Benedict Michel, (58)
BW72761	*Hfr(PO2A) leu-63::Tn10 fhuA22 Δ(argF-lac)169 ompF627 relA1 spoT1*	*E. coli* Genetic Stock Center
RW82	Δ*(umuDC)595*::*cat*	(59)
RW880	F- λ^- *rph-* Δ*(umuDC)595*::*cat*	MG1655 x P1.RW82
SSH037	F- λ^- *rph- dnaX-YPet*::kan Δ*(umuDC)595*::*cat*	JJC5945 x P1.RW880
SSH073	as SSH037, but harboring pJM1337	This work
SSH074	as SSH037, but harboring pJM1350	This work
EAW287	F- λ^- *rph- recA730 sulA*-	(9)
SSH116	F- λ^- *rph- recA730 sulA- dnaX-YPet*	EAW287 x P1.AR164

SSH117	F- *λ⁻ rph- recA730 sulA- dnaX-YPet* Δ*(umuDC)595*::*cat*	SSH116 x P1.RW880
SSH118	as SSH117, but harboring pJM1324	This work
SSH119	as SSH117, but harboring pJM1334	This work
RW584[a]	*recA730 lexA51*(Def) Δ*(umuDC)596*::*ermGT*	(60)
RW1448[b,c]	*recA730 lexA51*(Def) Δ*(umuDC)596*::*ermGT* Δ*dinB61*::*ble*	RW698 x BW7261
NR9566	*dnaE915 yafC502*::Tn*10*	Roel Schaaper, (61)
RW1560[b]	*recA730 lexA51*(Def) Δ*(umuDC)596*::*ermGT* Δ*dinB61*::*ble dnaE915 yafC502*::Tn*10*	RW1448 x P1.NR9566
RW698[a]	*recA730 lexA51*(Def) Δ*(umuDC)596*::*ermGT* Δ*dinB61*::*ble*	(25)
RW838[a]	*recA730 lexA51*(Def) Δ*(umuDC)596*::*ermGT* Δ*dinB61*::*ble* Δ*rnhB782*::Kan	(25)
RW902[a]	*recA730 lexA51*(Def) Δ*(umuDC)596*::*ermGT* Δ*dinB61*::*ble* Δ*uvrA753*::Kan	(25)

RW1044[a]	*recA730 lexA51*(Def) Δ*(umuDC)596*::*ermGT* Δ*dinB61*::*ble* Δ*rnhA319*::*cat*	(25)
RW1092[a]	*recA730 lexA51*(Def) Δ*(umuDC)596*:: *ermGT* Δ*dinB61*::*ble* Δ*rnhB782* Δ*rnhA319*::*cat*	(25)
RW990[a]	*recA730 lexA51*(Def) Δ*(umuDC)596*::*ermGT* Δ*dinB61*::*ble* Δ*rnhB782* Δ*uvrA753*::Kan	(26)
RW1190[a]	*recA730 lexA51*(Def) Δ*(umuDC)596*::*ermGT* Δ*dinB61*::*ble* Δ*rnhB782* Δ*rnhA319*::*cat* Δ*uvrA753*::Kan	(26)
RW1450[b,c]	*recA730 lexA51*(Def) Δ*(umuDC)596*::*ermGT* Δ*dinB61*::*ble* Δ*rnhB782*::Kan	RW838 x BW7261
EC9998[b,c]	*recA730 lexA51*(Def) Δ*(umuDC)596*::*ermGT* Δ*dinB61*::*ble* Δ*uvrA753*::Kan	RW902 x BW7261
RW1510[b,c]	*recA730 lexA51*(Def) Δ*(umuDC)596*::*ermGT* Δ*dinB61*::*ble* Δ*rnhB782* Δ*uvrA753*::Kan	RW990 x BW7261

[a]: Full genotype: *thr-1 araD139* Δ*(gpt-proA)62 lacY1 tsx-33 glnV44 galK2 hisG4 rpsL31 xyl-5 mtl-1 argE3 thi-1 sulA211 lexA51*(Def) *recA730* Δ(*umuDC*)*596*::*ermGT* Δ*dinB61*::*ble*

[b]: As “a”, but *gpt*$^{+}$ *proA*$^{+}$ Δ*(argF-lac)169*

[c]: For the *lacZ* reversion assay, the above strains[b] were used to construct pairs of *lacZ* derivatives, as described in (33). These strains carry a chromosomal copy of the *lacZ* missense allele from strain CC105 (32), in one of the two orientations, with respect to the origin of replication (Left or Right).

Table 2. *E. coli* plasmids used in this study

Plasmid	Relevant Characteristics	Source or Reference
pGB2	Low-copy-number, Spc^R vector	(62)
pRW134	pGB2, *umuD'C*	(34)
pJM963	pGB2, *umuD'C*_Y11A [steric gate mutant]	(63)
pRW320	pGB2, *rumA'B*	(34)
pJM1282	pGB2, *rumA'B*_Y13A [steric gate mutant]	This work
pJM1324	pGB2, *rumA' mKate2-rumB*	This work
pJM1334	pGB2, *umuD' umuC-mKate2*	This work
pJM1347	pGB2, *rumA' mKate2-rumB*_D103A-E104A [catalytically dead]	This work
pJM1350	pGB2, *rumA' mKate2-rumB*_ Q358A-L361A-F364A [β-clamp mutant]	This work
pARA1	High copy, Amp^R, RumA′ expressed from the *Ara* promoter	(35)
pHRB1	pGB2, Kan^R, low expression of His-Tagged RumB	(35)
pJM1295	pHRB1, but expressing His-Tagged RumB_Y13A	This work

Table 3. Spontaneous mutagenesis promoted by wild type and steric gate variants of pol V and pol V_{ICE391} in *E. coli recA730 lexA*(Def) Δ*dinB* Δ*umuDC* strains

	Status of rNMP repair genes	pGB2	pol V homologs	Wild-type polymerase	Steric Gate polymerase	SG[a] % of WT
1	wt	3.2 ± 0.2	pol V	691 ± 9	73 ± 5	11
			pol V_{ICE391}	>3000	27 ± 3	<1
2	Δ*rnhB*	2.8 ± 0.6	pol V	671 ± 12	207 ± 4	31
			pol V_{ICE391}	>3000	338 ± 6	~10
3	Δ*rnhA*	2.7 ± 0.3	pol V	~3000	127 ± 3	~4
			pol V_{ICE391}	≫3000	14 ± 1	<0.5
4	Δ*uvrA*	2.9 ± 0.6	pol V	439 ± 2	65 ± 1	15
			pol V_{ICE391}	>3000	44 ± 1	~1.5
5	Δ*rnhB* Δ*uvrA*	2.9 ± 0.4	pol V	382 ± 14	236 ± 15	62
			pol V_{ICE391}	>3000	503 ± 67	~17

[a]: SG: Steric gate mutant polymerase

Table 4. Leading- and lagging- strand mutagenesis promoted by wild type and steric gate variant of pol V_{ICE391} determined by assaying *lacZ* reversion via an A·T→T·A transversion

	Status of rNMP repair genes	Strand	Frequency per10^8 cells		SG % of WT
			WT pol	SG pol	
1	wt	leading	28.9 ± 3.9	0.8 ± 0.3	3%
2		lagging	591.2 ± 58.4	0.3 ± 0.1	0.1%
3	Δ*rnhB*	leading	34.2 ± 5.8	17.2 ± 2.5	50%
4		lagging	575.1 ± 55.3	4.8 ± 0.9	0.8%
5	Δ*uvrA*	leading	22.4 ± 2.6	1.3 ± 0.3	6%
6		lagging	607.6 ± 86.7	2.0 ± 0.6	0.3%
7	Δ*rnhB*	leading	25.2 ± 3.4	19.9 ± 2.8	79%
8	Δ*uvrA*	lagging	435.1 ± 56.4	17.4 ± 2.4	4%

7.6 Supplementary Figures and Legends

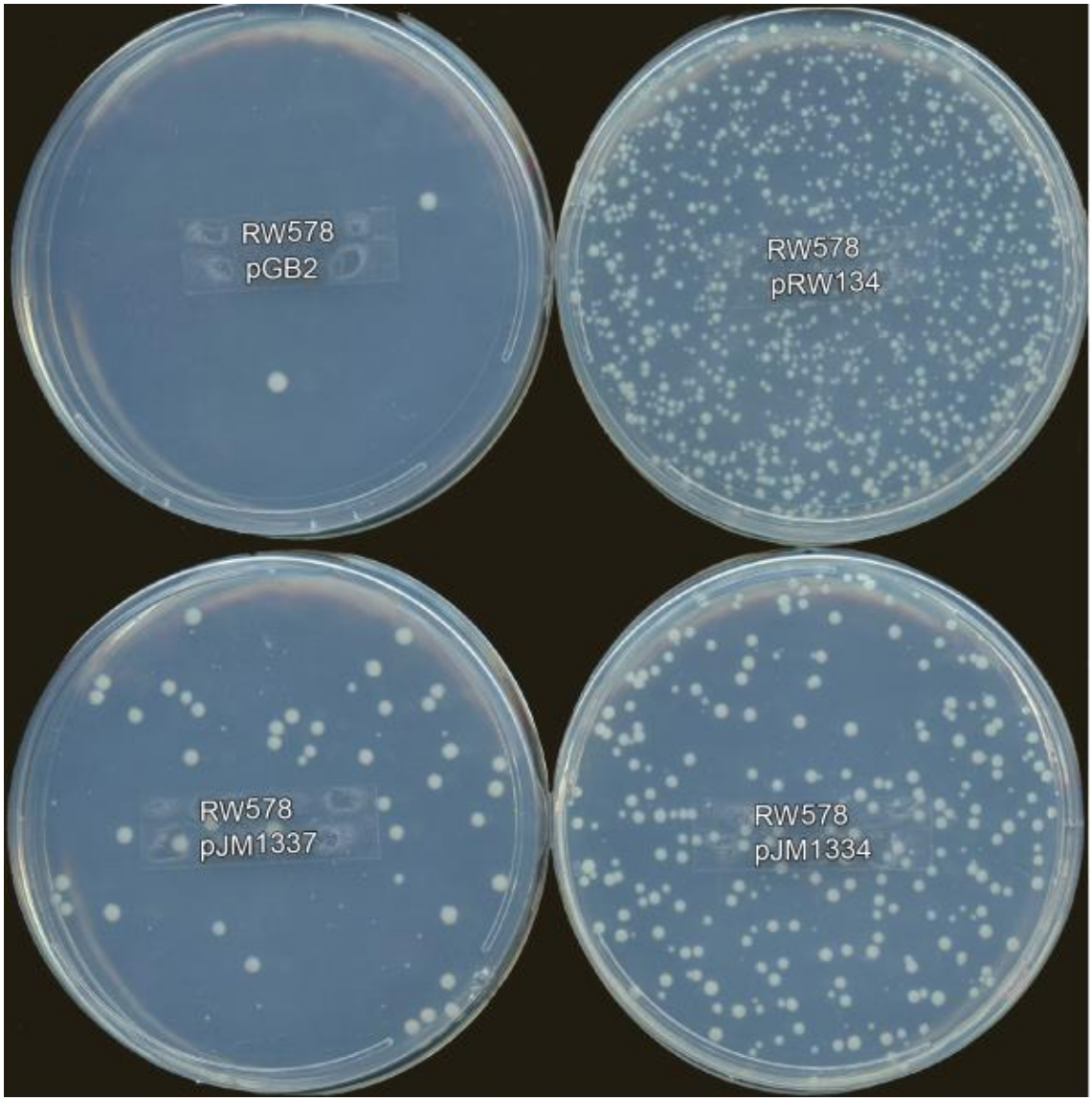

Supplemental Figure 1A: Spontaneous mutagenesis promoted by wild-type pol V and N- or C- terminal mKate2 fusion proteins. pGB2: Vector pRW134: Wild-type pol V (UmuD' - UmuC) pJM1337: UmuD' - mKate2-UmuC pJM1334: UmuD' - UmuC-mKate2 Colonies growing on the plate are His+ revertants and reflect the extent of spontaneous mutagenesis in the various strains.

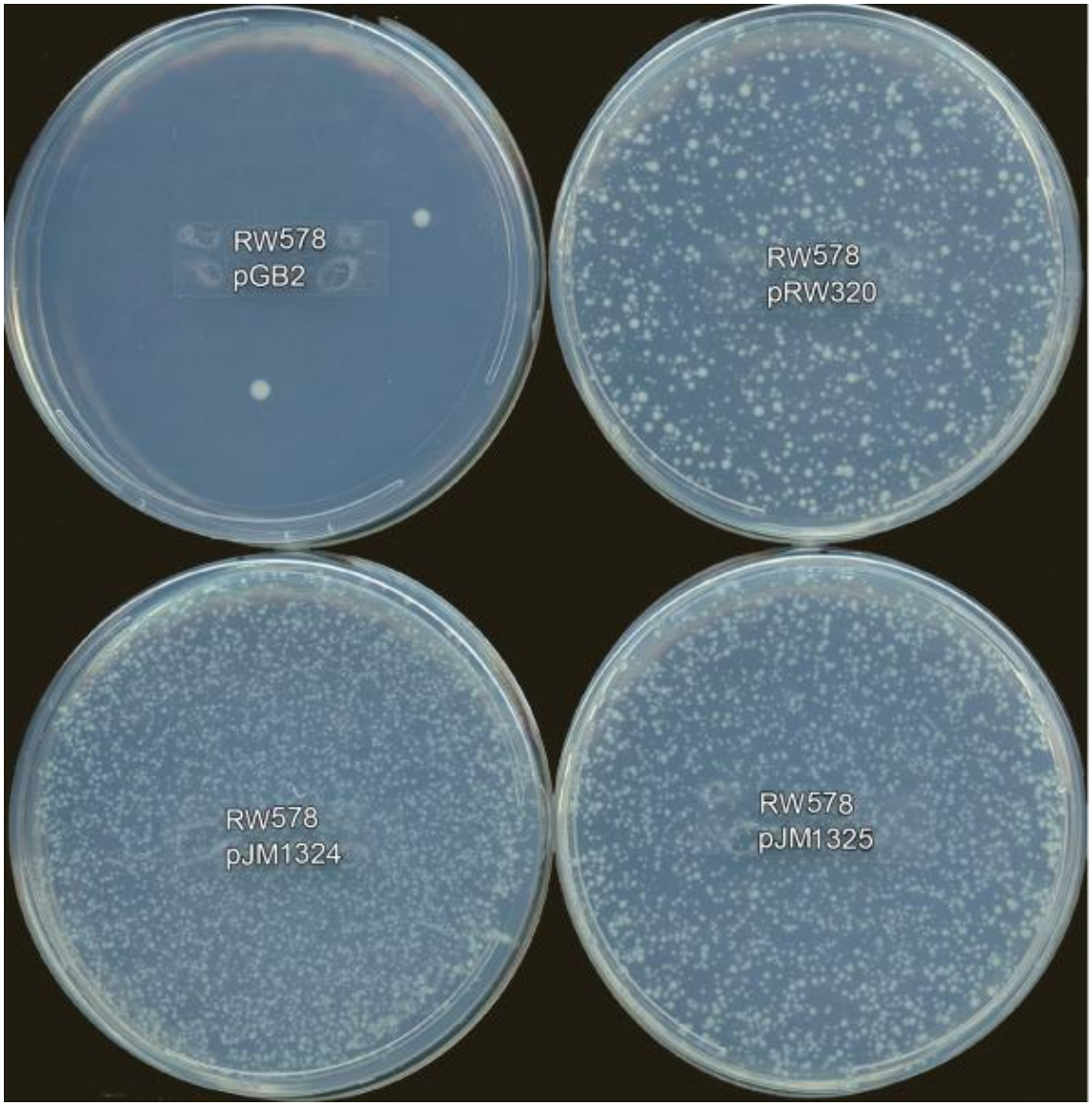

Supplemental Figure 1B: Spontaneous mutagenesis promoted by wild-type pol VICE391 and N- or C-terminal mKate2 fusion proteins. pGB2: Vector pRW320: Wild-type pol VICE391 (RumA' - RumB) pJM1324: RumA' - mKate2-RumB pJM1325: RumA' - RumB-mKate2 Colonies growing on the plate are His+ revertants and reflect the extent of spontaneous mutagenesis in the various strains.

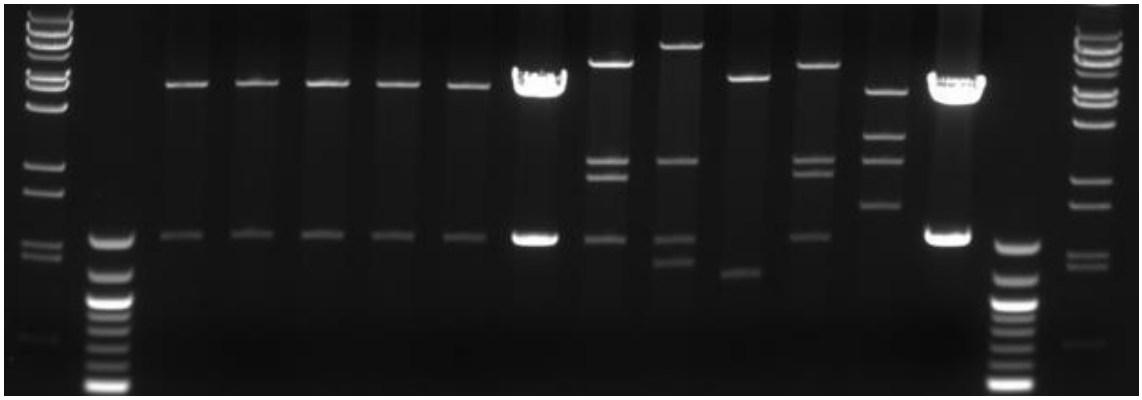

Supplemental Figure 2: Plasmid DNAs isolated from RW1190 (ΔrnhB ΔrnhA ΔuvrA). Lanes designated λ and 100 indicate lambda DNA BstEII digested marker and 100 bp marker (New England Biolabs). Plasmids pRW320 (wild-type RumA'-RumB) or pJM1282 (RumA'-RumB Y13A steric gate) were freshly transformed into RW1190 (ΔrnhB ΔrnhA ΔuvrA) and one-day old transformant colonies were inoculated into liquid LB and grown overnight. Miniprep DNA was prepared using the QIAprep Spin Miniprep Kit (Qiagen). Miniprep DNA was digested with the HindIII restriction enzyme (New England Biolabs) for an hour and subsequently electrophoresed on a 0.9% agarose gel. Lanes designated DH indicate stock midi-prep plasmid DNAs (HiSpeed Plasmid Midi Kit, Qiagen) isolated from DH5a which were also digested with HindIII. These stock plasmid DNAs were used for the transformations into RW1190. HindIII digest of intact plasmid pRW320, or pJM1282, should result in two DNA bands of ~4.4 kb and ~1.5 kb. None of the HindIII digests of the RW1190/pRW320 miniprep DNAs show any rearrangements. In contrast, all of the miniprep DNAs from RW1190/pJM1282 transformants showed various drastic rearrangements or deletions leading to the inactivation of the Pol VICE391_Y13A steric gate DNA polymerase.

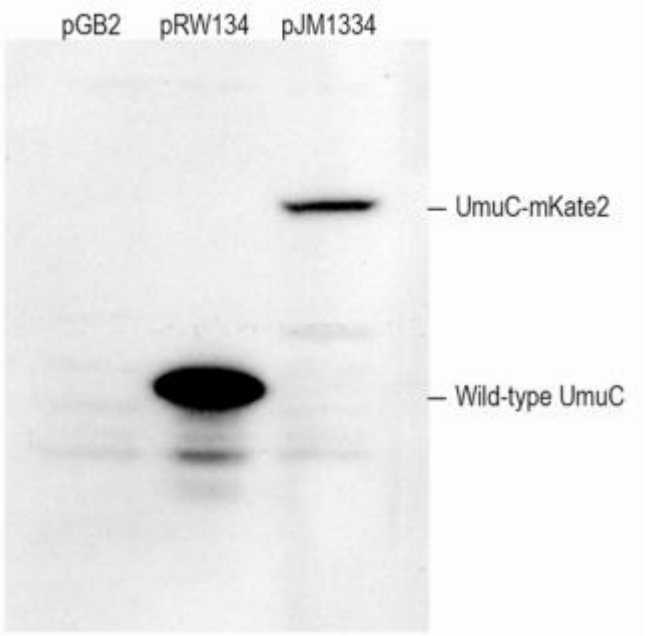

Supplemental Figure 3. Western blot of wild-type UmuC and UmuC-mKate2 expressed in RW584 (*recA730 lexA*(Def) Δ*umuDC*). pGB2: low copy vector. pRW134: wild-type UmuD'C expressed in pGB2. pJM1334: UmuD'-UmuC-mKate2 expressed in pGB2.

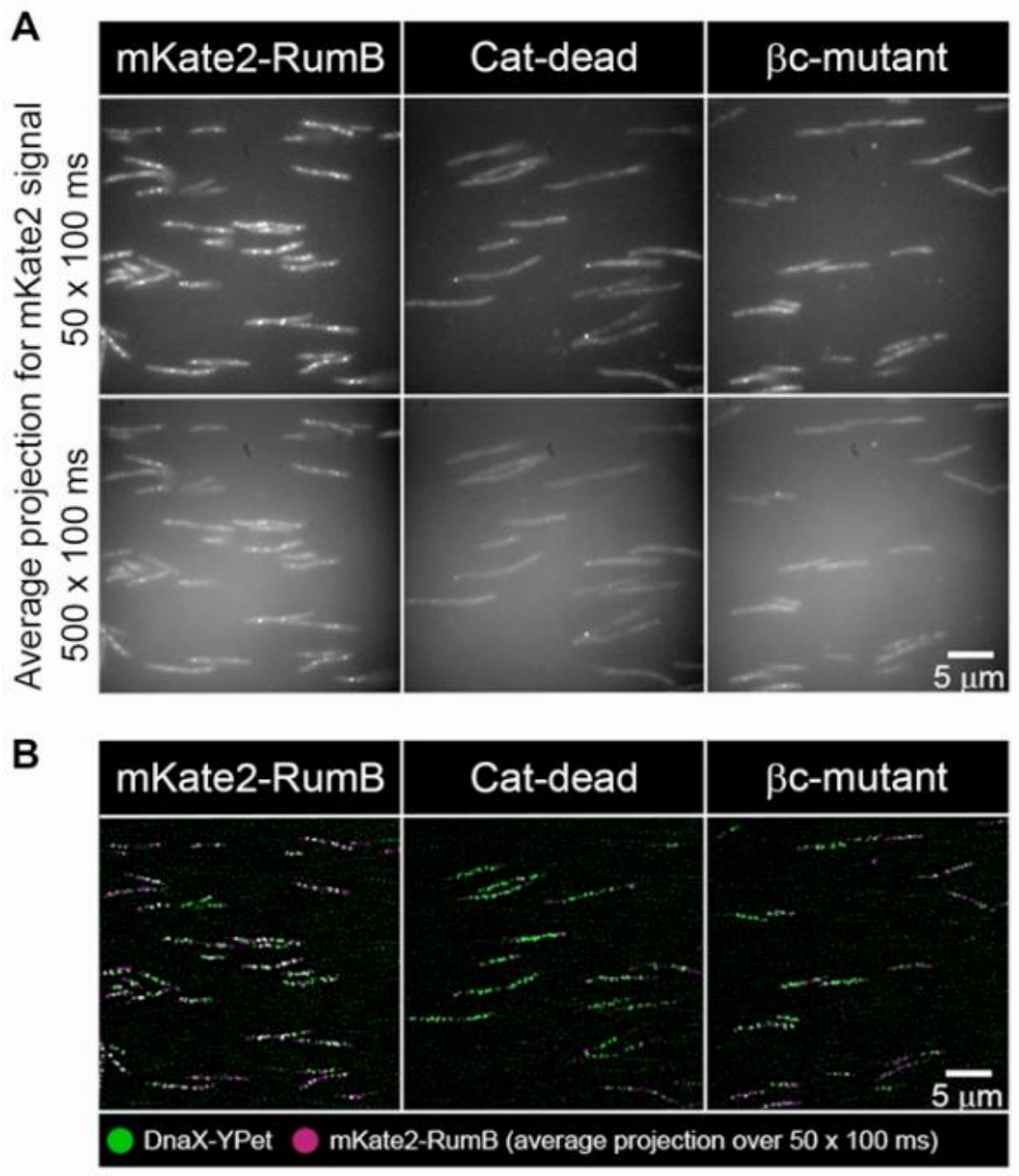

Supplemental Figure 4. Images of mKate2-RumB and catalytically inactive- or β-binding site variants in *ΔumuDC recA*$^{+}$ at 60-90 min after 10 J/m^2 UV light. A, Upper panels: Average projection over 5 s for mKate2-RumB and its catalytically dead and β- binding site mutant from left to right. Bottom panels: Average projection over 50 s for mKate2- RumB and its catalytically dead and β-binding site mutant from left to right. Scale bar: 5 µm. B, Merged images of DnaX-YPet (green) and mKate2-RumB and mutants (magenta, foci bound for 5 s). Scale bar: 5 µm.

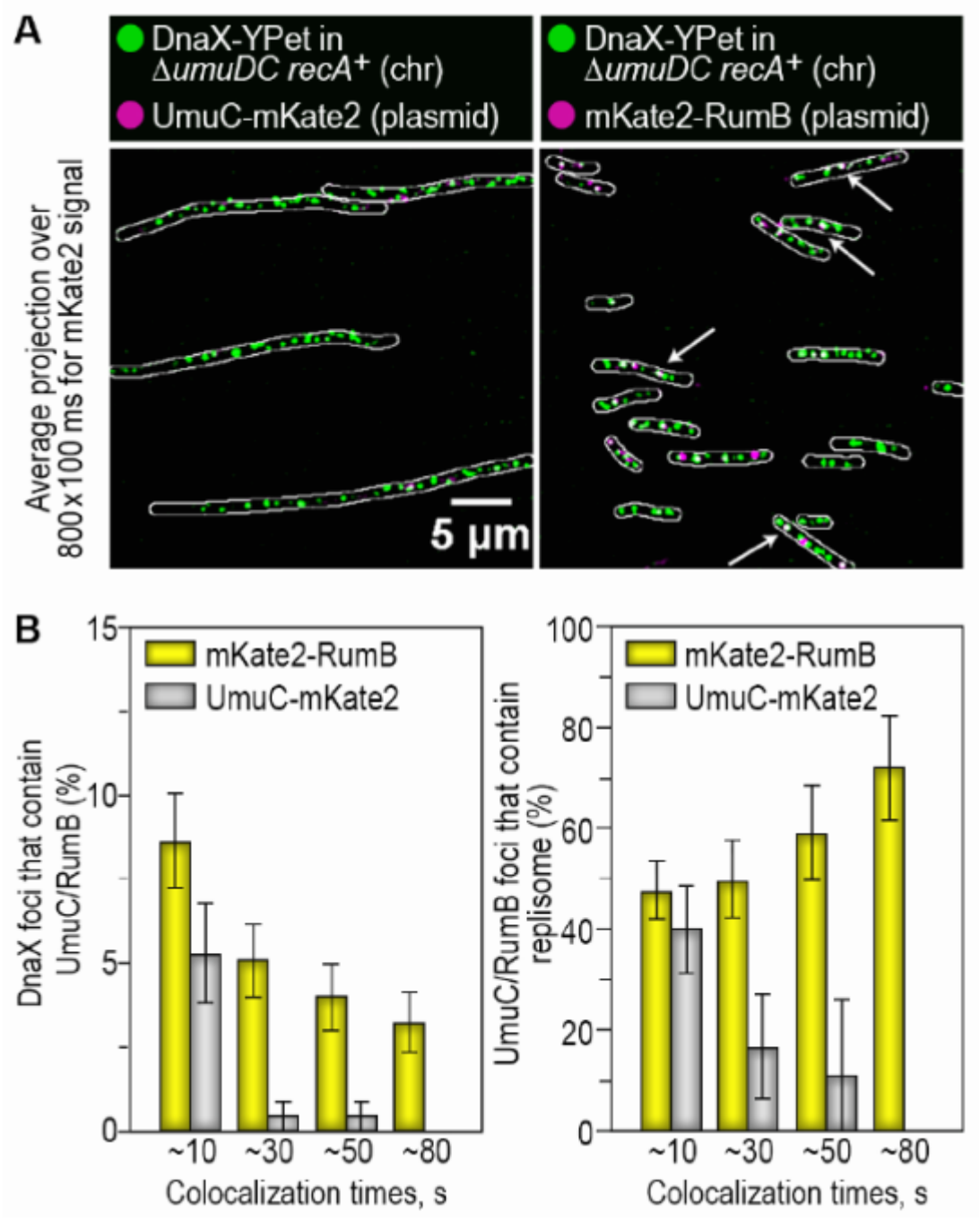

Supplemental Figure 5. Colocalization measurements of DnaX-YPet with UmuC-mKate2 or mKate2-RumB in a DumuDC recA strain 60-90 min after 10 J/m UV light. A, Left panel: Merged images of DnaX-YPet (green) and UmuC-mKate2 (magenta, foci bound for 30s). Right panel: Merged images of DnaX-YPet (green) and mKate2-RumB (magenta, foci bound for 30s). Scale bar: 5 µm. B, Left panel: Percentage of DnaX foci that contain a UmuC (grey), RumB focus (yellow) at different effective exposure times of 10, 30, 50 and 80s. Right panel: Percentage of UmuC (grey) or RumB foci (yellow), that overlap with DnaX foci at different effective exposure times of 10, 30, 50 and 80s.

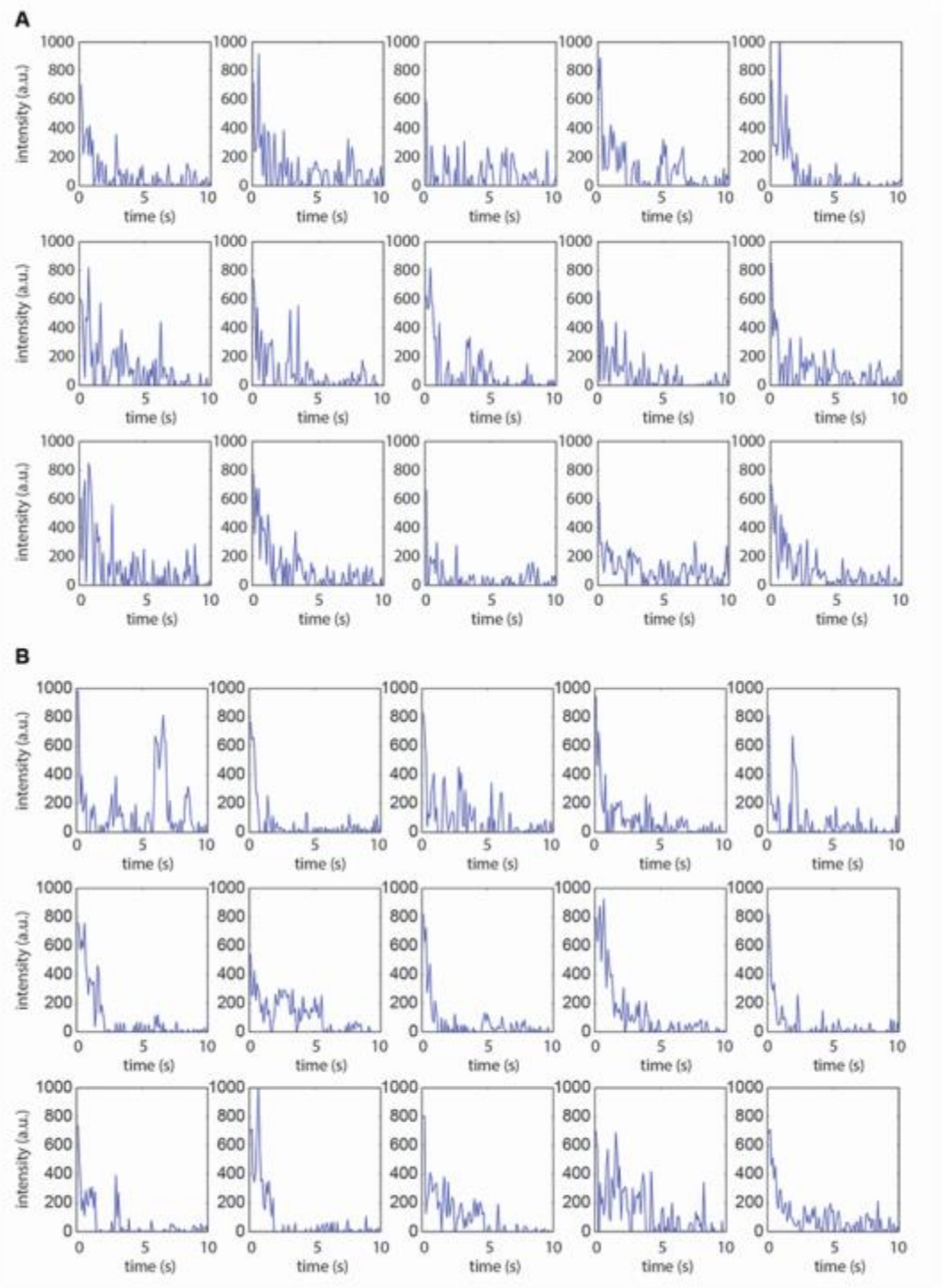

Supplemental Figure 6. Example intensity versus time trajectories for UmuC-mKate2 and mKate2-RumB signals at replisomal positions. Regions-of interest placed at DnaX-YPet markers were used to monitor fluctuations in UmuC- mKate2 and mKate2-RumB signals within fluorescence movies. Trajectories were locally background corrected to minimize the contributions of signals arising from molecules that were not bound in the vicinity of replisomes.

7.7 References

1. Tang M, Shen X, Frank EG, O'Donnell M, Woodgate R, Goodman MF, UmuD'$_2$C is an error-prone DNA polymerase, *Escherichia coli*, DNA pol V. *Proc Natl Acad Sci USA.* 1999;96:8919-8924.
2. Ohmori H, Friedberg EC, Fuchs RPP, Goodman MF, Hanaoka F, Hinkle D, Kunkel TA, Lawrence CW, Livneh Z, Nohmi T, Prakash L, Prakash S, Todo T, Walker GC, Wang Z, Woodgate R. The Y-family of DNA polymerases. *Mol Cell*. 2001;8:7-8.
3. Kato T, Shinoura Y. Isolation and characterization of mutants of *Escherichia coli* deficient in induction of mutations by ultraviolet light. *Mol Gen Genet*. 1997;156:121-131.
4. Steinborn G. Uvm mutants of *Escherichia coli* K12 deficient in UV mutagenesis. I. Isolation of *uvm* mutants and their phenotypical characterization in DNA repair and mutagenesis. *Mol Gen Genet*. 1978;165:87-93.
5. Woodgate R. Evolution of the two-step model for UV-mutagenesis. *Mutat Res.* 2001;485:83-92.
6. Jaszczur M, Bertram JG, Robinson A, van Oijen AM, Woodgate R, Cox MM, Goodman MF. Mutations for worse or better: low-fidelity DNA synthesis by SOS DNA polymerase V Is a tightly regulated double-edged sword. *Biochemistry*. 2016;55:2309-2318.
7. Goodman MF, McDonald JP, Jaszczur M.M, Woodgate R. Insights into the complex levels of regulation imposed on *Escherichia coli* DNA polymerase V. *DNA Repair*. 2016;44:42-50.
8. Sweasy JB, Witkin EM, Sinha N, Roegner-Maniscalco V. RecA protein of *Escherichia coli* has a third essential role in SOS mutator activity. *J Bacteriol*. 1990;172:3030-3036.
9. Robinson A, McDonald JP, Caldas VE, Patel M, Wood EA, Punter CM, Ghodke H, Cox MM, Woodgate R, Goodman MF, van Oijen AM. Regulation of mutagenic DNA polymerase V: activation in space and time. *PLoS Genet.* 2015;11:e1005482.
10. Fijalkowska IJ, Dunn RL, Schaaper RM. Genetic requirements and mutational specificity of the *Escherichia coli* SOS mutator activity. *J Bacteriol*. 1997;179:7435-7445.
11. Maliszewska-Tkaczyk M, Jonczyk P, Bialoskorska M, Schaaper RM, Fijalkowska IJ. SOS mutator activity: unequal mutagenesis on leading and lagging strands. *Proc Natl Acad Sci USA.* 2000;97:12678-12683.
12. Neuhard J, Nygaard P. Purines and pyrimidines, in: J.L. Ingraham, K.B. Low, F.C. Neidhardt, B. Magasanik, M. Schaechter, H.E. Umbarger (Eds.) EcoSal:*Escherichia coli* and *Salmonella*, Cellular and Molecular Biology, American Society for Microbiology, Washington D.C., 1987, pp. 445-473.
13. Buckstein MH, He J, Rubin H. Characterization of nucleotide pools as a function of physiological state in *Escherichia coli*. *J Bacteriol*. 2008;190:718-726.
14. Ferraro P, Franzolin E, Pontarin G, Reichard P, Bianchi V. Quantitation of cellular deoxynucleoside triphosphates. *Nucleic Acids Res*. 2010;38:e85.
15. Joyce CM. Choosing the right sugar: how polymerases select a nucleotide substrate. *Proc Natl Acad Sci USA*. 1997;94:1619-1622.

16. Astatke M, Ng K, Grindley ND, Joyce CM. A single side chain prevents *Escherichia coli* DNA polymerase I (Klenow fragment) from incorporating ribonucleotides. *Proc Natl Acad Sci USA*. 1998;95:3402-3407.
17. Vaisman A, Woodgate R. Redundancy in ribonucleotide excision repair: Competition, compensation, and cooperation. *DNA Repair*. 2015;29:74-82.
18. Nick McElhinny SA, Kumar D, Clark AB, Watt DL, Watts BE, Lundstrom EB, Johansson E,. Chabes A, Kunkel TA. Genome instability due to ribonucleotide incorporation into DNA *Nat Chem Biol*. 2010;6:774-781.
19. Nick McElhinny SA, Watts BE, Kumar D, Watt DL, Lundstrom EB, Burgers PM, Johansson E, Chabes A, Kunkel TA. Abundant ribonucleotide incorporation into DNA by yeast replicative polymerases. *Proc Natl Acad Sci USA*. 2010;107:4949-4954.
20. Lazzaro F, Novarina D, Amara F, Watt DL, Stone JE, Costanzo V, Burgers PM, Kunkel TA, Plevani P, Muzi-Falconi M. RNase H and postreplication repair protect cells from ribonucleotides incorporated in DNA. *Mol Cell.* 2012;45:99-110.
21. Sparks JL, Chon H, Cerritelli SM, Kunkel TA, Johansson E, Crouch RJ, Burgers PM. RNase H2-initiated ribonucleotide excision repair. *Mol Cell.* 2012;47:980-986.
22. Williams JS, Gehle DB, Kunkel TA. The role of RNase H2 in processing ribonucleotides incorporated during DNA replication. *DNA Repair*. 2017;53:52-58.
23. Vaisman A, Woodgate R. Ribonucleotide discrimination by translesion synthesis DNA polymerases. *Crit Rev Biochem Mol Biol*. 2018;53:382-402.
24. Vaisman A, Kuban W, McDonald JP, Karata K, Yang W, Goodman MF, Woodgate R. Critical amino acids in *Escherichia coli* responsible for sugar discrimination and base-substitution fidelity. *Nucleic Acids Res*. 2012;40:6144-6157.
25. McDonald JP, Vaisman A, Kuban W, Goodman MF, Woodgate R. Mechanisms employed by *Escherichia coli* to prevent ribonucleotide incorporation into genomic DNA by pol V. *PLoS Genet*. 2012;8:e1003030.
26. Vaisman A, McDonald JP, Huston D, Kuban W, Liu L, Van Houten B, Woodgate R. Removal of misincorporated ribonucleotides from prokaryotic genomes: an unexpected role for nucleotide excision repair. *PLoS Genet*. 2013;9:e1003878.
27. McCann JC, Springarn NE, Kobari J, Ames BN. Detection of carcinogens as mutagens: bacterial tester strains with R factor plasmids. *Proc Natl Acad Sci USA.*1975;72:979-983.
28. Ho C, Kulaeva OI, Levine AS, Woodgate R. A rapid method for cloning mutagenic DNA repair genes: isolation of *umu*-complementing genes from multidrug resistance plasmids R391, R446b, and R471a. *J Bacteriol*. 1993;175:5411-5419.
29. Kulaeva OI, Wootton JC, Levine AS, Woodgate R. Characterization of the *umu*-complementing operon from R391. *J Bacteriol*. 1995;77:2737-2743.
30. Mead S, Vaisman A, Valjavec-Gratian M, Karata K, Vandewiele D, Woodgate R. Characterization of polV_{R391}: a Y-family polymerase encoded by *rumA'B* from the IncJ conjugative transposon, R391. *Mol Microbiol*. 2007;63:797-810.

31. Miller JH. A short course in bacterial genetics: a laboratory manual and handbook for *Escherichia coli* and related bacteria. *Cold Spring Harbor Laboratory Press, Cold Spring Harbor*, N.Y, 1992.

32. Cupples CG, Miller JH. A set of *lacZ* mutations in *Escherichia coli* that allow rapid detection of each of the six base substitutions. *Proc Natl Acad Sci USA*. 1989;86:5345-5349.

33. Fijalkowska IJ, Jonczyk P, Tkaczyk MM, Bialoskorska M, Schaaper RM. Unequal fidelity of leading strand and lagging strand DNA replication on the *Escherichia coli* chromosome. *Proc Natl Acad Sci USA*. 1998;95:10020-10025.

34. Szekeres ESJ, Woodgate R, Lawrence CW. Substitution of *mucAB* or *rumAB* for *umuDC* alters the relative frequencies of the two classes of mutations induced by a site-specific T-T cyclobutane dimer and the efficiency of translesion DNA synthesis. *J Bacteriol*. 1996;178:2559-2563.

35. Gruber AJ, Erdem AL, Sabat G, Karata K, Jaszczur MM, Vo DD, Olsen TM, Woodgate R, Goodman M.F, Cox MM. A RecA protein surface required for activation of DNA polymerase V. *PLoS Genet*. 2015;11:e1005066.

36. Davis BD, Mingioli ES. Mutants of *Escherichia coli* requiring methionine or vitamin B12. *J Bacteriol*. 1950;60:17-28.

37. Karata K, Vaisman A, Goodman MF, Woodgate R. Simple and efficient purification of *Escherichia coli* DNA polymerase V: cofactor requirements for optimal activity and processivity *in vitro*. *DNA Repair*. 2012;11:431-440.

38. Jiang Q, Karata K, Woodgate R, Cox MM, Goodman MF. The active form of DNA polymerase V is UmuD'$_2$C-RecA-ATP. *Nature*. 2009;460:359-363.

39. Boosalis MS, Petruska J, Goodman MF. DNA polymerase insertion fidelity. Gel assay for site-specific kinetics. *J Biol Chem*. 1987;262:14689-14696.

40. Fijalkowska IJ, Schaaper RM. Effects of *Escherichia coli dnaE* antimutator alleles in a proofreading- deficient *mutD5* strain. *J Bacteriol*. 1995;177:5979-5986.

41. Henrikus SS, Wood EA, McDonald JP, Cox MM, Woodgate R, Goodman MF, van Oijen AM, Robinson A. DNA polymerase IV primarily operates outside of DNA replication forks in *Escherichia coli*. *PLoS Genet*. 2018;14:e1007161.

42. Schneider CA,.Rasband WS, Eliceiri KW. NIH Image to ImageJ: 25 years of image analysis. *Nat Methods*. 2012;9:671-675.

43. Sliusarenko O, Heinritz J, Emonet T, Jacobs-Wagner C. High-throughput, subpixel precision analysis of bacterial morphogenesis and intracellular spatio-temporal dynamics. *Mol Microbiol*. 2011;80:612-627.

44. Wozniak R.A, Fouts DE, Spagnoletti M, Colombo M.M, Ceccarelli D, Garriss G, Dery C, Burrus V, Waldor MK. Comparative ICE genomics: insights into the evolution of the SXT/R391 family of ICEs. *PLoS Genet*. 2009;5:e1000786.

45. Pinney RJ. Distribution among incompatibility groups of plasmids that confer UV mutability and UV resistance. *Mutat Res*. 1980;72:155-159.

46. Upton C, Pinney RJ. Expression of eight unrelated Muc^+ plasmids in eleven DNA repair-deficient *E. coli* strains. *Mutat Res*. 1983;112:261-273.
47. Fijalkowska IJ, Schaaper RM. Antimutator mutations in the a subunit of *Escherichia coli* DNA polymerase III: identification of the responsible mutations and alignment with other DNA polymerases. *Genetics.* 1993;134:1039-1044.
48. Banach-Orlowska M, Fijalkowska IJ, Schaaper RM, Jonczyk P. DNA polymerase II as a fidelity factor in chromosomal DNA synthesis in *Escherichia coli*. *Mol Microbiol.* 2005;58:61-70.
49. Maslowska KH, Makiela-Dzbenska K, Mo JY, Fijalkowska IJ, Schaaper RM. High-accuracy lagging-strand DNA replication mediated by DNA polymerase dissociation. *Proc Natl Acad Sci USA.* 2018;115:4212-4217.
50. Elf J, Li GW, Xie XS. Probing transcription factor dynamics at the single-molecule level in a living cell. *Science.* 2007;316:1191-1194.
51. Lewis JS, Spenkelink LM, Jergic S, Wood EA, Monachino E, Horan NP, Duderstadt KE, Cox MM, Robinson A, Dixon NE, van Oijen AM. Single-molecule visualization of fast polymerase turnover in the bacterial replisome. *Elife*. 2017;6:e23932.
52. Schlacher K, Leslie K, Wyman C, Woodgate R, Cox MM, Goodman MF. DNA polymerase V and RecA protein, a minimal mutasome. *Mol Cell*. 2005;17:561-572.
53. Schlacher K, Cox MM, Woodgate R, Goodman MF. RecA acts in trans to allow replication of damaged DNA by DNA polymerase V. *Nature*. 2006;442:883-887.
54. Vlašić I, Šimatović A, Brčić-Kostić K. Genetic requirements for high constitutive SOS expression in *recA730* mutants of *Escherichia coli*. *J Bacteriol*. 2011;193:4643-4651.
55. Watanabe-Akanuma M, Woodgate R, Ohta T. Enhanced generation of A:T→T:A transversions in a *recA730 lexA51*(Def) mutant of *Escherichia coli*. *Mutat Res*. 1997;373:61-66.
56. Curti E, McDonald JP, Mead S, Woodgate R. DNA polymerase switching: effects on spontaneous mutagenesis in *Escherichia coli*. *Mol Microbiol*. 2009;71:315-331.
57. Gonzalez M, Huston D, McLenigan MP, McDonald JP, Garcia AM, Borden KS, Woodgate R. $SetR_{ICE391}$, a negative transcriptional regulator of the integrating conjugative element 391 mutagenic response. *DNA Repair*. 2019;73:99-109.
58. Lia G, Michel B, Allemand JF. Polymerase exchange during Okazaki fragment synthesis observed in living cells. *Science*. 2012;335:328-331.
59. Woodgate R. Construction of a *umuDC* operon substitution mutation in *Escherichia coli*. *Mutat Res*. 1992;281:221-225.
60. Vandewiele D, Fernández de Henestrosa AR, Timms AR, Bridges BA, Woodgate R. Sequence analysis and phenotypes of five temperature sensitive mutator alleles of *dnaE*, encoding modified a-catalytic subunits of *Escherichia coli* DNA polymerase III holoenzyme. *Mutat Res*. 2002;499:85-95.
61. Schaaper RM. The mutational specificity of two *Escherichia coli dnaE* antimutator alleles as determined from *lacI* mutation spectra. *Genetics*. 1993;134:1031-1038.

62. Churchward G, Belin D, Nagamine Y. A pSC101-derived plasmid which shows no sequence homology to other commonly used cloning vectors. *Gene*. 1984;31:165-171.

63. Kuban W, Vaisman A, McDonald JP, Karata K, Yang W, Goodman MF, Woodgate R. *Escherichia coli* UmuC active site mutants: effects on translesion DNA synthesis, mutagenesis and cell survival. *DNA Repair*. 2012;11:726-732.

8 Concluding remarks

8.1 The regulation of the DNA damage response

According to the conventional model, the SOS response is triggered by RecA* filaments that form on single-stranded DNA gaps (ssDNA) and/or double-strand breaks (DSBs) (1–3). The RecA* filaments facilitate the cleavage of the SOS repressor LexA (3). Consequently, proteins are expressed that are involved in DNA repair and damage tolerance pathways, such as the error-prone DNA polymerases IV and V (pols IV and V) (4,5). In the early stages of the SOS response, RecA and SulA (an inhibitor of cell division) are strongly upregulated (6). 50 min after DNA damage induction, pol IV is expressed at higher levels (Chapter 3). In the later stages of the SOS response (90 min), cells begin to produce more pol V (7). These results indicate several control mechanisms for the SOS regulon and match with previous findings. For instance, pol V expression underlies a strong LexA repressor box and is thus expressed late in the SOS response (8,9). The study described in Chapter 4 however questions the conventional model of the SOS response. Following thymine starvation, DSBs are the major trigger for SOS induction, whereas single-stranded gaps only have a minor contribution.

8.1.1 Is double-strand break resection the key step for SOS induction?

During thymine starvation, ssDNA regions are converted to DSBs by reactive oxygen species or ROS (Figure 8.1 A, (10)). Trimethoprim starves cells from thymine by inhibiting dihydrofolate reductase, a pre-cursor in the synthesis of thymine (11–13). Under oxidising conditions, trimethoprim treatment causes the formation of DSBs, triggering the SOS response (Figure 8.1 A, Chapter 4). SOS induction is however blocked under radical-scavenging conditions (< 1% of SOS induction levels), even though persistent ssDNA regions are generated (Figure 8.1 A). Consistent with the levels of SOS induction, trimethoprim treatment under oxidising conditions triggered pol IV upregulation, whereas, the addition of a ROS scavenger fully repressed pol IV expression (Chapter 4). Pol V activation however differed from the results described for SOS induction and pol IV upregulation (Chapter 4). After trimethoprim treatment under oxidising conditions, pol V is only slightly upregulated and localises to the cell membrane, thus suggesting that pol V is not converted into its mutagenic active form, pol V Mut. In agreement, low levels of UmuD and UmuD′ are observed when treating with trimethoprim (Chapter 4). These observations reveal that ROS-induced DSBs trigger pol IV upregulation but not pol V upregulation/activation following trimethoprim treatment.

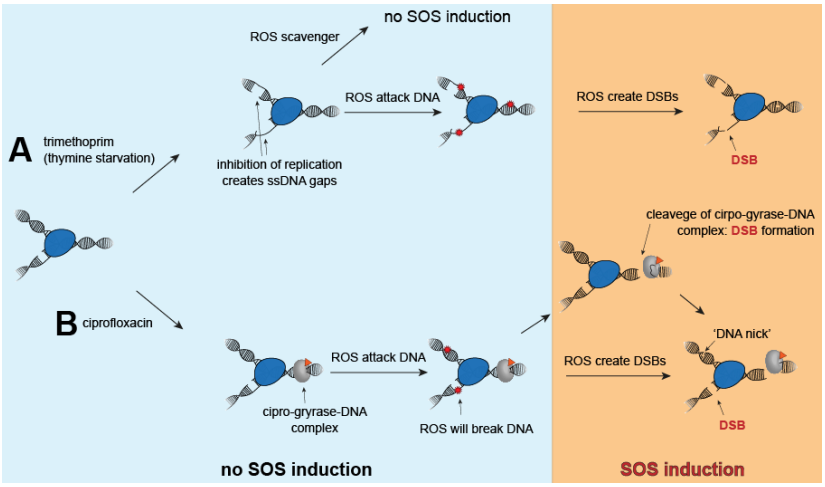

Figure 8.1. Treatment with trimethoprim and ciprofloxacin induces DSBs under oxidised conditions, triggering the SOS response. (A) Trimethoprim treatment depletes the nucleotide pool, starving cells from thymine (12). Ultimately, single-stranded regions are accumulated due to inhibition of replication (10). These ssDNA regions however only marginally trigger SOS induction (Chapter 4); pols IV and V are not upregulated. Under oxidised conditions, ssDNA are converted into DSBs, starting the SOS response. SOS induction can be blocked using ROS scavengers. (B) Following ciprofloxacin treatment, stabilised ciprofloxacin-gyrase-DNA complexes are formed. These stabilised complexes contain broken DNA and form at and away from replisomes (cartoon does not illustrate DSB formation away from replisomes). Cleavage of ciprofloxacin-enzyme-DNA complexes generates DSBs which induce the SOS response. In addition, ciprofloxacin treatment leads to the accumulation of ROS which also induce DSBs, potentiating SOS induction.

Ciprofloxacin, an antibiotic of the quinolone class, inhibits DNA gyrase (Figure 8.1 B) as well as Topoisomerase IV. These complexes contain broken DNA (14). When DNA is cleaved from these ciprofloxacin-enzyme-DNA complexes, lethal DSBs are generated (Figure 8.1B, (14)). A recent study revealed that gyrase foci form in the vicinity of replisomes with ~10 enzymes per focus (15). The vast majority of gyrase foci are however bound elsewhere on the DNA, indicating that DSBs are formed at and away from replisomes. It has been proposed that lethality may underlie gyrase inhibition and/or endonuclease activity (14). In addition, killing by ciprofloxacin is potentiated by the accumulation of reactive oxygen species (ROS), inducing DNA damage such as DSBs (Figure 8.1 B, (16)). During ciprofloxacin treatment, the SOS response is induced following DSB processing (Chapter 4). Cells then express pols IV and V at higher levels. In cells lacking *recB*, double-strand break resection is blocked as well as SOS induction. *recB* mutants however still exhibited very low levels of SOS induction (< 1%) which could be caused due to the formation ssDNA regions or RecJ activity at DSBs (2). During ciprofloxacin treatment, the addition of a reactive oxygen species scavenger largely reduced SOS induction by ~50%, suggestive of ROS generating DSBs. The addition of the ROS scavenger also reduced the expression levels of each pols IV and V by ~50%. Independent of ROS levels, pol V is released from the membrane and binds to DNA from 90 min after ciprofloxacin treatment (Chapter 4). Consequently, ciprofloxacin-induced DSBs and ROS-induced DSBs during ciprofloxacin treatment cause an increase in the expression level of pols IV and V.

Interestingly, during ciprofloxacin treatment, ROS induce non-replisomal binding sites for pol IV, consistent with the production non-replisomal DSB. This observation raises many questions. How do

ROS create non-replisomal binding sites for pol IV? Do ROS contribute to the cleavage of ciprofloxacin-enzyme-DNA complexes, generating DSBs? Are DSBs processed differently when formed in the vicinity of replisomes or away from replisomes, implying differences in toxicity?

Under the conditions described in this thesis, ciprofloxacin-induced DSBs cause pol V activation, whereas following trimethoprim treatment, ROS-induced DSBs do not trigger pol V activation. The difference in the cellular response to ciprofloxacin and trimethoprim treatment might be due to the severity of DNA damage cells are experiencing. Ciprofloxacin immobilises gyrase on the DNA at and away from replisomes (15), causing fragmentation of the entire bacterial chromosome. Starvation from thymine however destroys the replication origin, leading to local fragmentation of the chromosome (17). These results bring forward that further studies are necessary to fully understand the regulation of the SOS response and its major triggers, such as RecA loading on ssDNA gaps or DSBs (18–20). Initial data were recorded to understand the involvement of the recombination mediators RecF and RecO in forming RecA* structures after UV irradiation (Chapter 6.7).

8.1.2 Molecular dynamics during homology search

Largely fragmented chromosomes (i.e. after ciprofloxacin treatment) and local fragmentation (i.e. after trimethoprim treatment) show a difference in pol V activation, and thus, in the DNA damage response. This suggests that the DNA damage caused by trimethoprim might be not as severe as the DNA damage induced by ciprofloxacin. These variations might stem from the molecular dynamics of the players involved (i.e. DNA substrates). Three main factors might influence the cellular response:

1. Local fragmentation might be repaired faster than largely fragmented chromosomes. To repair largely fragmented and locally fragmented chromosomes, fragments must encounter its DNA partner for homology pairing. Due to cells containing many recombinant DNA fragments, DNA strands will anneal and peel off until finding the correct DNA sequence. The rate of homology search depends on the number of DNA sequences; more DNA substrates imply a longer homology search. A heavily fragmented chromosome produces many different DNA sequences as the chromosome is non-specifically broken into DNA fragments. Local fragmentation at the origin is however specific, generating DNA fragments from a smaller pool of DNA sequences. This implies that DNA repair of largely fragmented chromosomes will take longer than DNA repair of locally fragmented chromosomes. In multichromosomal cells, resected DSBs could undergo intra- and interchromosomal recombination, adding a different layer of complexity.

2. Scaffolding proteins might also change the molecular dynamics during homology search. It has been shown that the chromosome gets compacted directly after UV exposure (21). DNA compaction depends on the recombination mediator proteins RecA, RecO, RecR and RecN, suggesting that recombination might compact the nucleoid. In the later stages of the UV-induced DNA damage response, the chromosome relaxes and appears fragmented independently of recombination mediator proteins (21), probably implying DSB formation. Similarly, following ciprofloxacin treatment, the chromosome appears relaxed and fragmented (data not shown), presumably impeding recombinant search. Locally fragmented chromosomes might still have a partially intact DNA scaffold, like a compacted nucleoid structure, possibly allowing a faster homology search.

3. RecA* polymers are loaded on the 3′ overhang of DSBs, displacing the single-stranded binding protein SSB (22). The lengths of these RecA* polymers could also play into molecular dynamics. RecA* filaments grow directionally, extending the single-stranded DNA. In a cell with a largely fragmented chromosome, one would imagine that many RecA* bundles are formed, probably imposing steric hindrance and hampering homology search.

Beyond these three main factors, unknown interactions between other DNA damage response proteins, which wait to be discovered, are also likely to play into the dynamics of the DNA damage response.

8.2 Regulation of DNA polymerase IV

8.2.1 Pol IV has a role in double-strand break repair

In 1999, *Escherichia coli* was found to encode DNA polymerase IV (pol IV), promoting mutagenesis when overexpressed (4). Biochemical experiments demonstrated that pol IV can bypass various lesions (23-26). *In vivo*, pol IV was found to be involved in tolerating N^2-guanine adducts (27, 28). Similar to the replicative DNA polymerase, processivity of pol IV is increased in the presence of the β sliding clamp (29). Binding to the β sliding clamp allows pol IV to exchange for the replicative DNA polymerase within the replisome *in vitro* (30, 31). In addition, the pol IV-β interaction supports mutagenesis *in vivo* (32). Taking together these observations, pol IV has been described to carry out translesion synthesis (TLS) at the replication fork.

Based on these biochemistry and genetics data, it was however not possible to visualize the main binding sites of pol IV in living cells. Employing single-molecule live-cell imaging, the study described in Chapter 2, 4 and 5 demonstrated that only 10% of pol IV binding events happen at replisomes for different DNA damaging agents. This observation suggested that restart of stalled replisomes might thus be a minor activity of pol IV. Nonetheless, it is unclear if each pol IV binding event represents DNA synthesis.

Besides TLS, pol IV has also been demonstrated to participate in homologous recombination reactions. Work from the Rosenberg and Foster lab showed that pol IV is involved in mutagenic double-strand break repair (DSBR), under the control of the transcriptional activator RpoS (33-37). Additionally, the O'Donnell and Goodman labs demonstrated that pol IV is significantly more error-prone at recombination intermediates, called D-loops (38, 39). In agreement with pol IV working in DSBR, the study described in Chapter 4 (Figure 8.2) demonstrated that double-strand break (DSB) resection is crucial for the DNA binding activity of pol IV. To facilitate DSBR, DSBs are resected and RecA is loaded onto the single-stranded DNA (ssDNA) region, forming a RecA* nucleoprotein filament. Consistent with pol IV having a major role in DSBR, Chapter 5 describes that RecA* recruits pol IV to DNA (Figure 8.2). Replisomal pol IV foci might also form at RecA* structures, consistent with RecA* structures forming frequently at replisomes (40). In summary, this thesis supports the notion that pol IV may be a recombination protein.

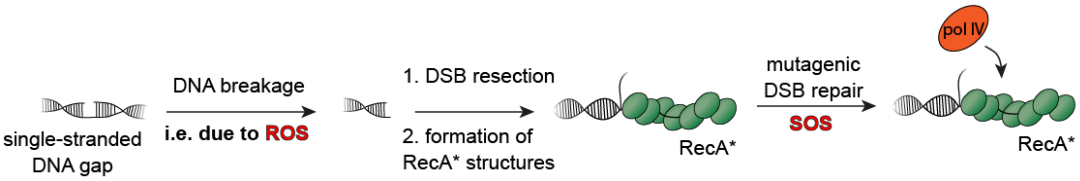

Figure 8.2. Pol IV primarily works in homologous recombination. Single-stranded DNA can be converted to DSBs by ROS. Following DSBs resection, RecA* structures are stabilised on the ssDNA overhang. Pol IV is recruited to DNA by RecA* structures.

Interestingly, preliminary data indicate that pol IV and the recombination mediator protein RecO do not share binding sites (percentage of colocalisation is below chance; data not shown). This initial finding leads to a fundamental question: Under the conditions presented here, is RecO and/or RecBCD involved in forming the RecA* filaments that recruit pol IV to the nucleoid? If RecO is involved in RecA loading, pol IV would bind at RecA* structures after RecO has dissociated. Beyond this, the role of pol IV with respect to antibiotics with different mechanisms has to be investigate in the future to paint a full picture of pol IV in living cells. Additionally, the role of pol IV in transcription-coupled repair needs to be further investigated (41).

8.2.2 UmuD and UmuD′ regulate pol IV DNA binding activity

$UmuD_2$ and $UmuD'_2$ physically interact with pol IV, modulating its mutagenic activity (Figure 8.3 A, (42)). Pol IV by itself introduces -1 frameshifts (42). In the presence of UmuD, pol IV operates error-free, whereas, UmuD′ reduces -1 frameshift mutations introduced by pol IV (42). The study in Chapter 5 describes uncleavable UmuDK97A increasing the binding lifetime of pol IV and the number of binding events (pol IV foci per cell) compared to the *umuD* deletion background (Figure 8.3 B). In contrast, UmuD′ reduces the binding lifetime of pol IV compared to the *umuD* deletion background (Figure 8.3 B). Notably, UmuDK97A and UmuD′ were expressed from a plasmid at levels 4-5 times higher than chromosomal expression levels.

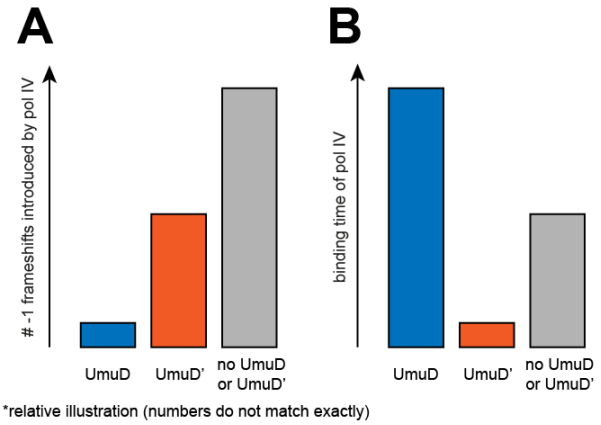

Figure 8.3. UmuD is a biochemical switch for pol IV binding and regulates the mutagenic activity of pol IV. (A) Pol IV works mostly error-free in the presence of UmuD (42). In the presence of UmuD′, -1 frameshift mutations introduced by pol IV are however increased. Curiously, UmuD′ has an inhibitory effect on the generation of -1 frameshifts. (B) UmuD promotes long-lived pol IV binding events at the nucleoid (Chapter 5). UmuD′ however strongly reduces pol IV binding time. In the absence of UmuD and UmuD′, pol IV foci are longer lived than in the presence of UmuD′ but shorter lived than in the presence of UmuD.

The fact that UmuD variants differentially affect pol IV lifetimes could also be a result of the interaction of the pol IV-UmuD complexes with RecA*. It has been reported that pol IV, $UmuD_2$ and RecA as well as pol IV, $UmuD'_2$ and RecA form ternary complexes (42). Thus, differences in the binding times of pol IV could also reflect the binding times of UmuD variants in complex with pol IV. Long-lived pol IV foci in the presence of uncleavable UmuDK97A could originate from binding events of pol IV-UmuDK97A complexes to RecA*. Thereby, uncleavable UmuDK97A (complexed with pol IV) could be trapped at RecA* structures, captured in a state in which UmuD would usually catalyse its cleavage. Short-lived pol IV foci in the presence of UmuD′ could reflect the activity of a pol IV-$UmuD'_2$ (pol IV-$UmuD'_2$-RecA respectively) which might unproductively bind to DNA or induce -1 frameshifts. This complex might also have an error-free mode, consistent with UmuD′ reducing pol IV-dependent mutation rates (42). The complex containing $UmuD'_2$ is reminiscent of pol V Mut ($UmuD'_2$C-RecA-ATP, (43)). The function of such ternary complexes of pol IV are however unknown and only speculative. Additionally, these observations might point towards a mechanism where UmuD or UmuD′ enable or block access of pol IV to the replisome must be further tested in the future.

Beyond this, alternative explanations for UmuD or UmuD′ enabling or blocking pol IV access to the replisome might be competition between, for instance, pol IV and UmuD′ for binding partners or the possibility that UmuD might allow pol IV to bind to certain binding sites which it cannot in the absence of UmuD. The latter might be reflected in UmuD increasing the binding time of pol IV, allowing pol IV to be recruited to certain binding sites, which might not necessarily reflect active DNA synthesis.

8.2.3 The recombination mediator protein RecF excludes pol IV from replisomes

In vitro, pol IV is capable of translesion synthesis at stalled replisomes, synthesising a DNA patch over a lesion. *In vivo* however, (Chapter 2), pol IV rarely binds at replisomes. Initial findings suggest that the recombination mediator RecF excludes pol IV from replisomes (Chapter 4.8, Figure 6). Three points support this hypothesis: 1. At 30 min after DNA damage induction, colocalisation of RecF with replisomes is increased (Chapter 6), while the colocalisation of pol IV with replisomes is decreased (Chapter 4). 2. In cells lacking *recF*, the decrease in pol IV-replisome colocalisation is not observed (Chapter 4.8). 3. Pol IV-RecF colocalisation is below chance colocalisation (data not shown), showing that RecF and pol IV do not share binding sites.

RecF processes stalled replisomes after UV exposure, restarting replication (44). Following repriming, this restart process might generate a gap left behind the replisome (post-replicative gap, Figure 8.4). Restart in this way might be valuable when replisomes encounter DNA lesions; RecF might be involved in lesion skipping, creating post-replicative gaps that contain a lesion (Figure 8.4). Four observations agree with RecF working in replisomes, especially after UV damage: 1. RecF is involved in replication restart after UV irradiation (45). 2. Following DNA damage induction, RecF-replisome colocalisation is increased (Chapter 6). 3. Impaired replication permits increased RecF binding at replisomes. In cells expressing a mutant of the replicative helicase DnaB (*dnaB8*[Ts]), RecF-replisome colocalisation is enhanced in the absence of DNA damage (Chapter 6). This DnaB mutant has impaired ATPase activity at its permissive temperature, consistent with replication inhibition (46), where RecF foci depend on active DNA replication.

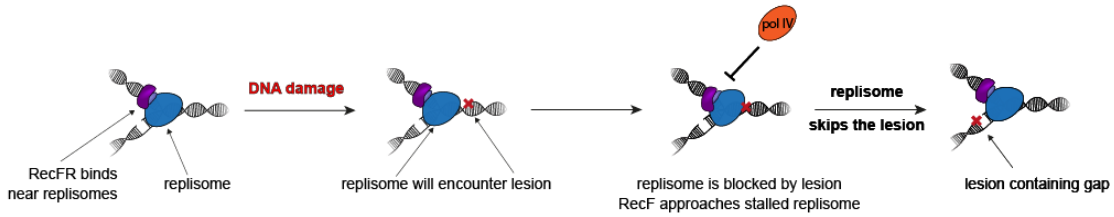

Figure 8.4. RecF processes stalled replisomes, creating post-replicative gaps. RecF frequently binds at replisomes. Following DNA damage (t = 30 min), RecF block pol IV from binding at replisomes. Thereby, RecF might allow repriming, generating a post-replicative gap.

These observations raise many questions. 1. What is the molecular basis of RecF inhibiting pol IV binding to the replisome? 2. Which substrate does RecF block from pol IV binding? Is RecF involved in producing a binding substrate for pol IV? Alternatively, does RecF generate binding sites for pol IV elsewhere on the chromosome? 3. Does a *recR* deletion also result in increased pol IV-replisome colocalisation compared to wild-type cells? RecR has been shown to increase the DNA binding activity of RecF (47). 4. Does the deletion of *recO* change the percentage of pol IV-replisome colocalisation? RecO might be involved in loading the RecA* filaments which recruit pol IV to DNA at and away from replisomes (40). If the deletion of *recO* does not affect pol IV-replisome colocalisation, RecBCD might be the primary factor for RecA* loading under the conditions described here. 4. Do *recF*, *recR* and *recO* deletions affect the activity of DNA polymerase II (pol II) at or away from replisomes? 5. Do *recF*, *recR* and *recO* deletions affect the activation of the highly mutagenic DNA polymerase V (pol V) and its binding activity at or away from replisomes? To form active pol V Mut, pol V has to form a complex with a RecA monomer from the 3′ end of a RecA* filament (48). In recombination deficient strains, RecA loading is impaired which presumably impedes the activation of pol V. In recombination deficient strains a change in pol V-replisome colocalisation might be observed. This would reveal that non-replisomal pol V foci are due to pol V activation at RecA* filaments (7). Curiously, and similar to pol IV, initial findings indicate that pol V does not share binding sites with RecO or RecF (data not shown).

8.3 Do reactive oxygen species contribute to resistance development?

Many antibiotics lead to the accumulation of reactive oxygen species (38). For instance, β-lactams (cell wall synthesis inhibitor) and quinolones (DNA gyrase and Topoisomerase IV inhibitors) potentiate ROS accumulation in bacteria (16,50). Even though β-lactams and quinolones have different bacterial targets, both treatments alter the bacterial metabolism, accumulating ROS. Consequently, ROS damage DNA, contributing to bacterial death. The phenomenon in which different antibiotic classes trigger ROS-induced damage contributing to cell death has been described as the common killing mechanism (49).

During quinolone treatment, ROS accumulation follows SOS induction using subinhibitory concentration of ciprofloxacin (Chapter 4, (51,52)). Furthermore, ROS potentiates SOS induction levels (Chapter 4, (51)). For instance, ROS-induced damage upregulates pol IV (Chapter 4). Beyond this, ROS create binding sites for pol IV. Since pol IV binding to the nucleoid is dependent on DSB resection (RecB activity, Chapter 4), pol IV may thus work at ROS-induced DSBs. Previous studies revealed that DSBs are mutagenic hotspots for pol IV activity and other error-prone polymerases (33–39), indicating that

ROS-induced DSBs might contribute to the mutagenicity of pol IV. This leads to the question if ROS accumulation is in favour of bacterial killing or if ROS-induced DSBs contribute to the emergence of resistant bacteria. The answer might however lie in between.

ROS also oxidise the nucleotide pool, creating chemically altered nucleotides (42). To counter nucleotide pool oxidation, cells express proteins that cleanse the nucleotide pool from chemically altered nucleotides (i.e. *Escherichia coli* MutT, (53,54)), thus preventing altered nucleotides being incorporated by error-prone polymerases. Pol IV, for instance, has been shown to incorporate oxidised guanines (8-oxo-dGs), generating a DNA lesion (53). It is however unknown in which context pol IV incorporates 8-oxo-dG. Since DSB resection is essential for pol IV DNA binding activity, oxidised guanines might be incorporated during DSBR or mutagenic DSBR respectively. Furthermore, incorporation of 8-oxo-dG might be mutagenic because it can base-pair with adenine and cytosine (53). In contrast to *E. coli* pol IV, its human homolog pol κ (55–57) preferentially pairs 8-oxo-dG with adenine (58). Additionally, pol κ reduces inflammation-induced mutagenesis in mice (59). These observations indicate that the human polymerase pol κ might differ from *E. coli* pol IV in its mutagenicity. Future studies are likely to shed light on the activity differences of pol κ and pol IV.

8.5 Perspectives

The studies described throughout this thesis emphasise the complexity of the DNA damage response. Within the DNA damage response, multiple proteins may compete for the same substrate (i.e. RecF and pol IV, Chapter 4.8). Some proteins might stimulate the activity of another protein (i.e. UmuD and pol IV, Chapter 5). Some proteins show differences in mutagenicity even though they are close homologs (i.e. pol V Mut and pol V_{ICE} Mut, Chapter 7).

Using single-molecule microscopy, the complex interplay of proteins within the DNA damage response can be monitored in live cells. With the introduction of single-molecule live-cell imaging in recent years, it is possible to monitor the behaviour of proteins in live cells. In combination with mutants that alter the protein's behaviour, the protein's role within cells can be functionally dissected. Besides mutants, different DNA damaging sources can also give clues about the protein's role with in the DNA damage response. Furthermore, when studying proteins of the same pathway, it can be determined if these proteins collectively or sequentially perform their function. For instance, in the case of the RecFOR pathway, RecF, RecO and RecR were described to form an active RecFOR complex. Chapter 6 however shows that RecF and RecO have distinct binding sites in cells and thus presumably different functions within the recombination pathway.

In the future, new single-molecule *in vivo* assays are likely to give further insights into the complexity of the DNA damage response. For instance, the introduction of protein-based *in vivo* DNA 'road-blocks' (dCas9, (60)) could be used to explore replisome dynamics when encountering a protein DNA complex (i.e. transcription-coupled repair). Beyond this, DNA polymerases could be studied by using fluorescent nucleotides, enabling a scientist to watch a polymerase as it synthesises DNA (Figure 8.5). This could be further used to develop a FRET-based assay that detect incorporation GA opposite of TT by pol V, giving insights into its mutagenic behaviour *in vivo*. However, to understand mechanisms in

detail, it is important to combine single-molecule assays with biochemical assays and structural studies, employing for instance cryogenic electron microscopy.

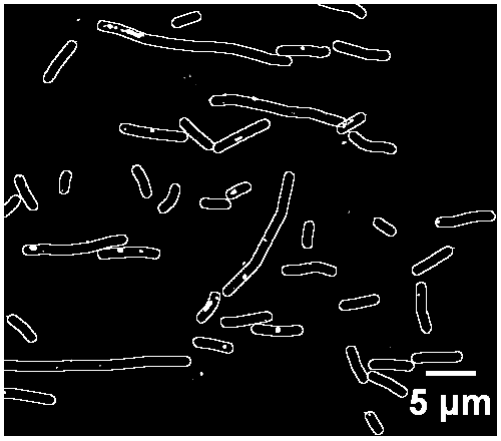

Figure 8.5. Cells contain tetramethylrhodamine-dUTP foci. Prior to imaging cells were grown in the presence of tetramethylrhodamine-dUTP and the detergent F68 Poloxamer (61). Using an exposure time of 500 ms, some foci locate to the nucleoid region, whereas other foci from at the membrane. Image is discoidal filtered. Scale bar: 5 µm.

Breaking down the complexity of the DNA damage response could uncover important mechanisms underlying the emergence of antibiotic resistance mutations. Understanding these mechanisms may allow the design of new drugs that are less likely to be overcome by bacteria. Furthermore, the DNA repair and damage tolerance mechanisms found in simple bacterial organisms might also translate to higher organism (i.e. *S. cerevisiae* and humans), having implications for the field of cancer research.

8.5 References

1. Indiani C, O'Donnell M. A Proposal: Source of single strand DNA that elicits the SOS response. *Front Biosci*. 2013;18:312–323.

2. Vlašić I, Ivančić-Baće I, Imešek M, Mihaljević B, Brčić-Kostić K. RecJ nuclease is required for SOS induction after introduction of a double-strand break in a RecA loading deficient *recB* mutant of *Escherichia coli*. *Biochimie*. 2008;90:1347–1355.

3. Simmons LA, Foti JJ, Cohen SE, Walker GC. The SOS regulatory network. *EcoSal* Plus. 2008;3:doi:10.1128/ecosalplus.5.4.3.

4. Wagner J, Gruz P, Kim SR, Yamada M, Matsui K, Fuchs RPP, et al. The dinB gene encodes a novel *E. coli* DNA polymerase, DNA pol IV, involved in mutagenesis. *Mol Cell*. 1999;4:281–286.

5. Yeiser B, Pepper ED, Goodman MF, Finkel SE. SOS-induced DNA polymerases enhance long-term survival and evolutionary fitness. *Proc Natl Acad Sci USA*. 2002;99:8737–8741.

6. Courcelle J, Khodursky A, Peter B, Brown PO, Hanawalt PC. Comparative gene expression profiles following UV exposure in wild-type and SOS-deficient. *Genetics*. 2001;158:41–64.

7. Robinson A, McDonald JP, Caldas VEA, Patel M, Wood EA, Punter CM, et al. Regulation of mutagenic DNA Polymerase V activation in space and time. *PLoS Genet*. 2015;11:e1005482.

8. Sommer S, Bailone A, Devoret R. The appearance of the UmuD′C protein complex in Escherichia coli switches repair from homologous recombination to SOS mutagenesis. *Mol Microbiol*. 1993;10:963–971.

9. Goodman MF, Woodgate R. Translesion DNA polymerases. *Cold Spring Harb Perspect Biol*. 2013;5:a010363.

10. Hong Y, Li L, Luan G, Drlica K, Zhao X. Contribution of reactive oxygen species to thymineless death in *Escherichia coli. Nat Microbiol*. 2017;2:1667–1675.

11. Birdsall B, Roberts GC, Feeney J, Dann J, Burgen A. Trimethoprim binding to bacterial and mammalian dihydrofolate reductase: a comparison by proton and carbon-13 nuclear magnetic resonance. *Biochemistry*. 1983;22:5597–604.

12. Gleckman R, Blagg N, Joubert DW. Trimethoprim: Mechanisms of action, antimicrobial activity, bacterial resistance, pharmacokinetics, adverse reactions, and therapeutic indications. *Pharmacotherapy*. 1981;1:14–19.

13. Queener SF, Cody V, Pace J, Torkelson P, Gangjee A. Trimethoprim resistance of dihydrofolate reductase variants from clinical isolates of *Pneumocystis jirovecii. Antimicrob Agents Chemother*. 2013;57:4990–4998.

14. Drlica K, Zhao X. DNA gyrase, topoisomerase IV, and the 4-quinolones. *Microbiol Mol Biol Rev.* 1997;61:377–392.

15. Stracy M, Wollman AJM, Kaja E, Gapinski J, Lee JE, Leek VA, et al. Single-molecule imaging of DNA gyrase activity in living *Escherichia coli. Nucleic Acids Res*. 2019;47:210-220.

16. Goswami M, Mangoli SH, Jawali N. Involvement of reactive oxygen species in the action of ciprofloxacin against *Escherichia coli. Future Microbiol*. 2014;6:949–954.

17. Sangurdekar DP, Hamann BL, Smirnov D, Srienc F, Hanawalt PC, Khodursky AB. Thymineless death is associated with loss of essential genetic information from the replication origin. *Mol Microbiol.* 2010;75:1455–1467.

18. Morimatsu K, Kowalczykowski SC. RecFOR proteins load RecA protein onto gapped DNA to accelerate DNA strand exchange: A universal step of recombinational repair. *Mol Cell*. 2003;11:1337–1347.

19. Sakai A, Cox MM. RecFOR and RecOR as distinct RecA loading pathways. *J Bio*. 2009;284:3264–3272.

20. Lesterlin C, Ball G, Schermelleh L, Sherratt DJ. RecA bundles mediate homology pairing between distant sisters during DNA break repair. *Nature*. 2014;506:249–253.

21. Odsbu I, Skarstad K. DNA compaction in the early part of the SOS response is dependent on RecN and RecA. *Microbiology*. 2014;160:872–882.

22. Cox MM. Regulation of bacterial RecA protein function. *Crit Rev Biochem Mol Biol*. 2007;42:41–63.

23. Tang M, Pham P, Shen X, Taylor JS, O'Donnell M, Woodgate R, Goodman MF. Roles of *E. coli* DNA polymerases IV and V in lesion-targeted and untargeted SOS mutagenesis. *Nature.* 2000; 404):1014–1018.

24. Suzuki N, Ohashi E, Hayashi K, Ohmori H, Grollman AP, Shibutani S. Translesional synthesis past acetylaminofluorene-derived DNA adducts catalyzed by human DNA polymerase kappa and *Escherichia coli* DNA polymerase IV. *Biochemistry.* 2001;40:15176–15183.

25. Shen X, Sayer JM, Kroth H, Ponten I, O'Donnell M, Woodgate R, Jerina DM, Goodman MF. Efficiency and accuracy of SOS-induced DNA polymerases replicating benzo[*a*]pyrene-7,8-diol 9,10-epoxide A and G adducts. *J Biol Chem.* 2002; 277:5265–5274.

26. Maor-Shoshani A, Hayashi K, Ohmori H, Livneh Z. Analysis of translesion replication across an abasic site by DNA polymerase IV of *Escherichia coli*. *DNA Repair.* 2003; 2:1227–1238.

27. Napolitano R, Janel-Bintz R, Wagner J, Fuchs RP. All three SOS-inducible DNA polymerases (Pol II, Pol IV and Pol V) are involved in induced mutagenesis. *EMBO J.* 2000; 19:6259–6265.

28. Kim SR, Matsui K, Yamada M, Gruz P, Nohmi T. Roles of chromosomal and episomal *dinB* genes encoding DNA pol IV in targeted and untargeted mutagenesis in *Escherichia coli*. *Mol Genet Genomics.* 2001; 266:207–215.

29. Wagner J, Fujii S, Gruz P, Nohmi T, Fuchs RP. The β clamp targets DNA polymerase IV to DNA and strongly increases its processivity. *EMBO Rep.* 2000; 1:484–488.

30. Indiani C, McInerney P, Georgescu R, Goodman MF, O'Donnell M. A sliding-clamp toolbelt binds high- and low-fidelity DNA polymerases simultaneously. *Mol Cell.* 2005; 19:805–815.

31. Furukohri A, Goodman MF, Maki H. A dynamic polymerase exchange with *Escherichia coli* DNA polymerase IV replacing DNA polymerase III on the sliding clamp. *J Biol Chem.* 2008; 283:11260–11269.

32. Becherel OJ, Fuchs RP, Wagner J. Pivotal role of the beta-clamp in translesion DNA synthesis and mutagenesis in *E. coli* cells. *DNA Repair.* 2002 Sep 4; 1:703–708.

33. Shee C, Gibson JL, Rosenberg SM. Two mechanisms produce mutation hotspots at DNA breaks in *Escherichia coli*. *Cell Rep.* 2012;2:714–721.

34. Rosenberg SM, Shee C, Frisch RL, Hastings PJ. Stress-induced mutation *via* DNA breaks in *Escherichia coli*: A molecular mechanism with implications for evolution and medicine. *Bioessays*. 2012;34:885–892.

35. Frisch RL, Su Y, Thornton PC, Gibson JL, Rosenberg SM, Hastings PJ. Separate DNA Pol II- and Pol IV-dependent pathways of stress-induced mutation during double-strand-break repair in *Escherichia coli* are controlled by RpoS. *J Bacteriol*. 2010;192:4694–4700.

36. Ponder RG, Fonville NC, Rosenberg SM. A switch from high-fidelity to error-prone DNA double-strand break repair underlies stress-induced mutation. *Mol Cell*. 2005;19:791–804.

37. Mallik S, Popodi EM, Hanson AJ, Foster PL. Interactions and localization of *Escherichia coli* error-prone DNA Polymerase IV after DNA damage. *J Bacteriol*. 2015;197:2792–2809.

38. Pomerantz RT, Kurth I, Goodman MF, O'Donnell M. Preferential D-loop extension by a translesion DNA polymerase underlies error-prone recombination. *Nat Struct Mol Biol*. 2013;20:748–755.

39. Pomerantz RT, Goodman MF, O'Donnell ME. DNA polymerases are error-prone at RecA-mediated recombination intermediates. *Cell Cycle*. 2013;12:2558–2563.

40. Ghodke H, Paudel B, Lewis JS, Jergic S, Gopal K, Romero Z, et al. Spatial and temporal organization of RecA in the *Escherichia coli* DNA-damage response. *Elife*. 2019;8:e42761.

41. Cohen SE, Lewis CA, Mooney RA, Kohanski MA, Collins JJ, Landick R, Walker GC. Roles for the transcription elongation factor NusA in both DNA repair and damage tolerance pathways in *Escherichia coli*. *Proc Natl Acad Sci U S A.* 2010; 107:15517–15522.

42. Godoy VG, Jarosz DF, Simon SM, Abyzov A, Walker GC. UmuD and RecA directly modulate the mutagenic potential of the Y-family DNA polymerase DinB. *Mol Cell*. 2007;28:1058–1070.

43. Erdem AL, Jaszczur M, Bertram JG, Woodgate R, Cox MM, Goodman MF. DNA polymerase V activity is autoregulated by a novel intrinsic DNA-dependent ATPase. *Elife*. 2014;3:1–14.

44. Courcelle J, Carswell-Crumpton C, Hanawalt PC. recF and recR are required for the resumption of replication at DNA replication forks in Escherichia coli. *Proc Natl Acad Sci USA*. 1997;94:3714–3719.

45. Fujii S, Isogawa A, Fuchs RP. RecFOR proteins are essential for Pol V-mediated translesion synthesis and mutagenesis. *EMBO J*. 2006;25:5754–5763.

46. Saluja D, Godson GN. Biochemical characterization of Escherichia coli temperature-sensitive *dnaB* mutants *dnaB8*, *dnaB252*, *dnaB70*, *dnaB43*, and *dnaB454*. *J Bacteriol*. 1995;177:1104–1111.

47. Webb BL, Cox MM, Inman RB. An interaction between the *Escherichia coli* RecF and RecR proteins dependent on ATP and double-stranded DNA. *J Biol Chem*. 1995;270:31397–31404.

48. Gruber AJ, Erdem AL, Sabat G, Karata K, Jaszczur MM, Vo DD, et al. A RecA protein surface required for activation of DNA polymerase V. *PLoS Genet.* 2015;11:e1005066.

49. Kohanski MA, Dwyer DJ, Hayete B, Lawrence CA, Collins JJ. A common mechanism of cellular death induced by bactericidal antibiotics. *Cell.* 2007;130:797–810.

50. Dwyer DJ, Belenky PA, Yang JH, MacDonald IC, Martell JD, Takahashi N, et al. Antibiotics induce redox-related physiological alterations as part of their lethality. *Proc Natl Acad Sci USA*. 2014;111:E2100–9.

51. Rodriguez- Rosado A, Valencia EY, Rodriguez- Rojas A, Coloma C, Galhardo RS, Blazquez J, et al. Reactive oxygen species are major contributors to SOS-mediated mutagenesis induced by fluoroquinolones. *bioRχiv*. 2018;http://dx.doi.org/10.1101/428961.

52. Pribis JP, Garcia-Villada L, Zhai Y, Lewin-Epstein O, Wang A, Liu J, et al. Gamblers: an antibiotic-induced evolvable cell subpopulation differentiated by reactive-oxygen-induced general stress response. *Mol Cell*. 2019;74:785-800.

53. Foti JJ, Devadoss B, Winkler JA, Collins JJ, Walker GC. Oxidation of the guinine nucleotide pool underlies cell death by bactericidial antibiotics. *Science*. 2012;336:315–319.

54. Friedberg EC, Walker GC, Wolfram S, Wood RD, Schultz RA, Ellenberger T. DNA Repair and Mutagenesis. 2005.

55. Washington MT, Johnson RE, Prakash L, Prakash S. Human DINB1-encoded DNA polymerase is a promiscuous extender of mispaired primer termini. *Proc Natl Acad Sci USA.* 2002;99:1910–1914.

56. Gerlach VL, Aravind L, Gotway G, Friedberg EC, Schultz RA, Koonin E V. Human and mouse homologs of Escherichia coli DinB (DNA polymerase IV), members of the UmuC/DinB superfamily. *Proc Natl Acad Sci USA*. 2002;96:11922–11927.

57. Velasco-Miguel S, Richardson JA, Gerlach VL, Lai WC, Gao T, Russell LD, et al. Constitutive and regulated expression of the mouse Dinb (Polκ) gene encoding DNA polymerase kappa. *DNA Repair*. 2003;2:91–106.

58. Katafuchi A, Sassa A, Niimi N, Grúz P, Fujimoto H, Masutani C, et al. Critical amino acids in human DNA polymerases η and κ involved in erroneous incorporation of oxidized nucleotides. *Nucleic Acids Res*. 2009;38:859–867.

59. Hakura A, Sui H, Sonoda J, Matsuda T, Nohmi T. DNA polymerase kappa counteracts inflammation-induced mutagenesis in multiple organs of mice. *Environ Mol Mutagen Mutagen*. 2019;60:320-330.

60. Whinn K, Kaur G, Lewis JS, Schauer G, Müller S, Jergic S, et al. Nuclease dead Cas9 is a programmable roadblock for DNA replication. *bioRχiv*. https://doi.org/10.1101/455543.

61. Berlatzky IA, Rouvinski A, Ben-Yehuda S. Spatial organization of a replicating bacterial chromosome. *Proc Natl Acad Sci USA*. 2008;105:14136–14140.